Durability of steel fibre reinforced concrete in corrosive environments

PhD thesis

20th July 2019

Victor Marcos Meson
vicmes@byg.dtu.dk
Department of Civil Engineering, Technical University of Denmark
Kongens Lyngby, Denmark

Supervisors:

Associate Professor Gregor Fischer. *Department of Civil Engineering, Technical University of Denmark (DTU), Denmark.*

Assistant Professor Alexander Michel. *Department of Civil Engineering, Technical University of Denmark (DTU), Denmark.*

Dr. Carola Edvardsen. *Department of Tunnels and Underground Infrastructure, COWI A/S, Denmark.*

Dr. Anders Ole Stubbe Solgaard. *Department of Tunnels and Underground Infrastructure, COWI A/S, Denmark.*

Associate Professor Torben Lund Skovhus. *Centre of Applied Research and Development in Building, Energy & Environment, VIA University College (VIA UC), Denmark.*

Assessment committee:

Professor Henrik Stang. *Department of Civil Engineering, Technical University of Denmark (DTU), Denmark.*

Professor Giovanni Plizzari. *Department of Civil, Environmental, Architectural Engineering and Mathematics (DICATAM), University of Brescia, Italy.*

Professor Terje Kanstad. *Department of Structural Engineering, Norwegian University of Science and Technology (NTNU), Norway.*

Durability of steel fibre reinforced concrete under corrosive environments

Printed by

Department of Civil Engineering

Technical University of Denmark

ISBN: 87-7877-532-9

ISSN:

Preface

This thesis is submitted as partial fulfilment of the requirements for obtaining the Danish Industrial PhD degree. The study has been undertaken at the Department of Civil Engineering, Technical University of Denmark, under the supervision of Associate Professor Gregor Fischer and co-supervised by Assistant Professor Alexander Michel, and at COWI A/S under the supervision of Dr. Carola Edvardsen and co-supervision of Dr. Anders Solgaard. Co-supervision at VIA University College was provided by Associate Professor Torben L. Skovhus.

This thesis is part of the industrial PhD project: *"Corrosion resistance of steel fibre reinforced concrete structures"*, carried out in collaboration with the department of Tunnels and Underground Infrastructure of COWI A/S and the Centre of Applied Research and Development in Building, Energy & Environment of VIA University College.

The project covered the period between September 2015 and July 2019, and comprised three years of PhD education where the candidate was employed at the department of Tunnels and Underground Infrastructure of COWI A/S, and two voluntary leave of absences at the Department of Civil Engineering of DTU comprising ten months: four months in connection with the project *"Enhanced mechanical evaluation of fresh and harden properties of oil&gas well barrier material quality in underground conditions"* at and six months in connection with the project *"Grøn Beton II"*.

This study was co-funded by InnovationsFonden Denmark (grant number 5016-00103B) and COWIfonden (grant number C-129.02). The work was carried out at the Technical University of Denmark (DTU), COWI A/S and VIA University College, in the period from September 2015 to July 2019. The experimental work was co-financed by the VDS members (KrampeHarex, Arcelor Mittal, Bekaert and BM-Underground Solutions), Mapei Denmark, and VejDirektoratet.

Victor Marcos Meson

Kgs. Lyngby July 2019

Preface to published version

This thesis was defended at a public defence on Monday the 29th of October 2019. The PhD degree was awarded by the Technical University of Denmark.

A few minor changes were made to the published version, compared to the version submitted for defence. The status of the papers has been updated on March of 2020:

Papers V and VIII are published and are printed in this thesis in the Publisher's formatted version. The doi reference numbers have been included in the thesis.

Paper VII is published and is printed in this thesis as the original manuscript with the authors' formatting. The doi reference number to the published version has been included.

Paper VI is under review. The status has been updated in the thesis, and the paper is printed in this thesis as the original manuscript with the authors' formatting. The status of the paper is referred to as "under-review".

Papers III and IV have been resubmitted to the journal: "Journal of Sustainable Cement-Based Materials (Taylor & Francis)". Further changes may be expected to the final accepted version. The papers are printed in this thesis as the original manuscript with the authors' formatting and their status is referred to as "unpublished".

Victor Marcos Meson

Kgs. Lyngby March 2020

Acknowledgements

First, I would like to express my gratitude to my supervisors Associate Professor Gregor Fischer and Assistant Professor Alexander Michel from the Department of Civil Engineering at the Technical University of Denmark (DTU), Dr. Carola Edvardsen and Dr. Anders Solgaard from COWI, and Associate Professor Torben L. Skovhus from VIA University College (VIA) for their support and guidance during this time. My special thanks to Alexander Michel and Anders Solgaard for their day to day work with me and long discussions, I would not have reached the finish line without you.

Second, I would like to thank my colleagues at DTU, VIA and COWI. Thanks to the staff at the structural and material laboratories at DTU and the laboratories at VIA, that have contributed with their work to the experimental campaigns. Mange tak Hans Erik, Klaus, Michael og Christian.

I would like to acknowledge the contribution of the students whose dissertations I co-supervised at DTU during this period. Their work, even if not included, has helped in great share to this thesis: Simon Bozik & Viktor Balaz, Jakob Jensen & Oliver Thorpe, Lisa Alm, Andreas Kragh & Martin Carlsen, Anna Adamczyk, Daniel Mois & Vlad Chiriac, Robert Havlik & Ivan Galik, and Mathias Thorsen & Patrick Christensen.

Also, I would like to acknowledge the contribution to experiments and publications in this thesis from: Prof. Mette Geiker (NTNU), Dr. Ulla Jakobsen (TI), Dr. Tobias Danner (SINTEF) and Dr. Carsten Grundlach (DTU 3DIM).

Third, I want to thank the financial and technical support from our partners during the planning and execution of the project: the VDS members (KrampeHarex, Arcelor Mittal, Bekaert and BM-Underground Solutions), Mapei Denmark, and VejDirektoratet. Special thanks in this aspect to VIA University College in Horsens: Gitte N. Munch-Petersen, Søren E. Poulsen and Torben Brøchner for their support during the preparation of this project.

Last but foremost, I would like to thank my family and friends for their warmth and support during these years. *A mis padres y hermano, que me habéis apoyado y enseñado tanto, nunca habría escrito esta tesis sin vosotros, os quiero. Y a Maria, que durante estos años has sido amiga, compañera, consejera, reviewer, editora… esta tesis es también tuya, maite zaitut.*

Abstract

Steel Fibre Reinforced Concrete (SFRC) is increasingly used worldwide for the construction of civil infrastructure under aggressive exposure conditions. The use of carbon-steel fibres in concrete as partial or total replacement of conventional steel reinforcement bars is becoming an attractive solution to the industry, considering its simplified production processes, cost-effectiveness and overall durability in compressed elements subject to corrosive exposures.

However, the durability aspect is still under discussion when addressing the corrosion of carbon-steel fibres bridging cracks in concrete under some exposures, such as wet-dry conditions. Contradictions in design guidelines and in former studies regarding the durability of cracked SFRC under these exposures hampers further development of SFRC infrastructure. In particular, the deterioration mechanisms affecting cracked SFRC under wet-dry cyclic exposures are not well-understood.

This thesis presents an experimentally-focused multiscale investigation that aims at identifying the main variables influencing steel fibre corrosion in concrete subject to wet-dry cycles and quantifying the effect of fibre corrosion on the mechanical performance of SFRC. The experimental campaign covered studies of SFRC exposed to wet-dry cycles under chloride and carbon-dioxide exposure, at the composite and single-fibre level, with focus on the deterioration inside cracks.

Experiments at the composite level confirmed that corrosion damage in uncracked SFRC is negligible and does not entail damage to the mechanical performance of the uncracked material. Corrosion damage of steel fibres inside cracks narrower than 0.3 mm occurred at the outermost 20 – 40 mm of the crack and had a limited impact on the mechanical performance of the cracked SFRC over a period of two years.

Significant increases of the residual tensile strength of the cracked SFRC after exposure were observed at the composite and single fibre level. A semi-empirical multiscale model based on the fibre bundle approach was developed to connect observations at the single-fibre and composite levels. The model confirmed that, under wet-dry cyclic exposure conditions, fibre corrosion may not be the dominant deterioration mechanism affecting the mechanical performance of cracked SFRC during exposure. An increase of the fibre-matrix bond strength was responsible for a large share of the variations observed in the toughness of the cracked SFRC.

An investigation of the damage mechanisms showed that concurring deterioration and recovery processes reduce the tensile capacity of the steel fibres and alter the cement matrix adjacent to the crack and surrounding the steel fibres. Autogenous healing of mechanical damage at the cement matrix around the fibre hook was identified as the main recovery mechanism responsible of the increase in the fibre-matrix bond strength during the exposure. A conceptual deterioration model considering these processes was described and compared to experimental data.

The work presented in this thesis concluded that, under the exposure conditions and time-scales investigated, corrosion damage of steel fibres inside cracks below 0.3 mm has a subordinate impact on the alterations of the tensile toughness of cracked SFRC. Changes in the toughness of the cracked SFRC after exposure were related mainly to the alteration of the cement matrix surrounding the steel fibres.

Resume

På verdensplan benyttes stålfiberarmeret beton (SFRC) i stigende grad til konstruktioner til infrastrukturen udsat for aggressiv miljøeksponering. Fordelene ved brug af (kulstof) stålfibre som hel eller delvis erstatning for traditionelle armeringsjern er mange, deriblandt simplificerede produktionsprocesser og reducerede produktions-omkostninger ved udstøbning af beton, samt en generel og bred anerkendelse af deres gode holdbarhed når blot de bruges i betonelementer udsat for trykpåvirkning.

Holdbarheden af SFRC, mht. risikoen for korrosion af stålfibre der krydser revner i betonen når denne er udsat for bestemte miljøpåvirkninger, f.eks. cyklisk vådt-tørt miljø, debatteres stadig. Modstridende information i designguidelines samt tidligere studier vedrørende holdbarheden af revnet SFRC udsat for disse miljøpåvirkninger vanskeliggør brugen og den videre udvikling af SFRC til beton i infrastrukturen. Særligt er nedbrydningsmekanismerne for revnet SFRC udsat for cyklisk våd-tør miljø-påvirkning ikke tilstrækkeligt beskrevet og afdækket.

Denne afhandling præsenterer resultater fra et eksperimentelt-fokuseret multiskala PhD projekt, hvis formål har været at identificere primære parametre, der har en indflydelse på korrosion af stålfibre i beton udsat for våd-tør miljøpåvirkning samt kvantificere indflydelsen af fiberkorrosion på de mekaniske egenskaber af SFRC. De eksperimentelle undersøgelser indeholdt studier af SFRC eksponeret for våd-tør cykler inklusiv klorid og CO_2, på kompositniveau såvel som på fiberniveau med fokus på nedbrydning i betonens revner.

Forsøgene på kompositniveau bekræftede at korrosion i urevnet SFRC er negligibel og at dette ikke fører til en reduktion af de mekaniske egenskaber af det urevnede materiale. Korrosion af stålfibre i revner mindre end 0.3mm forekom ved de yderste 20-40 mm, og dette havde kun en begrænset indflydelse på de mekaniske egenskaber af revnet SFRC målt over forsøgenes varighed, dvs. to år.

En væsentlig forøgelse af den maksimale residualtrækstyrke af revnet SFRC efter eksponering blev observeret på kompositniveau såvel som på fiberniveau. En semiemperisk multiskalamodel baseret på teorien om fibre-bundter blev udviklet til at forbinde observationerne på fiberniveau med observationerne på kompositnievau. Resulater fra modellen bekræftede, at fiberkorrosion formentlig ikke er den dominerende nedbrydningsmekanisme influerende de mekaniske egenskaber af revnet SFRC under våd-tør eksponering. Forøgelse af vedhæftningen mellem fiber og matrice var primær årsag til de observerede variationer i sejheden af revnet SFRC.

En undersøgelse af skadesmekanismerne viste at der på samme tid sker en reduktion af stålfibrenes trækstyrke og en ændring af cementmatricen omkring revnen og stålfibrene. Autogen heling af de mekanisk opståede skader omkring fiberens endekroge blev identificeret som den primære helingsmekanisme ansvarlig for forøgelsen af vedhæftningen mellem fiberen og matricen under eksponeringen. En konceptuel nedbrydningsmodel som tager disse processer i betragtning blev beskrev og sammenlignet med eksperimentelle data.

Studierne præsenteret i denne afhandling konkluderer, at, korrosionsskader af stålfibre i revner mindre end 0.3 mm har kun en sekundær effekt på ændringer af sejheden af revnet SFRC udsat for trækpåvirkning under de undersøgte miljøpåvirkninger samt varighed af forsøg. Ændringer i sejheden af revnet SFRC efter eksponering blev primært tilskrevet ændringer i cementmatricen omkring stålfibrene.

Table of contents

Publications included in the thesis

Paper I Marcos-Meson, V., Michel, A., Solgaard, A., Fischer, G., Edvardsen, C., Skovhus, T.L., 2018. Corrosion resistance of steel fibre reinforced concrete - A literature review. Cem. Concr. Res. 103, 1–20. doi:10.1016/j.cemconres.2017.05.016.

Paper II Marcos-Meson, V., Fischer, G., Edvardsen, C., Skovhus, T.L., Michel, A., 2019. Durability of Steel Fibre Reinforced Concrete (SFRC) exposed to acid attack – A literature review. Constr. Build. Mater. 200, 490–501. doi:10.1016/j.conbuildmat.2018.12.051.

Paper III Marcos-Meson, V., Fischer, G., Edvardsen, C., Solgaard, A., Michel, A., 2019. Mechanical performance of steel fibre reinforced concrete exposed to chlorides and carbon dioxide: results after one year (unpublished).

Paper IV Marcos-Meson, V., Fischer, G., Solgaard, A., Edvardsen, C., Michel, A., 2020. Development of the mechanical performance of steel fibre reinforced concrete exposed to wet-dry cycles of chlorides and carbon dioxide: results after two years (unpublished).

Paper V Marcos-Meson, V., Fischer, G., Edvardsen, C., Solgaard, A., Michel, A., 2020. Pull-out behaviour of hooked-end steel fibres in cracked concrete exposed to wet-dry cycles of chlorides and carbon dioxide – mechanical performance. Constr. Build. Mater. 240 (2020) 117764. doi:10.1016/j.conbuildmat.2019.117764.

Paper VI Marcos-Meson, V., Geiker, M., Fischer, G., Solgaard, A., Jakobsen, U.H., Edvardsen, C., Danner, T., Skovhus, T.L., Michel, A., 2020. Durability of cracked SFRC exposed to wet-dry cycles of chlorides and carbon dioxide – multiscale deterioration phenomena (Under review). Cem. Concr. Res.

Paper VII Marcos-Meson, V., Solgaard, A., Skovhus, T.L., Jakobsen, U.H., Fischer, G., Edvardsen, C., Michel, A. 2020. Pull-out behaviour of steel fibres in cracked concrete under wet-dry cycles – deterioration phenomena. Mag. Concr. Res. (2020) 1–32. doi:10.1680/jmacr.19.00448.

Paper VIII Marcos-Meson, V., Fischer, G., Edvardsen, C., Solgaard, A., Michel, A., 2020. Mechanical performance of cracked SFRC exposed to corrosive environments – a multiscale modelling approach. Constr. Build. Mater. 234 (2020) 117847.doi:10.1016/j.conbuildmat.2019.117847.

Additional publications (not appended)

Marcos-Meson, V., Michel, A., Solgaard, A., Fischer, G., Edvardsen, C., Skovhus, T.L., 2016. Corrosion Resistance of Steel Fibre Reinforced Concrete – a Literature Review, in: Beushausen, H. (Ed.), Fib Symposium 2016. Performance-Based Approaches for Concrete Structures. FIB, Cape Town, ZA, pp. 121–122.

Marcos-Meson, V., Michel, A., 2016. Multi-scale testing of fibre reinforced concrete under corrosion deterioration. In: 1st International Symposium on Multi-Scale Experimental Mechanics. Roskilde, DK, pp. 33–34.

Marcos-Meson V., Michel A., Fischer G., Solgaard A., Edvardsen C., Skovhus T.L., 2018. Accelerated weathering of steel fibre reinforced concrete exposed to chlorides. In: 17th Nordic Corrosion Congress. Kgs. Lyngby, DK.

Michel, A., Meson, V.M., Stang, H., Geiker, M.R., Lepech, M., 2018. Coupled mass transport, chemical, and mechanical modelling in cementitious materials: A dual-lattice approach, in: Caspeele, R., Taerwe, L., Frangopol, D.M. (Eds.), Life Cycle Analysis and Assessment in Civil Engineering: Towards an Integrated Vision: Proceedings of the Sixth International Symposium on Life-Cycle Civil Engineering (IALCCE 2018). CRC Press, Ghent, Belgium, pp. 965–972.

Michel, A., Geiker, M., Marcos, V., 2020. Microstructural changes and mass transport in cement-based materials: a modeling approach (Under Review). Cem. Concr. Res.

Kragh, A.K., Carlsen, M.E., Marcos-Meson, V., Fischer, G., Michel, A., 2019. The influence of concrete maturity on the pull-out behaviour of steel fibres at early-ages, in: Fib SYMPOSIUM 2019 Concrete - innovations in materials, design and structures. Krakow, Poland.

Addassi, M., Michel, A., Meson, V.M., Kunther, W., 2019. Modelling and testing of carbonation effects on hydrated oil-well cements, in: IFFSAR (Ed.), International Workshop. CO2 Storage in Concrete. Marne La Vallée, FR.

Marcos-Meson, Victor, I. Paegle, and G Fischer. 2019. “Characterization of the Initiation and Development of Cracks in Cement Sheath around Oil&gas Well Casing.” In 4th International Conference. Innovative Materials, Structures and Technologies. Riga, Latvia.

Chapter 1
Introduction

1.1 Background and motivation

Steel fibre reinforced concrete (SFRC) is increasingly used to produce in-situ and prefabricated concrete structures. The use of carbon-steel fibres, henceforth "steel fibres" for structural applications, as partial or total replacement of conventional reinforcement bars has become a popular solution, among others, for the construction of prefabricated segmental linings for bored tunnels and in-situ industrial slabs (Abbas, 2014; de Rivaz, 2009; Meda and Plizzari, 2005).

One of the major arguments used in favour of this technology is the overall improved performance of SFRC under aggressive exposure conditions compared to conventional reinforcement and unreinforced concrete; both standalone (ACI Committee 544, 2010, 2002) or combined with reinforcement bars (Berrocal, 2015; Solgaard, 2014). Despite the positive perspective, the total replacement of conventional steel reinforcement with steel fibres is still controversial, especially when the long-term durability of cracked SFRC under corrosive exposure conditions is addressed.

1.1.1 Design guidance for SFRC exposed to corrosive environments

To date, there is no international standard available for the design of SFRC structures, yet an EN standard in the framework of Eurocode-2 is currently under preparation (European Commitee for Standardization (CEN), 1993). Therefore, the design of SFRC infrastructure primarily relies on national guidelines and international design codes, which are often not coherent with respect to the applicability within certain exposure classes that involve the risk of reinforcement corrosion, such as: chloride attack (EN-206 exposure class XS2-3 and XD2-3) (European Commitee for Standardization (CEN), 2013), carbonation attack (XC3-4) or chemical attack (XA1-3), as shown in **Table 1**.

Most of the guidelines cover the design of SFRC subject to carbonation (XC) and chloride (XS and XD) exposure. These guidelines primarily specify prescriptive design rules in terms of: i) identifying a sacrificial layer of SFRC to discount from the original cross-section for uncracked SFRC (Δ_h); ii) defining a critical characteristic crack width for cracked SFRC ($w_{k,crit}$); iii) using specific types of steel fibres, e.g. stainless-steel; iv) considering special design actions, such as experimental proof of the durability under certain exposures. However, some of the national guidelines do not cover the design of SFRC under the most aggressive exposure classes (e.g. XS2-3, XD2-3) or do not mention specific limitations in terms of durability.

The regulation for SFRC under chemical exposure class (XA) is special, since there are limited national guidelines covering this exposure and prescriptions rely on very limited research to support recommendations in terms of, e.g., a sacrificial layer (Δh), a critical characteristic crack width ($w_{k,crit}$) or a fibre material.

In other cases, guidance is given on basis of unclear recommendations (Norsk Beton, 2011; The Concrete Society, 2007); or specific recommendations are not given (International Federation for Structural Concrete, 2010; New Zealand Standards, 2006), so that consideration of the same design recommendations as for conventional steel reinforcement may be left to the interpretation of designers.

Table 1. Summary of recommendations in design guidelines, after (Marcos-Meson et al., 2018).

Standard		**Carbonation**		**Chlorides**		**Chemical / acids**	
		XC2 XC3	**XC4**	**XS2 XD2**	**XS3 XD3**	**XA1 XA2**	**XA3**
ACI-544-1R-96 (US) (ACI Committee 544, 2002)	w_k^{50}	0.30	0.30	0.10	0.10	-	-
	Δ_h^{50}	-	-	2.5	2.5	-	-
RILEM TC 162-TDF (EU) (RILEM, 2000)	w_k^{50}	0.30	0.30	Special	Special	Special	Special
	Δ_h^{50}	10	10				
DBV-Merkblatt Stahlfaserbeton (DE) (German Society for Concrete and Construction Technology, 2001)	w_k^{50}	0.30	0.20	0.20	0.20	0.2 0.15	0.15
	Δ_h^{50}	20	25	40	40	40	40
CNR-DT 204/2006 (IT) (CRN, 2006)	w_k^{50}	0.30	0.30	0.30	0.30	-	-
	$*\Delta_h^{>50}$	10	10	10	10	10	10
	Fibre	C-G-S	G-S	G-S C-G-S	S G-S	G-S	S
EHE 2008 (ES) (Spanish Development Ministry, 2009)	w_k^{50}	0.30	0.30	Test	Test	Test	Test
	Fibre	C-G-S	C-G-S	G-S	G-S		
DAfStb Stahlfaserbeton (DE) (DAfStb, 2012)	w_k^{50}	0.30	0.30	N/A	N/A	-	-
Design guideline for structural applications of SFRC (DK) (SFRC Consortium, 2013)	w_k^{50}	0.30	0.20	N/A	N/A	-	-
AFTES-GT38R1A1 (FR) (AFTES, 2013)	w_k^{50}	0.20	0.20	0.15	0	0.15	0
	Fibre	C-G-S	C-G-S	C-G-S	G-S	C-G-S	G-S
SS-812310: 2014 (SE) (Swedish Standards Institute, 2014)	w_k^{50}	0.50	0.40	0.30	0.20	-	-
	w_k^{100}	0.40	0.30	0.20	0.10		

Abbreviations: (N/A) Not applicable; (C) Carbon-steel steel fibres can be used; (G) Coated carbon-steel fibres can be used; (S) Stainless-steel fibres required; (Test) Experimental verification required; (Special) Special crack limitations required; (w_k) maximum crack width allowed, expressed in mm; (Δ_h) minimum sacrificial layer on exposed surfaces, expressed in mm; (XC, XS, XD) EN 206 exposure classes; (Δ_h^{50}, $\Delta_h^{>50}$, w_k^{50}, w_k^{100}) Design service life for 50 years, over 50 years and 100 years.
* The minimum sacrificial layer (Δ_h) shall be considered for a design service life superior to 50 years.

1.1.2 Durability of SFRC exposed to corrosive environments

The observed contradictions in design guidelines are generally motivated by a lack of consensus at the scientific level regarding the impact of critical design aspects, such as the admissible crack width and exposure conditions, on the long-term mechanical performance of SFRC. Additionally, the main deterioration processes connecting exposure, corrosion damage and mechanical damage are not fully understood and described.

Deterioration processes

The corrosion deterioration process of carbon-steel fibres in SFRC is not fully understood. So far, studies describing the deterioration processes of SFRC due to corrosion of steel fibres (Dauberschmidt, 2006; Nordström, 2005) have related these to conceptual models used for conventional reinforcement in concrete (Tuutti, 1982). This conceptual model for conventional reinforcement describes the deterioration process due to corrosion of reinforcing steel in concrete as a two-phase process: the initiation phase and the propagation phase. In the discussion below, a critical stage in the propagation phase was added, as shown in **Figure 1**; which describes the point in time where either critical corrosion damage to the steel fibres is reached or else the corrosion process stagnates.

The initiation phase is governed by the time to depassivation of the steel due to reduction of the pH in the pore solution of the cement matrix (e.g. carbonation or acid attack) and/or by the ingress of halides (e.g. chloride ions) through the cement matrix or cracks. Corrosion damage of steel fibres induced by DC stray-currents was shown unlikely under typical design conditions in Solgaard et al. (2013a), and is not discussed herein.

Generally, transport and chemical deterioration processes in uncracked SFRC have been considered comparable to those of plain concrete, for example: moisture or gas transport properties (Frazão et al., 2015, 2013), carbonation rates (Cangiano et al., 2005; T. Teruzzi et al., 2004) or the diffusion of chloride ions (Abbas et al., 2015, 2014). The latter showed substantial discrepancy when electrical fields were applied (Abbas et al., 2014; Frazão et al., 2015, 2013). Investigations covering transport of aggressive species inside cracks, e.g. chlorides (Mangat and Gurusamy, 1987a) or freshwater and carbon

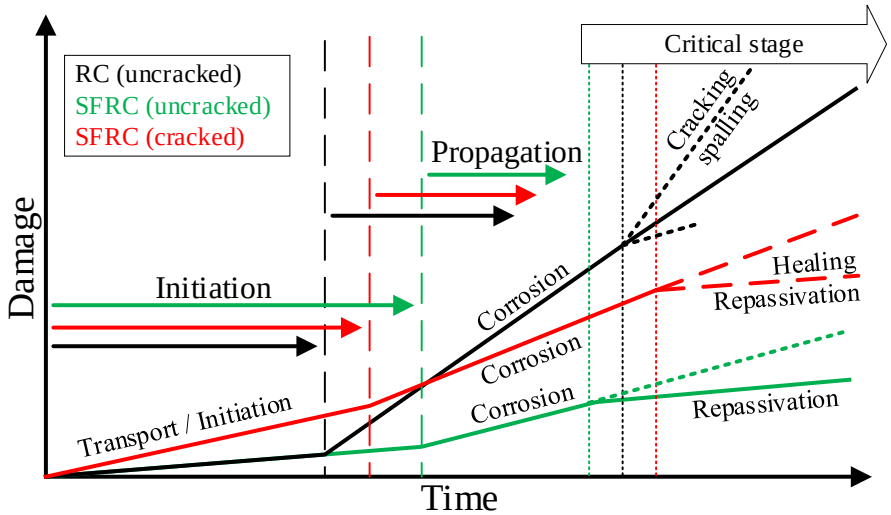

Figure 1 Representation of conceptual deterioration model for corrosion damage of reinforced concrete (RC) and SFRC based on existing conceptual models for reinforced concrete (Tuutti, 1982).

dioxide (Nemegeer et al., 2000) or acids (Roque et al., 2009) did not compare the ingress in SFRC to observations in plain concrete.

The transition from the initiation to the corrosion propagation phase is traditionally defined by localized or general depassivation of the steel. This is generally estimated by e.g. exceeding a specific free chloride threshold limit at the steel fibre surface and/or a critical reduction of the pH around the steel below a certain threshold (e.g. the carbonation threshold). Yet, there is disagreement regarding the applicability of these parameters as the sole indicators for depassivation and propagation of corrosion in steel reinforcement (Angst et al., 2009; Stefanoni et al., 2018).

In the case of SFRC exposed to chlorides, research indicates five- to ten-fold free-chloride threshold limit values for cold-drawn steel fibres relative to steel reinforcement bars (Dauberschmidt, 2012; Mangat and Gurusamy, 1988). This behaviour has been related to several parameters such as: a more homogeneous surface of the steel and a denser and more homogeneous steel-concrete interface for the SFRC, compared to conventional steel reinforcement (Dauberschmidt, 2012). To the author's knowledge, no research investigated pH values in the pore solution leading to depassivation of steel fibres embedded in concrete for carbonation or acid exposure of SFRC.

The propagation phase in conventional steel rebar is generally governed by the amount of mass-loss of the steel due to corrosion over time (i.e. corrosion rate). This process is governed by numerous factors, for example: exposure conditions, moisture content, temperature and concrete composition and microstructure (Bertolini et al., 2013).

Corrosion rates of steel fibres mixed in SFRC have, to the author's knowledge, not been measured so far. Studies investigating this aspect only comprised single fibres embedded in mortar with mixed-in chlorides, and showed questionable current density values up to 400 mA/m^2 (Hwang et al., 2015). Other electrochemical studies covered measurement of half-cell potentials (Dauberschmidt, 2006; Mangat and Gurusamy, 1988; Nemegeer et al., 2000; Nordström, 2005) and polarization resistance experiments (Dauberschmidt, 2006; Frazão et al., 2016), that identified initiation of corrosion and ongoing corrosion but did not quantify corrosion rates.

Based on the conceptual model described in **Figure 1**, progressing corrosion damage of steel fibres embedded in uncracked SFRC or bridging cracks, leads to a general or localized cross-sectional reduction of the steel, depending on the exposure and local conditions, that progressively reduces the tensile capacity of the steel fibre. Unlike for conventional steel reinforcement, additional damage to the cement matrix, such as corrosion induced cracking or spalling have not been identified in SFRC explained by the small size of the fibres (Balouch et al., 2010; Granju and Balouch, 2005).

This conceptual model approach (**Figure 1**) would correlate corrosion damage to the eventual rupture of the fibre during pull-out, provided that the tensile forces transferred through the fibre exceed the tensile capacity of the corroded cross-section of the steel. Therefore, at the composite level, the corrosion of individual steel fibres eventually leads to their rupture during the opening of the crack and reduces progressive the residual tensile capacity of the SFRC over time (Nordström, 2005).

Corrosion damage and mechanical performance of SFRC

The long-term durability and mechanical performance of SFRC exposed to corrosive environments has been the subject of numerous field and laboratory investigations (Marcos-Meson et al., 2018). The main goals of these studies were to quantify the extent of corrosion damage of the steel fibres and to describe its impact on the strength and

elastic mechanical performance of the uncracked SFRC (e.g. compressive, tensile strength or elastic moduli) and on the residual mechanical performance of uncracked and cracked SFRC (e.g. residual tensile strength and tensile toughness).

Former investigations of the durability of SFRC have covered a large number of design parameters such as: type of fibres, type of concrete, exposure time and exposure conditions, specimen dimensions or the presence and width of cracks. Such large amount of study variables generally hinders a direct comparison of the results, and complicates the elaboration of solid conclusions (Marcos-Meson et al., 2018). However, the presence and size of cracks in the SFRC has been identified as one of the main governing parameters that influence the deterioration of SFRC due to corrosion of steel fibres.

Investigations covering the mechanical properties of uncracked SFRC under chloride and carbonation exposures have shown minor corrosion damage of steel fibres embedded in uncracked SFRC, limited to the outermost 5 – 10 mm of the specimen's cross-section. There was negligible detriment to the mechanical properties of the uncracked SFRC, either immersed (Roque et al., 2009), or under wet-dry conditions (Kamal and El-Refai, 1987; O'Neil and Devlin, 1999; Schupack, 1985). Loss of mechanical performance of uncracked SFRC under acidic exposure was related to chemical damage to the cement matrix rather than solely corrosion damage of the steel fibres (Roque et al., 2009).

Corrosion damage of steel fibres in cracked SFRC depended strongly on the width of the crack and the type of exposure. Corrosion damage was generally larger inside larger cracks and when the exposure conditions involved wet-dry cycles. The discussion hereafter groups the observations in cracks larger and smaller than 0.3 mm, and focuses on wet-dry exposure conditions.

Studies investigating cracks wider than approx. 0.3 mm reported substantial corrosion damage of steel fibres under partial immersion and exposure to wet-dry cycles of freshwater or rainwater, which entailed a moderate reduction of the residual tensile strength of the SFRC (Bernard, 2004; Nordström, 2005; Weydert and Schiessl, 1998). Corrosion damage was much more severe when the wet-dry cycles involved chloride exposure, leading to substantial reduction of the residual tensile strength (Mangat and Gurusamy, 1987b; Nordström, 2005; Weydert and Schiessl, 1998). Exposure of SFRC cracked within the same range to acids lead as well to substantial residual tensile strength reductions, attributed to corrosion damage of the steel fibres (Kaufmann, 2014).

Investigations of SFRC with crack widths smaller than 0.3 mm, exposed to rainwater or wet-dry cycles of freshwater, reported minor corrosion damage of fibres bridging the cracks (Bernard, 2004; Nordström, 2005); which did not result in a substantial deterioration of the mechanical performance due to fibre corrosion. Similar investigations under chloride exposure lead to moderate corrosion damage of fibres, but entailed negligible reductions of the mechanical performance over the exposure (Bernard, 2004; Mangat and Gurusamy, 1987b; Nordström, 2005). Investigations covering exposure of SFRC to acidic environments reported critical reductions of the residual tensile strength of the cracked SFRC, comprising corrosion damage of the fibres and chemical erosion of the concrete matrix (Roque et al., 2009).

Milder exposure conditions, involving immersion in freshwater and saltwater (Roque et al., 2009) or airborne exposure to chlorides (Granju and Balouch, 2005) entailed less

corrosion damage compared to wet-dry conditions and negligible loss of mechanical performance. Percolation of corrosive solutions through cracks has not been fully covered in former studies, but results available indicate that deterioration of the concrete matrix, e.g. due to leaching , may be as severe as corrosion of the steel fibres (Hagelia, 2011a).

Insight about additional damage mechanisms

The results discussed above show deterioration trends generally in agreement with the deterioration model described in **Figure 1**. Exposure of uncracked SFRC to corrosive environments leads to minimal corrosion damage of the steel fibres and caused negligible variations of the mechanical performance of the SFRC. The extent of corrosion of steel fibres inside cracks seemed to correlate with the loss of the residual tensile strength in the cracked SFRC.

However, some of these studies also report observations that do not agree with the deterioration mechanisms presented above. Corrosion damage of the steel fibres did not always lead to a reduction of the residual tensile strength of the SFRC. Or else, a critical reduction of the residual strength of the SFRC was reported, even though corrosion damage of the steel fibres was minimal.

Reductions of the toughness of cracked SFRC partially immersed in seawater (Bernard, 2004) or exposed to rainwater (Bernard, 2015a) have been linked to an excessive increase of the fibre-matrix bond strength during the exposure, rather than corrosion damage of the steel fibres. Similar mechanisms were attributed to reductions of the tensile toughness of SFRC with cracks larger than e.g. 0.3 mm (Bernard, 2004); or in other cases to moderate increases of the residual tensile strength of cracked SFRC (Granju and Balouch, 2005; Nemegeer et al., 2000), which was substantial for cracks smaller than 0.2 mm (Bernard, 2004; Mangat and Gurusamy, 1987b; Nordström, 2005).

Contradictory observations also have been reported for uncracked SFRC, where variations of the residual tensile strength of SFRC over time were related to the development of the fibre-matrix bond strength. Few studies have reported critical loss of tensile toughness in uncracked SFRC immersed in freshwater (Bernard, 2015a, 2008), which were attributed to an unaccounted increase of the fibre-matrix bond strength over time. While similar studies have shown a steady increase over time (Šušteršič et al., 2000; Teixeira Buttignol et al., 2016).

These inconsistencies indicate that; either there are fundamental flaws in the methodology of some of these studies, or else the assumptions considered in conventional conceptual models for corrosion of reinforced concrete are limited, and additional deterioration and recovery mechanisms have to be taken into account.

1.1.3 Motivation for the study

The increasing use of SFRC in the construction sector to produce in-situ and prefabricated concrete structures is hampered by concerns regarding the long-term durability of SFRC at the scientific level, which are reflected in the discrepancies found in international design guidelines.

Published research has investigated a number of design parameters that may affect the durability of SFRC under corrosive exposures. However, methodologies and results are diverse, and studies are either based on macroscopic mechanical observations at the composite level or on studies of specific deterioration processes at the single-fibre level; yet, not connecting both.

Discrepancies found among macroscopic observations at the composite level and current deterioration models, indicate limitations in both. There is a need to develop a more detailed description of the relation between the corrosion damage of steel fibres and the variations of the mechanical performance of SFRC exposed to corrosive environments.

1.2 Aim and objectives of the thesis

This project aims at identifying the main variables influencing steel fibre corrosion in concrete subject to corrosive environments and quantifying the effect of fibre corrosion on the mechanical performance of SFRC. Special focus is set on the deterioration processes occurring inside cracked SFRC exposed to wet-dry conditions. Achieving the project aim comprised the following objectives:

- The identification of the principal design and service conditions leading to corrosion of steel fibres in concrete exposed to chlorides, carbon dioxide and acidic exposures.
- The quantification of the extent and impact of fibre corrosion on the macroscopic mechanical behaviour of SFRC subject to wet-dry cycles under chloride and carbon dioxide exposure.
- The description of the underlying mechanisms responsible for the deterioration of SFRC subject to wet-dry cycles under chlorides and carbon dioxide exposure.
- The connection between the damage mechanisms affecting SFRC exposed to corrosive exposures and changes in the mechanical performance of the cracked SFRC at the composite and single-fibre levels.

1.3 Research hypotheses

Following the aim and objectives of the project, the following scientific hypotheses will be tested:

- Exposure of uncracked SFRC to corrosive exposures is not expected to produce significant corrosion damage, nor alter the strength of the uncracked concrete.
- The presence and size of cracks in SFRC is expected to determine the extent of corrosion damage of steel fibres embedded in cracked and uncracked SFRC. A crack width in the range of 0.1 – 0.3 mm is expected to result in a moderate corrosion damage of most fibres crossing cracks.
- Corrosion damage of steel fibres in cracks exposed to chlorides is expected to be significantly more severe than corrosion due to carbonation. Reduction of the tensile toughness of the cracked SFRC under chloride exposure is expected to be substantially larger than under carbonation exposure.
- Corrosion damage of steel fibres bridging cracks is expected to lead to a net reduction of the tensile toughness of the cracked SFRC. Loss of tensile toughness after cracking must be linked to a change in the failure mode of the fibre from fibre pull-out to rupture of the fibre.
- The tensile behaviour of the cracked SFRC can be explained through the pull-out behaviour of single fibres. Changes in the fibre-matrix bond or reduction of

the tensile capacity of the fibre due to corrosion can explain variations in the tensile performance of the SFRC.

- The build-up of corrosion and healing products in small cracks is expected to limit the access of aggressive species (e.g. Cl^-, CO_2) in cracked SFRC. Chemical alteration of the cement matrix around the fibres is expected to influence the strength of the fibre-matrix bond.

1.4 Research approach

The study comprises four work packages (WP), which are described schematically in **Figure 2**. The first work package (WP1) comprises a literature review, which identified the main research questions concerning corrosion damage in SFRC. The experimental investigations were designed based on the research questions and hypotheses defined around the issue of corrosion damage of cracked SFRC exposed to wet-dry cycles.

The experimental and analytical studies were constructed as a multiscale investigation, structured into three work packages: (WP2) quantification of the corrosion damage and mechanical performance at the composite level, (WP3) description of the deterioration mechanisms governing the behaviour observed at the composite level at the macro- and microscale and (WP4) connection of the damage mechanisms observed at the single-fibre level at the macro- and microscale to the performance observed at the composite level.

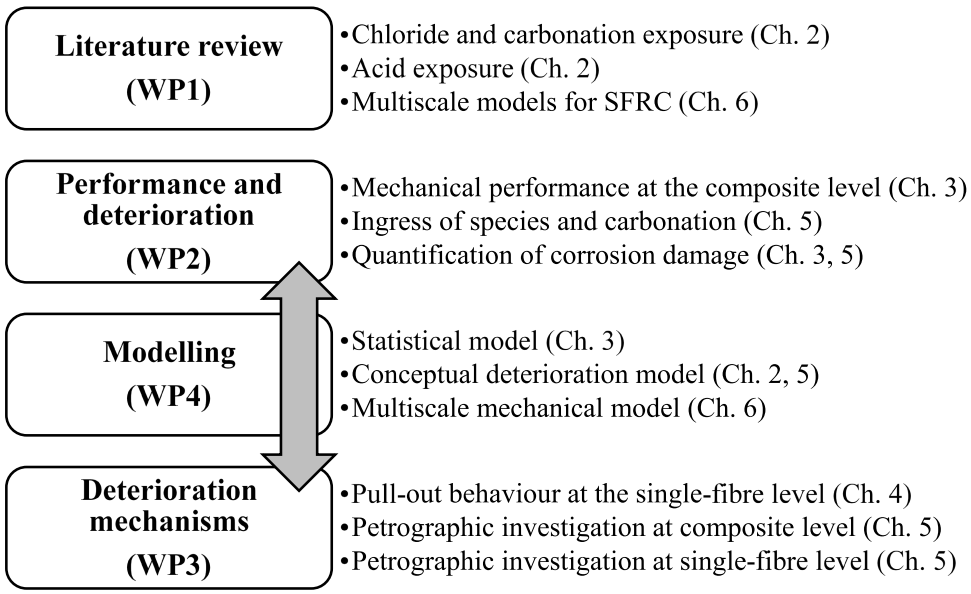

Figure 2 Structure of investigations and chapters

1.4.1 Summary of investigations

A summary of the main investigations carried out in this study is shown in **Table 2**. The techniques used are shown divided into experimental and analytical studies. Details regarding the specific methods are given in the appended publications in Chapters 2 – 6.

The experimental investigations presented in this thesis cover the preparation, exposure, mechanical testing and inspection of three types of specimens: i) three-point bending notched beams, ii) single notched coupons tested in uniaxial tension and iii)

single-fibre pull-out specimens. The experimental campaign comprised approx. 500 SFRC specimens and 150 single-fibre pull-out specimens. The SFRC specimens were tested both uncracked and with induced crack widths of 0.15 and 0.3 mm and were exposed to wet-dry cycles for two years. The single-fibre pull-out specimens were tested un-pulled and pre-pulled to a displacement of 0.15 mm and exposed to wet-dry cycles for six months. The mix-design and configuration of the exposure setup used for SFRC and single-fibre specimens were analogous. Experimental investigations are enumerated in **Table 2**.

The analysis of the experimental data and modelling comprised statistical evaluation and modelling of the experimental data and the development of a multiscale numerical model that connects the pull-out performance of single fibres to the tensile performance of the composite. The statistical techniques were used consistently through the chapters, following the same methodology. The main methods used are listed in **Table 2**.

Table 2. Summary of main investigation techniques used and corresponding chapters and work packages

Study		Chapter				
		2	**3**	**4**	**5**	**6**
	Experimental					
Exposure	Wet-dry cycles		C	F	C - F	C - F
Mechanical	Pull-out			F	F	F
	Uniaxial tension		C			C
	Three-point bending		C		C	
	Compression		C	F		
Visual inspection	Fibre counting		C		C	
	Colorimetric profiles				C	
Chemical	Chloride profiles				C	
	X-ray fluorescence				C	
Petrographic	Thin sections			F - C	F - C	
	Polished sections			C	F - C	
	X-ray tomography			F - C		
	Analytical					
Statistical	Exploratory data analysis	L	C	S	F - C	
	Confirmatory data analysis		C	S		
Modelling	Statistical modelling	L	C			
	Multiscale mechanical model					F - C
Work Package (Figure 2)		WP1	WP2 WP4	WP3	WP2 WP3 WP4	WP1 WP4

Abbreviations: (L) data from literature, (C) investigation at composite level, (F) investigation at single-fibre level

1.5 Scope and limitations

The scope of work of this study comprises the following aspects:

- A critical analysis of the literature that identifies the principal research questions and hypotheses that require investigation.
- Design and operation of an exposure setup to simulate wet-dry cyclic exposure in SFRC and single-fibre pull-out specimens. Five different exposure environments, comprising chloride and carbonation exposure were investigated.
- Preparation, exposure and testing of approx. 500 SFRC specimens and 150 single-fibre specimens. Investigations of SFRC specimens covered two types of

steel fibre and one concrete mix-design. Investigations of single-fibres comprise four fibre types and two concrete mix-designs.

- The experiments comprised: mechanical, chemical and petrographic investigations, mainly on cracked specimens. The evaluation of the experimental data comprised: exploratory and confirmatory data analysis, and statistical modelling.
- Development and testing of a mathematical model that connects results at the single-fibre level to results in SFRC.

The scope of work was limited to:

- The analysis of results from the literature was restricted by the lack of raw data available and heterogeneous testing and analysis methods.
- Experimental investigations covered chloride and carbonation exposure under wet-dry cycles. Other exposure conditions such as immersed conditions, percolation through cracks or exposure to acids were not covered experimentally in this study.
- The crack widths investigated in SFRC specimens were limited to cracks in the range of 0.15 – 0.3 mm. Single-fibre pull-out specimens were partially pulled to slip values of 0.15 mm.
- Long-term exposure was not covered experimentally in this study. The exposure time of the SFRC specimens tested was limited to two years, and the exposure of pull-out specimens lasted six months.
- Investigations on additional concrete compositions or types of fibres were not covered. The study only covered investigations of hooked-end fibres made of cold-drawn carbon-steel wire.
- Mechanical studies of cracked SFRC and single fibres were limited to tensile forces normal to the crack plane (e.g. Mode I opening). Fracture modes involving shear (e.g. Mode II and III opening) were not investigated.
- Electrochemical investigations of steel fibres were not included in the experimental studies. Petrographic and chemical studies were restricted to selected companion specimens to the ones conforming the main studies.
- Modelling of experimental results was limited by the early stage of development of the model approach and current understanding of the pull-out processes of steel fibres in concrete.

1.6 Outline and reading guide

The thesis is organized as a “collection of papers”, that cover the deterioration phenomena observed in cracked and uncracked SFRC. First, from the perspective of former studies and design codes in a critical review of the literature. And later, as two experimental campaigns that describe chemical, microstructural and mechanical changes in SFRC exposed to wet-dry cycles at the composite and at the single-fibre level. A list of the chapters comprising the core of this thesis and its publications is given in **Table 3**.

Chapter 1 describes the background of the project and the general methodology used throughout the investigation.

Subsequent chapters (Chapters 2 to 7) present the investigations carried out. These chapters are written as "paper-based", where the summary and conclusions to the chapter are given as an extended abstract, followed by the appended publications that describe the contents of the chapter in detail.

Chapter 2 presents the state-of-the-art of SFRC under corrosive exposures. The chapter comprises two publications (Papers I and II) that cover: i) the deterioration of SFRC exposed to chlorides and carbon dioxide, and ii) the deterioration of SFRC exposed to acids. The chapter serves as a basis for the specific research questions investigated in Chapters 3 to 6.

Chapter 3 covers a study of the corrosion damage and mechanical performance of SFRC specimens exposed to wet-dry cycles of chlorides and carbon dioxide over a period of two years. The chapter comprises two publications (Papers III and IV) that describe: i) the quantification of the extent of corrosion damage of fibres crossing cracks and its correlation to variations in the mechanical performance of the composite, and ii) the evolution of corrosion damage and mechanical performance of the exposed SFRC coupons over time. Findings of this chapter provide the basis for the investigations carried out in Chapter 4 and Chapter 5.

Chapter 4 comprises a study of the pull-out behaviour of hooked-end fibres under simulated crack conditions, involving wet-dry cycles of chlorides and carbon dioxide. The chapter is composed by one publication (Paper V), which describes the pull-out mechanisms of straight hooked-end fibres in concrete and identifies changes in those due to exposure. Additional publications and investigations carried out during the PhD project in this area are referenced but not appended. The findings of this chapter serve as an explanation to the macroscopic observations reported in Chapter 3 and are used further in **Table 3**.

Chapter 5 describes the deterioration mechanisms involved in the exposure of complementary SFRC specimens to the ones investigated in Chapter 3. The chapter is composed by two publications (Paper VI and VII), that describe: i) the transport, reaction and corrosion processes taking place inside the cracks and updates the conceptual deterioration model for SFRC exposed to chlorides and carbon dioxide presented in Chapter 2; and ii) the mechanisms responsible for the alteration of the pull-out behaviour of the single fibres investigated in *Chapter 4*. The findings of this chapter serve as a link between the deterioration mechanisms described in Chapter 2, based on former studies, and the observations presented in Chapter 3 and Chapter 4 at the composite and single-fibre level.

Chapter 6 presents a multi-scale modelling approach (Paper VIII), which connects the findings regarding alteration of the fibre-matrix bond strength of single fibres presented in Chapter 4 to the macroscopic observations reported in Chapter 3. The deterioration mechanisms involved were explained in a broader context by the multi-scale deterioration model described in Chapter 5.

Chapter 7 comprises a summary of the discussion presented in Chapter 2 to Chapter 6, which connects the results presented in this study to the conclusions from former research and discusses the implications of these results in current design approaches.

Chapter 8 presents the conclusions of the study and discusses research areas within the scope of this investigation where further work is needed.

Table 3. List of chapters and publications

Chapter	Description	Publication	
1	Introduction		
2	State-of-the-art on the durability of SFRC subject to corrosive exposures	I + II	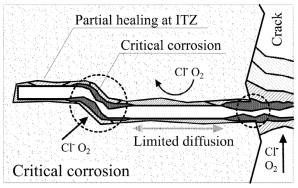
3	Investigation of the mechanical performance and corrosion damage of cracked and uncracked SFRC	III + IV	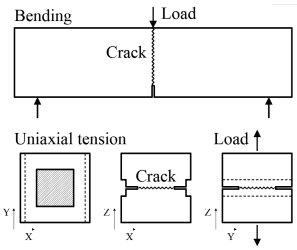
4	Investigation of pull-out mechanisms of hooked-end steel fibres in cracked concrete	V	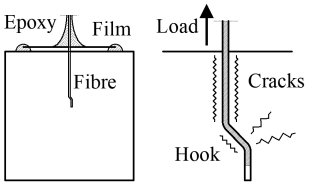
5	Investigation of the deterioration mechanisms affecting cracked SFRC exposed to wet-dry cycles	VI + VII	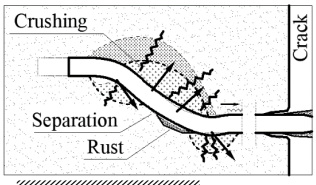
6	Connection of the damage observed at the single-fibre level to the changes in the mechanical performance at the composite level	VIII	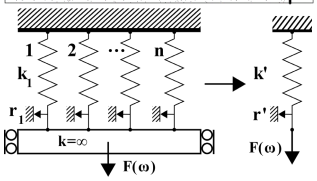
7	Closing discussion and design implications		
8	Conclusions and future work		

1.7 Contribution to the field

The investigations presented in this project will contribute to connect the conclusions of former investigations regarding the durability of SFRC under aggressive environments and provide an explanation for some of the discrepancies observed both at the technical and scientific level.

This study will contribute to the field with a set of experimental data with a significant level of detail, a multiscale and multidisciplinary scope (e.g. mechanical, chemical and microstructural) and a robust discussion based on a statistical interpretation of the data. The identification of the specific deterioration mechanisms affecting SFRC structures undergoing fibre corrosion will contribute to bridge the gap between transport processes of aggressive agents in SFRC and changes in its mechanical performance.

The results of this study contribute to the further development of the necessary tools for the service-life design of new SFRC structures, as well as increased knowledge for the maintenance and preservation of existing infrastructure built of SFRC.

Chapter 2
Literature review

The background presented in Chapter 1 highlighted that there is a general discrepancy at the technical and scientific level concerning the corrosion damage and mechanical performance of cracked SFRC. Part of this discrepancy is motivated by the lack of an overview of the research available that connects observations and deterioration phenomena.

This chapter provides an objective evaluation of the literature available covering corrosion damage of SFRC exposed to chlorides (Paper I), carbon dioxide and acids (Paper II). The focus of the review is to identify key conditions that lead to fibre corrosion and understand its impact on the mechanical performance of the SFRC.

Chloride and carbonation induced corrosion

A review of the existing literature investigating chloride and carbonation induced corrosion of SFRC was carried out in Paper I. The paper discusses the main factors affecting corrosion of carbon-steel fibres under these exposures and describes a conceptual deterioration model based on findings from former studies investigating concurring damage mechanisms under such exposures.

The review concluded that there is overall agreement among academics regarding the durability of uncracked SFRC exposed to chlorides and carbon dioxide; which is reflected in the consensus found in design guidelines and standards. The superior durability against corrosion of carbon-steel fibres embedded in uncracked SFRC relative to conventional steel was attributed to: i) the discrete nature of the fibres, ii) a more homogeneous steel surface due to production processes of cold-drawn wire steel fibres versus a rougher surface for conventional reinforcing bars, and iii) a denser and more homogeneous fibre-matrix interface compared to conventional steel reinforcement.

There is overall disagreement regarding the durability of cracked SFRC exposed to chlorides and carbonation; while investigations showed a general trend for larger

deterioration with increasing crack width. Yet, there was discrepancy regarding the extent and role of fibre corrosion inside cracks in the range of 0.2 – 0.3 mm, and its impact on the residual performance of cracked SFRC.

Discrepancies were attributed, among others, to the lack of understanding of the mechanisms governing corrosion of carbon-steel fibres in cracked SFRC subject to chloride and carbonation exposure. In this aspect, the conceptual deterioration model proposed suggests that corrosion damage of steel fibres bridging cracks may be governed by damage and healing processes at the fibre-matrix interface and the main crack. Insight that fibre corrosion may not be the dominant damage mechanism responsible for the loss of post-crack ductility of cracked SFRC under these exposures was discussed.

Corrosion damage induced by acid attack

A review of the existing literature investigating corrosion and chemical erosion damage of SFRC exposed to acids was carried out in Paper II. The paper focused on presenting the main deterioration processes taking place under this exposure, being corrosion of the steel among them.

The review concluded that exposure of uncracked SFRC to acids results in damage similar to unreinforced concrete, governed by the loss of structural integrity of the concrete matrix due to chemical erosion. Corrosion of the steel fibres embedded in uncracked concrete due to neutralization of the cement matrix was regarded as secondary compared to the microstructural damage of the cement matrix.

Deterioration of cracked SFRC exposed to acids may be governed instead by a combination of corrosion damage and deterioration of the cement matrix surrounding the fibres. Former studies reported that severe exposure of cracked SFRC to acids entails a significantly larger deterioration of the residual mechanical performance of the composite, relative to other exposures (i.e. carbonation or chloride exposure). However, the contribution of fibre corrosion to that damage is not clear. Insight suggests that this deterioration may be governed by the dissolution of the cement matrix surrounding the fibre, instead of corrosion damage of the steel fibres. Yet, the contribution of these mechanisms may be strongly dependent on the crack widths investigated.

All in all, deterioration of the mechanical performance of SFRC under this exposure seems to be mostly related to damage of the cement matrix rather than corrosion damage of the fibres, including fibres bridging cracks below e.g. 0.3 mm.

2.1 Paper I. A review of chloride and carbonation induced corrosion of SFRC

The following publication, referred as “paper I”, has been published in Cement and Concrete Research.

Marcos-Meson, V., Michel, A., Solgaard, A., Fischer, G., Edvardsen, C., Skovhus, T.L., 2018. Corrosion resistance of steel fibre reinforced concrete - A literature review. Cem. Concr. Res. 103, 1–20. doi:10.1016/j.cemconres.2017.05.016.

Cement and Concrete Research 103 (2018) 1–20

Contents lists available at ScienceDirect

Cement and Concrete Research

journal homepage: www.elsevier.com/locate/cemconres

Corrosion resistance of steel fibre reinforced concrete - A literature review

Victor Marcos-Meson[a,b,c,*], Alexander Michel[a], Anders Solgaard[b], Gregor Fischer[a], Carola Edvardsen[b], Torben Lund Skovhus[c]

[a] Department of Civil Engineering, Technical University of Denmark, Copenhagen, Denmark
[b] COWI A/S, Copenhagen, Denmark
[c] VIA Building, Energy & Environment, VIA University College, Horsens, Denmark

ARTICLE INFO

Keywords:
Steel fibre reinforced concrete (SFRC)
Corrosion mechanisms
Chlorides
Carbonation
Cracks

ABSTRACT

Steel fibre reinforced concrete (SFRC) is increasingly being used in the construction of civil infrastructure. However, there are inconsistencies among international standards and guidelines regarding the consideration of carbon-steel fibres for the structural verification of SFRC exposed to corrosive environments. This paper presents a review of the published research regarding carbonation- and chloride-induced corrosion of SFRC, and proposes a deterioration theory for cracked SFRC exposed to chlorides and carbonation, based on the damage at the fibre-matrix interface. The review confirms an overall agreement among academics and regulators regarding the durability of uncracked SFRC exposed to chlorides and carbonation. Contrariwise, the durability of cracked SFRC is under discussion at the technical and scientific level, as there is a large dispersion on the experimental results and some of the mechanisms governing the corrosion of carbon-steel fibres in cracks and its effects on the fracture behaviour of SFRC are not fully understood.

1. Introduction

Steel fibre reinforced concrete (SFRC) is a composite material, combining a cementitious matrix and a discontinuous reinforcement, consisting of steel fibres randomly distributed in the matrix. In this paper, the term SFRC refers to mix-designs based on Portland cement binders, with mix-proportions and elastic mechanical properties (i.e. in the uncracked state) similar to conventional concrete. SFRC is increasingly being adopted for the production of in-situ and prefabricated concrete structures as: a) auxiliary reinforcement for temporary load cases, e.g. arresting shrinkage cracks, limiting cracks occurring during transport or installation of precast members, b) partial substitution of the conventional reinforcement, i.e. combined reinforcement systems, and c) total replacement of the conventional reinforcement in elements in overall compression, e.g. ground-supported slabs, tunnel linings, foundations, thin-shell structures [1–3].

In particular, the use of steel fibres as partial or total replacement of conventional reinforcement bars has become a popular solution for the construction of prefabricated segmental linings for bored tunnels, due to its overall good durability and performance in compression [4–9]. Nevertheless, the total replacement of conventional steel reinforcement is still controversial according to some experts, especially when the long-term durability of SFRC under severe chloride and carbonation exposure is addressed [10–13].

At present, there is no international standard available for the design of SFRC structures. However, an EN standard is currently in preparation. Moreover, the national guidelines available for design of SFRC are not coherent with respect to the applicability within certain exposure classes. Table 1 presents a summary of the main design recommendations for the EN 206 exposure classes: i) XC, hereafter referred to as “carbonation exposure”, and entailing the exposure to air, CO_2 and moisture; ii) XS, seawater exposure, comprising concrete exposed to chlorides from sea water; iii) XD, other-chloride exposure, covering chloride sources other than seawater, i.e. de-icing salts [14].

There is an overall agreement among the standards and guidelines regarding the design of SFRC under carbonation exposure, with a crack width limit in the range 0.20–0.40 mm for mild exposure conditions (i.e. XC2-3, immersed concrete and concrete sheltered from rain), presenting similar limitations to conventional reinforcement, Table 1. On the contrary, there is disagreement on the durability of SFRC exposed to cyclic wet and dry conditions (i.e. XC4), where some of the guidelines do not recommend the use of carbon-steel fibres in cracked SFRC [18,19].

The case of chloride exposure is more controversial, and four main design approaches can be identified, as shown in Table 1: i) crack limitation in the range 0.10–0.20 mm [15,17,20,26]; ii) special measures such as experimental validation [16,22]; iii) use of coated carbon-steel or stainless-steel fibres [18,19,27]; iv) no applicability for these

* Corresponding author at: Department of Civil Engineering, Technical University of Denmark, Copenhagen, Denmark.
E-mail address: vicmes@byg.dtu.dk (V. Marcos-Meson).

http://dx.doi.org/10.1016/j.cemconres.2017.05.016
Received 24 October 2016; Received in revised form 25 April 2017; Accepted 17 May 2017
Available online 26 October 2017

Table 1
Summary table, design recommendations for SFRC exposed to chlorides and carbonation.

Standard	Ref.		Carbonation			Chlorides			
			XC2	XC3	XC4	XS2	XS3	XD2	XD3
ACI-544-1R-96 (US)	[15]	w_k^{50} Δ_h^{50}	0.30 –	0.30 –	0.30 –	0.10 2.5	0.10 2.5	0.10 2.5	0.10 2.5
RILEM TC 162-TDF (EU)	[16]	w_k^{50} Δ_h^{50} Fibre	0.30 10 C-G-S	0.30 10 C-G-S	0.30 10 C-G-S	Special Special –	Special Special –	Special Special –	Special Special –
DBV-Merkblatt Stahlfaserbeton (DE)	[17]	w_k^{50} Δ_h^{50}	0.30 20	0.30 20	0.20 25	0.20 40	0.20 40	0.20 40	0.20 40
UNI/CIS/SC4:2004 (IT)	[18]	w_k^{50} $\Delta_h^{>50}$ [a] Fibre	0.30 10 C-G-S	0.30 10 C-G-S	0.30 10 G-S	0.30 10 C-G-S	0.30 10 G-S	0.30 10 C-G-S	0.30 10 G-S
CNR-DT 204/2006 (IT)	[19]	w_k^{50} $\Delta_h^{>50}$ [a] Fibre	0.30 10 C-G-S	0.30 10 C-G-S	0.30 10 G-S	0.30 10 G-S	0.30 10 S	0.30 10 C-G-S	0.30 10 G-S
NZS 3101-2:2006 (NZ)	[20]	w_k^{50}	0.30	0.30	0.30	0.20	0.20	0.20	0.20
TR-63 (UK)	[21]	w_k^{50}	0.30	0.30	0.30	0.30	0.30	0.30	0.30
EHE 2008 (ES)	[22]	w_k^{50} Fibre	0.30 C-G-S	0.30 C-G-S	0.30 C-G-S	Test G-S	Test G-S	Test G-S	Test G-S
DAfStb Stahlfaserbeton (DE)	[23]	w_k^{50} Fibre	0.30 C-G-S	0.30 C-G-S	0.30 C-G-S	N/A –	N/A –	N/A –	N/A –
Design guideline for structural applications of SFRC (DK)	[24]	w_k^{50} Fibre	0.30 C-G-S	0.30 C-G-S	0.20 C-G-S	N/A –	N/A –	N/A –	N/A –
AFTES-GT38R1A1 (FR)	[25]	w_k^{50} Fibre	0.20 C-G-S	0.20 C-G-S	0.20 C-G-S	0.15 C-G-S	0 G-S	0.15 C-G-S	0 G-S
SS-812310:2014 (SE)	[26]	w_k^{50} w_k^{100}	0.50 0.40	0.50 0.40	0.40 0.30	0.30 0.20	0.20 0.10	0.30 0.20	0.20 0.10
NB-Publication no. 7. Sprayed concrete for rock support:2014 (NO)	[27]	Fibre	C-G-S	C-G-S	C-G-S	G-S[b]	G-S[b]	G-S[b]	G-S[b]

Abbreviations: (N/A) Not applicable; (C) Carbon-steel steel fibres can be used; (G) Coated carbon-steel fibres can be used; (S) Stainless-steel fibres required; (Test) Experimental verification required; (Special) Special crack limitations required; (w_k) maximum crack width allowed, expressed in mm; (Δ_h) minimum sacrificial layer on exposed surfaces, expressed in mm; (XC, XS, XD) EN 206 exposure classes; (Δ_h^{50}, $\Delta_h^{>50}$, w_k^{50}, w_k^{100}) Design service life for 50 years, over 50 years and 100 years.

[a] The minimum sacrificial layer (Δ_h) shall be considered for a design service life superior to 50 years.

[b] Galvanized fibres may be considered provided that hydrogen formation at the zinc coating is prevented.

exposure classes [23,24], or limitation to the uncracked state, i.e. the contribution of the steel fibres cannot be considered for the serviceability limit state [25].

Other national guidelines do not mention specific limitations for durability, but highlight the improved durability of SFRC relative to conventional reinforcement [21,28], refer to other guidelines and standards [29–31], or express imprecise recommendations for special measures under aggressive exposures [16,22,32].

The inconsistencies observed regarding the consideration of steel fibres for SFRC exposed to the most aggressive exposure classes, e.g. XC4, XS2-3 and XD2-3, indicate a limited understanding about the probability of fibre corrosion for exposed SFRC and its impact on the structural integrity of structures built of SFRC. In particular, the durability of cracked SFRC subjected to wet and dry cycles under chloride and carbonation exposure, for cracks below 0.30 mm, is in focus and under discussion at the technical level. Furthermore, these discrepancies suggest a limited understanding of the mechanisms governing chloride- and carbonation-induced corrosion of steel fibres in cracked concrete and its effects on the long-term mechanical behaviour of SFRC.

This paper reviews the existing literature investigating chloride- and carbonation-induced corrosion of steel fibres in concrete, evaluating the main variables influencing the durability of SFRC exposed to chlorides and carbonation, and mechanisms responsible for this deterioration. The paper is divided into two sections: SFRC exposed to chlorides (EN 206 exposure classes XS1-3, XD1-3 and XF3-4) and SFRC exposed to carbonation (EN 206 exposure class XC1-4). Each of those sections concludes with a discussion of the various mechanisms associated to the results presented on the experimental work and proposes deterioration models covering the corrosion of steel fibres for uncracked and cracked SFRC exposed to chlorides and carbonation.

2. Durability of SFRC exposed to chlorides

There is abundant research investigating the durability of SFRC exposed to different chloride contaminated environments, as shown in Table 2. However, there is a large amount of variables influencing the results, which hinders the direct comparison among studies, namely: i) quality of concrete; ii) type, material and quantity of fibres; iii) exposure time and conditions; iv) existence and size of cracks.

The test results published from the studies presented in Table 2, have been categorized and introduced in a database. The database contains the information of the design-variables characterizing the SFRC, exposure conditions and the main indicators defining the

Table 2
List of studies investigating durability of SFRC exposed to chlorides.

First author	Year	Ref.	Bind (kg/m^3)	w/c (−)	Fibre (steel) (type)	Fibre content (kg/m^3)	Exp. class (EN)	Exp. type	Age (mo.)	Crack w_k (mm)	Crack crit. $w_{k,\ crit}$ (mm)	Scr. layer Δ_h (mm)
Hannant	1975	[33]	393	0.49	L/M	94	XS3	Field	11	Uncracked	0.10–0.30	5–17
			480	0.75	D	107			57	0.10–0.30		
Batson	1977	[34]	386	0.59	L	62	XS3	Lab	2	0.10–0.20	0.10–0.20	–
					S	123			6			
Morse	1977	[35]	446	0.50	L	119	XS3	Lab	2	Uncracked	0.25	1–5
					D/M		XF4	Field	18	0.25–3.20		
Rider	1978	[36]	308	0.50	L/S	94	XS3	Lab	9	0.10–0.20	0.25[b]	1–13
				0.60	D/E	101	XF4	Field	12			
Schupack (WES)	1976	[37]	468	0.45	L/B/S	114	XS3	Field	132	Uncracked	–	3
					D		XF4					
Schupack (Long Island)	1972	[37]	560	0.46	L/B	114	XS3	Field	120	Uncracked	0	2
					D/M		XF4			0.10–0.60		
Schupack (Australia)	1971	[37]	580	0.51	L	160	XS3	Field	120	Uncracked	–	3
					D		XC4[a]					
Schupack (Battelle)	1978	[37]	445	0.45	L/B	89	XS3	Lab	120	Uncracked	–	1–3
				0.62	D/S	153	XD3	Field				
Kamal	1987	[38]	350	0.50	L	60	XS2	Lab	12	Uncracked	–	3
					M	120						
Mangat	1987	[39–44]	590	0.40	L/Z/S	130	XS3	Lab	20	Uncracked	0.10–0.25	3–15
	1988				D/E	230	XC4	Field	41	0.20–0.70		
Kosa	1990	[45,46]	530	0.42	L	153	XS3	Lab	9	Uncracked	0	40
	1991		860	0.70	D		XC4	(HT)		0.10–0.20		
Weydert	1998	[47,48]	350	0.40	L/Z	30	XS3	Lab	14	0.10–0.40	0–0.10[c]	1–10
				0.50	D/M	120			17			
O'neil	1999	[49]	468	0.45	L/B/S	114	XS3	Field	216	Uncracked	–	2
					D/M		XF4					
Hansen	1999	[50,51]	305	0.38	L	30	XS3	Lab	7	0.10–0.20	0.20	0–10
			358	0.52	D				13			
Balouch	1999	[52–54]	250	0.36	L	40	XS3	Lab	3	Uncracked	0.10	1–3
	2010		470	0.78	D				12	0.50		
Dhanasekar	1999	[55]	475	0.36	L	56	XS2	Lab	4	Uncracked	–	1–3
					S							
Nemegeer	2000	[56–58]	350	0.45	L/Z	78	XS3	Lab	18	0.20–0.50	0.50	(1–5)
					D		XC4					
Mantegazza	2004	[59]	320	0.55	L	39	XS3	Lab	2	0.20	0.20[b]	–
					D							
Bernard	2004	[13]	420	0.42	L	50	XS2	Field	24	0.10–1.00	0.10	–
					D							
Nordstrom	2005	[60,61]	510	0.30	L/M	65	XD3	Field	60	Uncracked	0.10–0.20	(1–5)
				0.42	D	70	XC4			0.10–1.00		
Kopecksko	2008	[62]	300	0.42	L/M	25	XD3	Lab	1	Uncracked	–	1
			400	0.54	D	75	XF4					
Serna	2008	[63]	350	0.50	L/Z	60	XS3	Lab	12	Uncracked	< 0.50[a]	(1–5)
					D/S					0.50–1.50		
Roque	2009	[64]	362	0.37	L	71	XS2	Lab	27	Uncracked	0.10–0.20	(1–5)
			446	0.44	D		XS3			0.20		
Graeff	2010	[65,66]	300	0.35	L	47	XS3	Lab	10	Uncracked	–	(1–5)
			380	0.50	D	51						
Sanchez	2009	[67,68]	426	0.45	L-Z	40	XS1	Field	18	Uncracked	–	(1–5)
					D		XC4					
Sun	2011	[69,70]	494	0.47	L/Z	77	XS3	Lab	1	Uncracked	–	1
					D							
Buratti	2011	[71]	350	0.50	L	25	XS3	Lab	8	0.50	0.50	–
					D							
Abbas	2014	[6,72]	647	0.29	L	60	XS3	Lab	16	Uncracked	0.20	3–5
	2015				D			(HT)		0.20		
Anandan	2014	[73]	449	0.30	L	115	XS3	Lab	6	Uncracked	–	(1–5)
					D							
Kaufmann	2014	[74]	450	0.40	M	35	XS3	Lab	12	0.50–1.20	< 0.50[a]	1–5
					D			Field				
Bernard	2015	[75]	586	0.29	L	40	XS1	Field	37	0.10–0.30	0–0.10	(1–5)
					D		XC4					

Abbreviations: (Bind) total binder content, expressed in kg/m^3; (w/c) water to binder ratio; (Fibre) description of the steel fibre, being steel the steel type (L)ow- (M)edium- (H)igh-carbon and (S)tainless steel, the type of coating (B)rass- and (Z)inc-plated and the type of fibre cold-(D)rawn, melt-(E)xtract, cut-(S)heet or cut-(M)ill; (Dose) the quantity of steel fibres, expressed in kg/m^3; (Exp. class) the exposure class, according to the EN 206 standard classes; (Exp. type) the exposure type, being laboratory or field exposure; (Age) the exposure time, expressed in months; (Crack) the state of the matrix prior to exposure, and characteristic crack width in mm; (Crack crit.) the critical characteristic crack width recommended by the authors, expressed in mm; (Scr. layer) the sacrificial layer, from the exposed surface, containing corroded steel fibres, expressed in mm.

() Values obtained from qualitative description of the exposed specimens.

[a] The crack range studied is above the critical crack width for fibre corrosion-protection, i.e. outside SLS limits ($w_k > w_{k,\ crit}$).

[b] Consideration of critical corrosion by the author of the reference is based on small reductions on the mechanical properties, relative to an insufficient number of replicates tested.

[c] The author of the reference observes non-critical corrosion observed at fibres bridging cracks for $w_k > w_{k,\ crit}$, but expect larger deterioration on the long-term and do not recommend cracked SFRC.

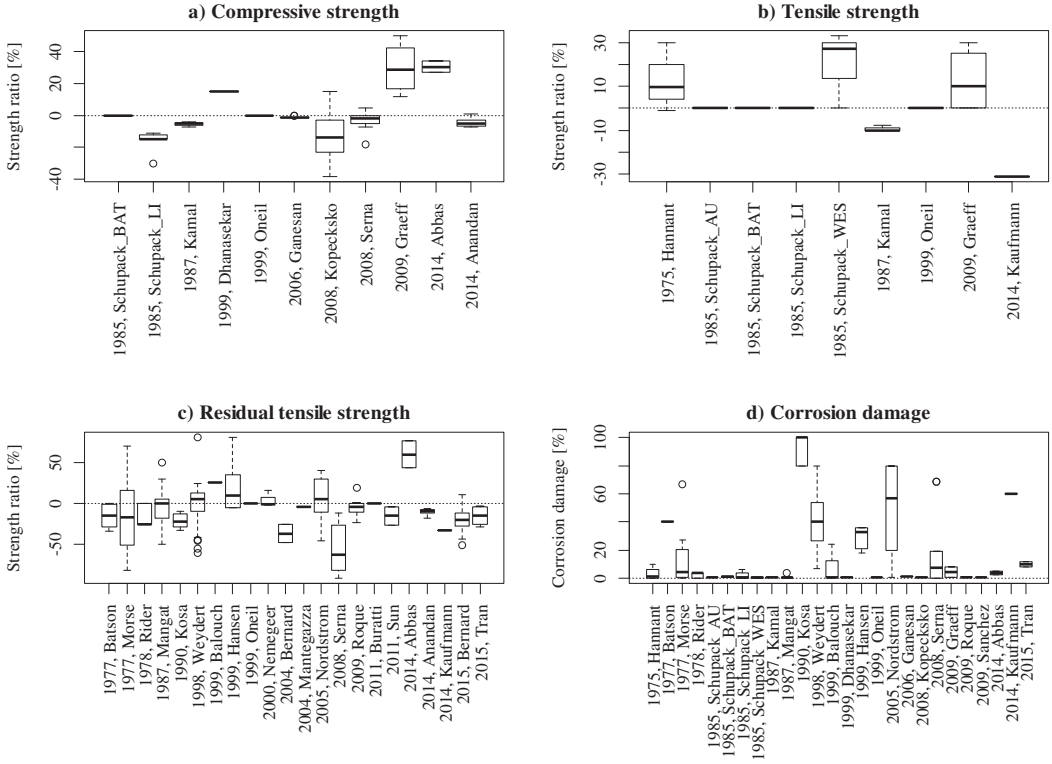

Fig. 1. Deterioration of SFRC exposed to chlorides, summary of results for: a) compressive strength ratio; b) tensile strength ratio; c) residual-tensile strength ratio; d) corrosion damage.

performance of SFRC after exposure, e.g. mechanical properties, chloride penetration depth, corrosion damage.

The database contains the performance indicators calculated systematically for each replicate reported in the literature, when available. The following order of preference was applied to pre-process and introduce the data: i) raw data published in tables or graphs was utilized to calculate directly the performance indicators; ii) centrality and dispersion indicators provided in tables and graphs, were included in the database as three records (i.e. the average value, the upper- and lower-bounds); iii) the value reported was entered as a single record in the database, if none of the former data sources were available or no information about the number of replicates was given. No correction or weighing factors have been applied to the original data. The performance indicators for the reference specimens, used to calculate the relative performance on exposed specimens, have been averaged to the arithmetic mean value.

The data has been evaluated using descriptive statistics, and the results presented comprise exploratory data analysis, presented in boxplots. Statistical modelling, i.e. linear regression analysis and principal component analysis, did not provide clear indication of correlation among the study variables, attributed to the limited amount of available data and the large variability among data sources, limiting further analysis.

Among those indicators, four variables are used to define the relative performance of exposed SFRC: i) the compressive strength ratio (Fig. 1a), tensile strength ratio (Fig. 1b) and residual-tensile strength ratio (Fig. 1c), expressed as the percentage-ratio of strength after exposure relative to the reference strength of the companion specimens; ii) the corrosion damage (Fig. 1d), expressed as the product of: the subjective classification of the corrosion damage at the fibres (converted to a 0–5 scale) and the ratio of the cross section of the specimen affected by fibre corrosion, as measured by the original authors, expressed as a percentage, i.e. being 0% undamaged and 100% fully damaged. When available, the description of the corrosion damage given by the original authors was verified trough analysis of images published of the crack planes (i.e. digital image correlation) and detailed images of corroding fibres.

The limit of proportionality (LOP), when specimens were pre-cracked prior to exposure and re-tested after the exposure [33,65,74], has been included within the tensile strength ratio group, whereas the residual tensile strength ratio comprises investigations on the flexural and tensile toughness of the material [44,46,61].

A direct comparison of the collected results reveals a large scatter within and between studies, indicating a great variability of the results depending on the material properties and exposure conditions. As an example, reference is made to the large variation (40–60%) observed on the residual-tensile strength ratio within some of the studies [35,43,50,61,63], Fig. 1c, or the large dispersion registered on the corrosion damage ratios between studies, Fig. 1d. Therefore, further analysis on the effects of each of the individual variables influencing the durability of SFRC exposed to chlorides is necessary to generalize the test results and research conclusions for SFRC structures exposed to chlorides.

2.1. Variables influencing the durability of SFRC exposed to chlorides

This review gathers the results and conclusions from published investigations available and classifies them according to: 1) exposure conditions and age; 2) type and size of the steel fibres; 3) quality of the concrete matrix; 4) structural integrity of the SFRC matrix (i.e. cracks).

2.1.1.1. Exposure conditions and age. The exposure conditions for testing the durability of SFRC subjected to chlorides can be divided into two groups, field exposure and laboratory exposure under accelerated conditions. Laboratory conditions are expected to accelerate the deterioration processes for the same exposure times by a factor of around 1:50, depending on the exposure conditions and materials (i.e. one year of accelerated exposure is equivalent to 50 years of field exposure) [61].

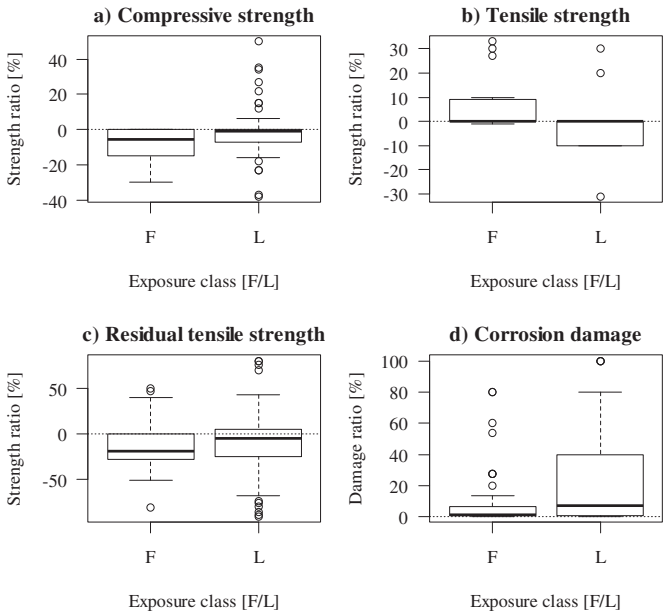

Fig. 2. Deterioration of SFRC exposed to chlorides, comparison of results for field (F) and laboratory (L) exposure for: a) compressive strength ratio; b) tensile strength ratio; c) residual-tensile strength ratio; d) corrosion damage.

The results presented in Fig. 2d, indicate larger corrosion damage for laboratory-exposed specimens, compared to field-exposure. However, the decay on mechanical properties does not follow the trend and field-exposed specimens tend to reach similar strength ratios within the large scatter previously mentioned (Fig. 2a–c). It is expected that the rest of test variables (e.g. crack width, type of fibres and quality of the concrete) have a large impact on the deterioration and would confound the direct comparison between the studies, hindering the elaboration of conclusions regarding the efficiency of laboratory and field exposure tests, e.g. the large dispersion observed at the residual-tensile strength ratios (Fig. 2c). There is limited research combining laboratory and field-exposed testing under comparable conditions and the available results are reported to be very sensitive to variations on the specimen dimensions [61] and exposure conditions [43,61].

2.1.1.1.1. Field exposure. Field tests comprise the exposure of several SFRC test coupons to in-situ exposure conditions at representative locations, using a limited exposure time (e.g. 1–20 years) to extrapolate the durability of SFRC structures to longer exposures. Variables such as temperature and exposure-cycles are uncontrolled and may vary from: a) extreme conditions, with large temperature variations and shorter cycles (e.g. seawater splash- or tidal-zone, splash of de-icing brines at road margins); b) to milder conditions, with even temperatures and longer cycles (e.g. partial immersion). Moreover, the salinity of the aqueous media may vary in the range of 3.0–3.8 wt% NaCl for sea exposure up to 20–30 wt% NaCl, or $CaCl_2$ for de-icing brines. It should be mentioned that accumulation and crystallization of salts at cracks and crevices might increase this concentration up to four-fold values [76,77].

Exposure of SFRC specimens for shorter periods (e.g. 1–3 years) to coastal environment, seawater or de-icing salts, showed limited damage for both uncracked and cracked ($w_k \leq 0.30$ mm) SFRC [13,33,35,40,43]. The damage was limited to aesthetics due to the rusting on external fibres, with a maximum depth of damage of a few millimetres (an assumed sacrificial layer would range between 1 and 5 mm). Uncracked specimens showed negligible reduction in compressive and flexural strength, along with increased residual-tensile strength, which can be attributed to a higher fibre-matrix friction as a result of limited corrosion of fibres and densification of the matrix [33,40]. Similar results for specimens with small cracks ($w_k \leq 0.20$ mm), suggest autogenous-healing of cracks and non-harmful corrosion on the fibres (i.e. limited cross-sectional reduction), leading to increased residual-tensile strength [13,35,40,44].

Extended exposure times (5–20 years) to analogous aggressive conditions (e.g. seawater splash- or tidal-zone, splash of de-icing brines at road margins) provide similar results, comprising limited damage of SFRC for both uncracked and cracked ($w_k \leq 0.20$ mm) scenarios [37,49,61,78–80]. The observations substantiate that corrosion of both cracked ($w_k \leq 0.20$ mm) and uncracked SFRC is limited to staining on external fibres, i.e. a sacrificial layer of 1–5 mm for uncracked SFRC and 10–25 mm for cracked SFRC, without additional corrosion-induced cracking or spalling of the matrix. The evolution of the mechanical behaviour and reduction in fibre cross section relative to shorter exposures suggests an early stabilization of the deterioration process during the first 2–3 years of exposure (e.g. calculated corrosion rates inside cracks at first year are four- to five-times the corrosion rates at five years) [61].

2.1.1.1.2. Accelerated laboratory conditions. A larger number of controlled variables is found for laboratory exposure: a) type of exposure; b) the type of salt (e.g. sodium chloride or calcium chloride); c) salinity; d) duration of the exposure; e) temperature, among others. This section classifies former research based on the type of exposure.

The use of wet-dry cycles has been proven an effective method to accelerate corrosion-induced damage of SFRC. Shorter exposures (up to six months) to average salinities (3–5 wt% NaCl and $CaCl_2$), typically show damage limited to staining at external surfaces (limited to outer 1–5 mm) on uncracked specimens, accompanied with negligible loss on compressive, flexural and residual-tensile strength [34,38,62,73,78,81,82]. Results on cracked SFRC indicate negligible residual-tensile strength loss for small cracks ($w_k \leq 0.20$ mm) [61,83]. At the same time, contradictive results showing significant reduction of the residual-tensile strength for cracked and uncracked SFRC are presented in [34,59,73,84,85].

Extended exposures (from 6 months to 3 years) to wet-dry cycles at average salinities, i.e. 3–5 wt% NaCl, generally showed similar results for uncracked SFRC, compared to shorter exposures, suggesting an early stabilization of the deterioration of the steel fibres [6,12,36,63,64]. Contradictive results are found for cracked SFRC; while positive results for smaller cracks ($w_k \leq 0.20$ mm), entailing minor corrosion of the fibres, negligible reductions of the residual-tensile strength and self-healing of the crack have been reported in e.g. [6,64,65,86], severe fibre corrosion and strong loss of residual-tensile strength for larger cracks ($w_k > 0.20$ mm), leading to further deterioration for longer exposures have been presented in e.g. [46,48,63].

Alternatively, the use of salt-fog spraying has been less common among researchers. The exposure time did not influence the corrosion damage for uncracked specimens for shorter exposure times, i.e. exposures of 6–12 months showed similar damage, limited to surface staining of external fibres (sacrificial layer of 1–3 mm) [40,54,78,87]. While, for cracked SFRC, extended exposure times to salt-fog spray (up to 3.5 years) revealed significant fibre corrosion and residual-tensile strength loss for larger cracks ($w_k > 0.20$ mm) [44,53].

Partial- and full-immersion have been reported ineffective on accelerating corrosion of SFRC. Short exposures (below 4 months) revealed negligible damage on uncracked specimens, limited to stains at the surface [55]. Whereas longer exposures (up to 10 years), resulted in limited corrosion in the outer 3 mm of the specimens and slight reductions on the flexural strength during the initial 2 years [78].

Early-age immersion of SFRC exposed to sodium chloride (i.e. curing of specimens in chloride solutions) and mixed-in $CaCl_2$ induced severe pitting damage on the fibres and significantly reduced the fibre pull-out resistance. These results contradict the moderate deterioration observed for uncracked SFRC tested with the previously mentioned exposure methods; which indicates the incompatibility of marine curing

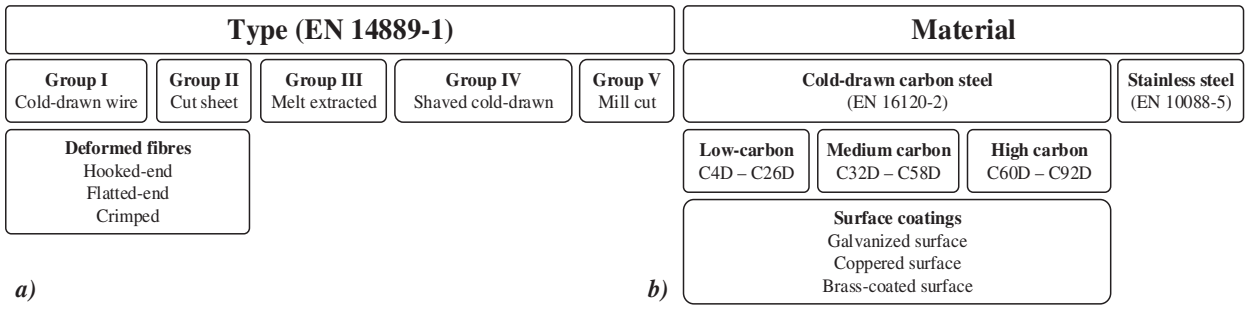

Fig. 3. Classification of steel fibres: a) type of steel fibre for concrete according to EN 14889-1 b) type of steel according to EN 10016-2 and EN 10088-5.

of SFRC and proves the inadequacy of this method to test the corrosion resistance of SFRC under accelerated chloride exposures [84,88,89].

The use of elevated temperatures (e.g. 30–80 °C) to accelerate the corrosion of SFRC has been proven highly effective on increasing the deterioration of SFRC for shorter exposure times (3–6 months) [6,45,46,64]. However, substantial changes in the damage mechanisms are responsible for the accelerated deterioration at elevated temperature (e.g. > 50 °C), due to the alteration of the cement chemistry, i.e. formation of Friedel's salt, leading to a rapid disintegration of the matrix [6,45,46]. Temperatures of 30–40 °C in combination with wet and dry cycles led to more realistic deterioration [64], although, no companion data for SFRC exposed under standard temperatures (e.g. 20 °C) is available in the study, impeding the estimation of the acceleration factor at higher temperature.

2.1.1.2. Type, material and size of the steel fibre. Limited amount of research has focused on the influence of type, material and dimension of the steel fibres on the durability of SFRC exposed to chlorides. The EN-14889-1 standard [90] proposes a classification of steel fibres according to the production process, as shown in Fig. 3a.

Cold-drawn carbon-steel and stainless-steel for groups I, III and IV are specified according to EN 16120-2 and EN 10088-5, respectively in Fig. 3b [91,92]. According to this classification, the main design variables influencing the durability of SFRC to chlorides are: a) fibre type (e.g. production method); b) type of steel and coatings; c) fibre dimensions (i.e. length and diameter).

Cold-drawn wire, typically deformed with hooked-ends, is used in most of the durability investigations of SFRC [12,13,33,35,40,49,52,56,83]. Other types of fibres, such as cut-sheet fibres have been only used in some of the research [34,49], limiting the scope of interpretation.

There is insight about significant variations of the likelihood of fibre corrosion and damage depending on the type of steel-fibres, e.g.: mill-cut fibres showed larger probability of corrosion and stronger reductions on the residual-tensile strength of SFRC, relative to cold-drawn wire, Fig. 4c–d, [12]. Conversely, cold-drawn and cut-sheet fibres showed a similar corrosion resistance under comparable exposure conditions, Fig. 4d, but the exposure of the latter resulted in larger reductions of the residual-tensile strength, Fig. 4c, [49,63]. The large corrosion resistance and negligible mechanical deterioration of melt extract fibres, Fig. 4c–d, responds primarily to the material properties, as this type of fibre is produced of stainless-steel [36,43].

Additionally, recent research indicates that deformed cold-drawn steel fibres (e.g. hooked ends) have a higher probability for initiation of chloride-induced corrosion, relative to un-machined cold-drawn steel wire, due to early initiation of pitting corrosion at micro-flaws at the bended regions [93].

Former research has reported increased resistance of stainless-steel to pitting corrosion relative to carbon-steel, limiting the formation of rust at the surface as well as ensuring negligible corrosion-damage in cracked SFRC [36,40,49]. Coated steel fibres (i.e. brass- or zinc-plated) showed contradictory results: a) reaching a similar long-term performance compared to carbon-steel wire, extending the time-to corrosion initiation for pitting corrosion [12,69,78]; b) or alternatively showing a total protection against corrosion for long-term exposures (i.e. 6–12 months of accelerated exposure and 18 years of field exposure) [49,56,63].

The influence of the fibre dimensions on the electrochemical behaviour of SFRC exposed to chlorides is unclear. Contradictory results observed in [61], showed increased corrosion rates for longer steel fibres at initial times of exposure to NaCl but opposite results for water-exposed specimens, accompanied with a large scatter of the results. Whereas a limited effect of the wire length on the corrosion of carbon-steel wire embedded in concrete exposed to chloride solution was observed by Mangat and Molloy [93]. Additionally, it has been reported that the fibre diameter plays a minor role on the initiation of corrosion of steel fibres, relative to the fibre length [93,94].

2.1.1.3. Quality of the concrete matrix. The quality of the concrete matrix has been suggested as a critical factor to consider when preventing chloride-induced corrosion of conventional steel reinforcement in concrete e.g. [76]. It is expected, that the main mix-design variables affecting the durability of conventional reinforced concrete have similar effects on SFRC, i.e. the water to binder ratio (w/b) and the type and quantity of binder.

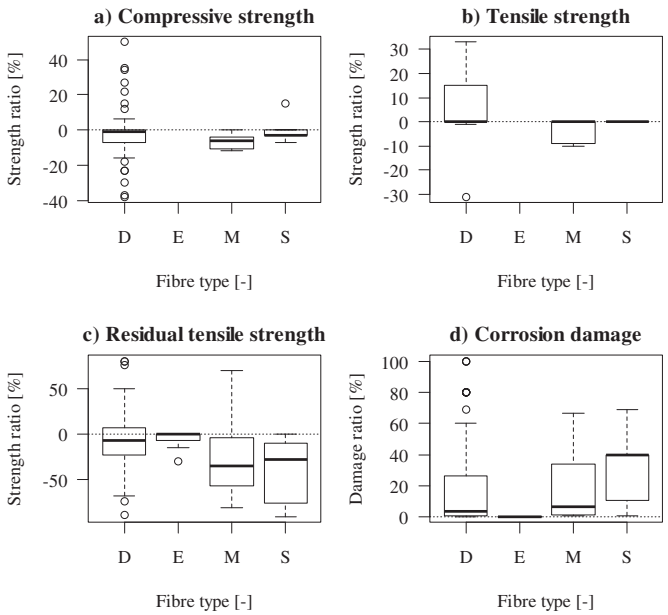

Fig. 4. Deterioration of SFRC exposed to chlorides, comparison of results for different types of fibre: a) compressive strength ratio; b) tensile strength ratio; c) residual-tensile strength ratio; d) corrosion damage.
Abbreviations: (Fibre type) type of fibre according to EN-14889-1: cold-(D)rawn, melt-(E)xtract, cut-(M)ill, or cut-(S)heet.

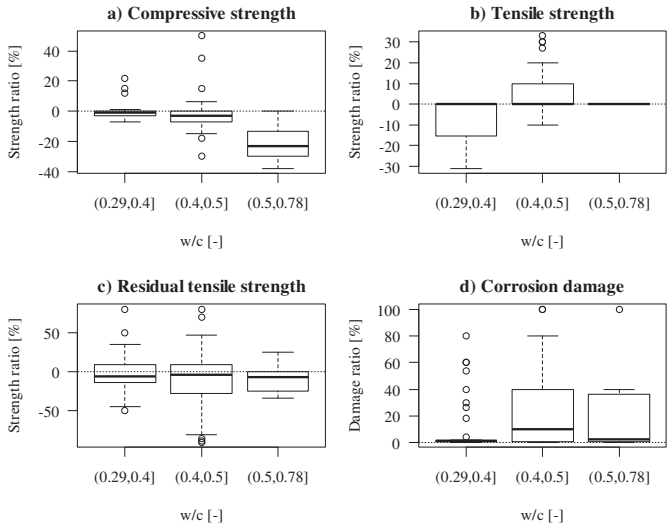

Fig. 5. Deterioration of SFRC exposed to chlorides, influence of the water to binder ratio on: a) compressive strength ratio; b) tensile strength ratio; c) residual-tensile strength ratio; d) corrosion damage.

A wide range of w/b ratios have been tested for SFRC, ranging from 0.30–0.70 [33,61,64,79]. An upper limit for w/b of 0.50 has been proposed by Granju and Balouch [52] for cracked and uncracked SFRC, ensuring a sacrificial layer < 1 mm for uncracked SFRC and limited corrosion for small cracks (w_k < 0.20 mm). However, other research suggests lower values (e.g. w/b < 0.40–0.45) in order to ensure durability of steel fibres in cracked SFRC [13,40,49,61]. An analysis of results presented in the literature indicates significantly higher degradation of the compressive strength (i.e. uncracked SFRC) for w/b > 0.50 (Fig. 5a), and larger corrosion damage for w/b > 0.40 for cracked SFRC (Fig. 5d). However, there is no clear trend on the detrimental effect on the residual-tensile strength for cracked SFRC, as shown in Fig. 5c. It should be noted, that there is limited data available regarding the impact of chloride exposure on the tensile strength of SFRC (Fig. 5b). The data available suggest a larger deterioration on the tensile strength at lower w/c ratios, discrepant with the observations on the compressive strength ratio and the expected corrosion behaviour of steel embedded in concrete, e.g. higher w/c ratios are expected to lead to larger corrosion damage.

Mineral admixtures (i.e. supplementary cementitious materials) are widely used, among others, to improve the durability of concrete subject to aggressive exposures [95]. A substantial share of the research on SFRC uses either: a) blended cements optimized for aggressive exposures, e.g. EN 197-1 type CEM II [37,49,51,63] or b) mineral cement replacements, i.e. Portland cement replacement with: fly ash, blast furnace slag or/and silica fume [6,12,43]. However, limited information is available on the efficiency of mineral admixtures on preventing chloride-induced corrosion in SFRC [41].

The minimum quantity of binder is specified in some of the principal design standards in Europe (e.g. EN-206 and national guidelines), this value ranges between 300–360 kg/m^3, depending on the aggressiveness of the exposure class. However, these limitations are so far only applicable to conventional reinforcement [96]. A wide range of binder content (250–750 kg/m^3) is found when comparing research related to chloride-induced corrosion on SFRC [6,40,53,54,64]. Nevertheless, there is strong criticism regarding the influence of the quantity of binder on the protection of steel against corrosion [97,98] and only limited information for SFRC can be found in the literature to elaborate definite conclusions.

2.1.1.4. Cracks. Limited corrosion damage is found in uncracked SFRC when sufficient concrete qualities are used, i.e. w/c ≤ 0.5 [54]. The potential damage due to extended exposures is restricted to formation of rust at the surface and light fibre corrosion in the outer 1–5 mm, appearing during the initial months of exposure but resulting in negligible long-term damage [6,12,35,37,43,49,54,64]. The investigations on uncracked concrete reveal negligible corrosion damage (Fig. 6b), except for isolated outliers. However, some investigations report reductions up to 40% of the residual tensile strength (Fig. 6a), with a large scatter among studies.

The durability of cracked SFRC is controversially discussed in the literature and conclusions can be divided according to three crack widths (w_k), labelled in this study as: a) wide cracks: w_k > 0.5 mm; b) narrow cracks: 0.5 mm ≥ w_k > 0.2 mm; c) hairline cracks: w_k ≤ 0.2 mm.

There is general consensus regarding the high probability of corrosion on carbon-steel fibres bridging cracks wider than 0.5 mm e.g. [12,35,44,53,83]. The formation of pits at weaker spots, i.e. the crack-bridging region of the fibres and the deformed areas, leads to a significant reduction of the fibre cross-section and provokes notable reductions of the residual-tensile strength (Fig. 6a), due to a subsequent change in the failure mode from fibre pull-out to fibre failure, after short periods under moderate exposure to chlorides [12,13,46,53,56,61,63]. Crack widths larger than 0.5 mm, show no evidence of self-healing in the cracks and despite local damage at the crack region, there is no extended damage due to cracking or spalling of the adjacent matrix caused by fibre corrosion [44,46,53].

The risk of fibre corrosion in narrow cracks is controversial, and the results reported show a great variation on the corrosion damage and residual tensile strength ratios (Fig. 6a–b). A greater share of the research supports the scenario in which carbon-steel fibres corrode up to critical reductions of the fibre cross-section in the long-term [12,13,33,34,44,46,63,75], leading to substantial decay of the residual-tensile strength of SFRC exposed to chlorides. The use of galvanized steel fibres extended the time to initiation but did not prevent the propagation of corrosion for longer exposures [12,63]. Other results indicate limited corrosion of carbon-steel as well as no corrosion for galvanized and stainless steel fibres bridging narrow cracks, together with minor loss of residual-tensile strength [53,56].

However, there is research supporting that a significant share of the reduction on the residual tensile strength observed after exposure is related to the embrittlement of the SFRC due to densification of the

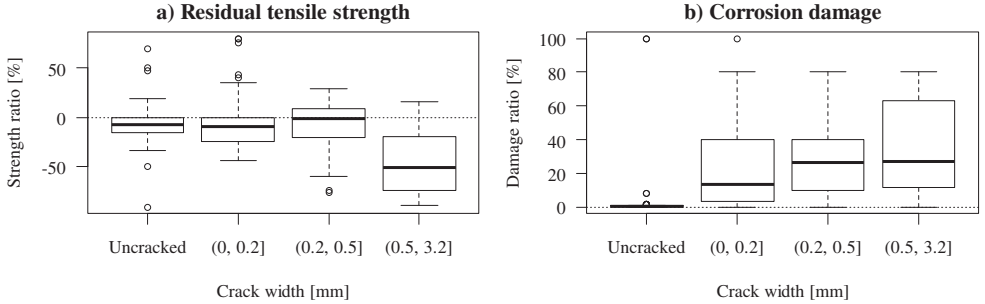

Fig. 6. Deterioration of SFRC exposed to chlorides, influence of crack width on: a) residual-tensile strength ratio; b) corrosion damage.

matrix [13,75,99]. Since the hydration process promotes an increase on the compactness and strength of the matrix, and therefore alters the fibre-matrix bond and mechanical anchorage of the fibre, changing the failure mode from fibre pull-out to fibre yield. This issue may be solved by an adequate dimensioning of the fibre type, dimensions and steel strength, considering the long-term mechanical behaviour instead of the 28 days or early age maturity one [99].

Corrosion of steel fibres bridging hairline cracks is currently under discussion. There is a large scatter in the results presented in the literature, i.e. large variation of corrosion damage and residual strength ratios (Fig. 6a–b). Some research points towards limited corrosion of carbon-steel fibres bridging cracks smaller than 0.15–0.20 mm, accompanied by negligible reductions of the residual-tensile strength [6,44,51,53,56,61]. More restrictively, other investigations point towards crack limits of 0.05–0.10 mm, in order to avoid corrosion on carbon-steel fibres bridging cracks, ensuring negligible reductions of the residual-tensile strength [10,13,35]. For those crack limits, self-healing at the crack is commonly reported, often leading to greater peak residual-tensile strengths relative to unexposed SFRC [35,44,53,56,61].

Conversely, a share of the research refutes the existence of a crack width limit for corrosion of carbon-steel fibres, recommending the incompatibility of cracked SFRC exposed to chlorides. The argumentation is based on the fact that exposure times are insufficient to induce sufficient damage and early corrosion will proceed until complete failure of the fibre [12,79] or else, results show a strong reduction on the residual tensile capacity during the exposure [34,46,59,83,84].

2.2. Mechanisms of chloride-induced corrosion in SFRC

Steel embedded in uncontaminated concrete remains passive due to the high alkalinity of the concrete. The ingress and build-up of chloride ions into the matrix surrounding the steel disrupts the passive layer, leading to the dissolution of iron and promoting a local reduction of the pH at the steel surface, initiating pitting-corrosion [95].

Following a generalized conceptual model for corrosion of steel in concrete [100], the deterioration of SFRC exposed to chlorides can be divided into two stages: a) initiation phase, where dissolved chlorides penetrate into the concrete and reach the steel surface and, b) propagation phase, once the chloride threshold at the steel surface is exceeded and the corrosion process of the steel embedded in the contaminated concrete proceeds.

2.2.1.1. Transport properties of SFRC, chloride exposure. The transport properties of uncracked SFRC have been reported similar to the properties of un-reinforced concrete. Contrary to earlier assumptions, the fibre-matrix interface does not provide a preferential path for the ingress of chlorides [42,67,101–103]. Moreover, Abbas et al. [72,104] suggest a lower chloride penetration in uncracked SFRC relative to plain concrete, attributed in similar research to the arresting of microcracks by steel fibres during curing and handling [105].

The transport properties of cracked SFRC are also unaffected by the fibres, excluding the assumed crack arresting effect of the fibres, i.e. reduced cracking at same load conditions compared to plain concrete [72]. The build-up of chlorides in cracks due to wet-dry cycles, evaporation, and limited wash-out, increases the chloride concentration inside the crack. This leads to similar chloride concentrations inside the crack faces compared to external exposed surfaces, i.e. the crack faces act as free surfaces [51].

2.2.1.2. Chloride-induced pitting corrosion of steel fibres in concrete. It is generally assumed that once a critical concentration of chlorides (i.e. the critical chloride threshold) is reached at the steel surface, the steel de-passivates locally. Typically, this leads to initiation of pitting corrosion at weaker regions or micro-flaws in the oxide layer, as shown by the dotted lines in the Eh-pH diagram with superimposed

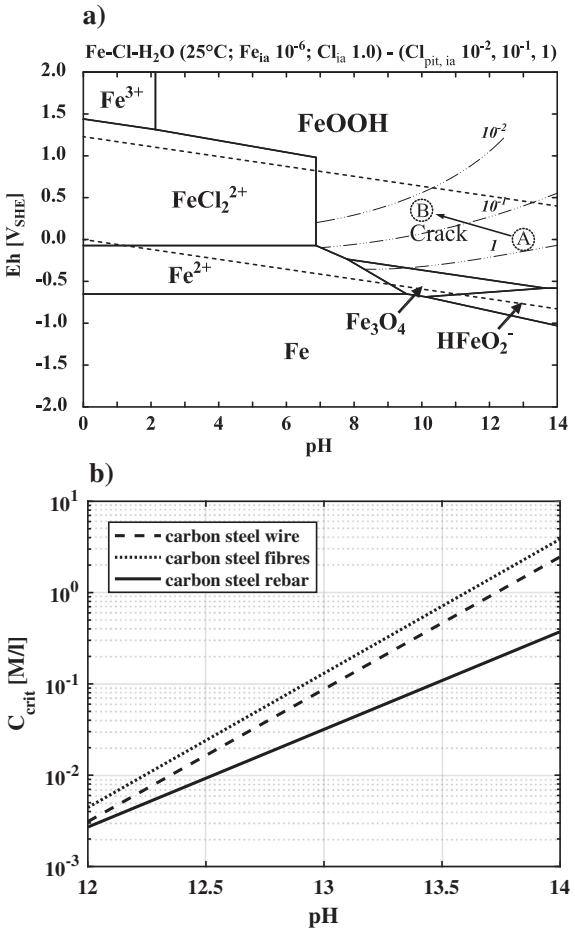

Fig. 7. Critical chloride concentrations for pitting corrosion on: a) Potential-pH diagram with superimposed pitting-potential curves for conventional steel, after Küter et al. [106], (A) indicative potential of steel in uncracked concrete and (B) indicative potential of steel in cracked concrete; b) critical chloride content at different pH values for conventional steel and steel fibres, after Dauberschmidt [93,108].

pitting-potential (E_{pit}-pH vs Cl^-) curves, Fig. 7a [106]. The literature suggests chloride threshold values in the range of 0.1–2.0 wt% Cl^-/wt % cem. for conventional carbon-steel reinforcement, depending on several variables: e.g. oxygen concentration, pH, binder type, w/c ratio, steel grade, test conditions (e.g. temperature, measurement technique) [107].

Significantly higher chloride threshold values have been found for SFRC, i.e. 2.1–5.6 wt% Cl^-/wt% cem. tested in simulated pore solution [40,93], as shown in Fig. 7b. The higher resistance of carbon cold-drawn steel fibres towards initiation of pitting corrosion is explained by the combination of several factors: a) more uniform steel surface due to the cold-drawing process, which restrains the initiation of pitting-corrosion; b) smaller dimension of fibres limiting the cathodic area and leading to slower corrosion rates; and c) denser and more uniform steel-matrix interface of SFRC, which effectively protects the fibres against chlorides and oxygen ingress [61,93].

2.2.1.2.1. Mechanisms governing chloride-induced corrosion of uncracked SFRC. The limited corrosion observed for uncracked SFRC exposed to chlorides, relative to conventional reinforcement has been primarily attributed to three components: a) the discontinuous nature of the fibres; b) the uniform steel surface due to the cold-drawing process; c) the dense and uniform fibre-matrix interfacial transition zone (ITZ) [61,94,108].

The positive influence of the discontinuous nature of the fibres on the improved corrosion resistance of uncracked SFRC exposed to chlorides, relative to conventional reinforcement, has been theorized by

several researchers [61,108]. The greater stability against corrosion has been related to smaller potential difference along the steel surface and smaller cathode/anode ratios [61,108] compared to conventional reinforcement. Nevertheless, the impact of the fibre size-effect is still unclear, i.e. Mangat and Molloy [94] suggest a negligible length-effect for wire lengths in the range of 0–160 mm and an anodically-controlled reaction (i.e. the oxidation rate of iron limits the redox reaction).

The beneficial role of the cold-drawing process for steel-wire fibres has been shown by Dauberschmidt (2006) who observed a greater stability against chloride-induced corrosion of steel fibres in pore solution, compared to conventional steel, due to a more uniform surface structure of the steel, as proposed earlier by Mangat and Molloy [94].

There is limited research investigating the impact of galvanic coatings (e.g. zinc or brass alloys) on the corrosion mechanisms of steel fibres embedded in chloride contaminated concrete. There is overall insight on the protection given by zinc-alloy coatings under short-term chloride exposure [12,40,56,61,63], which raises the corrosion potential and reduces corrosion rates at the steel by consumption of the zinc coating in the anodic process [70]. However, some investigations concerning long term exposure of galvanized steel wire to chlorides in cracked and uncracked concrete show pitting corrosion at the steel surface similar to uncoated carbon-steel fibres [12,40,61]. Additionally, there is insight of increased risk of hydrogen embrittlement for galvanized high-carbon steel wire in alkaline media due to hydrogen development at the zinc coating before full passivation of the zinc layer [109], which may be minimized by pre-passivation treatment of the coating [110]. Other coatings, such as brass-alloys, are also expected to provide temporary protection against chlorides [49,78], due to the combination of the anodic protection provided by the zinc phases and the dense and stable copper oxide phases formed at high pH values even in the presence of chlorides [111,112]. However, there is insight of larger corrosion rates once the coating is removed due to local damage or large strains in the steel, due to galvanic coupling of the iron-copper phases [111].

Stainless steel fibres have been reported to provide full protection against chloride-induced corrosion in uncracked and cracked SFRC in the majority of published research [36,40,49]. However, most of the publications focus on macroscale investigations and there is limited knowledge on the particular protection and deterioration mechanisms. There is insight of pitting threshold values around 0.5 M Cl^- (i.e. 3.5% NaCl) for certain high-strength stainless steel wires tested in pore solution (i.e. pH = 12.5), decreasing to 0.25 M Cl^- at pH = 9.5 (i.e. carbonated or cracked concrete) [113].

This section will focus on the insight regarding the beneficial effects of a denser and more uniform fibre-matrix ITZ, as reported in [61,108]. In particular, Dauberschmidt [108], discussed the presence of a larger and more uniform calcium hydroxide (CH) layer around the fibre, which results in an increased protection of fibres in the bulk SFRC against chloride and oxygen ingress. As shown in Fig. 8b, the microstructure of the steel fibre-matrix ITZ is composed of a significantly larger CH layer, followed by a thinner and denser “porous layer”, relative to conventional steel reinforcement (Fig. 8a). The duplex film, a 1–2 μm bilayer structure composed of CH crystals deposited perpendicular to the steel surface covered by a single layer of calcium silicate hydrate gel (C–S–H), is reported to be similar for steel fibres [114] and conventional steel rebar [115].

The overall thickness of the fibre-matrix ITZ is expected to be smaller compared to conventional reinforcement, which would explain the similar bulk chloride diffusion coefficients between SFRC and plain concrete observed in the literature [114]. Furthermore, it is expected that limited pores and defects occur at the fibre-matrix ITZ, as fibres “float” inside the fresh-concrete matrix similarly to the aggregates, hindering the formation of weak spots at the fibre surface where pitting corrosion might initiate [108].

2.2.1.2.2. Mechanisms governing chloride-induced corrosion of cracked SFRC. The mechanisms responsible for corrosion in cracked SFRC are not well understood. A great share of publications base their

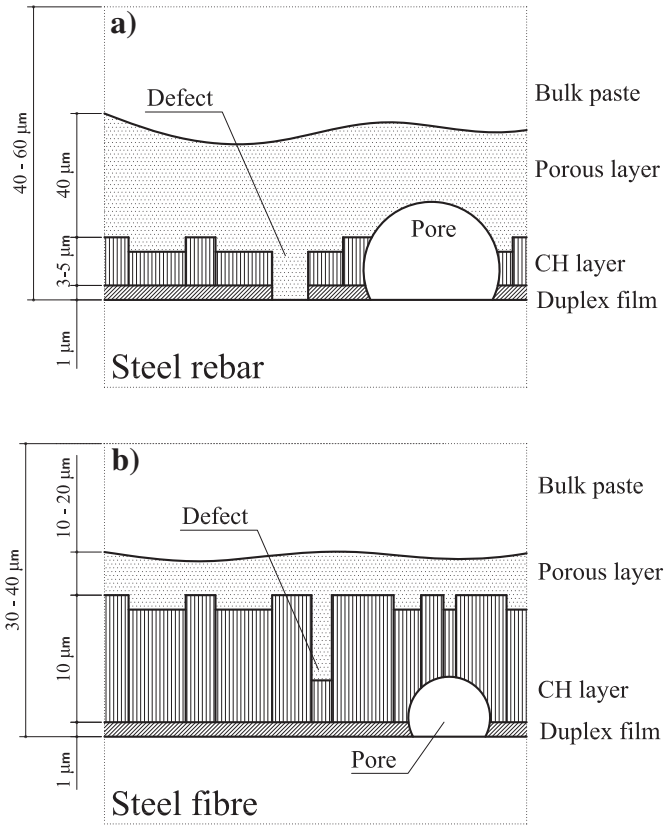

Fig. 8. Microstructure of the steel-matrix ITZ for: a) conventional steel, after Poole and Sims [115]; b) steel fibres, after Bentur et al. [114].

conclusions on a critical crack width (e.g. $w_k < 0.20$ mm), where ingress of chlorides and oxygen is limited and autogenous-healing and corrosion products completely seal the crack within a short time, preventing the evolution of corrosion at the fibre section bridging the crack [6,39,61]. Although in agreement with the abovementioned experimental data, this theory provides a limited explanation for the often observed increase on the residual strength of cracked SFRC exposed to chlorides.

The authors suggest a model governed by the damage at the fibre-matrix ITZ, as suggested by Granju and Balouch [53], corresponding to recent research on the impact of load-induced cracks on the corrosion of conventional reinforcement in chloride-contaminated concrete [116]. The protective role of the fibre-matrix ITZ prevents the initiation of pitting corrosion on the steel fibres of uncracked SFRC; once the matrix cracks, the strain in the fibres bridging the crack induces the damage at the ITZ, promoting corrosion at the weakest regions. Four stages may be identified:

1) The steel-matrix ITZ of steel fibres is denser and more uniform than for conventional steel, as shown in Fig. 8. This layer acts as a protective coating (Fig. 9a): preventing the access of aggressive agents (e.g. oxygen, chlorides), binding the free chlorides surrounding the steel surface, and isolating the steel surface from the electrolyte (i.e. limiting ionic diffusion along the steel surface). However, there is limited data available on the properties and structure of the fibre-matrix interface; even though several investigations support the hypothesis of a denser interface with limited defects [61,108,114,117], recent studies show significant porosity surrounding the fibre [118,119].
2) When the tensile capacity of the concrete is exceeded, the matrix cracks and the fibre-matrix bond is “activated”. The strain at the fibre-matrix interface damages the ITZ. The extent of this damage is directly related to the strain (i.e. larger crack widths induce larger

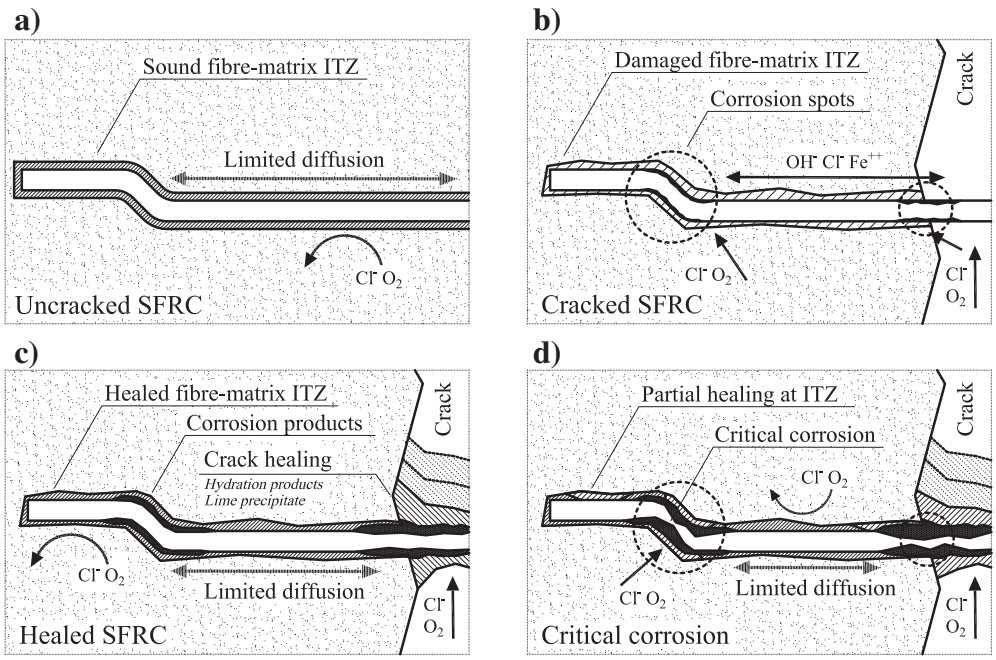

Fig. 9. Structure and corrosion mechanisms for SFRC exposed to chlorides, for: a) uncracked SFRC; b) cracked SFRC at an early stage; c) cracked SFRC after autogenous healing; d) cracked SFRC with critical corrosion on fibres.

damage at the ITZ and a greater exposed area of the steel fibre within the crack) and the shape of the fibres, i.e. Granju and Balouch [53] and Nemegeer et al. [56] observed localized corrosion damage at the hook and at the fibre region intersecting the crack. The damaged ITZ would provide a preferential path for transport of chlorides, metal ions and oxygen, promoting corrosion at the areas with greater damage (Fig. 9b). Furthermore, it can be assumed that the area of the fibre crossing the crack will be more susceptible to pitting corrosion and may present larger corrosion rates compared to the embedded steel [120,121]. Since the electrolyte inside the crack would present higher chloride concentrations, higher oxygen mobility and lower pH values (i.e. due to carbonation and leaching) compared to the regions at the fibre-matrix interface, as presented in the indicative shift on the of the potential of the steel from point A to point B shown in Fig. 7a.

3) In the case that the composite does not reach a critical strain (i.e. up to a critical crack width), the damaged fibre-matrix interface would eventually heal [122], recovering similar conditions to the original state “stage 1” (Fig. 9a). The fibre-matrix ITZ, rich in CH would assist the binding of chlorides and the corroding steel would eventually re-passivate. The increase in fibre roughness due to corrosion and expansion of the corrosion products, in combination with autogenous healing at the interface and the accumulation of products resulting from the chemical binding of chlorides (i.e. Friedel's salt), may increase the fibre-matrix frictional bond (Fig. 9c), as suggested in [123]. Which would explain the improved residual-tensile strength observed in part of the literature [12,53,56,123]. Finally, a combination of hydrating cement, calcium carbonate, corrosion products and salt crystals would eventually seal the crack, limiting the ingress of chlorides and oxygen; the fibres bridging the crack would serve as preferential surfaces for deposition of these compounds [122].
4) Excessive damage at the fibre-matrix interface (i.e. due to larger strain) would result in delayed or defective healing at the ITZ at the regions with greater damage (e.g. deformed regions, fibre-crack intersection), which would result in a progressive and localized reduction of the fibre cross-section due to corrosion. Once a critical cross-section is reached (i.e. the tensile capacity of the steel is lower that the fibre-matrix bond strength) the failure mode of the SFRC would change from fibre pull-out to fibre yield and the residual-tensile strength would decrease (Fig. 9d), as reported in previous research [13,34,46,61].

3. Carbonation-induced corrosion of steel fibres in concrete

There is significantly less data available investigating the corrosion resistance of SFRC exposed to carbonation, compared to chloride attack, as shown in Table 3. Most of the research investigates uncracked SFRC and the exposure conditions often consist of a combination of several agents besides carbon dioxide (e.g. freeze-thaw, thermal loads, soft/acid water attack, airborne chloride attack), which confound the analysis of the direct effect of carbonation. The scarce data and the large amount of variables influencing the results hinders establishing solid conclusions and defining limit states, such as e.g. a critical crack width and sacrificial layer for long-term exposures.

There is limited data regarding the impact of steel fibre corrosion on the compressive and tensile strength of SFRC exposed to carbonation (Fig. 10a–b) [37,38]. However, the compressive and tensile strength are primarily related to the performance of the uncracked matrix. Fibre corrosion would only have an impact in case of corrosion-induced cracking of the concrete matrix, reported unlikely by several researchers [6,53]. The limited corrosion damage presented in studies investigating durability of uncracked SFRC supports the hypothesis that corrosion-induced damage in the matrix due to carbonation is minimal (Fig. 10d).

Conversely, significant corrosion damage has been reported for cracked SFRC (Fig. 10c) [12,61,74]; leading to significant detriment on the residual tensile strength for some of these studies [74]; or small average reductions with a large scatter for others [12,56,61] (Fig. 10c). However, the direct comparison of studies is obstructed by the large quantity of variables influencing the results (e.g. crack width, exposure time, exposure conditions, fibre properties, concrete quality) and the limited quantity of research available. Therefore, further investigation of the parameters influencing steel fibre corrosion in carbonated SFRC is required.

3.1. Influencing parameters

Carbonation-induced corrosion in SFRC is generally considered less aggressive than chloride-induced corrosion, as the carbonation process is much slower than chloride ingress and the risk of corrosion-induced

Table 3
List of studies investigating durability of SFRC exposed to carbonation.

First author	Year	Ref.	Bind (kg/m^3)	w/c (−)	Fibre (steel) (type)	Dose	Exp. class (EN)	Exp. type	Age (mo.)	Crack w_k (mm)	Crack crit. $w_{k,\ crit}$ (mm)	Scr. layer Δ_h (mm)
Hannant	1975	[33]	393 420	0.62 0.75	L D	94	XC4 XA3	Field	57	Uncracked	–	1–6
Schupack (Australia)	1971	[37]	580	0.51	L D	160	XC4 XS1	Field	120	Uncracked	–	3
Kamal	1987	[38]	350	0.50	L M	60 120	XC4	Lab	12	Uncracked	–	3
Kern	1991	[80]	580	0.47	L D	160	XC4	Field	276	Uncracked	–	1–2
Weydert	1998	[47,48]	350 400	0.40 0.50	L/Z D/M	30 120	XC4	Lab Field	17 120	0.15–0.40	0–0.10[b]	5–15
Nemegeer	2000	[56–58]	350	0.45	L/Z D	78	XC4	Lab	18	0.20–0.50	0.50	(1–5)
Bernard	2004	[13]	420	0.42	L D	50	XC3 XC4	Field	24	0.10–1.00	0–0.10	–
Nordstrom	2005	[60,61]	500 510	0.30 0.42	M D	65 70	XC4 XD1	Field	60	Uncracked 0.10–1.00	0.10–0.20	1–5
Sanchez	2009	[67,68]	426	0.45	L-Z D	40	XC4 XS1	Field	18	Uncracked	–	1–5
Kaufmann	2014	[74]	450	0.40	M D	35	XC4 XF3	Field	12	0.50–1.50	< 0.50[a]	1–5
Bernard	2015	[75]	586	0.29	L D	40	XC3 XC4 XS1	Field	37	0.10–0.30	0–0.10	(1–5)

Abbreviations: (Bind) total binder content, expressed in kg/m^3, without considering replacement efficiency factors; (w/c) water to binder ratio, without considering replacement efficiency factors; (Fibre) description of the steel fibre, being steel the steel type: (L)ow- (M)edium- (H)igh-carbon and (S)tainless steel, the type of coating (B)rass- and (Z)inc-plated and the type of fibre cold-(D)rawn, melt-(E)xtract, cut-(S)heet or cut-(M)ill; (Dose) the quantity of steel fibres, expressed in kg/m^3; (Exp. class) the exposure class, according to the EN 206 standard classes; (Exp. type) the exposure type, being laboratory or field exposure; (Age) the exposure time, expressed in months; (crack) the state of the matrix prior to exposure, and characteristic crack width in mm; (Crack crit.) the critical characteristic crack width recommended by the authors, expressed in mm; (Scr. layer) the sacrificial layer, from the exposed surface, containing corroded steel fibres, expressed in mm.

() Values obtained from qualitative description of the exposed specimens.

[a] The crack range studied is above the critical crack with for fibre corrosion-protection ($w_{k,\ crit} < w_k$).

[b] Non-critical corrosion observed at fibres bridging cracks for $w_k > w_{k,\ crit}$, the authors expect larger deterioration on the long-term and do not recommend cracked SFRC.

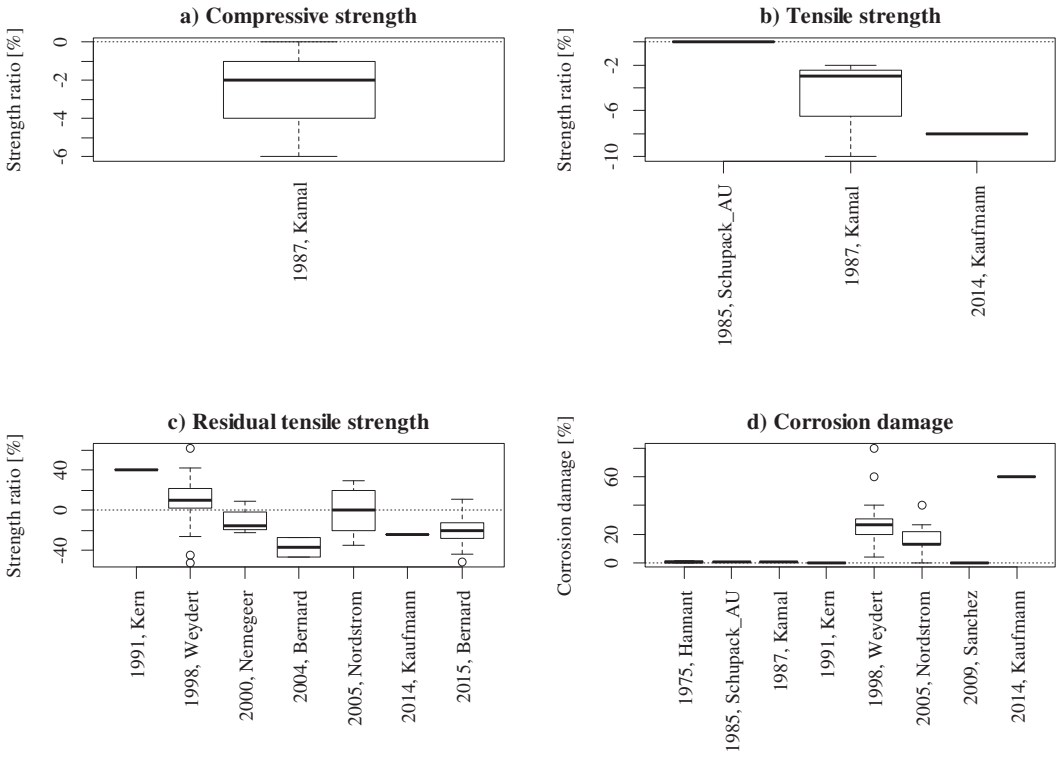

Fig. 10. Deterioration of SFRC exposed to carbonation, summary of results for: a) compressive strength ratio; b) tensile strength ratio; c) residual-tensile strength ratio; d) corrosion damage.

cracking or spalling in SFRC is minimal [124]. The same classification as used for chloride-induced corrosion of SFRC will be used in the following for the discussion of the influencing parameters: 1) exposure conditions and age; 2) type and dimensions of the steel fibres; 3) quality of concrete matrix; 4) presence of cracks.

3.1.1.1. Exposure conditions and age. The exposure conditions are classified into field exposure and accelerated laboratory exposure. The results shown in Fig. 11d indicate a larger average corrosion damage for laboratory-exposed specimens. However, within the range of damage observed for field exposed specimens. The decay of mechanical properties follows the opposite trend (Fig. 11b–c), as field-exposed specimens present lower strength ratios, within a large scatter. This remark could be explained by the additional damage caused by natural agents, such as erosion, freeze-thaw, or temperature variations, typically present under field experimentation. Furthermore, there is limited experimental data on the variation of compressive and tensile strength, Fig. 11a, available results indicate minimal strength variations, below 10% [38].

3.1.1.1.1. Field exposure. Field tests for durability of carbonated SFRC comprise the exposure under atmospheric conditions and natural agents (e.g. rain, freeze-thaw, and direct insolation), extrapolating a limited exposure time to longer lifetimes. Variables such as temperature, CO_2 concentration and exposure-cycles (e.g. wetting-drying, freeze-thaw) are uncontrolled and might vary from: a) extreme conditions with large variations in temperature and/or moisture, freeze-thaw and high concentrations of carbon dioxide (e.g. outside exposure at industrial areas, urban areas exposed to exhaust gases); b) to milder conditions with lower CO_2 concentrations, even temperatures and dry conditions (e.g. rural areas, covered structures).

Exposure of SFRC to aggressive environments for short periods (< 5 years) typically result in limited penetration of CO_2, primarily absorbed by the alkaline buffer of the concrete. Therefore, resulting in a shallow penetration of the carbonation front (i.e. internal area of the concrete with pH < 9 is < 1–3 mm) and negligible damage due to corrosion of fibres, which typically concerns corrosion stains at the surface of uncracked SFRC [33,42,61,68]. In the presence of cracks, the carbonation front progresses up to 20–25 mm, with decreasing

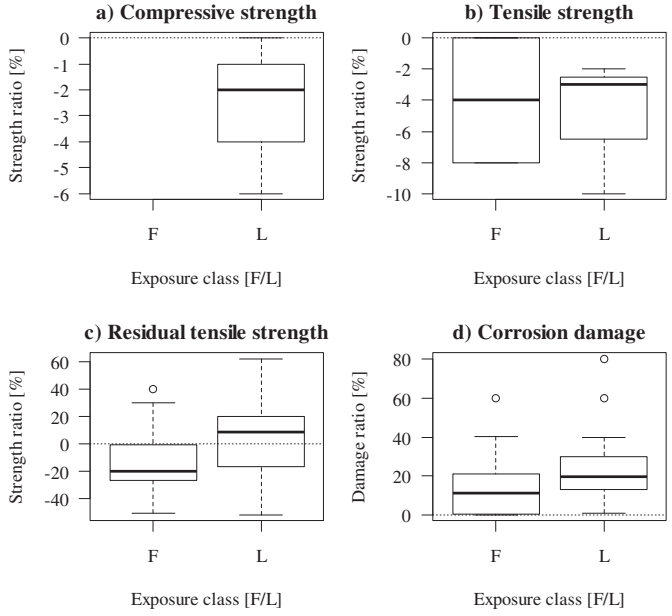

Fig. 11. Deterioration of SFRC exposed to carbonation, comparison of results for field (F) and laboratory (L) exposure for: a) compressive strength ratio; b) tensile strength ratio; c) residual-tensile strength ratio; d) corrosion damage.

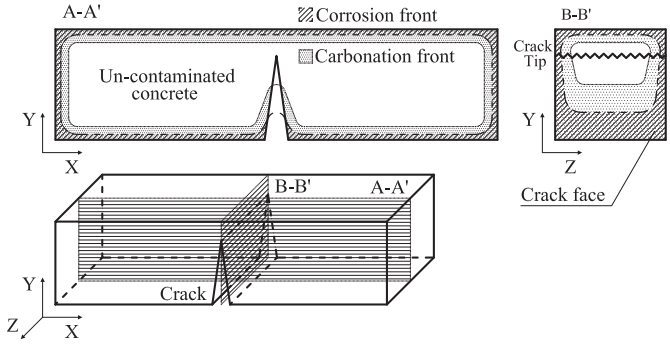

Fig. 12. Description of carbonation and corrosion front for carbonation exposure. A-A′) longitudinal cross-section; B-B′) transversal cross-section. Please note: dimensions for carbonation and corrosion penetration fronts are indicative.

carbonation depth at the crack faces (e.g. 1–3 mm), resulting in limited mechanical damage [33]. Conversely, Bernard [13,75] suggests a similar deterioration of cracked SFRC subjected to 2 years of inland-atmospheric and seawater-immersed exposure, reporting severe corrosion of crack-bridging steel fibres and significant reductions of the residual-tensile strength.

Field exposure of uncracked SFRC for longer periods (5–20 years) results in greater carbonation depths (4–20 mm), with a great variability on the results depending on the conditions and time of exposure. Nevertheless, the damage of the SFRC due to corrosion of fibres is typically limited to staining at the surface (outer 1–2 mm) with absence of cracking or spalling [12,37,49,80]. Conversely, the carbonation front inside cracks propagates at the first 3–5 mm of the inner crack faces (as described by the longitudinal cross-section A-A′ in Fig. 12), decreasing up to depths of 20–40 mm inside the crack, and encountering heavy corrosion on fibres at the outer 2–5 mm (transversal cross-section B-B′ in Fig. 12) [12,79].

3.1.1.1.2. Laboratory exposure. Laboratory exposure entails a stronger acceleration of the carbonation process. The main variables affecting the results are: a) type of exposure, e.g. standard carbonation testing, pre-carbonation, wet-dry cycles; b) CO_2 concentration; c) duration of the exposure; d) temperature and relative humidity.

Standard carbonation testing involves the use of a carbonation cell for smaller specimens, mainly in order to evaluate the progress of the carbonation front using chemical indicators (e.g. phenolphthalein), and additionally, assessing the corrosion of the embedded steel fibres [79,125]. These tests cause strong acceleration rates of the carbonation process (i.e. exposure for 56 days at 50 vol% CO_2 is equivalent to about 100 years of a mild environment), reaching carbonation depths of 50–60 mm, but conversely observing no signs of fibre corrosion [79,101,102,125].

The use of pre-carbonated specimens exposed to simulated atmospheric corrosion (e.g. wet-dry cycles) has been proven more effective reproducing actual corrosion of steel fibres. Weydert & Schiessl [12], exposed pre-carbonated SFRC beams (3 vol% CO_2 for 3 months) to a mild-environment (including rain and freezing) for 18 months, resulting in carbonation depths of 6–10 mm with corroding fibres at the outer 2 mm and negligible mechanical damage for uncracked SFRC. Conversely, the presence of cracks resulted in severe corrosion of the fibres in 20–80% of the cross section of the beams, increasing for larger crack widths, but with limited effect on the residual-tensile strength.

Nemegeer et al. [56], exposed uncracked and pre-cracked SFRC to wet-dry cycles with demineralized water and saltwater (5 wt% NaCl solution), employing a CO_2-rich environment during the drying cycles, for a total exposure time of 18 months. Results presented a shallow carbonation depth, below 2 mm, with limited rusting at the surface and no reductions of the residual-tensile strength for the uncracked specimens. The pre-cracked specimens showed limited carbonation at the crack faces (1–2 mm), accompanied by minor rusting of fibres bridging

cracks and negligible reductions of the residual-tensile strength.

Alternatively, Kosa and Naaman [45,46], exposed pre-carbonated SFRC beams (50 vol% CO_2 for 21 days) to wet-dry cycles with saltwater (3.5 wt% NaCl) for 9 months, observing an increase of the corrosion damage relative to un-carbonated SFRC and larger reductions of the fibre diameter and residual-tensile strength.

3.1.1.2. Type and size of steel fibres. There is limited research focusing on the influence of the fibre type on the durability of SFRC subjected to carbonation. The classification as used for chloride-induced corrosion will be used in the following: a) fibre type; b) type of steel and coatings; c) fibre dimensions; d) volume fraction of fibres.

The majority of research focuses on cold-drawn steel fibres. Earlier research mainly deals with un-deformed cold-drawn wire [33,37,80], showing limited corrosion and mechanical damage, but lacking a detailed analysis of the fibre role. Recent studies focus on hooked-end fibres; agreeing on a reasonably good durability for uncracked SFRC, but disagreeing on the effect of cracks on fibre corrosion [48,79]. Alternatively, the comparison of cold-drawn wire with other fibre types (i.e. Mill-cut fibres) does not show significant differences on the electrochemical behaviour, possibly covered by the scatter of the results (Fig. 13d) [12,49]. However, the variation of the residual tensile strength after exposure shows a significantly larger deterioration for mill-cut fibres (Fig. 13c). There is limited experimental data available to explain the variations of compressive and tensile strength, and the reported results show minor strength variation for exposed SFRC with cold-drawn carbon-steel fibres and melt extract stainless-steel fibres (Fig. 13a–b), suggesting negligible damage of the matrix due to fibre corrosion.

Carbon-steel fibres show an overall good performance in uncracked SFRC [12,13,80], but some studies report severe corrosion of fibres bridging cracks [12,79], which in some cases leads to significant reductions of the residual-tensile strength of the SFRC [13,74]. Stainless steel fibres have been reported to provide full long-term protection against corrosion, even for cracked SFRC [49]. Galvanized and brass-coated fibres showed a similar long-term behaviour to un-coated carbon-steel fibres [12,49,56,79]. Moreover, Ferrara et al. [79], reported higher corrosion rates for brass-coated fibres, attributed to copper-iron galvanic coupling at small flaws on the coating.

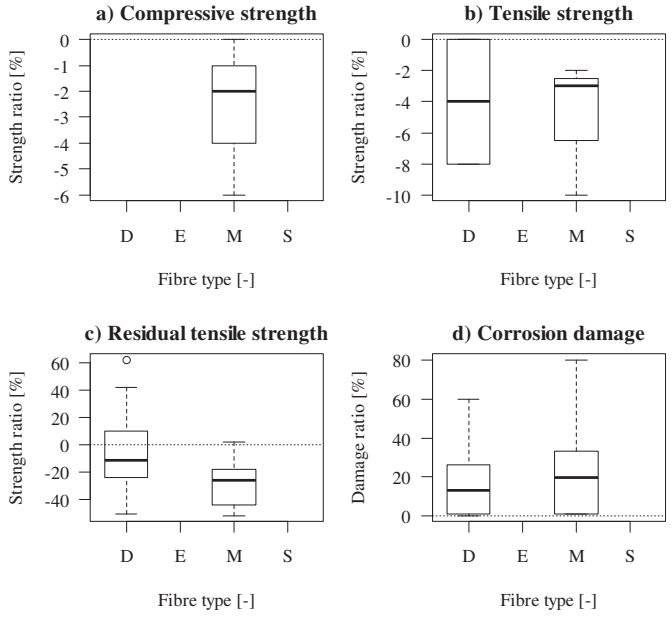

Fig. 13. Deterioration of SFRC exposed to carbonation, influence the type of fibre on: a) compressive strength ratio; b) tensile strength ratio; c) residual-tensile strength ratio; d) corrosion damage.
Abbreviations: (Fibre type) type of fibre according to EN-14889-1: cold-(D)rawn, melt-(E)xtract, cut-(M)ill, or cut-(S)heet.

3.1.1.3. Quality of concrete. As assumed in the general practice, lower water to cement ratios are expected to produce a denser matrix, which leads to a lower penetration of CO_2 and consequently lower carbonation rates [76,95]. Water to binder ratios (w/b) in the range of 0.29–0.78 have been investigated [33,48,79,102,126]; showing an overall good behaviour of SFRC against carbonation for w/c < 0.50, i.e. carbonation rates below 1.0 mm/√y and corrosion limited to fibres directly exposed at the SFRC surface [12,79].

The analysis of the experimental data available reveals a lack of data for higher w/b ratios presenting contradictive results for the corrosion damage ratio (Fig. 14d). The results available are inconsistent and despite the decreasing average corrosion damage for lower water-binder ratios, the results overlap within a large scatter (Fig. 14d). The variations of the residual tensile strength reported for SFRC at low- (w/b = 0.30–0.40) and medium- (w/b = 0.40–0.50) water to binder ratios are similar, and present large variations, i.e. ± 20% (Fig. 14c). The limited data available for the compressive and tensile strength ratios hampers the elaboration of conclusions based on published results (Fig. 14a–b).

There is limited research focusing on the effect of the binder type and content on the corrosion resistance of SFRC subjected to carbonation, hindering the elaboration of design guidelines. A large share of the research typically uses plain Portland cement with contents ranging from 350 to 580 kg/m^3 [12,33,37,80], in some cases combined with minor mineral replacements [13]. The total binder content does not show a significant impact on the corrosion durability, relative to the other variables (e.g. crack width, water to binder ratios, exposure conditions).

3.1.1.4. Cracks. Carbonation of uncracked SFRC causes limited long-term damage, restricted to fibre corrosion progressing at low rates in the outer region of the carbonated area (i.e. 1–10 mm) and aesthetical damage with no cracking or spalling of the matrix [12,33,37,80], as seen from the collection of results presented in Fig. 15b. Negligible reductions of the residual-tensile strength of carbonated SFRC are reported in e.g., [12,33], even in combination with chlorides [12,46,56]. However, the large scatter observed for the results (Fig. 15a) has been related to the progressive embrittlement of the SFRC, i.e. for a 10-year period for some of the investigations [75,99].

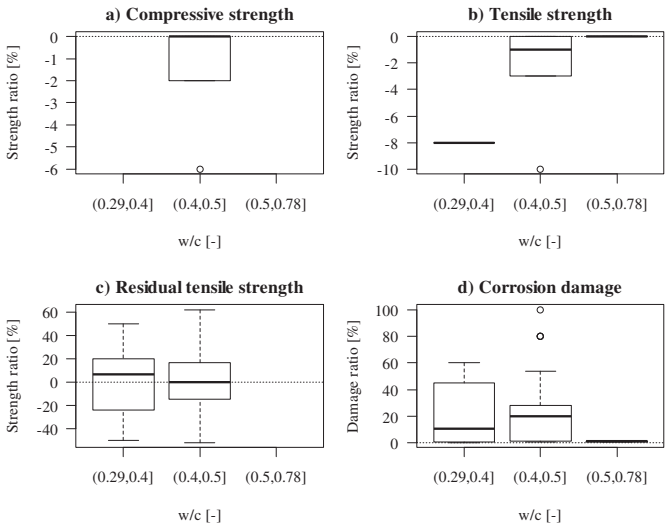

Fig. 14. Deterioration of SFRC exposed to carbonation, influence the water to cement ratio on: a) compressive strength ratio; b) tensile strength ratio; c) residual-tensile strength ratio; d) corrosion damage.

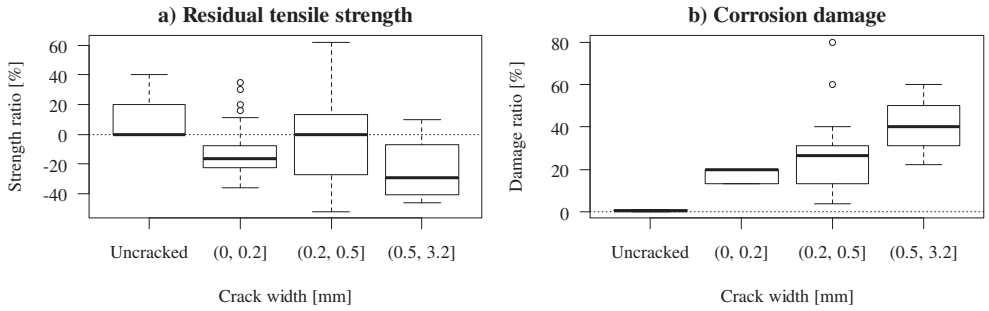

Fig. 15. Deterioration of SFRC exposed to carbonation, influence of the crack width on: a) residual-tensile strength ratio; b) corrosion damage ratio.

Such a change of the fracture behaviour of SFRC has been linked to the continuous hydration and densification of the matrix, rather than the deterioration of the steel fibres [13,99]. A detailed discussion on the mechanisms is provided in chapter 3.2 of this paper.

There is controversy regarding the durability of carbonated cracked SFRC, depending on the crack width, divided into: a) wide cracks, $w_k > 0.50$ mm; b) narrow cracks, 0.50 mm $> w_k >$ 0.20 mm; c) hairline cracks, $w_k < 0.20$ mm.

The presence of wider cracks ($w_k > 0.50$ mm) promotes early initiation of corrosion of steel fibres bridging the crack (Fig. 15b), especially in the outer crack region (Fig. 12, transversal cross-section B-B′), covering up to 90% of the fibre's cross section for longer exposures [12]. Fibre corrosion inside cracks wider than 0.50 mm resulted in a significant loss of the residual-tensile strength (Fig. 15a), estimated around 30–40% by Bernard [13].

Narrow cracks (0.20–0.50 mm) resulted in initiation of corrosion of 70–90% of the fibres bridging the crack (Fig. 15b), with limited reductions of the residual-tensile strength for long accelerated exposure [12]. Conversely, [13,74] reported a substantial decrease of the total energy absorption (30 to 40% loss) of pre-cracked SFRC, at cracks wider than 0.20 mm, after 24 and 37 months of field exposure. These discrepancies regarding the deterioration on the residual-tensile strength of exposed SFRC for cracks wider than 0.20 mm are reflected in the large scatter presented in Fig. 15a.

The durability of carbonated SFRC with smaller cracks ($w_k < 0.10$–0.20 mm) is currently under discussion. Although initiation of fibre corrosion is found in the outer 10–40% of the crack's cross-section (Fig. 15b), the residual-tensile strength at small deformations is unaffected and even slightly improved when compared to unexposed SFRC [12], accounting for negligible reductions of the total energy absorption for large deformations [13]. However, the large scatter reported among research for this exposure, as presented in Fig. 15a, complicates the definition of limit states, such as e.g. a critical crack width, for the most aggressive exposure classes (i.e. XC4).

3.2. Mechanisms of carbonation-induced corrosion in SFRC

Steel embedded in concrete remains passive due to the high alkalinity of the surrounding environment (i.e. pH 13–14). The dissolution of CO_2 into the pore solution through the concrete surface leads to the formation of carbonic acid (H_2CO_3), which reacts with the calcium hydroxide forming calcium carbonate, thus lowering the pH below 10 and promoting the de-passivation of the steel surface [95].

Following Tuutti's model for corrosion of reinforced concrete [100], the deterioration of SFRC due to carbonation can be divided into: a) initiation phase, where CO_2 dissolves into the pore solution, reacts with calcium hydroxide and progressively lowers the pH at the steel surface; b) propagation phase, once the pH of the electrolyte at the steel surface is lower than the pH threshold (pH < 8–9), the passive layer at the steel surface starts to dissolve and corrosion initiates.

3.2.1.1. Carbonation of SFRC. The initiation phase is governed by the progress of the carbonation front, which defines the region of the concrete with pH < 8–9, where corrosion of steel is expected to initiate, described in Fig. 16 as the process A–B [106]. The rate of carbonation is highly dependent on several variables: e.g. the concentration of CO_2 at the surface, moisture content, concrete composition (e.g. w/c ratio and binder composition) and temperature. Carbonation rates for uncracked SFRC have been found similar to plain concrete (e.g. k = 0.4–1.4 mm/√y), suggesting that the fibre-matrix interface does not provide a weaker path for CO_2 to diffuse into the concrete [67,79,102,125].

The presence of cracks increases the depth of the penetration front locally (Fig. 12); the crack faces act as new surfaces carbonating at a lower rate, e.g. calculated carbonation coefficients inside cracks and perpendicular to the crack faces are 70–80% lower than the ones for external surfaces, and decrease along the crack depth [12,57].

3.2.1.2. Carbonation-induced corrosion of steel fibres. The propagation phase described in Tutti's model, corresponds to the initiation of corrosion, governed by the dissolution of the passive layer of the steel at decreasing pH (Fig. 16B–C–D). When the pH of the electrolyte surrounding the steel interface decreases below the threshold for reinforcing steel (typically assumed in the range of pH = 8–9 for carbon-steel), the dissolution of the passive layer of iron oxyhydroxide at localized anodic sites (Fig. 16C) promotes the initiation of corrosion, which would propagate through the dissolution of iron as Fe^+ ions, as presented in the active corrosion area of the Eh-pH diagram (Fig. 16D) [106], reaching corrosion rates in the order of 5–50 μm/year for conventional reinforcement in uncracked concrete

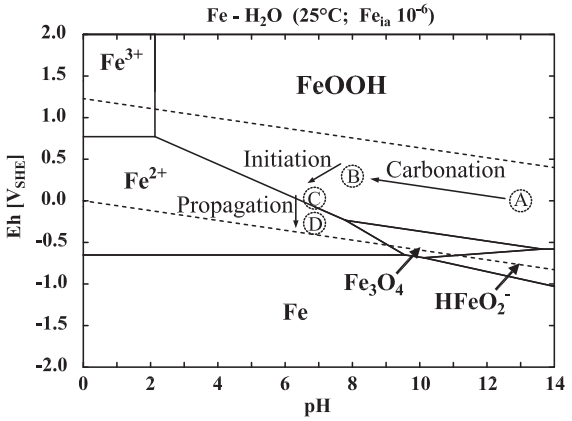

Fig. 16. Potential-pH diagram for conventional steel in carbonated concrete, pH-potential for: A) steel embedded in un-carbonated concrete (mixed potential); B) steel embedded in carbonated concrete (mixed potential); C) corrosion initiation of steel embedded in carbonated concrete, anodic region; D) corrosion propagation of steel embedded in carbonated concrete, anodic region. After Küter et al. [106].

[95,127].

There is limited research on the corrosion rate of steel fibres embedded in carbonated concrete. Nevertheless, the absence of steel fibre corrosion with cold-drawn carbon-steel wire embedded in uncracked carbonated SFRC, suggests an improved resistance to carbonation-induced corrosion. Published research presents limited corrosion in the outer 1–5 mm of the concrete regardless of the penetration depth of the carbonation rim (10–20 mm) [12,37,79,80]. The case of cracked SFRC is more complex; corrosion has been observed for most of the fibres bridging the crack, as the carbonation front propagates along the whole crack region. Severe corrosion is observed particularly at the outer crack rim, as shown in Fig. 12, whereas deeper fibres show milder signs of corrosion, i.e. rusting, [47,56].

The mechanisms governing carbonation-induced corrosion of steel fibres in cracked SFRC have not been clarified yet, but it is expected that some of the mechanisms responsible for the increased resistance to chloride-induced pitting corrosion might apply as well for carbonation-induced corrosion: a) smaller dimension of fibres limiting the cathodic area and leading to slower corrosion rates; b) denser and more uniform steel-matrix interface of SFRC, which effectively protects fibres against oxygen ingress and limits ionic transport at the steel surface.

There is limited data available investigating the chemical stability of coated steel fibres in carbonated SFRC. There is overall agreement regarding the full protection of galvanized steel fibres in uncracked carbonated SFRC, as presented in macroscopic investigations [12,56,79]. However there is disagreement on the stability of galvanized fibres inside cracks [12,56,61], since there is insight of fibre corrosion for long-term exposures [12,61]. Electrochemical testing of galvanized fibres embedded in un-carbonated concrete show limited corrosion rates at the coating, leading to passivation of the zinc coating at the fibre [70]. It is reported that carbonation of the uncracked concrete (i.e. pH ≈ 9.5) promotes the formation of additional passive zinc-oxide phases, unless the concentration of carbonates (i.e. HCO_3^-, CO_3^{2-}) and alkali in the pore solution drops significantly, which leads to the dissolution of the zinc coating [128,129], such as in the case of leaching inside large cracks and at surfaces exposed to rain or running water [129,130].

Macroscopic investigations report higher corrosion rates on brass-coated carbon-steel fibres in cracked and uncracked SFRC under long-term exposures, relative to carbon-steel wire, attributed to galvanic coupling between the copper-steel phases at local damage in the coating [79]. These observations agree with the deterioration model proposed in [112], presented as a combination of: i) iron-zinc galvanic coupling, which decelerates the initiation of corrosion at the exposed steel through the consumption of the zinc phases, i.e. dezincification; ii) iron-copper galvanic coupling, which increases corrosion rates at the steel once the zinc is locally depleted.

Stainless steel fibres have been reported effective on preventing corrosion in cracked and uncracked SFRC subjected to carbonation in the long-tem [49]. Published research indicates negligible corrosion rates for stainless steel wire tested in pore solution simulating carbonated concrete (i.e. pH = 9.5), showing an electrochemical behaviour similar to un-carbonated pore solution (i.e. pH = 12.5). However, there is insight of a large impact of a decreasing pH in the pore solution on the pitting corrosion resistance of stainless-steel wire embedded in carbonated concrete exposed to chlorides [113].

3.2.1.3. Mechanisms governing carbonation-induced corrosion of uncracked SFRC. The limited corrosion observed on steel fibres embedded in carbonated uncracked SFRC, relative to conventional reinforcement might be attributed to two of the main components influencing the improved resistance against chloride-induced pitting corrosion [61,94,108]: a) the discontinuous nature of the fibres; b) the dense and uniform fibre-matrix interfacial transition zone (ITZ). So far, there is, to the authors' knowledge, no research describing the relevance of these mechanisms or proposing a theory explaining the improved behaviour of SFRC against carbonation-induced corrosion relative to conventional reinforcement.

The positive influence of the discontinuous nature of the fibres on the improved corrosion resistance of uncracked carbonated SFRC, relative to conventional reinforcement, might be associated (as for chloride-induced pitting corrosion) to smaller potential difference along the steel surface and smaller cathode/anode ratios [61,108]. Criticism about the impact of the fibre size-effect for chloride-induced corrosion may apply as well for the carbonation scenario, where the length-effect for wire lengths in the range of 0–160 mm is negligible and the corrosion reaction might be anodically controlled [94].

The insight of the authors on this issue is that: even though the initiation of corrosion (i.e. depassivation) of the embedded steel may be anodically controlled, the small length (e.g. 30–70 mm) and discrete nature of the fibres relative to conventional reinforcement would limit the development of large potential gradients along each single fibre, reducing corrosion rates in the event of propagation of corrosion macrocells, such as in the case of heterogeneous exposure conditions or localized defects at the steel interface. Similar behaviour (i.e. repassivation of the steel after initiation of corrosion) has been reported in cracked SFRC subjected to carbonation in wet-dry cycles [56]. In the event of fibre corrosion, the accumulation of expansive corrosion products would block the surrounding pore structure, limiting further diffusion of oxygen and ions through the steel-concrete interface, thus limiting further propagation of corrosion, as the expansive stresses originated from corroding steel fibres are not expected to induce cracking of the surrounding matrix [61,131]. It is expected as well that the densification of the cement microstructure surrounding the fibres due to carbonation will limit ionic and oxygen transport at the interface [132,133], reducing corrosion rates in uncracked SFRC.

The role of a denser and more uniform fibre-matrix ITZ is expected to be of major importance for the corrosion protection of carbon-steel fibres in uncracked carbonated SFRC, as already theorized for chloride-induced corrosion [61,108]. The presence of a larger and more uniform calcium hydroxide (CH) layer around the fibre (Fig. 17b), as proposed

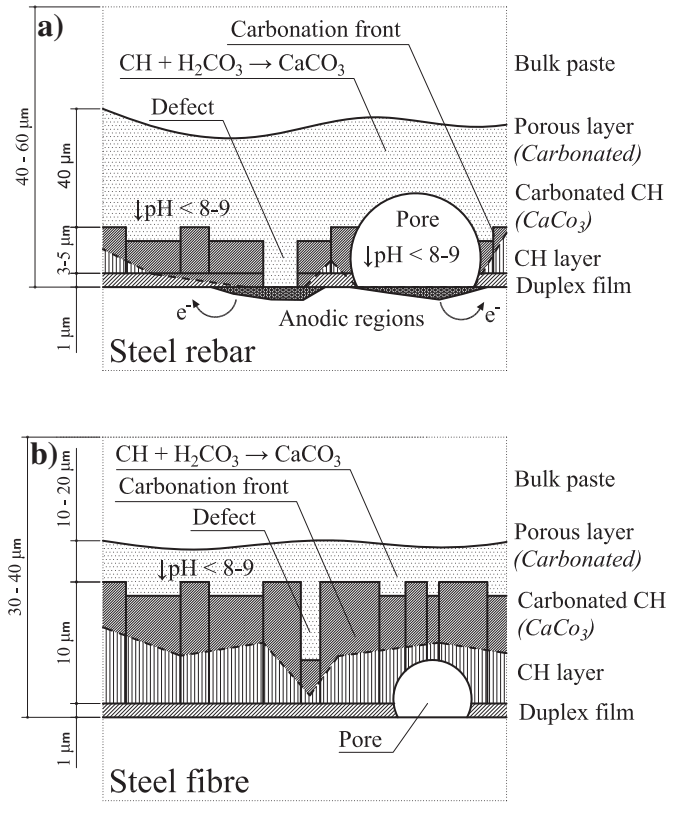

Fig. 17. Microstructure and mechanisms of carbonation-induced corrosion in uncracked concrete, for: a) conventional reinforcement; b) steel fibre reinforced concrete.

by [108,114], would have a beneficial effect in two aspects: i) the denser ITZ would increase the protection of fibres in the bulk SFRC against oxygen ingress and would prevent ionic transport; ii) the thicker CH layer (i.e. 10 μm), estimated two- to three-fold as for conventional steel (Fig. 17a–b), would provide a larger calcium-buffer for the absorption of H_2CO_3 and its densification due to the formation of calcium carbonate would potentially prevent further carbonation at deeper layers (i.e. the duplex film), see Fig. 17b.

Furthermore, the limited amount of pores and defects at the fibre-matrix ITZ, as fibres "float" inside the fresh-concrete matrix similarly to aggregates, would hinder the formation of weak spots where localized corrosion might initiate (Fig. 17b) [108]. It has been shown that these weaker spots represent the preferential points for initiation of reinforcement corrosion on conventional reinforcement in carbonated concrete [106].

3.2.1.3.1. Mechanisms governing carbonation-induced corrosion of cracked SFRC. There is limited research available investigating the mechanisms responsible for carbonation-induced corrosion of carbon-steel fibres in cracked SFRC. The published investigations evaluate the performance of the exposed SFRC at the macroscale level, and conclusions are based on a critical crack width (e.g. w_k < 0.10–0.20 mm); where limited access of oxygen due to the natural tortuosity of the crack and sealing of the crack by autogenous-healing, calcium leaching and corrosion products prevents the evolution of corrosion at the fibre regions bridging the crack [56,61]. These observations provide a limited explanation for the increase of the peak residual strength and the decrease of the residual tensile strength for larger deformations, viz. "stiffening" effect, observed for cracked SFRC exposed to rainwater or wet-dry cycles [13,61,75,99,134].

Studies report a change in the failure mode of cracked SFRC (w_k > 0.20–0.30 mm), shifting from fibre pull-out to fibre yield, in particular at larger strains: e.g. 3 mm central span deflection (CMOD ≈ 2.6 mm) on ASTM C1609 beams exposed to coastal weather (i.e. XC4, XS1) [75], or 10 mm cumulative central deflection on ASTM C1550 round panels exposed to high relative humidity environments (i.e. XC3) [99].

However, there is an open discussion on the issue, as several practitioners attribute such changes to an inadequate selection of the fibre type and dosage [135,136], arguing that the change in failure mode obeys to the densification of the fibre-matrix interface, not accounted for at early-age testing, but on the other hand possible to be estimated via accelerated ageing and testing. Similar issues have been already discussed for other types of fibres, e.g. alkali-resistant glass fibres and cellulose fibres, concluding that the main mechanisms responsible for long-term embrittlement were related to the abovementioned densification of the fibre-matrix interface during time [124].

The authors suggest a model governed by the damage at the fibre-matrix ITZ, complementary to the deterioration model proposed for steel fibres in chloride-contaminated concrete, presented in the previous section. The protective role of the fibre-matrix ITZ prevents the initiation of corrosion of steel fibres in uncracked SFRC and hinders further hydration at the fibre-matrix interface; as the matrix cracks, the strain in the fibres bridging the crack damages the fibre-matrix ITZ, promoting corrosion at the exposed region of the fibre as the pH decreases. Autogenous-healing at the fibre-matrix interface improves the fibre-matrix bond and eventually hinders fibre corrosion. Four stages may be identified:

1) The dense and uniform steel-matrix ITZ surrounding the steel fibre acts as a protective 'coating' (Fig. 18a): limiting the access of oxygen and isolating the steel surface from the electrolyte (i.e. limiting ionic diffusion along the steel surface). The thicker and more uniform CH layer compared to conventional steel acts as a "calcium buffer" delaying the progress of carbonation at the steel-concrete interface.
2) When the tensile capacity of the concrete is exceeded, the matrix cracks and the strain at the fibre-matrix interface damages the ITZ (Fig. 18b). The damaged ITZ facilitates O_2 and ionic transport along the steel surface; the bridging region of the fibre acts as anode, while the embedded area will act as the cathode due to the pH gradient formed at the crack face (i.e. corrosion macro-cell), as presented for conventional reinforcement in [120]. Furthermore, the cracked interface provides a preferential path for the dissolution of calcium, towards the crack face, where the pH is lower due to access of surrounding water (e.g. rain, running water). The dissolved calcium depositing at the broken interface together with the hydration of unhydrated cement facilitates the autogenous healing of the damaged fibre-matrix interface [122]. Finally, the pH at the inner faces of the crack will decrease as a combination of leaching and carbonation (i.e. ingress of CO_2, dissolved as H_2CO_3 at the crack); carbonation of calcium at the fibre-matrix interface would further increase the

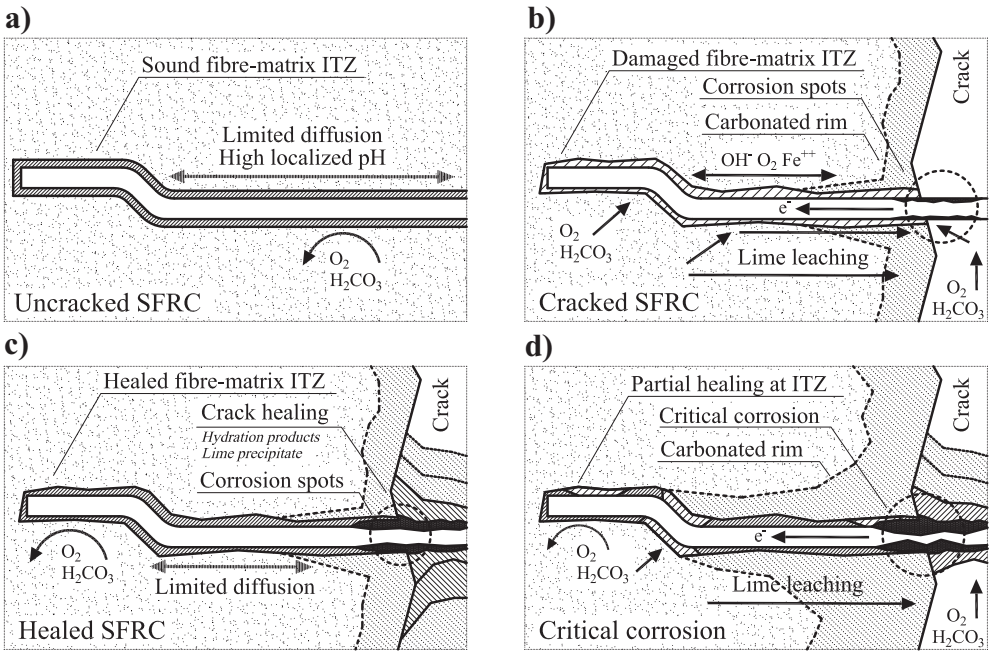

Fig. 18. Structure and corrosion mechanisms of carbonated SFRC, for: a) uncracked SFRC; b) cracked SFRC at an early stage; c) cracked SFRC after autogenous healing; d) cracked SFRC with critical corrosion of fibres.

density of the depositing healing products.

3) If the fibre does not reach a critical strain (i.e. critical crack width), the damaged fibre-matrix interface may heal completely [122], recovering to similar conditions as the uncracked state (Fig. 18a). The fibre-matrix ITZ, rich in CH would limit the decrease of the pH at the steel surface, re-passivating the steel at anodic regions (Fig. 18c). Carbonation of the healing products (e.g. calcium and C—S—H) at the interface would densify the surroundings of the fibre, improving the fibre-matrix mechanical bond; explaining the improved peak residual tensile strength reported in the literature [12,58,75]. Finally, the crack would progressively seal with un-hydrated cement, leaching, and corrosion products, limiting the diffusion of oxygen and CO_2; the surface of the fibres bridging the crack would serve as preferential surfaces for deposition of these compounds [122,137].
4) At larger strains, i.e. above critical crack width, excessive damage at the fibre-matrix interface would result in defective healing of the ITZ at the regions with greater damage (e.g. hooked ends, fibre-crack intersection), as shown in Fig. 18d. This defective healing may facilitate the evolution of fibre corrosion at anodic sites, as previously described in Fig. 18b, which would result in a progressive reduction of the fibre cross-section. Furthermore, progress of carbonation at the fibre-matrix interface and the surrounding matrix will increase the fibre matrix bond and mechanical anchorage of deformed fibres (e.g. hooked-end or crimped fibres). Once a critical cross-section reduction is reached (i.e. the tensile capacity of the steel is lower than the fibre-matrix bond strength) the failure mode of the SFRC would change from fibre pull-out to fibre yield and the residual tensile strength for larger strains would decrease, as reported in previous research [61,75,99]. In the case of a large increase of the fibre-matrix bond and mechanical anchorage due to autogenous healing and carbonation, the failure mode would change to fibre yield even for negligible corrosion of fibres, as the original design assumptions (e.g. post-crack behaviour at 28 days maturity) would be no longer applicable [75,99].

4. Summary and discussion

A summary of the analysis of the existing literature on durability of SFRC exposed to chlorides and carbonation is presented in Table 4. The table classifies the results according to: mild carbonation exposure (EN 206 classes: XC2-3), aggressive carbonation exposure (XC4), mild chloride exposure (XS2, XD2) and aggressive chloride exposure (XS3, XD3). Furthermore, the case of mixed-in chlorides (e.g. 3.5 wt% NaCl) is included, despite the fact that it is generally disapproved and not covered by standards.

For carbonation exposure, there is significant disagreement between the limitations stated in international standards and guidelines and the results extracted from published research, the latter being more restrictive with respect to limit states, such as the critical crack width for wet-dry cycles (XC4). The restrictions of the maximum crack width presented in the standards ($w_k \leq 0.20$–0.40 mm), seem somehow permissive when compared to the substantial corrosion damage ratios reported in the literature and the large scatter observed for residual tensile strength ratios (Fig. 15a–b). Conversely, for the least aggressive exposure classes (XC2-3), the limitations regarding the maximum crack width ($w_k \leq 0.30$–0.50 mm) might be too strict, if compared to the limited corrosion damage expected.

For chloride exposure, the results from the scientific literature partially agree with the limitations observed in the standards and guidelines. The limitations of the maximum crack width (w_k), in the range of 0.10–0.30 mm, proposed by some of the international standards and guidelines [15,17,26], are in agreement with the increased damage observed for narrow cracks ($0.50 > w_k > 0.20$ mm) compared to hairline cracks ($w_k \leq 0.20$ mm). Nevertheless, there is still disagreement at the technical and scientific level regarding the extent of fibre corrosion and reduction of residual tensile-strength of SFRC. Nonetheless, the significantly lower degree of deterioration observed for immersed exposures (XS2, XD2) is not covered by most of the standards and guidelines, which tend to overestimate the deterioration and apply similar limitations to aggressive exposures (XS3, XD3).

The analysis of macro-scale investigations suggests significant differences of the durability of uncracked and cracked SFRC exposed to chlorides and carbonation, distinguishing two main scenarios: corrosion of cracked and uncracked SFRC.

There is an overall good understanding of the improved corrosion of carbon-steel fibres in uncracked SFRC, relative to conventional reinforcement. There is overall agreement among researchers regarding the durability of uncracked SFRC to chloride and carbonation exposure, despite the fact that the damage mechanisms are not fully understood, particularly for the case of carbonation-induced corrosion. Investigations of the topic indicate transport properties for uncracked SFRC similar to plain concrete, fibre corrosion is expected to occur at

Table 4
Summary table, design parameters and mechanical behaviour of SFRC exposed to chlorides and carbonation.

	Carbonation		Chlorides		
	Mild XC2-3	Aggressive XC4	Mild XS1-2/XD1-2	Aggressive XS3/XD3	Mixed-in chlorides
Maximum water/binder ratio	< 0.50–0.60	< 0.40–0.50	< 0.50	< 0.40–0.50	–
Mineral additions	PC, SF	PC, SF	PFA, GGBS	PFA, GGBS	
Type of steel	Carbon-steel Galvanized	Carbon-steel Galvanized Stainless	Carbon-steel	Carbon-steel Stainless	
Critical crack width (mm)	0.30–0.50	0–0.30	0.20–0.30	0–0.20	
Sacrificial layer (mm)	< 1	1–5	1–5	1–15	
Cracking/spalling	No	No	No	No	Yes
Compressive strength loss	None	None	None	Low–none[a]	Medium
Tensile strength loss	None	Low–none[a]	None	Low–none[a]	High
Residual tensile strength loss					
Uncracked	Low–none[b]	Low–none[b]	Low–none[b]	Low–none[b]	High
Wide cracks ($w_k > 0.50$ mm)	Low	High	Medium	High	
Narrow cracks ($w_k < 0.50$ mm)	Low	Medium	Medium	Medium–high	
Hairline cracks ($w_k < 0.20$ mm)	Low–none	Medium–none	Low–none	Medium–none	

Abbreviations: (PC) Portland cement; (SF) silica fume; (PFA) pulverized fly ash; (GGBS) ground granulated blast-furnace slag; (w_k) characteristic crack width.

[a] Detriment on elastic properties of SFRC related to chemical degradation of the matrix. Corrosion of steel fibres do not alter the structural integrity of the matrix.

[b] Embrittlement due to continuous hydration and carbonation shall be prevented by considering a larger matrix compressive strength, e.g. avoid fibre-yield failure by selecting medium- or high-strength steel fibres at appropriate doses.

the outer 1–5 mm, without inducing cracking or spalling of the matrix due to the expansion of corrosion products.

Conversely, there are significant disparities between the experimental results from published research investigating the durability of cracked SFRC exposed to corrosive environments. There is no consensus regarding the design parameters that can guarantee the durability of cracked SFRC under chloride and carbonation exposure, namely: the maximum water to cement ratio, the critical crack width and the minimum sacrificial layer. A comparison of experimental results from former investigations, show a large scatter of the results (deviation of 20–50% for the damage ratios) for similar design parameters, hindering the elaboration of solid conclusions.

The mechanisms governing the deterioration of the mechanical properties of SFRC exposed to chlorides and carbonation are not fully understood. Despite the fact that there is recent research investigating the mechanisms responsible of chloride-induced corrosion of carbon-steel fibres in uncracked SFRC, there is limited information on the mechanisms influencing corrosion inside cracks, the latter being the main issue concerning durability of SFRC. The authors propose a deterioration theory for cracked SFRC based on the damage at the fibre-matrix interface during fibre pull-out. However, there is limited information covering the damage of the fibre-matrix ITZ during pull-out and the development of autogenous healing of corroding SFRC is still unclear.

5. Conclusions

This paper reviews the existing literature investigating chloride- and carbonation-induced corrosion of SFRC. The paper reviews the main factors influencing the durability of SFRC exposed to corrosive environments and analyses systematically the published experimental data on the deterioration of SFRC subject to chloride and carbonation exposure.

There is overall agreement among academics and regulators regarding the durability of uncracked SFRC exposed to chlorides (exposure classes: XC2-4) and carbonation (exposure classes: XS2-3, XD2-3). The superior durability against corrosion of carbon-steel fibres embedded in uncracked SFRC relative to conventional steel, obeys to three main components: the discrete nature of the fibres, the more homogeneous steel surface due to production processes of cold-drawn wire steel fibres (cold-drawing) versus a rougher surface for conventional reinforcing bars (hot-rolling mill), and the denser and more homogeneous fibre-matrix interface compared to conventional steel reinforcement.

The durability of cracked SFRC exposed to chlorides and carbonation is under discussion at the technical and scientific level. There is substantial insight among academics regarding the existence of a critical crack width, below 0.20 mm, where fibre corrosion is limited and the structural integrity of SFRC can be ensured for long-term exposures. However, the mechanisms governing corrosion of carbon-steel fibres in cracked SFRC subject to chloride and carbonation exposure are still unclear. In particular, the influence of fibre corrosion on the residual strength of SFRC is in focus and under discussion.

This paper proposes an alternative deterioration theory for corrosion of steel fibres bridging cracks in SFRC exposed to chlorides and carbonation, focusing on the damage and healing at the fibre-matrix interface. Further research in this field is required, in particular focusing on the damage and healing mechanisms at the fibre-matrix interface during partial fibre pull-out.

Acknowledgements

The first author would like to express his gratitude to: CowiFonden, InnovationsFonden, the German association of steel fibre producers (VDS), VejDirektoratet and Mapei-Denmark, for supporting this project.

References

[1] V.C. Li, Large volume, high performance applications of fibers in civil engineering, J. Appl. Polym. Sci. 83 (2002) 660–686, http://dx.doi.org/10.1002/app.
[2] M. di Prisco, G.A. Plizzari, Precast SFRC elements: from material properties to structural applications, in: M. di Prisco, R. Felicetti, G.A. Plizzari (Eds.), 6th RILEM Symp. Fibre-Reinforced Concr. - BEFIB 2004, RILEM Publications SARL, Varenna, Italy, 2004, pp. 81–100.
[3] P. Serna, S. Arango, T. Ribeiro, A.M. Núñez, E. Garcia-Taengua, Structural cast-in-place SFRC: technology, control criteria and recent applications in spain, Mater. Struct. 42 (2009) 1233–1246, http://dx.doi.org/10.1617/s11527-009-9540-9.
[4] S. Wallis, Steel fibre developments in South Africa, Tunnels Tunn. Int. 27 (1995) 22–24.
[5] R.G.A. De-Waal, Steel Fibre Reinforced Tunnel Segments for the Application in Shield Driven Tunnel Linings, Delft University of Technology, 1999.
[6] S. Abbas, Structural and Durability Performance of Precast Segmental Tunnel Linings, University of Western Ontario, 2014.
[7] G.A. Plizzari, G. Tiberti, Steel fibers as reinforcement for precast tunnel segments, Tunn. Undergr. Sp. Technol. 21 (2006) 438–439, http://dx.doi.org/10.1016/j.tust.2005.12.079.
[8] B. Schnütgen, Design of precast steel fibre reinforced tunnel elements, in: B. Schnütgen, L. Vandewalle (Eds.), Int. RILEM Work. Test Des. Methods Steelfibre Reinf. Concr, RILEM Publications SARL, Bochum, Germany, 2003, pp. 145–152.
[9] B. De Rivaz, Durability issue for SFRC precast segment in tunnelling application, in: S.W. Meng, C.K. Siong (Eds.), WUTC2010, World Urban Transit Conference, Sentosa, Singapore, 2010, pp. 1–10, , http://dx.doi.org/10.3850/978-981-08-6396-8_P223.
[10] G.T. Halvorsen, C.E. Kesler, A.R. Robinson, J.A. Stout, Durability and Physical Properties of Steel Fiber Reinforced Concrete, Illinois, US, (1976).
[11] R. Winterberg, Performance and durability improvements of precast concrete lining segments with fibre reinforcement, in: Australasian Institute of Mining and Metallurgy (Ed.), 14th Australas. Tunn. Conf. 2011 Dev. Undergr. Space, Proc, Australasian Institute of Mining and Metallurgy, Auckland, New Zealand, 2011, pp. 645–656.
[12] R. Weydert, P. Schiessl, Korrosion von Stahlfasern in gerissenem und ungerissenem Stahlfaserbeton, Abschlussbericht, Bergisch Gladbach (Germany), 1998.
[13] E.S. Bernard, Durability of cracked fibre reinforced shotcrete, in: E.S. Bernard (Ed.), Shotcrete More Eng. Dev. Proc. Second Int. Conf. Eng. Dev. Shotcrete, A.A. Balkema Publishers, Sydney, Australia, 2004, pp. 59–66.
[14] CEN, EN 206 - Concrete, Specification, Performance, Production and Conformity, European Union, 2013.
[15] ACI Committee 544, State-of-the-art Report on Fiber Reinforced Concrete, United States, (2002).
[16] RILEM, Test and Design Methods for Steel Fibre Reinforced Concrete, France, (2000).
[17] German Society for Concrete and Construction Technology, Guide to Good Practice: Steel Fibre Concrete, Germany, (2001).
[18] UNI, UNI/CIS/SC4–SFRC, Elementi Strutturali in Calcestruzzo Rinforzato Con Fibre D'Acciaio, Italy, (2004).
[19] CRN, Guide for the Design and Construction of Fiber-Reinforced Concrete Structures, Italy, (2006).
[20] New Zealand Standards, NZS 3101:2006 - Concrete Structures Standard, New Zealand, (2006).
[21] The Concrete Society, TR-63, Guidance for the Design of Steel-Fibre-Reinforced Concrete, United Kingdom, (2007).
[22] Spanish Development Ministry, EHE-08 instrucción de hormigón estructural, Ministerio de Fonmento, Spain, (2009).
[23] DAfStb, DAfStb Stahlfaserbeton, Deutscher Ausschuss für Stahlbeton e. V. - DAfStb, Germany, (2012).
[24] T. Kasper, B.T. Jensen, H. Stang, P. Mjoernell, H. Slot, G. Vitt, L.N. Thrane, L. Reimer, Design Guideline for Structural Applications of Steel Fibre Reinforced Concrete, SFRC Consortium, Copenhagen, Denmark, Denmark, 2013.
[25] P. Guedon, AFTES-GT38R1A1. Design, Dimensioning and Execution of Precast Steel Fibre Reinforced Concrete Arch Segments, France, (2013).
[26] Swedish Standards Institute, SS 812310:2014. Fibre Concrete – Design of Fibre Concrete Structures, Sweden, (2014).
[27] Norsk Beton, Sprayed Concrete for Rock Support, Norway, (2011).
[28] JSCE, Recommendation for Design and Construction of Steel Fiber Reinforced Concrete, Tokio, Japan, Japan, (1984).
[29] Standards Australia, AS 3600-2009 Supp 1:2014 Concrete Structures, Australia, (2014).
[30] ITAtech, ITAtech Report n°7 - Design Guidance for Precast Fibre Reinforced Concrete Segments, ITA, Avignon, France, 2015.
[31] CUR, Staalvezelbeton inventarisatie van regelgeving, CUR Bouw & Infra, Gouda, Netherlands, Netherlands, 2012.
[32] SIA - Schweizer Ingenieur und Architekt, Sia 162/6 - Stahlfaserbeton, Switzerland, (1999).
[33] D.J. Hannant, J. Edgington, Durability of steel fibre concrete, in: A. Neville (Ed.), Rilem Symp. 1975 Fibre Reinf. Cem. Concr, The Construction Press, Leeds, UK, 1975, pp. 159–169.
[34] G.B. Batson, Strength of Steel Fiber Concrete in Adverse Environments, Champaign, Illinois (US), 1977.
[35] D.C. Morse, G.R. Williamson, Corrosion Behavior of Steel Fibrous Concrete, Dept. of Defense Dept. of the Army Corps of Engineers Construction Engineering

Research Laboratory, Champaign Ill, 1977.
[36] R. Rider, R. Heidersbach, Degradation of metal-fiber reinforced concrete exposed to a marine environment, in: D.E. Tonini, J.M. Gaidis (Eds.), Corros. Reinf. Steel Concr, ASTM International, Philadelphia, US, 1978, pp. 75–92.
[37] M. Schupack, Steel fiber concrete, in: S.P. Shah, A. Skarendahl (Eds.), Steel Fiber Concr. US-Sweden Jt. Semin, Elsevier, Stockholm, Sweden, 1985, pp. 479–496.
[38] M.M. Kamal, F.E. El-Refai, Durability of steel fibre reinforced concrete, Proc. Fourth Int. Conf. Durab. Build. Mater. Components, Elsevier, Singapore, 1987, pp. 235–247, , http://dx.doi.org/10.1016/B978-1-4832-8386-9.50034-6.
[39] P.S. Mangat, K. Gurusamy, Chloride diffusion in steel fibre reinforced marine concrete, Cem. Concr. Res. 17 (1987) 385–396, http://dx.doi.org/10.1016/0008-8846(87)90002-0.
[40] P.S. Mangat, K. Gurusamy, Corrosion resistance of steel fibres in concrete under marine exposure, Cem. Concr. Res. 18 (1988) 44–54, http://dx.doi.org/10.1016/0008-8846(88)90120-2.
[41] P.S. Mangat, K. Gurusamy, Chloride diffusion in steel fibre reinforced concrete containing PFA, Cem. Concr. Res. 17 (1987) 640–650, http://dx.doi.org/10.1016/0008-8846(87)90137-2.
[42] P.S. Mangat, K. Gurusamy, Pore fluid composition under marine exposure of steel fibre reinforced concrete, Cem. Concr. Res. 17 (1987) 734–742, http://dx.doi.org/10.1016/0008-8846(87)90036-6.
[43] P.S. Mangat, Long-term properties of steel fibre reinforced marine concrete, Mater. Struct. Matériaux Constr. 20 (1987) 273–282.
[44] P.S. Mangat, K. Gurusamy, Permissible crack widths in steel fibre reinforced marine concrete, Mater. Struct. 20 (1987) 338–347, http://dx.doi.org/10.1007/BF02472580.
[45] K. Kosa, A.E. Naaman, W. Hansen, Durability of fiber reinforced mortar, ACI Mater. J. Mater. J. 88 (1991) 310–319.
[46] K. Kosa, A.E. Naaman, Corrosion of steel fiber reinforced concrete, ACI Mater. J. 87 (1990) 27–37.
[47] R. Weydert, P. Schiessl, Corrosion of steel fibres in cracked and uncracked steel fibre reinforced concrete, IBAC 61 (1996) 1310–1315.
[48] P. Schiessl, Y. Weydert, Korrosion von Stahlfasern in gerissenem und ungerissenem Stahlfaserbeton, Kurzberichte Aus Der Bauforsch. 39 (1998) 331–336.
[49] E. O'Neil, J.T. Devlin, Durability of Fiber-Reinforced Concrete Under Flexural Stress in a Severe Marine Environment, Defense Technical Information Center, Vicksburg, US, 1999.
[50] E.J. de P. Hansen, Holdbarhed af fiberarmeret beton, Eksperimentelle undersøgelser, Copenhagen, Denmark, 1999.
[51] E.J. de P. Hansen, T. Ekman, K.K. Hansen, Durability of cracked fibre reinforced concrete structures exposed to chlorides, in: M.A. Lacasse, D.J. Vanier (Eds.), Durab. Build. Mater. Components, NRC Research Press, Vancouver, Canada, 1999, pp. 280–289.
[52] S.U. Balouch, Corrosion of Steel Fibre Reinforced Concrete, (1999).
[53] J.-L. Granju, S.U. Balouch, Corrosion of steel fibre reinforced concrete from the cracks, Cem. Concr. Res. 35 (2005) 572–577, http://dx.doi.org/10.1016/j.cemconres.2004.06.032.
[54] S.U. Balouch, J.P. Forth, J.-L. Granju, Surface corrosion of steel fibre reinforced concrete, Cem. Concr. Res. 40 (2010) 410–414, http://dx.doi.org/10.1016/j.cemconres.2009.10.001.
[55] R. Dhanasekar, C. Hudson, Durability of high strength steel fibre reinforced concrete, in: M.A. Bradford, R.Q. Bridge, S.J. Foster (Eds.), 16th Australas. Conf. Mech. Struct. Mater, A.A. Balkema Publishers, Sidney, Australia, 1999, pp. 525–530.
[56] D. Nemegeer, J. Vanbrabant, H. Stang, Final Report on Durability of Steel Fibre Reinforced Concrete, Copenhagen, Denmark, (2000).
[57] D. Nemegeer, J. Vanbrabant, H. Stang, Brite euram program on steel fibre concrete. Subtask: durability: corrosion resistance of cracked fibre reinforced concrete, in: B. Schnütgen, L. Vandewalle (Eds.), Int. RILEM Work. Test Des. Methods Steelfibre Reinf. Concr, RILEM Publications SARL, Bochum, Germany, 2003, pp. 47–66, , http://dx.doi.org/10.1617/2351580168.004.
[58] A. Lambrechts, D. Nemegeer, J. Vanbrabant, H. Stang, Durability of Steel Fibre Reinforced Concrete, (2003).
[59] G. Mantegazza, A. Gatti, Aspects of durability of fiber reinforced concrete: workability and stress-corrosion, in: M. di Prisco, R. Felicetti, G.A. Plizzari (Eds.), 6th RILEM Symp. Fibre-Reinforced Cocnretes - BEFIB 2004, RILEM Publications SARL, Varenna, Italy, 2004, pp. 593–602.
[60] E. Nordström, Durability of Sprayed Concrete Steel Fibre Corrosion in Cracks, Lulea Technical University, 2000.
[61] E. Nordström, Durability of Sprayed Concrete Steel Fibre Corrosion in Cracks, Lulea University of Technology, 2005.
[62] A. Erdélyi, E. Csányi, K. Kopecskó, A. Borosnyói, O. Fenyvesi, Deterioration of steel fibre reinforced concrete by freeze-thaw and de-icing salts, Concr. Struct. 9 (2008) 33–44.
[63] P. Serna, S.E. Arango, Evolution of the flexural behaviour of precracked SFRC in marine environment, in: R. Gettu (Ed.), 7th RILEM Int. Symp. Fibre Reinf. Concr. Des. Appl. - BEFIB 2008, RILEM Publications SARL, Chennai, India, 2008, pp. 595–605.
[64] R. Roque, N. Kim, B. Kim, G. Lopp, Durability of Fiber-reinforced Concrete in Florida Environments, Florida, USA, 2009.
[65] A.G. Graeff, K. Pilakoutas, C. Lynsdale, K. Neocleous, Corrosion durability of recycled steel fibre reinforced concrete, Intersections/IntersectII 6 (2009) 77–89.
[66] A.G. Graeff, K. Pilakoutas, K. Neocleous, C. Lynsdale, Behaviour of concrete reinforced with recycled steel fibres exposed to chloride contaminated environment, in: A.K.C. vysoké učení technické v P.K. betonových a zděných Konstrukcí (Ed.), Fibre Concr. 2011, Czech Technical University, Praghe, Czech Republic, 2011, pp. 9–10.
[67] M. Sanchez, M.C. Alonso, Durability performance of plain and fiber reinforced self-compacting concrete, Concr. Plant Int. (2009) 62–66.
[68] J.L. García, M. Sánchez, Durabilidad de hormigones autocompactantes con prestaciones especiales expuestos en atmosferas marinas y urbanas, 2° Congr. Ibérico Sobre Hormigón Autocompactante, Minho University, Guimarães, ES, 2010, pp. 1–10.
[69] M. Sun, D.J. Wen, P. Xie, Bending toughness of zinc phosphate steel fiber reinforced concrete before and after corrosion, Adv. Mater. Res. 168–170 (2011) 1762–1766.
[70] M. Sun, D.-J. Wen, H.-W. Wang, Influence of corrosion on the interface between zinc phosphate steel fiber and cement, Mater. Corros. 63 (2012) 67–72, http://dx.doi.org/10.1002/maco.200905580.
[71] N. Buratti, C. Mazzotti, M. Savoia, Long-term behavior of cracked SFRC elements exposed to chloride solutions, ACI Spec. Publ. 280 (2011) 1–14.
[72] S. Abbas, A.M. Soliman, M.L. Nehdi, Chloride ion penetration in reinforced concrete and steel fiber-reinforced concrete precast tunnel lining segments, ACI Mater. J. 111 (2014) 613–622, http://dx.doi.org/10.14359/51686991.
[73] S. Anandan, S.V. Manoharan, T. Sengottian, Corrosion effects on the strength properties of steel fibre reinforced concrete containing slag and corrosion inhibitor, Int. J. Corros. 2014 (2014) 1–8.
[74] J.P. Kaufmann, Durability performance of fiber reinforced shotcrete in aggressive environment, in: A. Negro, W. Bilfinger, M.O. Cecilio (Eds.), WTC 2014 – Tunnels a Better Life, ITA-AITES, Iguaçu, Brazil, 2014, pp. 1–7.
[75] E.S. Bernard, Effect of exposure on post-crack performance of FRC for tunnel segments, in: I. Vrkljan, Z. Dekovic, M. Dobrilovic, J. Likar, P. Miscevic (Eds.), SEE TunnelPromoting Tunneling SEE Reg. - ITA WTC 2015, ITA-AITES, Dubrovnik, Croatia, 2015, p. 13.
[76] A. Bentur, N. Berke, S. Diamond, Steel Corrosion in Concrete: Fundamentals and Civil Engineering Practice, First, CRC Press, London, UK, 1997.
[77] O. Gjørv, Durability Design of Concrete Structures in Severe Environments, First, Taylor & Francis, London; New York, 2009.
[78] G.C. Hoff, Durability of fiber reinforced concrete in a severe marine environment, Spec. Publ. 100 (1987) 997–1042.
[79] L. Ferrara, R. Fratesi, S. Signorini, F. Sonzogni, M. Building, Durability of steel fibre-reinforced cocnrete precast elements: experiments and proposal of design recommendations, in: M. Di Prisco, R. Felicetti, G.A. Plizzari (Eds.), 6th RILEM Symp. Fibre-Reinforced Cocnretes - BEFIB 2004, RILEM Publications SARL, Varenna, Italy, 2004, pp. 565–574.
[80] E. Kern, H. Schorn, 23 Jahre alter Stahlfaserbeton, Beton-Und Stahlbetonbau 86 (1991) 205–208, http://dx.doi.org/10.1002/best.199100380.
[81] N. Ganesan, P.V. Indira, P.T.S. Kumar, Durability aspects of steel fibre-reinforced SCC, Indian Concr. J. 80 (2006) 31–37.
[82] N.T. Narayan, S. Ramakrishnan, Steel Fibre Reinforced Concrete for Ports Infrastructure, The Masterbuilder, 2013, pp. 144–147.
[83] C. Frazão, A. Camões, J. Barros, D. Gonçalves, Durability of steel fiber reinforced self-compacting concrete, Constr. Build. Mater. 80 (2015) 155–166, http://dx.doi.org/10.1016/j.conbuildmat.2015.01.061.
[84] E. Alizade, F.J. Alaee, S. Zabihi, Effect of steel fiber corrosion on mechanical properties of steel fiber reinforced concrete, Asian J. Civ. Eng. 17 (2016) 147–158.
[85] G. Chen, M.N.S. Hadi, D. Gao, L. Zhao, Experimental study on the properties of corroded steel fibres, Constr. Build. Mater. 79 (2015) 165–172, http://dx.doi.org/10.1016/j.conbuildmat.2014.12.082.
[86] B. Kim, A.J. Boyd, J.-Y. Lee, Durability performance of fiber-reinforced concrete in severe environments, J. Compos. Mater. 45 (2011) 2379–2389, http://dx.doi.org/10.1177/0021998311401089.
[87] Y. La-Palme, P. La-plante, P.C. Aitcin, Use of Fibre Reinforced Concrete for Highway Rehabilitation, Waterloo, Canada, (1985).
[88] N. Banthia, C. Foy, Marine curing of steel fiber composites, J. Mater. Civ. Eng. 1 (1989) 86–96, http://dx.doi.org/10.1061/(ASCE)0899-1561(1989)1:2(86).
[89] I. Janotka, Ľ. Krajčí, K. Komloš, D. Fŕalová, Chloride corrosion of steel fibre reinforcement in cement mortar, Int. J. Cem. Compos. Light. Concr. 11 (1989) 221–228, http://dx.doi.org/10.1016/0262-5075(89)90102-4.
[90] EN, Fibres for Concrete - Part 1: Steel Fibres - Definitions, Specifications and Conformity, EU, 2006.
[91] EN, Non-alloy Steel Wire rod for Conversion to Wire, EU, 2011.
[92] EN, Stainless Steels - Part 5: Techni; Rods; Sections and Bright Products of Corrosion Resistin; Wire, EU, 2009.
[93] C. Dauberschmidt, Corrosion Mechanism of Steel Fibres in Concrete, München, (2012).
[94] P.S. Mangat, B.T. Molloy, Size effect of reinforcement on corrosion initiation, in: P. Rossi, G. Chanvillard (Eds.), PRO 15 5th RILEM Symp. Fibre-reinforced Concr. - BEFIB' 2000, RILEM Publications SARL, Lyon, France, 2000, pp. 691–701.
[95] L. Bertolini, B. Elsener, P. Pedeferri, E. Redaelli, R.B. Polder, Corrosion of Steel in Concrete: Prevention, Diagnosis, Repair, Second, John Wiley & Sons, 2013.
[96] P. Hagelia, Does the EN 206-1 exposure classification apply to tunnel concrete? Nord. Expo. Sites - Input to Revis. EN 206-1, Hirtshals, Denmark, 2008, pp. 241–264.
[97] P. Mehta, Effect of cement composition on corrosion of reinforcing steel in concrete, in: D. Tonini, S. Dean (Eds.), Chloride Corros. Steel Concr, ASTM International, West Conshohocken, PA, 1977, pp. 12–19, , http://dx.doi.org/10.1520/STP629-EB.
[98] A.D. Medagoda-Arachchige, Influence of cement content on corrosion resistance, Proc. ICE - Constr. Mater. 161 (2008) 31–39, http://dx.doi.org/10.1680/coma.2008.161.1.31.
[99] E.S. Bernard, Age-dependent changes in post-crack performance of fibre reinforced

shotcrete linings, Tunn. Undergr. Sp. Technol. 49 (2015) 241–248, http://dx.doi.org/10.1016/j.tust.2015.05.006.
[100] K. Tuutti, Corrosion of Steel in Concrete, First, Swedish Cement and Concrete Research Institute, Stockholm, 1982.
[101] T. Teruzzi, E. Cadoni, G. Frigeri, S. Cangiano, G.A.a. Plizzari, T. Teruzzi, E. Cadoni, G. Frigeri, S. Cangiano, G.A.a. Plizzari, Durability aspects of steel fibre reinforced concrete, in: M. Di Prisco, R. Felicetti, G.A. Plizzari (Eds.), 6th Int. RILEM Symp. Fibre Reinf. Concr, RILEM Publications SARL, Varenna, Italy, 2004, pp. 625–634 (doi:2912143748).
[102] S. Cangiano, G. a Plizzari, E. Cadoni, G. Frigeri, T. Teruzzi, On durability of steel fibre reinforced concrete, in: R.K. Dhir, T.A. Harrison, M.D. Newlands (Eds.), Int. Conf. Cem. Comb. Durable Concr, Thomas Telford, Dundee, Scotland, 2005, pp. 477–486, , http://dx.doi.org/10.1680/ccfdc.34013.
[103] Experimental investigation on rebar corrosion in combination with fibres, in: C.G. Berrocal, I. Löfgren, K. Lundgren, Nordic Concrete Federation (Eds.), XXII Nord. Concr. Res. Symp, Nordic Concrete Federation, Reykjavik, Iceland, 2014, pp. 1–4.
[104] S. Abbas, A.M. Soliman, M.L. Nehdi, Experimental study on settlement and punching behavior of full-scale RC and SFRC precast tunnel lining segments, Eng. Struct. 72 (2014) 1–10, http://dx.doi.org/10.1016/j.engstruct.2014.04.024.
[105] V. Corinaldesi, G. Moriconi, Mechanical and thermal evaluation of ultra high performance fiber reinforced concretes for engineering applications, Constr. Build. Mater. 26 (2012) 289–294, http://dx.doi.org/10.1016/j.conbuildmat.2011.06.023.
[106] A. Küter, M.R. Geiker, P. Møller, Management of Reinforcement Corrosion, DTU, 2006.
[107] U. Angst, B. Elsener, C.K. Larsen, Ø. Vennesland, Critical chloride content in reinforced concrete — a review, Cem. Concr. Res. 39 (2009) 1122–1138, http://dx.doi.org/10.1016/j.cemconres.2009.08.006.
[108] C. Dauberschmidt, Untersuchungen zu den Korrosionsmechanismen von Stahlfasern in chloridhaltigem Beton, Munich University, 2006.
[109] F.J. Recio, M.C. Alonso, L. Gaillet, M. Sánchez, Hydrogen embrittlement risk of high strength galvanized steel in contact with alkaline media, Corros. Sci. 53 (2011) 2853–2860, http://dx.doi.org/10.1016/j.corsci.2011.05.023.
[110] S.R. Yeomans, 6 – Galvanized steel reinforcement, Corros. Steel Concr. Struct, 2016, pp. 111–129, , http://dx.doi.org/10.1016/B978-1-78242-381-2.00006-7.
[111] V. Vignal, V. Rault, H. Krawiec, A. Lukaszczyk, F. Dufour, Microstructure and corrosion behaviour of deformed pearlitic and brass-coated pearlitic steels in sodium chloride solution, Electrochim. Acta 203 (2016) 416–425, http://dx.doi.org/10.1016/j.electacta.2016.03.005.
[112] S. Chanel, N. Pébère, Investigation on the corrosion of brass-coated steel cords for tyres by electrochemical techniques, Corros. Sci. 43 (2001) 413–427, http://dx.doi.org/10.1016/S0010-938X(00)00093-7.
[113] R.D. Moser, P.M. Singh, L.F. Kahn, K.E. Kurtis, Chloride-induced corrosion resistance of high-strength stainless steels in simulated alkaline and carbonated concrete pore solutions, Corros. Sci. 57 (2012) 241–253, http://dx.doi.org/10.1016/j.corsci.2011.12.012.
[114] A. Bentur, S. Diamond, S. Mindess, The microstructure of the steel fibre-cement interface, J. Mater. Sci. 20 (1985) 3610–3620, http://dx.doi.org/10.1007/BF01113768.
[115] A.B. Poole, I. Sims, Concrete Petrography: A Handbook of Investigative Techniques, Second edition, CRC Press, 2015.
[116] A. Michel, A.O.S. Solgaard, B.J. Pease, M.R. Geiker, H. Stang, J.F. Olesen, Experimental investigation of the relation between damage at the concrete-steel interface and initiation of reinforcement corrosion in plain and fibre reinforced concrete, Corros. Sci. 77 (2013) 308–321, http://dx.doi.org/10.1016/j.corsci.2013.08.019.
[117] D.J. Pinchin, D. Tabor, Interfacial phenomena in steel fibre reinforced cement I: structure and strength of interfacial region, Cem. Concr. Res. 8 (1978) 15–24, http://dx.doi.org/10.1016/0008-8846(78)90054-6.
[118] J.P. Hwang, M.S. Jung, M. Kim, K.Y. Ann, Corrosion risk of steel fibre in concrete, Constr. Build. Mater. 101 (2015) 239–245, http://dx.doi.org/10.1016/j.conbuildmat.2015.10.072.
[119] J.C. Scheydt, Mechanismen der Korrosion bei ultrahochfestem Beton, Karlsruhe Institute of Technology, KIT, 2013.
[120] P. Schiessl, M. Raupach, Laboratory studies and calculations on the influence of crack width on chloride-induced corrosion of steel in concrete, ACI Mater. J. 94 (1997) 56–62.
[121] M. Raupach, Investigations on the influence of oxygen on corrosion of steel in concrete—part 2, Mater. Struct. 29 (1996) 226–232, http://dx.doi.org/10.1007/BF02485944.
[122] D. Homma, H. Mihashi, T. Nishiwaki, Self-healing capability of fibre reinforced cementitious composites, J. Adv. Concr. Technol. 7 (2009) 217–228, http://dx.doi.org/10.3151/jact.7.217.
[123] C. Frazão, J. Barros, A. Camões, A.C. Alves, L. Rocha, Corrosion effects on pullout behavior of hooked steel fibers in self-compacting concrete, Cem. Concr. Res. (2015), http://dx.doi.org/10.1016/j.cemconres.2015.09.005.
[124] A. Bentur, S. Mindess, Fibre Reinforced Cementitious Composites, Second edition, CRC Press, 2006 (Second).
[125] Y. Wang, D. Niu, Z. Dong, Experimental study on carbonation of steel fiber reinforced concrete, in: J. Olek, W. Weiss (Eds.), 4th Int. Conf. Durab. Concr. Struct, Purdue University Press, West Lafayette, USA, 2014, pp. 55–59.
[126] Y.Y. Miao, D.T. Niu, Y. Wang, Steel fiber reinforced concrete carbonation simulation research, Adv. Mater. Res. 243–249 (2011) 108–111.
[127] C. Andrade, C. Alonso, Life time of rebars in carbonated concrete, in: J. Costa, Mercer (Eds.), Prog. Underst. Prev. Corros, Institute of Materials, UK, Barcelona, Spain, 1993.
[128] S.B. Farina, G.S. Duffó, Corrosion of zinc in simulated carbonated concrete pore solutions, Electrochim. Acta 52 (2007) 5131–5139, http://dx.doi.org/10.1016/j.electacta.2007.01.014.
[129] G. Roventi, T. Bellezze, G. Giuliani, C. Conti, Corrosion resistance of galvanized steel reinforcements in carbonated concrete: effect of wet-dry cycles in tap water and in chloride solution on the passivating layer, Cem. Concr. Res. 65 (2014) 76–84, http://dx.doi.org/10.1016/j.cemconres.2014.07.014.
[130] E. Sistonen, A. Cwirzen, J. Puttonen, Corrosion mechanism of hot-dip galvanised reinforcement bar in cracked concrete, Corros. Sci. 50 (2008) 3416–3428, http://dx.doi.org/10.1016/j.corsci.2008.08.050.
[131] M. Raupach, C. Dauberschmidt, Untersuchungen zum kritischen korrosionsauslösenden Chloridgehalt von Stahlfasern in künstlicher Betonporenlösung, Mater. Corros. 53 (2002) 408–416, http://dx.doi.org/10.1002/1521-4176(200206)53:6<408::AID-MACO408>3.0.CO;2-G.
[132] Q. Shen, G. Pan, H. Zhan, Effect of interfacial transition zone on the carbonation of cement-based materials, J. Mater. Civ. Eng. 4017020 (2017), http://dx.doi.org/10.1061/(ASCE)MT.1943-5533.0001860.
[133] B. Šavija, M. Luković, Carbonation of cement paste: understanding, challenges, and opportunities, Constr. Build. Mater. 117 (2016) 285–301, http://dx.doi.org/10.1016/j.conbuildmat.2016.04.138.
[134] E.S. Bernard, Embrinlement of Fiber-Reinforced Shotcrete, Shotcrete, (2008), pp. 16–21.
[135] C. Allen, Review of FRC brittle failure considerations, TunnelTECH - TunnelTalk, Vol. 3 2015.
[136] P. Rossi, Critique of synthetic fiber FRS paper, TunnelTECH - TunnelTalk, Vol. 7 2014.
[137] H. Huang, G. Ye, C. Qian, E. Schlangen, Self-healing in cementitious materials: materials, methods and service conditions, Mater. Des. 92 (2016) 499–511, http://dx.doi.org/10.1016/j.matdes.2015.12.091.

2.2 Paper II. A review of the deterioration of SFRC exposed to acids

The following publication, referred as “paper II”, has been published in Construction and Building Materials.

Paper II Marcos-Meson, V., Fischer, G., Edvardsen, C., Skovhus, T.L., Michel, A., 2019. Durability of Steel Fibre Reinforced Concrete (SFRC) exposed to acid attack – A literature review. Constr. Build. Mater. 200, 490–501. doi:10.1016/j.conbuildmat.2018.12.051.

Construction and Building Materials 200 (2019) 490–501

Contents lists available at ScienceDirect

Construction and Building Materials

journal homepage: www.elsevier.com/locate/conbuildmat

Review

Durability of Steel Fibre Reinforced Concrete (SFRC) exposed to acid attack – A literature review

V. Marcos-Meson [a,b,c,*], G. Fischer [a], C. Edvardsen [b], T.L. Skovhus [c], A. Michel [a]

[a] Department of Civil Engineering, Technical University of Denmark, Copenhagen, Denmark
[b] COWI A/S, Copenhagen, Denmark
[c] VIA Building, Energy & Environment, VIA University College, Horsens, Denmark

ARTICLE INFO

Article history:
Received 8 September 2018
Received in revised form 29 November 2018
Accepted 11 December 2018

Keywords:
Steel Fibre Reinforced Concrete
SFRC
Acid
Durability
Corrosion
Cracks

ABSTRACT

Steel Fibre Reinforced Concrete (SFRC) is increasingly used in the construction of civil infrastructure. There is particular interest in the behaviour of SFRC under chemical and bio-chemical exposure, since it can be utilized, among others, for the construction of waste-water and agricultural infrastructure. However, the applicability of SFRC exposed to acidic environments is hindered by inconsistencies among international regulations. This paper reviews the published literature concerning the durability of SFRC exposed to acid attack. Research suggests that the exposure to acids of uncracked SFRC results in damage similar to what would occur in Plain Concrete (PC). There is insight into the non-critical corrosion of steel fibres embedded in the neutralized concrete layer, not entailing corrosion-induced cracking or spalling and steel fibres have been reported to limit secondary damage by bridging cracks and restraining the progress of the chemical-erosion front. However, there is limited data regarding the residual mechanical performance of cracked SFRC that has been exposed to acids. Published research suggests the existence of a critical crack width, below 0.3 mm, where the corrosion damage to the steel fibre is non-critical and there is a limited loss of fracture toughness. However, it has been observed that the exposure of cracked SFRC to acids leads to a larger deterioration of its residual mechanical performance compared to other exposures.

Contents

* Corresponding author.

https://doi.org/10.1016/j.conbuildmat.2018.12.051
0950-0618/

1. Introduction

Steel Fibre Reinforced Concrete (SFRC) is a composite material, combining a cementitious matrix with a discontinuous reinforcement, consisting of steel fibres randomly distributed in the matrix. SFRC is increasingly being adopted for the production of in-situ and prefabricated concrete structures as: i) auxiliary reinforcement for temporary load cases [1], ii) partial substitution of conventional reinforcement [2,3], and iii) total replacement of conventional reinforcement in elements in overall compression [4,5]. The use of steel fibres for structural applications, as partial or total replacement of conventional reinforcement bars has become a popular solution for the construction of concrete infrastructure, due to its overall good durability and mechanical performance in statically indeterminate structures, e.g. by promoting the formation of several smaller cracks of greater tortuosity instead of few larger cracks [2,6–9]. However, the total replacement of conventional steel reinforcement is still controversial, especially when the long-term durability of SFRC under severe exposure conditions is addressed [10–13].

At present, there is no international standard available for the design of SFRC structures, so the design of infrastructure primarily relies on: national standards [14–16], national guidelines [17–19] and international design codes [20]; yet an EN standard is currently in preparation. However, some of these standards and guidelines are not coherent with respect to the applicability within certain exposure classes: chloride attack (EN 206 exposure class XS2-3, XD2-3), carbonation attack (XC3-4), freeze-thaw attack (XF2-4), or chemical attack (XA1-3) [21,22]. The latter is gaining interest for designers of SFRC infrastructure, as there is an increasing trend towards using steel fibres for the construction of bored [11,23–25] and sprayed linings [26] for sewer tunnels.

There are limited national guidelines covering the design of SFRC under XA exposure class [14,16,17,27,28] and prescriptions rely on limited research to support recommendations in terms of, e.g. a sacrificial layer (Δ_h), a critical characteristic crack width ($w_{k,crit}$), or a fibre material. Technical guidelines fully covering all exposure classes, including XA class [27], are being replaced by more restrictive national guidelines, which do not cover the most aggressive exposure classes (i.e. XS2-3, XD2-3) and do not mention other exposures (i.e. XF, XA) [29]. Technical recommendations applicable to XA exposure specify a "non-cracking in service" limitation for SFRC where the characteristic tensile capacity of the element cannot be exceeded for the SLS structural verification for the XA3 exposure class, and a critical crack width of 0.2 mm for the exposure classes XA1-2, but does not consider any minimum sacrificial layer for the service life verification [17]. Other national guidelines propose special measures such as the use of galvanized and/or stainless steel fibres [16,28] or the application of special protection measures verified through experience or experimental proof [14].

This paper summarizes the literature concerning the performance of SFRC exposed to acid attack and discusses the deterioration mechanisms responsible for the degradation of the concrete matrix and for corrosion of the embedded steel.

2. Acid attack in SFRC infrastructure

The exposure of cement-based materials to low-pH solutions promotes the decomposition and dissolution of the main hardened cement paste phases and certain aggregates (i.e. calcium-based), leading to loss of alkalinity and basicity in the pore solution, increased porosity and a deterioration of the mechanical properties of the hardened concrete matrix [30–32]. This phenomenon is generally defined as "corrosion of cement or concrete" [31–34] or "decalcification" [35] in the literature. However, this process is termed "chemical-erosion of cement or concrete" in this paper, corresponding to the terminology used in geological science [36], in order to avoid confusion with corrosion of steel (i.e. a redox reaction).

The loss of alkalinity and basicity in the pore solution (i.e. neutralization front) leads to depassivation of the reinforcing steel, as the neutralization front reaches the steel surface. This process may lead to uniform corrosion, similar to carbonation-induced corrosion for uncracked concrete [37,38]; or to the formation of localized corrosion macro-cells in the presence of cracks reaching the reinforcement, as observed for carbonation-induced corrosion in cracked concrete [39,40]. However, there is limited data available about this phenomenon in SFRC exposed to acids [41,42].

There are many fields of application where this deterioration process is of key importance and limits the service life of structures built from mass and reinforced concrete:

i) Sewage and industrial wastewater tunnels and treatment plants: where the intrados of the conduit is exposed to chemical and microbiological acid attack (i.e. sulphuric acid attack) [11,23,43–46]. In particular, for densely reinforced sections, i.e. treatment plants, there is large risk of reinforcement corrosion [43,47].
ii) Cooling towers at power plants: pure water from condensation neutralizes the pH at the surface of the concrete, favouring the growth of sulphur oxidizing bacteria inducing sulphuric acid attack at the concrete surface [30,48].
iii) Agricultural silos and fermenters: where the decomposition of biological matter and silage effluents expose concrete structures to organic acid attack produced by bacteria and fungi (e.g. lactic or acetic acid) [34,38,49]. This exposure scenario is applicable to biogas fermenters and anaerobic digesters [50].
iv) Industrial floors, slabs and concrete overlays exposed to acidic rainwater: the damage is related to the dissolution of CO_2, SO_2 and NO_x in rainwater, which are then transformed to carbonic, sulphuric and nitric acid respectively; lowering the pH of the water to more acidic levels (e.g. pH $\approx$ 4–5) and promoting the dissolution and neutralization of the cement paste [51–53].

Steel fibres are increasingly used as a total or partial replacement of the conventional reinforcement for some of these applications, such as prefabricated bored tunnels for sewers [11,24,25,54] or industrial floors and heavy duty slabs exposed to acidic rainwater [55–60]. However, the lack of experience with SFRC subject to acid attack and limited normative regulating the use of SFRC under these conditions, hampers the development of such infrastructure built of SFRC and in most cases introduces severe restrictions to designers, such as the installation of High-Density Polyethylene (HDPE) membranes in tunnels [24], the provision of thick sacrificial layers [11] and crack limitations (e.g. elements in overall compression in service) [23–25,61].

3. Deterioration mechanisms

There is limited research focusing on the deterioration mechanisms responsible for acid attack in steel fibre reinforced concrete [41,62,63], as most of the investigations focus on the impact of the material performance (e.g. residual tensile strength). However, the limited research available for SFRC can be complemented with the more developed research on cement paste [30,49,64,65], plain concrete [30,32,66] and reinforced concrete [37,38], which provides a sufficient background to understand some of the deterioration phenomena related to acid attack.

The general deterioration mechanism responsible for acid attack on SFRC may follow the scheme presented in Fig 1: the exposure to acidic environments (i), leads to neutralization and dissolution of the cement paste (ii), which promotes the damage and spalling of concrete (iii) and, finally, leads to the depassivation of the embedded steel and propagation of corrosion (iv).

3.1. Type and source of acids

The type of acid attack in concrete can be differentiated according to the type and source of the acid neutralizing the cement paste (i.e. decreasing the pH at the pore solution and consuming the alkaline buffer). A summary of the main acids affecting concrete infrastructure classified according to their source, nature and strength is presented in Table 1. The table includes general information regarding the pH of the pure acid, reported aggressiveness of the attack in concrete and references of investigations on SFRC exposed to each acid.

A first classification can be done according to the source of the acid. Two main sources can be identified: biotic and abiotic sources.

3.1.1. Biotic sources

A larger share of the potentially attacked SFRC infrastructure would be affected by biologically produced acids, e.g. prefabricated tunnels for sewers [11,24,25] or some cases of sprayed tunnels [42]. The mechanisms responsible for the production of the acid depend on the exposure conditions and source:

i) Biogenic Sulphuric Acid (BSA) produced by sulphate-reducing and sulphur-oxidizing bacteria, leading to sulphuric acid (H_2SO_4) attack [43,44,50,73,74]. This source of sulphuric acid production takes place in partially-filled sewers, under two main bacterial processes: i) sulphates present in the raw sewage are reduced into sulphides by anaerobic bacteria (i.e. the *Desulfovibrio* species), this process takes place typically at the slime layer on the pipe-walls at near-zero oxygen levels; ii) the sulphur ions released by the anaerobic bacteria combine with dissolved hydrogen in the wastewater and form hydrogen sulphide gas (H_2S), which enters the atmosphere and dissolves in the moisture layer at the surface of the above-water structure; iii) aerobic sulphur-oxidizing bacteria (i.e. the *Thiobacillus* species) colonize the surface of carbonated concrete and oxidize the dissolved hydrogen sulphide (H_2S) into sulphuric acid (H_2SO_4). Acid attack on cooling towers has been reported, following a similar deterioration process as before: as the combination of pure water attack from condensation of water vapour at the surface of the concrete and the growth of sulphur oxidizing and nitrifying bacteria [30,48].
ii) Organic acids resulting from fermentation of organic matter [50] and livestock silage and manure [34,49,50], leading to acetic acid ($C_2H_4O_2$) and lactic acid ($C_3H_6O_3$) attack. The sources of these organic acids comprise complex processes not addressed in this paper. However, there is increasing research on the impact of these acids in the durability of concrete for the construction of biogas plants [50] and agricultural infrastructure [34].
iii) Manganese-Iron biofilms, composed of Mn- and Fe-oxidizing bacteria (*Leptothrix* and *Gallionella* species) [42,75]. This type of attack has been recently reported at the intrados of sprayed liners for subsea tunnels [75]. The mechanisms responsible for the acidification at these biofilms (i.e. pH ≈ 5–6) are not clearly understood, the decrease in pH has been linked to oxidation of iron and manganese from the corroding steel reinforcement (i.e. steel fibres) and infiltration of seawater from the ground, respectively.

3.1.2. Abiotic sources

In particular, this deterioration is related to human activity, as in the case of acidic rain and acidification of groundwater due to pollution:

i) Acidic rain, primarily composed of carbonic acid (H_2CO_3) sulphuric acid (H_2SO_4) and nitric acid (HNO_3), reaches pH values in the range 3.5–5.0, depending on levels of pollution and local climate conditions [51,76,77]. It has been reported as a major threat to civil infrastructure in industrial areas and highly polluted regions [52,77]. The formation of the three major acidic components is explained by: i) carbonic

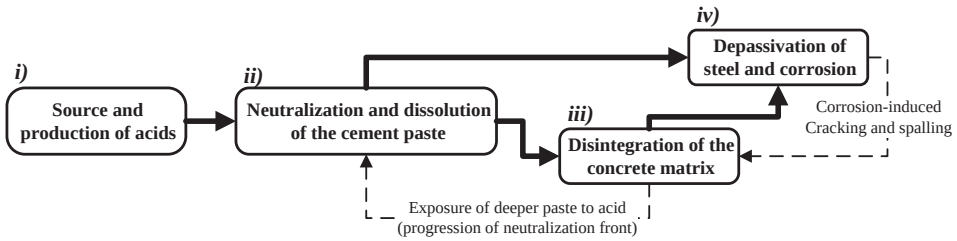

Fig. 1. Deterioration phenomena due to acid attack in (reinforced) concrete.

Table 1
Summary of sources of acids and classification.

Acid	Formula	pH*	Source	Nature	Strength**	Attack	Refs.
Sulphuric acid	H_2SO_4	1 – 3	abiotic/biotic	inorganic	strong (−3.0)	Very high	[34,37,38,50,67]
Hydrochloric acid	HCl	1 – 3	abiotic	inorganic	strong (−7.0)	High	[68]
Nitric acid	HNO_3	1 – 3	abiotic	inorganic	strong (−1.3)	High	[51,52,68–70]
Carbonic acid	H_2CO_3	4 – 5	abiotic	inorganic	weak (6.3)	Low	[51,52,69,70]
Acetic acid	$C_2H_4O_2$	3 – 4	biotic	organic	weak (4.8)	High	[34,41,49,50,71]
Lactic acid	$C_3H_6O_3$	2 – 4	biotic	organic	weak (3.9)	High	[34,49,50]
Citric acid	$C_6H_8O_7$	2 – 3	biotic	organic	weak (6.3)	Low	[72]

* pH values rounded to a single integer and given for a conce range: 100 mM–1 mM.
** Strength of acid dissolved in water, expressed as the negative-logarithmic acidity constant (pK_a).

acid (H_2CO_3) produced by the dissolution of carbon dioxide in rainwater; ii) sulphuric acid (H_2SO_4) formed from the dissolution, oxidation and hydrolysis of sulphur dioxide in rainwater; ii) nitric acid (HNO_3) formed by hydrolysis of nitrogen oxides (NO_x) in rainwater and water vapour.

ii) Acidic groundwater originating from different sources, such as: i) percolation and filtration of acids generated directly from human activity, e.g. spillage, industrial waste, agricultural activity; ii) percolation and diffusion of acidic rainfall into the soil [78]; iii) natural decomposition of organic matter in the subsoil; iv) natural weathering or corrosion of mineral formations, e.g. sulphuric acid production from oxidation of pyrite in alum-shale formations [42,79].

3.2. Dissolution and neutralization of cement paste

The contact of a pure acid, or acidic water, with a cementitious composite promotes the dissolution and neutralization of the cement paste. The chemical-erosion (i.e. cement corrosion) process takes place as a combination of three main mechanisms [32,80,81]:

i) Ingress of the acid into the pore solution, as a result of contact between two very differentiated environments. The ingress of the acid (H(x)) and H^+ ions, i.e. due to dissociation of the acid molecule and hydration to its stable aqueous form H_3O^+, as shown in Eqs. 1 and 2; is governed by the equilibrium of species (i.e. diffusion) and electro-neutrality within the pore structure of the cement, as shown in Fig. 2a, resulting in a progressive decrease of the pH in the pore solution, as reported in [32,80].

$$H(x) + H_2O \rightleftharpoons (x)^- + H^+ \quad (1)$$

$$H_2O + H^+ \rightleftharpoons H_3O^+ \quad (2)$$

ii) Leaching of dissolved calcium, hydroxyl, alkali and other ions present in the pore solution, as a result of the concentration gradient of ionic species (Fig. 2a). The free OH^- and alkali (i.e. $(a)^+$) are progressively consumed by neutralizing the H^+ ions (i.e. stable in solution as H_3O^+) and acid radicals (i.e. $(x)^-$) that diffuse into the pore solution, producing water molecules and salts as shown in Eqs. 3–5, therefore reducing the pH of the pore solution at the outermost layers below neutrality and progressing deeper into the microstructure. In the case of Portland cement, leaching of calcium to the outermost layers promotes the formation of salts when reacting with the acid molecules, forming e.g. $CaCO_3$ (H_2CO_3), $CaSO_4$ (H_2SO_4) or $CaCl_2$ (HCl). A deeper discussion of transport and reaction kinetics is required to accurately define these processes [32,35,80].

$$H(x) + (a)OH \rightarrow ax + H_2O \quad (3)$$

$$H_3O^+ + OH^- \rightleftharpoons 2H_2O \quad (4)$$

$$(x)^- + (a)^+ \rightarrow ax \quad (5)$$

iii) The dissolution of the hydration products, primarily ruled by three factors: i) the reduction of the pH in the pore solution brings some of the hydration products out of their stability region, the dissolution of portlandite (CH) Fig. 2b precedes the dissolution of C-S-H or calcite (CC), more stable at lower pH values, as shown in Fig. 2c and d; ii) the decreasing concentration of calcium ion (Ca^{++}) in the pore solution due to leaching also promotes the dissolution of CH (Fig. 2b), over C-S-H and CC (Fig. 2b), which will start dissolving as the CH buffer decreases; iii) The reaction of the dissolved alkali (e.g. CaOH, NaOH) with the acid, consumes hydrogen molecules to form water and salts (e.g. $CaSO_4$, Na_2SO_4), the alkali and acid molecules are replenished by the previously mentioned mechanisms.

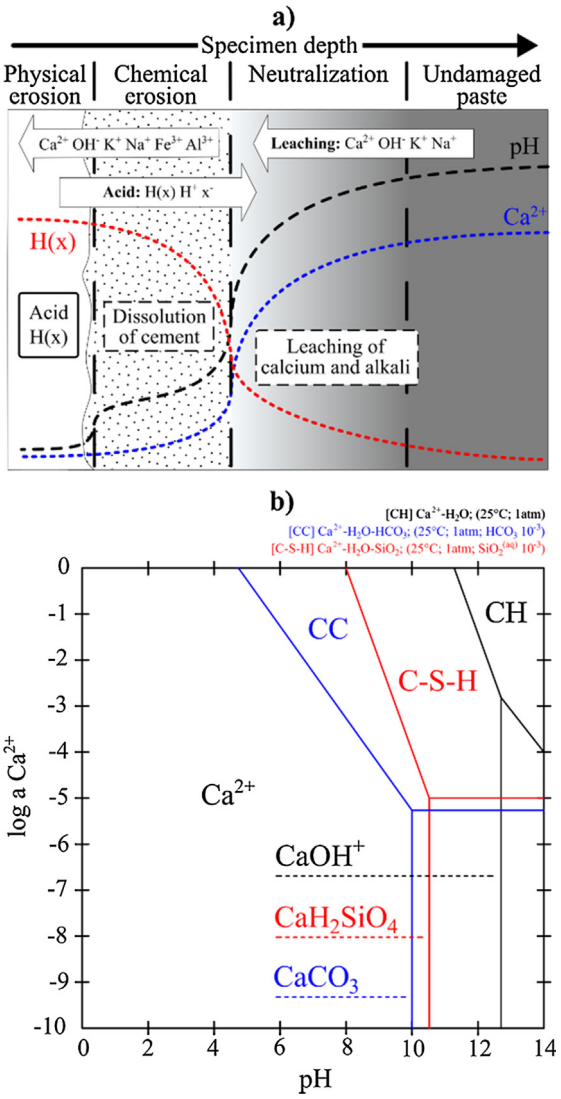

Fig. 2. Dissolution and neutralization of the cement paste. a) dissolution mechanisms for a given acid H(x) [32,80]; b) stability diagram for portlandite (CH, C-S-H and Calcite) depending on Ca++ concentration and pH.

For certain acids, secondary reactions take place. For example, sulphuric acid (H_2SO_4), the dissolution of the calcium hydroxide ($Ca(OH)_2$) is followed by the formation of gypsum ($CaSO_4{\cdot}2H_2O$). This process introduces further damage due to sulphate attack, i.e. expansion due to Ettringite formation and subsequent cracking, as reported in [31]. The deterioration process is self-sustaining as long as the acidic source replenishes, and the chemically-eroded layer of cement paste provides room for further leaching of calcium, alkali and dissolved hydration products, as shown in Fig. 2a.

3.3. Chemical erosion of concrete

The progressive dissolution of the cement paste leads to exposure of the aggregates to the acidic environment. At this stage, two scenarios are considered [32]: i) the presence of inert (i.e. acid-resistant) aggregate such as quartz, which does not dissolve in the acidic environment and will therefore not deteriorate; ii)

the presence of acid-soluble aggregate, such as limestone or dolomite, which will dissolve following mechanisms similar to those presented in figure Fig. 2a (i.e. dissolution of calcite Fig. 2b).

The dissolution of acid-soluble aggregate in addition to the dissolution of the cement matrix will contribute to the re-establishment of the neutrality and calcium equilibrium in the pore solution; whereas on the other hand, it will increase porosity and therefore facilitate ionic transport. It has been proven that a balance between these two variables can improve the acid-erosion resistance of the concrete, as certain acid-soluble aggregate (i.e. travertine or limestone) would provide slower chemical-erosion rates for the concrete compared to acid-resistant aggregate [32].

For certain exposure cases, such as sulphuric acid attack, secondary reactions (i.e. sulphate attack) can accelerate the erosion damage by causing expansion-induced cracks, which provide a preferential path for ionic diffusion and increases the depth of the attack [32,80]. At this stage of the deterioration process, the use of fibre reinforcement has been suggested as being effective in restraining the propagation of the erosion front by limiting the propagation of cracks within the matrix and avoiding the spalling of concrete [71,82]. The use of steel fibres has been reported to limit the propagation of the chemical-erosion front and decrease the mass-loss rate of acid-exposed SFRC [62,70,71,83], particularly in the case of sulphuric acid attack, where secondary sulphate attack introduces expansion cracking that deepens the acid attack [62].

However, this generalization may not apply to certain exposures, such as Mn-Fe biofilm attack [42], where the iron hydroxides from the corrosion of steel fibres at cracks provide a source of iron for the Fe-oxidizing bacteria and promote the deterioration process [42,84]. There are contradictory results regarding the efficiency of steel fibres relative to other materials (e.g. glass, polymer): most investigations report an improved performance of SFRC relative to glass or plastic fibres for uncracked concrete [41,62,71,82]; whereas for cracked SFRC, severe corrosion of steel fibres bridging cracks has been reported [41,71,85].

Furthermore, the shape of the pH profile through the depth of the uncracked concrete depends on a large number of parameters, for example: the type and proportion of cementitious materials, the Water-Binder (w/b) ratio, the reactivity of the aggregate, and especially the type and concentration of the acid.

In example, recent research has shown that strong acids (i.e. high dissociation factors) at high concentrations, e.g. sulphuric acid at pH = 2–4 [80], produce a sharp decrease of the pH and a narrow neutralization front. Whereas, weaker acids at pH values approaching neutrality, e.g. boric acid at pH = 5–6 [86,87], would produce a wider neutralization front with a smooth decrease in the pH. The depth of the chemical erosion front would decrease significantly for weaker acids or lower concentrations, as described in [80], and it is very dependent of secondary reactions and the stability of the salts formed, see Fig. 3. However, there is still limited research available predicting the transport and chemical reaction processes of acids attacking cement paste.

The main phases composing the cement paste are not stable within the neutralization front, i.e. pH ≈ 8–9 for C-S-H and pH ≈ 11–12 for CH at $Ca^{2+} \approx 10^{-1}$–10^{-2} mol/l, see Figs. 2b and 3. Therefore, a gradual transformation of the cement paste is expected at still high pH values, i.e. pH ≈ 8–11, while calcium ions leach. These changes in the cement paste surrounding fibres have been reported to cause significant detriment of the fibre-matrix bond, corresponding with the discussion presented in [88] for leaching studies with ammonium nitrate on Polyvinyl Alcohol (PVA) fibres embedded in mortar and in [89] for stainless-steel fibres embedded in concrete.

Yet, to the authors' knowledge, there is limited data available investigating the abovementioned deterioration mechanisms for deformed steel fibres, e.g. hooked-ended steel fibres, where a substantial share of the stresses transferred to the cement matrix are localized next to the deformed regions and deterioration of the surrounding matrix could have a significant impact on the mechanical performance of the composite.

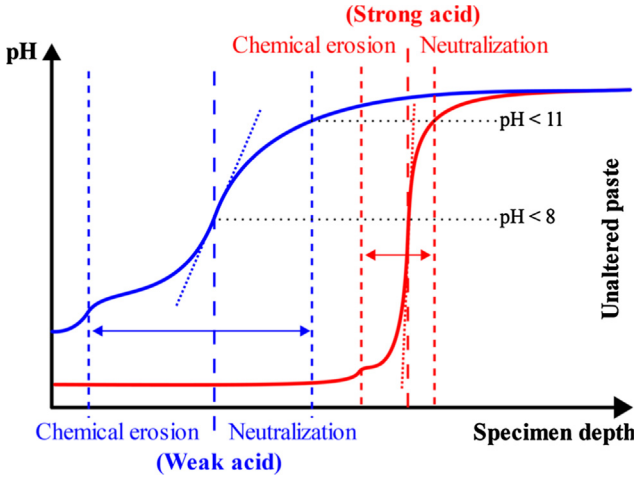

Fig. 3. Indicative pH profiles for concrete exposed to weak and strong acids, after [80,86,87]. * The distances and graphs shown in the figure are indicative.

3.4. Depassivation and corrosion of steel

The last stage of the deterioration process corresponds to the depassivation and corrosion of the embedded steel. As the neutralization front penetrates inside the concrete, the pH of the pore solution decreases gradually due to the diffusion of OH^- and H^+ from and towards the unaffected matrix. Additionally, the diffusion of alkali and Ca^{2+} towards the surface reduces the buffer capacity of the pore solution near the corrosion front, as shown in Fig. 4.

Once the pH of the pore solution falls close to neutrality values, i.e. pH < 7–8, the embedded steel de-passivates (Fig. 4) and corrosion initiates in a similar fashion to carbonation-induced corrosion [37,38], as shown in Fig. 5a (point B of pH curve, pH = 7–8).

In the case of conventional reinforcing steel, the pressure generated due to the expansion of corrosion products eventually leads to cracking of the matrix and further propagation of both the corrosion process and the acid attack, as shown in Fig. 5a (point B-B′) [37,38]. For this reason, as presented in Fig. 4, the critical depth

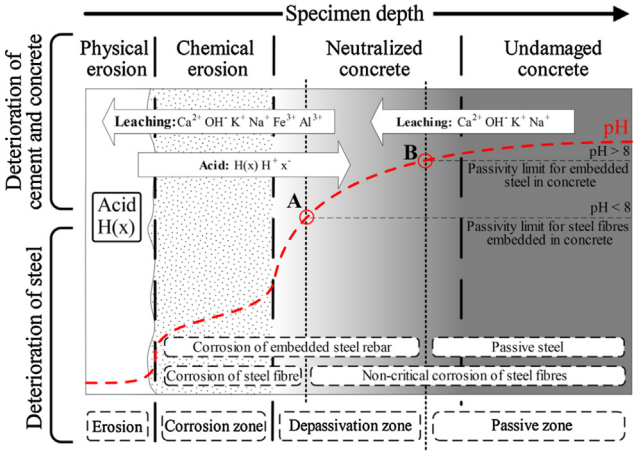

Fig. 4. Corrosion of steel in acidic environment. Deterioration of conventional reinforcement and steel fibre reinforced concrete exposed to acid attack. Legend: Electrochemical equilibrium regions for steel: (A) stability limit for steel fibres embedded in neutralized concrete; (B) passivity limit for steel embedded in concrete. * The distances and graphs shown in the figure are indicative.

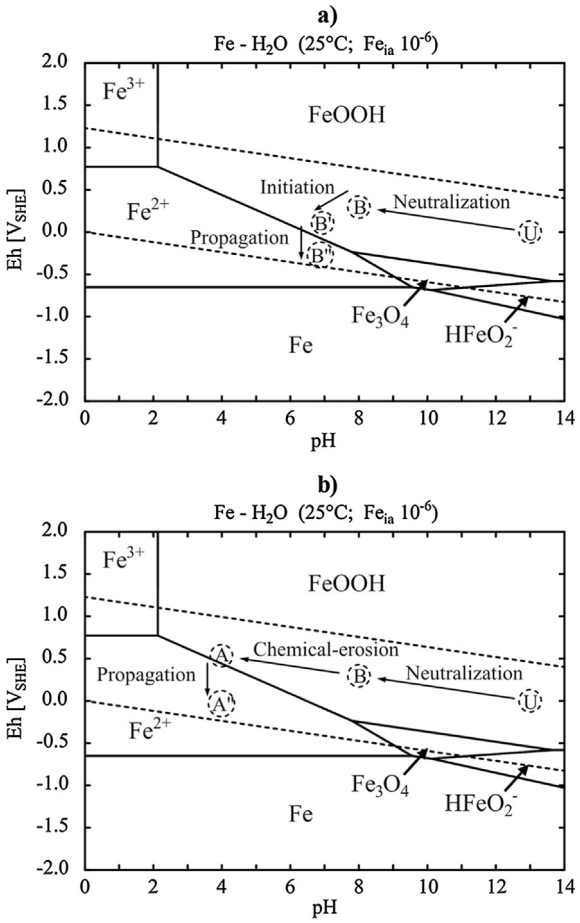

Fig. 5. Corrosion of steel in acidic environment. a) Eh-pH diagram for steel rebar embedded in carbonated concrete, after [95]; b) Eh-pH diagram for cold-drawn steel fibres embedded in concrete exposed to acids. Legend: Electrochemical equilibrium regions for steel, according to Fig. 4: (U) unaltered concrete, (B) passivity limit for steel embedded in concrete; (B′) corrosion initiation phase for steel embedded in neutralized concrete; (B″) corrosion propagation phase for steel embedded in neutralized concrete; (A) stability limit for steel fibres embedded in neutralized concrete; (A′) corrosion propagation phase for steel fibres embedded in neutralized concrete. * The graphs shown in the figure are indicative.

of corrosion for conventional reinforcing steel would be closer to the depassivation limit (point B of Fig. 4), i.e. closer to the edge of the undamaged concrete. However, there is limited research investigating these phenomena and the thickness of the neutralized concrete layer varies depending on the type and quality of concrete and the aggressiveness of the exposure: a very thin neutralization zone (1–5 mm) for aggressive exposures (e.g. sulphuric acid attack) and high concrete qualities [90]; or a thicker neutralization zone for lower concrete qualities and weaker acids (e.g. carbonic acid or acetic acid attack) [69,71].

Steel fibres have been proven stable when embedded in uncracked concrete at pH values in the pore solution of the bulk matrix below the stability region for iron (i.e. pH < 8), as observed in carbonated SFRC [12,91–94]. There is research suggesting that the small dimensions of the fibres prevent the corrosion-induced cracking, that is responsible for the larger share of the deterioration due to uniform-corrosion of steel reinforcement [12,91,94]. According to these observations, the critical corrosion region for embedded steel fibres would be closer to the chemical-erosion front, as de-passivation of the steel does not lead directly to the propagation phase (i.e. cracking); therefore, as presented in Fig. 5a, neutralization of the pore solution (U-B) would lead to depassivation of the steel fibre (B-B′) but not to critical propagation of corrosion. As the chemical erosion front reaches the steel fibre, porosity at the cement paste increases significantly and the pH drops further (e.g. pH < 4–6), initiating the dissolution of the Interfacial Transition Zone (ITZ) [32] and finally promoting corrosion propagation of the steel fibre (Fig. 4, point A). According to this deterioration model, the steel fibres do not follow the neutralization-initiation-propagation course presented in Fig. 5a (U-B-B′-B″) for conventional steel when the pH drops around 8; instead, further reduction of the pH and dissolution at the cement matrix must first take place to force the shift from depassivation to propagation, as shown in Fig. 5b (U-B-A-A′).

There is scientific insight into a larger deterioration of the residual mechanical properties (i.e. residual tensile strength) of cracked SFRC exposed to acids relative to other aggressive exposures, such as chloride or carbonation exposure [41,71,85]. Yet, to the authors' judgement, this detriment of the residual mechanical performance cannot be solely related to fibre corrosion; since additional leaching and dissolution of solid phases at the fibre-matrix interface may have a significant impact on the fibre-matrix bond, corresponding with the previous discussion based on results from [88,89]. However, there is insufficient experimental data on the specific deterioration mechanisms and performance of SFRC exposed to acidic environments to draw solid conclusions that could be translated into specific design guidelines.

4. SFRC exposed to acid attack

Compared to studies on other environment exposures, such as chloride or carbonation exposure, there is limited research investigating the durability of SFRC exposed to acidic environments. Most of the studies address the performance of the uncracked matrix, in terms of loss of compressive strength and decrease of density and mass [62,70,72,82,83,96,97], while a small share of the published research focuses on the impact of acid exposure on the residual mechanical properties [41,63,71,85], or on the deterioration phenomena for cracked SFRC [41,42,63,71,85]. The evaluation of the performance of uncracked SFRC (i.e. the elastic region) provides indication of the penetration depth and rate of the acid-erosion front, in addition to the overall impact on the mechanical and physical properties of the concrete matrix, but neglects the impact of the exposure on the fibre reinforcement. There are limited amount of studies focusing on the residual mechanical performance of the material after acid exposure, i.e. characterizing the toughness or residual tensile strength [41,63,71,85]. A summary of the published research on this topic is presented in Table 2.

The principal variables affecting the studies are discussed in the following paragraphs, including: i) type of exposure and exposure time; ii) binder composition and quality; iii) type and quantity of steel fibres; iv) cracks.

4.1. Type of exposure

The type of exposure greatly influences the progress of the deterioration front through the cement paste and therefore the chemical-erosion of the concrete and corrosion of the steel. Table 2 presents a summary of the exposure conditions and methods used in former research. The rate of deterioration of uncracked SFRC has been calculated as the chemical erosion rate ($k_{a,e}$) and neutralization rate ($k_{a,n}$); which are calculated as the penetration depth of the chemically-eroded layer and neutralization front (i.e. the front where the pH drops below pH 9) respectively, divided by the square root of the exposure time and expressed in mm/$\sqrt{y}$.

The majority of the studies have used sulphuric acid as the exposure agent at concentrations in the range 2–10 wt-%, resulting in initial pH values of 0–0.4, increasing up to pH 2.5 in some cases

Table 2
Summary of studies investigating durability of SFRC exposed to acid attack.

First author	Year	Refs.	Binder content (kg/m^3)	w/b (–)	Exp. Class (EN 206)		Exp. type	Acid Type	pH	Test methods	Crack w_k (mm)	Crack crit. $w_{k,crit}$ (mm)	Erosion rate $k_{a,e}$ ($mm/\sqrt{y}$)
					Main	Second							
Hannant	1975	[96]	390 480	0.49 0.75	XA2 XA3[*1]	SA	Field (FL)	BSA	?	3 PB (3) C (3) VI - CI	–	–	2.3–4.6
Bassuoni	2007	[62]	470	0.38	XA3	SA	Lab (IM)	H_2SO_4	0.9 – 2.5	C (3) XRD SEM – EDS ML	–	–	20
Hagelia	2008 2016	[42,75, 79,84, 98,99]	485 550	0.38 0.47	XA2 XA3[*2]	SA XS2	Field (FL)	Mn-Fe-b H_2SO_4	5.5 – 6.5 5.2 – 7.0	PI – TS SEM-EDS XRD VI - CI	0.10 0.20	*** <0.10 –0.20	8.9–44.7
Roque	2009 2015	[41,63, 71]	303 446	0.37 0.44	XA2 XA3	–	Lab (WD)	$C_2H_4O_2$	4.5	3 PB (3)[*4] C (3) ST (3) SEM – EDS VI - CI	– 0.20	0.10– 0.20	6.7–10
Hai-tang	2010 2013	[83,100–102]	370 475	0.54	XA XA2[*2]	SA	Lab (IM)	BSA	6.3	3PB (3) C (3) VI	–	–	?
Yue	2011	[72]	360 444	0.37 0.44	XA3	SA XC3	Lab (IM)	$C_6H_8O_7$ H_2SO_4	1.4	3PB (?) C (?) VI	–	–	?
Niu	2013 2017	[70,103, 104]	370 475	0.45	XA3	SA	Lab (WD)	H_2SO_4 HNO_3	3.0	ST (3)[*5] ML SEM MIP VI - CI	–	–	1.7–5.2
Kaufmann	2014	[85]	450	0.40	XA3	SA	Lab (WD)	H_2SO_4	0.4	SPT (1) VI PI	0.50 2.00	<0.50	?
Narendra Kumar	2015	[97]	700	0.21	XA3	SA	Lab (WD)	H_2SO_4 HCl	<0–0.1 <0 – 0.2	C (?) ML	–	–	?
Badagha	2015	[82]	220	0.40	XA3	–	Lab (IM)	HCl	0.2	C (3)[*5] IR (3)[*5] SS (3)[*5]	–	–	?
Koenig	2016	[50]	345	0.45	XA3	SA	Lab Field (WD)	BSA $C_2H_4O_2$ $C_3H_6O_3$	3.5 4	VI – CI PI SEM - EDS	–	–	1.0–2.1

Abbreviations: (Exp. class) the main and secondary exposure class according to EN 206; (Exp. type) the exposure type, being field or laboratory exposure and exposure method being (IM) Immersed, (FL) flowing solution or (WD) wet-dry cycles; (Acid type) the type of acidic exposure; (pH) the range of pH investigated; (Crack) the crack widths investigated, expressed in mm; (Crack crit.) the critical characteristic crack width recommended by the authors, expressed in mm; (Erosion rate) erosion rates at the exposed surface, comprising chemically-eroded concrete, expressed in $mm/\sqrt{y}$; and (Test methods) the main experiments and inspection done for the study, being (3 PB) 3-point bending test and (n. of replicates), (C) compression tests and (n. of replicates), (ST) splitting tension test and (n. of replicates),(SS) shear strength based on L-shaped test and (n. of replicates), (SPT) square panel test and (n. of replicates), (VI) visual inspection and photography and (CI) colorimetric indicators for pH, (PI) petrographic investigation in light microscope of polished sections and (TS) thin-sections, (XRD) phase composition by x-ray diffraction, (SEM) scanning electron microscope images and (EDS) elemental mapping by X-ray spectroscopy, (MIP) mercury intrusion porosimetry, (ML) mass loss measurements.
[*1] No record of pH values or chemical analysis of exposure media. Exposed described as: "very high pollution with sulphur compounds". Exposure class XA2 - XA3 due to BSA.
[*2] pH values measured at surface, local pH due to microbial activity expected to be lower than measured. Exposure class expected by the authors.
[*3] Crack widths are not expressed quantitatively, but are described as "leaking cracks" and "microcracking". Reference to estimated cracks in the range 0.1–0.2 mm given in [84]. Large deterioration observed inside the cracks investigated.
[*4] the total number of replicates was 5, but the highest and lowest result were rejected for the analysis.
[*5] the number of replicates is not directly stated in the publications and is inferred based on reference to standards, graphical documentation or the total number of specimens tested.
[?] Question marks refer to unknown values.

due to leaching [62]. The chemical erosion rates ($k_{a,e}$) are highly dependent on the pH of the solution: a higher acid concentration with constant renovation of the acid source results in large erosion rates, i.e. $k_{a,e} \approx 20$ $mm/\sqrt{y}$ for a pH = 0.9–2.5 [62]; while higher pH values (pH ≈ 3) lead to lower chemical-erosion rates ($k_{a,e}$ = 1.7–5.2 $mm/\sqrt{y}$) [70,103]. The neutralization front (i.e. pH < 9) propagates deeper into the sample, i.e. at neutralization rates ($k_{a,n}$) of 10–14 $mm/\sqrt{y}$ for wet-dry cycles, reaching values similar to those at the front achieved in a fast carbonation exposure (20 vol-% CO_2) [70,103]. The exposure of carbonated SFRC to sulphuric acid increases the penetration rate of the chemical-erosion front ($k_{a,e}$ = 14–28 $mm/\sqrt{y}$) [70].

In some cases, the source of the sulphuric acid is sulphur-oxidizing bacteria (i.e. BSA) [83,96,100–102]. The pH values measured in the solution (pH ≈ 6.3) [83,100–102] are in agreement with previous literature in the field of BSA [43,105], but often disregard local conditions at the surface of the specimen, i.e. pH ≈ 1.6–3 reported in other studies [43,46,105]. There is disagreement on whether steel fibres have a negligible impact on the propagation of the chemical-erosion front in SFRC exposed to BSA attack [50], or whether the corrosion of steel fibres in the vicinity of the chemical-erosion front may seal nearby pores and cracks and does not induce cracking or spalling of the adjacent matrix [50].

The exposure to sulphuric acid entails sulphate attack as a secondary deterioration mechanism, which facilitates the ingress of the acid and leaching due to internal cracking of the matrix. There is ongoing discussion on the effect of steel fibres on arresting these cracks under sulphuric acid exposure [42,50] or sulphate attack [106–111]. In particular, whether the addition of steel fibres has a positive impact on the performance of concrete subjected to sulphate attack, i.e. by arresting ettringite-induced cracks and ensuring the cohesiveness of the matrix at later damage stages [106–108]; or that the fibre reinforcement plays a minor role in the deterioration kinetics when compared to other variables (e.g. water-binder ratio or cement type) [109,110].

There is limited research studying exposure to other inorganic acids, such as hydrochloric acid [82,97] or nitric acid [70,103]. However, there is data suggesting that the chemical erosion rates are slower compared to those of sulphuric acid (i.e. HCl) [97]; these results support the hypothesis that secondary sulphate attack promotes deterioration by leading to cracking of the matrix and additional ingress of acid and leaching [97]. For the studies using Nitric acid, the solution was composed of a mixture of nitric- and sulphuric acid, which hampers the elaboration of further conclusions [82].

The exposure to organic acids such as: acetic acid [41,50,71], citric acid [72] or lactic acid [50], caused deterioration similar to what was induced by inorganic compounds. As a reference, the exposure to acetic acid (pH = 4.5) resulted in neutralization rates ($k_{a,n}$) of 6.7–10 mm/$\sqrt{y}$ for cracked and uncracked SFRC respectively [41,50,71]. The investigation reported severe corrosion of steel fibres at the surface of the specimen, with a larger deterioration relative to wet-dry cycles of NaCl, but no corrosion-induced cracking or spalling of the matrix. The residual mechanical performance (i.e. residual-tensile strength and toughness indices) decreased for the uncracked SFRC matrix exposed to the acid, relative to other exposures (e.g. wet-dry cycles under carbonation or chloride exposure), but showed a similar degree of deterioration for cracked and uncracked SFRC, which suggests a limited impact of cracks on the corrosion of steel fibres [41,50,71].

Some of the experiments with citric acid reported a larger chemical-erosion damage, relative to inorganic acids (H_2SO_4) at similar acidity level (e.g. pH = 3.0) [72]. This phenomenon has been attributed in the literature to the lower dissociation rates of organic acids compared to most inorganic acids, which provides a "buffer effect" at the same pH level and leads to greater deterioration under certain exposure conditions (e.g. immersion in stagnant solution) [30,81,112].

Other deterioration phenomena, such as biologically-induced chemical erosion of concrete due to Fe- Mn-oxidizing bacteria, have only been reported for SFRC under very specific conditions (e.g. leaking-cracks in sprayed liners in Norwegian subsea tunnels) [42,75,99] and further research is needed to understand the deterioration phenomena and their influence on the performance of concrete and SFRC. The data available suggest a synergetic effect between chloride-induced corrosion of the steel and the growth of certain species of bacteria, which promote acidification at the crack rim, leading to multiple deterioration mechanisms: i) decalcification of the crack surfaces due to leaching and percolation, and ingress of chlorides; ii) pitting corrosion of the steel fibres bridging the crack; iii) further biological oxidation of the corrosion products, producing H^+ and promoting further decalcification at the crack.

4.2. Binder type and quality

The type of binder and the quality of the cement matrix are the principal factors influencing the deterioration of concrete exposed to acids, since the degradation process is governed by the dissolution of the binder. So far, there are limited data providing information on the impact of the binder properties on the mechanical and chemical performance of SFRC exposed to acids. The following discussion includes also results from research on plain binder paste, mortar and concrete.

There is a large focus on identifying adequate binder compositions and optimizing mix-designs in order to enhance the resistance of concrete and cementitious composites to acid-erosion attack [32,46,65,68,73,81,113]. In general terms, the governing factor determining the resistance of concrete to acidic-erosion is the density of the microstructure, mainly dependent on the water-binder ratio and proper curing [114]. The use of pozzolanic admixtures, such as fly ash, has been reported effective in reducing acidic-erosion in concrete, which has been attributed to a finer pore structure [49,62,67]. However, published results for field exposure do not show a clear improvement [115].

There is overall disagreement regarding the impact of partial and total replacement of Portland cement by Ground Granulated Blast-Furnace Slag (GGBS or GGBFS): A significant amount of publications indicate a positive influence of GGBS addition on the acid-resistance of binary and ternary mixes [42,43,48,49,115–117], while, some research has shown a lower performance under acid exposure at high replacement ratios (i.e. GGBS-binder ratio above 40–50 wt-%), relative to Portland cement binders [43,66,67].

The addition of Silica Fume (SF) has been proposed effective on restraining the ingress of the chemical erosion front; the refinement of the pore-structure is proposed as the governing mechanism [49,66]. However, differing results suggest a lower performance of SF in ternary blends under acid exposure [65,67].

In general, lower water-binder ratios have been shown to produce a denser microstructure with a larger resistance to acid attack [46,50,65,115]. As a general practice for this type of exposure, the EN-206 standard recommends water-binder ratios below 0.45–0.55 for the exposure classes XA1-3, decreasing for more aggressive exposure classes. These values comply in general with the SFRC mix-designs presented in Table 2. However, the results presented in [41,63,71] indicate a limited influence of the water-binder ratio (w/b = 0.37–0.44) and binder content (cem = 360–444 kg/m^3) on the mechanical performance and chemical-erosion rate of SFRC exposed to acetic acid.

4.3. Type and quantity of fibres

So far there is no research comparing the performance of different types of steel fibres in concrete subject to acid exposure. The published research available mainly reports studies of cold-drawn carbon-steel fibres (EN 14889–1: Group I) [41,62,81–83,85,97,101,102]. For some of the investigations, cold-rolled sheet carbon-steel fibres (Group II) were used [72].

There are reports comparing the performance of different fibre materials such as: steel (S), polypropylene (PP), polyethylene (PE), polyester (PET), polyvinyl-alcohol (PVA) and glass (G) fibres [41,62,63,71,82,85]. For some of these studies, there is a similar loss of performance on the residual-mechanical properties for all of the different fibre materials. A general decrease in the toughness index for all the fibre types (e.g. PVA, PP and steel fibres) relative to limewater-cured references was reported for both uncracked and cracked FRC, suggesting a similar durability performance of polymer- and steel-fibres subject to acid-attack [41,63,71]. Nevertheless, some authors have reported a larger deterioration for steel fibres compared to polymer fibres for uncracked [62] and cracked FRC [85]. There is an ongoing discussion regarding the validity of comparisons of the long-term mechanical- and durability-performance of steel and polymer fibres under aggressive exposure conditions (e.g. carbonation, chloride or acid attack) [13,118–121], as polymer fibres have typically not been considered for structural applications [122]; although, recent studies show potential struc-

tural applications of polymer fibres in precast tunnel linings [123–125], slabs-on-ground [126] or in combination with steel fibres [127,128].

There are several investigations focusing on the influence of the fibre content on the deterioration of SFRC exposed to acids [62,70,72,82,83,100–103]. There is general agreement concerning the overall improvement in performance at higher fibre contents (e.g. fibre content 20–80 kg/m^3). Some investigations suggest a decrease in performance for fibre contents above 80 kg/m^3 [70,72,83,100–103]. Nevertheless, the abovementioned conclusions are based on investigations of the uncracked properties of SFRC, with a limited number of replicates (i.e. one to three replicates), which provides only a limited basis for interpretation supported on a comprehensive statistical analysis.

4.4. Cracks

Most of the research available concerning the durability of SFRC exposed to acids focuses on the performance of uncracked SFRC. For most of the investigations, the analysis takes into account only the elastic mechanical performance of the material (e.g. loss of compressive-, tensile- or shear-strength) and the physical properties of the matrix (e.g. depth of chemical-erosion and neutralization front, mass-loss) [62,70,72,82,83,97,100–103]. This approach provides some information regarding the effect of fibre reinforcement on the overall integrity of the matrix but offers only limited insight into the deterioration phenomena affecting the fibres themselves. Research investigating the residual-mechanical performance of uncracked SFRC exposed to acids shows a large drop in performance, relative to limewater cured references [41,63,71]. However, the above-mentioned effect was also observed on polymer fibres, which suggests that the damage observed might be an overall deterioration of the matrix, particularly at the fibre-matrix interface, rather than a specific fibre corrosion issue.

Corrosion-induced cracking and spalling have been reported as negligible in most investigations [41,63,71,103,129,130] and there is overall agreement on the positive effect of fibre addition in terms of reduced mass loss and slower propagation of the chemical-erosion front [50]. It has been suggested that the corrosion of steel fibres in the vicinity of the chemical-erosion front seals nearby pores and cracks and does not induce cracking or spalling of the adjacent matrix [50]. However, disagreement is still expressed in certain publications [62].

There is limited research investigating the durability of cracked SFRC exposed to acids [41,63,71,85]. The research available shows a similar deterioration for cracks below 0.20 mm, compared to uncracked SFRC for lower quality mixes (i.e. w/c = 0.44, cem = 303 kg/m^3); whereas for higher quality mixes (w/c = 0.37, cem = 446 kg/m^3) there was a significant reduction of residual-tensile strength and toughness relative to uncracked SFRC [41,63,71]. The reduction of residual-tensile strength is more pronounced at larger crack widths (i.e. $W_{k,crit}$ = 0.5–1.0 mm) and was larger than the deterioration observed in plastic fibres for exposure to 2 wt-% sulphuric acid (pH = 0–1) [85]. However, it is noted that cracks wider than $w_{k,crit}$ = 0.3–0.5 mm are typically not considered for SLS calculations under any aggressive exposure.

Précising, there is general disagreement regarding the long-term mechanical- and durability-performance of cracked SFRC exposed to acidic environments; as there is no clear understanding of the influence of the exposure on the fibre-matrix bond and its effect on the long-term fracture behaviour of SFRC [13,118–121].

5. Conclusions

Steel Fibre Reinforced Concrete (SFRC) is increasingly being used for the construction of civil infrastructure subjected to severe chemical and bio-chemical exposure. However, the lack of detailed state-of-the-art reports on this topic and imprecise regulation hinders the further development of such infrastructure.

Former research indicates that exposure of uncracked SFRC to acids results in damage similar to what occurs in Plain Concrete (PC), as the corrosion damage of steel fibres is limited to the fibres enclosed within the chemically-eroded concrete.

The fibres embedded in the chemically-eroded concrete layer may corrode but will not lead to expansion-induced cracking or spalling, and the loss of tensile capacity of the fibre may be accompanied by a significant loss of strength of the surrounding matrix due to the acid attack on the cement paste, which in any case leads to total loss of bearing capacity. Whereas, non-critical corrosion has been observed on steel fibres embedded in the neutralized concrete layer, entailing no corrosion-induced cracking or spalling.

To date, there is limited data regarding the residual mechanical performance of cracked SFRC exposed to acids. The research available suggests the possible existence of a critical crack width in the range of $w_{k,crit} \approx 0.1 - 0.3$ mm, where the corrosion damage of the steel fibre is non-critical and there is limited damage to the surrounding cement matrix that leads to a limited loss of residual mechanical performance.

It has been observed that severe exposure of cracked and uncracked SFRC to acids entails a significantly larger deterioration of the residual mechanical performance of the composite, relative to other exposures (i.e. carbonation or chloride exposure). However, there is insight suggesting that this deterioration may be governed by the changes of the matrix surrounding the fibre, due to progressive dissolution of the main calcium phases, i.e. CH and CSH, instead of corrosion damage of the steel fibres.

However, there is limited data available to provide a clear understanding of the specific deterioration mechanisms affecting the mechanical performance of steel fibres embedded in concrete exposed to acids, which is key to develop consistent guidance at the technical level regarding the design of fibre-reinforced infrastructure.

There is a need for further research focusing on reactive mass transport modelling in cement exposed to acids, as well as on the experimental characterization of the changes at the fibre-matrix interface and their impact on the fibre-matrix bond due to acid attack.

Acknowledgments

The first author would like to express his gratitude to: CowiFonden, InnovationsFonden, the German association of steel fibre producers (VDS), VejDirektoratet and Mapei-Denmark, for supporting this project; and Dr. Anders Solgaard for his contribution to supervision during this project.

References

[1] M. Bakhshi, Design of Segmental Tunnel Linings for Serviceability Limit State, (2015) 48.
[2] R.G.A. De-Waal, Steel, fibre Reinforced Tunnel Segments for the Application in Shield Driven Tunnel Linings, Delft University of Technology, 1999.
[3] R. Gettu, B. Barragán, T. García, C. Fernández, R. Oliver, Steel fiber reinforced concrete for the Barcelona metro line 9 tunnel lining, in: M. di Prisco, R. Felicetti, G.A. Plizzari (Eds.), 6th Int. RILEM Symp. Fibre Reinf. Concr., RILEM Publications SARL, 2004, pp. 141–156.
[4] M. di Prisco, G.A. Plizzari, Precast SFRC elements: From material properties to structural applications, in: M. di Prisco, R. Felicetti, G.A. Plizzari (Eds.), 6th RILEM Symp. Fibre-Reinforced Concr. - BEFIB 2004, RILEM Publications SARL, Varenna, Italy, 2004, pp. 81–100.
[5] P. Serna, S. Arango, T. Ribeiro, A.M. Núñez, E. Garcia-Taengua, Structural cast-in-place SFRC: technology, control criteria and recent applications in Spain, Mater. Struct. 42 (2009) 1233–1246, https://doi.org/10.1617/s11527-009-9540-9.
[6] S. Wallis, Steel fibre developments in South Africa, Tunnels Tunn. Int. 27 (1995) 22–24.

[7] S. Abbas, Structural and Durability Performance of Precast Segmental Tunnel Linings, University of Western, Ontario, 2014.
[8] G.A. Plizzari, G. Tiberti, Steel fibers as reinforcement for precast tunnel segments, Tunn. Undergr. Sp. Technol. 21 (2006) 438–439, https://doi.org/10.1016/j.tust.2005.12.079.
[9] B. De Rivaz, Durability issue for SFRC precast segment in tunnelling application, in: S.W. Meng, C.K. Siong (Eds.), WUTC2010, World Urban Transit Conference, 2010, pp. 1–10, https://doi.org/10.3850/978-981-08-6396-8_P223. Sentosa, Singapore.
[10] G.T. Halvorsen, C.E. Kesler, A.R. Robinson, J.A. Stout, Durability and Physical Properties of Steel Fiber Reinforced Concrete, 1976. Illinois, US.
[11] R. Winterberg, Performance and durability improvements of precast concrete lining segments with fibre reinforcement, in: Australasian Institute of Mining and Metallurgy (Ed.), 14th Australas. Tunn. Conf. 2011 Dev. Undergr. Space, Proc., Australasian Institute of Mining and Metallurgy, 2011, pp. 645–656. Auckland, New Zealand.
[12] R. Weydert, P. Schiessl, Korrosion von Stahlfasern in gerissenem und ungerissenem Stahlfaserbeton, Abschlussbericht, Bergisch Gladbach (Germany), 1998.
[13] E.S. Bernard, Durability of cracked fibre reinforced shotcrete, in: E.S. Bernard (Ed.), Shotcrete More Eng. Dev. Proc. Second Int. Conf. Eng. Dev. Shotcrete, A. A. Balkema Publishers, Sydney, Australia, 2004, pp. 59–66.
[14] Spanish Development Ministry, EHE-08 instrucción de hormigón estructural, Ministerio de Fonmento, Spain, 2009.
[15] Swedish Standards Institute, SS 812310:2014. Fibre Concrete – Design of Fibre Concrete Structures, Sweden, 2014.
[16] UNI, UNI/CIS/SC4–SFRC. Elementi Strutturali in Calcestruzzo Rinforzato Con Fibre D'Acciaio, Italy, 2004.
[17] P. Guedon, AFTES-GT38R1A1. Design, Dimensioning and Execution of Precast Steel Fibre Reinforced Concrete arch Segments France, 2013.
[18] JSCE, Recommendation for design and construction of steel fiber reinforced concrete, Tokio, Japan, Japan, 1984.
[19] T. Kasper, B.T. Jensen, H. Stang, P. Mjoernell, H. Slot, G. Vitt, L.N. Thrane, L. Reimer, Design Guideline for Structural Applications of Steel Fibre Reinforced Concrete, SFRC Consortium, Copenhagen, Denmark, Denmark, 2013.
[20] International Federation for Structural Concrete, FIB Model Code for concrete structures 2010, Lausanne, Switzerland, 2010.
[21] CEN, EN 206 - Concrete. Specification, performance, production and conformity, European Union, 2013.
[22] European Commission, Eurocode 2, Part1 - Design of concrete structures, European Union, 2002.
[23] J. Greenhalgh, C. Roberts, J. Brown, Developments in the Use of Steel Fibre Reinforced Concrete (SFRC) in Precast Segments for Tunnel Linings, in: A.T. Society, A.I. of M. and Metallurgy (Ed.), 13th Aust. Tunn. Conf., Australasian Institute of Mining and Metallurgy, Melbourne, Australia, 2008, pp. 77–82.
[24] C. Edvardsen, P. Jackson, K. Lyngby, Durability Design of steel fibre reinforced concrete for severe exposure conditions ZA, in: H. Beushausen (Ed.), Fib Symp. 2016. Performance-Based Approaches Concr. Struct., 2016, pp. 120–121. FIB, Cape Town.
[25] R. Winterberg, G. Vollmann, Use of steelfiber reinforced concrete in precast tunnel segment production, BTF Int. 75 (2009) 4–15.
[26] T. Franzen, K.F. Garshol, N. Tomisawa, Sprayed concrete for final linings: ITA working group report, Tunn. Undergr. Sp. Technol. 16 (2001) 295–309, https://doi.org/10.1016/S0886-7798(01)00052-9.
[27] German Society for Concrete and Construction Technology, Guide to Good Practice: Steel fibre concrete, Germany, 2001.
[28] CRN, Guide for the Design and Construction of Fiber-Reinforced Concrete Structures, Italy, 2006.
[29] DAfStb, DAfStb Stahlfaserbeton, Deutscher Ausschuss für Stahlbeton e. V. - DAfStb, Germany, 2012.
[30] A. Koenig, N. Erkenntnisse, Concepts for concrete exposed to acidic fluids, BFT Int. (2016) 1–3.
[31] M. Alexander, A. Bertron, N. De Belie, Performance of cement-based materials in aggressive aqueous environments, in: M. Alexander, A. Bertron, N. De Belie (Eds.), RILEM State-of-the-Art Reports 10, Springer, Netherlands, Dordrecht, 2013, p. 462, https://doi.org/10.1007/978-94-007-5413-3.
[32] R.E. Beddoe, Modelling acid attack on concrete: part I. The essential mechanisms, Cem. Concr. Res. 35 (2005) 2333–2339, https://doi.org/10.1016/j.cemconres.2005.04.002.
[33] C. Parker, The corrosion of concrete 1. The isolation of a species of bacterium associated with the corrosion of concrete exposed to atmospheres containing hydrogen sulphides, Aust. J. Exp. Biol. Med. Sci. 23 (1945) 81–90, https://doi.org/10.1038/icb.1945.13.
[34] N. De Belie, J.J. Lenehan, C.R. Braam, B. Svennerstedt, M. Richardson, B. Sonck, Durability of building materials and components in the agricultural environment, part III: concrete structures, J. Agric. Eng. Res. 76 (2000) 3–16, https://doi.org/10.1006/jaer.1999.0520.
[35] F.P. Glasser, J. Marchand, E. Samson, Durability of concrete — degradation phenomena involving detrimental chemical reactions, Cem. Concr. Res. 38 (2008) 226–246, https://doi.org/10.1016/j.cemconres.2007.09.015.
[36] R. Stallard, Relating chemical and physical erosion, Rev. Mineral. Geochem. 31 (1995) 543–564.
[37] H. Gerengi, Y. Kocak, A. Jazdzewska, M. Kurtay, H. Durgun, Electrochemical investigations on the corrosion behaviour of reinforcing steel in diatomite- and zeolite-containing concrete exposed to sulphuric acid, Constr. Build. Mater. 49 (2013) 471–477, https://doi.org/10.1016/j.conbuildmat.2013.08.033.
[38] A.F. Idriss, S.C. Negi, J.C. Jofriet, G.L. Hayward, Corrosion of steel reinforcement in mortar specimens exposed to hydrogen sulphide, part 1: impressed voltage and electrochemical potential tests, J. Agric. Eng. Res. 79 (2001) 223–230, https://doi.org/10.1006/jaer.2001.0701.
[39] S. Miyazato, N. Otsuki, Steel corrosion induced by chloride or carbonation in mortar with bending cracks or joints, J. Adv. Concr. Technol. 8 (2010) 135–144, https://doi.org/10.3151/jact.8.135.
[40] Y.S. Ji, J.L. Shen, L. Wang, C.Y. Xu, Corrosion characteristics and corrosion current distribution of steel bar in carbonated concrete, Adv. Mater. Res. 239–242 (2011) 3371–3376, https://doi.org/10.4028/www.scientific.net/AMR.239-242.3371.
[41] R. Roque, N. Kim, B. Kim, G. Lopp, Durability of Fiber-Reinforced Concrete in Florida Environments, Florida, USA, 2009.
[42] P. Hagelia, Deterioration Mechanisms and Durability of Sprayed Concrete for Rock Support in Tunnels, Technical University of Deltf, 2011.
[43] I. Fernandes, M. Pericão, P. Hagelia, F. Noronha, M.A. Ribeiro, J. Maia, Identification of acid attack on concrete of a sewage system, Mater. Struct. 45 (2012) 337–350, https://doi.org/10.1617/s11527-011-9769-y.
[44] M. O'Connell, C. McNally, M.G. Richardson, Biochemical attack on concrete in wastewater applications: a state of the art review, Cem. Concr. Compos. 32 (2010) 479–485, https://doi.org/10.1016/j.cemconcomp.2010.05.001.
[45] K. Olonade, A review of the effects of wastewater on reinforced concrete structures in Nigeria, Niger. J. Technol. 35 (2016) 234, https://doi.org/10.4314/njt.v35i2.2.
[46] M.G.D. Gutiérrez-Padilla, A. Bielefeldt, S. Ovtchinnikov, M. Hernandez, J. Silverstein, Biogenic sulfuric acid attack on different types of commercially produced concrete sewer pipes, Cem. Concr. Res. 40 (2010) 293–301, https://doi.org/10.1016/j.cemconres.2009.10.002.
[47] M.A. Abd El-Aziz, W.H. Sufe, Effect of sewage wastes on the physico-mechanical properties of cement and reinforced steel, Ain Shams Eng. J. 4 (2013) 387–391, https://doi.org/10.1016/j.asej.2012.04.011.
[48] M.L. Berndt, Evaluation of coatings, mortars and mix design for protection of concrete against sulphur oxidising bacteria, Constr. Build. Mater. 25 (2011) 3893–3902, https://doi.org/10.1016/j.conbuildmat.2011.04.014.
[49] A. Bertron, J. Duchesne, G. Escadeillas, Attack of cement pastes exposed to organic acids in manure, Cem. Concr. Compos. 27 (2005) 898–909, https://doi.org/10.1016/j.cemconcomp.2005.06.003.
[50] A. Koenig, F. Dehn, Biogenic acid attack on concretes in biogas plants, Biosyst. Eng. 147 (2016) 226–237, https://doi.org/10.1016/j.biosystemseng.2016.03.007.
[51] H. Okochi, H. Kameda, S.I. Hasegawa, N. Saito, K. Kubota, M. Igawa, Deterioration of concrete structures by acid deposition - an assessment of the role of rainwater on deterioration by laboratory and field exposure experiments using mortar specimens, Atmos. Environ. 34 (2000) 2937–2945, https://doi.org/10.1016/S1352-2310(99)00523-3.
[52] S. Xie, L. Qi, D. Zhou, Investigation of the effects of acid rain on the deterioration of cement concrete using accelerated tests established in laboratory, Atmos. Environ. 38 (2004) 4457–4466, https://doi.org/10.1016/j.atmosenv.2004.05.017.
[53] Y.F. Fan, Z.Q. Hu, Y.Z. Zhang, J.L. Liu, Deterioration of compressive property of concrete under simulated acid rain environment, Constr. Build. Mater. 24 (2010) 1975–1983, https://doi.org/10.1016/j.conbuildmat.2010.04.002.
[54] Macaferri, Case History. Hobson Bay sewer tunnel, 2011.
[55] N.T. Narayan, S. Ramakrishnan, Steel Fibre Reinforced Concrete for Ports Infrastructure, The Masterbuilder, 2013, pp. 144–147.
[56] A. Meda, G.A. Plizzari, New design approach for steel fiber-reinforced concrete slabs-on-ground based on fracture mechanics, ACI Struct. J. 101 (2005) 3–8.
[57] T. Teruzzi, E. Cadoni, G. Frigeri, S. Cangiano, G.A. a Plizzari,, Durability aspects of steel fibre reinforced concrete, in: M. Di Prisco, R. Felicetti, G.A. Plizzari (Eds.), 6th Int. RILEM Symp. Fibre Reinf. Concr., RILEM Publications SARL,, Varenna, Italy, 2004, pp. 625–634. 2912143748.
[58] D. Fall, Steel Fibres in Reinforced Concrete Structures of Complex Shapes, Chalmers University of Technology, 2014.
[59] L. Facconi, F. Minelli, G. Plizzari, Steel fiber reinforced self-compacting concrete thin slabs – experimental study and verification against Model Code provisions, Eng. Struct. 122 (2016) (2010) 226–237, https://doi.org/10.1016/j.engstruct.2016.04.030.
[60] J. Ošlejs, New frontiers for steel fiber-reinforced concrete: experience from the Baltics and Scandinavia, Concr. Int. 3 (2008) 45–50.
[61] F. Papworth, M. Marosszeky, Durability assessment of tunnels, in: Concrete Institute of Australia (Ed.), Concr. 11, Concrete Institute of Australia, Perth, Australia, 2011, p. 10..
[62] M.T.T. Bassuoni, M.L.L. Nehdi, Resistance of self-consolidating concrete to sulfuric acid attack with consecutive pH reduction, Cem. Concr. Res. 37 (2007) 1070–1084, https://doi.org/10.1016/j.cemconres.2007.04.014.
[63] B. Kim, A.J. Boyd, J.-Y. Lee, Durability performance of fiber-reinforced concrete in severe environments, J. Compos. Mater. 45 (2011) 2379–2389, https://doi.org/10.1177/0021998311401089.
[64] J.L. Brady, L.L. Gantt, D.M. Fife, D.A. Rich, S.W. Almond, D.A. Ross, Cement solubility in acids, in: SPE (Ed.), SPE 18986 Low Permeability Reserv. Symp., Society of Petroleum Engineers, Denver US, 1989, pp. 569–576, https://doi.org/10.2118/18986-MS.

[65] R. Sersale, G. Frigione, L. Bonavita, Acid depositions and concrete attack: main influences, Cem. Concr. Res. 28 (1998) 19–24, https://doi.org/10.1016/S0008-8846(97)00193-2.
[66] F. Girardi, W. Vaona, R. Di Maggio, Resistance of different types of concretes to cyclic sulfuric acid and sodium sulfate attack, Cem. Concr. Compos. 32 (2010) 595–602, https://doi.org/10.1016/j.cemconcomp.2010.07.002.
[67] Z.T. Chang, X.J. Song, R. Munn, M. Marosszeky, Using limestone aggregates and different cements for enhancing resistance of concrete to sulphuric acid attack, Cem. Concr. Res. 35 (2005) 1486–1494, https://doi.org/10.1016/j.cemconres.2005.03.006.
[68] H. Gay, T. Meynet, J. Colombani, Local study of the corrosion kinetics of hardened Portland cement under acid attack, Cem. Concr. Res. 90 (2016) 36–42, https://doi.org/10.1016/j.cemconres.2016.09.007.
[69] M.C. Chen, K. Wang, L. Xie, Deterioration mechanism of cementitious materials under acid rain attack, Eng. Fail. Anal. 27 (2013) 272–285, https://doi.org/10.1016/j.engfailanal.2012.08.007.
[70] D. Niu, Y. Wang, Neutralization of steel fiber reinforced concrete under multiple influential factors, J. Earthq. Tsunami 7 (2013) 1–13, https://doi.org/10.1142/S1793431113500152.
[71] B. Kim, A.J. Boyd, H.S. Kim, S.H. Lee, Steel and synthetic types of fibre reinforced concrete exposed to chemical erosion, Constr. Build. Mater. 93 (2015) 720–728, https://doi.org/10.1016/j.conbuildmat.2015.06.023.
[72] Q. Yue, L. Li, Z.P. He, Experiment research on the steel fiber reinforced concrete in the acid environment, Adv. Mater. Res. 224 (2011) 224–228, https://doi.org/10.4028/www.scientific.net/AMR.224.224.
[73] H. Yuan, P. Dangla, P. Chatellier, T. Chaussadent, Degradation modeling of concrete submitted to biogenic acid attack, Cem. Concr. Res. 70 (2015) 29–38, https://doi.org/10.1016/j.cemconres.2015.01.002.
[74] E. Fjerdingstad, Bacterial corrosion of concrete in water, Water Res. 3 (1969) 21–30, https://doi.org/10.1016/0043-1354(69)90063-3.
[75] P. Hagelia, Deterioration mechanisms and durability of sprayed concrete in Norwegian tunnels, in: K. Berg, ITA-AITES (Eds.), 5th Int. Symp. Sprayed Concr. - Mod. Use Wet Mix Sprayed Concr. Undergr. Support, Norwegian Tunnelling Society, Lillehammer, Norway, 2008, pp. 149–170.
[76] F.C. Menz, H.M. Seip, Acid rain in Europe and the United States: an update, Environ. Sci. Policy 7 (2004) 253–265, https://doi.org/10.1016/j.envsci.2004.05.005.
[77] S. Fujita, A. Takahashi, J.-H. Weng, L.-F. Huang, H.-K. Kim, C.-K. Li, F.T.C. Huang, F.-T. Jeng, Precipitation chemistry in East Asia, Atmos. Environ. 34 (2000) 525–537, https://doi.org/10.1016/S1352-2310(99)00261-7.
[78] G.P. Ayers, L.C. Peng, R.W. Gillett, L.S. Fook, Rainwater composition and acidity at five sites in Malaysia, Water Air. Soil Pollut. 133 (2002) (1996) 15–30, https://doi.org/10.1023/A:1012967614759.
[79] P. Hagelia, Does the EN 206-1 Exposure Classification Apply to Tunnel Concrete? Hirtshals, Denmark, in: Nord Expo. Sites - Input to Revis. EN 206-1, 2008, pp. 241–264.
[80] R.E. Beddoe, Modelling acid attack on concrete: part II. A computer model, Cem. Concr. Res. 88 (2016) 20–35, https://doi.org/10.1016/j.cemconres.2015.10.012.
[81] A. Koenig, F. Dehn, Main considerations for the determination and evaluation of the acid resistance of cementitious materials, Mater. Struct. 49 (2016) 1693–1703, https://doi.org/10.1617/s11527-015-0605-7.
[82] D. Badagha, C.D. Modhera, An experimental approach to investigate effects of curing regimes on mechanical properties and durability of different fibrous mortars, in: Adv. Struct. Eng. Mater. Vol. Three, Springer India, New Delhi, 2015, pp. 1917–1929, https://doi.org/10.1007/978-81-322-2187-6_148.
[83] Z. Hai-tang, F. Xiang-qian, Z. Qi-ming, L. Jin-zhang, Experimental study on the damage of steel fiber reinforced concrete by simulation domestic sewage, Adv. Mater. Res. 168–170 (2011) 1801–1805.
[84] P. Hagelia, Sprayed concrete in aggressive subsea environment the Oslofjord test site, in: 6th Int. Symp. Sprayed Concr. - Mod. Use Wet Mix Sprayed Concr. Undergr. Support, Tromsø, Norway, 2011 p. 15.
[85] J.P. Kaufmann, Durability performance of fiber reinforced shotcrete in aggressive environment, in: A. Negro, W. Bilfinger, M.O. Cecilio (Eds.), WTC 2014 – Tunnels a Better Life, ITA-AITES, Iguaçu, Brazil, 2014, pp. 1–7.
[86] R.T. Pabalan, L. Yang, K.-T.K. Chiang, Boric Acid Degradation of Reinforced Concrete, San Antonio, US, 2011. doi:10.13140/RG.2.1.3257.6400.
[87] R.T. Pabalan, K.-T.K. Chiang, Experimental study and reactive transport modeling of boric acid leaching of concrete, in: EPJ Web Conf., 2013, p. 01009, https://doi.org/10.1051/epjconf/20135601009.
[88] B.H. Oh, P. Kabele, Durability under chemical loads, in: F. Wittmann, G. Van Zijl (Eds.), Durab. Strain-Hardening Fibre-Reinforced Cem. Compos, first ed., Springer, Netherlands, Dordrecht, 2011, p. 152, https://doi.org/10.1007/978-94-007-0338-4.
[89] G. Camps, A. Sellier, A. Turatsinze, G. Escadeillas, X. Bourbon, Modelling of leaching effects on fibre-reinforced concrete properties Toulouse, FR, in: Concr. Aggress. Aqueous Environ. Performance, Test. Model., 2009, pp. 179–186.
[90] F. Jahani, J. Devinny, F. Mansfeld, I.G. Rosen, Z. Sun, C. Wang, Investigations of sulfuric acid corrosion of concrete. II: electrochemical and visual observations, J. Environ. Eng. 127 (2001) 580–584, https://doi.org/10.1061/(ASCE)0733-9372(2001).
[91] S. Cangiano, G.A. Plizzari, E. Cadoni, G. Frigeri, T. Teruzzi, On durability of steel fibre reinforced concrete, in: R.K. Dhir, T.A. Harrison, M.D. Newlands (Eds.), Int. Conf. Cem. Comb. Durable Concr., 2005, pp. 477–486, https://doi.org/10.1680/ccfdc.34013. Thomas Telford, Dundee, Scotland.
[92] M. Schupack, Steel fiber concrete, in: S.P. Shah, A. Skarendahl (Eds.), Steel Fiber Concr. US-Sweden Jt. Semin., Elsevier, Stockholm, Sweden, 1985, pp. 479–496.
[93] E. Kern, H. Schorn, 23 Jahre alter Stahlfaserbeton, Beton- Und Stahlbetonbau. 86 (1991) 205–208, https://doi.org/10.1002/best.199100380.
[94] L. Ferrara, R. Fratesi, S. Signorini, F. Sonzogni, Durability of steel fibre-reinforced cocnrete precast elements: experiments and proposal of design recommendations, in: M. Di Prisco, R. Felicetti, G.A. Plizzari (Eds.), 6th RILEM Symp. Fibre-Reinforced Cocnretes - BEFIB 2004, RILEM Publications SARL, Varenna, Italy, 2004, pp. 565–574.
[95] A. Küter, M.R. Geiker, P. Møller, Management of Reinforcement Corrosion, DTU, 2006.
[96] D.J. Hannant, J. Edgington, Durability of steel fibre concrete, in: A. Neville (Ed.), Rilem Symp. 1975 Fibre Reinf. Cem. Concr., The Construction Press, Leeds, UK, 1975, pp. 159–169.
[97] B. Narendra Kumar, Physical and chemical durability studies on high performance self compacting hybrid fibre reinforced concrete, Indian Concr. J. 89 (2015) 73–82.
[98] P. Hagelia, Deterioration mechanisms and durability of sprayed concrete in Norwegian tunnels, Publication 17, in: K. Fossum, G. Gjæringen, E. Moe (Eds.), Undergr. Openings - Oper. Maint. Repair, Norwegian Tunnelling Society, Oslo, SE, 2008, pp. 45–58.
[99] P. Hagelia, Interaction of abiotic and biochemical reactions and their role in concrete deterioration, Concrete 49–51 (2016).
[100] Z. Hai-tang, F. Xiang-qian, G. Dan-ying, Z. Qi-ming, Experimental study on corrosion of steel fiber reinforced concrete under industrial wastewater environment, J. Southeast Univ. 2 (2010).
[101] Z. Hai-tang, F. Xiang-qian, Z. Qi-ming, G. Dan-ying, Experimental research on corrosion behavior of SFRC subjected to wastewater and dry-wet cycling, J. North China Inst. Water Conserv. Hydroelectr. Power 1 (2013).
[102] F. Xiang-qian, H. Shao-wei, Z. Hai-tang, SFRC subjected to domestic sewage and sustained load, J. Wuhan Univ. Technol. Sci. Ed. 27 (2012) 797–804, https://doi.org/10.1007/s11595-012-0551-y.
[103] J. Wang, Study of neutralization of steel fiber reinforced self-compacting concrete in action of various factors, Nanjing Hangkong Hangtian Daxue Xuebao/Journal Nanjing Univ Aeronaut. Astronaut. 45 (2013).
[104] Y. Wang, D. Niu, Z. Song, Effect of acid rain erosion on steel fiber reinforced concrete, J. Wuhan Univ. Technol. Mater. Sci. Ed. 32 (2017) 121–128, https://doi.org/10.1007/s11595-017-1569-y.
[105] S. Okabe, M. Odagiri, T. Ito, H. Satoh, Succession of sulfur-oxidizing bacteria in the microbial community on corroding concrete in sewer systems, Appl. Environ. Microbiol. 73 (2007) 971–980, https://doi.org/10.1128/AEM.02054-06.
[106] M.T. Bassuoni, M.L. Nehdi, Durability of self-consolidating concrete to sulfate attack under combined cyclic environments and flexural loading, Cem. Concr. Res. 39 (2009) 206–226, https://doi.org/10.1016/j.cemconres.2008.12.003.
[107] M.T. Bassuoni, M.L. Nehdi, Durability of self-consolidating concrete to different exposure regimes of sodium sulfate attack, Mater. Struct. 42 (2008) 1039–1057, https://doi.org/10.1617/s11527-008-9442-2.
[108] M.T. Bassuoni, M.L. Nehdi, Resistance of self-consolidating concrete to ammonium sulphate attack, Mater. Struct. Constr. 45 (2012) 977–994, https://doi.org/10.1617/s11527-011-9811-0.
[109] C. Miao, R. Mu, Q. Tian, W. Sun, Effect of sulfate solution on the frost resistance of concrete with and without steel fiber reinforcement, Cem. Concr. Res. 32 (2002) 31–34, https://doi.org/10.1016/S0008-8846(01)00624-X.
[110] A.S. El-Dieb, Mechanical, durability and microstructural characteristics of ultra-high-strength self-compacting concrete incorporating steel fibers, Mater. Des. 30 (2009) 4286–4292, https://doi.org/10.1016/j.matdes.2009.04.024.
[111] E. Alizade, F.J. Alaee, S. Zabihi, Effect of steel fiber corrosion on mechanical properties of steel fiber reinforced concrete, Asian J. Civ. Eng. 17 (2016) 147–158.
[112] A. Koenig, F. Dehn, Acid Resistance of Ultra High-Performance Concrete (UHPC), in: Nanotechnol. Constr., Springer International Publishing, Cham, 2015, pp. 317–323, https://doi.org/10.1007/978-3-319-17088-6_41.
[113] N. De Belie, J. Monteny, A. Beeldens, E. Vincke, D. Van Gemert, W. Verstraete, Experimental research and prediction of the effect of chemical and biogenic sulfuric acid on different types of commercially produced concrete sewer pipes, Cem. Concr. Res. 34 (2004) 2223–2236, https://doi.org/10.1016/j.cemconres.2004.02.015.
[114] A.M. Neville, Properties of Concrete IV, IVPrentice Hall, Harlow, UK, 2012.
[115] F. Bellmann, W. Erfurt, H.M. Ludwig, Field performance of concrete exposed to sulphate and low pH conditions from natural and industrial sources, Cem. Concr. Compos. 34 (2012) 86–93, https://doi.org/10.1016/j.cemconcomp.2011.07.009.
[116] O.B. Ozger, F. Girardi, G.M. Giannuzzi, V.A. Salomoni, C.E. Majorana, L. Fambri, N. Baldassino, R. Di Maggio, Effect of nylon fibres on mechanical and thermal properties of hardened concrete for energy storage systems, Mater. Des. 51 (2013) 989–997, https://doi.org/10.1016/j.matdes.2013.04.085.
[117] E. Gruyaert, P. Van Den Heede, M. Maes, N. De Belie, Investigation of the influence of blast-furnace slag on the resistance of concrete against organic acid or sulphate attack by means of accelerated degradation tests, Cem. Concr. Res. 42 (2012) 173–185, https://doi.org/10.1016/j.cemconres.2011.09.009.

[118] E.S. Bernard, Embrinlement of Fiber-Reinforced Shotcrete, Shotcrete (2008) 16–21.
[119] C. Allen, In the land of the blind. . ., Tunneling J. (2014) 39–40.
[120] P. Rossi, Critique of synthetic fiber FRS paper, TunnelTECH - TunnelTalk. (2014) 7.
[121] D. Wimpenny, W. Angerer, T. Cooper, S. Bernard, The use of steel and synthetic fibres in concrete under extreme conditions Sidney, Australia, in: Concr. Inst. Austrialia. Conf., 2009, pp. 1–10.
[122] N. Buratti, C. Mazzotti, M. Savoia, Post-cracking behaviour of steel and macro-synthetic fibre-reinforced concretes, Constr. Build. Mater. 25 (2011) 2713–2722, https://doi.org/10.1016/j.conbuildmat.2010.12.022.
[123] R. Winterberg, L.M. Rodríguez, R. Justa-Cámara, D. Sualdea-Abad, T. Orfila-Farràs, Design of segmental linings with macro synthetic fibre reinforcement, in: P.D. Jakobsen, B. Nilsen, K.G. Holter (Eds.), World Tunn. Congr. 2017 – Surf. Challenges – Undergr. Solut., Norwegian Tunnelling Society, Bergen, NO, 2017, pp. 1–7.
[124] R.I. Gilbert, E.S. Bernard, Post-cracking ductility of fibre reinforced concrete linings in combined bending and compression, Tunn. Undergr. Sp. Technol. 76 (2018) 1–9, https://doi.org/10.1016/j.tust.2018.02.010.
[125] A. Conforti, I. Trabucchi, G. Tiberti, G. Plizzari, A. Caratelli, A. Meda, S. Moro, M. Hunger, An experimental study on the use of polypropylene fibers in precast segments for hydraulic and metro tunnel lining, in: B. Massicotte, F. Minelli, B. Mobasher, G. Plizzari (Eds.), FRC2018 Fibre Reinf2018 FRC2018 Fibre Reinf. Concr. from Des. to Struct. Appl. Jt. ACI-Fib-RILEM Int. Work., 2018, pp. 138–139. Cartolibreria Snoopy, Desenzano, IT.
[126] J.R. Roesler, S.A. Altoubat, D.A. Lange, K.A. Rieder, G.R. Ulreich, Effect of synthetic fibers on structural behavior of concrete slabs-on-ground, ACI Mater. J. 103 (2006) 3–10, https://doi.org/10.14359/15121.
[127] B. Li, Y. Chi, L. Xu, Y. Shi, C. Li, Experimental investigation on the flexural behavior of steel-polypropylene hybrid fiber reinforced concrete, Constr. Build. Mater. 191 (2018) 80–94, https://doi.org/10.1016/J.CONBUILDMAT.2018.09.202.
[128] N. Banthia, M. Sappakittipakorn, Toughness enhancement in steel fiber reinforced concrete through fiber hybridization, Cem. Concr. Res. 37 (2007) 1366–1372, https://doi.org/10.1016/j.cemconres.2007.05.005.
[129] Y. Wang, D. Niu, Z. Dong, Experimental study on carbonation of steel fiber reinforced concrete, in: J. Olek, W. Weiss (Eds.), 4th Int. Conf. Durab. Concr. Struct., Purdue University Press, West Lafayette, USA, 2014, pp. 55–59.
[130] J. Gao, Z. Yu, L. Song, T. Wang, S. Wei, Durability of concrete exposed to sulfate attack under flexural loading and drying-wetting cycles, Constr. Build. Mater. (2013) 33–38, https://doi.org/10.1016/j.conbuildmat.2012.05.033.

Chapter 3
Corrosion damage and mechanical performance of SFRC

The literature review presented in Chapter 2 showed discrepancy at the technical and scientific level regarding the corrosion damage and mechanical performance of cracked SFRC exposed to wet-dry cycles involving chloride and carbonation exposure. There is particular interest regarding the extent of the corrosion deterioration of steel fibres inside cracks in the range of 0.1 to 0.3 mm and its impact on the residual tensile performance of the cracked SFRC.

In order to investigate these aspects, an experimental study comprising the preparation, exposure and testing of approx. 500 cracked SFRC specimens, exposed to wet-dry cycles under laboratory conditions during a period of two years was carried out. The objective of this chapter is to present a quantitative evaluation of the extent of corrosion damage of fibres bridging cracks and its impact on the residual performance of SFRC, based on a detailed statistical study. The chapter comprises two publications that cover the quantification and description of the corrosion and mechanical damage and its evolution over time.

The investigation presented in Paper III comprised the quantification of the extent of fibre corrosion in cracked and uncracked SFRC exposed to wet-dry cycles of chlorides and carbon dioxide, and a statistical evaluation of its impact on the mechanical performance of SFRC. The evolution of the corrosion damage over time and subsequent changes in the mechanical performance of the composite are covered in Paper IV.

The investigations confirmed that fibre corrosion in uncracked SFRC was limited to the concrete surface and produced aesthetical damage, i.e. formation of rust stains, but did not cause cracking or spalling of the uncracked concrete matrix. There was no observable progression of fibre corrosion inside the uncracked composite within the time-scale investigated. There was no statistically significant detriment to the

compressive strength of the uncracked concrete matrix due to corrosion under wet-dry cycle exposure.

Investigations of SFRC with crack widths of 0.15 and 0.3 mm, respectively, indicated that fibres bridging cracks may corrode up to depths of 10 – 40 mm inside the crack, depending on the exposure and crack width; developing slightly over time. Corrosion of fibres inside the crack increased the probability of fibre rupture, but had a limited impact on the global count of ruptured fibres. The ratio of fibres rupturing due to corrosion did not vary significantly over time and was only statistically significant for specimens with small cross-sections.

However, there were substantial changes in the residual mechanical performance of the cracked SFRC after exposure relative to the uncracked SFRC, which comprised increases in the residual tensile and flexural forces transferred at crack openings below 1.5 mm. The observed increase was consistent over time and was related to an increase of the fibre-matrix bond strength during the exposure. Only moderate reductions in the total toughness were observed in specimens with small cross-sections (i.e. 80x80 mm) cracked at 0.3 mm and exposed to large chloride concentrations (i.e. 7 -wt.% NaCl). It was concluded that the impact of fibre corrosion on the performance of the cracked composite over time is subject to a size-effect and may only be significant for specimens with small cross-sections.

A correlation was observed between the increase of the residual mechanical performance of the cracked SFRC and a larger number of ruptured fibres after exposure. Yet, these changes were secondary compared to the toughness variation due to the fibre distribution. Fibre corrosion had a subordinate, yet statistically significant, impact on the changes in toughness over time. The exposure time had a negligible impact on the variations of the residual tensile performance, considering the time-scales investigated.

This study concluded that changes in the residual performance of cracked SFRC exposed to chlorides and carbon dioxide, are not exclusively a result of fibre damage due to corrosion and may be related to localized changes at the fibre-matrix interface due to the exposure. Yet, macroscopic observations at the composite level do not provide a clear explanation for those changes. Therefore, the following chapters focus on: i) investigating the changes in the pull-out behaviour of single fibres in cracked SFRC exposed to wet-dry cycles and ii) characterizing the microstructural changes at the fibre-matrix interface of cracked SFRC exposed to wet-dry cycles.

3.1 Paper III. Corrosion damage and mechanical performance of SFRC exposed to wet-dry cycles

The following publication, referred as “paper III”, has been submitted to Journal of Sustainable Cement-Based Materials.

Marcos-Meson, V., Fischer, G., Edvardsen, C., Solgaard, A., Michel, A., 2020. Mechanical performance of steel fibre reinforced concrete exposed to chlorides and carbon dioxide: results after one year (unpublished).

Printed in this thesis as the original manuscript with the authors’ formatting.

Submitted to Journal of Sustainable Cement-Based Materials (2020)

Mechanical performance of steel fibre reinforced concrete exposed to chlorides and carbon dioxide: results after one year

Victor Marcos-Meson[1,2,3*], Gregor Fischer[1], Carola Edvardsen[2], Anders Solgaard[2], Alexander Michel[1]
[1] Department of Civil Engineering, Technical University of Denmark, Kgs. Lyngby, Denmark
[2] COWI A/S, Kgs. Lyngby, Denmark
[3] VIA Building, Energy, Water & Climate, VIA University College, Horsens, Denmark

Abstract

This paper presents an experimental study addressing the corrosion damage and mechanical performance of steel fibre reinforced concrete (SFRC) exposed to chloride and carbon dioxide wet-dry cycles for one year. Results presented indicated negligible corrosion damage to uncracked SFRC exposed to chlorides and carbon dioxide. Fibre corrosion inside the crack occurred at the outermost fibres, yet it had a minor impact on the toughness of the material compared to the impact of the fibre content for the crack widths studied. Changes in the residual performance of cracked SFRC after 1-year exposure lead to a moderate increase of the toughness small cracks. This was partly attributed to an increase of the fibre-matrix bond strength. This indicates that there may be additional damage mechanisms besides fibre corrosion that explain the changes in the residual performance of the composite material, likely related to alteration of the fibre-matrix interface.

Keywords

Steel Fibre Reinforced Concrete (SFRC), durability, corrosion, chlorides, carbonation, cracks

1. Introduction

Steel fibre reinforced concrete (SFRC) is widely used in the construction industry as partial or total replacement of conventional reinforcing steel [1–3]. There is substantial research describing the beneficial impact of the addition of carbon-steel fibres, henceforth “steel fibres”, on the durability of conventional carbon-steel reinforcement in concrete [4]. However, the total replacement of conventional carbon-steel reinforcement with steel fibres is still controversial when considering the long-term durability of cracked SFRC under corrosive exposures, leading to discrepancy in the applicability among regulators [5].

Previous research investigating the performance of SFRC exposed to chlorides reports limited corrosion damage for uncracked SFRC, restricted to formation of rust stains due to corrosion of steel fibres adjacent to the concrete surface, which resulted in negligible long-term damage with no cracking or spalling of the matrix [6–10]. However, the durability of cracked SFRC exposed to chlorides is controversially discussed in the literature and the conclusions are, among others, highly dependent on the crack width [5].

There is substantial corrosion damage reported for carbon-steel fibres bridging cracks wider than 0.5 mm, leading to notable reductions of the residual-tensile strength and no healing inside the cracks, but not causing additional damage due to cracking or spalling of the matrix adjacent to the fibres due to fibre corrosion [7,11–15]. Whereas, there is discrepancy regarding the corrosion of carbon-steel fibres bridging cracks below 0.5 mm [5]. There is insight of substantial decay of the residual-tensile strength of SFRC cracked in the range 0.2 – 0.5 mm exposed to chlorides [11,14,16–20]. However, research indicates that a share of the toughness loss reported after exposure may be related to an excessive strengthening of the fibre-matrix bond due to the densification of the matrix, referred as “embrittlement” in some publications [18,20,21], which may lead to premature fibre rupture during pull-out.

Most research reports negligible reductions of the residual-tensile strength and limited corrosion of

carbon-steel fibres bridging cracks smaller than 0.2 mm [11,13,22–25] and 0.1 mm [7,18,26] in SFRC exposed to chlorides. Greater peak residual-tensile strengths relative to unexposed SFRC have been attributed to self-healing inside the crack [7,11,13,22,23]. However, part of the research suggested that cracks should not be allowed in SFRC under chloride exposure, based on two arguments: insufficient exposure time to induce sufficient corrosion-damage on the steel fibres [14,27], and the observation of a strong decay of the residual tensile capacity after exposure [15,17,19,28].

Previous research agrees that carbonation of uncracked SFRC caused limited long-term corrosion damage [5], restricted to fibre corrosion progressing at low rates in the outer region of the carbonated area and aesthetical damage with no cracking or spalling of the matrix [8,14,16,29]. Negligible reductions of the residual-tensile strength of carbonated SFRC are reported in [14,16], also in combination with chlorides [14,15,23]. Changes of the fracture behaviour of SFRC, i.e. leading to loss of ductility, reported over a 10-year period were linked to the continuous densification of the matrix, rather than the deterioration of the steel fibres [18,20,21]. However, there is limited research investigating the durability of cracked SFRC exposed to carbon dioxide [5].

There is confirmation of critical corrosion of steel fibres bridging cracks wider than 0.50 mm in carbonated concrete exposed to rainwater, especially in the outer crack region (e.g. up to 20 – 40 mm) [14], which in some cases resulted in a significant loss of residual-tensile strength [18]. There is discrepancy regarding the effect of corrosion on the performance of SFRC cracked in the range 0.2 – 0.5 mm: some studies report limited long-term reduction of the residual-tensile strength regardless of initiation of corrosion in most of the fibres bridging the crack [14], whereas other studies report a substantial decrease of the total energy absorption of pre-cracked SFRC with cracks larger than 0.2 mm [18,20]. Carbonation of SFRC in cracks smaller than 0.2 mm, promoted initiation of fibre corrosion at the outer crack's cross-section, but resulted in increased residual-tensile strength at small deformations compared to unexposed SFRC [14] and negligible reductions of the total energy absorption for large deformations [18].

This paper investigates the corrosion damage of carbon-steel fibres and the mechanical performance of uncracked and cracked SFRC exposed to chlorides and carbon dioxide. The investigation covers the exposure, mechanical testing and visual inspection of bending and uniaxial tension specimens, cracked at 0.15 and 0.3 mm, and exposed to wet-dry cycles for one year. The discussion presented in this paper focuses on the extent of fibre corrosion and its impact on the mechanical performance of cracked SFRC, based on a statistical study of the test data.

Table 1. Mix-design.

Component	Quantity (kg/m^3)
Cement (CEM I 52.5N)	326.3
Fly Ash	100.0
Water	145.0
Sand 00/02	626.5
Sea gravel 04/08	175.1
Sea gravel 08/16	933.6
Steel fibres	40.0

2. Methodology

The investigation presented in this paper covers the preparation, exposure, mechanical testing and visual inspection of 220 SFRC specimens, with induced crack widths of 0.15 and 0.3 mm and exposed to wet-dry cycles for one year. The exposures investigated comprise chloride and carbon dioxide in wet-dry cycles. Two types of specimens have been investigated: 110 three-point bending notched beams according to EN 14651:2007 [30] and 110 single notched coupon tests in uniaxial tension based on the experiments presented in [31].

The analysis of the mechanical performance of the material is made by the comparison of the stress-CMOD and work-CMOD response (i.e. the energy absorption) for the investigated material in bending and uniaxial tension. Visual inspection of the crack surface and fibres bridging the crack were used to determine the degree of fibre damage due to corrosion.

Discussions regarding the extent and impact of fibre corrosion are based on descriptive statistics of the fibre distribution and regression analysis comparing the correlation between exposure conditions, crack width, fibre damage due to corrosion and mechanical performance.

2.1 Preparation of specimens

The specimens were prepared following a mix-design in compliance with the recommendations for minimum binder content and water-to-binder ratio specified for conventional reinforced concrete in DS/EN 206-1: 2011 for the exposure classes XC4 – XS3. The total binder content was 426.3 kg/m^3 with 31% fly ash replacement of the Portland cement. The water to binder ratio was 0.34 and the equivalent water to cement ratio was 0.40, considering an effective k-factor for the fly ash of 0.40, see **Table 1**.

The superplasticizer and air-entrainer content were adjusted in the subsequent mixes to reach a slump of

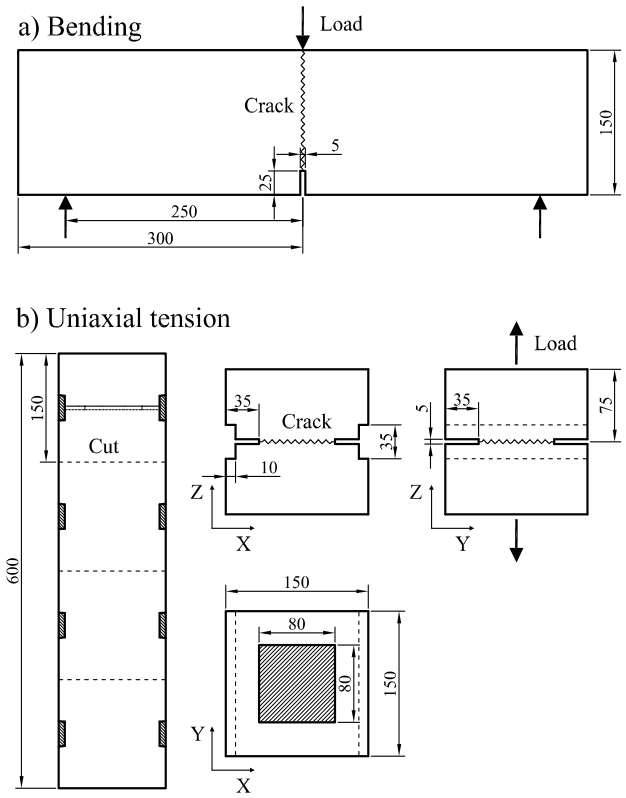

Fig. 1. Dimensions of specimens: a) bending test, b) uniaxial tension test. Dimensions are expressed in mm.

100±20 mm and an entrained air content of 4.5±0.5 %, measured according to EN 12350-2 and EN 12350-7 respectively. The fibres were added in two steps: 50 % of the fibres where pre-mixed with the dry material, the rest was added to the mixer once the wet mix was ready, if clumps of fibres were found they were removed by the operators.

The steel fibre used was a cold-drawn hooked-ended fibre (type 1 according to EN 14889-1:2006 [32]), with a length of 60 mm and diameter of 0.75 mm (aspect ratio: l/d = 80). The fibre was made of high-carbon cold-drawn steel with a characteristic ultimate tensile strength of 1900 MPa.

The production of the bending specimens was done in a prefabrication plant, using an industrial mixing plant. The casting was made by direct pumping of the concrete from a truck on coated plywood forms over an industrial vibration table. Each formwork contained 5 beam elements (600×150×150 mm) that were filled from one end in two steps and were vibrated for 4 minutes in total at approx. 50 Hz. The specimens were cast in 3 separate batches in consecutive days, demoulded after one day and cured indoors, moist covered with plastic for 56 days at 20 °C.

The uniaxial tension specimens were cast in the laboratory with a 300 L planetary mixer. The specimens were cast in 600×150×150 mm steel formworks over a vibration table in two steps and were vibrated in total for 4 minutes at 50 Hz. The lateral grooves shown in **Fig. 1** were cast with eight hardened PVC inserts glued to the side of each of the formworks. The specimens were cast in 5 separate batches in consecutive days, demoulded after one day and cured indoors, moist covered with plastic for 56 days at 20 °C. The specimens were cut in cubes after 28 days of curing and thereafter cured for additional 28 days.

The final dimensions of the three-point bending beam specimens were 600×150×150 mm, with a 25 mm deep and 5 mm thick notch cut at the centre, along the transversal direction, according to [30], see **Fig. 1a**. The effective cross-section at the notch was 150x125 mm. The dimensions of the uniaxial tension cube specimens were 150×150×150 mm, with a 35 mm deep and 5 mm thick notch cut along the perimeter, leaving an effective cross-section of 80×80 mm inside the notch, as shown in **Fig. 1b**.

The bending specimens were grouped in samples of 9 replicates and the uniaxial tension specimens were grouped in samples of 10 replicates. The specimens were distributed uniformly in the samples from the batches they were casted. Cubes for additional compression tests were cut off the last 150 mm of the bending beams after testing and 10 replicates were tested for every exposure.

Table 2. Test samples and exposure conditions.

Code name (sample)	Crack width (w) [mm]	Wet cycle (s)	Dry cycle (c)
w0 - s0 - c0 - t0	0 (w0)	Covered (s0)	Covered (c0)
w0 - s0 - c0	0 (w0)	Covered (s0)	Covered (c0)
w15 - s0 - c0	0.15 (w15)	Limewater (s0)	Air (c0)
w30 - s0 - c0	0.30 (w30)		
w15 - s3 - c0	0.15 (w15)	3.5 %-wt. NaCl (s3)	Air (c0)
w30 - s3 - c0	0.30 (w30)		
w15 - s7 - c0	0.15 (w15)	7.0 %-wt. NaCl (s7)	Air (c0)
w30 - s7 - c0	0.30 (w30)		
w15 - s0 - c5	0.15 (w15)	Fresh water (s0)	0.5 %-vol. CO_2 (c5)
w30 - s0 - c5	0.30 (w30)		
w15 - s3 - c5	0.15 (w15)	3.5 %-wt. NaCl (s3)	0.5 %-vol. CO_2 (c5)
w30 - s3 - c5	0.30 (w30)		

2.2 Exposure setup

The exposure environments are described in **Table 2** and comprise wet-dry cycles (i.e. two days each) of cracked specimens and reference specimens.

The samples (i.e. test-groups) were coded as follows: (w) crack width being 0.15 and 0.3 mm, (s) salinity of wet cycle being 3.5% and 7.0%, and (c) carbon dioxide concentration being 0.05 %vol. for ambient exposure and 0.5 %vol for accelerated carbonation exposure.

Two reference scenarios were investigated: i) uncracked samples that were kept covered, which were tested after 56 days (w0s0c0t0) and after one year of curing (w0s0c0); and ii) cracked samples that were exposed to wet-dry cycles of limewater and air for one year (w15s0c0 and w30s0c0). The cracked samples exposed to corrosive environments for one year were subjected to four different exposures, as shown in **Table 2**.

The exposure setup consisted of 10 polyethylene containers of 1 m^3, connected in pairs, providing the possibility of five different exposures, see **Fig. 2**. Each pair of tanks was connected with two membrane pumps that circulated the solution to the tank running the wet cycle, while specimens in the other tank were exposed to the dry cycle in the meantime. The execution of the cycles was set automatically from a controller. The tanks were filled with 500 l of solution and the solution was pumped at a rate of 4.5 l/min, covering the specimens by at least 20 cm of solution.

The drying cycle for the air exposed specimens was provided by a 100 mm fan placed at the centre of the upper side of the tank, with a nominal flow of 93 m^3/h. The fan created an air flow towards four outlets of 100 mm diameter placed at the top four corners, see **Fig. 2**. The air was mixed with the laboratory air and was kept at stable temperature and humidity by the ventilation system of the building. The drying cycle of the carbon dioxide exposure ran through a closed loop and utilized a heat exchanger cooled with two Peltier modules of 60 W to condensate moisture from the air flux before the inlet (see **Fig. 2**); the nominal air flow was also 93 m^3/h.

The specimens were placed vertically with the crack in horizontal position, leaving a minimum separation of 50 mm between specimens to ensure sufficient air circulation inside the tank. The beam specimens were placed with an approx. 5° inclination, leaving the crack mouth facing upwards to facilitate the release of entrapped air inside the crack.

The solution was replaced every two weeks during the first three months of the exposure and then monthly until 6 months of exposure. After that, the solution was replaced every two months. The composition of the solution was checked by means of total dissolved solids (TDS) and pH measurements weekly, the Cl- concentration of the saltwater solutions was measured before replacing the solution by spectrophotometry [33] and was compared against the TDS values registered. The solution of the cracked references (w15s0c0 and w30s0c0) was not replaced, and a 20/80 mixture of saturated sodium and calcium hydroxide (pH = 13.5) was added weekly, keeping the pH value in the solution in the range of 10 – 13.5. Non-chlorinated fresh water (pH = 7.5 – 8.0, $Cl^- < 50$ mg/l, 13 – 15 °dH) was used as exposure media for the specimens subjected to carbon dioxide cycles (w15s0c5 and w30s0c5) and to prepare the saltwater solutions.

The temperature and relative humidity inside the room were monitored, varying in the range 20±2 °C and 50±10 % respectively. The CO_2 concentration in the room and inside the carbon dioxide loop were measured weekly and were 500±100 ppm for the room and 5000±1000 ppm inside the carbon dioxide loop.

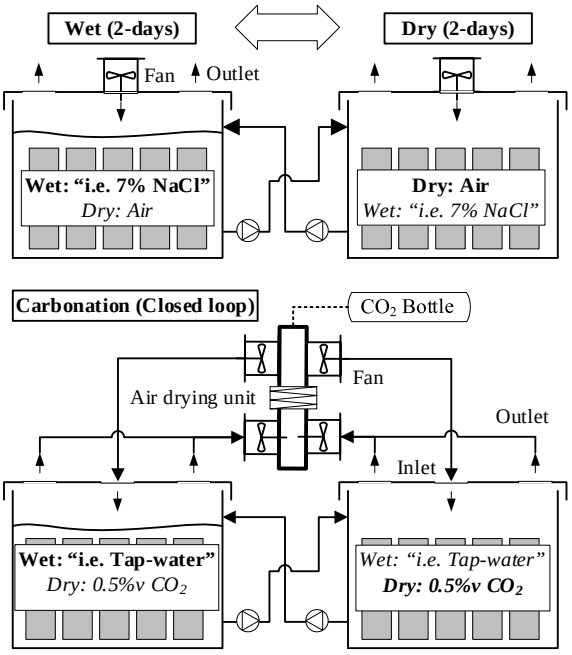

Fig. 2. Exposure setup.

2.3 Mechanical testing

The workflow of the experiments comprised: i) testing of specimens at 56 days; ii) cracking of the specimens at 56 days and preparation for exposure; iii) exposure for one year; iv) testing after one year of exposure.

The three-point bending tests were conducted in a 100 kN capacity flexural test frame, with a span of 500 mm between the supports and a and a central loading rod, according to [30], see **Fig. 3a**. The crack mouth opening displacement at the end of the notch

($CMOD_N$) was measured at the centre of the notch with a clip-gage with a total travel length of 5 mm, connected to two steel pins glued to the face of the notch.

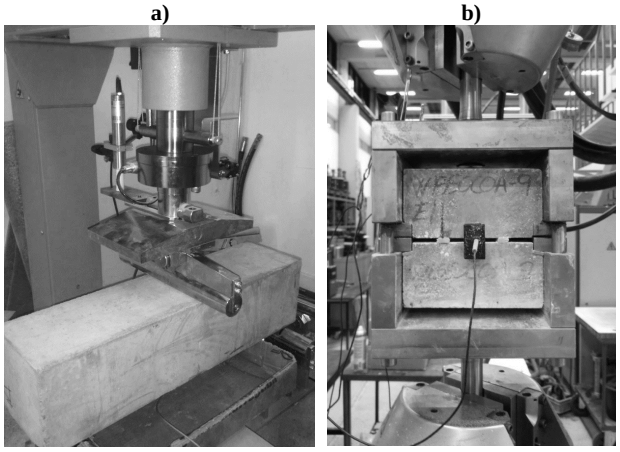

Fig. 3. Test setups, mechanics: a) bending test, b) uniaxial tension test.

The uniaxial tension tests were performed in a 500 kN capacity universal test frame. The uniaxial tension setup consisted of two steel grips hydraulically clamped at the two ends of the test frame, based on the setup in [31]. The test rig transferred the tensile load through the two indentations placed at the sides of the specimen; while the two steel grips were coupled with four sliding steel rails at the corners of the rig to restrain rotation and torsion at the specimen during the test, see **Fig. 3b**. The $CMOD_N$ was measured by two clip gages, each with a total travel length of 5 mm, connected to two steel pins glued to the centre of opposite faces, as shown in **Fig. 3b**.

The compression tests were executed in a 4000 kN capacity compression frame, according to the specifications of EN 12390-3:2012 [34].

The testing of the residual-flexural and -tensile strengths of uncracked reference specimens and tests of cracked specimens was done in accordance to the displacement rates specified in [30], i.e. steps 1 – 3 in **Table 3**. The sampling frequency of the raw data was 100 Hz. After reaching a crack width of 5 mm, the displacement rate was increased up to 1 mm/min, until the specimen was split open completely.

The specimens were cracked before the exposure, at cracks of 0.15 and 0.3 mm calculated at the crack mouth ($CMOD_M$). The loading rates corresponded to the first three steps described in **Table 3**. After the target crack width was reached, the displacement of the crosshead was locked, and the crack was maintained with HDPE inserts inside the notch, then the crosshead was released letting the cracked section load against the plastic inserts. The crack opening at the notch was monitored after releasing the crosshead until the $CMOD_N$ values were constant and the final value was recorded.

After the preparation tests, the opening at the crack mouth for the bending specimens was CMOD = 0.10±0.01 and 0.25±0.03 mm for the specimens cracked at 0.15 mm and 0.3 mm, respectively. The opening at the crack mouth for the uniaxial tension specimens was CMOD = 0.13±0.03 for the specimens cracked at 0.15 mm and CMOD = 0.25±0.04 mm for the specimens cracked at 0.3 mm. Additionally, the crack opening was measured at the notch ($CMOD_N$) with a digital micrometre after the cracking and at the time of testing (i.e. after one year). The comparison of both groups of measurements for any of the specimen types (e.g. bending and uniaxial tension) showed minor variations in the mean $CMOD_N$ during the exposure (e.g. mean variations were approx. 1 %), which were statistically non-significant according to the results of a two-tailed t-test comparing the distributions (e.g. p-values were in the range 0.4 – 0.5). For simplicity, crack widths will refer only to the target crack opening at the crack mouth hereafter, i.e. 0.15 and 0.3 mm CMOD.

Table 3. Load rates.

	Step	Displacement rate (mm/min)	Range
1	Preload	0.10	0 – 100 N
2	Cracking	0.05	0 – 0.1 mm
3	Residual	0.20	0.1 – 5.0 mm
4	Opening	1.00	5.0 – >35 mm

2.3.1 Processing of data from experiments

The load – $CMOD_N$ data from each specimen was first resampled to a resolution of 1 µm. Then, the data was filtered and smoothed, using a 1-dimensional median filter with a block size of 5 and a moving average filter with a block size of 3 respectively.

The opening displacement at the crack mouth (CMOD) for the bending specimens was calculated from the $CMOD_N$ measurements based on inverse calculation of the neutral axis position applying the cracked-hinge model [35]. The CMOD values for the uniaxial tension specimens was calculated as the mean value from the two $CMOD_N$ measurements registered. Hereafter, crack opening values discussed in this paper will only refer to the opening displacement at the crack mouth (CMOD).

The residual-flexural and -tensile strengths were calculated for the bending and uniaxial tension tests, respectively. The calculation of the residual flexural strength was done according to [30], considering that: there is a single crack, that initiates at the notch and propagates perpendicular to the length of the beam, which covers the entire cross-section. The residual tensile strength of the uniaxial tension tests was

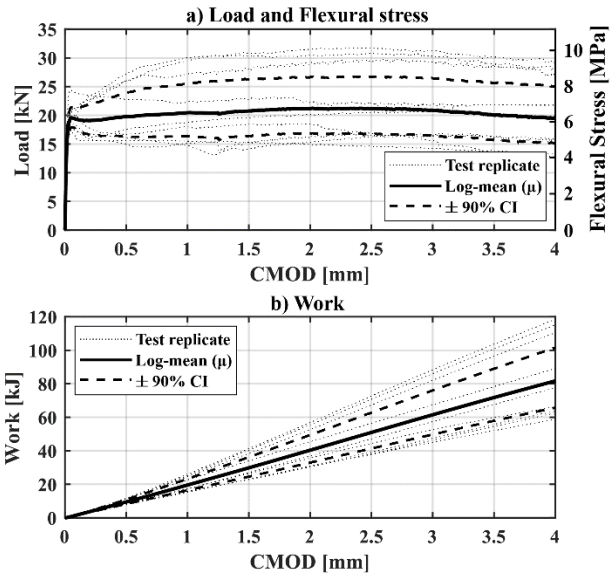

Fig. 4. Data processing and distribution fit for: a) load vs CMOD and flexural stress vs CMOD, b) work vs CMOD.

calculated as the ratio of the load and cross-section, assuming a single crack with a uniform crack width.

The energy absorbed by the system during the test, denoted as "work", was calculated as the integration of the area below the load – CMOD curve for both bending and uniaxial tension specimens.

Finally, a lognormal probability distribution was fitted to each sample of data (i.e. group of specimens), the final filtered data is presented as the mean value of the load at each CMOD value with its upper and lower confidence bounds at 90% confidence interval (90% CI). An example of the filtered data and the fitted curves for the reference bending sample that was tested uncracked (w0s0c0) is shown in **Fig. 4**.

2.4 Visual inspection and fibre counting

After finalizing the mechanical tests, the crack was opened completely, and the fibres crossing the crack were counted and classified according to the degree of corrosion observed, see **Fig. 5**. The fibres marked according to the following categories:

- Level 1, no corrosion (green): uncorroded fibres. Under the assumption that the fibre contributed to the residual mechanical performance of the specimen, see **Fig. 5a**.
- Level 2, minor corrosion (yellow): rust spots at the surface with no visible loss of cross-section. Presuming that there was no impact of corrosion on the fibre contribution to the residual mechanical performance of the specimen, see **Fig. 5b**.
- Level 3, moderate corrosion (orange): presence of pits and small loss of cross-section. Presuming that fibre corrosion had an impact on the fibre contribution to the residual mechanical performance of the specimen, see **Fig. 5c**.
- Level 4, severe corrosion (red): presence of large pits and total or major loss of cross-section. Presuming that the fibre had no contribution to the residual mechanical performance of the specimen, see **Fig. 5d**.
- Fibre rupture, (blue): additional indicator to mark fibres that ruptured instead of pulled-out, see **Fig. 5a** and **Fig. 5c**. Fibre rupture was always assumed for fibres with major corrosion (level 4), see **Fig. 5d**.

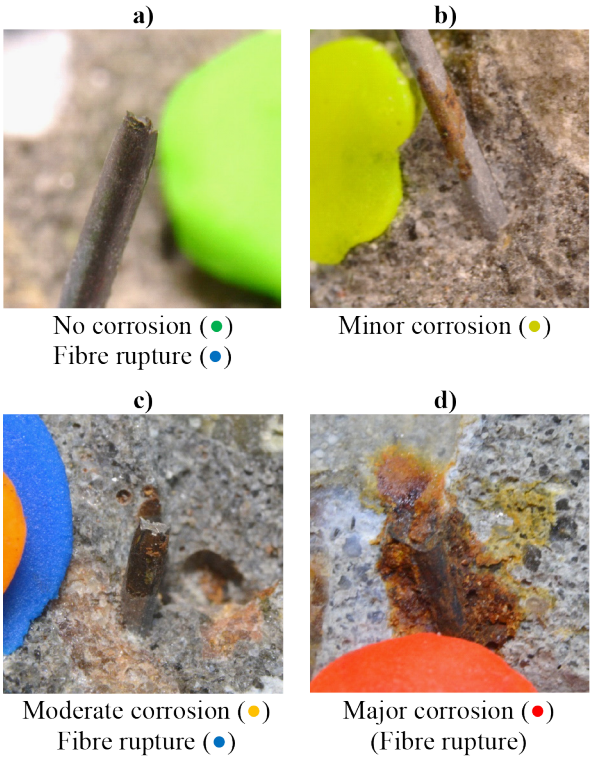

Fig. 5. Visual inspection, fibre classification: a) no corrosion (level 1), b) minor corrosion (level 2), c) moderate corrosion (level 3), d) major corrosion (level 4).

The fibre counting was made by visual inspection, placing a bit of acrylic modelling paste of selected colours at the intersection of each fibre with the crack face, as shown **Fig. 6a**. Afterwards, a high-resolution image of the surface of the open crack was taken and analysed in batches using an image analysis algorithm: the location and classification of each fibre was calculated by means of colour segmentation on the HSV representation of the image and subsequent calculation of the centroids of each point in the mask, see an example in **Fig. 6b**.

Furthermore, colorimetric tests were done on the cracked surface to measure the penetration of free chlorides spraying 0.1N $AgNO_3$; and the carbonation depth inside the crack, spraying a 1-wt.% phenolphthalein solution (pH threshold ≈ 9) and rainbow indicator (pH thresholds in the range: 5-7-9-11-13).

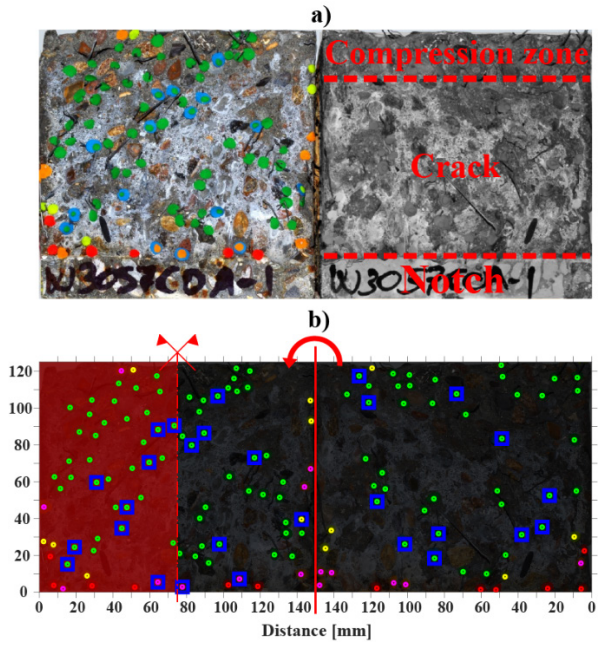

Fig. 6. Visual inspection, fibre counting: a) original cracked specimen with marked fibres and main features of the crack, b) processed data showing symmetry axes and final calculated area (highlighted in red).

The location and degree of corrosion of the fibres are presented in **Sections 3.2.2** and **3.3.2** as discrete contours of the average number of fibres per dm^2 of each group of specimens (i.e. density of fibres), see **Fig. 7**. The contours represent the density of fibres, categorized according to the degree of corrosion damage observed, shown in **Fig. 7a-e**. Furthermore, an additional contour: "severe corrosion" (black) shows the areas with a density of fibres with a significant level of corrosion (i.e. combination of levels 3 and 4), see **Fig. 7f**.

For illustrative purposes, the contours of each group of fibres were combined into one figure for each sample. Therefore, only one representative contour is plotted for each group (e.g. shown highlighted in **Fig. 7a-f**) which is then combined in a single plot (see **Fig. 7g**). The following thresholds were used to plot the contours: the non-corroded fibres (level 1) are plotted for a density over 50 fibres/dm^2, the fibres with corrosion (level 2 – 4) and ruptured fibres are plotted for a density of 10 fibres/dm^2 (see **Fig. 7**b-**f**).

2.5 Statistical analyses

The discussion section includes two main types of statistical analyses: comparison of samples based on the Student's t-test, used in **Sections 4.1, 4.2 and 4.4,** and a regression model used in **Section 4.5**.

For consistency, the results and discussion section will use statistical terminology: The word "specimen" refers to a single sampling unit (i.e. each of the tests executed); the word "sample" refers to a group of specimens exposed to the same environment and cracked at the same CMOD (i.e. each sample is a group of 9 specimens for the bending tests and 10 specimens for the uniaxial tension tests). Discussion will be primarily based on comparison of samples and individual specimens will not be compared hereafter.

2.5.1 Comparison of samples

The comparison of samples, discussed in **Sections 4.1, 4.2 and 4.4**, was performed by the Welch's approximation of the Student's t-test for samples with unequal variance [36]. The test was used to calculate the probability value (p-value) for the null hypothesis (H_0) being true, i.e. the mean value for both distributions being equal. If the p-values for the H_0

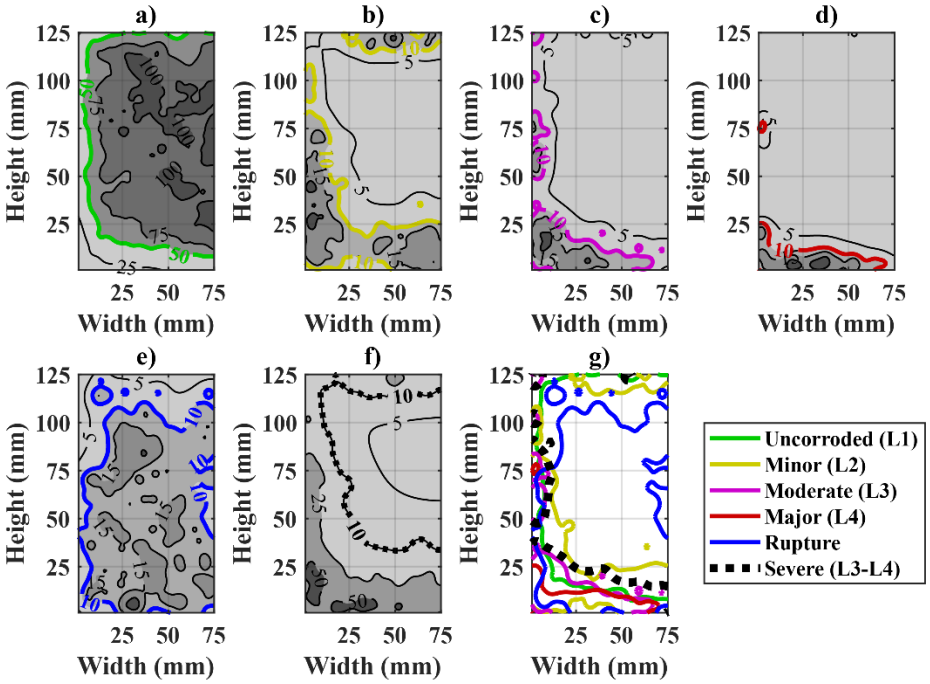

Fig. 7. Representation example of fibre counting results for bending sample (w30s3c0), displaying example of full contour data and selected contours for representation: a) no corrosion (L1); b) minor corrosion (L2); c) moderate corrosion (L3); d) major corrosion (L4); e) fibre rupture; f) severely corroded fibres (L3-L4), g) combined plot. Corrosion levels correspond to the ones described in **Fig. 5**. Contour value are given as fibres/dm^2.

are lower than the level of significance (α), there is an indication that the alternative hypothesis (H_a) might be correct, i.e. the sample reaching significantly higher or lower values than the reference.

$$\begin{aligned} &i + x1*x2 + x1*x3 + x1*x4 + x1*x5 + \\ &x1*x6 + x2*x3 + x2*x4 + x2*x5 + x2*x6 \\ &+ x3*x4 + x3*x5 + x3*x6 + x4*x5 + \\ &x4*x6 + x5*x6 \end{aligned} \quad \textbf{Eq. 1}$$

In **section 4.1**, a two-tailed Welch's T-test is used to test the following alternative hypothesis (H_a): i) the mean values of the compressive strength for the three batches being different among each other, ii) the mean value of the compressive strength for the exposed sample being different than the unexposed reference tested at 56 days, i.e. s0c0t0. The statistical significance level was set to α = 10%.

In **section 4.2**, the mean values of the work – CMOD curves for the bending and uniaxial tension samples are compared to the references by a one-tailed Welch's T-test. The following alternative hypotheses (H_a) were tested: i) the probability of the mean value of the sample being smaller than the reference and ii) the probability of the mean value of the sample being greater than the reference. The statistical significance level was set to various levels: i.e. α = 5, 15 and 25%.

In **section 4.4**, the mean value of the ratio of ruptured fibres is compared to the mean value of the uncorroded reference (level 1) by a two-tailed Welch's T-test with a statistical significance level of α = 10%.

2.5.2 Regression model

The effect of fibre damage and crack width on the mechanical performance, discussed in **section 4.5**, was evaluated based on a multiple linear regression analysis. The analysis covers the contribution of the fibre content, fibre damage (i.e. corrosion and rupture) and crack width to the toughness of the material, expressed as the total work at a crack opening 0.5 – 4.0 mm in bending and tension.

The regression model covers the main effects and 2-factor interactions for the following variables: fibre content (x1), ratio of corroding fibres for levels 2 – 4 (x2-4), ratio of ruptured fibres (x5) and crack width (x6). The initial model is described in **Eq. 1** in Wilkinson notation [37].

The independent and response variables were standardized. The predictor coefficients were fitted to the data using robust regression, i.e. least trimmed squares (LTS) with a bisquare weight function for the residuals. The model was reduced iteratively by backwards component selection applied to the interaction terms (threshold α = 5%).

3. Experimental results

The experimental results are described in this section separated in compression tests, bending tests and uniaxial tension tests. The results of the two latter are divided into mechanical performance results and fibre counting results, in order to evaluate and compare the extent and severity of fibre corrosion depending on the crack width and exposure conditions and identify its relation to changes in the mechanical performance of the exposed SFRC.

3.1 Compression tests

The compression test results after one year of exposure are presented in **Fig. 8**, including the unexposed samples (w0s0c0t0 and w0s0c0) which are presented in **Fig. 8a** as "REF". The results showed a significant scatter within each sample, with a standard deviation in each sample close to 8 MPa. The large deviation was related to production variations between the three batches (batch A-C), as shown in **Fig. 8b**. The mean values of the samples grouped by exposure are similar to each other, within 72 – 75 MPa, as shown in **Fig. 8a** and indicate negligible change of the compressive strength comparing the exposures. However, there is indication of skewness on each sample group, as observed in the median values, that lie away from the mean values, see **Fig. 8a**.

3.2 Bending tests

3.2.1 Mechanical performance

The results from the bending tests for reference and cracked samples are presented as the residual-

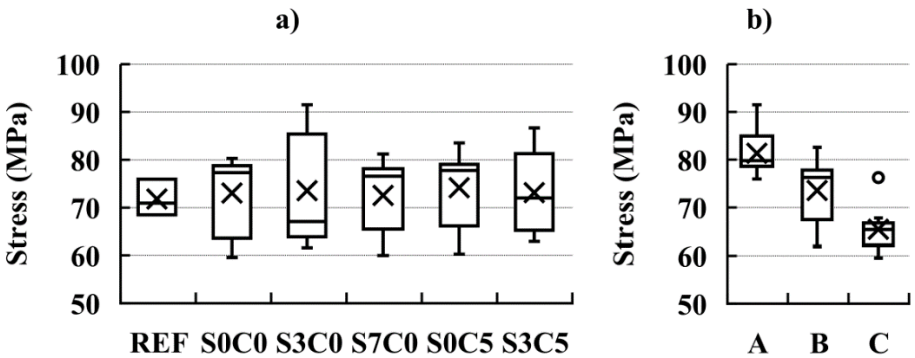

Fig. 8. Compression tests results, grouped by: a) exposure, b) batch. The median value is shown as "—", the mean (arithmetic) value is shown as "X" and outliers are shown as "o". The "REF" group comprises the combined results from the unexposed reference samples tested after 56 days and one year.

strength (i.e. stress vs CMOD curves) and as toughness (i.e. work – CMOD curves) in **Fig. 9** and **Fig. 10**, respectively. Solid lines present the mean values (μ), while the dotted lines show the upper and lower bounds of the 90% confidence interval (90% CI) for the mean value.

From the results presented in **Fig. 9a** and **Fig. 10a**, respectively, it can be seen that the mean value and confidence bounds for strength and work of the uncracked references at 56 days and one year are close to each other, indicating limited strength and toughness variation after one year.

The results for the beams cracked at CMOD = 0.15 mm show that the exposed samples reach higher or overlapping mean strength (**Fig. 9a**) and work values (**Fig. 10a**), relative to the uncracked reference samples. There is a significant increase in the spread of the confidence bounds observed for the cracked samples exposed to carbonation (s0c5 and s3c5). The rest of the samples presented a spread of the mean similar to the uncracked references.

The results for samples with a larger crack width, i.e. CMOD = 0.3 mm, show that the mean residual strength (**Fig. 9b**) and work curves (**Fig. 10b**) are generally similar to or above the uncracked references. Except for the sample exposed to 3.5%-wt. NaCl (w30s3c0), which dropped significantly relative to its 0.15 mm counterpart. There is also a slight drop in the mean residual strength values for the samples exposed to carbonation (i.e. w30s0c5 and w30s3c5) in addition to a reduction of the spread of the confidence interval of the mean compared to their counterparts cracked at 0.15 mm.

The mean values of the exposed cracked references (w15s0c0 and w30s0c0) are generally above the rest of the exposed samples, see **Fig. 9** and **Fig. 10**. Except for the 0.15 mm sample exposed to 3.5% NaCl (w15s3c0), which reached values similar to the cracked reference (w15s0c0), see **Fig. 9a** and **Fig. 10a**

3.2.2 Visual inspection and fibre count

The results from the fibre counting of the bending specimens are presented in **Fig. 11**, as discrete contours of the total density of fibres for each sample, i.e. the mean number of fibres per m^2 of each group of specimens. The contours describe the density of fibres, categorized according to the degree of damage: (level 1, green) no corrosion, (level 2, yellow) minor corrosion, (level 3, magenta) moderate corrosion, (level 4, red) major corrosion and (blue) fibre rupture.

The original surface of the crack (150×125 mm) has been divided by its vertical symmetry axis, showing

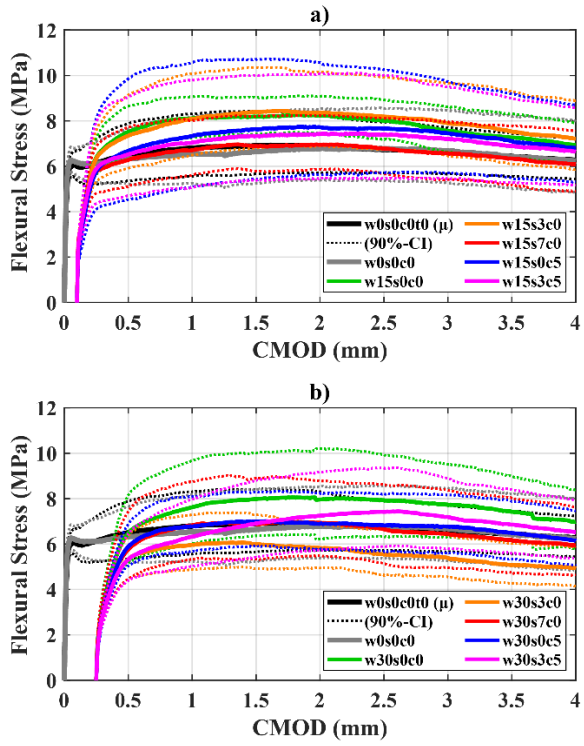

Fig. 9. Bending test, Stress-CMOD plot for samples: a) cracked at 0.15 mm, b) cracked at 0.3 mm.
Full lines represent the log-mean value (μ) of the sample and dotted lines represent the upper- and lower- confidence bounds at 90% CI. Sample names correspond to code names described in Table 2.

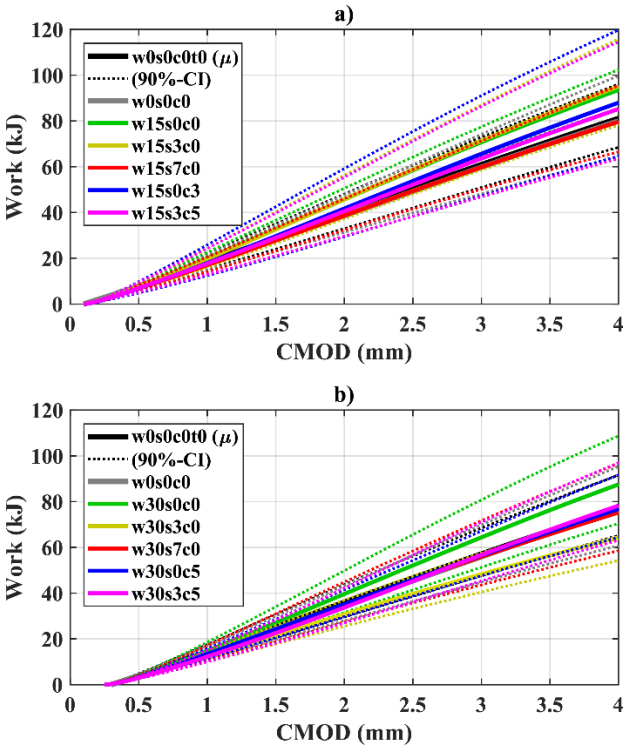

Fig. 10. Bending test, Work-CMOD plot for samples: a) cracked at 0.15 mm, b) cracked at 0.3 mm.
Full lines represent the log-mean value (μ) of the sample and dotted lines represent the upper- and lower- confidence bounds at 90% CI. Sample names correspond to code names described in Table 2.

a surface of 75×125mm. The edges exposed to the solution are marked with a dotted red line (lower, left and upper axis). Furthermore, the crack width is shown at the right axis for the cracked samples, including the position of the neutral axis from the top of the sample; calculated at 35 mm and 25 mm for the 0.15 mm and 0.3 mm crack width samples respectively, see **Fig. 11b-k**.

For illustrative purposes, the contours are shown with the following thresholds: the non-corroded fibres (level 1) are plotted for a density over 50 fibres/dm^2, corroded fibres (level 2 to level 4) and ruptured fibres are plotted for a density of 10 fibres/dm^2. An additional contour, plotted as a black dashed line, shows the areas with a density of fibres with a "severe" level of corrosion (i.e. combination of levels 3 and 4) over 10 fibres/dm^2. Additionally, the uncracked reference (w0s0c0) is presented in **Fig. 11a**, with the following thresholds for the total density of fibres (level 1) and ruptured fibres: 50 and 100 fibres/dm^2.

The uncracked reference sample (w0s0c0) presents a homogeneous fibre distribution, with a density of fibres between 50 – 100 fibres/dm^2. The density of ruptured fibres is 5 – 25 fibres/dm^2 and is higher at the centre and lower end of the sample (**Fig. 11a**). For the rest of the cracked samples, the density of non-corroded fibres throughout the whole sample area is in the same range, i.e. 50 – 100 fibres/dm^2, and decreases at the exposed edges. The cracked reference samples exposed to limewater (w15s0c0 and w30s0c0) show fibres with minor signs of corrosion (level 2) at the outer 10 mm, regardless of the crack width (**Fig. 11b-c**). Ruptured fibres appear uniformly distributed throughout the crack.

The samples exposed to chlorides are presented in **Fig. 11** for these exposures: i) 3.5wt.% NaCl solution (w15s3c0 and w30s3c0), shown in **Fig. 11d-e**; ii) 7.0wt.% NaCl solution (w15s7c0 and w30s7c0), shown in **Fig. 11f-g**; and iii) carbon dioxide and 3.5wt.% NaCl solution (w15s3c5 and w30s3c5), shown in **Fig. 11d-e**. These show a similar spread of the contour of minor corrosion (level 2) and severe corrosion (levels 3 – 4), in the range 10 – 25 mm inside the crack, decreasing both for smaller crack widths and lower NaCl concentrations.

The samples exposed to carbon dioxide and fresh water (w15s0c5 and w30s0c5) displayed a limited extent of corrosion into the crack (**Fig. 11h-i**); fibres with minor corrosion (level 2) were found at the outermost 10 – 20 mm of the crack and fibres presenting sever corrosion (levels 3 – 4) were found at the outermost 5 – 10 mm of the crack, increasing for the larger crack width. However, there is no clear evidence of a larger share of ruptured fibres in the corrosion front.

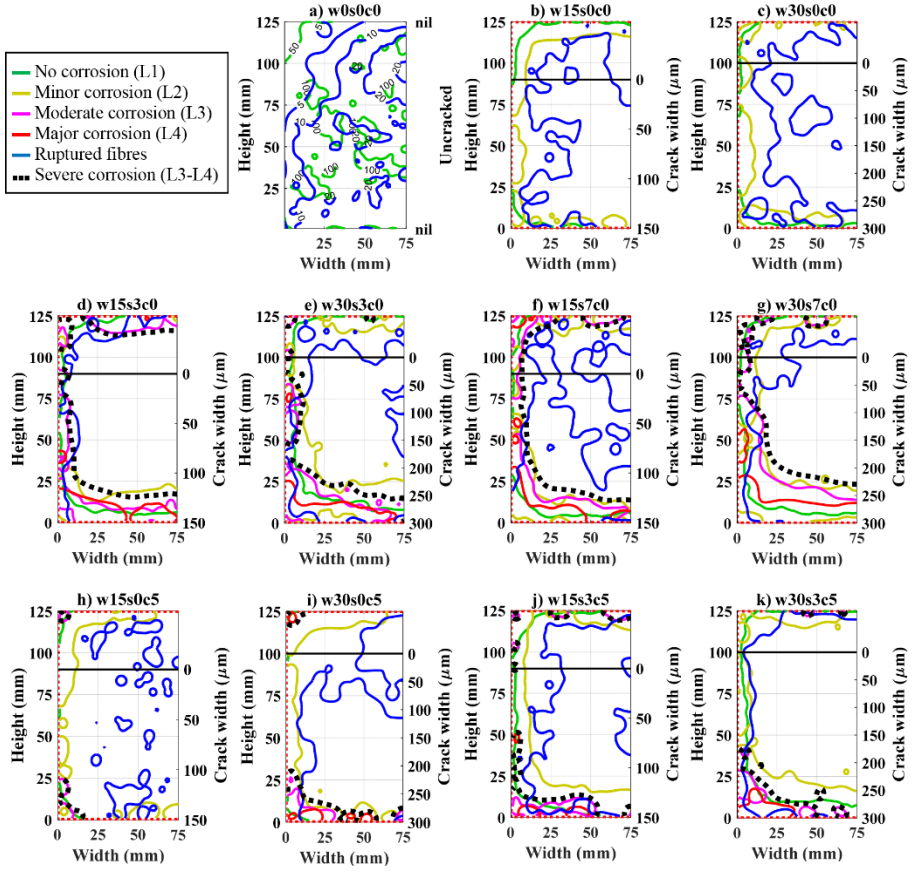

Fig. 11. Fibre counting for bending tests, contour plots for: a) uncracked reference, w0s0c0; b,c) cracked reference, s0c0; d,e) 3.5 %-wt. NaCl exposure, s3c0; f,g) 7.0 %-wt. NaCl exposure, s7c0; h,i) carbon dioxide and fresh-water exposure, s0c5; j,k) carbon dioxide and 3.5 %-wt. NaCl exposure, s3c5.

The inner crack surface of the exposed samples was covered by a white precipitate, which was not present at the outer 5 – 15 mm of the crack for the 0.15 and 0.3 mm CMOD, respectively. The pH in the vicinity of the precipitate was in the range of 9 – 10, dropping below the phenolphthalein indicator threshold at the outer areas not covered by the precipitate, i.e. pH in the range of 7 – 9 measured with rainbow indicator. Deeper inside the crack, areas still covered by the precipitate showed pH values above the higher threshold of the rainbow indicator, i.e. pH > 13.

Free chlorides were identified using the $AgNO_3$ colorimetric test inside most of the original crack surface for the samples cracked at 0.3 mm CMOD exposed to NaCl solution, i.e. excluding the compression zone. The free chloride profile inside the crack surface of samples cracked at 0.15mm CMOD was irregular and penetrated in the range 30 – 50 mm inside the crack, increasing with a higher NaCl concentration in the solution.

3.3 Uniaxial tension tests

3.3.1 Mechanical performance

The results from the uniaxial tension tests for reference and cracked samples are presented as the residual-strength (i.e. stress vs CMOD curves) (**Fig. 12**) and toughness (i.e. work – CMOD curves) (**Fig. 13**), correspondingly to their bending counterparts presented above. The reference values for the uncracked samples are only plotted for the sample tested at 56 days (i.e. w0s0c0t0), since there is no significant difference relative to the sample tested at one year (i.e. w0s0c0), as observed in the bending test.

Results presented in **Fig. 12a** and **Fig. 13a** for the samples cracked at 0.15 mm CMOD show higher mean strength values up to a CMOD of 2.5 – 3.5 mm and higher work values, relative to the uncracked reference samples (w0s0c0t0). Moreover, the results indicate that the confidence bounds of the mean observed for the cracked samples is similar to the uncracked references.

The results for samples cracked at 0.3 mm CMOD, show that in general, the mean strength (**Fig. 12b**) and work responses (**Fig. 13b**) decrease relative to their 0.15 mm counterparts (**Fig. 12a** and **Fig. 13a**); there is a significant drop in the performance of the cracked reference samples (w30s0c0) compared to the samples cracked at 0.15 mm CMOD (w15s0c0).

Except for the cracked reference (w30s0c0), the mean strength of the samples cracked at 0.3 mm CMOD are above the uncracked reference (w0s0c0t0) up to a CMOD = 1.5 – 2.5 mm but produce significantly lower values at the end of the tail, i.e. CMOD = 4.0 mm (**Fig. 12b**). The mean work curves for the

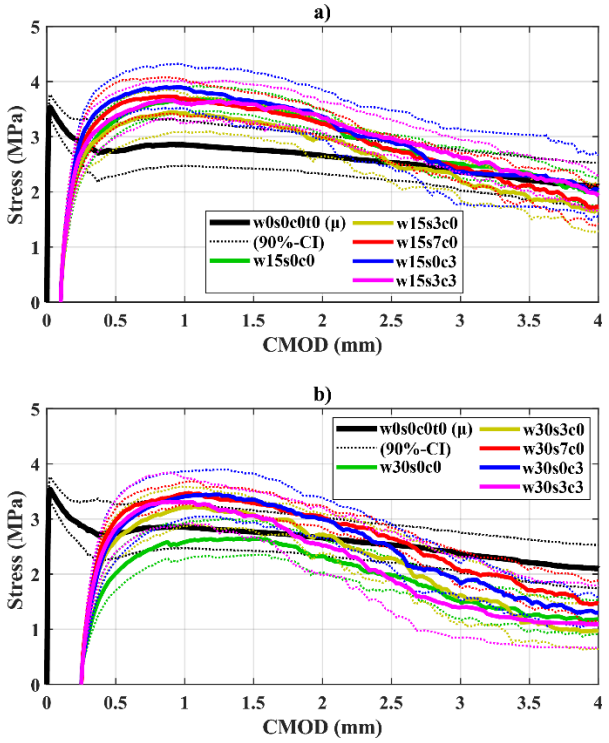

Fig. 12. Uniaxial tension test, Stress-CMOD curves for samples: a) cracked at 0.15 mm, b) cracked at 0.3 mm. Full lines represent the log-mean value (μ) of the sample and dotted lines represent the upper- and lower- confidence bounds at 90% CI. Sample names correspond to code names described in Table 2.

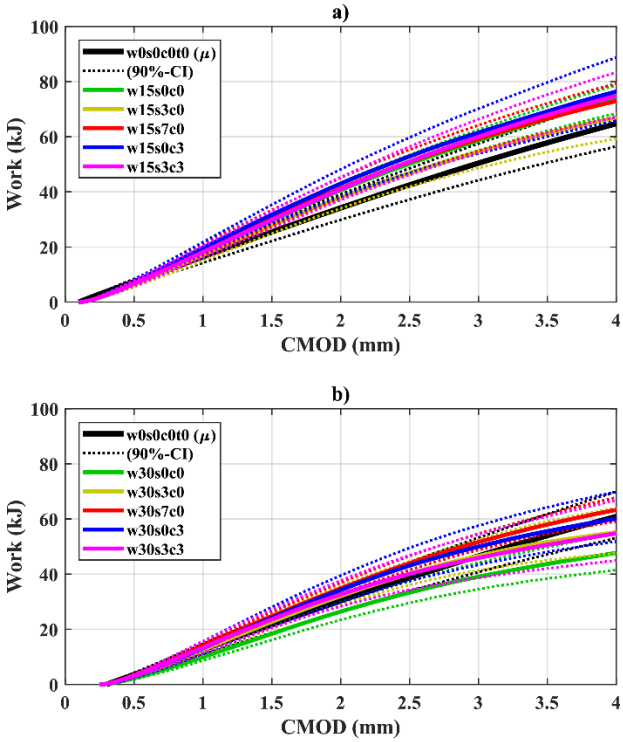

Fig. 13. Uniaxial tension test, Work-CMOD plot for samples: a) cracked at 0.15 mm, b) cracked at 0.3 mm. Full lines represent the log-mean value (μ) of the sample and dotted lines represent the upper- and lower- confidence bounds at 90% CI. Sample names correspond to code names described in Table 2.

exposed samples cracked at 0.3 mm are within the 90% CI the mean of the uncracked reference (**Fig. 13b**), except for the cracked reference (w30s0c0) which is significantly lower.

The mean value of the exposed cracked reference at 0.15 mm CMOD (w15s0c0) lies within the rest of the exposed samples for the same crack width, see **Fig. 12a** and **Fig. 13a**, considering the confidence interval of the mean. In the case of the sample cracked at 0.3 mm CMOD, the cracked reference (w30s0c0) shows strength values below the rest of the samples (**Fig. 13a**), up to CMOD values of 2.0 – 2.5 mm, but shows similar strength values at the end of the tail. The cracked reference (w30s0c0) produces lower work values, compared to the rest of the cracked samples, which show a similar mean performance within the 90% CI, see **Fig. 13b.**

3.3.2 Visual inspection and fibre count

The results of the fibre counting for the uniaxial tension tests are shown in **Fig. 14**, as contours of the mean fibre density per sample for the levels of fibre corrosion described in the previous section for the bending samples. The surface of the crack, initially 80×80 mm, was divided by its symmetry axis, showing a crack surface of 40×40mm with a diagonal symmetry axis crossing the area from bottom-left to top-right. The exposed edges are marked with dotted red lines (left and lower axis).

For illustrative purposes, the contours show regions with a density of fibres over 10 fibres/dm^2 for each group, except for the uncorroded fibres (level 1) that are plotted for a density of 50 fibres/dm^2. The plots follow the same scheme as previously described for the bending samples. The crack width is assumed constant throughout the whole area, i.e. 0.15 mm and 0.3 mm.

The uncracked reference sample presents a homogeneous fibre distribution with a fibre density between 50 – 100 fibres/dm^2. The density of ruptured fibres lies around 10 fibres/dm^2 and is uniformly distributed throughout the cross-section of the crack, see **Fig. 14a**. The cracked reference samples show fibres with minor corrosion (level 2) at the outer 10 – 30 mm of the crack, increasing for the larger crack width, see **Fig. 14b-c**. There are no fibres presenting a critical level of corrosion (levels 3 – 4) and ruptured fibres seem uniformly distributed throughout the crack.

The samples exposed to chlorides are presented in **Fig. 14** for these exposures: i) 3.5wt.% NaCl solution (w15s3c0 and w30s3c0), shown in **Fig. 14d-e**; ii) 7.0wt.% NaCl solution (w15s7c0 and w30s7c0), shown in **Fig. 14f-g**; and iii) carbon dioxide and 3.5wt.% NaCl solution (w15s3c5 and w30s3c5), shown in **Fig. 14d-e**. These show a similar spread of the contour of minor corrosion (level 2), that extends from the exposed edges to the full depth of the crack. Fibres presenting critical corrosion are found up to 10 – 25 mm inside the crack, decreasing both for smaller crack widths and lower NaCl concentrations. The corroding areas show a slightly larger share of rupturing fibres.

The samples exposed to carbon dioxide and fresh water (w15s0c5 and w30s0c5) displayed a moderate extent of corrosion into the crack (**Fig. 14h-i**); fibres with minor corrosion (level 2) were found at the outermost 10 – 20 mm of the crack for the sample

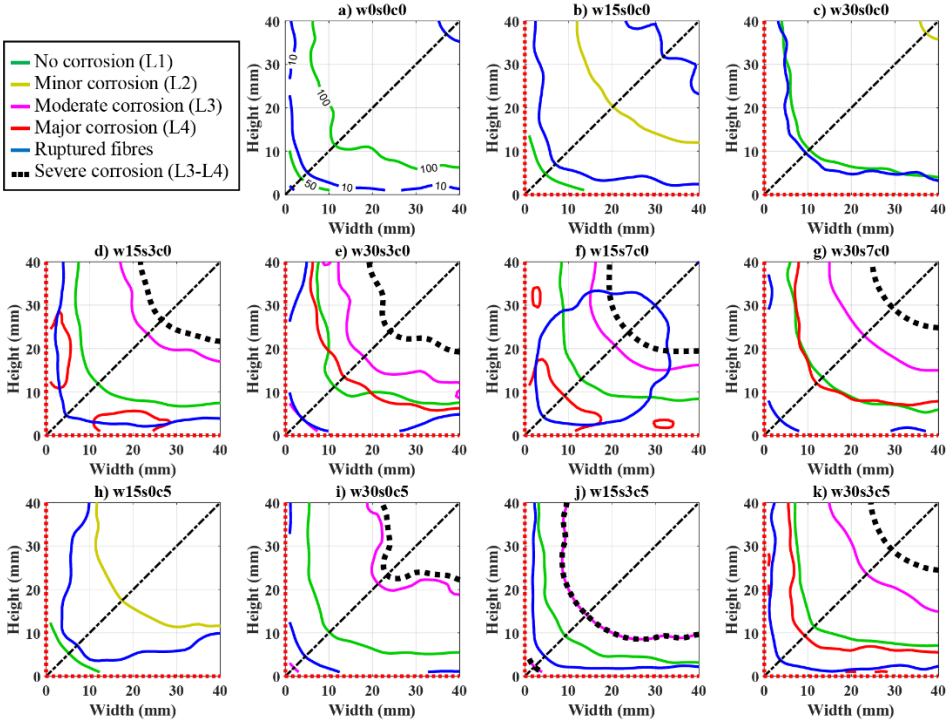

Fig. 14. Fibre counting for uniaxial tension tests, contour plots for: a) uncracked reference, w0s0c0; b,c) cracked reference, s0c0; d,e) standard chloride exposure, s3c0; f,g) high chloride exposure, s7c0; h,i) carbon dioxide and standard chloride exposure, s0c5; j,k) carbon dioxide and standard chloride exposure, s3c5.

cracked at 0.15 mm CMOD, but covered the whole crack in the sample cracked at 0.3 mm. Fibres presenting sever corrosion (levels 3 – 4) were only found at the outer 20 mm of the crack in the sample cracked at 0.3 mm. Whereas, there is no clear evidence of a larger share of ruptured fibres at the outermost part of the crack.

The same white precipitate found in the bending samples was also found at the inner crack faces of all the exposed specimens. The precipitate faded at the outer 10 – 20 mm of the crack, for the 0.15- and 0.3-mm cracks respectively. The pH at the precipitate was in the range 9 – 10 and dropped below the phenolphthalein indicator threshold at the areas not covered by the white deposit, i.e. pH in the range 7 – 9 measured with rainbow indicator.

Free chlorides were identified (i.e. by the $AgNO_3$ spray test) inside the whole crack surface for the samples cracked at 0.3 mm cracks exposed to NaCl solution. While ingress inside samples cracked at 0.15mm was irregular and was found from 20 mm up to full penetration inside the crack, depending on the NaCl concentration of the solution.

4. Discussion

The discussion focuses on five aspects: i) the impact of the exposure conditions on the elastic properties of uncracked SFRC; ii) the impact of the exposure conditions on the toughness of cracked SFRC; iii) the impact of the exposure on fibre corrosion; iv) the correlation between fibre corrosion and fibre rupture; v) the correlation between fibre damage and the residual mechanical performance of the cracked SFRC.

4.1 Impact of exposure on the strength of uncracked SFRC

The compressive strength of the bulk concrete was not influenced by the exposure conditions, compared to the unexposed and exposed references, based on the results from the compression tests presented in **Fig. 8**. The mean ($\bar{x}$), and variations of the mean ($\Delta\bar{x}$) and median ($\Delta\tilde{x}$) values are presented in **Table 4**, the table includes the probability value for the null hypothesis (H_0) for a two-tailed Welch's t-test.

There is limited variation of the mean values, when comparing the reference exposed samples (s0c0) and unexposed reference tested at 56 days w0s0c0, the high p-value of the t-test supports the observation. The mean value for the rest of the exposures show no significant variation relative to the exposed reference s0c0, supported by the large p-values reported. The large variations observed in the median can be explained by the differences in the mean compressive strength between the three batches, confirmed as significant by the t-test (**Table 4**).

The tensile strength of the matrix was not measured on uncracked exposed specimens in this study. However, the abovementioned discussion for compressive strength results may be translated to the tensile strength of the uncracked matrix; under the assumption that compressive and tensile strength test results for SFRC are correlated [38].

The reported results confirm the observations of previous research [19,39,40], substantiating that fibre corrosion in uncracked SFRC affects surface fibres (i.e. fibres at the outer 0.1 – 1.0 mm depending on the w/c ratio [6]) and does not have a significant impact on the strength of the uncracked concrete matrix, i.e. there is no micro-cracking or spalling of matrix induced by fibre corrosion that would affect the strength of the uncracked concrete matrix. Furthermore, there is no indication that microstructural changes in the matrix at the surface due to exposure (e.g. chloride ingress, carbonation and leaching) have a significant impact on the strength of the bulk matrix.

Table 4. Comparison of compressive strength results

Sample	$\bar{x}$ (MPa)	$\Delta\bar{x}$ (MPa)	$\Delta\tilde{x}$ (MPa)	p-value (H_0) (-)
s0c0 (REF)	73.06	1.28	6.37	0.676
s3c0 (s0c0)	73.56	0.50	-10.19	0.909
s7c0 (s0c0)	72.54	-0.52	-0.71	0.865
s0c5 (s0c0)	74.18	1.11	0.45	0.728
s3c5 (s0c0)	73.11	0.05	-5.31	0.988
A (C)	81.36	+15.94	+14.40	0.000
B (A)	73.56	-7.80	-3.51	0.000
C (B)	65.42	-8.15	-10.88	0.000

Notes: *The names in brackets "(_)" in the sample column denote the reference sample used for the comparison and calculation of $\Delta\bar{x}$, $\Delta\tilde{x}$ and p-value for each of the samples.*

4.2 Impact of exposure on the residual mechanical performance of cracked SFRC

The residual mechanical performance of cracked SFRC was affected by the different exposure conditions, as shown in **Fig. 9-10** for the bending samples and **Fig. 12-13** for the uniaxial tension samples.

The toughness of the cracked material was described by the total energy absorbed during the tests, i.e. calculated as the total work, see **Fig. 15**. The total work was calculated as the cumulative integral of the load-CMOD curve in the range CMOD = 0.5 – 4.0 mm.

The uncracked reference sample tested at 1-year (w0s0c0) showed similar total work values relative to

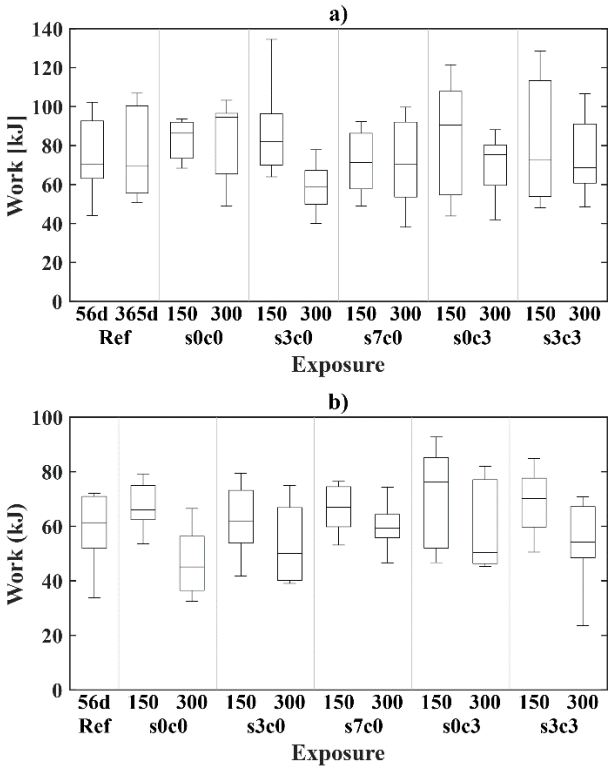

Fig. 15. Boxplot, total work for the uncracked reference and exposed samples for: a) bending test and b) uniaxial tension test. Sample names correspond to code names described in Table 2.

the uncracked reference sample tested at 56 days (w0s0c0t0), see **Fig. 15a**. This indicates a limited development of the total toughness of the unexposed uncracked material over the time investigated.

The total work calculated for the cracked references (s0c0) show overall higher mean values compared to the uncracked references (Ref), both for samples in bending and uniaxial tension, see **Fig. 15a-b**. However, the uniaxial tension reference sample cracked at 0.3 mm CMOD (**Fig. 15b and Fig. 17a**) presents a substantial decrease in the mean toughness relative to the uncracked reference. The visual inspection of the cracked specimens in this sample showed that in this case there were no traces of the precipitate observed in all the other samples, but instead a loose lime precipitate was found inside the crack.

The samples exposed to chlorides and carbonation showed an overall trend of lower mean toughness values for samples cracked at 0.3 mm compared to the samples cracked at 0.15 mm, for both bending (**Fig. 15a**) and uniaxial tension samples (**Fig. 15b**); except for the bending sample exposed to 7% NaCl (w30s7c0), that showed comparable values to its counterparts cracked at 0.15 mm. However, the large spread of the results complicates the direct comparison of the data.

The mean values of the work-CMOD curves for the bending and uniaxial tension samples are compared to the references by a one-tailed Welch's T-test, as shown in **Fig. 16** and **Fig. 17** respectively. The graph shows the probability (p-value) of the null hypothesis (H_0) for the following alternative hypotheses (Ha): a) the probability of the mean value of the sample being smaller than the reference (left tail); b) the probability of the mean value of the sample being greater than the reference (right tail).

The distribution of the work-CMOD curves of the exposed samples are compared to the uncracked reference tested at 56days (i.e. w0s0c0t0), see **Fig. 16a** and **Fig. 17a**, and to the cracked reference (i.e. w15s0c0 and w30s0c0), see **Fig. 16b** and **Fig. 17b**. Significance thresholds (α) of 95, 85 and 75% for the alternative hypotheses (Ha) are considered, leading to p-values of 0.05, 0.15 and 0.25 for the null hypothesis (H_0), displayed as dotted horizontal lines. For consistency, the term "significant" is reserved to refer to the statistical significance of the probability (p-values) of the sample mean being higher or lower than the reference, compared to the significance (α) values described above, for example: p-values in the range 0.25 – 0.75 correspond to non-significant variations in the mean.

A more detailed analysis to the evolution of the toughness over time for the uncracked sample tested after 1-year (w0s0c0), showed that significant toughness variations over time were only registered at the first 0 – 0.1 mm CMOD, i.e. within elastic range and low deformations (**Fig. 16a**). The significant

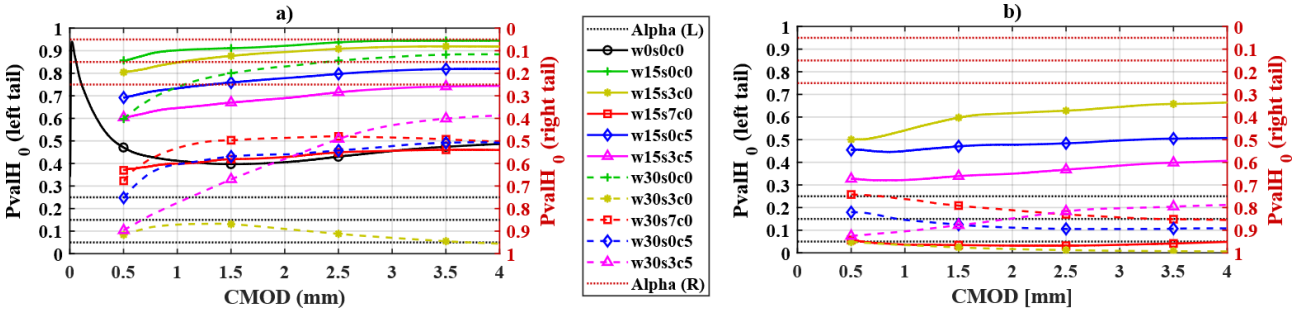

Fig. 16. T-test, comparison of bending samples to: a) uncracked reference at 56 days, b) cracked reference exposed to limewater (S0C0).

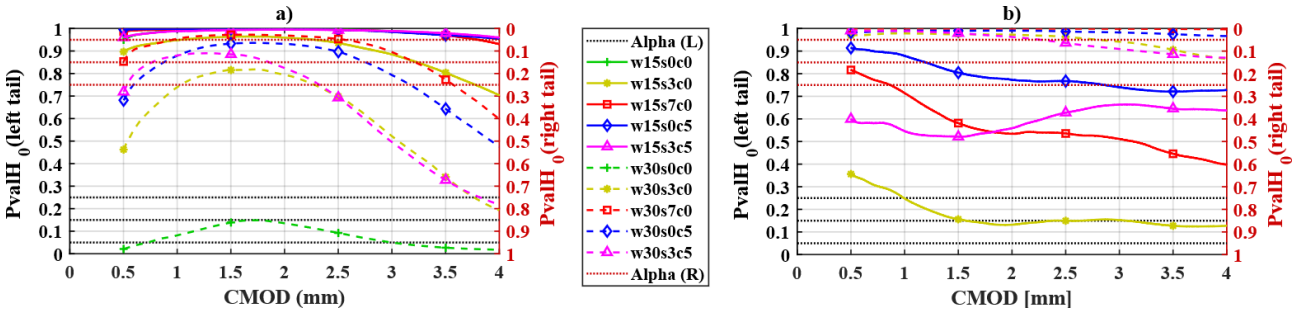

Fig. 17. T-test, comparison of uniaxial tension samples to: a) uncracked reference at 56 days, b) cracked reference exposed to limewater (S0C0).

increase in toughness was attributed to additional strength development of the uncracked matrix with time (i.e. the mean tensile strength increased approx. 1.5%). Yet, such slight development of the tensile strength had no implications in the analysis of the residual structural performance of the cracked material, e.g. regarded as the performance at CMOD values in the range 0.5 – 4 mm in this paper.

The samples cracked at 0.15 mm generally reached significantly higher toughness values through the whole CMOD range compared to the uncracked reference (Ref), see **Fig. 16a** and **Fig. 17a**. Except for the bending sample exposed to 7 -wt.% NaCl (w15s7c0), that showed non-significant variation of the work relative to the uncracked reference (**Fig. 16a**).

Comparison of the samples exposed to chlorides and carbonation cracked at 0.15 mm to their corresponding references exposed to limewater (w15s0c0) showed non-significant variation in the performance; except for the bending sample exposed to 7 -wt.% NaCl (w15s7c0) and the uniaxial tension sample exposed to 3.5 -wt.% NaCl (w15s3c0), that showed significantly lower values compared to their references (w15s0c0), see **Fig. 16b and Fig. 17b**.

The bending samples cracked at 0.3 mm (see **Fig. 16a**) generally showed non-significant toughness variations compared to the uncracked reference (Ref); except for the sample exposed to limewater (w30s0c0) and the one exposed to 3.5 -wt.% NaCl (w30s3c0) that respectively showed a significant increase and decrease of toughness, relative to the uncracked reference (Ref). Uniaxial tension samples cracked at 0.3 mm (**Fig. 17a**) generally showed a significant increase in the toughness at CMOD values in the range 1 – 3 mm, which decreased at larger CMOD values.

Comparison of the bending samples exposed to chlorides and carbonation cracked at 0.3 mm to their corresponding references exposed to limewater (w30s0c0) showed significantly lower toughness values over the whole CMOD range (see **Fig. 16**); which may be attributed to fibre corrosion. While, uniaxial tension samples reached significantly higher toughness values over the whole CMOD range; which in this case is attributed to the unexpectedly low toughness measured in the uniaxial tension sample exposed to limewater (w30s0c0), already discussed.

The discussion above indicates that there is a significant increase in the toughness of cracked SFRC exposed to wet-dry cycles; especially at small crack openings (i.e. CMOD < 2.5 mm) and for a small initial crack width (i.e. 0.15 mm CMOD). Whereas, there is no indication that fibre corrosion may lead to critical detriment to the residual performance of the material. These observations are in agreement with previous research investigating the performance of cracked SFRC exposed to chlorides [13,22–25] and carbon dioxide [14,22], that had identified increases in the residual performance of cracked SFRC at narrow cracks (i.e. crack width < 0.2 mm). Yet, some of these publications show a significant decrease in the toughness at larger deformations (i.e. equivalent CMOD > 2 – 2.5 mm) [18,22].

Visual inspection of the specimen surface during the tests revealed that, for 30 – 50% of the specimens composing the exposed samples, the original crack opened during the first 0.5 mm CMOD but additional branching and formation of new cracks at adjacent regions occurred at larger CMODs, as shown in **Fig.**

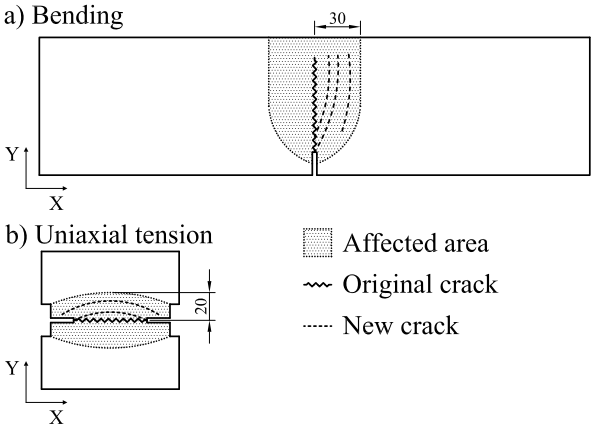

Fig. 18. Typical crack path with additional branching for exposed specimens: a) bending, b) uniaxial tension. Dotted lines represent the additional cracks forming, describing the various crack patters observed.

18. The branching and additional cracking in the bending specimens appeared within a region of 20 – 30 mm around the original crack, as shown in **Fig. 18a**. Additional cracking in uniaxial tension specimens occurred in a region up to 10 – 20 mm from the original crack plane, see **Fig. 18b**.

This phenomenon was not observed in uncracked reference samples and was more prominent in the bending samples cracked at 0.15 mm CMOD. This description correlates to the higher loads registered during the testing of cracked samples, see **Fig. 9** and **Fig. 12**, and may explain the larger scatter in the results of the cracked samples relative to the uncracked references. Insight on the topic suggests an increase of the fibre-matrix bond, as described in [5], leading to localized stresses near the crack larger than the tensile strength of the adjacent uncracked matrix. Furthermore, the formation of new cracks complicates the analysis of the mechanical performance for larger deformations, i.e. at CMOD values > 1 – 2 mm, since the test measures a combination of the residual strength of the exposed crack and the uncracked material. Similar behaviour was reported for cracked round panels (i.e. crack width < 0.1 mm) immersed in seawater and exposed to rainwater for 2 years [18].

4.3 Impact of exposure on fibre damage

The counting and classification of the fibres crossing the crack is presented as the percentage of fibres for each of the levels described in **Fig. 5** relative to the depth inside the crack, calculated from the lower exposed edge of the processed data described in **Fig. 11** for the bending samples and **Fig. 14** for the uniaxial tension samples. The mean values are plotted in **Fig. 19** for the bending samples and in **Fig. 20** for the uniaxial tension samples. The plots include a definition of two corrosion fronts: a) corrosion front, corresponding to any degree of fibre corrosion (levels 2-4), b) severe corrosion front, related to moderate and major corrosion of fibres (levels 3-4).

For the bending samples, **Fig. 19**, the outer 25 mm at the laterals of the crack are omitted from the analysis to consider just the corrosion extending from the crack mouth. Furthermore, the fibres located at the compression zone of the bending samples are not included in the analysis, i.e. from the position of the neutral axis described in **Fig. 11**. Therefore, the initial cross-section (150×125 mm), is reduced to an area of 100×90 mm for samples cracked at 0.15 mm CMOD and 100×100 mm for samples cracked at 0.3 mm CMOD. The uncracked reference samples (**Fig. 19a**) are evaluated in an area of 150×100 mm. The whole cross-section of the crack was considered for the uniaxial tension samples (**Fig. 20**), comprising an area of 80×80 mm.

The uncracked reference samples show a ratio of ruptured fibres in the range 10 – 20 %, varying through the depth of the crack (**Fig. 19-20a**). Similarly, there is no clear indication of increased fibre rupture at the outermost fibres of the cracked references exposed to limewater (**Fig. 19-20b-c**), being in the range 10 – 20 %; despite that up to 20 – 80 % of the fibres presented minor corrosion (level 2) at the outermost 10 – 30 mm of the crack.

For the exposed samples, fibre corrosion is only observed in the outer crack area, i.e. up to 20 – 40 mm from the crack mouth, see **Fig. 19-20b-k**. Severe fibre corrosion (i.e. levels 3 – 4) is observed at the outer 10

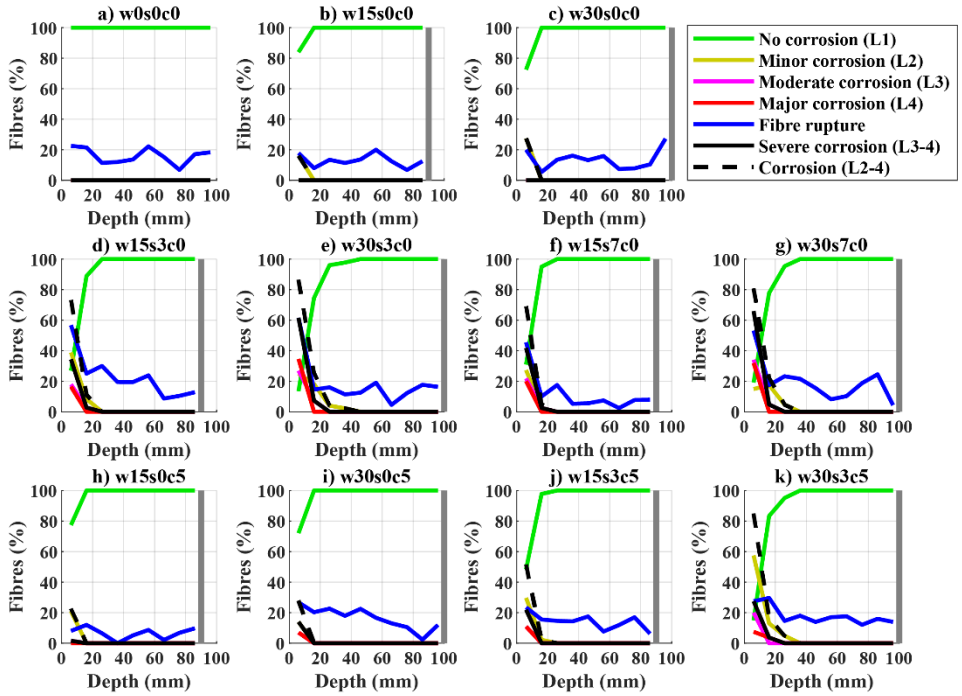

Fig. 19. Fibre corrosion versus crack depth for bending samples: a) uncracked reference, w0s0c0; b,c) cracked reference, s0c0; d,e) 3.5%-wt. NaCl exposure, s3c0; f,g) 7.0%-wt. NaCl exposure, s7c0; h,i) carbon dioxide and fresh water exposure, s0c5; j,k) carbon dioxide and 3.5%-wt. NaCl exposure, s3c5. The position of the neutral axis has been marked as a vertical grey line in the plot, at 90 mm and 100 mm from the surface for the samples cracked at 0.15 mm (w15) and 0.3 mm (w30), respectively.

– 20 mm of the crack, varying with the exposure and crack width.

Generally, corrosion is more severe and is observed deeper inside the crack for samples exposed to chlorides (**Fig. 19-20d-g** and **Fig. 19-20j-k**), compared to the carbonation samples (**Fig. 19-20h-i**) and the cracked references exposed to limewater (**Fig. 19-20b-c**). There is no clear increase in the number of fibres corroding when increasing the NaCl concentration of the solution from 3.5-wt.% NaCl (**Fig. 19-20d-e**) to 7-wt.% NaCl (**Fig. 19-20f-g**).

There is a significant increase in the percentage and spread of corroded fibres for larger cracks, i.e.: 0.3 mm cracks (**Fig. 19-20c,e,g,i,k**) over 0.15 mm cracks (**Fig. 19-20b,d,f,h,j**). While generally, fibre rupture tends to increase at depths where most fibres present severe corrosion (levels 3 – 4), i.e. the outer 10 – 20 mm of the crack depending on the exposure and crack width.

Generally, the results discussed in this section show that the extent and severity of fibre corrosion inside the crack increases both at larger initial crack width and for chloride exposures. Fibre corrosion was found at 10 – 40 mm inside the crack, with severely corroded fibres ranging 20 – 60 % of the total count, both increasing with crack width and the presence of chlorides. However, increase in fibre rupture was moderate and only evident up to approx. 10 mm inside the crack. Similar trends were found in previous research [14,22], yet former studies could not provide an accurate location and classification of the corroding and rupturing fibres. Furthermore, a large part of the literature did not provide a quantitative analysis of the extent and severity of fibre corrosion inside the crack [5], which does not allow further objective comparison of this data.

4.4 Correlation of fibre corrosion and fibre rupture

The detrimental effect of fibre corrosion on the residual mechanical performance of the SFRC is discussed in this section. In order to correlate corrosion damage of fibres bridging the crack to changes in the residual performance of the material, this section analyses the impact of corrosion on the quantity of fibres rupturing instead of pulling-out.

The discussion is based on the hypothesis that fibre corrosion mainly affects the residual performance of the cracked material by leading to critical reductions of the cross-section of the fibres bridging the crack. A critical reduction of the fibre's cross section would thus promote premature fibre rupture instead of a complete pull-out. Therefore, presuming that fibre corrosion does not have any significant impact on the residual mechanical performance of the cracked composite unless fibre corrosion leads to a premature rupture of the fibre during pull-out.

The impact of fibre corrosion on the number of fibres rupturing is presented in **Fig. 21**. The figure describes: i) the ratio of fibres ruptured at each corrosion level (L1-L4) and combinations of them as a boxplot (**Fig. 21a,c**) and ii) the amount of ruptured fibres and total fibres of every specimen at each corrosion level (L1-L4), as a correlation plot in **Fig. 21b,d**. The ratio of ruptured fibres is compared at each corrosion level to the uncorroded reference (L1) by a two-tailed Welch's T-test with a 90% confidence, which shows a significantly higher number of samples marked in red in **Fig. 21a,c**.

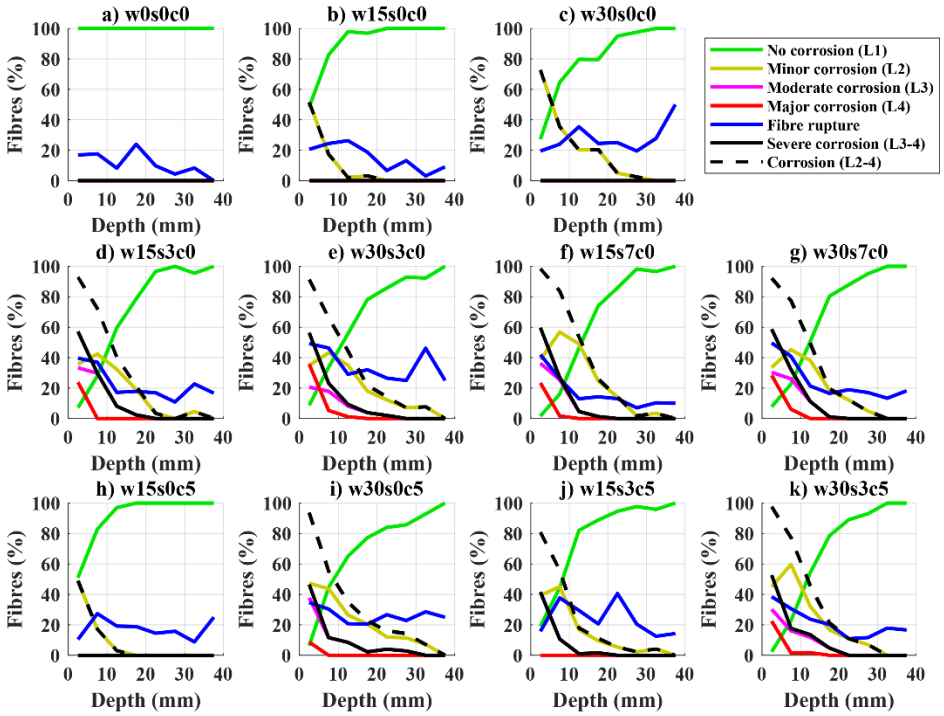

Fig. 20. Fibre corrosion versus crack depth for uniaxial tension samples: a) uncracked reference, w0s0c0; b,c) cracked reference, s0c0; d,e) 3.5%-wt. NaCl exposure, s3c0; f,g) 7.0%-wt. NaCl exposure, s7c0; h,i) carbon dioxide and fresh water exposure, s0c5; j,k) carbon dioxide and 3.5%-wt. NaCl exposure, s3c5.

The results presented in **Fig. 21a,c**, show that any degree of fibre corrosion, i.e. minor (L_1), moderate (L_2) or severe (L_4), leads to a significant increase in fibre rupture. The ratio of fibres rupturing increases with larger corrosion damage of the fibre, reaching 100% for the severe corrosion level (L_4). However, increase of fibre corrosion does not lead to significant increases of fibre rupture if non-corroded fibres are included in the analysis (see $L_{1,2}$, $L_{1,3}$ and $L_{1\text{-}3}$ in **Fig. 21a,c**), since the proportion of fibres presenting corrosion is still low compared to the total number of fibres. This is not the case for severely corroded fibres, i.e. L_4, which entail a significant increase in the fibre rupture ratio, see $L_{1,4}$ and $L_{1\text{-}4}$ in **Fig. 21a,c**. The correlation plots shown in **Fig. 21b,d** confirm that a higher corrosion level shifts the ratio of ruptured fibres towards the identity line, i.e. 1:1 ratio. However, the amount of fibres showing any corrosion level is almost one order of magnitude lower than the number of fibres showing no corrosion. The total number of fibres shows slightly higher ratios of ruptured fibres than the non-corroded ones, particularly for the uniaxial tension specimens **Fig. 21d**.

4.5 Impact of fibre behaviour on mechanical performance of cracked SFRC

The impact of the fibre damage and crack width on the mechanical performance was evaluated based on a multiple linear regression analysis described in **Section 2.5.2**. The analysis covers the contribution of the fibre content, fibre damage (i.e. corrosion and rupture) and crack width on the toughness of the material. The linear predictors are presented in Wilkinson notation for the bending tests in **Eq. 2** and for the uniaxial tension tests in **Eq. 3**.

$$i + x1 + x2 + x3 + x4 + x5 + x6 + x1{:}x4 + x1{:}x5 \quad \textbf{Eq. 2}$$

$$i + x1 + x2 + x3 + x4 + x5 + x6 + x2{:}x6 \quad \textbf{Eq. 3}$$

The resulting coefficient estimates and p-values of the linear terms and correlation coefficients (R^2 and adjusted R^2) are presented in **Table 5**.

Table 5. Multiple regression model results. Estimates and p-values for regressors and coefficients of determination.

		Bending		Uniaxial tension	
	Variable	**Estimate**	**p-value**	**Estimate**	**p-value**
i	Intercept	0.081	0.226	0.087	0.212
x1	Fibre count	0.936	0.000	0.760	0.000
x2	Corr. L2 (%)	-0.030	0.672	-0.017	0.838
x3	Corr. L3 (%)	-0.161	0.031	-0.064	0.439
x4	Corr. L4 (%)	-0.303	0.000	-0.122	0.161
x5	Rupture (%)	0.466	0.000	0.040	0.661
x6	Crack width	-0.085	0.223	-0.299	0.000
		R2	0.696	**R2**	0.633
		R2 adj.	0.669	**R2 adj.**	0.607

The coefficient-estimates and normalized residuals (i.e. Standardized and Pearson residuals) of the resulting models are presented in **Fig. 22a-b** for the bending and in **Fig. 22c-d** for the uniaxial tension tests. The adjusted correlation coefficients, in the range 0.6 to 0.7, indicate a modest fit; but the

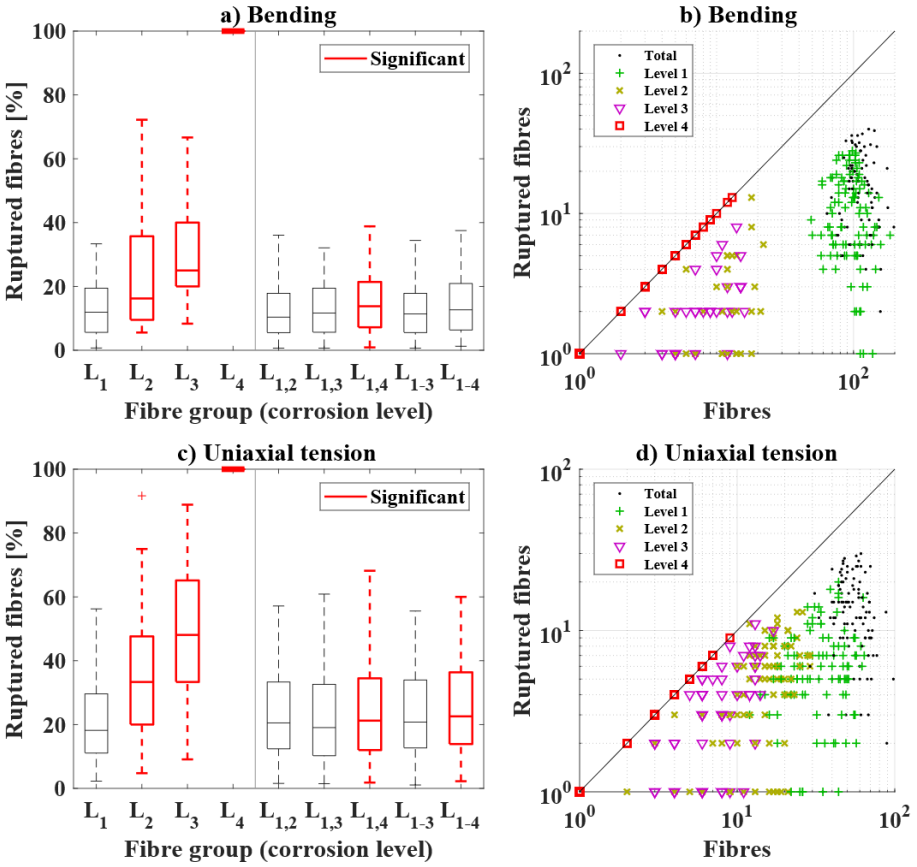

Fig. 21. Impact of fibre corrosion on fibre rupture for: a) boxplot for bending samples, b) correlation plot for bending specimens, c) boxplot for uniaxial tension samples, d) correlation plot for uniaxial tension specimens. The groups shown in "a)" and "c)" correspond to the corrosion levels described in **Fig. 5**. Group numbers separated by "," (e.g. $L_{1,3}$) represent discrete combinations (e.g. $L_1 + L_3$), and groups separated by "-" (e.g. $L_{1\text{-}3}$) represent full combinations (e.g. $L_1 + L_2 + L_3$).

normalized residual plots, see **Fig. 22b,d**, show a fair distribution, despite reaching large normalized residual values, e.g. up to 2-times the standard deviation.

The normalized coefficient estimates (z-scores) of the main predictors are presented in **Fig. 22a,c** and display the relative impact of each variable on the toughness of the material. Positive estimates indicate a positive effect of the variable on the toughness (i.e. increase) and negative values indicate a detrimental one. Non-significant estimate predictions, i.e. p-value larger than 0.05, are displayed in grey.

The coefficient estimates show that the impact of the fibre content (x1) dominates over the rest of the variables with respect to changes on the toughness of the material, for both bending and uniaxial tension. Minor corrosion of fibres bridging the crack (x2), i.e. level 2, does not have a significant impact on the toughness; while moderate (x3), i.e. level 3, and major corrosion (x4), i.e. level 4, only show a significant negative impact on the performance of the bending specimens. On the contrary, fibre rupture (x5) shows a positive correlation with the toughness of the material, only significant for the bending specimens. The crack width (x6) shows a significant negative impact on the toughness for the uniaxial tension specimens.

This analysis infers that, for bending and uniaxial tension specimens, the fibre content dominates over the rest of the variables studied and it is the main responsible for the changes in the residual performance of the material, which increases at higher fibre content.

The impact of fibre corrosion on the residual performance of the material is only statistically significant for the bending specimens, which show a substantial detrimental effect from fibres showing severe signs of corrosion (i.e. corrosion levels 3-4). Whereas, fibres with minor corrosion (level 2) do not show a significant impact on the residual performance of the material. The crack width showed a significant detrimental impact on the residual performance of the uniaxial tension specimens but was limited for the specimens in bending.

There was a positive correlation between a higher number of fibres rupturing and higher toughness values. Thus, suggesting that fibre rupture is not necessarily related to a decrease in toughness, i.e. described in this study as the total work; but may be the result of an increase of the fibre-matrix bond strength of the cracked composite during the exposure. Such increase of the fibre-matrix bond strength may be attributed to autogenous healing at the fibre-matrix interface, based on the discussion presented in [5], and corresponding to results from similar specimens under comparable exposure conditions [41].

Conversely, other studies have attributed such increase of the fibre-matrix bond strength to higher roughness of the fibre due to corrosion [13,42], yet with limited evidence. Whereas, in the authors' opinion, additional friction is not expected to have a dominant role on the mechanical anchorage of deformed fibres at pull-out displacements below 4 mm; which for the case of this study, is primarily governed by the plastic deformation of the steel wire at the hook bends, until reaching pull-out displacements in the range 4 – 5 mm [43,44].

Generally, this discussion presents evidence suggesting that variations observed in the mechanical performance of cracked SFRC under certain exposures may not be solely related to corrosion damage; so that the transport inside the crack and alteration of the matrix may have an important role to the mechanical performance of the cracked material.

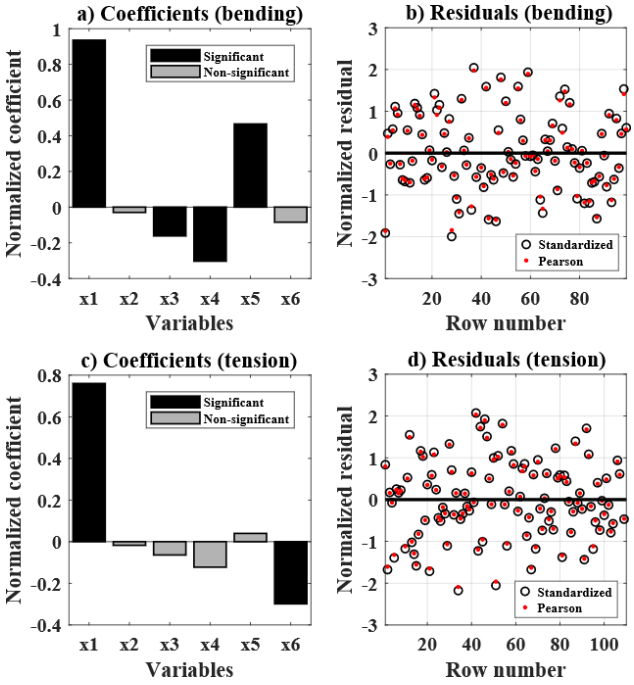

Fig. 22. Multiple regression for bending specimens and uniaxial tension specimens, showing: a) normalized coefficients for bending specimens, b) residuals for bending specimens, c) normalized coefficients for uniaxial tension specimens, d) residuals for uniaxial tension specimens.

4.6 Summary and engineering application

This study investigated the impact of fibre corrosion on the mechanical performance of cracked SFRC exposed to wet-dry cycles of various corrosive environments for one year. **Table 6** shows a summary of the results for each of the exposures tested. Exposure conditions are classified according to EN 206 as: limewater (XC1-XC4), 3.5%-wt. NaCl solution (XS3), 7.0%-wt. NaCl solution (XS3↑), fresh

water and CO_2 drying cycles (XC4) and 3.5%-wt. NaCl solution and CO_2 drying cycles (XS3 + XC4).

The results show negligible changes in the mechanical performance of the exposed uncracked material tested in compression compared to the unexposed references, as discussed in **section 4.1**; in agreement with the conclusions of previous research. Strength ratios, calculated as the strength of the exposed samples relative to the unexposed references (w0s0c0), are given in **Table 6**.

Conversely, substantial changes in the residual performance of the cracked material were observed after exposure, as discussed in **section 4.2**. There was a statistically significant increase in the toughness for smaller cracks (i.e. 0.15 mm) relative to the unexposed references. Whereas, a statistically significant drop in the toughness of the cracked material was only observed for a limited number of the samples with larger cracks (i.e. 0.3 mm). Toughness ratios, calculated as the total work up to CMOD = 4.0 mm for each of the exposures relative to the uncracked references, are given in **Table 6**. Additional cracking and branching during testing of the exposed specimens was attributed to changes of the fibre-matrix bond strength during exposure.

Fibre corrosion was observed at the outer 10 – 40 mm of the crack (see **section 4.3**), depending on the exposure and crack width, and was more severe for chloride exposure than for carbon dioxide exposure, similar to what has been described in previous research [14,22,45]; for specific values refer to **Table 6**. These observations suggest that the corrosion damage inside the crack is still governed by the ionic, moisture and gas transport inside the crack. Therefore, the composition of the solution inside the crack differs significantly from those at an external free surface, e.g. higher alkalinity and lower chloride concentration, similarly to what has been discussed for conventional steel in concrete in previous studies [46].

The analysis of the relative impact of the main experimental variables on the residual performance of the material (**section 4.5)**, showed that the total number of fibres bridging the crack dominated over the rest of the experimental variables. However, this variable depends on the production and test method and it is accounted for in current test and design standards [30,47,48], for example: by enforcing a minimum amount of test replicates, i.e. from 6 – 12 specimens, and using a probability distribution to calculate the safety factors and characteristic values of the material.

Corrosion damage at the fibres bridging the crack had a secondary impact on the residual performance of the material, compared to the variations observed due to the fibre distribution at the cracks. Whereas, the contribution of corrosion to the total count of fibres rupturing was negligible. Since corroding fibres crossing the crack represented a moderate fraction of the total fibre count; and only fully corroded fibres had a statistically significant, yet limited, impact on the total amount of ruptured fibres.

Therefore, fibre corrosion is only expected to have a negative impact on the residual performance of the material at the outer 10 – 25 mm of the specimen, provided that there is a significant reduction of the fibre cross-section and a large share of the fibres critically corrode. Thus, emphasizing the impact of

Table 6. Summary of results

Exposure (sample)	Exposure Class [EN 206]	Crack width [mm]	Corrosion depth [mm]		Severe corrosion depth [mm]		Toughness variation [-]		Strength variation [-]
			3PB	UTT	3PB	UTT	3PB	UTT	C
w15s0c0	XC1 (XC4)	0.15	10	-	-	-	1.20*	1.19*	1.02
w30s0c0		0.30	10	-	-	-	1.20	0.81*	
w15s3c0	XS3	0.15	20	20	20	20	1.22*	1.08	1.01
w30s3c0		0.30	25	25	25	25	0.88*	0.92	
w15s7c0	XS3↑	0.15	20	25	25	20	1.02	1.17*	0.99
w30s7c0		0.30	25	35	35	20	1.03	1.07	
w15s0c5	XC4	0.15	10	10	0	0	1.14	1.23*	1.02
w30s0c5		0.30	20	15	15	25	1.06	1.02	
w15s3c5	XC4 + XS3	0.15	20	10	15	20	1.10	1.21*	1.00
w30s3c5		0.30	25	20	25	25	1.08	0.92	

Abbreviations: *(Exposure "sample") codes of the experiment exposures according to Table 2, (Exposure class) corresponding exposure classes according to EN 206, (Crack width) crack width during the exposure expressed in mm, (Corrosion depth) depth of corrosion inside the crack measured from the exposed edges for any level of corrosion expressed in mm, (Severe corrosion depth) depth of severe corrosion "corrosion levels 3-4" inside the crack measured from the exposed edges expressed in mm, (Toughness variation) the ratio between the toughness of the cracked sample and the uncracked reference at 56 days, significant values are marked with "*", (Strength variation) the ratio between the compressive strength of the exposed sample and the unexposed reference (w0s0c0), significant values are marked with "*", (3PB) three-point bending specimens, (UTT) uniaxial tension test specimens, (C) compression specimens.*

the specimen size in the deterioration observed. This may result in an overestimation of the exposure damage in very small specimens and would not be representative for the extrapolation to typical engineering applications: e.g. cross-section thickness of a prefabricated segmental lining is in the range 200 – 400 mm [49].

The positive correlation between the number of fibres rupturing and the toughness variation of the cracked material has been related to an increase of the fibre-matrix bond strength during the exposure. Noting that, in this study, a significant share of the fibres (e.g. 75 – 85 %) did not rupture during the experiments. In this regard, an adequate selection of the fibre is critical to avoid general rupture of the fibres bridging the crack due to changes in the fibre-matrix bond strength over time and during exposure, as reported in [20,21]. For example, by selecting an appropriate steel strength and dimensions of the steel fibre, experimentally verified to the expected long-term strength class of the concrete matrix [5].

The discussion above indicates that there may be additional damage mechanisms besides fibre corrosion that explain the changes in the residual performance or the composite material. For example, alteration of the cement paste at the fibre-matrix interface [5]. Therefore, fibre corrosion cannot be regarded as the main deterioration mechanism affecting the residual performance of cracked SFRC. Yet, the discussion herein is based on a limited number of experiments at the composite scale and cannot be generalized to every type of fibre, concrete mix-design or exposure.

5. Conclusions

This paper investigated the corrosion of carbon-steel fibres and the mechanical performance of cracked and uncracked Steel Fibre Reinforced Concrete (SFRC) exposed to wet-dry cycles of chlorides and carbon dioxide over a period of one year.

The results presented in this paper confirm that there is a negligible detriment of the strength of uncracked SFRC exposed to chloride and carbon dioxide wet-dry cycles. However, there were substantial changes in the residual performance of the cracked SFRC after exposure, which have been attributed to changes of the fibre-matrix bond. Yet, macroscale observations at the composite scale do not provide a clear explanation for those changes.

Fibre corrosion in uncracked SFRC was limited to the concrete surface and produced aesthetical damage, i.e. forming rust stains, but did not cause cracking or spalling of the uncracked matrix. Whereas, fibre corrosion was only observed at 10 – 40 mm inside the crack, depending on the exposure and crack width (i.e. 0.15 mm and 0.3 mm). Furthermore, fibre corrosion had a secondary impact on the toughness variation of the material after exposure, compared to the variations observed due to the fibre distribution at the cracks.

Results showed that fibre corrosion inside the crack increased the probability of fibre rupture; yet, it had a limited impact on the global count of ruptured fibres. Increase in the number of ruptured fibres after exposure did not have a detrimental impact on the toughness of the material and was attributed to an increase in the fibre-matrix bond after the exposure. Therefore, changes in the residual performance of cracked SFRC exposed to chlorides and carbon dioxide, are not exclusively a result of fibre damage due to corrosion and may be related to localized changes at the fibre-matrix interface due to the exposure.

There is insight suggesting additional damage mechanisms, besides fibre damage, that explain the changes in the residual performance of the cracked SFRC and that those may be related to the dissolution and precipitation of solid phases at the fibre-matrix interface. Further research focusing on the pull-out performance of single fibres and the microstructural changes at the fibre-matrix interface exposed to wet-dry cycles is needed.

Acknowledgements

The first author would like to express his gratitude to: CowiFonden, InnovationsFonden, the German association of steel fibre producers (VDS), VejDirektoratet and Mapei-Denmark, for supporting this project; and Dr. Torben Lund Skovhus for his contribution to supervision during this project.

References

[1] V.C. Li, Large volume, high performance applications of fibers in civil engineering, J. Appl. Polym. Sci. 83 (2002) 660–686. doi:10.1002/app.

[2] M. di Prisco, G.A. Plizzari, Precast SFRC elements: From material properties to structural applications, in: M. di Prisco, R. Felicetti, G.A. Plizzari (Eds.), 6th RILEM Symp. Fibre-Reinforced Concr. - BEFIB 2004, RILEM Publications SARL, Varenna, Italy, 2004: pp. 81–100.

[3] P. Serna, S. Arango, T. Ribeiro, A.M. Núñez, E. Garcia-Taengua, Structural cast-in-place SFRC: technology, control criteria and recent applications in spain, Mater. Struct. 42 (2009) 1233–1246. doi:10.1617/s11527-009-9540-9.

[4] C.G. Berrocal, K. Lundgren, I. Löfgren, Corrosion of steel bars embedded in fibre reinforced concrete under chloride attack: State of the art, Cem. Concr. Res. 80 (2015) 69–85.

doi:10.1016/j.cemconres.2015.10.006.

[5] V. Marcos-Meson, A. Michel, A. Solgaard, G. Fischer, C. Edvardsen, T.L. Skovhus, Corrosion resistance of steel fibre reinforced concrete - A literature review, Cem. Concr. Res. 103 (2018) 1–20. doi:10.1016/j.cemconres.2017.05.016.

[6] S.U. Balouch, J.P. Forth, J.-L. Granju, Surface corrosion of steel fibre reinforced concrete, Cem. Concr. Res. 40 (2010) 410–414. doi:10.1016/j.cemconres.2009.10.001.

[7] D.C. Morse, G.R. Williamson, Corrosion behavior of steel fibrous concrete, Dept. of Defense Dept. of the Army Corps of Engineers Construction Engineering Research Laboratory ;, Champaign Ill., 1977.

[8] M. Schupack, Steel Fiber Concrete, in: S.P. Shah, A. Skarendahl (Eds.), Steel Fiber Concr. US-Sweden Jt. Semin., Elsevier, Stockholm, sweden, 1985: pp. 479–496.

[9] P.S. Mangat, Long-term properties of steel fibre reinforced marine concrete, Mater. Struct. Matériaux Constr. 20 (1987) 273–282.

[10] E. O'Neil, J.T. Devlin, Durability of Fiber-Reinforced Concrete Under Flexural Stress in a Severe Marine Environment, Defense Technical Information Center, Vicksburg, US, 1999.

[11] P.S. Mangat, K. Gurusamy, Permissible crack widths in steel fibre reinforced marine concrete, Mater. Struct. 20 (1987) 338–347. doi:10.1007/BF02472580.

[12] C. Frazão, A. Camões, J. Barros, D. Gonçalves, Durability of steel fiber reinforced self-compacting concrete, Constr. Build. Mater. 80 (2015) 155–166. doi:10.1016/j.conbuildmat.2015.01.061.

[13] J.-L. Granju, S.U. Balouch, Corrosion of steel fibre reinforced concrete from the cracks, Cem. Concr. Res. 35 (2005) 572–577. doi:10.1016/j.cemconres.2004.06.032.

[14] R. Weydert, P. Schiessl, Korrosion von Stahlfasern in gerissenem und ungerissenem Stahlfaserbeton. Abschlussbericht, Bergisch Gladbach (Germany), 1998.

[15] K. Kosa, A.E. Naaman, Corrosion of Steel Fiber Reinforced Concrete, ACI Mater. J. 87 (1990) 27–37.

[16] D.J. Hannant, J. Edgington, Durability of steel fibre concrete, in: A. Neville (Ed.), Rilem Symp. 1975 Fibre Reinf. Cem. Concr., The construction press, Leeds, UK, 1975: pp. 159–169.

[17] G.B. Batson, Strength of Steel Fiber Concrete in Adverse Environments, Champaign, Illinois (US), 1977.

[18] E.S. Bernard, Durability of cracked fibre reinforced shotcrete, in: E.S. Bernard (Ed.), Shotcrete More Eng. Dev. Proc. Second Int. Conf. Eng. Dev. Shotcrete, A.A. Balkema Publishers, Sydney, Australia, 2004: pp. 59–66.

[19] P. Serna, S.E. Arango, Evolution of the Flexural Behaviour of Precracked SFRC in Marine Environment, in: R. Gettu (Ed.), 7th RILEM Int. Symp. Fibre Reinf. Concr. Des. Appl. - BEFIB 2008, RILEM Publications SARL, Chennai, India, 2008: pp. 595–605.

[20] E.S. Bernard, Effect of Exposure on Post-crack Performance of FRC for Tunnel Segments, in: I. Vrkljan, Z. Dekovic, M. Dobrilovic, J. Likar, P. Miscevic (Eds.), SEE TunnelPromoting Tunneling SEE Reg. - ITA WTC 2015, ITA-AITES, Dubrovnik, Croatia, 2015: p. 13.

[21] E.S. Bernard, Age-dependent changes in post-crack performance of fibre reinforced shotcrete linings, Tunn. Undergr. Sp. Technol. 49 (2015) 241–248. doi:10.1016/j.tust.2015.05.006.

[22] E. Nordström, Durability of Sprayed Concrete Steel fibre corrosion in cracks, Lulea University of Technology, 2005.

[23] D. Nemegeer, J. Vanbrabant, H. Stang, Final report on Durability of Steel Fibre Reinforced Concrete, Copenhagen, Denmark, 2000.

[24] E.J. de P. Hansen, T. Ekman, K.K. Hansen, Durability of cracked fibre reinforced concrete structures exposed to chlorides, in: M.A. Lacasse, D.J. Vanier (Eds.), Durab. Build. Mater. Components, NRC Research Press, Vancouver, Canada, 1999: pp. 280–289.

[25] S. Abbas, Structural and Durability Performance of Precast Segmental Tunnel Linings, University of Western Ontario, 2014.

[26] G.T. Halvorsen, C.E. Kesler, A.R. Robinson, J.A. Stout, Durability and Physical Properties of Steel Fiber Reinforced Concrete, Illinois, US, 1976.

[27] L. Ferrara, R. Fratesi, S. Signorini, F. Sonzogni, Durability of Steel Fibre-Reinforced Cocnrete Precast Elements: Experiments and Proposal of design recommendations, in: M. Di Prisco, R. Felicetti, G.A. Plizzari (Eds.), 6th RILEM Symp. Fibre-Reinforced Cocnretes - BEFIB 2004, RILEM Publications SARL, Varenna, Italy, 2004: pp. 565–574.

[28] G. Mantegazza, A. Gatti, Aspects of Durability of Fiber Reinforced Concrete: Workability and Stress-Corrosion, in: M. di Prisco, R. Felicetti, G.A. Plizzari (Eds.), 6th RILEM Symp. Fibre-Reinforced Cocnretes - BEFIB 2004, RILEM Publications SARL, Varenna, Italy, 2004: pp. 593–602.

[29] E. Kern, H. Schorn, 23 Jahre alter Stahlfaserbeton, Beton- Und Stahlbetonbau. 86 (1991) 205–208. doi:10.1002/best.199100380.

[30] European Commitee for Standardization (CEN), Test method for metallic fibre concrete - Measuring the flexural tensile strenght (limit of proportionality (LOP), residual), EN 14651:2006 +A1, European Union, 2006.

[31] I. Paegle, F. Minelli, G. Fischer, Cracking and load-deformation behavior of fiber reinforced concrete: Influence of testing method, Cem. Concr. Compos. 73 (2016) 147–163. doi:10.1016/j.cemconcomp.2016.06.012.

[32] European Commitee for Standardization (CEN), Fibres for concrete - Part 1: Steel fibres - Definitions, specifications and conformity, EN 14889-1:2006, European Union, 2006.

[33] EPA, Methods for the Chemical Analysis of Water and Wastes, U.S.EPA National Exposure Research Laboratory (NERL), 1983.

[34] European Commitee for Standardization (CEN), Testing hardened concrete - Part 3: Compressive strength of test specimens, EN 12390-3 + AC:2012, European Union, 2012.

[35] J.F. Olesen, Fictitious Crack Propagation in Fiber-Reinforced Concrete Beams, J. Eng. Mech. March (2001) 272–280. doi:http://dx.doi.org/10.1061/(ASCE)0733-9399(2001)127:3(272).

[36] B.L. Welch, The generalisation of student's problems when several different population variances are involved, Biometrika. 34 (1947) 28–35. doi:10.1093/biomet/34.1-2.28.

[37] G.N. Wilkinson, C.E. Rogers, Symbolic Description of Factorial Models for Analysis of Variance, Appl. Stat. 22 (1973) 392. doi:10.2307/2346786.

[38] A. Behnood, K.P. Verian, M. Modiri Gharehveran, Evaluation of the splitting tensile strength in plain and steel fiber-reinforced concrete based on the compressive strength, Constr. Build. Mater. 98 (2015) 519–529. doi:10.1016/j.conbuildmat.2015.08.124.

[39] N. Ganesan, P. V Indira, P.T.S. Kumar, Durability aspects of steel fibre-reinforced SCC, Indian Concr. J. 80 (2006) 31–37.

[40] M.M. Kamal, F.E. El-Refai, Durability of steel fibre reinforced concrete, in: Proc. Fourth Int. Conf. Durab. Build. Mater. Components, Elsevier, Singapore, 1987: pp. 235–247. doi:10.1016/B978-1-4832-8386-9.50034-6.

[41] L. Ferrara, V. Krelani, F. Moretti, M. Roig Flores, P. Serna Ros, Effects of autogenous healing on the recovery of mechanical performance of High Performance Fibre Reinforced Cementitious Composites (HPFRCCs): Part 1, Cem. Concr. Compos. 83 (2017) 76–100. doi:10.1016/j.cemconcomp.2017.07.010.

[42] C. Frazão, J. Barros, A. Camões, A.C. Alves, L. Rocha, Corrosion effects on pullout behavior of hooked steel fibers in self-compacting concrete, Cem. Concr. Res. (2015). doi:10.1016/j.cemconres.2015.09.005.

[43] K. Georgiadi-Stefanidi, E. Mistakidis, D. Pantousa, M. Zygomalas, Numerical modelling of the pull-out of hooked steel fibres from high-strength cementitious matrix, supplemented by experimental results, Constr. Build. Mater. 24 (2010) 2489–2506. doi:10.1016/j.conbuildmat.2010.06.007.

[44] R. Breitenbücher, G. Meschke, F. Song, Y. Zhan, Experimental, analytical and numerical analysis of the pullout behaviour of steel fibres considering different fibre types, inclinations and concrete strengths, Struct. Concr. 15 (2014) 126–135. doi:10.1002/suco.201300058.

[45] R. Roque, N. Kim, B. Kim, G. Lopp, Durability of Fiber-Reinforced Concrete in Florida Environments, Florida, USA, 2009.

[46] P. Schiessl, M. Raupach, Laboratory studies and calculations on the influence of crack width on chloride-induced corrosion of steel in concrete, ACI Mater. Jounal. 94 (1997) 56–62.

[47] International Federation for Structural Concrete, FIB Model Code for concrete structures 2010, Lausanne, Switzerland, 2010.

[48] SFRC Consortium, Design guideline for structural applications of steel fibre reinforced concrete, SFRC Consortium, Copenhagen, Denmark, Denmark, 2013.

[49] Z. Guan, T. Deng, G. Wang, Y. Jiang, Studies on the key parameters in segmental lining design, J. Rock Mech. Geotech. Eng. 7 (2015) 674–683. doi:10.1016/j.jrmge.2015.08.008.

3.2 Paper IV. The role of exposure time in the deterioration of cracked SFRC under wet-dry cycles

The following publication, referred as "paper IV", has been submitted to Journal of Sustainable Cement-Based Materials.

Marcos-Meson, V., Fischer, G., Solgaard, A., Edvardsen, C., Michel, A., 2020. Development of the mechanical performance of steel fibre reinforced concrete exposed to wet-dry cycles of chlorides and carbon dioxide: results after two years (unpublished)

Printed in this thesis as the original manuscript with the authors' formatting.

Submitted to Journal of Sustainable Cement-Based Materials (2020)

Development of the mechanical performance of steel fibre reinforced concrete exposed to wet-dry cycles of chlorides and carbon dioxide: results after two years

Victor Marcos-Meson[1,2,3*], Gregor Fischer[1], Anders Solgaard[2], Carola Edvardsen[2], Alexander Michel[1]

[1] Department of Civil Engineering, Technical University of Denmark, Kgs. Lyngby, Denmark

[2] COWI A/S, Kgs. Lyngby, Denmark

[3] VIA Building, Energy, Water & Climate, VIA University College, Horsens, Denmark

* Corresponding author: vicmes@byg.dtu.dk

Abstract

This paper presents an experimental study investigating the evolution over time of corrosion damage of carbon-steel fibre reinforced concrete (SFRC) exposed to wet-dry cycles of chlorides and carbon dioxide for two years, and its effects on the mechanical performance of the composite over time. The results presented confirmed that corrosion damage of steel fibres embedded in uncracked SFRC under these exposures does not entail any detriment to the mechanical performance of the uncracked concrete over time. There was a moderate increase in the extent of corroding fibres inside cracks over time, within an approximate depth of 40 mm inside the crack. There was no significant detriment to the overall performance of the cracked composite over the time-scales investigated. Overall, the impact of fibre damage to the toughness variation of the cracked composite over time was still secondary compared to the toughness variation due to the fibre distribution. The impact of fibre corrosion to the performance of the cracked composite over time is subject to a size-effect and may only be significant for small cross-sections.

Keywords

Steel fibre reinforced concrete (SFRC), corrosion, chlorides, carbonation, cracks, wet-dry cycles, exposure time

1. Introduction

Steel fibre reinforced concrete (SFRC) is increasingly used in civil engineering as partial or total replacement of conventional reinforcing steel. Carbon-steel fibres (henceforth "steel fibres") are being used, among others, for the construction of infrastructure exposed to corrosive environments [1–3]. However, the total replacement of conventional reinforcement with steel fibres is still controversial when considering the durability of cracked SFRC under corrosive exposures [4].

Former studies investigating the performance of SFRC exposed to chlorides and carbon dioxide reported limited corrosion damage for uncracked SFRC [4], which occurred mainly at the steel fibres adjacent to the concrete surface, and led to negligible long-term detriment to the mechanical performance of the composite over exposure periods in the field up to 20 years to chloride [5–9] or carbonation exposure [7,10–12]. However, there is an open discussion regarding the corrosion of steel fibres bridging cracks in the range of 0.1 – 0.3 mm in SFRC under these exposures, and its impact on the residual mechanical performance of the cracked composite [4].

Field exposure of cracked SFRC to saltwater (i.e. exposure classes corresponding XS2-XS3 according to EN-206 classification) generally showed an early stabilization of the deterioration process during the first 2 – 3 years of exposure. Which entailed moderate corrosion damage during periods of 1 – 2 years [6,10,13], and even increased residual tensile strength over time for small crack widths [6,10,13–16]. Similarly, field exposure of cracked SFRC to

rainwater (i.e. XC4 exposure class) presents contradictory results: showing minor corrosion damage and limited strength loss [10], or else, critical corrosion damage [13] for short-term exposures (i.e. 1 – 2 years). Longer exposure times (i.e. up to 5 years) to similar conditions resulted in limited corrosion damage for cracks in the abovementioned range [16]. Unfortunately, long-term exposure data (e.g. up to 20 years) is scarce and mostly comprises qualitative results from visual inspection for both chloride [7,16] and carbonation exposure [11,17].

Alternatively, the use of laboratory exposure to wet-dry cycles has been proven effective to accelerate the deterioration of cracked SFRC exposed to chlorides and carbon dioxide compared to field-exposure [4], by a factor of around 1:7 [11] to 1:50 [16] for the same exposure times. However, experimental studies under laboratory conditions often show contradictory results, which are reported to be very sensitive to variations in various parameters: the specimen dimensions [16,18], exposure conditions [8,16,19] and exposure time [4].

Accelerated exposure to chlorides under wet-dry cycles for short times (e.g. up to 6 months) generally resulted in negligible toughness loss for cracked SFRC [16,20]; yet, some studies show contradicting results [6,21,22]. While extended exposures (e.g. 1 – 3 years) to corresponding conditions also showed discrepant results: entailing minor corrosion damage [19,23] or else a large deterioration [24,25]. Similarly, laboratory exposure of cracked SFRC (0.2 – 0.5 mm cracks) to wet-dry cycles of freshwater and high CO_2 concentrations during 18 months resulted in minor corrosion damage of the cracked composite [20], as also observed in pre-carbonated specimens under similar conditions [11].

To address those issues, a testing campaign was initiated were cracked SFRC exposed to wet-dry cycles involving chlorides and carbon dioxide during one year [26]. Results showed that fibre corrosion does not necessarily entail a substantial detriment to the residual performance of the composite. While the residual tensile strength over the exposure increased substantially, but was attributed to the alteration of the fibre-matrix bond strength over time instead [26–28]. However, the evolution of these processes over time is not well understood, which leads to inconsistent predications of the durability of cracked SFRC exposed to wet-dry cycles [4].

This paper investigates the evolution of the corrosion damage on cracked SFRC exposed to wet-dry cycles of chlorides and carbon dioxide over time, and its impact on the mechanical performance of the uncracked and cracked composite. The investigation covers the exposure, mechanical testing and visual inspection of bending and uniaxial tension specimens cracked at 0.15 and 0.3 mm and exposed to wet-dry cycles for two years. The discussion presented in this paper focuses on describing the impact of the exposure time on the extent of fibre corrosion and its subsequent impact on the mechanical performance of the cracked and uncracked SFRC, comparing the results to corresponding data gathered after one year exposure [26], based on a statistical analysis of the test data.

2. Methodology

The investigation presented in this paper covers the preparation, exposure, mechanical testing and visual inspection of 220 SFRC specimens with induced crack widths of 0.15 and 0.3 mm and exposed to wet-dry cycles for two years. The results presented in this study are compared to corresponding data for specimens tested after one year of exposure [26].

The exposures investigated comprise wet-dry cycles of saltwater, freshwater and carbon dioxide; where two types of specimens have been investigated: three-point bending notched beams and single-notched coupon tests in uniaxial tension. The analysis of the mechanical performance of the material is made comparing the stress and work response for the investigated material in bending and uniaxial tension. Visual inspection of the crack surface and counting of fibres bridging the crack were used to determine the degree of fibre damage due to corrosion.

Finally, discussions regarding the extent of fibre corrosion over time and its impact on the residual performance of the cracked SFRC are based on descriptive statistics of the fibre distribution and toughness data of the cracked composite. Furthermore, the relative impact of the main experimental variables on the mechanical performance of the cracked composite over time is discussed based on a regression analysis.

The results and discussion section will use the following terminology: The word “specimen” refers to a single sampling unit (i.e. each of the tests executed); the word “sample” refers to a group of specimens exposed to the same environment and cracked at the same CMOD. Discussion will be primarily based on comparison of samples and individual specimens will not be discussed hereafter, unless specified.

2.1 Preparation of specimens

The mix design used was specified in compliance with the recommendations for minimum binder content and water-to-binder ratio for conventional reinforced concrete in DS/EN 206-1:2011 [29] for the exposure classes XC4 and XS3. The total binder

content was 426.3 kg/m^3 with 31% fly ash replacement of the Portland cement (CEM I 52.5N), and the water to binder ratio was (w/b = 0.34). Detailed mix-design proportions can be found in [26]. The steel fibre used was made of high-carbon cold-drawn wire with hooked ends with a length of 60 mm and an aspect ratio l/d = 80 and were mixed in a proportion of 40 kg/m^3.

The production of the bending specimens was done in a prefabrication plant, using an industrial mixing plant, over an industrial vibration table. The specimens were cast in three separate batches on consecutive days, demoulded after one day and cured indoors, moist cured and covered with plastic for 56 days at 20 °C. The dimensions of the three-point bending beam specimens were 600×150×150 mm, with a 25 mm deep and 5 mm wide notch cut at the centre, along the transversal direction, according to EN-14651:2007 [30]; with an effective cross-section at the notch location of 150x125 mm (**Fig. 1a)**.

The uniaxial tension specimens were prepared in a laboratory, mixed with a 300-l planetary mixer and cast over a vibration table. The specimens were cast in five separate batches on consecutive days, demoulded after one day and cured indoors, moist cured and covered with plastic for 56 days at 20 °C. The uniaxial tension specimens were 150 mm cubes, with a 35 mm deep and 5 mm wide notch cut along the central perimeter, leaving an effective cross-section of 80×80 mm inside the notch, see **Fig. 1b**.

The bending and uniaxial tension specimens were grouped in samples of nine and ten replicates, respectively. The specimens were distributed uniformly in the samples from the individual batches. Cubes for additional compression tests were cut off the last 150 mm of the bending beams after testing and twelve replicates were tested for every exposure.

2.2 Exposure setup

The exposure environments are described in **Table 1** and comprise wet-dry cycles of four days (i.e. two days each). The samples (i.e. test-groups) were coded as follows: (w) crack width; being 0.15 and 0.3 mm; (s) salinity of wet cycle, being 3.5% and 7.0%; and (c) carbon dioxide concentration, being 0.05 %vol. for ambient exposure and 0.5 %vol for accelerated carbonation exposure. The exposure time for the specimen was marked with a letter: (A) for one-year exposure and (B) for two-year exposure.

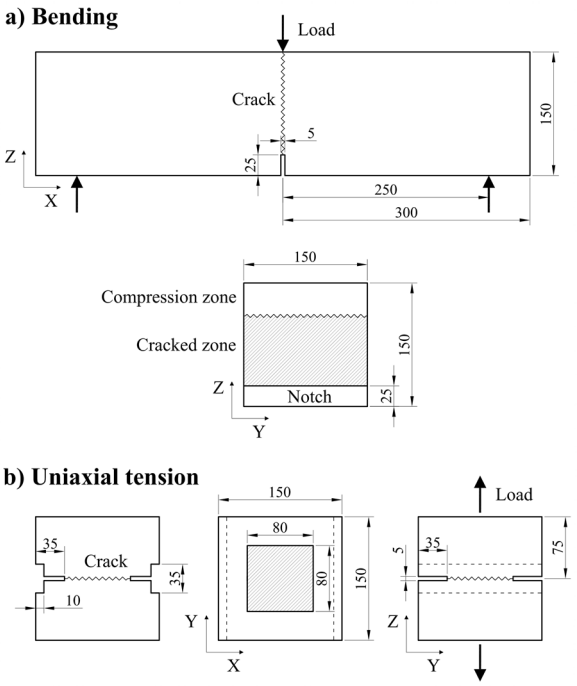

Fig. 1. Description of test specimens. After [26].

Two reference scenarios were tested: i) uncracked samples that were kept covered (w0s0c0t0 and w0s0c0B), and ii) cracked samples that were exposed to wet-dry cycles of limewater and air (w15s0c0 and w30s0c0). The cracked samples exposed to corrosive environments were divided into four exposures, shown in **Table 1**.

The exposure setup consisted of ten polyethylene containers connected in pairs, providing five different exposure conditions, further described in [26]. During the wet cycle the tanks were filled with 500 l of

Table 1. Test samples and exposure conditions, after [26].

Code name (sample)	Crack width (w) [mm]	Wet cycle (s)	Dry cycle (c)	Age (A / B)
w0 - s0 - c0t0	uncracked (w0)	-	-	56 days
w0 - s0 - c0B	uncracked (w0)	-	-	2 years
w15 - s0 - c0 - A / B	0.15 (w15)	Limewater (s0)	Air (c0)	1 / 2 years (A / B)
w30 - s0 - c0 - A / B	0.30 (w30)			
w15 - s3 - c0 - A / B	0.15 (w15)	3.5 wt.% NaCl (s3)	Air (c0)	1 / 2 years (A / B)
w30 - s3 - c0 - A / B	0.30 (w30)			
w15 - s7 - c0 - A / B	0.15 (w15)	7.0 wt.% NaCl (s7)	Air (c0)	1 / 2 years (A / B)
w30 - s7 - c0 - A / B	0.30 (w30)			
w15 - s0 - c5 - A / B	0.15 (w15)	Fresh water (s0)	0.5 %-vol. CO2 (c5)	1 / 2 years (A / B)
w30 - s0 - c5 - A / B	0.30 (w30)			
w15 - s3 - c5 - A / B	0.15 (w15)	3.5 wt.% NaCl (s3)	0.5 %-vol. CO2 (c5)	1 / 2 years (A / B)
w30 - s3 - c5 - A / B	0.30 (w30)			

solution; and during the drying cycle the tanks were emptied, and the specimens were dried with air circulating at nominal flow of 93 m^3/h. The drying cycle of the carbon dioxide exposure ran through a closed loop and utilized a cooled heatsink to condensate moisture from the air flux before the inlet; while the air of the rest of the exposures was mixed with the laboratory air.

The solution in the exposure tanks was replaced regularly, reducing the frequency with time, as described in [26]. The composition of the solution was checked weekly by means of total dissolved solids (TDS) from electrical conductivity measurements, and pH measurements. The solution of the limewater exposure was not replaced, and 0.3 l of a 20/80 mixture of saturated sodium and calcium hydroxide was added weekly, maintaining the pH value of the solution within the range of 10 – 13.5. Non-chlorinated fresh water (pH = 7.5 – 8.0, Cl^- < 50 mg/l, 13 – 15 °dH) was used as exposure media for the specimens subjected to carbon dioxide cycles and to prepare the saltwater brines. Furthermore, the temperature and relative humidity inside the room were monitored and fluctuated in the range 20±2 °C and 50±10 % respectively. The CO_2 concentration in the room and inside the carbon dioxide loop was measured weekly as approx. 0.05±0.01 %-vol. for the room and 0.5±0.1%-vol. inside the carbon dioxide loop.

2.3 Mechanical testing

The workflow of the experiments comprised: i) testing of reference specimens at 56 days; ii) cracking of the specimens at 56 days and preparation for exposure; iii) exposure for one- and two-years; iv) testing after one year of exposure; v) testing after two years of exposure. The data presented in this paper covers the experimental results after two years of exposure for experiments corresponding to the ones done after one year [26].

The bending tests were done in a 100 kN flexural test frame, according to [30]. The Crack Mouth Opening Displacement at the end of the notch ($CMOD_N$) was measured at the centre of the notch with a clip-gage connected to two steel pins glued to the face of the notch.

The testing of the uniaxial tension test specimens was done in a 500 kN capacity universal test frame. The uniaxial tension setup was described in [26], and is based on the design presented in [31]. The $CMOD_N$ was measured by two clip gages clipped onto two steel pins glued to the centre of opposite faces of the specimen.

The compression tests were executed in a 4000 kN capacity compression frame, according to the specifications of EN 12390-3:2012 [32].

The testing of the residual-flexural and residual -tensile strength of the specimens was done in accordance with the displacement rates specified in [30], with a sampling frequency rate of 100 Hz. After reaching a crack width of 5 mm, the displacement rate was increased up to 1 mm/min, until the specimen was split open completely.

The specimens were cracked before exposure with cracks of 0.15 and 0.3 mm calculated at the crack mouth ($CMOD_M$). After the target crack width was reached, the displacement of the crosshead was locked, and the crack was supported with HDPE inserts inside the notch. After the preparation tests, the opening at the crack mouth for the bending specimens was $CMOD_M$ = 0.10±0.01 and 0.25±0.03 mm for the specimens cracked at 0.15 mm and 0.3 mm, respectively; and $CMOD_N$ = 0.13±0.03 and 0.25±0.04 mm for the uniaxial tension specimens cracked at 0.15 mm and 0.3 mm, respectively. For simplicity, crack widths will refer only to the target crack opening at the crack mouth hereafter, i.e. 0.15 and 0.3 mm $CMOD_M$.

The load – $CMOD_N$ data from each specimen was first resampled to a resolution of 1 µm. Then, the data was filtered and smoothed, using a 1-dimensional median filter and a moving average filter.

The calculation of the opening displacement at the crack mouth ($CMOD_M$) from the $CMOD_N$ measurements for the bending and uniaxial tension specimens was done according to the following methods: i) inverse calculation of the neutral axis position, applying the cracked-hinge model [33] for the bending specimens; and ii) as the mean value from the two $CMOD_N$ measurements for the uniaxial tension specimens. Hereafter, crack opening values discussed in this paper will only refer to the opening displacement at the crack mouth (i.e. $CMOD_M$ → CMOD).

The residual -flexural and -tensile strengths were calculated for the bending and uniaxial tension tests, respectively. The calculation of the residual flexural strength was done according to [30], assuming a single crack that propagates from the notch perpendicular to the length of the beam and that covers the entire cross-section. The residual tensile strength of the uniaxial tension tests was calculated as the ratio of the load and cross-section, assuming a single crack with a uniform crack width. Finally, the total energy absorbed (work) was calculated for both bending and uniaxial tension specimens as the integral of the load – CMOD curve.

Fig. 2. Visual inspection, fibre classification: a) no corrosion (fibre rupture), b) minor corrosion, c) moderate corrosion (fibre rupture), d) major corrosion (fibre rupture). After [26].

The final filtered data for each sample (i.e. a group of specimens) was fitted by a lognormal probability distribution and presented as the mean value of the load at each CMOD value with its upper and lower confidence bounds at a 90% confidence interval (CI).

2.4 Visual inspection and fibre counting

After finalizing the mechanical tests, the crack was opened completely and the fibres crossing the crack were inspected and counted by taking a high-resolution image of the surface of the specimen, according to the method described in [26].

The fibres crossing the crack were classified according to the degree of corrosion observed (see **Fig. 2**), using the following categories: Level 1, for the uncorroded fibres (green); Level 2, for the fibres with minor corrosion (yellow), i.e. rust spots at the surface with no visible loss of cross-section; Level 3, for the fibres with moderate corrosion (magenta), i.e. presence of pits and small loss of cross-section; Level 4, for the fibres presenting severe corrosion (red), i.e. presence of large pits and total or major loss of cross-section. Additionally, fibres that ruptured instead of pulled-out were marked as "ruptured" (blue). Furthermore, fibre rupture was always assumed for fibres with major corrosion (Level 4).

The fibre distribution was computed from the digital images taken of every specimen exposed and processed in batches using the image analysis algorithm described in [26]. The processed data is presented in **Sections 3.2** and **3.3** as discrete contours of the total density of fibres for each sample, i.e. showing the average number of fibres per dm^2 of each group of specimens, see **Fig. 3**.

The contours represent the density of fibres, categorized according to the degree of corrosion damage observed: (Level 1, green) no corrosion, (Level 2, yellow) minor corrosion, (Level 3, magenta) moderate corrosion, (Level 4, red) major corrosion, and (blue) fibre rupture, shown in **Fig. 3a-e**. Furthermore, an additional contour: "severe corrosion" (black) shows the areas with a density of fibres with a significant level of corrosion (i.e. combination of levels 3 and 4), see **Fig. 3f**.

For illustrative purposes, the contours of each group of fibres were combined into one figure for each sample. Therefore, only one representative contour is

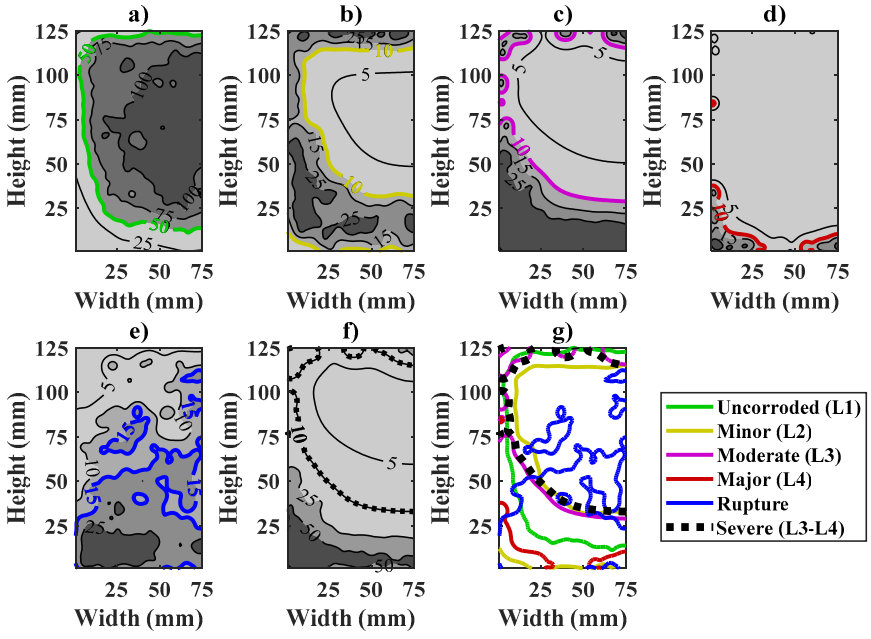

Fig. 3. Representation example of fibre counting results for bending sample (w30s7c0B), displaying example of full data and discretized contours for representation: a) no corrosion (L1); b) minor corrosion (L2); c) moderate corrosion (L3); d) major corrosion (L4); e) fibre rupture; f) significant corrosion (L3-L4), g) combined plot. Corrosion levels correspond to the ones described in **Fig. 2**. After [26].

plotted for each group (e.g. shown highlighted in **Fig. 3a-f**) which is then combined in a single plot (see **Fig. 3g**). The following thresholds were used to plot the contours: the non-corroded fibres (Level 1) are plotted for a density over 50 fibres/dm^2, the fibres with corrosion (Level 2 to Level 4) are plotted for a density of 10 fibres/dm^2, and the ruptured fibres are plotted for a density of 15 fibres/dm^2 (see **Fig. 3g**).

2.5 Statistical analyses

The discussion section includes two main types of statistical analysis: comparison of samples based on the Student's t-test, used in **Sections 4.1, 4.2 and 4.4,** and regression modelling used in **Section 4.5**.

2.5.1 Comparison of samples

The comparison of samples, discussed in **Sections 4.1, 4.2 and 4.4**, was performed by the Welch's approximation of the Student's t-test for samples with unequal variance [34], after the methodology used in [26]. The test calculates the probability value (p-value) for the null hypothesis (H_0) being true; being (H_0) the mean value for both distributions being equal. Therefore, p-values for the (H_0) which are lower than the level of significance (α), indicate that the null hypothesis (H_0) may be rejected; meaning that the alternative hypothesis (H_a) may be correct and the sample has a statistically-significant higher or lower mean value than the reference within a ($1-\alpha$) confidence.

In **section 4.1**, a two-tailed Welch's t-test is used to test the following alternative hypotheses (H_a): i) the mean values of the compressive strength for the three batches tested after two years of exposure being different to the ones tested after one year, ii) the mean value of the compressive strength for each of the exposed samples tested after two years of exposure being different than their corresponding sample tested after one year of exposure. The statistical significance level was set to $\alpha = 10\%$.

In **section 4.2**, the mean values of the work – CMOD curves for the bending and uniaxial tension samples are compared to the references by a one-tailed Welch's t-test (i.e. for both the right and left tails). The following alternative hypotheses (H_a) were tested: the probability of the mean value of the sample tested after two years of exposure being greater (right tail) or smaller (left tail) than its corresponding sample tested after one year of exposure. The statistical significance level was set to various levels: i.e. $\alpha = 5$, 15 and 25%.

In **section 4.4**, the mean value of the ratio of ruptured fibres tested after two years of exposure is compared twofold by a one-tailed Welch's t-test: i) to the mean value of the uncorroded reference (Level 1) after two-years exposure; and ii) to the mean values of each group, calculated for the samples tested after one-year exposure. The statistical significance level was set to $\alpha = 10\%$.

2.5.2 Regression model

The effect of the main study variables on the mechanical performance of the cracked SFRC were evaluated based on Partial Least-Squares Regression (PLS) analysis and Multiple Linear Regression (MLR) analysis in **section 4.5**.

First, the PLS analysis was used to identify the most dominant experimental variables (i.e. explanatory variables) in regard to explaining the variance observed in the toughness of the cracked composite after exposure during one and two years. The technique is a combination of Multiple Linear Regression (MLR) and Principal Component Analysis (PCA) techniques, described in [35]. The resulting model was used to identify the experimental variables that could have a dominant impact on the toughness of the material, i.e. expressed as the total work at a crack opening 0.5 – 4.0 mm in bending and tension. The following variables were investigated: the fibre content (v1), the ratio of fibres corroding (v2 – v4), the ratio of fibres rupturing (v5), the crack width (v6), the chloride concentration

(v7), the carbon dioxide concentration (v8) and the exposure time (v9).

Second, the MLR analysis was used to quantify the contribution of the main parameters to the variation in the toughness of the cracked SFRC tested after one- and two-years exposure, based on the results of the PLS analysis. Specifically, the model described the correlation of the fibre content, fibre damage (i.e. corrosion and rupture), crack width, exposure conditions and exposure time to the variation in toughness of the material, expressed as the total work at a crack opening 0.5 – 4.0 mm in bending and tension. The initial model is described in **Eq. 1** in Wilkinson notation [36]:

$$y \sim i + x1 : x2 : x3 : x4 : x5 : x6 : x7 \qquad \textbf{Eq. 1}$$

The regression model covers the main effects and 2-factor interactions of the following variables: fibre content (x1), ratio of corroding fibres for levels 2-4 (x2-4), ratio of ruptured fibres (x5), the crack width (x6) and the exposure time (x7). The independent and response variables were standardized. The predictor coefficients were fitted to the data using robust regression, i.e. least trimmed squares (LTS) with a bisquare weight function for the residuals. The model was reduced iteratively by backwards component selection applied to the interaction terms (threshold α

= 10%); while the main terms of the models were not reduced.

3. Experimental results

The experimental results after two-year exposure are described in this section divided into compression tests, bending tests and uniaxial tension tests. The corresponding results after one year were presented and discussed in [26]. The results of the bending tests and uniaxial tension tests are divided into mechanical performance results and fibre counting results.

3.1 Compression tests

The results of the compression test after two years of exposure are presented in **Fig. 4**. The data is presented classified by the exposure in **Fig. 4a**, with the sample names described in **Table 1** and the unexposed samples tested after two years (w0s0c0) presented in as "REF". Furthermore, the data is also presented classified by the concrete batch from which the specimens were produced (batch A-C), see **Fig. 4b**.

The results show a significant scatter within each sample (see **Fig. 4a**), corresponding to the results reported after one-year exposure [26], and related to production variations between the three batches (batch A-C), see **Fig. 4b**. The standard deviation for the whole population is around 7.5 MPa, i.e. approx. 10% of the mean value). The mean values of the samples grouped by exposure are comparable to each other, see **Fig. 4a**; which indicates a negligible change of the compressive strength comparing the exposures. Yet, the median values tend to lie skewed from the mean values, which is attributed to strength variations between batches (see **Fig. 4b**).

3.2 Bending tests

3.2.1 Mechanical performance

The results from the bending tests for uncracked and cracked samples are presented as the residual strength (i.e. stress – CMOD) in **Fig. 5** and as toughness (i.e. work – CMOD) in **Fig. 6**. Solid lines present the mean

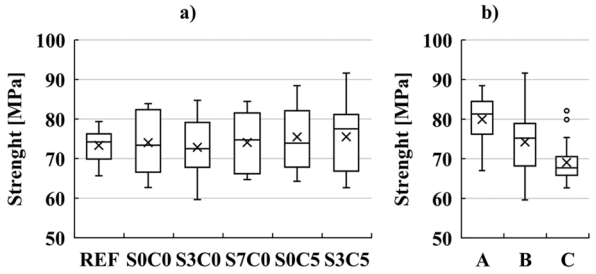

Fig. 4. Results for compression tests, grouped by: a) exposure, b) batch. The median value is shown as "—", the mean (arithmetic) value is shown as "X" and outliers are shown as "o". Sample names correspond to code names described in **Table 1**.

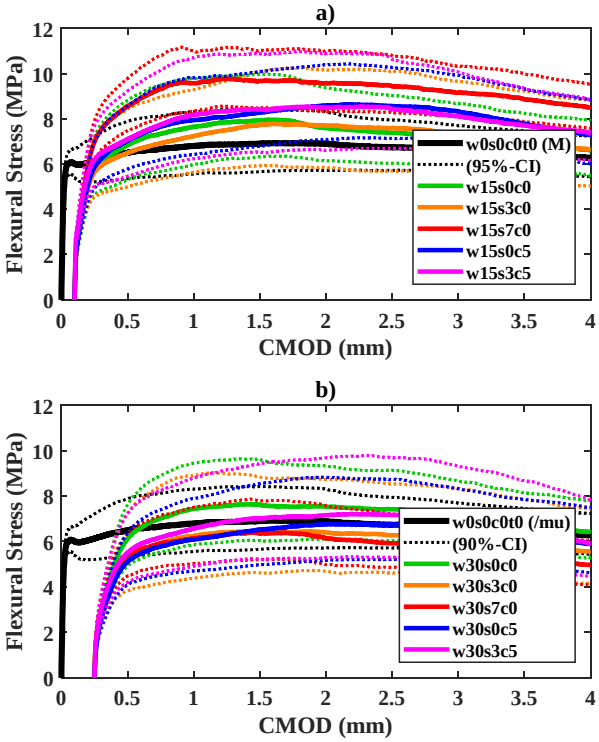

Fig. 5. Bending test after two-year exposure, Stress-CMOD plot for samples: a) cracked at 0.15 mm, b) cracked at 0.3 mm. Full lines represent the log-mean value (μ) of the sample and dotted lines represent the upper- and lower- confidence bounds at 90% CI. Sample names correspond to code names described in **Table 1**.

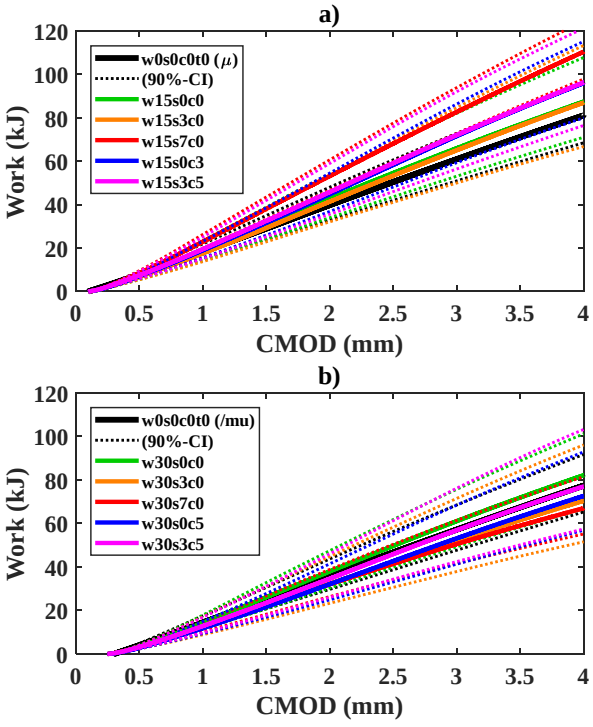

Fig. 6. Bending test after two-year exposure, Work-CMOD plot for samples: a) cracked at 0.15 mm, b) cracked at 0.30 mm. Full lines represent the log-mean value (μ) of the sample and dotted lines represent the upper- and lower- confidence bounds at 90% CI. Sample names correspond to code names described in **Table 1**.

values (μ), while the dotted lines show the upper and lower bounds of the 90% confidence interval (CI) for the mean value, assuming a lognormal distribution. Results for one-year exposure are presented and discussed in [26].

The results for the beams cracked at CMOD = 0.15 mm show that the exposed samples reach higher mean strength (**Fig. 5a**) and work values (**Fig. 6a**), relative to the uncracked reference samples tested at 56 days, similarly to as reported after one-year exposure in [26]. The spread of the confidence bounds of the mean for the exposed samples is generally higher compared to the spread observed for the uncracked references, especially for the cracked samples exposed to carbonation (s0c5 and s3c5).

The results for samples cracked at CMOD = 0.3 mm, show that the mean residual strength (**Fig. 5b**) and work curves (**Fig. 6b**) are generally similar to the uncracked references. However, the mean value of the samples exposed 3.5wt.% NaCl (w30s3c0) and 7.0wt.% NaCl (w30s7c0) dropped relative to the uncracked references. The spread of the confidence bounds of the mean for the exposed samples is generally higher compared to the spread observed for the uncracked references.

Generally, the mean value of the exposed cracked reference (s0c0) lies within the rest of the exposed samples for both crack widths, see **Fig. 5** and **Fig. 6**, except for the 0.15 mm sample exposed to 7.0% NaCl (w15s7c0), which reaches significantly higher values relative to the cracked reference (w15s0c0), see **Fig. 5a** and **Fig. 6a**.

3.2.2 Visual inspection and fibre count

The fibre count of the bending specimens is presented as discrete contours of the total density of fibres for each sample in **Fig. 7**, as described in **Fig. 3**. The contours represent the density of fibres, categorized according to the degree of corrosion damage observed: (Level 1, green) no corrosion, (Level 2, yellow) minor corrosion, (Level 3, magenta) moderate corrosion, (Level 4, red) major corrosion, (Levels 3-4, black) severe corrosion and (blue) fibre rupture. For illustrative purposes, the thresholds described in **Fig. 3** were used to plot the contours.

The surface of the crack (150×125 mm) has been divided by its vertical symmetry axis, showing an area of 75×125mm. The edges exposed to the solution are marked with a dotted red line (lower, left and upper edge); and the crack width of the cracked samples is plotted at the right axis. Finally, the position of the neutral axis of the cracked samples is

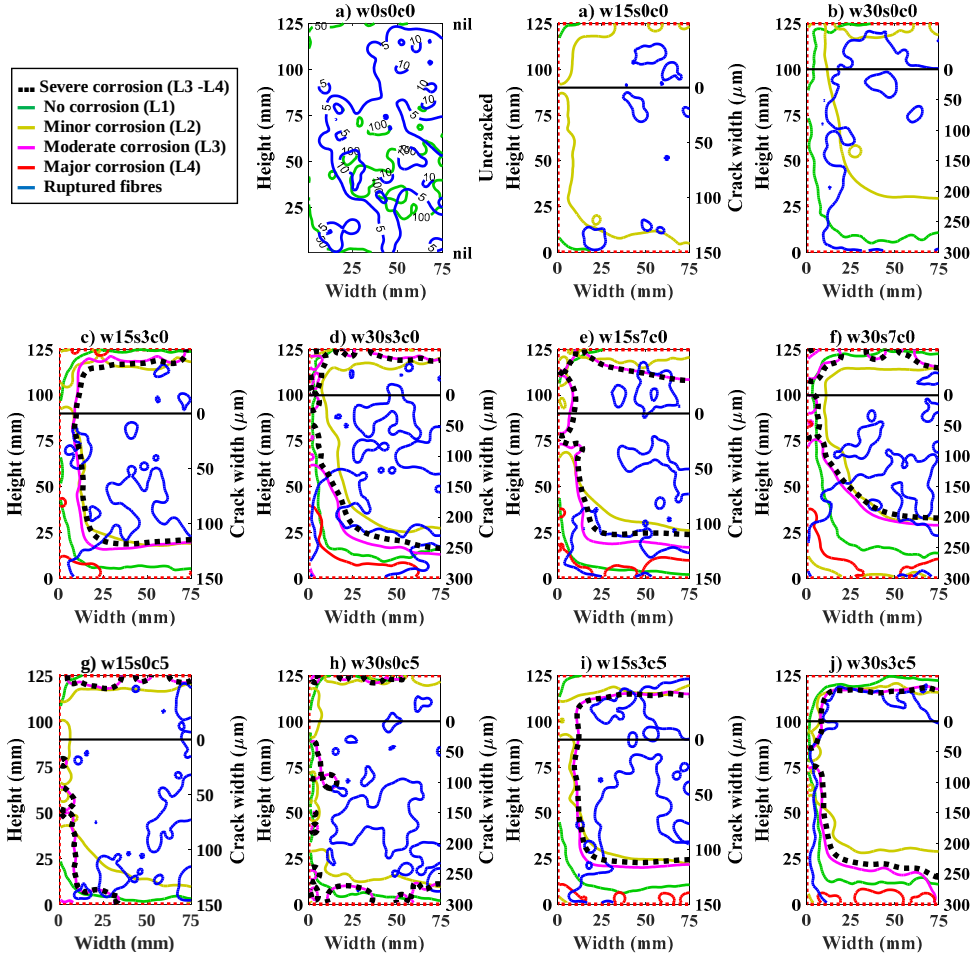

Fig. 7. Fibre counting for bending tests, contour plots for: a) uncracked reference, w0s0c0; b,c) cracked reference, s0c0; d,e) 3.5 wt.% NaCl exposure, s3c0; f,g) 7.0 wt.% NaCl exposure, s7c0; h,i) carbon dioxide and fresh-water exposure, s0c5; j,k) carbon dioxide and 3.5 wt.% NaCl exposure, s3c5. Sample names correspond to code names described in **Table 1**.

shown as a black horizontal line, and was calculated at 35 mm and 25 mm for the 0.15 mm and 0.3 mm CMOD samples respectively, see **Fig. 7b-k**. Additionally, the uncracked reference (w0s0c0) is presented with the following thresholds for the total density of fibres (Level 1) and ruptured fibres: 50-100 and 5-10 fibres/m^2, respectively (see **Fig. 7a)**.

The uncracked reference sample (w0s0c0) presents a homogeneous fibre distribution, with a total density of fibres between 50 – 100 fibres/dm^2 and a density of ruptured fibres in the range 5 – 10 fibres/dm^2, see **Fig. 7a**. Whereas, the cracked reference samples exposed to limewater (w15s0c0 and w30s0c0) show fibres with minor signs of corrosion (level 2) at the outer 10 – 25 mm, increasing for the larger crack width, see **Fig. 7b-c**. But do not show a larger share of rupturing fibres at the outermost regions of the crack.

The samples exposed to chlorides are presented in **Fig. 7** for these exposures: i) 3.5wt.% NaCl solution (w15s3c0 and w30s3c0), shown in **Fig. 7d-e**; ii) 7.0wt.% NaCl solution (w15s7c0 and w30s7c0), shown in **Fig. 7f-g**; and iii) carbon dioxide and 3.5wt.% NaCl solution (w15s3c5 and w30s3c5), shown in **Fig. 7d-e**. These show a similar spread of the contour of minor corrosion (Level 2) and the corrosion front (levels 3-4), that extend from the exposed edges up to 25 – 50 mm, decreasing both for smaller crack widths and lower NaCl concentrations.

The samples exposed to carbon dioxide and fresh water (w15s0c5 and w30s0c5) displayed a limited extent of corrosion into the crack (**Fig. 7h-i**), for example: the corrosion front (Levels 3-4) penetrated at approximately 10 mm from the exposed edges, and minor corrosion (Level 2) was observed up to 25 mm inside the cracked area, regardless of the crack width. Finally, the data indicates a larger share of rupturing fibres at the outermost regions of the cracks, corresponding to the corroding areas. Further analysis and discussion are provided in **Section 4.3**.

Additional results from visual inspection confirm the precipitate observed at the inner crack surface of the exposed samples reported in [26]; which changed its appearance and pH at the outer at the outer 10 – 25 mm (i.e. pH < 9) compared to the whiter coloration and higher pH deeper inside the crack (i.e. pH > 11). Furthermore, free chlorides were found inside most of the crack surface for the samples cracked at 0.3 mm CMOD exposed to NaCl, but only penetrated approx. 30 – 50 mm inside the crack for the specimens cracked at 0.15mm CMOD.

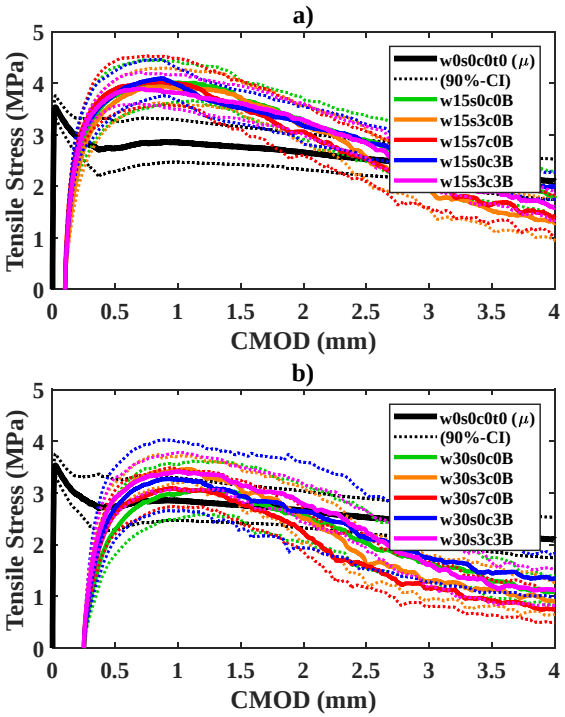

Fig. 8. Uniaxial tension test, Stress-CMOD curves for samples: a) cracked at 0.15 mm, b) cracked at 0.30 mm. Full lines represent the log-mean value (μ) of the sample and dotted lines represent the upper- and lower- confidence bounds at 90% CI. Sample names correspond to code names described in **Table 1**.

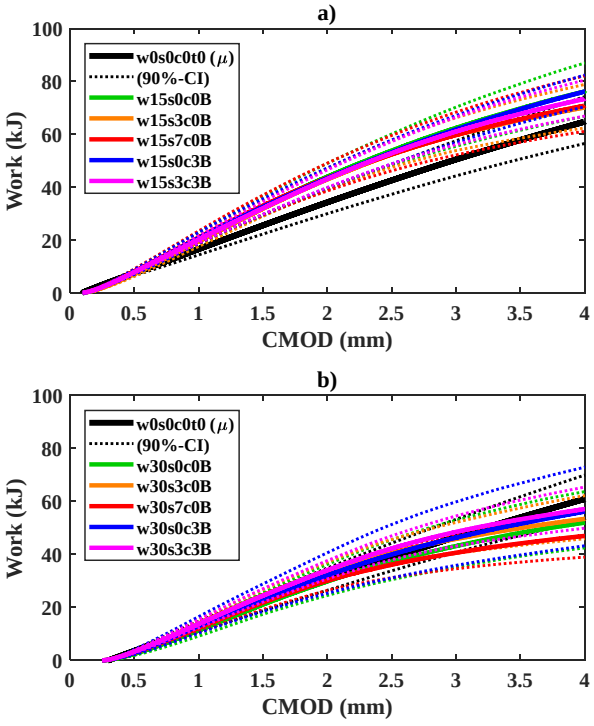

Fig. 9. Uniaxial tension test, Work-CMOD plot for samples: a) cracked at 0.15 mm, b) cracked at 0.30 mm. Full lines represent the log-mean value (μ) of the sample and dotted lines represent the upper- and lower- confidence bounds at 90% CI. Sample names correspond to code names described in **Table 1**.

3.3 Uniaxial tension tests

3.3.1 Mechanical performance

The results from the uniaxial tension tests for reference and cracked samples are shown as the residual strength (i.e. stress vs CMOD curves) (**Fig. 8**) and toughness (i.e. work – CMOD curves) (**Fig. 9**). The reference values for the uncracked samples are plotted for the sample tested at 56 days (i.e. w0s0c0).

Results presented in **Fig. 8a** and **Fig. 9a** for the samples cracked at 0.15 mm CMOD show higher mean strength values up to a CMOD of 2 – 3 mm and overall higher work values, relative to the uncracked reference samples (w0s0c0). Yet, showing similar confidence bounds of the mean observed to the uncracked references.

The results for samples cracked at 0.3 mm CMOD, show an overall decrease of the mean strength (**Fig. 8b**) and work responses (**Fig. 9b**) relative to the samples cracked at 0.15 mm CMOD (**Fig. 8a** and **Fig. 9a**). The drop in residual strength and work is more pronounced at CMOD values larger than 1.5 – 2.5 mm, where the mean strength of the samples cracked at 0.3 mm CMOD produce significantly lower values compared to the uncracked reference (w0s0c0), see **Fig. 8b**. Whereas, the slight increase in strength at CMOD ≈ 0.5 – 1.5 mm, relative to the uncracked reference (w0s0c0) compensates the drop at the end of the tail, and results in work curves for the exposed samples generally overlapping with the uncracked reference (**Fig. 9b**).

In general. the mean value of the exposed cracked reference at 0.15 mm CMOD (w15s0c0) and 0.30 mm CMOD (w30s0c0) lie within the rest of the exposed samples for the same crack width, see **Fig. 8** and **Fig. 9**, considering the confidence interval of the mean, and there is no distinct variation on the residual performance that can be directly linked to corrosion damage in fibres.

3.3.2 Visual inspection and fibre count

The fibre count results of the uniaxial tension specimens are presented as contours of the mean density of fibres for the levels of fibre corrosion described in the previous section for the bending samples, see **Fig. 10**. The surface of the crack (80×80 mm) was divided by its orthogonal symmetry axes, and the figure presents a crack surface of 40×40mm with a diagonal symmetry axis crossing the area from bottom-left to top-right; where the exposed edges are marked with dotted red lines (left and lower axis). The contours represent regions with a density of fibres over 10 fibres/dm^2 for each group, except for the uncorroded fibres (level 1) that are plotted for a density of 50 fibres/dm^2 and the ruptured fibres that are plotted for a density of 25 fibres/dm^2.

The uncracked reference sample presents a homogeneous fibre distribution, similar to the bending reference, with a fibre density between 50 – 100 fibres/dm^2, see **Fig. 10a**. The cracked reference samples exposed to limewater (w15s0c0 and w30s0c0) present mostly fibres with minor corrosion (level 2) at the outer 20 – 40 mm of the crack, respectively (see **Fig. 10b-c)**. Furthermore, the sample cracked at 0.3 mm (w30s0c0) also showed some fibres with a significant level of corrosion

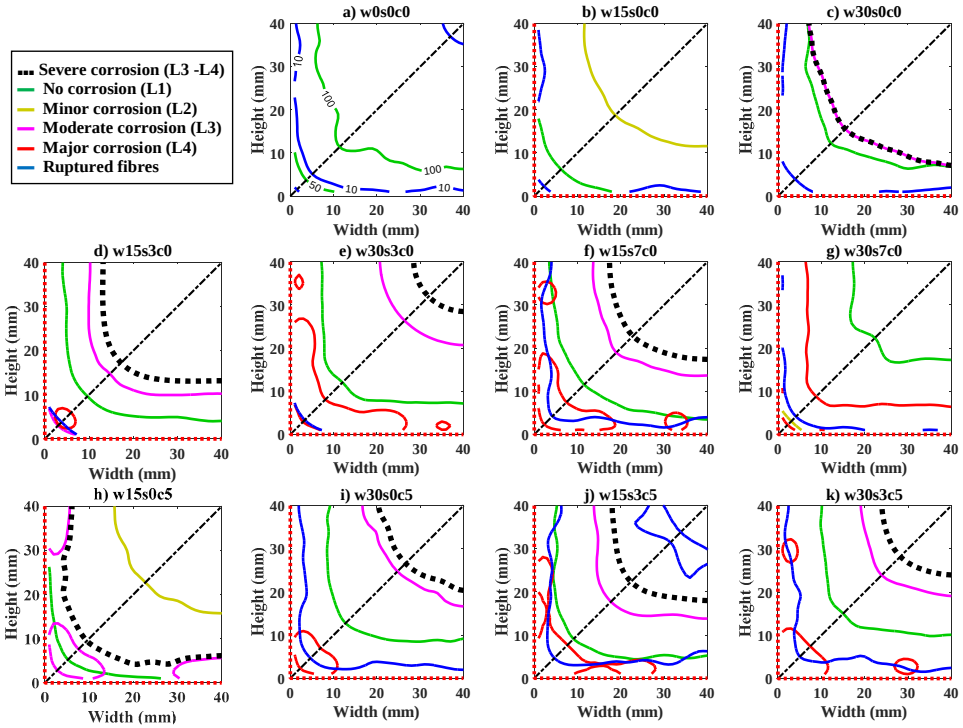

Fig. 10. Fibre counting for uniaxial tension tests, contour plots for: a) uncracked reference, w0s0c0; b,c) cracked reference, s0c0; d,e) standard chloride exposure, s3c0; f,g) high chloride exposure, s7c0; h,i) carbon dioxide and fresh-water exposure, s0c5; j,k) carbon dioxide and standard chloride exposure, s3c5. Sample names correspond to code names described in **Table 1**.

(levels 3 – 4) and a larger share of ruptured fibres at the outer 10 – 15 mm of the crack.

The samples exposed to chlorides are presented in **Fig. 10** for these exposures: i) 3.5wt.% NaCl solution (w15s3c0 and w30s3c0), shown in **Fig. 10d-e**; ii) 7.0wt.% NaCl solution (w15s7c0 and w30s7c0), shown in **Fig. 10f-g**; and iii) carbon dioxide and 3.5wt.% NaCl solution (w15s3c5 and w30s3c5), shown in **Fig. 10d-e**. These show a similar spread of the contour of minor corrosion (level 2) and the corrosion front (levels 3 – 4), that extend from the exposed edges from approx. 25 mm up to the full depth of the crack, decreasing both for smaller crack widths and lower NaCl concentrations.

The samples exposed to carbon dioxide and fresh water (w15s0c5 and w30s0c5) displayed a smaller extent of corrosion into the crack (**Fig. 10h-i**), for example: the corrosion front (levels 3 – 4) penetrated at approximately 10 – 25 mm from the exposed edges, but minor corrosion (level 1) was observed from 20 mm (**Fig. 10h**) up to the whole crack area (**Fig. 10i**), depending on the crack width. The corroding areas show a slightly larger share of rupturing fibres. Further analysis and discussion are provided in **Section 4.3**.

The visual inspection of the crack surface showed a precipitate at the inner crack faces of all the exposed samples, similar to that found in the bending samples, corresponding to the observations described in [26].

4. Discussion

The discussion below focuses on describing the role of the exposure time in the main aspects that describe the deterioration of SFRC: i) the strength of exposed uncracked SFRC (**Section 4.1**); ii) the toughness of exposed cracked SFRC (**Section 4.2**); iii) the extent and severity of fibre corrosion (**Section 4.3**); iv) the ratio of fibres rupturing and its relation to fibre corrosion (**Section 4.4**); v) the relative impact of the exposure time compared to the main variables affecting the toughness of the cracked material (**Section 4.5**).

The discussion finalizes in **Section 4.6** with a closing remark of the implications of the results presented in this paper on the design of SFRC infrastructure exposed to corrosive environments and a summary of the results presented in **Table 5**.

4.1 Variation of the strength of uncracked SFRC over time

This section discusses the variation of the strength of the uncracked composite over time. The results presented in **Section 3.1** show that there is no substantial variation in the compressive strength of the bulk concrete when comparing the exposures investigated (see **Fig. 4b**), and overall agree with the results presented in [26] for the specimens tested after one-year exposure.

Second, the variations of the mean ($\Delta\bar{x}$) and median ($\Delta\tilde{x}$) values over time (i.e. comparing results tested after one and two years of exposure) for each exposure and batch are presented in **Table 2**, including the probability value for the null hypothesis (H_0) for a two-tailed Welch's t-test. The results presented in **Table 2**, show a negligible variation of the mean values over time, when comparing one and two years of exposure, supported by the moderately high p-values of the t-test. Similarly, the variation of the compressive strength with time when comparing batches "A" and "B" with their counterparts tested at one year was statistically non-significant at α=10%. Batch "C" showed a statistically significant increase in the mean compressive strength over time of approximately 5%, which may be related to the still limited number of replicates tested (i.e. 12 replicates).

These results substantiate that under these exposure conditions, neither corrosion of fibres in uncracked concrete nor microstructural changes in the matrix at the surface due to exposure (e.g. chloride ingress, carbonation and leaching) may have a significant impact on the strength of the bulk concrete matrix over time, as discussed in [26] and in agreement with former studies [37–39].

Table 2. Comparison of compressive strength after two-year exposure, compared to results after one year.

Sample	Mean ($\bar{x}$) (MPa)	Δ. Mean ($\Delta\bar{x}$) (MPa)	Δ. Median ($\Delta\tilde{x}$) (MPa)	p-value (H_0) (-)
REF	73,3	1,5	3,3	0,619
s0c0B	74,0	1,0	-3,9	0,742
s3c0B	72,8	-0,7	5,4	0,870
s7c0B	74,1	1,5	-1,9	0,624
s0c5B	75,5	1,3	-3,8	0,718
s3c5B	75,5	2,4	5,5	0,514
A	80,0	-1,4	1,5	0,435
B	74,2	0,7	-1,1	0,719
C	69,1	3,7	2,3	0,035

Notes: *The mean value ($\bar{x}$) corresponds to the value for the results at two-years. The corresponding samples exposed for one year are used for calculation of $\Delta\bar{x}$, $\Delta\tilde{x}$ and p-value for each of the samples at two years. Data for samples exposed for one year was presented in* [26].

4.2 Variation of the residual mechanical performance of cracked SFRC over time

The results presented in **Sections 3.2.1 and 3.3.1** show that there are changes over time in the residual mechanical performance of cracked SFRC due to the different exposure conditions, relative to the uncracked reference sample, as shown in **Fig. 5-6** and

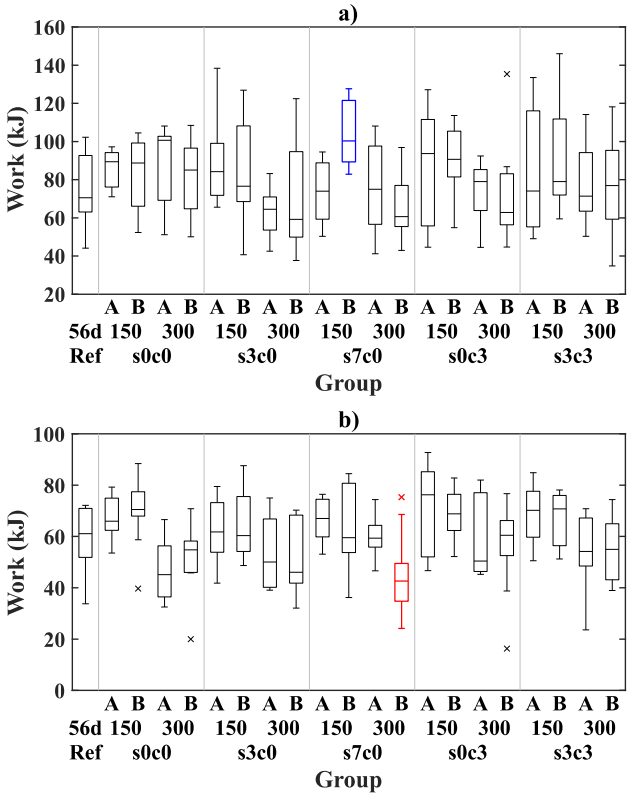

Fig. 11. Boxplot, total work at 4 mm CMOD for the uncracked reference and exposed samples after one year (A) and two years (B) for: a) bending test and b) uniaxial tension test. Sample names correspond to code names described in **Table 1**. Significant variations in work (at α=0.1) for samples exposed for two years compared to counterparts exposed for one year are highlighted in red (increase) and blue (decrease).

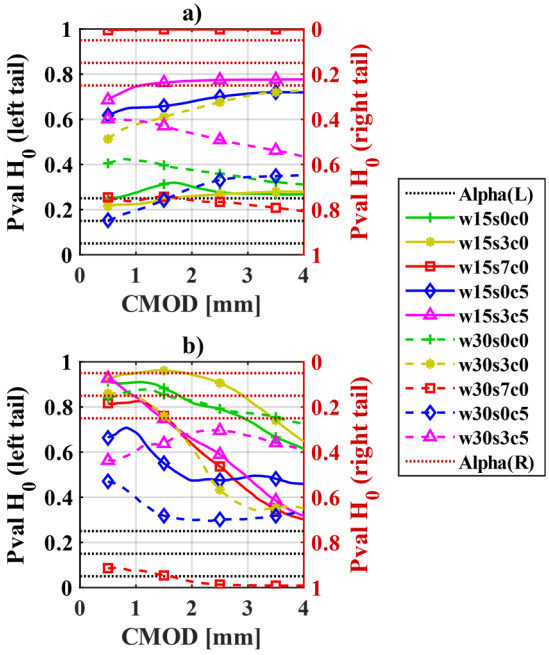

Fig. 12. T-test, comparison of samples after two years of exposure to cracked specimens exposed for one year, for: a) bending samples, and b) uniaxial tension samples. Sample names correspond to code names described in **Table 1**.

Fig. 8-9 for the bending and uniaxial tension samples, respectively. The variations of the toughness of the cracked composite over time (i.e. after two years exposure), compared to the data after one-year exposure [26], are discussed in this section.

The toughness of the cracked material was described by the total energy released during the tests (i.e. work); and was calculated below as the integral of the load-CMOD curve in the range of CMOD = 0.5 – 4.0 mm. The work values at 4 mm CMOD after one- and two-years exposure are presented as a boxplot in **Fig. 11**. The samples exposed for two years which show values significantly lower than their counterparts exposed for one year are highlighted in red, and the ones showing significantly higher values are highlighted in blue. The comparison was done by a one-tailed Welch's t-test, considering a significance level of α=10%.

The analysis of the data presented in **Fig. 11** shows that there is a generally large scatter of the toughness values, regardless of the crack width, exposure or age. There is no indication of a significant increase or decrease of the material toughness over time in bending or uniaxial tension when comparing data after one and two years of exposure to wet-dry cycles.

Except for two cases: i) the bending sample cracked at 0.15 mm and exposed to 7 wt.% NaCl, which showed a statistically significant increase in the toughness after two years exposure relative to one-year exposure (see w15s7c0B in **Fig. 11a**); and ii) the uniaxial tension sample cracked at 0.3 mm and exposed to 7 wt.% NaCl, which showed a statistically significant decrease in the toughness after two years exposure relative to one-year exposure (see w30s7c0B in **Fig. 11b**).

In the first case, i.e. w15s7c0B shown in **Fig. 11a**, the significant increase in performance may be related to the particularly low toughness of the sample tested after one year of exposure (w15s7c0B), as discussed in [26]. In the latter case, i.e. w30s7c0B shown in **Fig. 11b**, the significant decrease in toughness may be related to deterioration of the composite performance due to fibre corrosion, as observed in the large amount of fibres presenting moderate and major corrosion (levels 3-4) shown in **Fig. 10**. Further discussion on this issue is given in the following sections, see **Sections 4.3-4.5**.

The significance of the changes in the material toughness as a function of CMOD values was evaluated comparing the mean values of the work-CMOD curves for the bending and uniaxial tension samples to various references by means of a one-tailed Welch's t-test, as shown in **Fig. 12**. The figures show the probability (p-value) of: a) the mean value of the sample being smaller than the reference (left tail); b) the mean value of the sample being greater than the reference (right tail).

The distribution of the work-CMOD curves of the bending and uniaxial tension samples exposed during two years are compared to their corresponding samples exposed during one year, see **Fig. 12**. The significance thresholds (Alpha) considered for the alternative hypotheses (Ha) are: 95, 85 and 75%, which lead to p-values of 0.05, 0.15 and 0.25 for the null hypothesis (H_0), which are displayed as dotted horizontal lines.

Results show generally a non-significant variation on the toughness with time for most of the bending samples (see **Fig. 12a**), except for the sample cracked at 0.15 mm and exposed to 7 wt.% NaCl (w15s7c0), which presented a significant increase in the toughness over the whole CMOD range, see **Fig. 11a**. Uniaxial tension samples showed a trend of higher toughness values with time for CMOD < 2 mm which decreased at the end of the tail (i.e. at CMOD = 4 mm), see **Fig. 12b**; yet this was the case mostly for samples cracked at 0.15 mm. As discussed before, the uniaxial tension sample cracked at 0.3 mm and exposed to 7 wt.% NaCl (w30s7c0) showed a significantly lower toughness over the whole CMOD range.

These results show trends in toughness similar to as described in the data presented after one-year exposure in [26], presenting a general increase in toughness of cracked SFRC exposed to wet-dry cycles compared to uncracked SFRC at CMOD < 2.5 mm. Including additional branching and formation of new cracks in a region adjacent to the original crack (i.e. 10 – 30 mm around the crack) at CMODs larger than 0.5 mm.

Only the exposure to 7 wt.% NaCl resulted on a statistically significant decrease in work at larger deformations over time for the uniaxial tension samples cracked at 0.3 mm; though, bending samples under the same exposure and crack width did not show such a clear detriment to the performance over time. Which corroborates that there may be a "size-effect" to the deterioration of performance over time due to fibre corrosion, as discussed in[26] for corresponding data after 1 year exposure and in former studies [18,25].

4.3 Fibre corrosion over time

The results from the fibre counting described in Sections 3.2.2 and 3.3.2 are discussed below, presented as the percentage of fibres classified by the deterioration levels described in **Fig. 2** (Levels 1-4 and rupture), relative to the depth inside the crack. Results are shown for the bending samples in **Fig. 13** and uniaxial tension samples in **Fig. 14**. An additional profile represents all fibres with severe corrosion: e.g. the combination of fibres with moderate and major corrosion (Levels 3-4). Finally, the profiles of uncorroded fibres (Level 1) and fibres with severe corrosion (Levels 3-4) from the samples tested after one year, see [26], have been included as reference.

Furthermore, the outer 25 mm at the laterals of the crack and the fibres located at the compression zone of the cracked bending samples are omitted from the analysis in **Fig. 13**, to consider just the corrosion extending from the crack mouth. So that the initial cross-section (150×125 mm) is reduced to an area of 100×90 mm for samples cracked at 0.15 mm CMOD

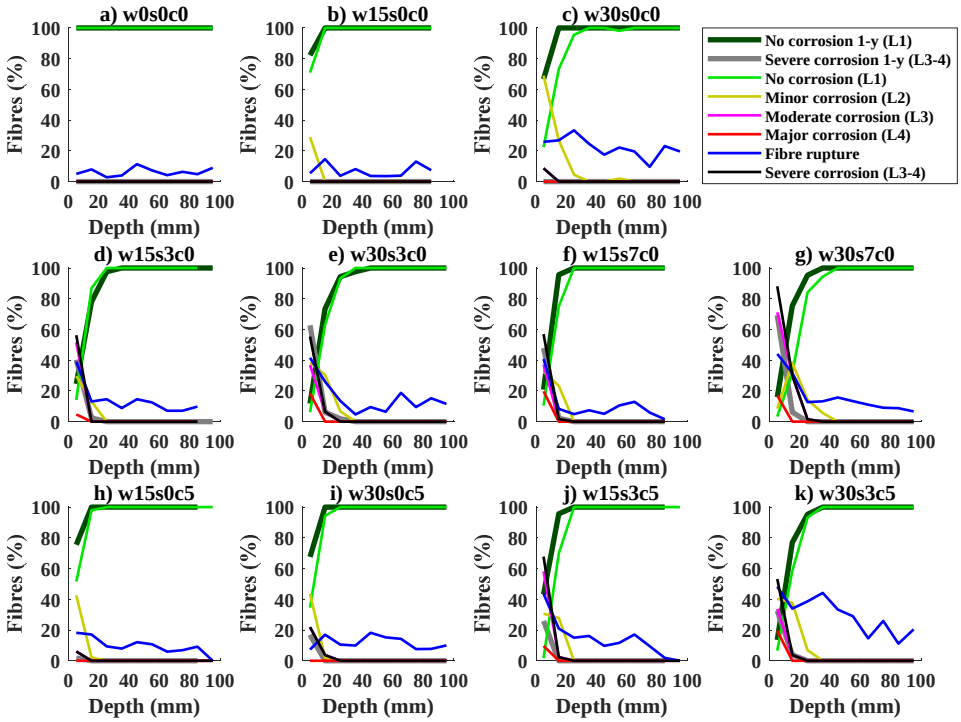

Fig. 13. Fibre corrosion versus crack depth for bending samples: a) uncracked reference, w0s0c0; b,c) cracked reference, s0c0; d,e) 3.5wt.% NaCl exposure, s3c0; f,g) 7.0wt.% NaCl exposure, s7c0; h,i) carbon dioxide and fresh water exposure, s0c5; j,k) carbon dioxide and 3.5wt.% NaCl exposure, s3c5. Sample names correspond to code names described in **Table 1**.

and 100×100 mm for samples cracked at 0.30 mm CMOD.

Fibre corrosion extends from the outer crack area, the ratio of corroding fibres and degree of corrosion decrease gradually up to approx. 20 – 40 mm from the crack mouth, see **Fig. 13-14b-k**. The extent and severity of fibre corrosion is generally larger for samples cracked at 0.3 mm (see **Fig. 13-14c,e,g,i,k**) compared to those cracked at 0.15 mm (see **Fig. 13-14b,d,f,h,j**). Exposure to chlorides mainly entails an increase in the severity of corrosion relative to the other exposed samples, i.e. larger share of fibres presenting moderate and major corrosion (Levels 3-4), see **Fig. 13-14d-g** and **Fig. 13-14j-k**. In general, fibre rupture tends to increase at depths where most fibres present severe corrosion (Levels 3-4), i.e. the outer 10 – 20 mm of the crack depending on the exposure and crack width. There is some trend of increase in the extent of fibre corrosion over time, when comparing the results presented in **Fig. 13-14** with the data after one year, discussed in [26].

Comparison of results from samples tested after one- and two-years exposure generally showed a negligible progress of the extent of fibre corrosion over time for the samples cracked at 0.15 mm, for both bending (see **Fig. 13 b,d,f,h,j**) and uniaxial tension samples (see **Fig. 14 b,d,f,h,j**). Whereas, the extent of fibre corrosion only increased over time for samples cracked at 0.3 mm exposed to: 7 wt.% NaCl (w30s7c0), see **Fig. 13-14c**; 0.5 vol.% CO_2 (w30s0c5), see **Fig. 13-14I**; and the reference sample exposed to limewater cycles (w30s0c0), see **Fig. 13-14c**. The additional corrosion damage was negligible in the two last ones (i.e. only related to fibres with minor corrosion).

Besides the aforementioned exceptions, the exposed samples showed corrosion damage agreeing with the data gathered after one-year exposure [26], for example: the extent of fibre corrosion inside the crack increased mainly with larger initial crack width and when exposed to carbon dioxide; while the presence of chlorides mainly increases the severity of fibre corrosion. The results suggest that fibre corrosion does not extend into the crack substantially with time, whereas the severity of fibre corrosion progresses gradually with time. Similar trends were found in previous research [11,16], but former studies do not provide an accurate location and classification of the corroding and rupturing fibres. The analysis of the extent and severity of fibre corrosion inside the crack is qualitative [4], which does not allow further objective comparison of this data.

4.4 Correlation of fibre corrosion and fibre rupture over time

The correlation of corrosion damage of fibres bridging the crack to changes in the residual performance of the material over time was investigated by quantifying the impact of fibre corrosion on the quantity of fibres rupturing instead of pulling out.

The relation of fibre corrosion to the number of fibres rupturing is presented in **Fig. 15**, as a boxplot showing the ratio of fibres ruptured at each corrosion level ($L_1 – L_4$) and combinations of them. The ratio of ruptured fibres is compared at each corrosion level to a reference by a two-tailed Welch's t-test with α=10%, which shows a significantly larger number of samples marked in red. The figure describes the following analyses: i) the percentage of fibres

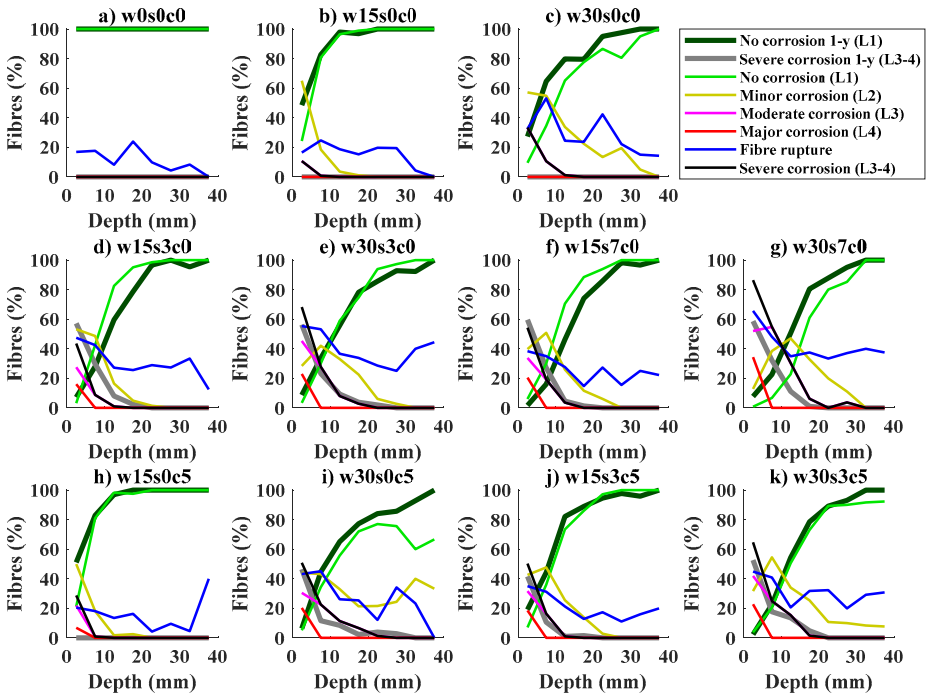

Fig. 14. Fibre corrosion versus crack depth for uniaxial tension samples: a) uncracked reference, w0s0c0; b,c) cracked reference, s0c0; d,e) 3.5wt.% NaCl exposure, s3c0; f,g) 7.0wt.% NaCl exposure, s7c0; h,i) carbon dioxide and fresh water exposure, s0c5; j,k) carbon dioxide and 3.5wt.% NaCl exposure, s3c5. Sample names correspond to code names described in **Table 1**.

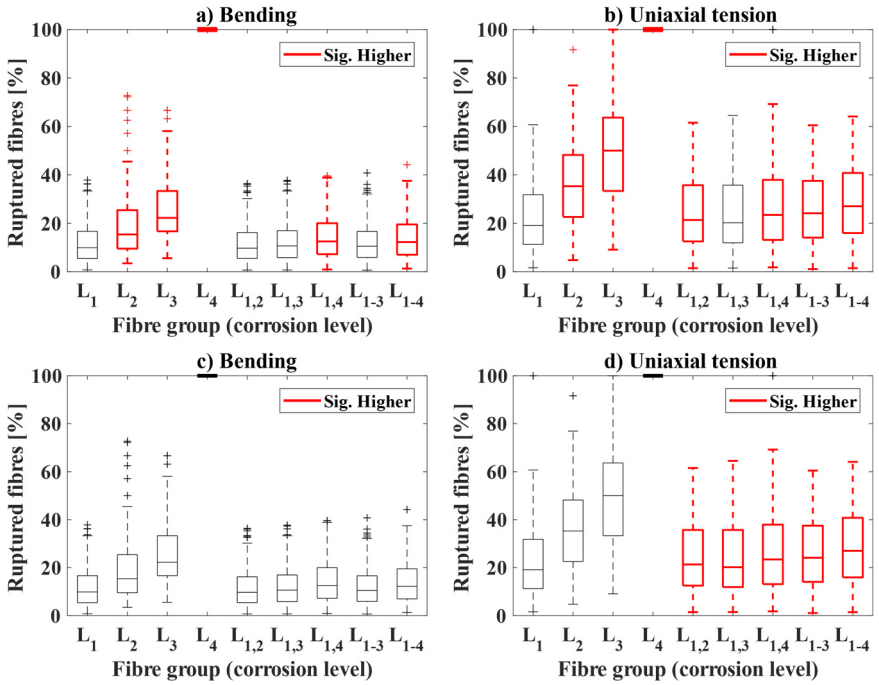

Fig. 15. Impact of fibre corrosion on fibre rupture over time for: a) bending samples after two years, b) uniaxial tension samples after two years, c) bending samples after one- and two-years d) uniaxial tension samples after one and two years.

rupturing depending on their degree of corrosion in the samples tested after two-years exposure for bending (**Fig. 15a)** and uniaxial tension samples (**Fig. 15b**), using the values measured for non-corroded fibres (L1) as reference in the t-test; ii) the total percentage of fibres rupturing depending on their degree of corrosion for the samples tested after one- and two-year exposure for bending (**Fig. 15c)** and uniaxial tension samples (**Fig. 15d**), indicating if there is a statistically significant increase in the ratio of ruptured fibres over time (i.e. using the data after one year of exposure as reference [26]).

The first analysis, see **Fig. 15a-b**, shows that for any degree of fibre corrosion (i.e. L2 to L4) there is a trend towards a significant increase in fibre rupture as corrosion is more severe; which corresponds well to the observations reported after one-year exposure [26]. The contribution of fibres rupturing due to corrosion to the total count of fibres was significant for some cases, i.e. see ($L_{1,4}$ and L_{1-4}) in **Fig. 15a** and ($L_{1,2}$, $L_{1,3}$, $L_{1,4}$, L_{1-3} and L_{1-4}) in **Fig. 15b**.

The second analysis, see **Fig. 15c-d**, shows that there is no significant increase in the ratios of fibres rupturing due to corrosion over time (see $L_{1,2}$, $L_{1,3}$ and $L_{1,4}$ in **Fig. 15c-d**). There is a statistically significant increase in the contribution of corroding fibres to the total amount of rupturing fibres over time for the uniaxial tension samples ($L_{1,2}$, $L_{1,3}$, $L_{1,4}$, L_{1-3} and L_{1-4} in **Fig. 15d**); yet, this increase in the contribution over time was not observed for the bending samples, as shown in ($L_{1,2}$, $L_{1,3}$, $L_{1,4}$, L_{1-3} and L_{1-4}) in **Fig. 15c**.

The discussion above corroborates that there must be a differentiation in the cause of fibre rupture in cracked SFRC, as presented in [26]; fibres crossing the crack may rupture due to: i) a critical reduction of the cross-section due to corrosion; or ii) an apparent increase in the fibre-matrix bond strength over the exposure. The data presented shows a slight increase over time in the first group for specimens with a small cross-section. Whereas, there does not seem to be an increase over time of the ruptured fibres belonging to the second group for the specimens tested in this study.

Consequently, it is inferred that the impact of the exposure time on the total number of fibres rupturing due to corrosion is strongly influenced by the size and shape of the specimen, since fibres corrode mostly at the outer 20 – 40 mm of the crack. For example, corroding fibres were found at 75 – 100% of the of the cross-section of uniaxial tension test samples (80x80 mm exposed at all edges) but comprised only 30 – 45 % of the cross-section of bending samples (150x125 mm exposed at three edges).

4.5 The contribution of exposure time to the mechanical performance of cracked SFRC

The relative impact of the exposure time on the mechanical performance of the cracked SFRC is discussed below by means of Partial least-squares (PLS) regression and multiple linear regression (MLR). The first analysis, based on the PLS technique, was utilized to identify the main variables affecting the mechanical performance of the composite measured in bending and uniaxial tension tests. Whereas, the second analysis, based on the MLR technique, was used to describe and quantify the contribution of these variables to the performance of the composite over time, based on the model described in **Section 2.5** and [26].

4.5.1 Partial least-squares regression (PLS)

The PLS method is applied to the two datasets (i.e. bending and uniaxial tension data) in separate models. The models cover the quantification of the contribution of the following variables to the toughness of the composite, integrated at a CMOD range 0.5 – 4 mm (y), being: the fibre content (v1), the ratio of fibres corroding (v2 – v4), the ratio of fibres rupturing (v5), the crack width (v6), the chloride concentration (v7), the carbon dioxide concentration (v8) and the exposure time (v9). The model was initially calculated for 8 principal components, and was subsequently reduced to 3 components, results are presented in **Table 3**; but for illustrative purposes the models presented in **Fig. 16-17** are shown for 5 principal components.

The resulting coefficient estimates (β) and normalized weights of the explanatory variables and coefficient of determination (R^2) are presented in **Table 3** for the two models. Furthermore, the variance explained by the first 5 principal components for the two models is presented in **Fig. 16-17a**, the plot of explained vs predicted variance is presented in **Fig. 16-17b**, and the cumulative normalized weights for the explanatory variables vs the first 5 components is presented in **Fig. 16-17c**.

The coefficients of determination (R^2) and the adjusted coefficients of determination are in the range 0.6 to 0.8, being slightly higher for the bending data. The coefficients of determination correspond well to the overall large scatter in the data observed in **Fig. 16-17b**. However, besides some signs of heteroskedasticity in **Fig. 16b** and a slightly uneven distribution observed in **Fig. 17b**, the fit may be sufficient for identifying the dominant variables in the study.

Table 3. Partial least-squares regression model results for 3 principal components for the bending and uniaxial tension data. Normalized weights for explanatory variables, regression coefficients (β) and coefficients of determination (R^2).

	Variables	Bending		Tension	
		Weight	β	Weight	β
i	*intercept*	-	0.000	-	0.000
v1	Fibre count	0.457	0.819	0.294	0.528
v2	Corr. L2 (%)	0.084	-0.054	0.104	-0.053
v3	Corr. L3 (%)	0.121	-0.230	0.104	-0.104
v4	Corr. L4 (%)	0.102	-0.179	0.087	-0.084
v5	Rupture (%)	0.127	0.402	0.160	-0.096
v6	Crack width	0.093	-0.067	0.174	-0.242
v7	Chlorides	0.002	-0.008	0.020	0.071
v8	Carbon dioxide	0.009	0.026	0.051	0.118
v9	Exposure cycles	0.005	-0.068	0.005	0.025
		R^2	0.728	R^2	0.632

The results presented in **Fig. 16-17c** present the normalized weight of the variables in the principal components. The figures show, that for both sets of data, the fibre content (v1) dominates over the rest of the variables; comprising 30 – 40 % of the explained variance within the first 2 – 3 components. Whereas, other variables such as the number of ruptured fibres (v5), the crack width (v6) or the ratios of corroding fibres (v2 – v4) have a secondary impact. Finally, the exposure time (v9) or the exposure conditions (v7 – v8) had a negligible normalized weight; which indicates that would have a non-significant contribution to the toughness of the cracked composite.

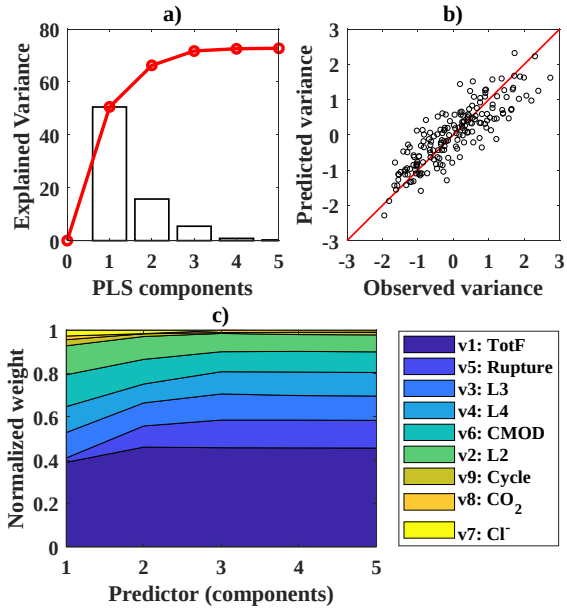

Fig. 16. Results from PLS regression for the bending data, showing: a) explained variance for main PLS components, b) predicted variance versus observed variance, c) cumulative normalized weight of variables trough PLS components.

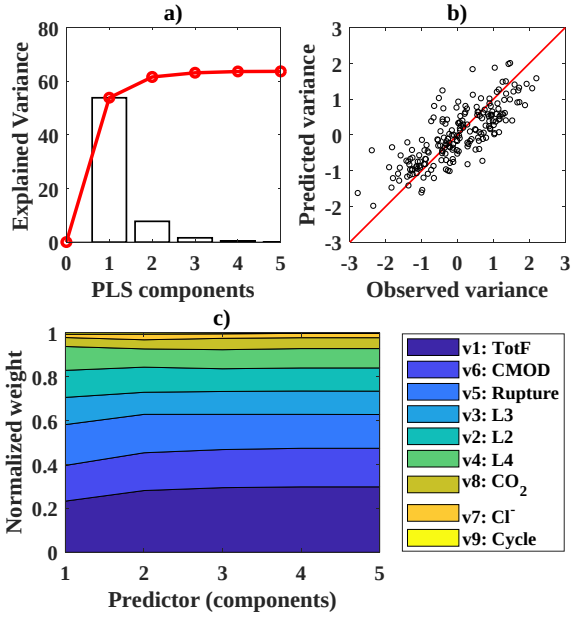

Fig. 17. Results from PLS regression for the uniaxial tension data, showing: a) explained variance for main PLS components, b) predicted variance versus observed variance, c) cumulative normalized weight of variables trough PLS components.

Therefore, this analysis confirms the discussion presented in [26], which showed a dominant role of the fibre content relative to the rest of the variables, when explaining the variations after exposure. Whereas, this study also suggests, that the exposure time may not have a substantial contribution to variations of the composite toughness at the time-scales investigated.

4.5.2 Multiple linear regression (MLR)

The previous analysis showed an indication of the relative impact of those variables in the toughness, but it did not provide a clear quantification of the correlation. Therefore, multiple linear regression analysis (MLR) was used to describe the contribution of those variables to the variations in toughness, by extending the model presented in [26] in order to include the contribution of the exposure time.

The model covers the quantification of the contribution of the following variables on the toughness of the composite up to a CMOD of 4 mm (y), being: the fibre content (x1), the ratio of fibres corroding (x2 – x4), the ratio of fibres rupturing (x5), the crack width (x6) and the exposure time (x7). The linear predictors for the main variables and two-factor interactions are presented in Wilkinson notation for the bending tests in **Eq. 2** and for the uniaxial tension tests in **Eq. 3**; where the non-statistically significant variables are presented between apostrophes ‘’ and non-significant interactions are omitted (i.e. considering $\alpha = 0.1$).

$$y \sim \text{‘i’} + x1 + \text{‘x2’} + x3 + x4 + x5 + x6 + \text{‘x7’} + x2{:}x6 + x5{:}x6 \quad \textbf{Eq. 2}$$

$$y \sim \text{‘i’} + x1 + \text{‘x2’} + \text{‘x3’} + x4 + \text{‘x5’} + x6 + \text{‘x7’} + x1{:}x4 + x4{:}x6 + x5{:}x6 + x6{:}x7 \quad \textbf{Eq. 3}$$

The resulting coefficient estimates and p-values of the linear terms and coefficients of determination (R^2 and adjusted R^2) are presented in **Table 4**. Furthermore, the coefficient-estimates and normalized residuals (i.e. Standardized and Pearson residuals) of the resulting models are presented in **Fig. 18a-b** for the bending tests and in **Fig. 18c-d** for the uniaxial tension tests.

Table 4. Multiple regression model results. Estimates and p-values for regressors and coefficients of determination.

		Bending		Uniaxial tension	
	Variable	**Estimate**	**p-value**	**Estimate**	**p-value**
i	Intercept	0.061	0.123	0.062	0.198
x1	Fibre count	0.859	0.000	0.674	0.000
x2	Corr. L2 (%)	0.062	0.157	0.049	0.367
x3	Corr. L3 (%)	-0.154	0.001	-0.060	0.348
x4	Corr. L4 (%)	-0.250	0.000	-0.139	0.027
x5	Rupture (%)	0.502	0.000	-0.004	0.952
x6	Crack width	-0.136	0.001	-0.270	0.000
x7	Exposure cycles	-0.012	0.784	-0.010	0.834
		R^2	0.788	**R^2**	0.633
		R^2 adj.	0.776	**R^2 adj.**	0.607

The coefficients of determination (R^2) and the adjusted coefficients of determination are in the range 0.6 to 0.8, being slightly higher for the bending data. These values indicate an overall moderate fit of the data; yet, the normalized residual plots, see **Fig. 18b,d**, show a fair distribution with no signs of self-correlation, but with large normalized residual values.

The normalized coefficient estimates (z-scores) for the main predictors are presented in **Fig. 18a,c**, which displays the relative impact of each variable on the toughness of the material. Positive estimates indicate an increase of the toughness when the variable increases. Non-significant estimate predictions, i.e. at α=10%, are displayed in grey.

The coefficient estimates presented in **Fig. 18a,c** agree with the results of the PLS model and show that the overall impact of the fibre content (x1) in the toughness of the cracked composite dominates over the relative impact of the other variables for both test methods.

The relative impact of fibre corrosion (x2-x4) on the toughness of the composite estimated by the model shows a non-statistically significant positive impact of the fibres with minor corrosion (x2) and a negative impact of fibres presenting moderate and major corrosion (x3-x4), which was statistically significant for both groups in the bending samples (see **Fig. 18a**) but only for the fibres presenting major corrosion (x4) for the uniaxial tension test (see **Fig. 18c**).

The ratio of ruptured fibres had a statistically significant positive relation to higher toughness

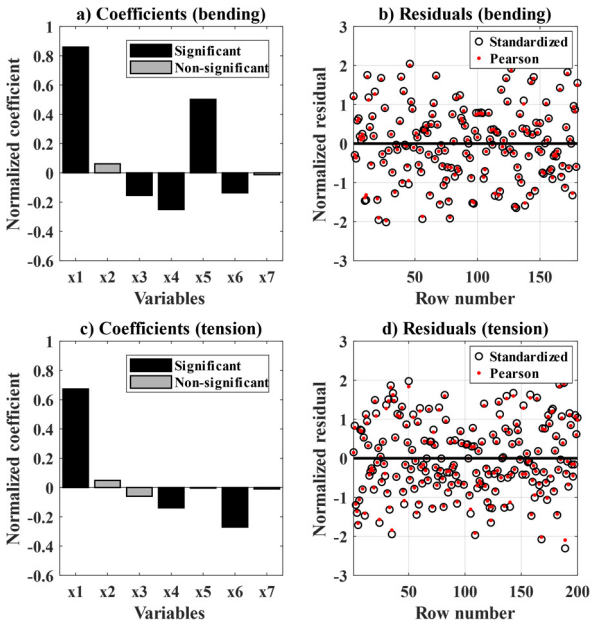

Fig. 18. First multiple regression model for bending specimens and uniaxial tension specimens, showing: a) normalized coefficients for bending specimens, b) residuals for bending specimens, c) normalized coefficients for uniaxial tension specimens, d) residuals for uniaxial tension specimens.

values for the bending samples (see **Fig. 18a**), but had a negligible impact on the uniaxial tension samples (see **Fig. 18b**). The crack width (x6) had a statistically significant negative impact on the toughness of the cracked composite for both datasets, see **Fig. 18a,c**. Finally, the number of cycles (x7) did not have a statistically significant contribution in the residual toughness for none of the datasets see **Fig. 18a,c**. Thus, suggesting some inconsistency in the expected negative contribution of the exposure time to the toughness of the cracked composite, which may be negligible at the scales investigated (i.e. comparing one and two years of exposure).

The analysis presented above generally agrees with the discussion presented in [26] for the experiments done after one year of exposure. Overall, the variability in the fibre distribution inherent to the production and test methods used have a dominant role over the rest of parameters when explaining changes in the residual mechanical performance of the exposed cracked composite over time.

4.6 Summary and design implications

This study investigated the impact of fibre corrosion on the mechanical performance of cracked SFRC exposed to wet-dry cycles of various corrosive environments over a period of two years. A summary of the results after two years of exposure to various environments is presented in **Table 5**, classified according to EN 206 as: limewater (XC0-1), 3.5wt.% NaCl solution (XS3), 7.0wt.% NaCl solution (XS3↑), fresh water and CO_2 drying cycles (XC4) and 3.5wt.% NaCl solution and CO_2 drying cycles (XS3 + XC4). Toughness ratios calculated as the mean total work up to CMOD = 4.0 mm for each of the exposures relative to the samples tested after one-year exposure are given in **Table 5**.

The discussion presented in **Section 4.1** indicates negligible changes in the elastic performance of the exposed uncracked material tested in compression over two years of exposure, for specific values refer to **Table 5**.

The residual mechanical performance of the cracked composite did not vary significantly with time for the time-scale studied, except for the samples cracked at 0.3 mm and exposed to 7wt.% NaCl, which showed a significant drop in toughness over time, see **Section 4.2**. In general, the changes in the residual mechanical behaviour of the cracked composite observed after one year of exposure in [26], were also observed after two years.

There was a minor increase in the extent and severity of fibre corrosion inside the crack over time, as discussed in **Section 4.3**, which was only significant for some of the specimens cracked at 0.3 mm. Anyhow, fibre corrosion was only observed at the outer 20 – 40 mm of the crack, depending on the exposure and crack width (for specific values refer to **Table 5**). The trends observed in fibre corrosion over time suggest that the corrosion damage inside the crack is governed by the transport of moisture and species through the crack.

The analysis of the contribution of fibre corrosion to the number of fibres that ruptured instead of pull-out of the matrix presented in **Section 4.4** showed that the ratio of ruptured fibres relative to the corrosion damage did not vary significantly over time. The total

Table 5. Summary of results

Exposure (sample)	Exposure Class [EN 206]	Crack width [mm]	Corrosion front depth [mm]		Severe corrosion front depth [mm]		Toughness variation [-]		Strength variation [-]
			3PB	UTT	3PB	C	3PB	UTT	C
w15s0c0	XC1 (XC4)	0.15	20	20	-	10	0.960	1.054	1.003
w30s0c0		0.30	30	>40	10	10	0.937	1.119	
w15s3c0	XS3	0.15	30	30	20	20	0.933	1.057	1.006
w30s3c0		0.30	40	40	30	20	1.153	0.969	
w15s7c0	XS3↑	0.15	30	30	30	20	1.378	0.990	1.004
w30s7c0		0.30	40	40	30	30	0.878*	0.779*	
w15s0c5	XC4	0.15	20	20	10	10	1.046	0.977	0.999
w30s0c5		0.30	30	>40	20	30	0.971	0.967	
w15s3c5	XC4 + XS3	0.15	30	30	20	20	1.105	0.981	1.033
w30s3c5		0.30	40	>40	30	20	1.012	1.024	

Abbreviations: *(Exposure "sample") codes of the experiment exposures according to* ***Table 1****, (Exposure class) corresponding exposure classes according to EN 206, (Crack width) crack width during the exposure expressed in mm, (Corrosion front depth) depth of corrosion inside the crack measured from the exposed edges for any level of corrosion expressed in mm, (Severe corrosion front depth) depth of severe corrosion "corrosion levels 3-4" inside the crack measured from the exposed edges expressed in mm, (Toughness variation) the ratio between the toughness of the sample tested after two-year exposure and the sample tested after one-year exposure, statistically-significant values (α = 0.2) are marked with "*", (Strength variation) the ratio between the compressive strength of the exposed sample and the unexposed reference (w0s0c0), significant values are marked with "*", (3PB) three-point bending specimens, (UTT) uniaxial tension test specimens, (C) compression specimens.*

count of rupturing fibres only increased significantly with time for the uniaxial tension samples; indicating that the percentage of fibres rupturing increase gradually as fibre corrosion proceeds, but it may be negligible in larger cross-sections.

Finally, the analysis presented in **Section 4.5** indicates that the contribution of the variation of the total number of fibres crossing the crack generally dominates over the rest of the experimental variables; including the exposure time, which showed a negligible impact on the toughness of the cracked composite for the time-scale investigated.

The discussion in this paper indicates minor deterioration over time of the toughness of the cracked composite due to fibre corrosion, i.e. disregarding the contribution of the outermost fibres (e.g. at approx. at the outer 10 – 40 mm of the crack), which could critically corrode, but may not compromise the long-term integrity of cross-sections larger than e.g. 150 mm. These observations correspond well to some of the results reported in field exposure of cracked SFRC exposed to chlorides (i.e. EN-206 classes XS2 and XS3) [6,10,13–16] and carbonation (i.e. EN-206 classes XC4) [10,16] during periods of 1 – 5 year. However, results presented herein still disagree with conclusions from former studies, that predicted substantial decrease in residual performance over time in cracked SFRC due to fibre corrosion [11] or that measured a substantial decrease in toughness attributed to an excessive increase in the fibre-matrix bond strength, described as "embrittlement" [13,40].

Based on this discussion, there is no indication suggesting that fibre corrosion may have a critical impact over time (i.e. for the timescales investigated) on the residual performance of SFRC cracked up to 0.3 mm exposed to wet-dry cycles for typical engineering applications. Considering for example that: the cross-section thickness of a prefabricated segmental lining is in the range 200 – 400 mm [2,41], or is approx. 400 – 600 mm for a slab-on-grade [42]. Yet, the time-scale investigated in this study is substantially shorter compared to the typical aims for service life of such infrastructure, i.e. the design service life of a bored tunnel may be as long as 100 – 120 years [2,43,44].

There is still limited data available from long-term studies that can be used to corroborate these observations, for example: inspection of SFRC infrastructure exposed to XS3 and XC4 environments during 20 years did not show substantial corrosion damage in steel fibres bridging small cracks, but did not provide any measure of the mechanical performance of the cracked composite [16].

Therefore, recommendations given in this paper may not be extrapolated to any design scenario or exposure time, since the discussion herein is still based on a limited number of experiments for short timescales and cannot be generalized to every type of fibre, concrete mix-design or exposure conditions.

5. Conclusions

The results presented in this study confirm that there is no substantial damage to uncracked SFRC exposed to wet-dry cycles of chloride and carbon dioxide, over the time-scale investigated. Fibres corroded primarily at the surface of the uncracked concrete and only produced aesthetical damage.

Corrosion of steel fibres bridging cracks did not progress substantially inside the crack over time after one-year exposure; and only entailed moderate reductions in the total toughness in small specimens cracked at 0.3 mm and exposed to large chloride concentrations. The moderate increase in the residual performance of the cracked SFRC at small deformations has been related to an increase of the fibre-matrix bond strength over time.

There is no indication of a larger probability of fibre rupture due to fibre corrosion over time. And there was only a statistically significant increase in the contribution of fibre corrosion to the global count of ruptured fibres over time for small cross-sections. Concluding that there was no clear detrimental relation between the number of ruptured fibres and the toughness of the material.

Fibre corrosion had a subordinate, yet statistically significant impact on the changes in toughness over time, relative to the toughness variation observed due to the fibre distribution; while the impact of the exposure time was negligible, considering the time-scales investigated.

The results presented in this paper do not indicate that fibre corrosion has a critical impact on the bulk toughness of cracked SFRC over time for typical engineering applications. Nonetheless, the extrapolation of these results to general design scenarios is still questionable, since the discussion herein is still based on a limited number of experiments under controlled conditions for a relatively short period of time compared to the expected service life of typical infrastructure. Further research focusing on the long-term chemical stability of cracked SFRC based on inspection of existing infrastructure is needed.

Acknowledgements

The first author would like to express his gratitude to: CowiFonden, InnovationsFonden, the German

association of steel fibre producers (VDS), VejDirektoratet and Mapei-Denmark, for supporting this project; and Dr. Torben Lund Skovhus for his contribution to supervision during this project.

References

[1] W. Angerer, M. Chappell, Design of Steel Fibre Reinforced Segmental Lining for the Gold Coast Desalination Tunnels, in: Australian Tunnelling Society, Australasian Institute of Mining and Metallurgy (Eds.), 13th Aust. Tunn. Conf., Australasian Institute of Mining and Metallurgy, Melbourne, Australia, 2008: pp. 4–7.

[2] T. Kasper, C. Edvardsen, G. Wittneben, D. Neumann, Lining design for the district heating tunnel in Copenhagen with steel fibre reinforced concrete segments, Tunn. Undergr. Sp. Technol. 23 (2008) 574–587. doi:10.1016/j.tust.2007.11.001.

[3] B. de Rivaz, Steel fiber reinforced concrete (SFRC): The use of SFRC in precast segment for tunnel lining, in: V.K. Kanjlia (Ed.), Water Energy Int., Indian Central Board of Irrigation & Power, Bekaert (France), 2009: pp. 75–84.

[4] V. Marcos-Meson, A. Michel, A. Solgaard, G. Fischer, C. Edvardsen, T.L. Skovhus, Corrosion resistance of steel fibre reinforced concrete - A literature review, Cem. Concr. Res. 103 (2018) 1–20. doi:10.1016/j.cemconres.2017.05.016.

[5] S.U. Balouch, J.P. Forth, J.-L. Granju, Surface corrosion of steel fibre reinforced concrete, Cem. Concr. Res. 40 (2010) 410–414. doi:10.1016/j.cemconres.2009.10.001.

[6] D.C. Morse, G.R. Williamson, Corrosion behavior of steel fibrous concrete, Dept. of Defense Dept. of the Army Corps of Engineers Construction Engineering Research Laboratory ;, Champaign Ill., 1977.

[7] M. Schupack, Steel Fiber Concrete, in: S.P. Shah, A. Skarendahl (Eds.), Steel Fiber Concr. US-Sweden Jt. Semin., Elsevier, Stockholm, sweden, 1985: pp. 479–496.

[8] P.S. Mangat, Long-term properties of steel fibre reinforced marine concrete, Mater. Struct. Matériaux Constr. 20 (1987) 273–282.

[9] E. O'Neil, J.T. Devlin, Durability of Fiber-Reinforced Concrete Under Flexural Stress in a Severe Marine Environment, Defense Technical Information Center, Vicksburg, US, 1999.

[10] D.J. Hannant, J. Edgington, Durability of steel fibre concrete, in: A. Neville (Ed.), Rilem Symp. 1975 Fibre Reinf. Cem. Concr., The construction press, Leeds, UK, 1975: pp. 159–169.

[11] R. Weydert, P. Schiessl, Korrosion von Stahlfasern in gerissenem und ungerissenem Stahlfaserbeton. Abschlussbericht, Bergisch Gladbach (Germany), 1998.

[12] E. Kern, H. Schorn, 23 Jahre alter Stahlfaserbeton, Beton- Und Stahlbetonbau. 86 (1991) 205–208. doi:10.1002/best.199100380.

[13] E.S. Bernard, Durability of cracked fibre reinforced shotcrete, in: E.S. Bernard (Ed.), Shotcrete More Eng. Dev. Proc. Second Int. Conf. Eng. Dev. Shotcrete, A.A. Balkema Publishers, Sydney, Australia, 2004: pp. 59–66.

[14] P.S. Mangat, K. Gurusamy, Corrosion resistance of steel fibres in concrete under marine exposure, Cem. Concr. Res. 18 (1988) 44–54. doi:10.1016/0008-8846(88)90120-2.

[15] P.S. Mangat, K. Gurusamy, Permissible crack widths in steel fibre reinforced marine concrete, Mater. Struct. 20 (1987) 338–347. doi:10.1007/BF02472580.

[16] E. Nordström, Durability of Sprayed Concrete Steel fibre corrosion in cracks, Lulea University of Technology, 2005.

[17] L. Ferrara, R. Fratesi, S. Signorini, F. Sonzogni, Durability of Steel Fibre-Reinforced Cocnrete Precast Elements: Experiments and Proposal of design recommendations, in: M. Di Prisco, R. Felicetti, G.A. Plizzari (Eds.), 6th RILEM Symp. Fibre-Reinforced Cocnretes - BEFIB 2004, RILEM Publications SARL, Varenna, Italy, 2004: pp. 565–574.

[18] K. Kosa, A.E. Naaman, W. Hansen, Durability of Fiber Reinforced Mortar, ACI Mater. JournalMaterials J. 88 (1991) 310–319.

[19] R. Roque, N. Kim, B. Kim, G. Lopp, Durability of Fiber-Reinforced Concrete in Florida Environments, Florida, USA, 2009.

[20] D. Nemegeer, J. Vanbrabant, H. Stang, Final report on Durability of Steel Fibre Reinforced Concrete, Copenhagen, Denmark, 2000.

[21] G.B. Batson, Strength of Steel Fiber Concrete in Adverse Environments, Champaign, Illinois (US), 1977.

[22] G. Mantegazza, A. Gatti, Aspects of Durability of Fiber Reinforced Concrete: Workability and Stress-Corrosion, in: M. di Prisco, R. Felicetti, G.A. Plizzari (Eds.), 6th RILEM Symp. Fibre-Reinforced Cocnretes - BEFIB 2004, RILEM Publications SARL, Varenna, Italy, 2004: pp. 593–602.

[23] S. Abbas, Structural and Durability Performance of Precast Segmental Tunnel Linings, University of Western Ontario, 2014.

[24] R. Weydert, P. Schiessl, Corrosion of Steel Fibres in Cracked and Uncracked Steel Fibre Reinforced Concrete, IBAC. 61 (1996) 1310–1315.

[25] K. Kosa, A.E. Naaman, Corrosion of Steel Fiber Reinforced Concrete, ACI Mater. J. 87 (1990) 27–37.

[26] V. Marcos-Meson, G. Fischer, C. Edvardsen, A. Solgaard, A. Michel, Mechanical performance of steel fibre reinforced concrete exposed to chlorides and carbon dioxide: results after one year (Manuscript submitted for publication), Cem. Concr. Compos. (2019).

[27] V. Marcos-Meson, G. Fischer, A. Solgaard, C. Edvardsen, M. Geiker, T. Danner, U.H. Jakobsen,

T.L. Skovhus, A. Michel, Durability of cracked SFRC exposed to wet-dry cycles of chlorides and carbon dioxide – multiscale deterioration phenomena (Manuscript submitted for publication), Cem. Concr. Res. (2019).

[28] L. Ferrara, V. Krelani, F. Moretti, M. Roig Flores, P. Serna Ros, Effects of autogenous healing on the recovery of mechanical performance of High Performance Fibre Reinforced Cementitious Composites (HPFRCCs): Part 1, Cem. Concr. Compos. 83 (2017) 76–100. doi:10.1016/j.cemconcomp.2017.07.010.

[29] European Commitee for Standardization (CEN), Concrete. Specification, performance, production and conformity. EN 206, European Union, 2013.

[30] European Commitee for Standardization (CEN), Test method for metallic fibre concrete - Measuring the flexural tensile strenght (limit of proportionality (LOP), residual), EN 14651:2006 +A1, European Union, 2006.

[31] I. Paegle, F. Minelli, G. Fischer, Cracking and load-deformation behavior of fiber reinforced concrete: Influence of testing method, Cem. Concr. Compos. 73 (2016) 147–163. doi:10.1016/j.cemconcomp.2016.06.012.

[32] European Commitee for Standardization (CEN), Testing hardened concrete - Part 3: Compressive strength of test specimens, EN 12390-3 + AC:2012, European Union, 2012.

[33] J.F. Olesen, Fictitious Crack Propagation in Fiber-Reinforced Concrete Beams, J. Eng. Mech. March (2001) 272–280. doi:http://dx.doi.org/10.1061/(ASCE)0733-9399(2001)127:3(272).

[34] B.L. Welch, The generalisation of student's problems when several different population variances are involved, Biometrika. 34 (1947) 28–35. doi:10.1093/biomet/34.1-2.28.

[35] S. Wold, M. Sjöström, L. Eriksson, PLS-regression: A basic tool of chemometrics, in: Chemom. Intell. Lab. Syst., Elsevier, 2001: pp. 109–130. doi:10.1016/S0169-7439(01)00155-1.

[36] G.N. Wilkinson, C.E. Rogers, Symbolic Description of Factorial Models for Analysis of Variance, Appl. Stat. 22 (1973) 392. doi:10.2307/2346786.

[37] P. Serna, S.E. Arango, Evolution of the Flexural Behaviour of Precracked SFRC in Marine Environment, in: R. Gettu (Ed.), 7th RILEM Int. Symp. Fibre Reinf. Concr. Des. Appl. - BEFIB 2008, RILEM Publications SARL, Chennai, India, 2008: pp. 595–605.

[38] N. Ganesan, P. V Indira, P.T.S. Kumar, Durability aspects of steel fibre-reinforced SCC, Indian Concr. J. 80 (2006) 31–37.

[39] M.M. Kamal, F.E. El-Refai, Durability of steel fibre reinforced concrete, in: Proc. Fourth Int. Conf. Durab. Build. Mater. Components, Elsevier, Singapore, 1987: pp. 235–247. doi:10.1016/B978-1-4832-8386-9.50034-6.

[40] E.S. Bernard, Effect of Exposure on Post-crack Performance of FRC for Tunnel Segments, in: I. Vrkljan, Z. Dekovic, M. Dobrilovic, J. Likar, P. Miscevic (Eds.), SEE TunnelPromoting Tunneling SEE Reg. - ITA WTC 2015, ITA-AITES, Dubrovnik, Croatia, 2015: p. 13.

[41] Z. Guan, T. Deng, G. Wang, Y. Jiang, Studies on the key parameters in segmental lining design, J. Rock Mech. Geotech. Eng. 7 (2015) 674–683. doi:10.1016/j.jrmge.2015.08.008.

[42] A. Meda, G.A. Plizzari, New Design Approach for Steel Fiber-Reinforced Concrete Slabs-on-Ground Based on Fracture Mechanics, ACI Struct. J. 101 (2005) 3–8.

[43] B. De Rivaz, Durability issue for SFRC precast segment in tunnelling application, in: S.W. Meng, C.K. Siong (Eds.), WUTC2010, World Urban Transit Conference, Sentosa, Singapore, 2010: pp. 1–10. doi:10.3850/978-981-08-6396-8_P223.

[44] C. Edvardsen, P. Jackson, K. Lyngby, Durability Design of Steel Fibre Reinforced Concrete for Severe Exposure Conditions, in: H. Beushausen (Ed.), Fib Symp. 2016. Performance-Based Approaches Concr. Struct., FIB, Cape Town, ZA, 2016: pp. 120–121.

Chapter 4
Pull-out mechanisms of single fibres in cracked SFRC under wet-dry exposure

The study presented in Chapter 3 concluded that there were significant changes in the residual performance of cracked SFRC specimens after exposure. There was insight suggesting that the increase on the residual strength measured at small deformations may be due to an alteration of the fibre-matrix bond strength during the exposure. However, macroscopic observations at the composite level provide a limited understanding of the nature of such changes in the residual performance of the cracked composite, and investigations at the single-fibre level are needed.

This chapter presents an experimental campaign that investigated the pull-out behaviour of four types of hooked-end fibres subjected to wet-dry cycles of freshwater and saltwater for six months. Single-fibre pull-out tests were performed on partially pulled fibres bridging an artificial crack. Results from the investigation are discussed in Paper V. The paper focuses on quantifying the variations of the fibre-matrix bond strength after the exposure to wet-dry cycles and relates these variations to the pull-out mechanisms of the fibre.

The results confirmed the hypotheses presented in Chapter 3, and showed that the exposure of partially pulled fibres to wet-dry cycles resulted in a significant increase of the pull-out forces transferred; which in some cases led to a substantial increase in the number of fibres rupturing after the exposure. Corrosion damage was mainly observed at the exposed steel surface for both freshwater and saltwater exposure, but there was only a noticeable cross-section reduction of the steel for the latter.

The variations in the fibre-matrix bond strength after the exposure affected both the adhesive and the mechanical bond. The adhesive bond was partially restored after the exposure, and a “new” deboning peak was observed in most experiments. There was an increase in the forces transferred during the mechanical bond phase, i.e. for slip values

in the range of 0.5 – 1 mm. Such increase in the mechanical bond strength, led in some cases to premature fibre rupture, which reduced significantly the total work transferred during pull-out. However, it was observed that fibre rupture did not necessarily occur at the highest force in the ascending branch of the curve, e.g. by exceeding the tensile capacity of the steel. In some cases, fibre rupture occurred at the hook during the descending branch of the test, e.g. at slip values of 2 – 3 mm, which corresponded to the last phase of the straightening process of the hook. It was found that increasing the steel strength for the same concrete strength was effective on reducing substantially the amount of fibres rupturing; ideally enabling cross-section reduction allowances due to corrosion of 10 – 30% in some cases.

The findings of this investigation support the hypothesis that a considerable share of the changes in the mechanical behaviour of cracked SFRC subject to wet-dry cyclic exposure, reported in former studies (Chapter 2) and in the experiments presented in Chapter 3, may be due to an increase of the fibre-matrix bond strength over the exposure, and not solely due to corrosion of the steel fibres. Thus, additional damage mechanisms, besides fibre corrosion, might explain the changes in the residual performance of the cracked SFRC. Former investigations and current observations propose that the alteration of the cement matrix surrounding the fibre during exposure to wet-dry cycles, e.g. due to autogenous healing, may be responsible for such changes.

The investigation reported in this chapter covered a detailed, yet limited, discussion of the effects of wet-dry exposure to the pull-out behaviour of steel fibres. The investigation presented covered the pull-out response of hooked-end fibres aligned with the pull-out direction with a fixed embedment length. Additional parameters influencing the pull-out behaviour of these fibres, such as: fibre inclination (Mois and Chiriac, 2017), concrete matrix maturity (Kragh et al., 2019; Kragh and Carlsen, 2017; Thorsen and Christensen, 2018) or sustained load conditions, such as creep (Havlik and Galik, 2017), were explored during the project through BSc and MSc theses. It was found that these parameters may play a critical role as well on the pull-out behaviour of hooked-end fibres under long-term exposure. Further experimental work and modelling are needed in order to extend these conclusions to general applications.

4.1 Paper V. Pull-out behaviour of hooked-end fibres in cracked concrete under corrosive exposures

The following publication, referred as “paper V”, has been published in Construction and Building Materials.

Marcos-Meson, V., Fischer, G., Edvardsen, C., Solgaard, A., Michel, A., 2020. Pull-out behaviour of hooked-end steel fibres in cracked concrete exposed to wet-dry cycles of chlorides and carbon dioxide – mechanical performance. Constr. Build. Mater. 240 (2020) 117764. doi:10.1016/j.conbuildmat.2019.117764.

Construction and Building Materials 240 (2020) 117764

Contents lists available at ScienceDirect

Construction and Building Materials

journal homepage: www.elsevier.com/locate/conbuildmat

Pull-out behaviour of hooked-end steel fibres in cracked concrete exposed to wet-dry cycles of chlorides and carbon dioxide – Mechanical performance

Victor Marcos-Meson [a,b,c,*], Anders Solgaard [b], Gregor Fischer [a], Carola Edvardsen [b], Alexander Michel [a]

[a] Department of Civil Engineering, Technical University of Denmark, Copenhagen, Denmark
[b] COWI A/S, Copenhagen, Denmark
[c] VIA Building, Energy, Water & Climate, VIA University College, Horsens, Denmark

HIGHLIGHTS

- Exposure to wet-dry cycles increased the fibre-matrix bond strength of steel fibres.
- The bond of partially pulled fibres was restored after exposure to wet-dry cycles.
- Corrosion damage mainly occurred at the steel exposed to the artificial crack.
- Fibre rupture occurred due to corrosion damage and increase in the bond strength.

ARTICLE INFO

Article history:
Received 19 June 2019
Received in revised form 28 November 2019
Accepted 29 November 2019

Keywords:
Steel fibre reinforced concrete (SFRC)
Durability
Corrosion
Chlorides
Carbonation
Cracks
Wet-dry cycles
Single fibre pull-out

ABSTRACT

This paper presents an experimental study investigating the pull-out behaviour of hooked-end carbon-steel fibres exposed to wet-dry cycles of freshwater and saltwater for six months. Experimental results from single-fibre pull-out tests of partially pulled fibres in a simulated crack were used to quantify the impact of corrosion damage at the fibre and alteration of fibre-matrix interface on the fibre-matrix bond strength after the exposure.

The results presented in this paper show that the maximum pull-out force and total work transferred by the fibres during pull-out increased both with increasing steel strength and matrix strength. Exposure of partially pulled steel fibres also resulted in an increase of the fibre-matrix bond strength over time. Thus, generally leading to higher maximum pull-out forces and moderate increase in toughness after exposure, provided that fibre rupture did not occur. Fibre rupture during pull-out occurred due to both the increase of the fibre-matrix bond strength after exposure and the reduction of the effective cross-section of the fibre as a result of corrosion. Overall, increasing the steel strength and reducing the bond-strength of the fibre was effective in reducing substantially the amount of fibres rupturing during pull-out.

This investigation substantiates ongoing discussion that proposes additional damage mechanisms, besides fibre corrosion, that explain the changes in the residual performance of the cracked Steel Fibre Reinforced Concrete (SFRC) exposed to wet-dry cycles of freshwater and saltwater.

1. Introduction

Hooked-end carbon-steel fibres are widely used in the construction industry as structural reinforcement in Steel Fibre Reinforced Concrete (SFRC) exposed to corrosive environments, such as saltwater, freshwater and carbon dioxide. To date, there is an open discussion regarding the long-term durability of cracked SFRC under these exposures due to fibre corrosion, particularly when involving wet-dry conditions [1].

Studies have reported substantial variations in the residual strength of the cracked composite, attributed in some cases to an increase in the fibre-matrix bond strength due to corrosion [2]. Or else, a substantial decrease in the toughness after exposure due to rupture of the fibres crossing the crack over time, yet not solely due to fibre corrosion [3,4]. There is scientific insight suggesting additional damage mechanisms to fibre corrosion that

* Corresponding author at: Department of Civil Engineering, Technical University of Denmark, Copenhagen, Denmark.
E-mail address: vicmes@byg.dtu.dk (V. Marcos-Meson).

https://doi.org/10.1016/j.conbuildmat.2019.117764
0950-0618/

may explain such changes in the fibre-matrix bond over the duration of the exposure [1].

Experimental results presented in [5] showed a moderate increase in the strength and toughness over the exposure, despite that some fibres ruptured due to corrosion. The study suggested that there is a twofold mechanism describing the changes in the performance of the cracked composite over time. First, the exposure of the cracked composite to wet-dry cycles may promote autogenous healing at the damaged matrix around the fibre which alters the fibre-matrix bond strength. Second, critical reductions in the cross-section of the fibres due to corrosion may reduce the load-bearing capacity of the cracked composite. However, these discussions are based on macroscopic observations, which cannot fully describe the changes in the pull-out behaviour of fibres due to exposure, nor the cause and mechanism of fibre rupture during pull-out [1].

Other test methods, such as the single-fibre pull-out test, may be used to describe variations to the fibre–matrix bond over time due to exposure. Among these, the use of single-sided pull-out experiments provide an accurate description of the forces transferred during the whole pull-out process of hooked-end fibres: during the debonding phase, the activation of the hook and the frictional phase [6,7]. The pull-out behaviour of the fibre through these phases is known to be partly governed by the degree of damage at the cement matrix that surrounds the steel fibre, e.g. at the "fibre–matrix interface"; comprising mostly crushing of the matrix around the hook [8–11], which facilitates the pull-out process of the fibre. However, the relation of this damage and corrosion to the pull-out performance of steel fibres in cracked SFRC is not well understood [1].

Studies investigating the pull-out behaviour of fibres exposed to wet-dry cycles of saltwater have reported increases in the maximum pull-out force and energy release after the exposure [12,13]. These changes were attributed to fibre corrosion, which increased the frictional resistance by: a localized expansion of corrosion products at the hook after three months of exposure [13], or the increase of the fibre roughness due to uniform corrosion of the steel over ten days [12]. The latter hypothesis was also suggested in studies using pre-corroded fibres embedded in mortar [14]; which observed an increase in the peak forces for fibres with an average reduction of 12% in the cross-section due to corrosion, but only reported fibre rupture during pull-out at reductions of the fibre cross-section of approx. 30 – 50%.

These studies generally suggest that the increase observed in the fibre–matrix bond strength after exposure is primarily explained by increase of friction due to corrosion. However, this hypothesis is not consistent with the increases observed in the fibre–matrix bond strength of de-bonded steel fibres reloaded after being cured in water [15] or for pre-pulled polymer fibres (PE and PVA) cured similarly [16,17], which did not entail corrosion damage. Further, these hypotheses do not explain some of the increased performance of cracked FRC exposed to non-corrosive environments, otherwise attributed to autogenous healing [18].

This investigation focuses on describing changes in the pull-out behaviour of partially pulled steel fibres from concrete exposed to wet-dry cycles of freshwater and saltwater for six months, under simulated crack conditions. Thus, quantifying the role of corrosion damage in the pull-out performance of hooked-end steel fibres in cracked concrete.

2. Methodology

The investigation presented in this paper covers the preparation, exposure and mechanical testing of approx. 180 single fibre pull-out specimens, partially pulled-out to induce mechanical damage equivalent to crack widths in the range of 0.2–0.3 mm and exposed to wet-dry cycles for six months. The exposures investigated comprise wet-dry cycles of saltwater and freshwater with a high carbon dioxide concentration.

Single-fibre specimens were investigated in a single-sided test, based on the setup described and tested in [19,20]. The analysis of the pull-out performance of the fibres was made by comparison of the force-slip and work-slip response for the investigated specimens. Visual inspection of the fibres after pull-out was used to determine the extent of fibre damage due to corrosion. Further, the discussion regarding the alteration of the fibre–matrix bond is based on descriptive statistics.

The results and discussion section use statistical terminology: hereafter, the word "specimen" refers to a single sampling unit (i.e. each of the tests executed), and the word "sample" refers to a group of specimens exposed to the same environment. Discussion will be primarily based on comparison of samples and individual specimens will not be discussed hereafter, unless specified otherwise.

2.1. Preparation of specimens

The pull-out specimens were cast using a mix-design based on the one utilized in [5], but reducing the maximum aggregate size from 24 to 8 mm. The total binder content was 426.3 kg/m^3 with 31-wt.% fly ash replacement of the Portland cement, and the water to binder ratio was 0.34, see Table 1. The superplasticizer content was adjusted in the subsequent mixes to reach a flow diameter of 120 ± 20 mm, measured according to EN 1015–3:1999 [21]; and the air-entrainer content was adjusted to reach two levels of entrained air: (A) 3.0 ± 0.5 vol% and (B) 6.0 ± 0.5 vol%, measured according to EN 413–2:2016 [22].

The steel fibres used were made of cold-drawn carbon-steel wire, with hooked ends (type 1 according to EN 14889–1:2006 [23]); with a length of 60 mm and a diameter of 0.75 mm. Four different fibres with the same length and aspect ratio, but different steel strength and hook shape were used in the study, see Table 2 and Fig. 1a.

The single-hook fibres used (Low (L), Medium (M) and High (H)) were distributed as loose fibres. Whereas, the double-hook fibres (D) were picked from glued fibre bundles; which were dissolved in limewater and dried with a paper cloth before the selection. The fibres used for the pull-out test were selected one by one, rejecting any fibre showing deformations or damage due to manufacture. The hook that was not embedded was clipped-off.

The specimens were cast using a 60 L planetary mixer, over a vibration table, using six PVC formworks that accommodated ten cubic specimens of 70 mm each, as used in [19,20,25]. The fibres were held to the bottom plate of the PVC formwork using a perforated rubber plug inserted into a conic gap at the centre of the bottom surface of the form, maintaining a 90° angle with the bottom of the formwork. Additionally, twelve 60 × 120 mm cylinders were casted for compression testing on each batch. Each fibre and matrix type were cast in a separate batch of 60 specimens in consecutive

Table 1
Mix-design.

Component	Quantity (kg/m^3)	
	Mix 1	Mix 2
Cement (CEM I 52.5 N)	326.3	326.3
Fly Ash	100	100
Water	145	145
Sand 00/02	787.4	752.3
Sea gravel 04/08	1036.5	990.3
Entrained air	3%	6%

Table 2
Fibre specifications.

Code	Hook type	Ultimate tensile strength		Steel grade*3		Length*2 (L)	Free length*2 (L')	Hook length*2 (h')	Diameter*1 (d)	Angle*2 (a)
		Characteristic ($R_{k,m}$) [MPa]	Mean $R_{u,m}$) [MPa]	ISO Grade	Carbon content [%-.wt]	[mm]	[mm]	[mm]	[mm]	[°]
Low (L)	Single	1200*1	1120 ± 7%*2	C7D	0.07	60	47	6.5	0.75	42
Medium (M)	Single	1500	1772 ± 3%	C18D	0.19	60	48	6.0	0.75	35
High (H)	Single	1900	2189 ± 3%	C38D	0.375	60	45	7.5	0.75	43
Double (D)	Double	1800	1825 ± 5%	C20D	0.205	60	49	5.5	0.75	25

*1Characteristic ultimate tensile strength of the cold-drawn steel wire ($R_{k,m}$), as given by the producer, from [24]. Measured according to (EN ISO 6892–1:2016) and specified according to (EN 14889–1:2006).
*2Mean ultimate tensile strength, measured at the fibre stem in a sample of 10 fibres, according to (EN ISO 6892–1:2016). Including the coefficient of variation (CV) for normally distributed values, expressed as a percentage.
*3Grade and mean carbon content of the carbon-steel rod used to produce the cold-drawn steel wire, from [24]. Specified according to (EN ISO 16120–2:2017).
*4Geometry given as rounded mean values, measured in a sample of 10 fibres.
*5Characteristic values of the wire diameter, as given by the producer

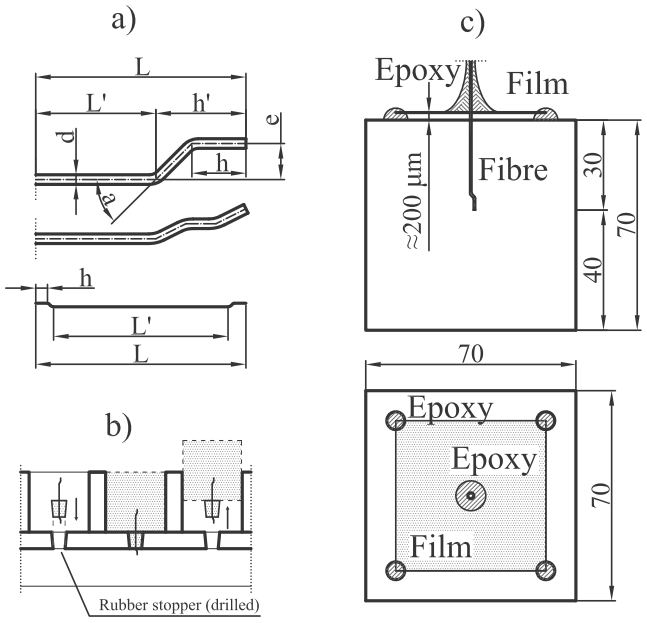

Fig. 1. Dimensions of specimens: a) fibre dimensions, b) formwork and fibre placement, c) pull-out specimen. Dimensions are expressed in mm.

days, demoulded after one day and cured immersed in limewater for 56 days at 20 °C.

The specimens exposed to saltwater and freshwater were partially pulled up to a slip value of 0.15 mm before the exposure; corresponding to the beginning of the mechanical anchorage phase of the fibre hook. Afterwards, the load was released, and the upper surface of the specimen was covered with a 50 × 50 mm acetate film, 0.05 mm thick; punching the fibre through and leaving a minimum separation between the film and the concrete surface of approx. 0.3 ± 0.1 mm, which simulated the crack. Finally, the part of the fibre exposed to the surface out was painted with two layers of heavy-duty marine-grade epoxy paint overlapping approx. 10 mm over the acetate film, see Fig. 1c.

2.2. Exposure setup

The exposure environments are described in Table 3 and comprise wet-dry cycles (i.e. two days each) of partially pulled specimens exposed to saltwater and freshwater. Furthermore, one sample of companion specimens (R) was tested after curing immersed in limewater for 56 days for each of the investigated groups of samples.

The pull-out samples (i.e. test-groups) were coded as follows: the fibre type according to Table 2 (i.e. L-M-H-D), the mix ID (i.e. 1 or 2), the age of the specimen in months (i.e. 2 or 6); and the exposure environment, being: immersed curing in limewater (R) and wet-dry cycle exposure to 7.5 -wt.% NaCl solution (S) and freshwater with 0.5%-vol. CO_2 exposure (C). Specimens exposed to saltwater (S) and freshwater (C) were exposed pre-pulled and specimens cured in limewater (R) were tested un-pulled.

The specimens cured in limewater were immersed in the solution at all times. The wet-dry exposure setup consisted of two rectangular polyethylene containers of approx. 200 L each, one used for each exposure. The specimens were stacked with the steel fibre in horizontal position.

The execution of the wet-dry cycles for the freshwater and saltwater exposure (S and C) was set automatically from a controller. During the wet cycle, the tanks were filled with approx. 120 L of solution, covering the specimens by at least 10 cm of solution.

The drying cycle for the air exposed specimens was provided by two fans placed at opposite ends of the upper side of the tank, with a nominal flow of 50 m^3/h each, and two outlets of 100 mm diameter placed at the top centre of the tank. The air was mixed with the laboratory air and was kept at stable temperature and humidity by the ventilation system of the building. The drying cycle of the carbon dioxide exposure had a nominal flow of approx. 90 m^3/h, provided by four fans in series running through a closed loop and utilized a heat exchanger to condense moisture from the air flux before the inlet, using three Peltier modules with a total cooling output of 90 W. The overall configuration of the exposure setups is based on the one described in [5], but at a smaller scale.

The solution of the wet-dry exposures was replaced regularly, every two weeks during the first two months of exposure and then monthly up to 6 months. The composition of the solution was checked weekly by means of total dissolved solids (TDS) and pH measurements. The solution of specimens cured in limewater was not replaced, and approx. 25 cl of saturated solution of calcium hydroxide was added every two weeks, keeping the pH value in the solution in the range of 10–13. Non-chlorinated fresh water (pH = 7.5–8.0, Cl^- < 100 mg/l, 16–17 °dH) was used as exposure media for the specimens subjected to freshwater cycles (e.g. exposure C) and to prepare the saltwater brine.

The temperature and relative humidity inside the room were monitored, varying in the range 20 ± 2 °C and 50 ± 10% respectively. The CO_2 concentration in the room and inside the carbon dioxide loop were measured weekly and were approx. 0.05 ± 0.01-vol.% for the room and 0.5 ± 0.1-vol.% inside the carbon dioxide loop.

Table 3
Test samples and exposure conditions.

Code name (sample)	Fibre type	Mix	Age [mo.]	Pull [mo.]	Wet cycle (s)	Dry cycle (c)
L1 – 2 – R	L	1	2	–	Limewater	–
L1 – 6 – C			6	0.15	Fresh water	0.5 -vol.% CO^2
L1 – 6 – S			6	0.15	7 -wt.% NaCl	Air
M1 – 2 – R	M	1	2	–	Limewater	-
M1 – 6 – C			6	0.15	Fresh water	0.5 -vol.% CO^2
M1 – 6 – S			6	0.15	7 -wt.% NaCl	Air
H1 – 2 – R	H	1	2	–	Limewater	–
H1 – 6 – C			6	0.15	Fresh water	0.5 -vol.% CO^2
H1 – 6 – S			6	0.15	7 -wt.% NaCl	Air
D1 – 2 – R	D	1	2	–	Limewater	–
D1 – 6 – C			6	0.15	Fresh water	0.5 -vol.% CO^2
D1 – 6 – S			6	0.15	7 -wt.% NaCl	Air
H2 – 2 – R	H	2	2	–	Limewater	–
H2 – 6 – C			6	0.15	Fresh water	0.5 -vol.% CO^2
H2 – 6 – S			6	0.15	7 -wt.% NaCl	Air
D2 – 2 – R	D	2	2	–	Limewater	–
D2 – 6 – C			6	0.15	Fresh water	0.5 -vol.% CO^2
D2 – 6 – S			6	0.15	7 -wt.% NaCl	Air

2.3. Mechanical testing

The workflow of the experiments comprised: i) full testing of reference specimens at 56 days; ii) partial pull-out of the specimens at 56 days and preparation for exposure; iii) exposure for six months; iv) testing of exposed specimens after six months of exposure.

The single-sided pull-out tests were performed on a 25 kN universal test frame, equipped with a 10 kN load-cell. The steel fibre was gripped with an ER-16 collet chuck holder designed for CNC milling, using a 1/32″ spring collet with a grip range of Ø ≈ 0.4 1–0.79 mm. The concrete cube was gripped by a tailored steel frame, as shown in Fig. 2. The experimental setup was designed in such a way that the fibre did not slip from the grip during the experiments.

The pull-out displacement of the fibre was measured as the displacement of the chuck holder relative to the surface of the concrete cube; assuming a firm connection between the collet chuck and the fibre. The displacement was measured with three LVDT-type extensometers with a total measurable travel length of 12.5 mm. These were attached around the holder at a 120° spacing and were aligned vertically to the chuck holder, as shown in Fig. 2.

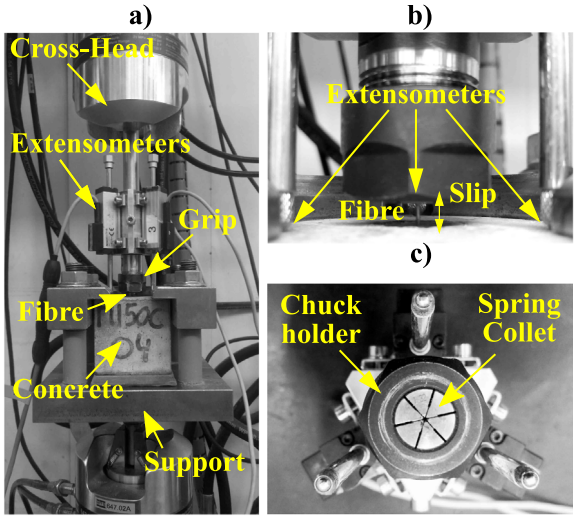

Fig. 2. Single-fibre pull-out setup: a) overall setup, b) connection of the grip and the fibre, c) front view of the spring collet and chuck holder.

The travel length of the extensometers was calibrated as installed in the abovementioned configuration to a calculated precision of 0.2‰.

The pull-out tests were executed based on the test methodology described in [19,20], with similar displacement rates to the ones specified in EN 14889–1:2006 [23] for three-point bending tests; using a sampling frequency rate of 100 Hz. The test was controlled by the displacement of the cross-head, measured with an integrated LVDT, and the average signal of the three extensometers was used to determine the end of each test-step, as described in Table 4. After reaching a pull-out displacement of 5.5 mm, the displacement rate was increased up to 1 mm/min, until the steel fibre was pulled-out completely.

The compression tests were performed on the pull-out cubes (70 mm) after the complete pull-out of the fibre. The test was executed in a 4000 kN capacity compression frame, according to the specifications of EN 12390–3:2012 [26]. Whereas, measurement of elastic modulus in compression and compressive strength of companion cylinders were executed in a 2000 kN capacity compression frame, after eight months of curing in limewater, according to the specifications of EN 12390–13:2012 [27] and [26], respectively.

The specimens exposed to chlorides and carbonation (i.e. groups S and C) were pre-pulled before the exposure at a slip value of 0.15 mm, calculated as the average of the value recorded by the three extensometers. After the target slip value was reached, the displacement of the crosshead was locked for two minutes and then released, measuring the recovery curve until the force reached a value in the range 0–5 N. The final slip value was recorded, reaching values of approx. 90 ± 10 μm. Afterwards, the specimens were prepared as described in Section 2.1.

2.4. Processing of data from experiments

The load – displacement data from each specimen was first resampled to a resolution of 1 μm. Then, the data was filtered

Table 4
Load rates for pull-out test.

	Step	Displacement rate (mm/min)	Range
1	Preload	0.10	0–10 N
2	Debond	0.05	0–0.1 mm
3	Pull-out	0.25	0.1–5.5 mm
4	Finish	1.00	5.5–35 mm

and smoothed, using a 1-dimensional median filter and a moving average filter, following a similar scheme as described in [5].

The pull-out slip of the fibre was calculated as the average displacement of the three extensometers. Hereafter, pull-out slip values discussed in this paper will only refer to this value as "slip". The results presented hereafter are based on load – slip data and work-slip data, the latter calculated as the integration of the area below the load – slip curve.

The processed data for each sample (i.e. a group of specimens) was fitted to a lognormal probability distribution and is presented as the mean value of the load at each slip value with its upper and lower confidence bounds at 90% confidence interval.

2.5. Visual inspection and fibre counting

After finalizing each pull-out test, the fibre was inspected with a magnifying glass and classified according to the degree of corrosion observed and the failure mode (i.e. pull-out or fibre rupture), according to the classification described in [5]. The fibres were classified according to the degree of corrosion observed (see Fig. 3) as follows:

- Level 1: for uncorroded fibres, which do not present any kind of corrosion damage. Only applicable to unexposed fibres in this study.
- Level 2: for fibres with minor corrosion, which present rust spots at the surface with no visible loss of cross-section, i.e. local loss of cross-section is below 5%.
- Level 3: for fibres with moderate corrosion, which present active corrosion with pits and a moderate loss of cross-section, i.e. approx. 5–30%.
- Level 4: for fibres with major corrosion, which present large pits and total or major loss of cross-section, i.e. larger than approx. 30%.

Furthermore, fibres that ruptured instead of pull-out during the test were inspected and counted. The location of the rupture was classified according to the categories shown in Fig. 3e: rupture occurring at the interface with the grip (1), at the intersection of the fibre and the concrete (2), at the embedded part of the fibre shaft (3), or at the hook (4).

2.6. Statistical analyses

The comparison of samples discussed in sections 4.1 and 4.3, was performed by the Welch's approximation of the Student's *t*-test for samples with unequal variance [28]. The test was used to calculate the probability value (p-value) for the null hypothesis (H_0) being true, i.e. the mean value for both distributions being equal. If the p-values for the H_0 are lower than the level of significance (α), there is an indication that the alternative hypothesis (H_a) might be correct, i.e. the sample reaching significantly higher or lower values than the reference.

In section 4.1, a one-tailed Welch's T-test is used to compare the mean values of the equivalent shear modulus of the fibre–matrix bond, testing the following alternative hypotheses (H_a): i) the mean value of the shear-modulus of the exposed samples being higher than the reference samples tested at 56 days, ii) the mean value of the shear-modulus of the exposed samples being lower than the reference samples tested at 56 days. The statistical significance level was set to α = 10%.

The equivalent shear modulus of the fibre–matrix bond at the elastic region was calculated as the mean of the derivative of the (shear) stress–strain relation of the experimental results in the slip range 0–15 μm. The shear stress was calculated assuming an idealised cylindrical fibre with a length equal to the embedded length, and the strain was calculated considering a unitary initial length.

In section 4.3, a one-tailed Welch's T-test is used to compare the mean values of the maximum pull-out force as well as the total work of reference and exposed samples, testing the following alternative hypotheses (H_a): i) the mean values of the exposed samples being higher than the reference samples tested at 56 days, ii) the mean values of the exposed samples being lower than the reference samples tested at 56 days. The statistical significance level was set to α = 10%.

Also, in section 4.3, the mean values of the work – slip curves for the exposed pull-out samples are compared to the references by a one-tailed Welch's T-test. The following alternative hypotheses (H_a) were tested: i) the probability of the mean value of the sample being smaller than the reference and ii) the probability of the mean value of the sample being greater than the reference. The statistical significance level was set to various levels: i.e. α = 5, 15 and 25%.

Finally, in section 4.4, the maximum pull-out forces measured in the experiments are compared to the characteristic idealised tensile capacity of the steel fibres (f_k^t). Calculated as the equivalent tensile force on a circular cross-section of 0.75 mm and a characteristic tensile strength of the steel in the range 1000–2000 MPa.

The maximum pull-out forces with varying steel strength was estimated by linear regression of the maximum pull-out force data presented in section 4.3. Approximated to a linear function with non-zero intercept: $f_{max}^p = mx + b$. The upper- and lower- prediction intervals at α = 2% and 10% were also calculated for comparison with the idealized tensile capacity of the fibre calculated above.

The excess of cross-section (henceforth "cross-section allowance") with increasing steel strength, was calculated as minimum cross-section variation, expressed as a percentage, that satisfied the relation: $f_k^t > f_{max}^p$. If the initial cross-section did not satisfy the relation above, the cross-section variation was calculated as the one satisfying $f_k^t = f_{max}^p$, writen as a negative value.

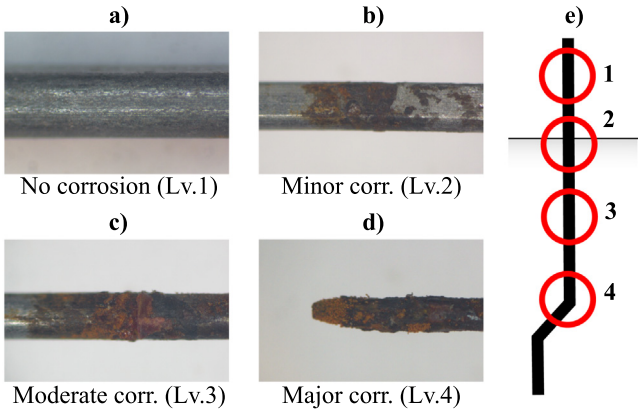

Fig. 3. Visual inspection, fibre classification after [5]: a) no corrosion (fibre rupture), b) minor corrosion, c) moderate corrosion (fibre rupture), d) major corrosion (fibre rupture); and e) locations of fibre rupture (1 to 4).

3. Experimental results

The experimental results described in this section are separated into compression and single-fibre pull-out tests. This second group of results is divided into mechanical performance results and fibre counting results.

3.1. Elastic properties

The results from the compression tests for each group are presented in Fig. 4. The figure shows the results of the compression

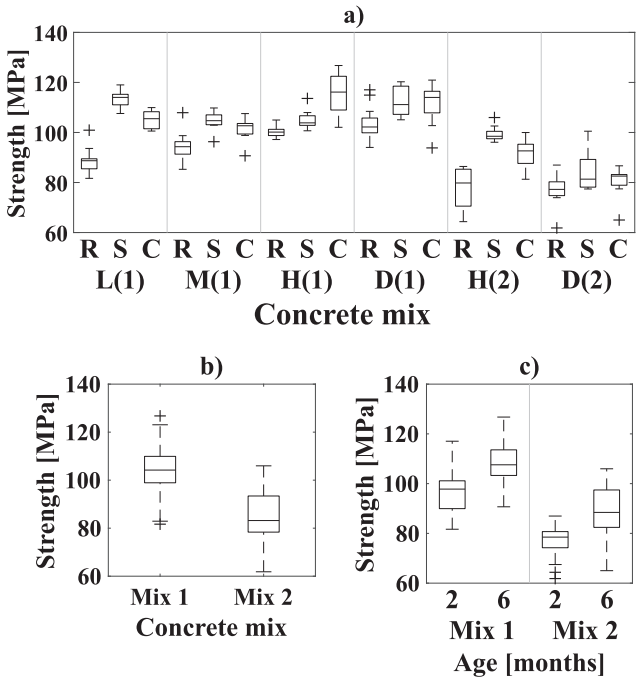

Fig. 4. Results for compression tests in pull-out samples, grouped by: a) the exposure, b) the concrete mix, and c) the age. The median value is shown as "—", the mean (arithmetic) value is shown as "X" and outliers are shown as "o".

tests for each test sample in Fig. 4a. As well as, the results grouped by the type of concrete mix used Fig. 4b and grouped by the age of the concrete in Fig. 4c.

The results show that the compressive strength of the matrix varies substantially between samples, see Fig. 4a. Overall variations due to the level of entrained air of the two mixes used (Fig. 4b), are consistent with the expected drop in strength due to an increase from 3 to 6 -vol.% in the entrained air content. Furthermore, the variation in compressive strength measured over time in Fig. 4c shows an increase of approx. 10% over the six months of exposure.

The mean values and standard deviation of the stabilized elastic modulus in compression of the two mixes, tested after eight months of curing in limewater were: 45 ± 2 GPa (Mix 1) and 41 ± 1.5 GPa (Mix 2), calculated according to [27]. And the mean values and standard deviation of the cylinder compressive strength were 92 ± 9 MPa (Mix 1) and 80 ± 6 MPa (Mix 2).

3.2. Single fibre pull-out tests

The results of the single-fibre pull-out tests are presented in this section, divided into the results of mechanical performance and the counting and inspection of the fibres after complete pull-out.

3.2.1. Mechanical performance

The results from the pull-out tests of reference specimens tested after 56 days of curing in limewater and the pre-pulled specimens exposed to wet-dry cycles for 6-months are presented as the pull-out force (i.e. force – slip) in Fig. 5 and as toughness (i.e. work – slip) in Fig. 6.

The results presented in Fig. 5 generally show an increase of the pull-out force at small slip values (i.e. at slip < 1 mm) for the samples exposed to freshwater and saltwater, relative to the reference specimens (R), which tend to approach the tail of the reference sample (R) at slip ≈ 4 mm. Whereas, the comparison of results from corresponding tests varying the concrete matrix, i.e. with a 3 and 6 -vol.% entrained air (Fig. 5c-d and Fig. 5e-f), showed a substantial drop on the pull-out forces of the reference specimens (R) and exposed specimens (S and C).

Furthermore, there are no clear differences in the pull-out behaviour of samples exposed to saltwater or freshwater. Except for an unexpected drop in the force at 0.5 – 2 mm slip of the double-hook

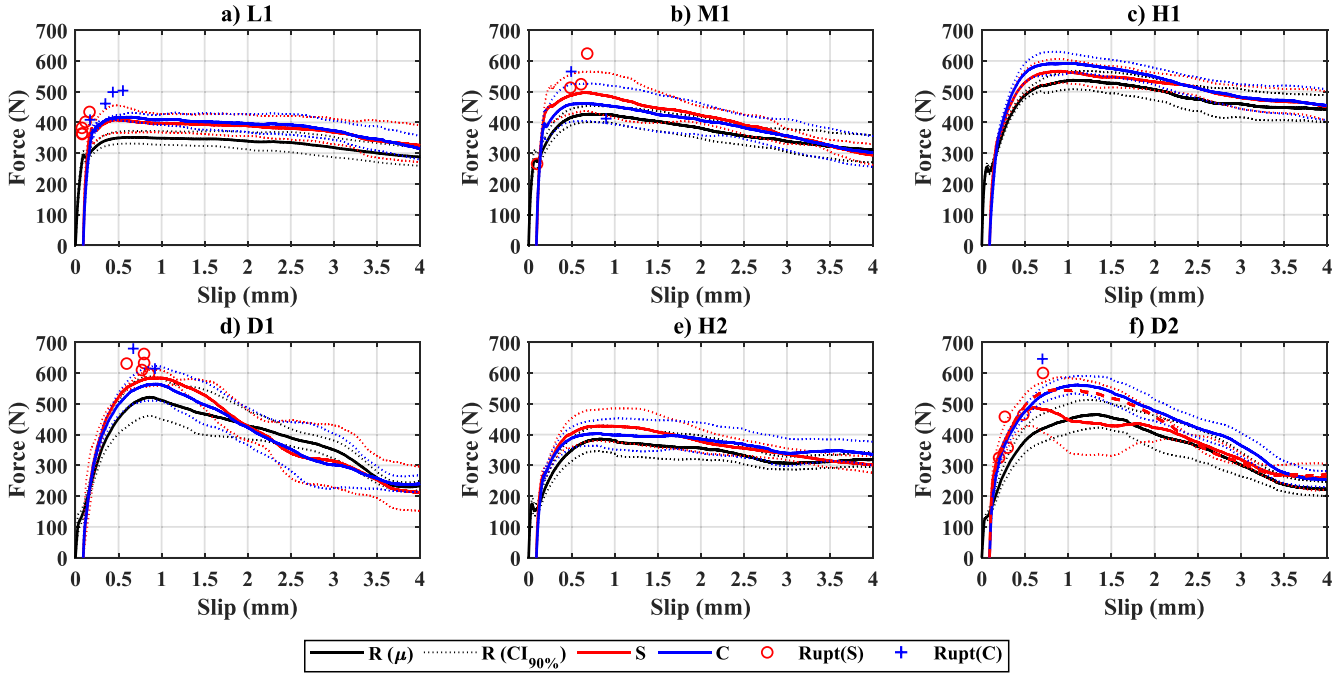

Fig. 5. Single fibre pull-out tests, Load-slip plot for samples: a) Low-strength fibre with mix 1 (L1), b) Medium-strength fibre with mix 1 (M1), c) High-strength fibre with mix 1 (H1), d) Double-hooked fibre with mix 1 (D1), e) High-strength fibre with mix 2 (H2), f) Double-hooked fibre with mix 2 (D2). Solid lines represent the log-mean value (μ) of the sample and dotted lines represent the upper- and lower- confidence bounds at 90% CI, for lognormal distribution. Sample names correspond to code names described in Table 3: (R) Limewater references, (S) Chloride exposure, (C) Carbonation exposure. The maximum force transferred by the specimens rupturing during pull-out (i.e. at slip values below 4 mm) are shown as marker points.

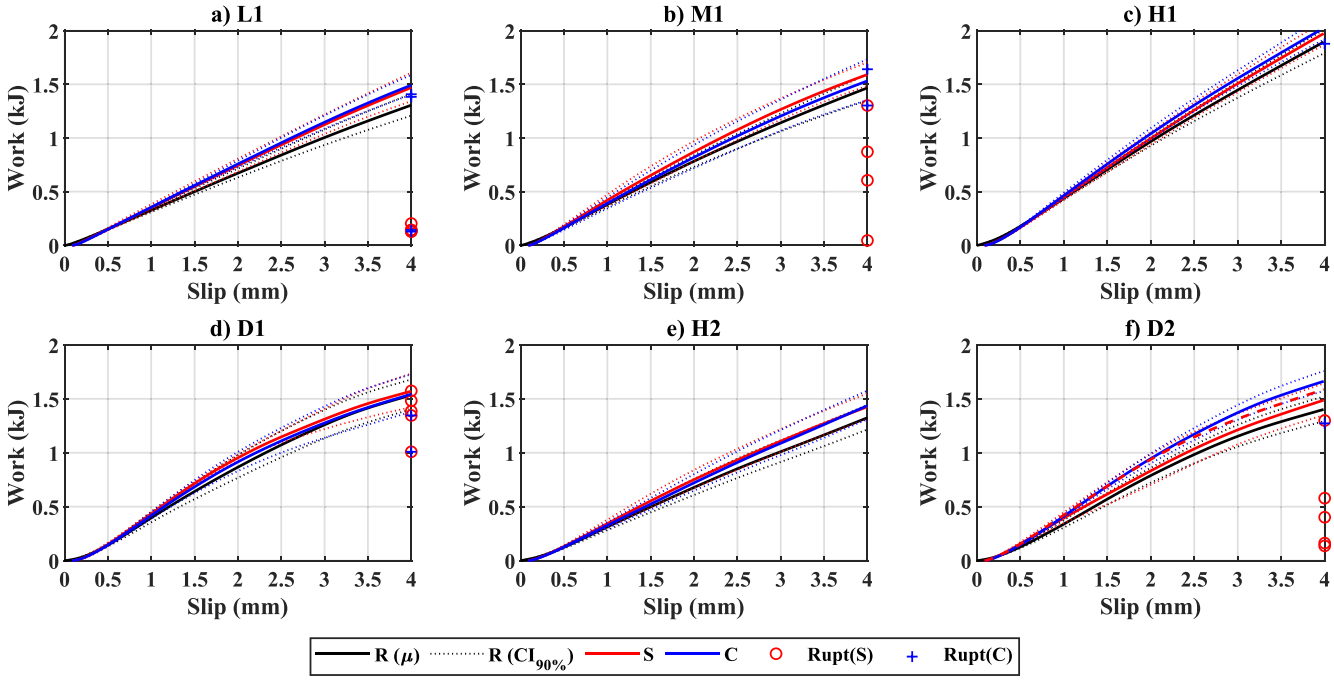

Fig. 6. Single fibre pull-out tests, Work-slip plot for samples: a) Low-strength fibre with mix 1 (L1), b) Medium-strength fibre with mix 1 (M1), c) High-strength fibre with mix 1 (H1), d) Double-hooked fibre with mix 1 (D1), e) High-strength fibre with mix 2 (H2), f) Double-hooked fibre with mix 2 (D2). Full lines represent the log-mean value (μ) of the sample and dotted lines represent the upper- and lower- confidence bounds at 90% CI, for lognormal distribution. Sample names correspond to code names described in Table 3: (R) Limewater references, (S) Chloride exposure, (C) Carbonation exposure. The total work transferred by the specimens rupturing during pull-out (i.e. at slip values below 4 mm) are shown as marker points at the 4 mm coordinate.

sample (D2) exposed to saltwater cycles, see Fig. 5f. Such a drop in the force was explained by the limited number of replicates that pulled-out completely during re-testing (i.e. the five rupturing specimens are not included in the calculation of the mean), which increased the impact of two specimens that pulled-out defectively, thus reducing the mean value and increasing the scatter. The mean value calculated for the three specimens left is shown as a red dashed line in Fig. 5f. Further discussion regarding the issue are given in Section 4.3.

Additionally, a number of fibres ruptured during pull-out of the exposed specimens for both saltwater (S) and freshwater (C) exposure; with the exception of the high-strength fibre samples (H1 and H2), that did not show any fibre rupturing during the tests, see Fig. 5c,e. The maximum force of these tests is marked as single points in Fig. 5 and reflects that, in some cases, fibre rupture occurs at loads higher than the upper confidence interval (90% CI). Further discussion is given in Section 4.3.

The work-slip diagrams, shown in Fig. 6 are presented following the same code as described above. Except for the representation of the specimens where the fibres ruptured, which show the work at 4 mm slip.

The results presented in Fig. 6 reflect the aforementioned increase of the pull-out loads at small slip values in the samples exposed to freshwater and saltwater (S and C), relative to the reference specimens (R). This increase in the force transferred at small slip values resulted in a progressive increase in the total work transferred during pull-out; which in most cases results on higher work values at 4 mm slip. However, the double-hook fibre sample embedded in the low entrained air content matrix (D1) only showed that increase in toughness at approx. 2–2.5 mm slip, see Fig. 6d.

Additionally, the results generally show an increase in the total toughness up to 4 mm for the reference samples tested after 56 days (R) with increasing steel strength (see Fig. 6a-c) and with lower entrained air content (see Fig. 6c,e and Fig. 6d,f). Whereas, the double hook samples (D1 and D2) showed a different behaviour compared to the single hooked fibres with similar strength (i.e. H1 and H2), with a smaller gradient at the tail after approx. 2 mm slip, see Fig. 6c,e and Fig. 6d,f. Which instead, reached toughness values at 4 mm slip similar to the medium strength fibres (M1), see Fig. 6b and Fig. 6d.

3.2.2. Visual inspection

The specimens were inspected before and after being pulled-out. The visual inspection focused on determining the corrosion damage of the fibre, as well as the location and occurrence of fibre rupture during the pull-out process.

Corrosion damage was mostly observed at three main locations of the fibre but may be classified in two groups as shown in Fig. 7. First, corrosion at the exposed surfaces of the steel ("location I" in Fig. 7a) that propagates into the concrete matrix and slightly through the interface of the steel and the epoxy coating. This damage entailed most of the cross-section reduction; which was more severe under chloride exposure.

Second, corrosion spots at the hook bends and at some locations of the fibre stem ("locations IIa and IIb" in Fig. 7a). These comprised minor rust and small pits smaller than a few micrometers, that did not entail a measurable reduction of the cross-section.

Similarly, there are various types of fibre failure that can be classified in three main types, as described in Fig. 7b. Type 1, which corresponds to tensile failure of the undamaged steel during pull-out (types 1 and 1′ in Fig. 7b). This failure generally occurred at large slip values (i.e. slip > 4 mm), mostly on the fibres with lower tensile strength (Types L and M), but regardless of the exposure or corrosion damage.

Type 2, mainly due to tensile failure of the steel at the corroded section, in some cases in combination with shear (types 2-2′ in Fig. 7b). This failure occurred primarily at small slip values (i.e. slip < 1 mm) during the ascending branch of the test and mostly affected fibres exposed to saltwater, which presented a moderate

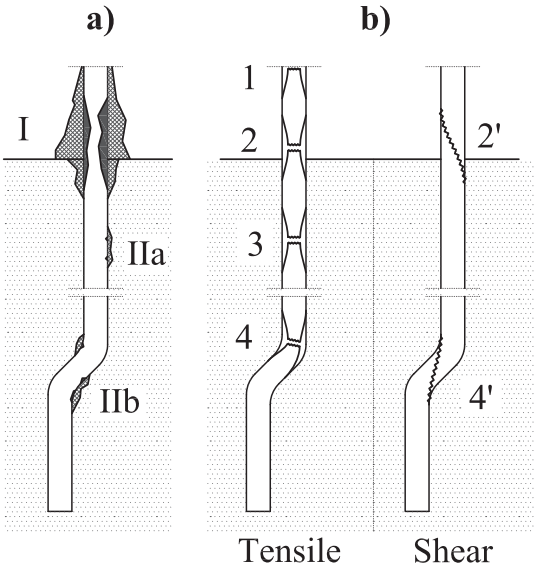

Fig. 7. Location and description of damage at fibres, showing: a) locations of corrosion damage; and b) types of fibre rupture.

or major reduction of the cross-section due to corrosion. This type of failure was more pronounced in fibres with lower tensile strength.

Type 3, which is related to tensile or shear failure at the hook bends (types 3-3′ in Fig. 7b). This failure occurred regardless of the exposure type or degree of corrosion damage, mainly at slip values in the range 1–3 mm, corresponding to the utilization of the mechanical bond. Mostly fibres with double hook embedded in the low-porosity matrix (Mix 1) showed this type of failure.

The results from the visual inspection of individual fibres after complete pull-out are presented in Fig. 8. The relative count of fibres classified according to: i) the location of the rupture at the fibre; ii) the occurrence of the rupture during the pull-out process, expressed as the slip value in mm; and iii) the severity of corrosion at the exposed part of the steel, classified according to the description given in Section 2.4.

The results presented in Fig. 8a-b show that, there is an overall decrease of the total amount of rupturing fibres with increasing fibre strength. Whereas, an increase in the entrained air content resulted on a moderate decrease in the number of rupturing fibres exposed to freshwater cycles (see H1 vs H2 and D1 vs D2). Furthermore, the total amount of fibres rupturing in the exposed samples (groups S and C) was substantially higher than for the reference samples (group R). Correspondingly, exposure to saltwater cycles (S) led to a higher percentage of rupturing fibres compared to freshwater cycles (C).

Comparison of the locations of fibre rupture (see Fig. 8a) showed that, rupture at the corroding regions (locations 2-2′ in Fig. 7b) only occurred at fibres exposed to saltwater cycles (S). Whereas, rupture of fibres cured in limewater (R) or exposed to freshwater cycles (C) mainly occurred at the fibre stem (locations 1 and 4 in Fig. 7b) and at the hook (locations 3-3′ in Fig. 7b). The slip range where rupture occurred during the pull-out process of each fibre is presented in Fig. 8b, expressed in mm. The results presented show that, fibres of reference samples cured in limewater (R) only ruptured at slip values over 4 mm (e.g. occurring mostly in the range 6–10 mm). Whereas, fibre rupture at fibres exposed to freshwater (C) and saltwater (S) cycles occurred at slip values below 2 mm in approx. 40% and 60% of the cases, respectively.

Finally, results classifying the severity of fibre corrosion on each sample are shown in Fig. 8c. The results show that there is no corrosion damage on samples cured in limewater (R). Whereas,

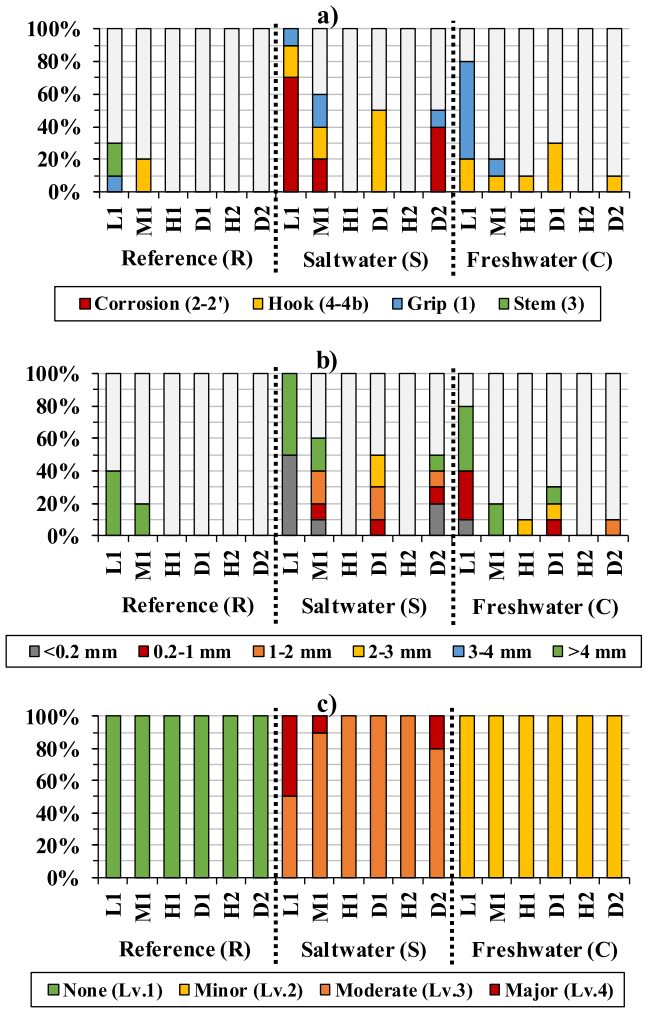

Fig. 8. Visual inspection of steel fibres after fibre pull-out tests, showing percentage of fibres classified by: a) the part of the fibre where rupture occurred (according to Fig. 7); b) the slip value at the moment of fibre rupture (expressed in mm); c) the degree of corrosion observed at the exposed part of the fibre (according to the corrosion levels described in Section 2.3.1).

samples exposed to freshwater (C) and saltwater (S) cycles present fibres with minor (Lv.2) and moderate-to-major (Lv.3 – Lv.4) corrosion damage, respectively.

4. Discussion

The pull-out results presented in section 3.2.1 showed that, after exposure to wet-dry cycles, there is an increase in the forces transferred by the fibre during pull-out, particularly at slip values below 1 mm. The following discussion aims at describing the changes in the pull-out behaviour of single fibres that were pre-pulled and exposed to wet-dry cycles. The discussion focuses on three main stages of the pull-out process of hooked-end fibres, as described in Fig. 9: i) the elastic phase, comprising the adhesive bond (see A in Fig. 9) and elastic reloading curve (A' in Fig. 9); ii) the process phase, comprising the fracture of the adhesive bond (see B-C in Fig. 9) and corresponding reloading curve during re-testing (B'-C' in Fig. 9); and iii) the pull-out phase, comprising the mechanical bond and load transfer through the hook (see D-E in and D'-E' Fig. 9). Whereas, the variations on the residual frictional bond after straightening of the hook (see F in Fig. 9) will not be fully covered in this discussion, since this stage corresponds to relatively large slip values (i.e. approx. 6 – 7 mm of slip)

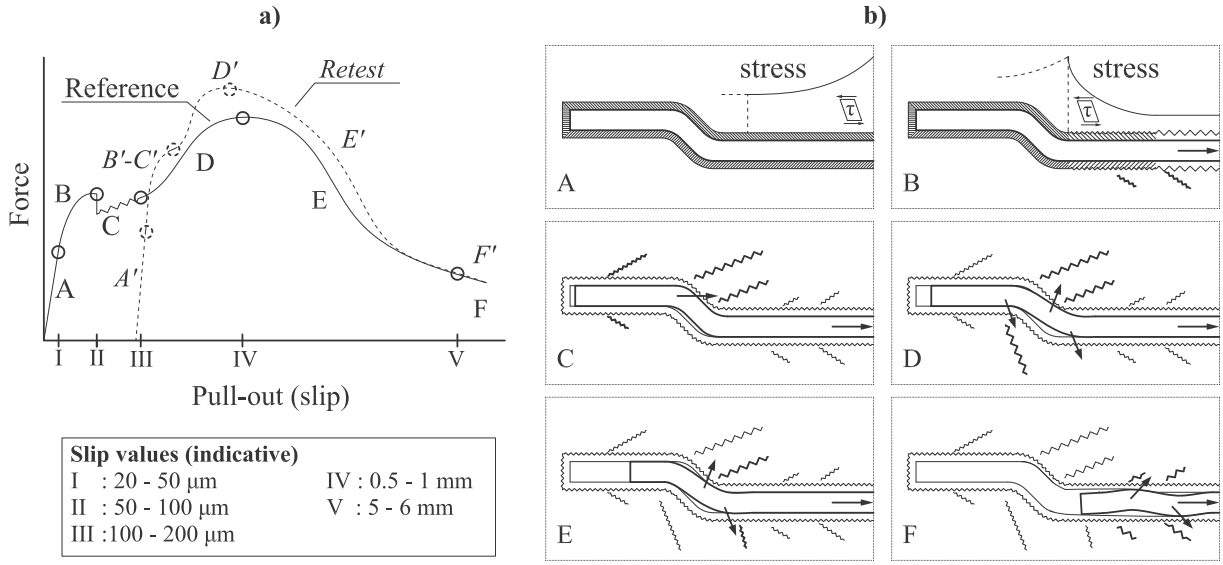

Fig. 9. Indicative description of the pull-out process of hooked-end fibres from concrete, showing: a) an indicative force-slip diagram of a hooked-end fibre with annotations of indicative slip values, and b) the corresponding load-transfer mechanisms at the hooked-end of the fibre. For illustrative purposes, the diagram in "a)" is not at scale and the images in "b)" describe a single-hook fibre.

compared to the range of interest for typical engineering applications (e.g. in the range 2.5–3.5 mm [29,30]), which are covered in this paper.

4.1. The elastic phase: The adhesive bond

The first phase of the pull-out process is expected to be governed by the strength and stiffness of the adhesive bond between the fibre and the matrix, see stage "A" in Fig. 9. Therefore, variations in the behaviour of this bond are expected to be closely related to variations in the elastic properties of the fibre–matrix interface. Fibre rupture was not observed at this phase in any of the specimens investigated.

The pull-out behaviour in the debonding phase of reference and re-tested fibres is presented in Fig. 10, as the mean force vs slip values at the initial 50 μm of the pull-out process of the reference samples (R) and exposed samples (S and C). The figure also shows the 90% CI of the mean as dotted lines. To ease the discussion, the representation of the reloading force-slip curve of the exposed samples (S and C) is shifted to the origin and is compared directly to the de-bonding force-slip curve of the reference samples (R). Results presented in Fig. 10 indicate a tendency towards an increase in the stiffness at the first 10 – 20 μm of slip for some of the exposed samples, see for example, the low- and medium-strength fibres (see L1 add M1 in Fig. 10a,b) and the double-hook fibres (see D1 and D2 in Fig. 10d,f). Whereas, the high-strength samples (H1 and H2) did not show a significant change in the initial stiffness after re-loading, see Fig. 10c,e.

The data presented indicate a general trend of a stiffer response of the fibre after reloading, which seems to diminish with increasing fibre strength for the single-hooked fibres. Specifically, comparing the stiffer response of the exposed samples (C and S) in L1 compared to the reference (R) in Fig. 10a with the progressive decrease in the stiffness gain observed for the medium-strength fibre (M1) Fig. 10b and the negligible change in the reloading stiffness measured in the high-strength fibre (H1 and H2) shown in Fig. 10c-e. Furthermore, it is observed that the change in the reloading stiffness of double-hook samples (D1 and D2) exposed to wet-dry cycles (S and C samples) was more pronounced when increasing the entrained air content of the mix, see Fig. 10d,f.

Furthermore, the equivalent shear modulus at the elastic region was calculated for the abovementioned data in the slip range 0–15 μm and is presented as a boxplot in Fig. 11. The plot also compares the shear modulus of the exposed samples (S and C) with the reference samples (R), where values significantly lower than the reference are highlighted in red and significantly higher values are highlighted in blue. The analysis was done by a one-tailed Welch's *t*-test, considering a significance level of $\alpha = 10\%$. The analysis presented in Fig. 11 confirms the aforementioned observations; i.e. a significantly stiffer bond for the some of the exposed samples, specifically the low-strength fibres (L1) and the double-hook fibres (D1 and D2). Whereas, the high-strength fibres (H1 and H2) showed a negligible increase or even a decrease in the re-loading stiffness.

The aforementioned observations indicate a tendency to a stiffening of the fibre–matrix bond after debonding and re-loading for some fibres. These observations agree with former investigations that observed an increase in the "interfacial bond" of pre-pulled straight steel fibres in mortar after curing in water [15] or for pre-pulled polymer fibres (PE and PVA) cured similarly for 28 days [16,17]; and attributed it to autogenous healing of the matrix surrounding the steel fibre. Although, such alteration of the fibre–matrix bond-strength has been also attributed to an increase of the frictional resistance due to fibre corrosion [12,13]."

Whereas, the extent of this recovery seems to depend on the fibre strength as well as on the fibre geometry; indicating that the recovery of the initial bond behaviour may be related to the damage of the fibre–matrix interface during the de-bonding process. Noting that, there is considerable damage occurring at the fibre–matrix interface during the de-bonding phase and the first 50 – 100 μm of the pull-out process, as described graphically in Fig. 9b (see stages "B" and "C") and reported in [8–11].

4.2. The process phase: Debonding and activation of the mechanical bond

The second phase of the pull-out process corresponds to the gradual breakage of the adhesive bond and the activation of the mechanical bond (i.e. loading of the hook), see stages "B" and "C" in Fig. 9. During the first part of this phase (Stage "B" in Fig. 9),

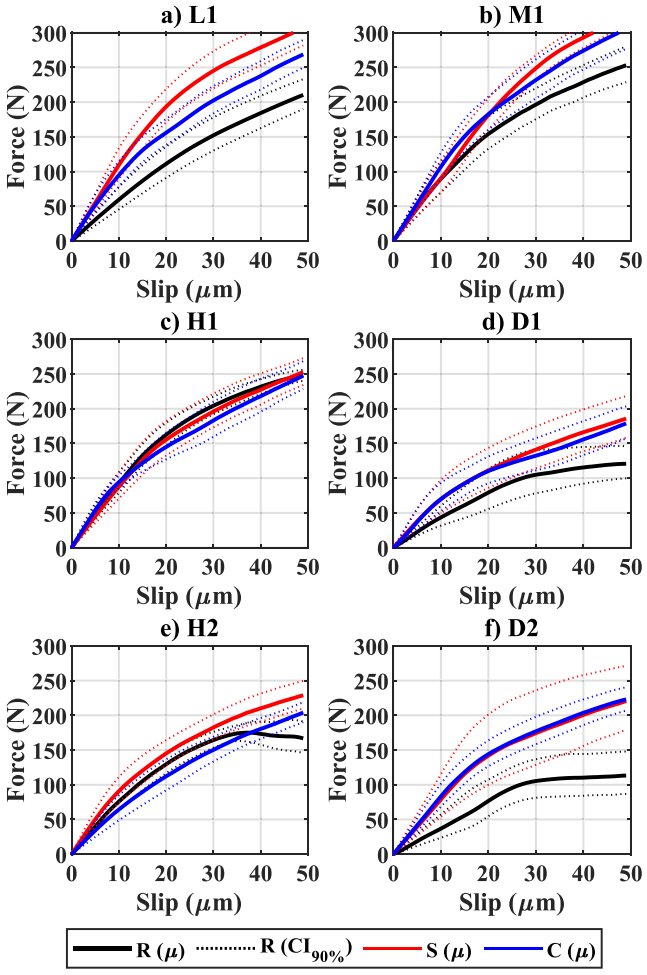

Fig. 10. Load-slip plot of the debonding phase, for samples: a) Low-strength fibre with mix 1 (L1), b) Medium-strength fibre with mix 1 (M1), c) High-strength fibre with mix 1 (H1), d) Double-hooked fibre with mix 1 (D1), e) High-strength fibre with mix 2 (H2), f) Double-hooked fibre with mix 2 (D2). Full lines represent the log-mean value (μ) of the sample and dotted lines represent the upper- and lower-confidence bounds at 90% CI, for lognormal distribution. Sample names correspond to code names described in Table 3: (R) Limewater references, (S) Chloride exposure, (C) Carbonation exposure.

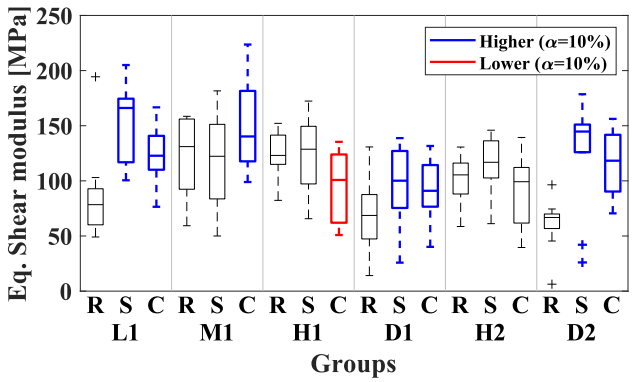

Fig. 11. Boxplot showing the equivalent shear modulus for debonding phase. Sample names correspond to code names described in Table 3: (R) Limewater references, (S) Chloride exposure, (C) Carbonation exposure. Significant variations in the shear modulus for exposed samples (S and C) compared to reference samples (R) are marked in red if lower and in blue if higher (α = 10%). Outliers are marked with a "+" symbol in the graph. (For interpretation of the references to colour in this figure legend, the reader is referred to the web version of this article.)

the fibre–matrix interface ruptures progressively from the intersection of the fibre and the crack towards the hook. Once the fractured interface reaches the hook, the fibre is displaced towards the adjacent matrix, and the deformed parts of the hook load against the adjacent matrix, crushing it (Stage "C" in Fig. 9). At this stage, variations in the pull-out behaviour are expected to be related to variations in the strength and stiffness of the matrix adjacent to the fibre (e.g. due to densification). Fibre rupture was only observed at this phase in the case of major reductions of the fibre cross-section for the low-strength fibres exposed to saltwater (i.e. L1-6-S).

The pull-out behaviour at this phase is presented in Fig. 12, as the gradient of the mean force vs slip (i.e. $dF/d\varepsilon$) of the initial 250 μm of the pull-out process of the reference samples (R) and exposed samples (S and C). For comparative purposes, the gradient to the re-tested specimens (S and C) is plotted both as tested (shown as red and blue full-lines in Fig. 12) and shifted to origin (shown as red and blue dashed-lines in Fig. 12). The data presented in Fig. 12 shows a higher gradient for exposed samples (S and C) at

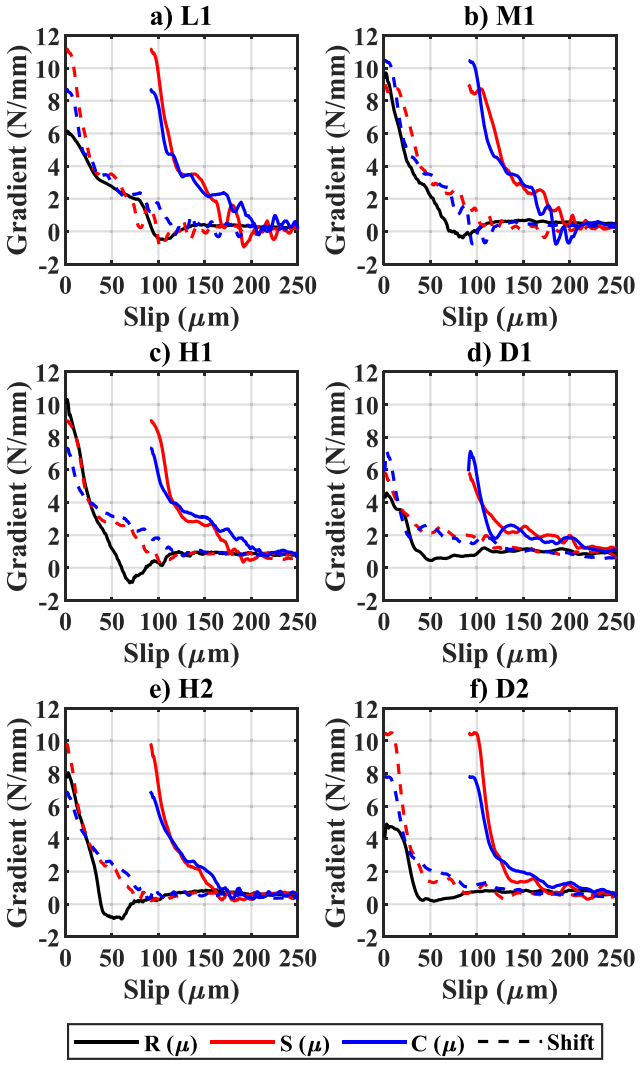

Fig. 12. Force-gradient vs slip plot in the debonding and mechanical loading phase, for samples: a) Low-strength fibre with mix 1 (L1), b) Medium-strength fibre with mix 1 (M1), c) High-strength fibre with mix 1 (H1), d) Double-hooked fibre with mix 1 (D1), e) High-strength fibre with mix 2 (H2), f) Double-hooked fibre with mix 2 (D2). Full lines represent the log-mean value (μ) of the sample and dotted lines represent the upper- and lower- confidence bounds at 90% CI, for lognormal distribution. Sample names correspond to code names described in Table 3: (R) Limewater references, (S) Chloride exposure, (C) Carbonation exposure.

smaller slip values (i.e. slip < 25 μm), compared to the reference samples (R); corresponding to the increase in the stiffness modulus after exposure discussed in Section 4.1.

After the elastic phase (i.e. the 10–20 μm of slip), the load gradient decreases gradually for all samples, reaching zero- or negative- values at a slip in the range 50–100 μm; where the adhesive bond breaks completely and the fibre fully de-bonds, see Fig. 12. At this stage, the reference samples show a clear drop in the gradient and a later stabilization (i.e. at slip > 80–100 μm), which marks the activation of the mechanical bond, see black full- lines in Fig. 12. Whereas, some of the exposed samples show a second failure zone after re-testing at similar slip values, i.e. fluctuations in the gradient at 50–100 μm of slip (Fig. 12a-b), which suggest additional fracture at the matrix after re-loading. This effect was evident in the fibres with lower strength (i.e. see L1 and M1 in Fig. 12a-b) but was faint in higher strength fibres (see H1-H2 and D1-D2 in Fig. 12c-f).

Finally, after the activation of the mechanical bond (i.e. at a slip ≳100–120 μm), the force gradient of the exposed samples (i.e. shifted S and C) and reference samples (R) tend to reach similar values, see Fig. 12. Whereas, comparing the gradient of the force-slip curves as measured (i.e. starting at slip ≈90 μm) for the exposed samples (S and C) with the references (R), shows that in any case the pull-out response of these follow a similar trend after a slip of 200–250 μm.

These observations correspond to the discussion initiated in Section 4.1, which suggests that there is a partial recovery of the original fibre–matrix bond on the re-tested samples (S and C) after exposure to wet-dry cycles of freshwater and saltwater during six months of exposure. Noting that, the exposed fibres were pre-pulled up to a slip value of 150 μm, where the adhesive bond was completely broken, and the mechanical bond was active for any of the samples tested.

The trends in the recovery of the stiffness discussed in Section 4.1, agree with the observations presented in Fig. 12. These suggest that the recovery and increase of the adhesive bond observed in Figs. 10–11 for the low- and medium-strength fibres (L1 and M1) may be related to a lower amount of damage at the fibre–matrix interface during the first stages of the pull-out. The authors expect that less damage may have facilitated the autogenous healing of the surrounding areas; similarly to as discussed at the single-fibre scale for analogous [31] and similar specimens [11,15,16], and also shown for cracked full-scale specimens exposed to analogous conditions during two years in [32]. Yet, other studies have indicated that such recovery may be due to increased friction due to expansion of corrosion products, as investigated at the single-fibre [12] and composite [2] scale.

4.3. The pull-out phase: Utilization of the mechanical bond

The last phase of the pull-out process described in this paper corresponds to the gradual utilisation of the mechanical bond (i.e. straightening of the hook), see stages "D" and "E" in Fig. 9. During the first part of this phase (phase "D" in Fig. 9), both bends of the hook are loading against the adjacent matrix and the load transferred increases with the slip, until reaching the maximum pull-out force (i.e. at a slip value of approx. 0.5–1 mm). After that point, the forces transferred decrease gradually as the hook-bends straighten; until reaching the frictional phase (i.e. at a slip value of approx. 5–6 mm), which is not covered in this discussion.

In the mechanical phase, the pull-out behaviour may be characterized by the maximum pull-out force and the energy-release capacity of the fibre along its slip (i.e. described as work). These are expected to be related to the properties and geometry of the steel wire as well as the mechanical properties of the matrix adjacent to the fibre. These two indicators are presented in Fig. 13 as a boxplot, showing the maximum pull-out force for each sample tested in Fig. 13a; and the total work of each sample in Fig. 13b, calculated in the slip range 0.2–4 mm. Furthermore, the exposed samples (S and C) are compared to the references (R) by means of a one-tailed Welch's *t*-test, which shows values significantly lower than reference samples (R) highlighted in red, and the ones showing significantly higher values highlighted in blue, considering a significance level of α = 10%.

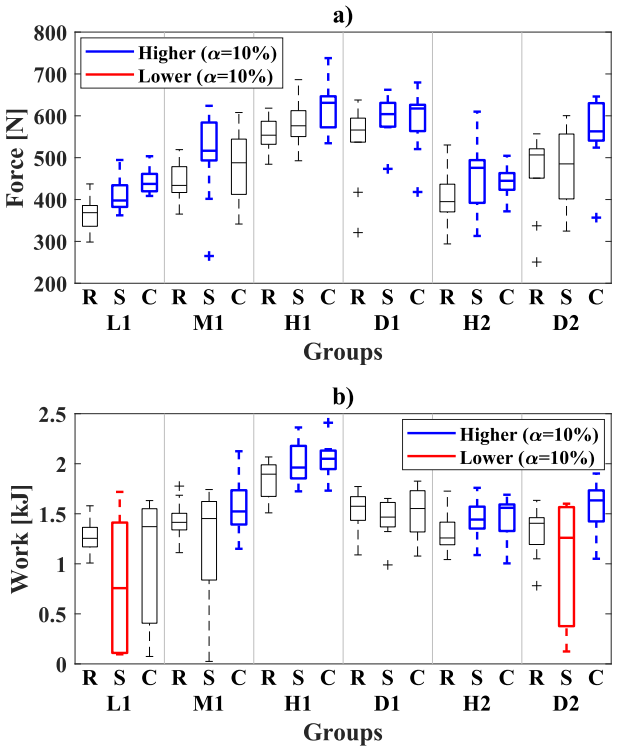

Fig. 13. Boxplot showing dispersion of the pull-out performance indicators: a) maximum pull-out force, and b) total pull-out work in the range (0.2 – 4 mm of slip). Sample names correspond to code names described in Table 3: (R) Limewater references, (S) Chloride exposure, (C) Carbonation exposure. Significant variations in the indicators for exposed samples (S and C) compared to reference samples (R) are marked in red if lower and in blue if higher (α = 10%). (For interpretation of the references to colour in this figure legend, the reader is referred to the web version of this article.)

The results presented in Fig. 13a show a general increase in the maximum pull-out force of exposed samples (S and C) relative to the corresponding references (R). However, this increase in the maximum force is not statistically significant in all cases and there is a trend of larger scatter in the exposed samples compared to the references. Furthermore, there is no statistically significant decrease in the maximum pull-out force in any of the cases, regardless of the exposure media, degree of corrosion damage or presence of rupturing fibres (see Fig. 8).

Likewise, the results discussed in Fig. 13b show an overall increase in the total work for some of the samples, particularly: the high-strength fibres (H1 and H2), as well as some other samples exposed to freshwater cycles (M1-6-C and D2-6-C). However, in this case, some samples showed a much larger scatter in the work as well as substantial drop of the total work, e.g. L1, M1 and D2 samples. Such a decrease in the total work corresponds to the contribution of fibres rupturing during the pull-out process (i.e. typically at slip values in the range 0–1 mm). This drop occurs mostly in the samples with the lower-strength steel types tested (L1 and M1); which otherwise correspond to the aforementioned increases in the maximum pull-out forces. Thus, suggesting that fibre rupture may occur due to the combination of two factors: i)

the reduction of the fibre cross-section due to corrosion, and ii) the increase of the load transferred by the fibre during pull-out.

Fibre rupture during pull-out, resulted in some cases in a divergence of the pull-out toughness of the samples tested; where specimens in which the fibre ruptured generally transfer substantially less work than the ones where the fibre pulled-out satisfactorily. In order to investigate this aspect, the work transferred during pull-out of exposed and reference samples is compared in Fig. 14, investigating each sample in two groups: the specimens with fibres not rupturing (solid lines), and all the specimens of the sample (dashed lines). The figure compares the mean accumulated energy released over the slip (i.e. the work-slip curves) of the exposed samples (S and C) to the corresponding reference samples (R) by means of a one-tailed Welch's *t*-test. The figure shows the probability (p-value) of the null hypothesis (H_0) for the alternative hypotheses (Ha): a) the probability of the mean value of the sample being smaller than the reference (left tail); b) the probability of the mean value of the sample being greater than the reference (right tail).

The results presented in Fig. 14 illustrate clearly the abovementioned divergence in the behaviour of the samples due to fibre rupture; particularly in the samples comprising low- and medium-strength fibres (L1 and M1), see Fig. 14a-b, as well as the double-hook fibres (D1 and D2), see Fig. 14d-f. In these cases, the exposed samples including non-rupturing fibres showed a significantly higher pull-out toughness over the whole slip range (0 – 4 mm) compared to the corresponding references. Whereas, fibre rupture led to a substantial drop in toughness over the slip, which depended on the location of the rupture (see Fig. 8a) and the slip value when the fibre ruptured during the test, (see Fig. 8b). Conversely, there was no detriment to the work of the exposed samples with high-strength fibres (H1 and H2) and only one fibre, corresponding to the low entrained-air content exposed to freshwater cycles, ruptured during the test (H1-6-C).

4.4. Corrosion damage and fibre rupture

The discussion above presents two main parameters that govern the rupture of fibres during pull-out: i) the tensile capacity of the fibre, and ii) the strength of the fibre–matrix bond. Fibre rupture occurs when the maximum force transferred exceeds the tensile- or shear-capacity of the steel wire. This may occur due to: a reduction of the load-bearing capacity of the fibre (i.e. reduction of the cross-section due to corrosion) and/or an increase of the forces transferred (i.e. an increase of the fibre–matrix bond strength).

The data presented in Fig. 15 shows the variation of the idealised tensile capacity of a fibre with a uniform reduction of its cross-section, assuming parameters corresponding to the ones studied in this paper: a fibre diameter of 0.75 mm and a characteristic steel strength in the range 1000–2000 MPa. The idealised tensile capacity is compared to the maximum pull-out forces measured in the experiments (shown in Fig. 13a); which were estimated by linear regression of the maximum pull-out force vs the steel strength, estimated to: $f^{p}_{max} = 0.270x + 79$, with an adjusted coefficient of determination of $R^2_{adj} = 0.6$.

The diagram shows the variation of the ideal tensile capacity of the fibre with varying steel strength in Fig. 15a at various percentages of cross-section reduction (0% to 60%). The predicted maximum pull-out force is plotted in red, as the mean as well as upper- and lower- prediction intervals at $\alpha = 10\%$. The second diagram (Fig. 15b) shows the ratio of cross-section that could be lost to corrosion, while maintaining a tensile capacity higher than the maximum pull-out force calculated for the maximum forces shown in Fig. 15a (henceforth "cross-section allowance") versus the characteristic strength of the steel. Negative values indicate an insufficient cross-section for the corresponding steel strength and predicted maximum pull-out force, therefore tensile rupture of

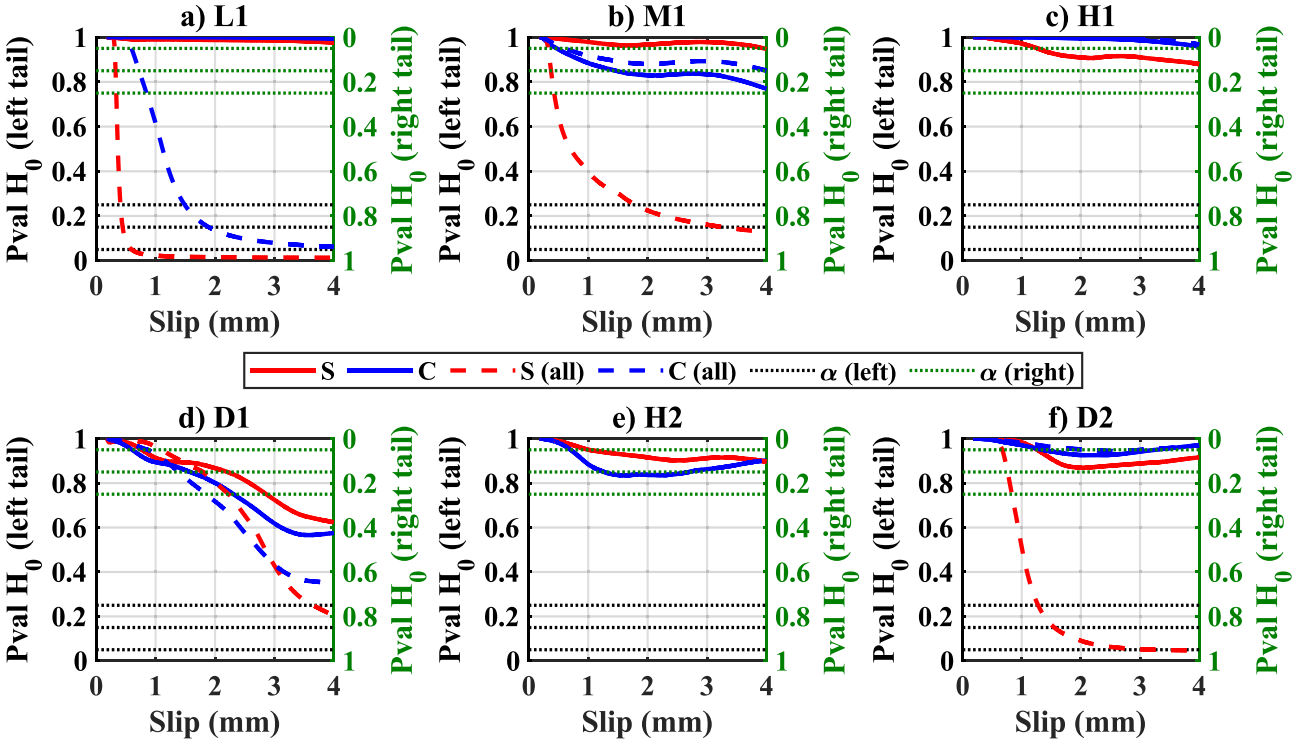

Fig. 14. T-test, comparison of work values for pull-out tests of exposed specimens (S and C) vs unexposed specimens (R), for: a) Low-strength fibre with mix 1 (L1), b) Medium-strength fibre with mix 1 (M1), c) High-strength fibre with mix 1 (H1), d) Double-hooked fibre with mix 1 (D1), e) High-strength fibre with mix 2 (H2), f) Double-hooked fibre with mix 2 (D2). Full lines represent the group containing specimens with non-rupturing fibres and dashed lines represent the group comprising all the specimens of the sample. Sample names correspond to code names described in Table 3: (S) Chloride exposure, (C) Carbonation exposure.

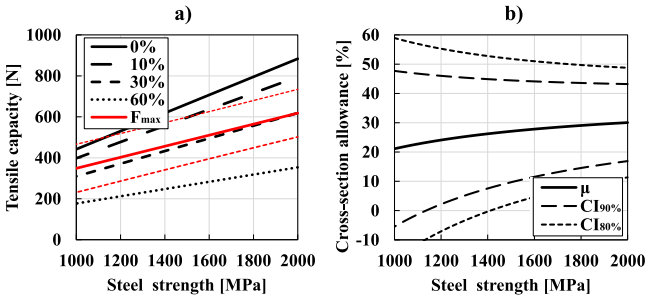

Fig. 15. Impact of cross-section reduction on the tensile capacity of the fibre during pull-out, depending of: a) the steel strength (cross-section reduction of 0–60%); and b) the cross-section reduction allowance due to e.g. corrosion (i.e. cross-section allowance) for the mean- upper- and lower- prediction intervals of the estimated maximum forces in the experiments at (α = 2% and 10%). The mean- upper- and lower-prediction intervals (α = 10%) of the maximum pull-out forces measured in the experiments ("pull") are plotted as red lines in "a)". (For interpretation of the references to colour in this figure legend, the reader is referred to the web version of this article.)

the fibre. While positive values indicate that additional cross-section could be lost due to, e.g. corrosion, without leading to tensile rupture of the fibre.

The data indicates that, the fibres tested would have an average corrosion allowance of 20–30% to result in tensile failure of the fibre at its maximum pull-out force (see Fig. 15b). Whereas, the upper prediction interval of the maximum pull-out forces registered would result in a steeper variation of the corrosion allowance in the range 0–20%, implying a tensile rupture of the lower-strength fibres regardless of the cross-section reduction. Thus, partly explaining the absence of fibre rupture in unexposed samples, which showed overall lower peak forces compared to their exposed counterparts.

Whereas, tensile rupture of the fibre (i.e. at the stem) would be expected for steel strengths above 1200 MPa, regardless of the cross-section reduction for 2–10% of the cases (see Fig. 15b). The measured increase in the cross-section allowance with increasing steel strength would explain the tensile failure observed in lower-strength fibres (types L and M) exposed to chlorides while higher-strength fibres (type H) did not show such behaviour. Yet, this analysis above is partly biased by the experimental nature of the data; since pull-out forces larger than the tensile capacity of the fibre cannot be measured as the steel would rupture, but substantially lower pull-out forces can be measured.

Furthermore, the discussion cannot explain the failure observed in most fibres under freshwater exposure, which did not present a significant loss of cross-section at the exposed steel; and often ruptured at the hook, at slip values much larger than the ones corresponding to the maximum pull-out force and regardless of the negligible cross-section reduction at the embedded steel due to corrosion. Therefore, it is expected that additional failure mechanisms may be affecting the pull-out process of hooked-end fibres at larger deformations, yet these are not fully described in the literature [33–35].

The discussion presented in this paper supports the hypotheses presented in [1,5], that suggest a twofold mechanism explaining the increase in toughness and the number of fibres rupturing observed in cracked SFRC: i) the fibre matrix-bond is altered after exposure of cracked SFRC to e.g. wet-dry cycles, disrupting the expected pull-out behaviour when the hook straightens; and ii) corrosion damage at the exposed fibres may reduce the tensile capacity of the steel at certain locations (i.e. at the intersection of the fibre with the crack). Noting that these mechanisms are not exclusive, and the overall pull-out behaviour is governed by both in the case of significant fibre corrosion.

Previous studies investigating the pull-out behaviour of fibres exposed under similar environments have shown corresponding increases in the maximum pull-out force and energy release to the ones reported in this paper [12,13]. Whereas, in both cases these changes were attributed to fibre corrosion. However, these assertions were based on limited data and, in the authors' opinion may not fully explain the increase in the fibre–matrix bond during the mechanical-bond phase, where forces are mainly transferred through yielding of the steel and crushing of the matrix adjacent to the hooks, as described in [11,15,16].

Additional mechanisms, such as the hydration of the binder over time, are expected to have a contribution to the increase observed in the fibre–matrix bond strength. The compressive strength data presented, indicated a development in the mechanical performance of the matrix over the exposure time, e.g. approx. 10% increase, yet the pull-out data included in this study could not provide sufficient data to isolate such effect. Variations in the pull-out strength over concrete maturity have been discussed in recent studies; showing a limited development of the pull-out force after 28 days in similar single-fibre specimens [20,36], also as reported in [13] for other matrix types. Yet, studies at the composite level have reported still substantial development in the residual strength of SFRC between 28 and 180 days in [3].

Similarly, cross-section reductions due to corrosion leading to fibre rupture agree partly with values estimated in former studies, i.e. at approx. 30–50% reduction [14], which would correspond to the fibres presenting major corrosion (Level 4), as described in Fig. 8c.

The discussion presented in this study complements former hypotheses that suggest a potential loss of toughness after exposure of cracked SFRC for some fibre types, yet not solely due to fibre corrosion [3,4]. Although, still agreeing with the discussion presented in [5], which suggest that an appropriate fibre type (i.e. steel strength and dimensions) may lead to a net increase in ductility over time, regardless of moderate corrosion damage at the fibres bridging the crack.

Generally, the investigation presented in this paper showed clear trends of variation of the fibre–matrix bond strength of straight fibres bridging cracks in SFRC exposed to wet-dry cycles. However, the results presented only cover a minor share of the variables that govern the pull-out behaviour of steel fibres embedded in cracked concrete. Parameters such as the fibre orientation, the type and strength of the matrix, the fibre shape or the level of damage at the interface were not investigated. Yet, these are expected to have a substantial impact on the pull-out behaviour of deformed fibres (e.g. hooked-end fibres) in cracked concrete exposed to similar environments.

5. Conclusions

This paper investigated the pull-out behaviour of hooked-end steel fibres in cracked concrete exposed to wet-dry cycles of corrosive environments. The results showed that the exposure to such environments entailed significant variations to the pull-out forces transferred during pull-out, while there was a substantial increase in the number of fibres rupturing after the exposure. Corrosion damage at the exposed steel surface was observed for both freshwater and saltwater exposure, while there was only a noticeable cross-section reduction at the steel for the latter.

There was an increase in the pull-out force transferred after the exposure during both the adhesive and the mechanical bond phase; which in some cases led to a premature rupture of the fibre during pull-out and a reduction of the work transferred during pull-out.

The amount of fibres rupturing during the test was governed by the reduction of the fibre's cross-section due to corrosion and the

increase of the fibre–matrix bond strength during exposure. Increasing the steel strength for the same concrete type was effective for reducing substantially the amount of fibres rupturing.

The findings of this investigation support current hypotheses that suggest additional damage mechanisms, besides fibre corrosion, that may contribute to the changes in the residual performance of the cracked SFRC. These additional mechanisms are related to an alteration of the matrix surrounding the fibre during exposure to wet-dry cycles.

This investigation provided a detailed discussion of the effects of wet-dry exposure to the pull-out behaviour of steel fibres bridging cracks and its governing damage mechanisms. Yet, the experimental variables investigated only covered a small share of the parameters governing the pull-out behaviour of steel fibres embedded in cracked concrete. Further experimental work and modelling are needed in order to extend these conclusions to general applications.

CRediT authorship contribution statement

Victor Marcos-Meson: Conceptualization, Methodology, Formal analysis, Investigation, Visualization, Project administration. **Anders Solgaard:** Conceptualization, Supervision, Funding acquisition. **Gregor Fischer:** Conceptualization, Supervision, Funding acquisition. **Carola Edvardsen:** Conceptualization, Supervision, Funding acquisition. **Alexander Michel:** Conceptualization, Supervision, Project administration, Funding acquisition.

Declaration of Competing Interest

The authors declare that they have no known competing financial interests or personal relationships that could have appeared to influence the work reported in this paper.

Acknowledgements

The first author would like to express his gratitude to: CowiFonden, InnovationsFonden, the German association of steel fibre producers (VDS), VejDirektoratet and Mapei-Denmark, for supporting this project; and Dr. Torben Lund Skovhus for his contribution to supervision during this project.

References

[1] V. Marcos-Meson, A. Michel, A. Solgaard, G. Fischer, C. Edvardsen, T.L. Skovhus, Corrosion resistance of steel fibre reinforced concrete – A literature review, Cem. Concr. Res. 103 (2018) 1–20, https://doi.org/10.1016/j.cemconres.2017.05.016.
[2] J.-L. Granju, S.U. Balouch, Corrosion of steel fibre reinforced concrete from the cracks, Cem. Concr. Res. 35 (2005) 572–577, https://doi.org/10.1016/j.cemconres.2004.06.032.
[3] E.S. Bernard, Age-dependent changes in post-crack performance of fibre reinforced shotcrete linings, Tunn. Undergr. Sp. Technol. 49 (2015) 241–248, https://doi.org/10.1016/j.tust.2015.05.006.
[4] E.S. Bernard, Effect of Exposure on Post-crack Performance of FRC for Tunnel Segments, in: I. Vrkljan, Z. Dekovic, M. Dobrilovic, J. Likar, P. Miscevic (Eds.), SEE TunnelPromoting Tunneling SEE Reg. - ITA WTC 2015, ITA-AITES, Dubrovnik, Croatia, 2015: p. 13.
[5] V. Marcos-Meson, G. Fischer, C. Edvardsen, A. Solgaard, A. Michel, Mechanical performance of steel fibre reinforced concrete exposed to chlorides and carbon dioxide: results after one year, J. Sustain. Cem. Mater. (2018) (Unpublished).
[6] R.J. Gray, Experimental techniques for measuring fibre/matrix interfacial bond shear strength, Int. J. Adhes. Adhes. 3 (1983) 197–202, https://doi.org/10.1016/0143-7496(83)90094-5.
[7] C. DiFrancia, T.C. Ward, R.O. Claus, The single-fibre pull-out test. 1: Review and interpretation, Compos. Part A Appl. Sci. Manuf. 27 (1996) 597–612, https://doi.org/10.1016/1359-835X(95)00069-E.
[8] I. Markovich, J.G.M. Van Mier, J.C. Walraven, Single fiber pullout from hybrid fiber reinforced concrete, Heron. 46 (2001) 191–200.
[9] P.D. Nieuwoudt, A.J. Babafemi, W.P. Boshoff, The response of cracked steel fibre reinforced concrete under various sustained stress levels on both the macro and single fibre level, Constr. Build. Mater. 156 (2017) 828–843, https://doi.org/10.1016/j.conbuildmat.2017.09.022.
[10] A. Bentur, S. Mindess, S. Diamond, Pull-out processes in steel fibre reinforced cement, Int. J. Cem. Compos. Light. Concr. 7 (1985) 29–37, https://doi.org/10.1016/0262-5075(85)90024-7.
[11] T.H. Ahn, D.J. Kim, S.H. Kang, Crack Self-Healing Behavior of High Performance Fiber Reinforced Cement Composites Under Various Environmental Conditions, in: Kris Zacny, R.B. Malla, W. Binienda (Eds.), Earth Sp. 2012, ASCE, Pasadena, United States, 2012: pp. 635–640.
[12] C. Frazão, J. Barros, A. Camões, A.C. Alves, L. Rocha, Corrosion effects on pullout behavior of hooked steel fibers in self-compacting concrete, Cem. Concr. Res. (2015), https://doi.org/10.1016/j.cemconres.2015.09.005.
[13] N. Banthia, C. Foy, Marine curing of steel fiber composites, J. Mater. Civ. Eng. 1 (1989) 86–96, https://doi.org/10.1061/(ASCE)0899-1561(1989) 1:2(86).
[14] E. Alizade, F.J. Alaee, S. Zabihi, Effect of steel fiber corrosion on mechanical properties of steel fiber reinforced concrete, Asian J. Civ. Eng. 17 (2016) 147–158.
[15] R.J. Gray, Autogenous healing of fibre/matrix interfacial bond in fibre-reinforced mortar, Cem. Concr. Res. 14 (1984) 315–317, https://doi.org/10.1016/0008-8846(84)90047-4.
[16] T. Nishiwaki, S. Kwon, D. Homma, M. Yamada, H. Mihashi, Self-healing capability of fiber-reinforced cementitious composites for recovery of watertightness and mechanical properties, Materials (Basel). 7 (2014) 2141–2154, https://doi.org/10.3390/ma7032141.
[17] D. Homma, H. Mihashi, T. Nishiwaki, Self-healing capability of fibre reinforced cementitious composites, J. Adv. Concr. Technol. 7 (2009) 217–228, https://doi.org/10.3151/jact.7.217.
[18] L. Ferrara, V. Krelani, F. Moretti, M. Roig Flores, P. Serna Ros, Effects of autogenous healing on the recovery of mechanical performance of High Performance Fibre Reinforced Cementitious Composites (HPFRCCs): Part 1, Cem. Concr. Compos. 83 (2017) 76–100, https://doi.org/10.1016/j.cemconcomp.2017.07.010.
[19] A.K. Kragh, M.E. Carlsen, Development of fibre-matrix bond over time, Technical University of Denmark, 2017.
[20] M.S. Thorsen, P. Christensen, Impact of w/c-ratio on development of fibre-matrix bond in steel fibre reinforced concrete over time - DTU Findit, Technical University of Denmark, 2018.
[21] European Commitee for Standardization (CEN), Methods of test for mortar for masonry. Determination of consistence of fresh mortar, European Union, 1999.
[22] European Commitee for Standardization (CEN), Masonry cement. Test methods, European Union, 2016.
[23] European Commitee for Standardization (CEN), Fibres for concrete - Part 1: Steel fibres - Definitions, specifications and conformity, EN 14889-1:2006, European Union, 2006.
[24] KrampeHarex, ArcelorMittal Fibres, Bekaert, Technical datasheets from suppliers (private communication), (2019)
[25] V.D. Mois, V. Chiriac, Response of single fibers to pull-out forces at different embedment angles, Technical University of Denmark, 2017.
[26] European Commitee for Standardization (CEN), Testing hardened concrete - Part 3: Compressive strength of test specimens, EN 12390-3 + AC:2012, European Union, 2012.
[27] European Commitee for Standardization (CEN), Testing hardened concrete. Determination of secant modulus of elasticity in compression, European Union, n.d.
[28] B.L. Welch, The generalisation of student's problems when several different population variances are involved, Biometrika. 34 (1947) 28–35, https://doi.org/10.1093/biomet/34.1-2.28.
[29] AFTES, AFTES-GT38R1A1. Design, dimensioning and execution of precast steel fibre reinforced concrete arch segments, France, 2013
[30] International Federation for Structural Concrete, FIB Model Code for concrete structures 2010, Lausanne, Switzerland, 2010.
[31] V. Marcos-Meson, G. Fischer, A. Solgaard, U.H. Jakobsen, C. Edvardsen, T.L. Skovhus, A. Michel, Pull-out behaviour of steel fibres in cracked concrete under wet-dry cycles – deterioration phenomena (In press), Mag. Concr. Res. (2019).
[32] V. Marcos-Meson, M. Geiker, G. Fischer, A. Solgaard, U.H. Jakobsen, C. Edvardsen, T. Danner, T.L. Skovhus, A. Michel, Durability of cracked SFRC exposed to wet-dry cycles of chlorides and carbon dioxide – multiscale deterioration phenomena (Unpublished), Cem. Concr. Res. (2019).
[33] S. Abdallah, M. Fan, Anchorage mechanisms of novel geometrical hooked-end steel fibres, Mater. Struct. Constr. 50 (2017) 139, https://doi.org/10.1617/s11527-016-0991-5.
[34] J.A.O. Barros, Steel fibre reinforced concrete: Material properties and structural applications, Fibrous Compos. Mater. Civ. Eng. Appl. (2011) 95–155, https://doi.org/10.1533/9780857095583.2.95.
[35] M. Maalej, V.C. Li, T. Hashida, Effect of fiber rupture on tensile properties of short fiber composites, J. Eng. Mech. 121 (1995) 903–913, https://doi.org/10.1061/(asce)0733-9399(1995) 121:8(903).

Chapter 5
Multiscale deterioration phenomena of cracked SFRC under wet-dry exposure

Investigations presented in Chapter 3 and Chapter 4 showed that the exposure of cracked SFRC to wet-dry cycles leads to significant changes in the residual performance of the cracked composite over time (Chapter 3), which were mainly related to an alteration of the fibre-matrix bond strength during the exposure (Chapter 4). Former studies have reported a similar behaviour, which was attributed in some cases to an increase of roughness due to fibre corrosion or to autogenous healing at the fibre-matrix interface in others. A conceptual deterioration model was proposed in Chapter 2 based on these arguments. However, there is limited data available to fully discuss these hypotheses.

The studies presented in this chapter cover the description of the microstructural and chemical changes occurring in cracked SFRC subject to wet-dry cycles. Two studies were conducted that covered macroscopic and microscopic investigations at the composite and single-fibre levels: the study presented in Paper VI investigated the multiscale deterioration phenomena at the composite level, the study presented in Paper VII was focused at the single-fibre level.

The study presented in Paper VI covers a multiscale chemical and petrographic study of SFRC bending specimens, exposed under the same conditions as the ones investigated in Chapter 3. The investigation focused on describing the transport processes inside the crack, the resulting changes in the microstructure at the concrete matrix adjacent to the crack and at the fibre-matrix interface; and the relation between these conditions and corrosion of the steel fibres crossing the crack.

The study presented in Paper VII investigated single-fibre pull-out specimens, exposed under the same conditions as the ones investigated in Chapter 4. The investigation focused on describing the contribution of fibre corrosion and alteration of the cement

matrix surrounding the fibre to the changes of the pull-out behaviour of single fibres reported in Chapter 4. The investigation comprised 3D optical profiles of single steel fibres extracted from pull-out specimens and a petrographic study of partially-pulled fibres embedded in the cracked matrix.

Results at the composite level (Paper VI) showed that corrosion of the steel fibres occurred mainly at the outer regions of the crack, for crack widths smaller than 0.3 mm, where the pH inside the crack dropped below values of 9 – 10; while the presence of chlorides was found to mainly affect the extent of corrosion damage. At the single-fibre level (Paper VII), corrosion damage was found to be mainly localized at the steel exposed to the solution inside the crack, as well as few rust spots around voids and cracks in the matrix. Corrosion products primarily accumulated around the exposed steel inside the crack, and a few millimetres inside the damaged fibre-matrix interface next to the crack, but were only related to a small part of the recovery of the adhesive bond between the fibre and the matrix.

Concurrently, exposure to wet-dry cycles led to substantial changes in the microstructure of the crack and surrounding cement matrix, as well as at the fibre-matrix interface of fibres crossing the crack. Results at the composite level (Paper VI) showed that the reactivity of the cement matrix surrounding the crack plays a dominant role in controlling deterioration reactions and promoting recovery processes inside cracks and at localized damage around fibres. Precipitation of secondary phases at the fibre-matrix interface of fibres bridging cracks was observed at the composite level (Paper VI) and at the single-fibre level (Paper VII). Investigations at the single-fibre level showed that the pull-out process is tightly related to damage of the cement matrix surrounding the hooked-end of the fibre. Autogenous healing processes of mechanical damage of the cement matrix around the hook were related to the alteration of the pull-out behaviour of single fibres observed in Chapter 4; and so these may explain the variations of the tensile performance of cracked SFRC reported in Chapter 3.

This chapter concluded that the deterioration mechanisms concurring in cracked SFRC exposed to wet-dry cycles are closely connected, and do not involve solely corrosion damage of the steel fibres bridging the crack. A conceptual deterioration model based on the model described in Paper II was presented in Paper VI. The model updates the hypotheses proposed in Chapter 2, and extends the description of the diverse mechanisms concurring inside the crack, which cause deterioration and/or recovery of the mechanical and transport properties of the cracked SFRC over time.

The finding presented in this chapter represent a step forward towards the estimation of the durability of the cracked SFRC over time. However, predictions rely on a precise understanding and accurate prediction of the aforementioned deterioration and recovery processes. Challenges arise when addressing such complex problems, which often require the use of advanced modelling techniques, such as reactive mass transport modelling (Addassi et al., 2019; Michel et al., 2019, 2018).

5.1 Paper VI. A conceptual deterioration model for cracked SFRC under wet-dry exposure conditions

The following publication, referred as “paper VI”, is under review in Cement and Concrete Research.

Marcos-Meson, V., Fischer, G., Solgaard, A., Edvardsen, C., Geiker, M., Danner, T., Jakobsen, U.H., Skovhus, T.L., Michel, A., 2020. Durability of cracked SFRC exposed to wet-dry cycles of chlorides and carbon dioxide – multiscale deterioration phenomena (Manuscript under review). Cem. Concr. Res.

Printed in this thesis as the original manuscript with the authors’ formatting.

Under review in Cement and Concrete Research (2020)

Durability of cracked SFRC exposed to wet-dry cycles of chlorides and carbon dioxide – multiscale deterioration phenomena

V. Marcos-Meson[1,2,3*], M. Geiker[4], G. Fischer[1], A. Solgaard[2], U.H. Jakobsen[5], T. Danner[6], C. Edvardsen[2], T.L. Skovhus[3] and A. Michel[1]

[1]Department of Civil Engineering, Technical University of Denmark, Kgs. Lyngby, Denmark

[2]COWI A/S, Kgs. Lyngby, Denmark

[3]VIA Building, Energy, Water & Climate, VIA University College, Horsens, Denmark

[4]Department of Structural Engineering, NTNU, Trondheim, Norway

[5]Danish Technological Institute, Taastrup, Denmark

[6]SINTEF, Trondheim, Norway

* Corresponding author: vicmes@byg.dtu.dk

Abstract

This paper describes an experimental study that comprised the exposure of cracked SFRC members to wet-dry cycles involving chloride and carbon-dioxide for two years. Results indicate that corrosion of steel fibres occurs mainly at the outer regions of the crack for cracks smaller than 0.3 mm, where the pH inside the crack drops below values of nine. The presence of chloride affected mainly the extent of corrosion. The results indicate that corrosion damage of the steel fibres does not necessarily play a dominant role on the overall deterioration of the composite; since changes in the microstructure of the matrix surrounding the crack and the fibre-matrix interface due to leaching and autogenous healing, may have a substantial impact on the long-term behaviour of the cracked composite. A conceptual deterioration model was developed, describing the deterioration and recovery mechanisms that alter the long-term mechanical performance of the cracked composite under wetting-drying conditions.

Keywords

Steel Fibre Reinforced Concrete (SFRC), cracks, chlorides, carbonation, corrosion, petrography, healing

1. Introduction

Steel Fibre Reinforced Concrete (SFRC) is used in the construction of infrastructure exposed to aggressive environment that often involve exposure to chlorides and carbon dioxide. Previous studies generally agree regarding the good long-term performance of uncracked SFRC exposed to aggressive environments; but are inconsistent regarding the extent of fibre corrosion inside cracks and its impact on the tensile toughness of the cracked composite for cracks in the range of 0.1 – 0.3 mm [1].

To date, there is a limited understanding of the deterioration processes of cracked SFRC in aggressive media, such as saline or fresh water. Earlier research has in general based its conclusions on macroscopic observations relating the mechanical performance of the composite to the corrosion of the carbon-steel fibres [1]. It is not clear whether toughness variations reported after exposure are related solely to corrosion damage at the fibres or if additional changes in the fibre-matrix bond due to alteration of the concrete matrix during exposure also plays a role [2,3], as also discussed in [1,4]. Ongoing studies have shown that exposure of cracked SFRC to some corrosive environments, e.g. wet-dry cycles of freshwater or saltwater, do not necessarily lead to a reduction of the mechanical performance of the cracked composite; and may even result on an

increase of the mechanical performance over time [4]. Yet, those changes cannot be explained by a conventional deterioration model, which accounts mainly for the detrimental contribution of fibre corrosion [5,6]. Thus, more detailed deterioration models were proposed [1]; which, however, lack data to substantiate their hypotheses.

The deterioration process of the material reported in macroscopic observations of cracked SFRC is initially triggered by the transport of moisture and other chemical species (henceforth "species") inside the crack. However, transport of species in cementitious composites involves multiple concurring processes: diffusion and convective transport of moisture and species, dissolution of primary phases of the binder and precipitation of secondary phases in voids [7]. These processes are increasingly complex when cracking of the concrete matrix facilitates the transport through the main cracks [8–10] and into the damaged matrix adjacent to the crack [11,12]. Concurringly, the reactivity of the hardened cement matrix surrounding the crack alters substantially the structure and transport properties (e.g. ionic, moisture or gas) along the crack with time; due to, among others: leaching in the surrounding matrix [13], binding of species (e.g. Cl^-) [14,15], carbonation of the cement paste [16,17] and autogenous healing [18–20].

The transport and reaction processes previously described eventually yield conditions inside the crack (in terms of e.g. pH, RH, $[O_2]$, $[Cl^-]$) that shift the electrochemical potential of the exposed steel locally and may lead to corrosion of the steel fibres bridging the crack. Whereas, additional damage that propagates along the steel-matrix interface during pull-out [21–23] is expected to play a significant role on the corrosion of steel fibres in cracked concrete [1]. Yet, there is limited data to support a conclusive discussion and there is insight indicating that "self-healing" processes may restore part of this damage with time under certain exposures (e.g. wet-dry cycles); which would lead to a strength regain of the fibre-matrix bond over time [24,25].

The foregoing discussion reflects the overall complexity involved in the long-term performance of cracked SFRC subject to aggressive corrosive exposures. Potential deterioration of the functionality of the cracked composite during exposure: e.g. structural and/or pervious; does not comprise a single progressive process that can be predicted based on macroscopic observations. Instead, requires a deeper understanding of several interconnected processes at various scales, which can lead in some cases to partial or total recovery of some of the properties of the bulk material.

2. Research significance and content

The aim of this study is to describe the main deterioration and recovery mechanisms observed in cracked SFRC subject to potential aggressive exposures and discuss its contribution to the long-term performance of the cracked composite. The paper presents the results of an experimental campaign investigating the durability of cracked SFRC exposed to wet-dry cycles of saltwater, freshwater and carbon dioxide for two years; and discusses the impact of these exposure conditions on the corrosion of the steel fibres bridging the cracks and the alteration of the matrix surrounding the crack.

The results section (**Section 4**) presents data from five experimental studies on analogous specimens, covering: i) the quantification of fibre corrosion at the composite scale by means of fibre counting (**Section 4.1**); ii) ingress of chloride ions and decrease of pH inside the crack based on colorimetric profiles and water-soluble chloride measurements (**Section 4.1 and 4.2**); iii) modification of the elemental composition of the matrix surrounding the crack after exposure based on X-ray fluorescence spectrometry mapping (**Section 4.3**); and iv) investigation of changes in microstructure around the crack due to exposure based on a petrographic study (**Section 4.4**).

The discussion section (**Section 5**) describes the main processes taking place during the exposure of cracked SFRC to wet-dry cycles and how these processes are interconnected at various scales, based on the data presented in (**Section 4**) and results from former studies. The main deterioration and recovery mechanisms are described indicatively in a conceptual model presented in **Section 5.1**, which reviews and updates the conceptual deterioration model proposed in [1]. The model is discussed afterwards covering the abovementioned processes at multiple scales: i) the deterioration of the matrix and fibre-matrix bond due to transport of species through the crack and alteration of the cement paste surrounding the crack (**Section 5.2**); ii) the deterioration of the steel fibres due to corrosion (**Section 5.3**); and iii) the recovery of the matrix due to transport of species through the bulk matrix, reactions with the matrix surrounding the crack and precipitation of secondary phases (**Section 5.4**).

3. Methodology

The investigation comprised the preparation, exposure, mechanical testing and characterization of 220 SFRC specimens, cracked in three-point bending at 0.15 and 0.30 mm and exposed to wet-dry cycles for one and two years. The investigated exposures comprised chloride and carbon dioxide, inducing steel corrosion. The characterization of the extent of

ingress of species and fibre corrosion comprised: descriptive statistics on the fibre distribution, visual inspection, chemical analyses and petrographic investigation. An overview of the samples, exposure and characterisation techniques is shown in **Table 1**.

For consistency, the results and discussion section will use the terminology described in [4]: The word "specimen" refers to a single sampling unit, the word "sample" refers to a group of specimens similarly exposed. The first section of the results chapter (**Sections 4.1**) presents data grouped in samples, individual specimens are evaluated in the following sections (**Sections 4.2, 4.3 and 4.4**).

3.1 Preparation of specimens

The specimens were prepared with mixture proportions in compliance with the recommendations for minimum binder content and water-to-binder (w/b) ratio specified in DS/EN 206-1:2011 [26] for the exposure classes XC4 – XS3 for conventional reinforced concrete. The total binder content was 426.3 kg/m^3, CEM-I was replaced by 31wt.% fly ash and the water-to-binder ratio (w/b) was 0.34, see **Table 2**. The superplasticizer and air entrainer content were adjusted in the subsequent mixes to reach a slump of 100±20 mm and an entrained air content of 3.5±1.0 vol.% The steel fibre used was a cold-drawn hooked-ended fibre (type 1 according to EN 14889-1 [27]), made of cold-drawn high-carbon steel, with a length of 60 mm and a diameter of 0.75 mm.

The production of the specimens was done in a prefabrication plant, using an industrial mixing plant. The casting was made by direct pumping of the concrete from a truck into coated plywood forms on an industrial vibration table. The specimens were cast in three batches in consecutive days, demoulded after one day and sealed cured indoors, covered with plastic for 56 days at 20°C. Additional details of the production process are given in [4]. The final dimensions of the three-point bending beam specimens was 600 x 150 x150 mm, with a 25 mm notch cut at the centre, along the transversal direction, according to EN-14651:2007 [28].

Table 2. Mix-design

Component	Quantity (kg/m^3)
Cement (CEM I 52.5N)	326.3
Fly Ash	100.0
Water	145.0
Sand 00/02	626.5
Sea gravel 04/08	175.1
Sea gravel 08/16	933.6
Steel fibres	40.0

3.2 Exposure setup

The exposure setup was built from ten plastic containers with a volume of 1 m^3, connected in pairs and alternating the wetting and drying cycle Specimens were exposed to wet-dry cycles of 2 + 2 days comprising different combinations of saturated limewater; sodium chloride solutions, (3.5 and 7.0 wt.% NaCl), and air with or without CO_2 (0.07 and 0.5 vol.% CO_2), named "air-exposure" and

Table 1. Samples, exposure in wet-dry cycles and characterization techniques. Abbreviations given in brackets (x) is used for sample identification. After [4].

Sample id.	Crack width (w) [mm]	Wet cycle (s)	Dry cycle (c)	Age (A / B)	Characterization		
					Profiles	XRF	TS
w15 s0 c0 A	0.15 (w15)	Limewater (s0)	Air (c0)	1 year (A)	pH	-	-
w30 s0 c0 A	0.30 (w30)					-	-
w15 s0 c0 B	0.15 (w15)	Limewater (s0)	Air (c0)	2 years (B)	pH	-	-
w30 s0 c0 B	0.30 (w30)					-	X
w15 s3 c0 A	0.15 (w15)	3.5 wt.% NaCl (s3)	Air (c0)	1 year (A)	pH, $AgNO_3$, Cl^-_{ws}	-	-
w30 s3 c0 A	0.30 (w30)					-	-
w15 s3 c0 B	0.15 (w15)	3.5 wt.% NaCl (s3)	Air (c0)	2 years (B)	pH, $AgNO_3$, Cl^-_{ws}	X	-
w30 s3 c0 B	0.30 (w30)					-	-
w15 s7 c0 A	0.15 (w15)	7.0 wt.% NaCl (s7)	Air (c0)	1 year (A)	pH, $AgNO_3$, Cl^-_{ws}	-	-
w30 s7 c0 A	0.30 (w30)					-	-
w15 s7 c0 B	0.15 (w15)	7.0 wt.% NaCl (s7)	Air (c0)	2 years (B)	pH, $AgNO_3$, Cl^-_{ws}	-	-
w30 s7 c0 B	0.30 (w30)					X	X
w15 s0 c5 A	0.15 (w15)	Fresh water (s0)	0.5 vol.% CO_2 (c5)	1 year (A)	pH	-	-
w30 s0 c5 A	0.30 (w30)					X	X
w15 s0 c5 B	0.15 (w15)	Fresh water (s0)	0.5 vol.% CO_2 (c5)	2 years (B)	pH	-	-
w30 s0 c5 B	0.30 (w30)					X	X
w15 s3 c5 A	0.15 (w15)	3.5 wt.% NaCl (s3)	0.5 vol.% CO_2 (c5)	1 year (A)	pH, $AgNO_3$, Cl^-_{ws}	-	-
w30 s3 c5 A	0.30 (w30)					-	-
w15 s3 c5 B	0.15 (w15)	3.5 wt.% NaCl (s3)	0.5 vol.% CO_2 (c5)	2 years (B)	pH, $AgNO_3$, Cl^-_{ws}	-	-
w30 s3 c5 B	0.30 (w30)					-	-

Abbreviations: (Profiles) refers to the colorimetric profiles for Phenolphthalein and universal indicator "pH"; (XRF) refers to X-Ray Fluorescence mapping in polished specimens; and (TS) refers to polarized-light microscopy on polished Thin-Sections.

"carbonation exposure" respectively, as described in **Table 1** and [4].

The drying cycle for the air-exposed samples was run in the laboratory air with a forced ventilation system on each tank with a nominal flow of 93 m^3/h. The drying cycle of the carbonation exposure ran through a closed loop with nominal air flow of 93 m^3/h and utilized a cooler to extract moisture from the air flow before the inlet. The samples were placed vertically with the crack in horizontal position, leaving a minimum separation of 50 mm between samples to ensure air circulation inside the tank.

The water solution (hereafter "solution") was replaced every two weeks during the first three months of the exposure and then monthly until six months of exposure. After that, the solution was replaced every two months. The composition of the solution was checked through weekly measurements of Total Dissolved Solids (TDS) and pH. Additionally, the Cl^- concentration of the saltwater solutions was measured by spectrophotometry (Hach Lange DR3900 and reagent LCK311), before replacing the solution and was compared against the TDS values registered. The solution of the cracked references was not replaced, and a 20/80 mixture of saturated sodium and calcium hydroxide (pH = 13.5) was added weekly, keeping the pH value in the range of 10 – 13.5. The temperature and relative humidity inside the room were monitored, varying in the range 20±2 °C and 50±10 % respectively. The CO_2 concentration in the room and inside the carbonation loop were measured weekly and ranged approximately 0.07±0.01 % and 0.5±0.1% vol., respectively.

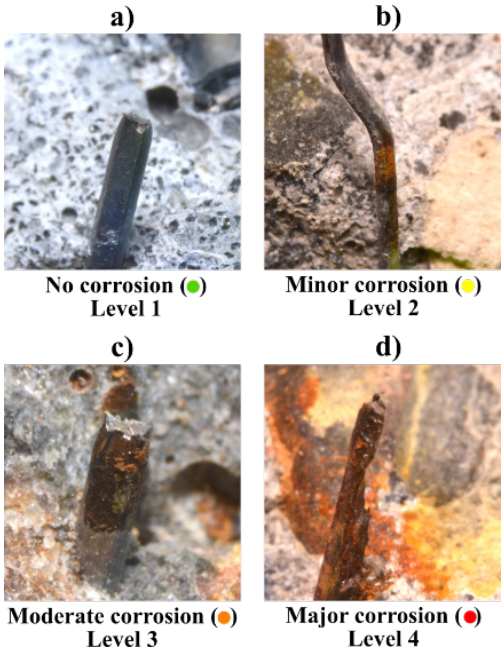

Fig. 1. Visual inspection, fibre classification: a) no corrosion (Level 1), b) minor corrosion (Level 2), c) moderate corrosion (Level 3), d) major corrosion (Level 4). After [4].

The specimens were cracked at 0.15 and 0.30 mm in 3-point bending before the exposure, measured at the crack mouth, following the procedure described in [4]. After one- and two-year exposure, the specimens were tested in 3-point bending. Further description of the mechanical-testing procedure and results can be found in [4].

3.3 Visual inspection, fibre counting and colorimetric profiles

After exposure and testing, the specimens were opened completely, and the fibres were counted and classified according to the degree of corrosion observed, see **Fig. 1**. The counting was made taking a digital image of the surface of the sample, as shown in **Fig. 2b**. The fibres were marked using oil-based modelling clay with the following colour code:

- Level 1, no corrosion (green): the fibre does not present any signs of corrosion, there is no rust or corrosion pits observable at the surface at 2× magnification.
- Level 2, minor corrosion (yellow): the fibre presents rust spots at the surface with no visible loss of cross-section at 2× magnification.
- Level 3, moderate corrosion (orange): the fibre presents localized corrosion pits and moderate loss of cross-section, i.e. localized reduction of cross-section larger than approx. 20%. The fibre did not rupture during pull-out or rupture showed clear signs of load transfer, e.g. necking at rupture section.
- Level 4, severe corrosion (red): the fibre presents large pits and major or total loss of cross-section. The fibre does not present signs of transferring load during pull-out (i.e. necking at the steel cross-section is not observed).

Furthermore, colorimetric tests were done on the cracked surface to measure the penetration of free chlorides using $AgNO_3$ [29] and to estimate the carbonation depth and pH inside the crack using phenolphthalein and rainbow indicator [30], as shown in **Fig. 2c**.

The fibre count and calculation of ingress profiles was done on every replicate of each of the samples exposed. The data was combined and analysed in batches using an image analysis script [31], where fibres were counted combining colour segmentation on the image and posterior calculation of the centroids of each point in the mask, see **Fig. 2b**. Whereas the free chloride and pH profiles are presented discretized as a trapezoid containing the boundary of the colour indicator for each specimen, according to **Fig. 2c**.

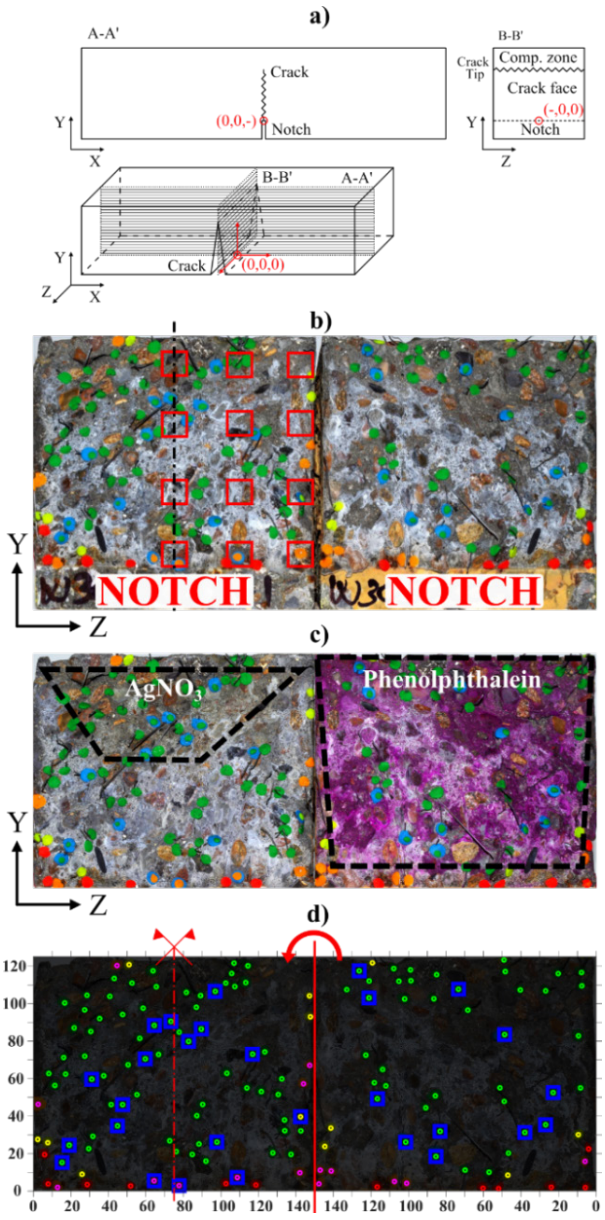

Fig. 2. Visual inspection and colorimetric analysis: a) specimen geometry and reference coordinates, b) crack surface and location of extraction points for grinding (red boxes); c) colorimetric indicators $AgNO_3$ for chloride detection (left) and e.g. the phenolphthalein for pH indication (right), and discrete profiles; and d) fibre counting and classification. After [4].

3.4 *Water-soluble chloride profile inside the crack*

The water-soluble chloride concentration inside the inner surface of the crack (hereafter "crack faces") was measured in one specimen of each sample, e.g. one of the split parts resulting from the complete opening of the test specimens of each sample.

The water-soluble chloride profiles were measured on dust samples, ground off from the surface of the crack, at the locations shown in **Fig. 2b**, on a 3x4 regular grid: at 0, 35, 70 mm from the centre of the crack in the x-axis and at 5, 35, 70 and 115 mm from the notch in the y-axis. Additionally, a sample was extracted at the surface of the specimen, at 0-1 mm depth.

The profile was grinded with a 5 mm spherical diamond drill bit, in an area of 10 x 10 mm area and to a depth of 0.2±0.1 mm, extracting a dust sample of 150±50 mg. The dust samples were leached in distilled water, by adapting the methods described in [32,33] as follows: i) approx. 100 mg was weighted to a 0.01 mg precision and 10 ml of distilled water were added; ii) the suspension was stirred for 24 h at 20 ºC; iii) the suspension was filtered and 0.5 ml of the filtrate were analysed by means of Ion Chromatography (Dionex Aquion from ThermoFisher Scientific). The chloride concentration was calculated to mg/g of dry material or wt.%

The water-soluble chloride profiles over the crack surface are calculated using 2-dimensional linear interpolation between the extraction points and were resampled to a 1 mm/pix resolution. Finally, the resulting profiles were smoothed using a 2-dimensional Gaussian convolution filter with $\sigma = 2$, see [34].

3.5 *Elemental chlorine profile transversal to the crack*

The elemental chlorine concentration in the cement paste was measured by means of micro X-ray fluorescence spectrometry mapping (µXRF), with the equipment and methods presented in [20] and data treatment following a similar methodology as [35]. Three specimens were analysed: the first specimen was used to investigate the ingress at two locations inside the crack, i.e. at the centre (coordinates x-y-0 mm in **Fig. 2a**) and at the edge (coordinates x-y-70 mm in **Fig. 2a**); the second and third specimens, were used to investigate the evolution of ingress at the centre of the crack (coordinates x-y-0 mm in **Fig. 2a**) with exposure time.

The first specimen was prepared after one-year exposure to wet-dry cycles with 3.5 wt.% NaCl solution. After the exposure, the specimen was dried in laboratory air for four weeks, and a 150 mm cube comprising the central section, i.e. at the location of the crack, was cut-off. Then, the crack was stabilized by vacuum epoxy-impregnation and was dry cut with a diamond saw, at two locations: at the centre of the crack and at 10 mm from the specimen face. The second and third specimen were prepared after one- and two-years of exposure to wet-dry cycles of 7.5 wt.% NaCl. The specimens were dried, cut and impregnated like the first one, but only at the centre of the crack.

The scanning was done on a Bruker® M4 Tornado, using a silver X-ray tube focused to a spot size of 25

µm and a silicon drift detector energy dispersive spectrometer (SDD-EDS). The elemental mapping was done at a current density of 600 µA and a voltage of 50 kV, with a chamber pressure of 20 mbar. The elemental mapping area was 120 x 120 mm. Mappings were taken with a speed of 1 ms/pixel for qualitative interpretation and 70 µm distance between each pixel. The resulting maps show percentage of the differential range measured, expressed as "counts".

The calibration of the measured elemental composition was made by means of four specimens of cement paste (10mm diameter cylinders) prepared with the same cement used in the main experiments and a w/c = 0.35, cut and dry-polished to 5 mm diameter discs. The analysed specimens comprised: i) one specimen with no mixed-in NaCl, ii) three specimens with 1, 2.5 and 5 wt.% of mixed-in NaCl, diluted in the mixing water. The references were scanned together with the specimens using the µXRF technique previously described. The calibration was done by means of linear regression, assuming a linear calibration function with a zero constant; a coefficient of 0.0572 wt.%/count was calculated with an R^2 = 0.99. Finally, the elemental maps were post-processed to segment-out the regions covered by aggregates, steel fibres and epoxy resin (i.e. cracks, notch and voids), leaving the resulting matrix comprised of cement paste. Furthermore, it was found that the epoxy impregnation of the crack did not affect the segmented chlorine maps by scanning a cracked specimen exposed to freshwater.

3.6 Petrographic study

The preparation techniques used correspond to those described in [36,37]. The preparation process comprised the following: i) drying of beams under laboratory for 4 weeks, ii) cutting petrographic specimens from the central crack section (150 mm cube), iii) vacuum resin impregnation of the petrographic specimens to stabilize crack, iii) sawing of the petrographic specimen at the central section (i.e. 150 x 150 x 75 mm prism) and drying in oven at 35°C for approx. 10 hours, iv) vacuum resin impregnation of the sawed face and subsequent grinding, lapping and polishing to prepare polished-sections and thin-sections.

Optical polarizing microscopy was used to characterize the extent of leaching and carbonation inside the crack, quantify the changes in porosity, describe mechanical damage and characterize secondary phases formed in the crack. Thin-sections were analysed using a Leica DM2500P optical polarizing microscope equipped with a fluorescent facility. The fluorescent filter combination used was a BG12 excitation filter and a K530 yellow blocking filter, as previously utilized in [38].

An overview image of the thin-sections was scanned using an Epson V850pro flatbed film scanner at 2400 dpi and 24bit depth. Plane sections were photographed under UV light at 24.5 MP resolution using a 60mm f2.8D macro lens.

3.7 Statistical, numerical and image analyses

The discussion section includes two main types of statistical analyses: comparison of samples based on the Student's t-test, used in Sections 4.1, 4.2 and 4.4, and a regression model used in Section 4.5.

The analysis of fibre corrosion and threshold values (**Section 5.1**) is based on the numerical interpolation to calculate the pH and Cl^- profiles for each specimen. The pH and water-soluble Cl^- concentration inside the cracks were calculated for every specimen using the profiles presented in **Section 4.1** and water-soluble Cl^- data presented in **Section 4.2**. First, the values of water-soluble Cl^- extracted from dust samples were recalculated to concentrations in the solution inside the crack, assuming a 1-1 ratio between the dry binder and surrounding solution inside the crack, based on the discussion presented in [32]. Whereas, pH values were assumed from the colorimetric profiles. Second, the pH and Cl^- profiles discussed in **Section 5.3.1** were correlated to the abovementioned results to reconstruct the $[OH^-]$ and $[Cl^-]$ profiles inside the crack of each specimen, using numerical correlation and interpolation based on digital-inpainting with the algorithm developed in [39].

The porosity change due to secondary reactions in the cement paste is discussed in **Section 5.2**. The analysis is based on the comparison of the relative luminance histograms of UV fluorescence images, calculated from the RGB space, see e.g. [37]. The subsequent discussion is based on descriptive statistics of the data, compared to a reference cement paste from an uncracked specimen.

4. Experimental results

4.1 Fibre counting, chloride and pH profiles

The results from the fibre counting after one- and two-year exposure are presented in **Fig. 3**, as discrete points for each fibre of each sample, classified by colour according to the degree of damage (see **Fig. 1**). The figure shows a surface of 75 x 125mm, corresponding to the original surface of the crack (150 x 125 mm) divided by its vertical symmetry axis. The edges exposed to the solution are marked in red (lower, left and upper edges). Furthermore, the crack width is shown at the right axis, including an estimation of the position of the neutral axis at 35 mm and 25 mm from the upper face for the 0.15 mm and 0.30 mm samples respectively, which was calculated

based on [4], see **Fig. 3**. Profiles are presented by a closed polygon corresponding to the 95% confidence interval of the boundary for each sample for the following colorimetric tests: a) free chloride profiles, based on the $AgNO_3$ spray test, i.e. free Cl^- ≷ 70 - 140 mmol/l [40,41], shown in brown; b) pH profiles from the phenolphthalein spray test, i.e. pH > 9, shown in purple for the samples exposed to chlorides; and c) pH profiles from universal indicator spray test, for pH > 11, shown in blue for the samples not exposed to chlorides.

In general, fibre corrosion occurs at zones near the exposed edges and extends deeper into the crack, up to the position of the Phenolphthalein front (i.e. pH < 9). The spread and intensity of fibres corroding increases for larger crack widths and for longer exposure times, see **Fig. 3**. Furthermore, fibre corrosion is more severe in the case of chloride exposure (**Fig. 3b,c,e,g,h,j** and **Fig. 3b,c,e,g,h,j**), compared to the reference (**Fig. 3a,f** and **Fig. 3k,p**) and carbonation exposure (**Fig. 3d,i** and **Fig. 3n,s**).

4.1.1 Limewater exposure (s0c0)

The samples exposed to limewater, cracked at 0.15 mm (w15s0c0) and 0.30 mm (w30s0c0) show fibres with minor corrosion (level 2) at the outer 10 – 20 mm of the samples cracked at 0.15 and 0.3 mm exposed for one year (**Fig. 3a,f**); and 15 – 25 mm for the samples exposed for 2 years (**Fig. 3p,k**). Fibre corrosion did not progress significantly with exposure time for the samples cracked at 0.15 mm (**Fig. 3a,k**). In contrast, the samples cracked at 0.3 mm show a

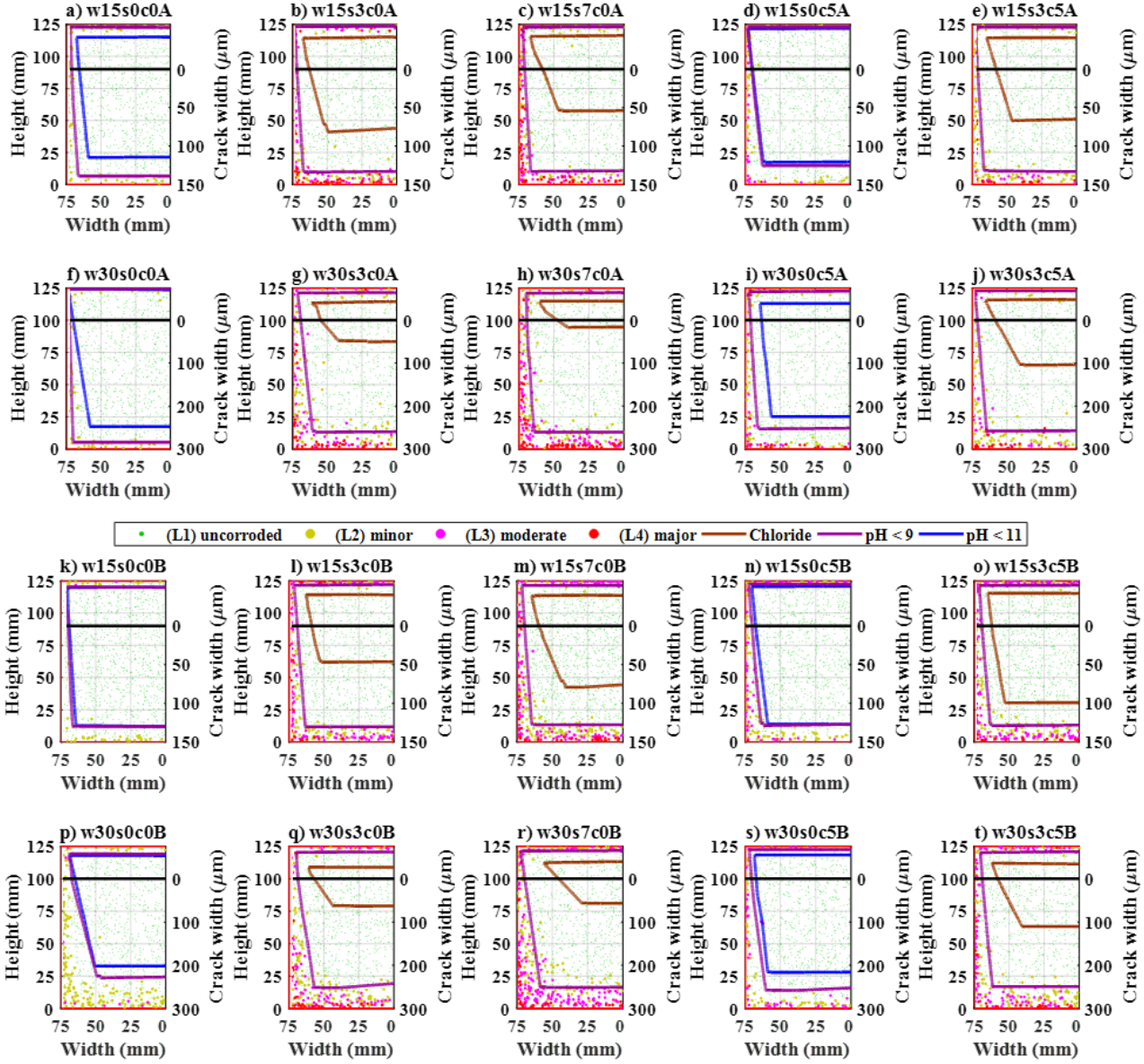

Fig. 3. Location of fibres and colorimetric profiles after one-year exposure for: a,f) cracked reference, s0c0; b,g) 3.5% NaCl exposure, s3c0; c,h) 7.0% NaCl exposure, s7c0; d,i) CO_2 exposure, s0c5; e,j) 3.5% NaCl and CO_2 exposure, s3c5. And results after two-years exposure for: k,p) cracked reference, s0c0; l,q) 3.5% NaCl exposure, s3c0; m,r) 7.0% NaCl exposure, s7c0; n,s) CO_2 exposure, s0c5; o,t) 3.5% NaCl and CO_2 exposure, s3c5. The fibres are classified according to corrosion level (levels 1 – 4), and the profiles plotted correspond to the mean value at 95% confidence (i.e. normal distribution).

significant increase in the extent of fibre corrosion with time, leading to moderate corrosion damage (level 3) for some fibres after two-years exposure (**Fig. 3f,p**). Fibre corrosion primarily occurs at pH < 9 and extends deeper into the crack for larger crack widths and progressed significantly with time, see **Fig. 3f,p**.

4.1.2 Chloride exposure (s3c0 and s7c0)

The samples exposed to chlorides are presented for: 3.5 wt.% NaCl cracked at 0.15 mm (w15s3c0) and 0.3 mm (w30s3c0), see **Fig. 3b,g** and **Fig. 3l,q**; and 7 wt.% NaCl cracked at 0.15 mm (w15s7c0) and 0.3 mm (w30s7c0), see **Fig. 3c,h** and **Fig. 3m,r**. Fibre corrosion within those samples comprise mainly fibres with minor corrosion (level 2) up to major corrosion (level 4) at the outer 15 – 25 mm; extending deeper into the crack for the 0.3 mm crack width and at higher NaCl concentration, but not progressing substantially with exposure time. The level of corrosion damage is higher at the outer regions of the crack (i.e. at the outer 10 mm).

Corroding fibres are primarily located at the zone where the pH falls below the Phenolphthalein threshold (i.e. pH < 9) for 0.15 mm cracks, see **Fig. 3b,g** and **Fig. 3l,q**. Whereas, for 0.3 mm cracks, there are also few fibres indicating minor and moderate corrosion (levels 2-3) in the zone with pH > 9, see **Fig. 3l,q** and **Fig. 3m,r**. Free chlorides measured by the $AgNO_3$ method, i.e. brown profile in **Fig. 3 b,g,l,q** and **Fig. 3c,h,m,r**, penetrated deeper into the samples cracked at 0.3 mm, relative to the samples cracked at 0.15 mm. However, free Cl^- penetration front did not progress significantly with time regardless of the crack width, since it already reached the neutral axis of the crack after one year (i.e. crack width < 0.05 mm). Corroding fibres are found inside the zone contaminated with chlorides, but close to the zone with pH < 9.

4.1.3 Carbon-dioxide exposure (s0c5 and s3c5)

The samples exposed to carbon dioxide and fresh water, cracked at 0.15 mm (w15s0c5) and 0.30 mm (w30s0c5) show a limited extent of corroding fibres inside the crack (**Fig. 3d,i** and **Fig. 3n,s**), approximately 10 – 20 mm for samples cracked at 0.15 and 0.30 mm, respectively. There seems to be an increase of the number of corroding fibres and severity of corrosion with time, but not in the spread of corroding fibres into the crack, see **Fig. 3n,s**. In general, most of the corroding fibres present minor corrosion (level 2), while moderate and major corrosion (levels 3 and 4) were found for fibres close to the surface. Fibre corrosion is mainly observed near the pH < 9 front and covers the outer 10 – 20 mm of the crack; whereas, there are limited cases of corrosion inside the pH > 11 front, only evident at the external regions of the compression zone.

The samples exposed to carbon dioxide and 3.5 wt.% NaCl, cracked at 0.15 mm (w15s3c5) and 0.30 mm (w30s3c5), see **Fig. 3e-j** and **Fig. 3o-t,** show a similar amount and extent of corroding fibres compared to the samples exposed to 3.5 wt.% NaCl (s3c0). Corroding fibres are found within the region where the pH falls below 9. The free chloride fronts are comparable to the ones measured for samples exposed to 3.5 wt.% NaCl, but do not reach as deep into the crack. There is no clear variation in the

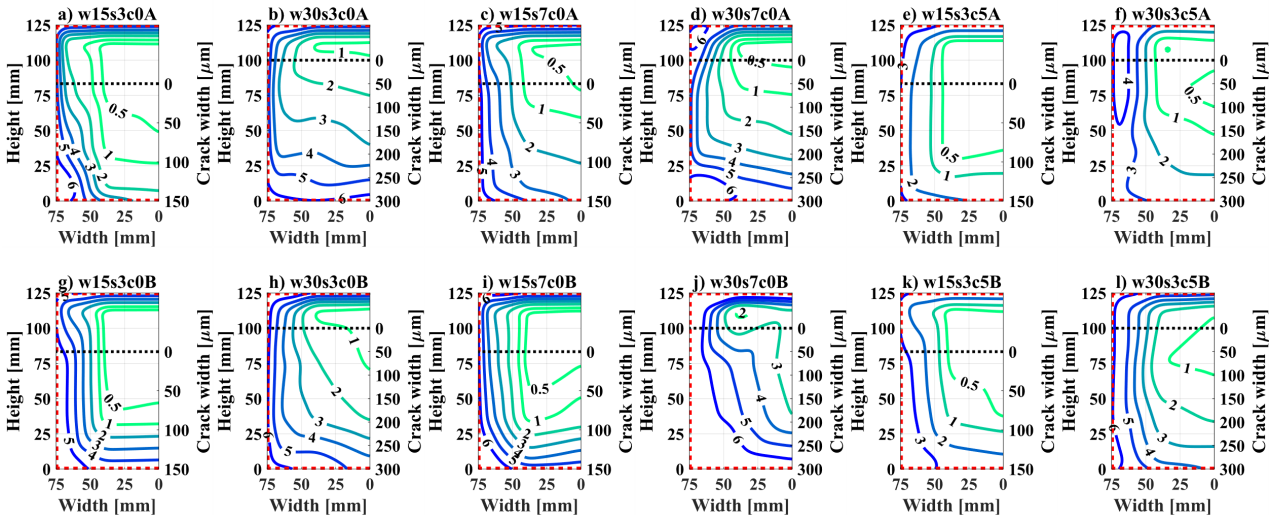

Fig. 4. Contour plots of water-soluble chloride profiles (mg/g) at the crack surface after one-year for: a,b) 3.5 wt.% NaCl exposure cracked at 0.15 and 0.3 mm, w15s3c0A and w30s3c0A; c,d) 7 wt.% NaCl exposure cracked at 0.15 and 0.3 mm, w15s7c0A and w30s7c0A; e,f) 3.5 wt.% NaCl and CO_2 exposure cracked at 0.15 and 0.3 mm, w15s3c5A and w30s3c5A. And contours after two-years exposure, for: g,h) 3.5 wt.% NaCl exposure cracked at 0.15 and 0.3 mm, w15s3c0B and w30s3c0B; i,j) 7 wt.% NaCl exposure cracked at 0.15 and 0.3 mm, w15s7c0B and w30s7c0B; k,l) 3.5 wt.% NaCl and CO_2 exposure cracked at 0.15 and 0.3 mm, w15s3c5B and w30s3c5B. Locations of extraction points are given in **Fig. 2b.**

penetration depth of the fronts with exposure time, which seem to stabilize and even recede at two years, see **Fig. 3e-j**. Corroding fibres found inside the zone contaminated with chlorides are still further from the $AgNO_3$ front relative to the Phenolphthalein profile, corresponding to the observations from the samples exposed at 3.5 wt.% and 7 wt.% NaCl.

4.2 Water soluble chloride profiles

The concentration of water-soluble chlorides ($[Cl^-]_{ws}$) measured after one- and two-years of exposure are presented in **Fig. 4**, as contours of water-soluble chlorides expressed as the relative weight to the hardened binder (i.e. mg/g). The figure shows the face of the crack split by its vertical symmetry axis, i.e. 75 x 125 mm, displaying on the horizontal axis the distance to the centre of the crack and on the left-vertical axis the depth inside the crack (i.e. the height of the specimen). Additionally, the right-vertical axis shows the crack width, expressed in µm, calculated according to [4]; whereas, the neutral axis, where the crack width is zero, is represented as a dotted horizontal line. The exposed edges (i.e. top, bottom and right) are marked in a red dotted line.

The results show that there is an overall increase in the extent and concentration of chlorides inside 0.3 mm cracks (**Fig. 4b,d,e,h,j,k**) compared to 0.15 mm ones (**Fig. 4a,c,e,g,i,k**). The increase in the extent of the chlorides inside larger cracks agrees with the results presented in **Fig. 3b,c,e** and **Fig. 3g,h,j,** for 0.15- and 0.3-mm cracks, respectively.

The impact of the exposure time on the concentration of $[Cl^-]_{ws}$ is well noticed in the specimens cracked at 0.3 mm, where there is a substantial increase of the water-soluble Cl^- concentration at deeper regions inside the crack; e.g. note the two- to three-fold increase in $[Cl^-]_{ws}$ concentration at 80 mm inside the crack for the specimens cracked at 0.3 mm exposed to 7 wt.% NaCl for one- and two-years (**Fig. 4d,j**). Specimens cracked at 0.15 mm do not show a clear increase in the water-soluble $[Cl^-]_{ws}$ concentration inside the crack after one-year exposure; e.g. note the negligible changes in the $[Cl^-]_{ws}$ concentration in any of the specimens tested after two years (**Fig. 4g,i,k**) relative to their counterparts tested after one-year (**Fig. 4a,c,e**).

4.3 Elemental chlorine profiles transversal to the crack

The total elemental chlorine (Cl) present in the cement matrix was measured by µ-XRF spectroscopy mapping, as described in **Section 3.5**. The results presented in **Fig. 5** show the total Cl content in the cement paste (expressed in wt.%) on a cut-section transverse to the crack (i.e. along the x-y axis of the beam according to **Fig. 2a**), for a specimen cracked at

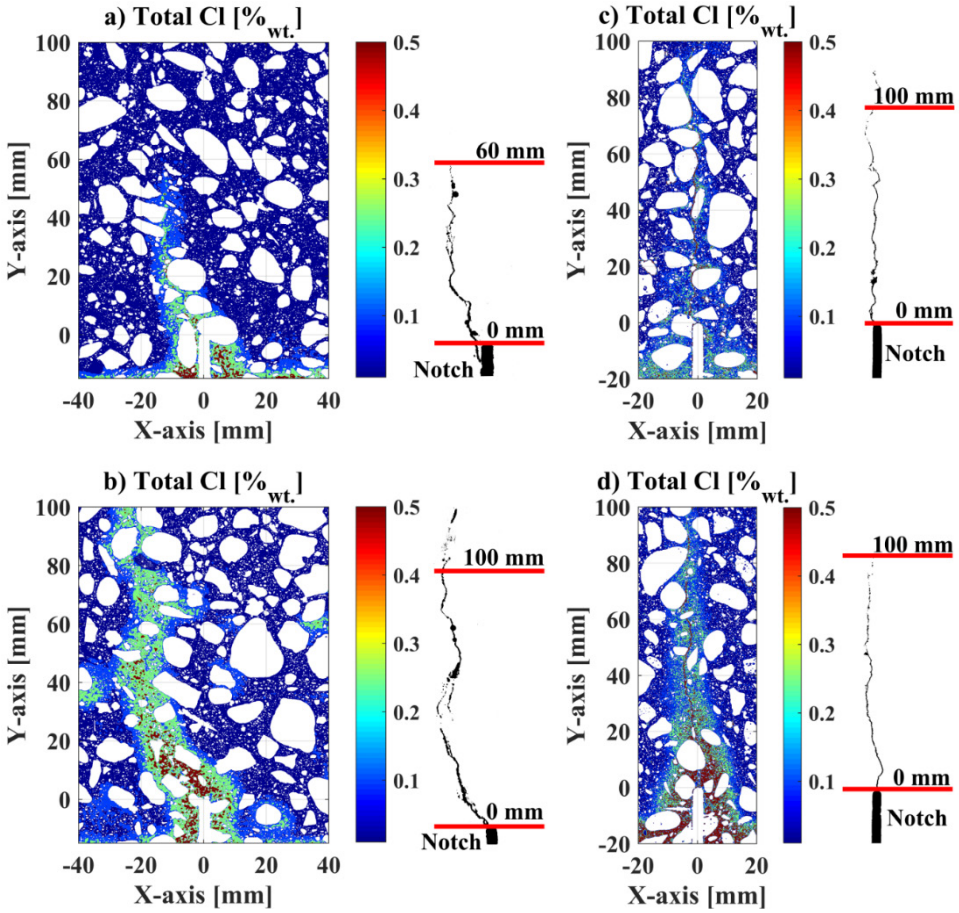

Fig. 5. Total chlorine concentration maps and segmented crack profiles for specimen cracked at 0.3mm exposed to 3.5 wt.% NaCl during one-year (w30s3c0A), at: a) cross-section at centre (75 mm from surface); b) cross-section at surface (10 mm from surface). And cross-section at centre for specimens cracked at 0.3mm exposed to 7 wt.% NaCl (w30s7c0) during: c) one-year (w30s7c0A); and d) two-years (w30s7c0B). The filled contours were plotted in Cl wt.%, with thresholds at: 0, 0.1, 0.25 and 0.5 wt.%

0.3 mm and exposed to wet-dry cycles of 3.5 wt.% NaCl for one year. The specimen was analysed at two locations: i) at the central cross-section, i.e. at 75 mm from the exposed sides of the beam (**Fig. 5a**); and ii) at the surface of the specimen, i.e. at 15 mm from the exposed side of the beam (**Fig. 5b**).

The distribution of chlorine at the centre of the specimen, see **Fig. 5a**, show a significant contribution of the matrix surrounding the crack to the transport of chloride ions inside the crack. The 5 – 10 mm of the paste adjacent to the crack at the vicinity of the notch (i.e. outer 20 mm) present a large Cl content (i.e. above 0.5 wt.%-cem), which agree with the $[Cl^-]_{ws}$ values presented in **Section 4.2** for its corresponding specimen (i.e. approx. 3 – 5 mg/g), but are much lower compared to the values expected in the solution (i.e. $[Cl^-] \approx 14$ mg/g). There is substantial chloride ingress transverse to the crack into the bulk cement matrix. Chlorine content up to 0.25 wt.%-cem was found primarily up to 60 mm inside the crack; which coincides with the depth that could be reached by the epoxy impregnation under vacuum, noting that the viscosity of the epoxy resin was higher than water (i.e. approx. 550 cP at 20° C [42]). Whereas, the chlorine content deeper inside the crack was in the range 0.1 – 0.2 wt.%-cem.

The Cl profile describing the ingress at the edge of the specimen, see **Fig. 5b**, showed a significantly larger Cl^- penetration compared to the central section. Total Cl concentrations above 0.5 wt.%-cem were registered following the crack pattern, on a band of approx. 10 – 20 mm of cement paste transversal to the crack. Additionally, there is substantial ingress in the bulk matrix around aggregates, e.g. see locations at "x,y" coordinates: (-40, 40), (40, 60), (10,40), due to out-of-plane ingress in the bulk matrix from the uncracked surface. Results at the first 20 mm inside the crack show significantly larger chloride penetration compared to the central section, indicating a clear influence of the exposure from two orthogonal directions to the chloride ingress inside the crack, viz. "corner effect" [43]. Furthermore, there seems to be a very small variation in the Cl content regardless of the crack width at shallow depths, i.e. the outer 10 – 20 mm of the crack.

The impact of the exposure time on the ingress is presented in **Fig. 5c-d**. The figures show the Cl profiles at the centre of the specimens exposed to wet-dry cycles at 7 wt.% NaCl during one- (**Fig. 5c**) and two-years (**Fig. 5d**) respectively. The depth of the $[Cl^-]_{ws}$ profile into the uncracked exposed surface (e.g. at the matrix around the notch) progresses substantially with time, and Cl content as high as 1 – 2 wt.%-cem are measured at the outer 10 – 15 mm over two years. The evolution of the Cl profile of the specimen exposed during two-years (**Fig. 5d**) compared to the one exposed for one year (**Fig. 5c**) shows that the

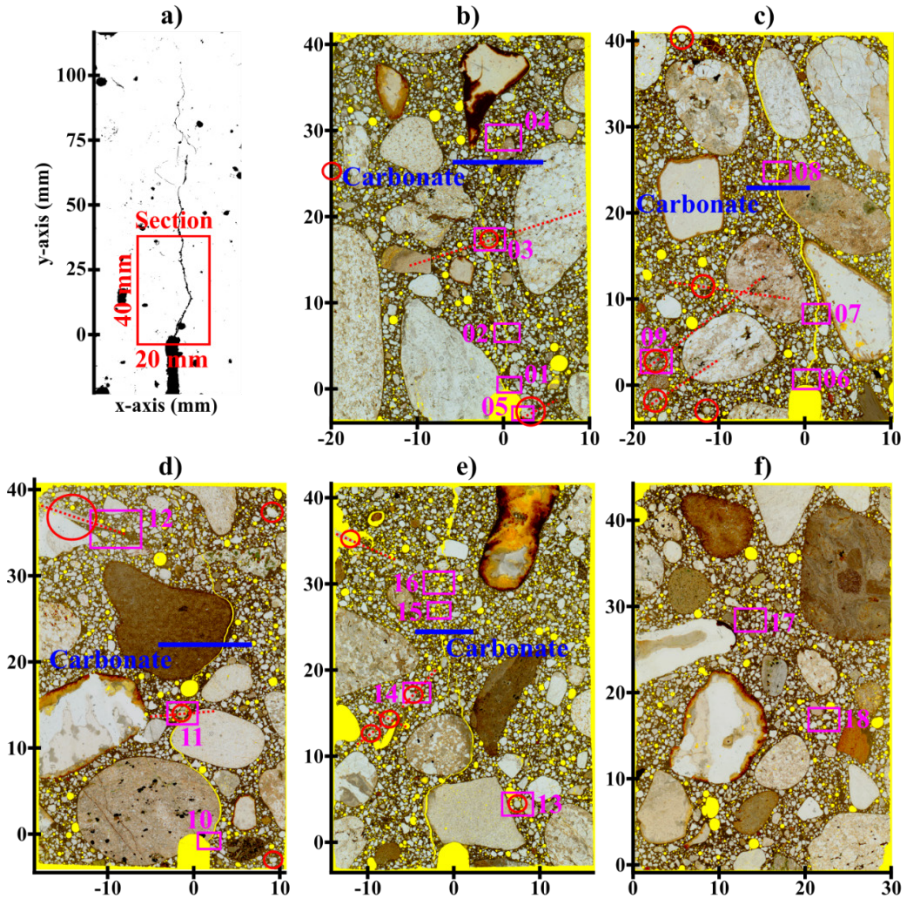

Fig. 6. Overview of thin-sections with study regions: a) schematic of location of thin-section at the crack; b) cracked specimen exposed to limewater cycles for one year, w30s0c0A; c) cracked specimen exposed to cycles of 7 wt.% NaCl for one year, w30s7c0A; d) cracked specimen exposed to cycles of fresh water and CO_2 for two years, w30s0c5B; e) cracked specimen exposed to cycles of 7 wt.% NaCl for two years, w30s7c0B; f) uncracked specimen exposed to limewater cycles for two years, w0s0c0B. The location of steel fibres is marked with a red circle, the areas investigated in the discussion section are marked in magenta and numbered and the depth of carbonation inside the crack is marked as a blue dashed line.

matrix surrounding the crack could absorb as well a substantial amount of Cl within one-year of exposure, and that transport of Cl^- transversal to the crack into the bulk matrix plays a leading role in the overall transport of Cl^- through the crack, i.e. the bulk matrix surrounding the crack acts as a buffer where the Cl^- that ingresses into the crack is transported and bound.

4.4 Petrographic study

A petrographic study was carried out to assess the extent of deterioration of the cracked specimens exposed to wet-dry cycles, focusing on the state of the matrix and fibres in the outer region of the crack. The study comprised the inspection of four specimens cracked at 0.3 mm and exposed to wet-dry cycles during one and two years. The specimens were extracted at the central section of the beam and covered the outer 40 mm of the crack, see **Fig. 6a**. The specimens are presented as a scanned image of the thin-section under polarized light, being: i) a specimen exposed to wet-dry cycles of limewater for one year, w30s0c0A (**Fig. 6b**); ii) a specimen exposed to wet-dry cycles of 7 wt.% of NaCl for one year, w30s7c0A (**Fig. 6c**); iii) a specimen exposed to wet-dry cycles of fresh water and CO_2 for two years, s0c5B (**Fig. 6d**); and iv) a specimen exposed to wet-dry cycles of 7 wt.% of NaCl for two years, w30s7c0B (**Fig. 6e**). Additionally, a specimen was extracted at the centre (i.e. at approx. 60mm from the exposed faces) of an uncracked beam, exposed to wet-dry cycles of limewater for two years, w0s0c0B (**Fig. 6f**).

The images presented in **Fig. 6** have been complemented with annotations regarding the location of areas which are examined and discussed in **Section 5**, see squares and text in magenta. The boundary where the precipitate inside the main crack does not comprise mostly carbonates, but it is instead composed of ettringite, portlandite and alkali-silica (ASR) gel has been marked with a blue line. Additionally, the position of the steel fibres intersecting the thin-section have been marked with a red circumference and the estimated orientation of fibres inclined relative to the crack has been marked with a dotted red line.

The cracked specimen exposed to wet-dry cycles of limewater for one year, i.e. w30s0c0A, is shown in **Fig. 6b**. The investigated section shows precipitation of secondary phases in the outer 30 mm of the main crack, primarily ettringite and calcite that does not close the crack mouth at the notch. Deeper inside the crack, precipitation of secondary phases occurs at discrete spots and comprises mostly ettringite. There is a fibre intercepting the crack at 15 mm inside the crack and the matrix surrounding the crack presents multiple cracking and branching. Additional branching is observed at 30 mm inside the crack, which disconnects the crack and is partly closed by secondary phases. Furthermore, there are two fibres intercepting the notch that are directly exposed to the surface. Corrosion is observed at the exposed areas of the steel.

The cracked specimen exposed to wet-dry cycles of 7% NaCl for one year, i.e. w30s7c0A, is shown in **Fig. 6c**. The analysis of the section indicates substantial precipitation of secondary phases up to 25 mm inside the crack, comprising mostly ettringite and calcite; the precipitate covers only a few µm inside the crack but closes almost fully the crack mouth, which is partially blocked with debris. Secondary phases precipitate locally deeper inside the crack, comprising mostly ettringite. The crack runs almost continuous through the whole section, up to 40 mm, where it is partially disconnected due to branching. There is a cluster of four fibres at the bottom-left corner, i.e. at 10 – 15 mm from the notch; three of these fibres were crossing the crack at a different plane from the sectioned, as observed in the counterparts resulting from the preparation of the thin section.

The cracked specimen exposed to wet-dry cycles of fresh water and CO_2 for two years, i.e. w30s0c5B, is shown in **Fig. 6d**. The studied section shows precipitation of secondary phases (e.g. mainly ettringite and calcite) at the crack faces within the outer 25 mm of the crack, not covering the cracked section (i.e. approx. 10 µm inside the crack), but fully closing the crack mouth. There is a fibre intersecting the crack at a depth of approx. 15 mm, which results in branching of the crack upstream and multiple cracking of the surrounding matrix. A second fibre, inclined relative to the crack, is located at the upper-left side of the section, i.e. at approx. 40 mm into the crack; which corresponds to the branching and multiple cracking observed at the main crack, near the estimated interception region with the main crack.

The cracked specimen exposed to wet-dry cycles of 7% NaCl for two years, i.e. w30s7c0B, is presented in **Fig. 6e**. The section shows that at this location the crack mouth does not fully connect to the external environment in this case. Precipitation of secondary phases inside the crack is similar to the previous cases. There is a cluster of four fibres at approx. 15 mm inside the crack. Two of the fibres are inclined relative to the crack and are expected to intersect the crack at other planes; contributing to the crack-branching observed at 15 – 20 mm inside the crack. A fibre inclined with respect to the crack, is located at the upper-left side of the section; corresponding to the branching and micro-cracking observed at approx. 30 mm inside the crack, which follows the expected trajectory of the fibre.

The uncracked specimen exposed to wet-dry cycles of limewater for two years, i.e. w0s0c0B, is presented in **Fig. 6f**. The section is used as a reference to evaluate the state of the cement paste and compare changes due to exposure. The analysis shows that there is a significant change in the coloration of the cement paste of the cracked specimens relative to this reference. The reference specimen shows a clear identification of primary phases under cross-polarized light and a substantial content of portlandite, which is not apparent in the previous ones.

5. Discussion

The data presented in the results section of this paper described the global transport in and out of the cracked SFRC. This promotes both the alteration of the matrix surrounding the crack, the precipitation of secondary phases inside the crack and eventually leads to fibre corrosion at the outermost fibres inside the crack.

In agreement with former studies [1], corresponding experiments investigating the mechanical performance of cracked SFRC have shown a substantial increase in the material toughness despite of the detrimental contribution of fibre corrosion [4]. These observations do not fully agree with former deterioration hypotheses, that associate changes in the mechanical performance primarily to fibre corrosion [2,44,45]. Therefore, more detailed conceptual deterioration models have been proposed, involving additional mechanisms, as discussed in [1]. The hypotheses proposed lead to the need of describing in more detail the processes involved in the deterioration of cracked SFRC exposed to wet-dry cycles. Since these mechanisms are often interconnected, and their analysis comprise a complex global picture.

The discussion presented below focuses on describing the main mechanisms that affect the chemical and microstructural integrity of the composite. The discussion is divided into the formulation of a conceptual deterioration model (**section 5.1**), which is correlated afterwards (**sections 5.2-5.4**) to the macroscopic and microscopic observations presented above.

5.1 Deterioration model

The conceptual model presented indicatively on a time-scale in **Fig. 7**, describes the overall damage at the composite "global deterioration", as the combination of various deterioration and recovery processes that take place simultaneously at the composite. The concept of global deterioration may correspond to, for example variations on the mechanical performance of the cracked composite or on its permeability to fluids.

The deterioration processes affecting the performance of the cracked composite comprise: i) ingress of external aggressive agents into the crack and adjacent matrix, e.g. Cl^- or CO_2; ii) transport of ions from the pore solution to the exterior, e.g. OH^- and Ca^{++}; iii) alteration of the cement paste matrix due to non-equilibrium between solids and pore solution; and iv) corrosion of the steel fibres bridging the crack.

The recovery processes affecting the performance of the steel fibres comprise: i) the transport of species transverse to the crack faces towards the unaltered cement paste, which smears the bulk ionic concentration of those species over a larger volume; ii) the dissolution of primary cement phases, which maintains equilibrium conditions inside the crack releasing e.g. OH and Ca^{++}; iii) the binding of aggressive species by the surrounding cement paste, e.g. chloride binding or neutralization of carbonic acid; and iv) the precipitation of secondary phases

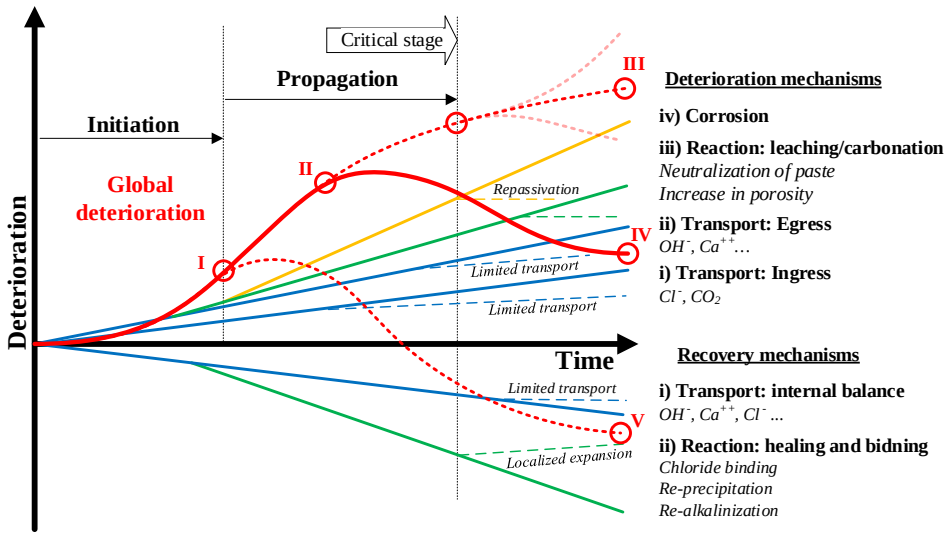

Fig. 7. Conceptual deterioration model. Individual mechanisms are separated into deterioration and recovery processes and are depicted as linear processes, while the global damage process is presented as a non-linear process. Distances and trends presented in the graphic are indicative. Roman numbers indicate relevant points of the global deterioration process in time, "stages", discussed in **Fig. 8**.

inside cracks and voids, which restrains transport inside the crack.

Following this conceptual model, individual processes (i.e. represented as linear trends in **Fig. 7**) that can be described based on specific experiments, would result in a highly non-linear global deterioration process, which may not be realistically understood and predicted based on macroscopic observations; such as mechanical experiments of exposed specimens, as discussed in [1]. Furthermore, even if most of the deterioration processes described are irreversible, the combination of those with recovery processes may lead to the effective partial- or full-recovery of some properties of the cracked composite, such as its mechanical performance or its perviousness.

The resulting contribution of the deterioration and recovery mechanisms described in the time-scale in **Fig. 7** are presented spatially in **Fig. 8**. The figure describes the main processes observed inside the crack at the macroscopic level, see **Fig. 8a**, and discusses the deterioration observed at the single-fibre level in **Fig. 8b-e**, based on the hypotheses presented in [1] and supported by the data presented in this paper as discussed in the following sections.

The discussion presented below and in **Sections 5.1-5.4** show that deterioration and recovery processes are tightly related and occur both at the composite scale and at the fibre scale, comprising:

i) Mechanical damage of the matrix (i.e. cracking) that facilitates the transport of ions and moisture into the matrix through the main crack and along the fibres bridging the crack.
ii) Transport of ions and moisture through the matrix surrounding the crack that leads to dissolution of primary phases and formation/precipitation of secondary phases.
iii) Variation of the conditions at the steel surface (i.e. pH, concentration of Cl^-, O_2, etc.) that may lead to corrosion of the steel fibres.

5.1.1 Composite scale

A summary of the main deterioration and recovery processes taking place in the main crack at the composite scale is presented in **Fig. 8a**, discussed in the following order: i) transport of substances, ii) reactions in the matrix surrounding the crack, iii) precipitation of secondary phases inside the crack, and iv) corrosion of steel fibres.

Transport of moisture, gas and ions through the uncracked concrete matrix is limited and leads to a slow deterioration of the composite. However, when the composite is subjected to large deformations, the matrix cracks and preferential paths for transport are formed. The observations reported in this paper and corresponding publications of this study [4], indicate that steel fibres restrain the formation of large cracks and increase the overall tortuosity of the crack, i.e. promoting the generation of crack branches and multiple cracking instead of a single crack, as described in **section 5.2.1** and shown schematically in **Fig. 8a**.

Ingress of extrinsic ions (e.g. Cl^-) or gasses (e.g. CO_2) and egress of intrinsic ions (e.g. OH^-, Ca^{2+}) as well as transport of moisture occur both along and transversal to the main crack, as described in **Fig. 8a**. Whereas, the bulk cement matrix provides a buffer of intrinsic ions and is able to accumulate a large amount of extrinsic ions, as discussed in **Sections 5.2.1** and **5.4.1**. Transport inside the crack may be partially impeded at the crack mouth and at deeper regions of the crack, where cracks are either: i) partially disconnected to the exterior due to branching and multiple micro-cracking, ii) not fully coalesced or locally blocked with debris, iii) locally blocked with precipitation of secondary phases, see **Fig. 8a**.

The transport of moisture, gasses and dissolved species through the main crack leads to chemical imbalances in the pore solution of the adjacent matrix; which promotes dissolution and precipitation processes in the hardened cement paste, as discussed in **sections 5.2.2** and **5.4.2** and depicted in **Fig. 8a**. The egress of intrinsic ions promotes the dissolution of cement phases (i.e. leaching); which weakens the matrix but also releases additional ions (e.g. Ca^{2+} or OH^-). Whereas, ingress of CO_2 promotes carbonation of the cement paste, which reduces the overall alkalinity of the solution inside the crack and transforms, primary phases, e.g. converting CH and C-S-H to calcite and silica gel. In the case of exposure to chlorides, the uncarbonated matrix is able to bind a substantial amount of Cl^- (e.g. calculated ratios of water-soluble Cl^- to total Cl were in the range 1:1 – 1:4 in this study).

Additional chemical reactions to those taking place at the matrix surrounding the crack generally involve precipitation of calcite and ettringite in cracks and voids, as described in **section 5.4.3**. The observed layer of precipitate was not homogeneous and did not fully close the main crack, but instead blocked the crack at discrete location, see **Fig. 8a**. In general, precipitation of secondary phases inside the crack seems to be tightly related to leaching of calcium and main cement phases from the adjacent matrix. The dissolution of primary phases and formation of secondary phases is in this case influenced by the variations in the moisture content inside the crack

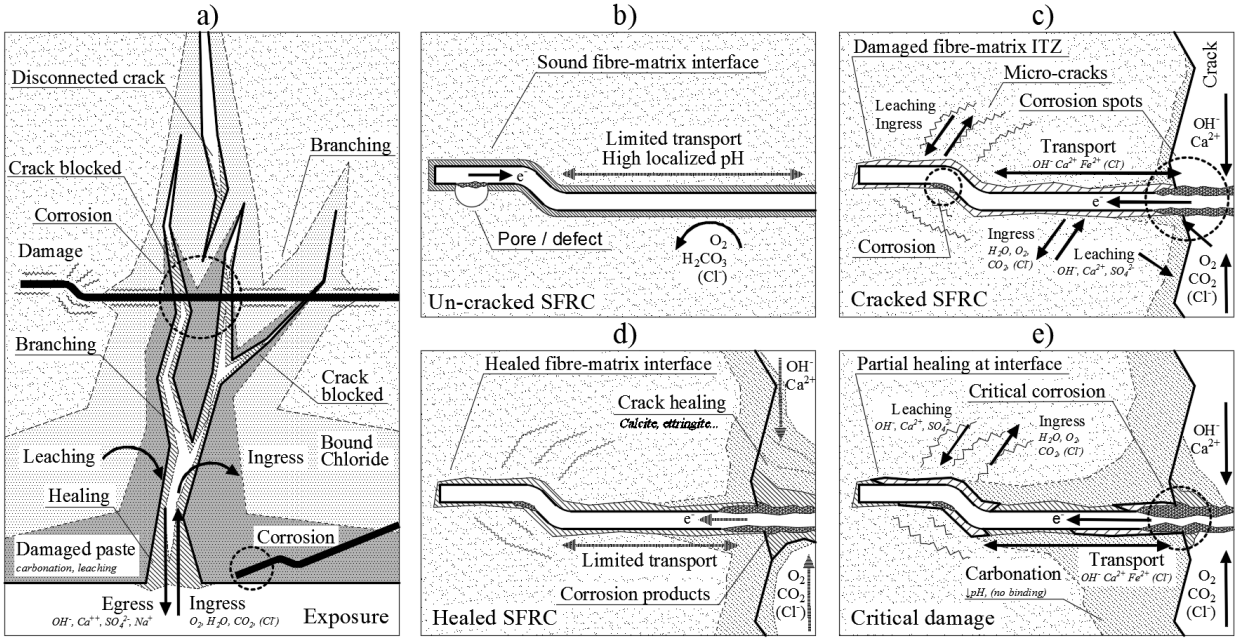

Fig. 8. Conceptual deterioration model showing: a) general processes at the composite scale (stage IV); b-e) processes at the single-fibre scale, after [1], for uncracked SFRC, at stages "I- II", (b), cracked SFRC, at stage "II" (c), healed SFRC, at stages "IV-V" (d), critical damage in cracked SFRC, at stage "III" (e) . Deterioration stages in roman numbers "I-V" refer to points marked in **Fig. 7**.

during the wetting and drying cycles, which alters the ionic concentration in the crack and matrix periodically, **Fig. 8a**.

Corrosion of steel fibres may result in a critical reduction of the fibre cross-section, eventually leading to a decrease in the residual mechanical performance of the composite. Corrosion of fibres embedded in uncracked SFRC occurred only on fibres that are directly exposed to the external environment (regardless of the exposure) or at some fibres near the surface under chloride exposure (i.e. outer 5 – 10 mm). Whereas, corrosion did not propagate in any case deep into the embedded parts of the steel and did not cause substantial damage to the surrounding cement matrix, as reported in former studies after 20 years of marine exposure [46]. Corrosion of fibres bridging cracks occurred primarily at the exposed steel surface and adjacent to the crack. The discussion presented in **section 5.3** suggests that the pH inside the crack tends to dominate over the Cl^- concentration in terms of probability of fibre corrosion.

5.1.2 Fibre scale

Similar deterioration and recovery processes as described at the composite scale take place at the fibre scale, which are presented in **Fig. 8b-e** and are discussed in the same order.

In uncracked SFRC, steel fibres are embedded in a generally well-defined layer of cement paste, not significantly different than the bulk cement matrix but still prone to a certain extent to local defects or inhomogeneities, as discussed in **sections 5.2.2**, **5.3.2** and **5.4.3**. When the matrix cracks, the fibres bridging the main crack are partially pulled-out, which produces micro-cracking and crushing of the matrix along the fibre-matrix interface and at the deformed regions of the fibre (e.g. the hooked-end of the fibre). This network of cracks is expected to be partially connected to the main crack through the damaged interface along the stem of the fibre, as described schematically in **Fig. 8c**.

The transport processes described above at the macroscopic level extend to the crack network that originates around the fibres bridging the crack due to partial pull-out, see **Fig. 8c**. The discussion presented in **section 5.2.2** shows carbonation and leaching of the cement paste surrounding the regions of the fibre crossing the crack, as shown schematically in **Fig. 8c-e**; but did not clearly indicate whether this profile progresses deep through the fibre-matrix interface. Overall, lime-rich paste is present around the damaged fibre-matrix interface of pulled fibres at the investigated sections, as discussed in **section 5.4.3**.

Precipitation of secondary phases, i.e. healing, at the fibre-matrix interface (i.e. small cracks 1-5 µm) was expected to seal leaching and ingress paths, see **Fig. 8d-e**. Based on previous studies and results reported in [1] and the discussion published in [4], part of this healing may be responsible for substantial increase in the residual performance of the cracked composite. The fibre-matrix interface of fibres crossing the crack showed several radial micro-cracks but minor slip-separation damage, i.e. a zone of approx. 10 – 20 µm

around the fibre presented larger porosity compared to the bulk matrix. The discussion presented in **section 5.4.3** did not show a clear sign of substantial precipitation in these; which comprised a narrow band of approx. 2 – 5 µm composed mainly of CH around the fibre. Results provide limited evidence supporting whether this may have some contribution to the mechanical performance of the cracked composite after exposure.

Corrosion of embedded fibres tends to occur at local defects at the fibre-matrix interface, such as pores or crevices, provided that locally low-pH and/or high Cl^- concentrations concur, as described in **section 5.3.2**. These conditions are expected to lead to a corrosion macro-cell which did not seem to progress at fast rates in the few cases observed, see **Fig. 8b**. Inside cracks, the part of the fibre directly exposed to the solution corrodes, since the interface is damaged it may facilitate cathodic reaction and promote faster corrosion rates, see **Fig. 8d-e**. However, there were no clear signs of corrosion at the hook region of fibres embedded in the matrix, as described in previous research [44] and reported in [1].

5.2 Deterioration: Ingress, leaching and carbonation inside crack

The processes described in this section comprise alteration of the matrix surrounding the steel fibres, which are affected by: i) the transport of species through the crack, both ingress of extrinsic into the adjacent cement matrix and egress of intrinsic ions from the pore solution of the adjacent cement matrix; and ii) the alteration of the microstructure and composition of the cement solid matrix.

5.2.1 Transport of species through the crack

Transport of species in uncracked concrete is typically obstructed by the complex and tortuous pore structure of cement paste. Whereas, cracks represent a preferential path for transport of moisture and species from and into the bulk concrete matrix. The results presented in this study cover the exposure to wet-dry cycles, leading to a complex transport scenario, which involves both diffusive and advective transport of dissolved species (i.e. by convection).

During the wetting-cycle, moisture flows inwards through the crack, transporting extrinsic ions (e.g. Cl^-) through advection into the crack and the adjacent matrix. As the crack reaches full moisture saturation, transport of dissolved species inwards and outwards would occur mainly by diffusion, and gas transport (i.e. water vapour, oxygen or CO_2) would be limited.

During the drying cycle, moisture flows as liquid outwards through the crack, which transports part of the dissolved species towards the exterior. However, as the moisture saturation decreases, moisture transport gradually also takes place in the gas phase causing ions to accumulate at the evaporation front. The increased concentration of dissolved species inside the crack is compensated by transport into the adjacent matrix. Once the RH inside the crack is low, transport of dissolved species is hindered and transport of species through the crack is dominated by gaseous species, e.g. water vapour, oxygen and CO_2.

As a result, concentration of extrinsic species localizes at the outer regions of the crack. For example, the Cl^- and total Cl profiles (see **Fig. 4** and **Fig. 5**, respectively), show a tendency for large Cl contents at the outer 20 mm of the crack, i.e. approximate values of $[Cl^-]_{ws} \approx 0.6$ wt.%-cem and total Cl ≈ 2 wt.%-cem; which fall progressively at deeper zones of the crack. Additionally, precipitation of carbonates inside the crack at the outer 20 – 40 mm suggest that transport of gaseous species may be limited along the depth of the crack, see **Fig. 6**.

Egress of intrinsic species is well observed in the pH profiles presented in **Fig. 3**, which show a decrease of several orders of magnitude in the $[OH^-]$ at the outer 20 – 30 mm inside the crack (i.e. from pH 14 to pH 9), as well as corresponding leaching of the paste discussed in **Section 5.2.2**. However, elemental maps for the main elements composing cement (e.g. Ca, Al, Fe, K and S) investigated by XRF (not presented in this publication) did not show a clear drop of these elements along the crack (see **Fig. 5**).

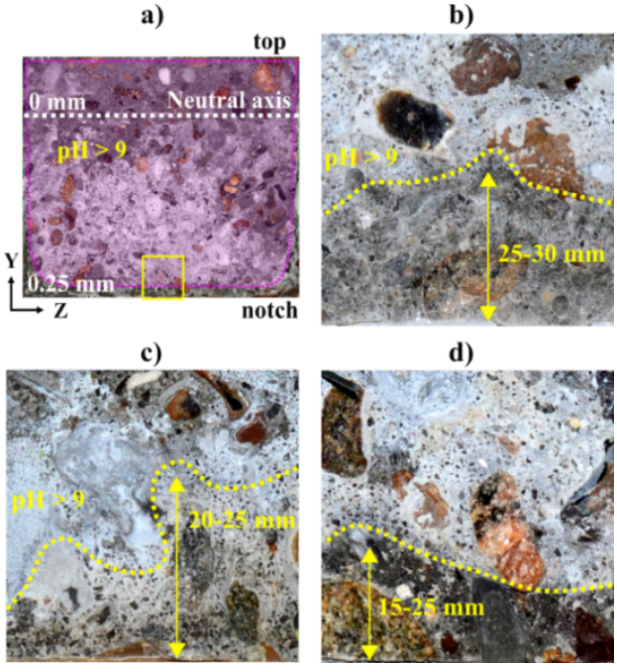

Fig. 9. Precipitate inside crack (on the crack faces), detail of coloration at outer edge. a) schematic view; and image for: b) 0.3 mm crack exposed to limewater cycles for two years (w30s0c0); c) 0.3 mm crack exposed to 7% NaCl cycles for two years (w30s7c0); d) 0.3 mm crack exposed to fresh water and CO_2 cycles for two years (w30s0c5).

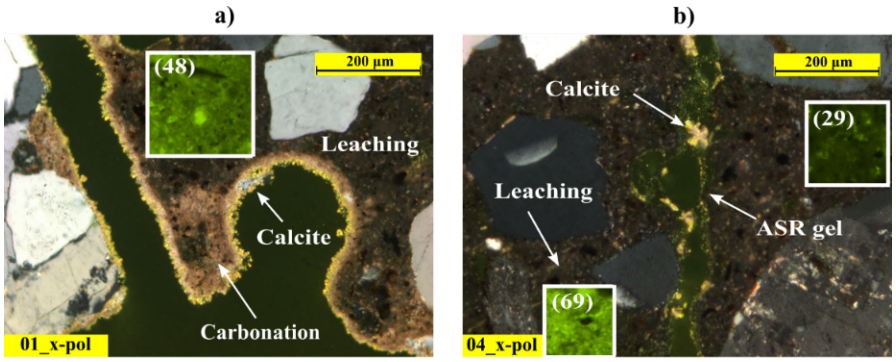

Fig. 10. Leaching and carbonation of cracked specimen exposed to limewater, w30s0c0A, inspection images at: a) crack mouth under cross-polarized light and UV fluorescent light; b) 30 mm inside crack under cross-polarized light and UV fluorescent light. Mean luminance values under fluorescent light ($\bar{L}_{RGB}$) for selected areas shown as numbers in brackets.

The main implications of these processes to the overall performance of the cracked composite are related to: i) changes in the concentrations of $[OH^-]$ and/or $[Cl^-]$ in the solution inside the crack, leading to corrosion of the steel fibres; and ii) alteration of the microstructure of the matrix adjacent to the crack, which leads to changes in the transport properties of the matrix and alterations of the fibre-matrix bond, e.g. as discussed in [4] for corresponding specimens to the ones described in this study.

5.2.2 Alteration of cement paste microstructure

Macroscopic observations of cracked specimens revealed a white precipitate covering the entire crack face, fading at the compression zone, see **Fig. 9**. The appearance and coloration of the precipitate changes at the outer 10 – 30 mm of the crack, at the boundary where the pH drops below pH 9, i.e. the Phenolphthalein threshold, see **Fig. 9b-d**. This region also comprises the area where fibre corrosion is typically observed. The area increases with longer exposure time and for larger crack widths. These macroscopic observations indicate changes in the matrix surrounding the crack, particularly at the outermost regions.

In addition to changes in pH and chloride content, the extent and nature of the transformation of the matrix adjacent to the crack has been characterized by means of a petrographic study on thin-sections, shown in **Fig. 6** using luminance values. The cement paste in the thin-section of the uncracked specimen exposed to limewater cycles for two years (s0c0B shown in **Fig. 6f**), has been used as reference, see **Fig. 11**. The reference cement matrix presents a grey, opaline shine under cross-polarized light, with abundant portlandite (i.e. white specs) visible, see **Fig. 11a**. Luminance values at inspected magnifications are presented in **Fig. 11b** for reference.

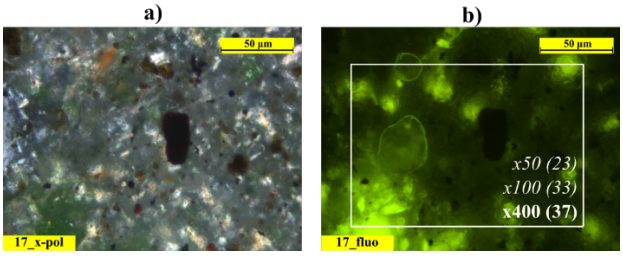

Fig. 11. Reference cement, uncracked specimen cured in limewater (w0s0c0A), at x400 magnification, viewed under: a) x-polarized light and b) UV-fluorescent light. Mean luminance values ($\bar{L}_{RGB}$) at inspected magnifications are shown in brackets for reference.

The results presented in **Fig. 10** correspond to the case of leaching and carbonation inside the crack for the specimen exposed to wet-dry cycles of limewater, s0c0. Results are presented at three locations inside the crack: i) at the crack mouth in **Fig. 10a**, ii) at 10 mm inside the crack in **Fig. 10b**. The exact locations of the inspection areas are given in **Fig. 6**.

There is minimal leaching and carbonation of the paste at the crack mouth, which extends approx. 10 – 20 µm inside the paste adjacent to the crack, and only a thin layer of carbonate precipitate, i.e. approx. 2 – 5 µm, formed at the crack face, see **Fig. 10a**. There is no significant difference in the volume of capillary porosity (characterized by luminance value) relative to the reference paste at the same magnification, see **Fig. 11b**. Deeper inside the crack, the precipitation of calcite gradually stops and there is mainly precipitation of ettringite and discrete carbonate crystals forming inside the crack, see **Fig. 10b**. At this area, there is negligible increase in porosity of the bulk cement paste, except for local defects corresponding to bleeding areas, see value at x50 in **Fig. 11b.**

The results presented in **Fig. 12** show the deterioration of the cement paste of the specimen exposed to 7 wt.% NaCl for one year, s7c0A. Results are presented at three locations inside the crack: i) at the crack mouth in **Fig. 12a**, ii) at 10 mm inside the crack in **Fig. 12b**, and iii) at 30 mm inside the crack in **Fig. 12c**.

The results show that there is substantial leaching and carbonation of the cement paste near the crack mouth, entailing an increase of the porosity at the region, see coloration in cross-polarized image and UV luminance in **Fig. 12a**. The thickness of the area around the crack that presents leaching and carbonation of the cement paste decreases gradually inside the crack, i.e. up to approx. 200 µm around the

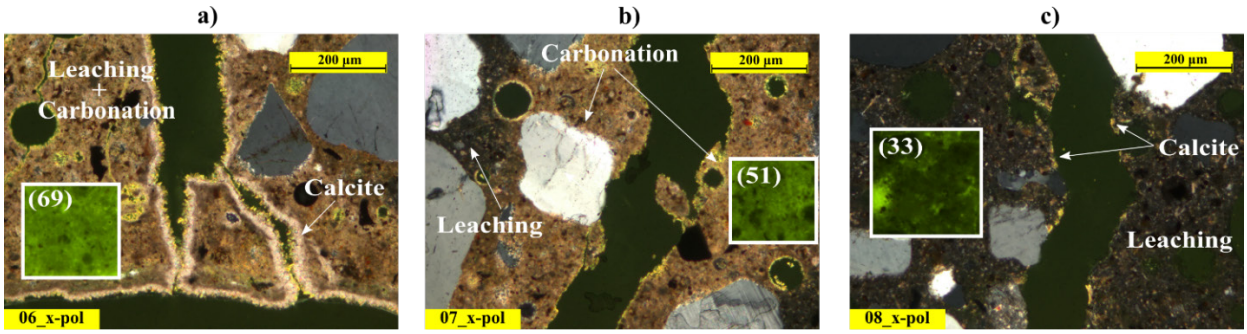

Fig. 12. Leaching and carbonation of cracked specimen exposed to 7% NaCl, w30s7c0A, inspection images at: a) crack mouth under cross-polarized light and UV fluorescent light; b) 10 mm inside crack under cross-polarized light and UV fluorescent light; c) 30 mm inside crack under cross-polarized light and UV fluorescent light. Mean luminance values under fluorescent light ($\bar{L}_{RGB}$) for selected areas shown as numbers in brackets.

crack at 10 mm depth, see **Fig. 12b**. Whereas, at approx. 30 mm depth inside the crack, the cement paste surrounding the crack does not show significant deterioration due to leaching, see coloration of paste in cross-polarized light and UV luminance in **Fig. 12c**.

The deterioration observed at the fibre-matrix interface and areas surrounding steel fibres are presented in **Fig. 13**. The figure shows the embedded region of two fibres that cross the crack: i) a fibre located at 15 mm inside the crack, at approx. 5 mm from the crack face **Fig. 13a**, and ii) at 40 mm inside the crack, at approx. 5 mm from the crack face **Fig. 13b-d**. Exact locations are given in **Fig. 6**.

As the main crack is generated in the matrix, the fibres bridging the crack are partially pulled-out from the matrix, which transfer the strain through as micro-cracking and crushing at the interface, see **Fig. 13a,b**; in particular at the hooked-ends of the fibre, see **Fig. 13b**. Such damage is expected to increase significantly the connectivity of the matrix surrounding the fibre through the micro-cracks (i.e. approx. 1 – 5 µm) to the main crack, as shown in the local changes of luminance following the fibre path in **Fig. 13b**. The aspect of the cracks presented in this paper corresponds well to observations on single-fibres reported in [21–23,47].

The damaged volume around the steel fibres may represent a preferential path for leaching of ions (e.g. Ca^{2+} and OH^-), as well as ingress of aggressive agents (e.g. Cl^- and CO_2) at the fibre matrix interface. Which would have two main implications: i) increasing the spread and degree of fibre corrosion and so reducing the cross-section of the steel fibre, i.e. promoting fibre rupture during the pull-out; ii) decreasing the overall integrity of the matrix around the fibre hook due to leaching and dissolution of primary phases (e.g. portlandite) which reduces the strength of the fibre-matrix bond.

Observations for fibres located at the outer 10 – 40 mm of the crack after one- and two-years of exposure did not show a substantial impact of leaching and ingress on the microstructure of the matrix around the fibre. Yet, there were some local areas around cracks

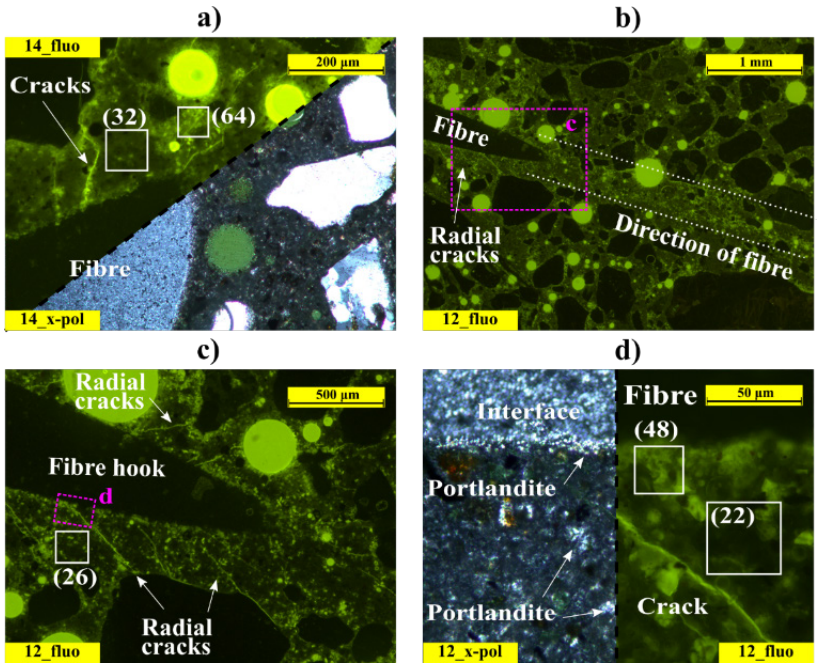

Fig. 13. Damage and leaching at fibre-matrix interface for: a) steel fibre bridging crack of specimen w30s7c0B, under cross-polarized and UV fluorescent light; b-c) steel fibre bridging crack of specimen w30s0c5B, under UV-fluorescent light; and d) detail of lower part of corresponding fibre presented in "c" under cross-polarized light and UV-fluorescent light. Mean luminance values under fluorescent light ($\bar{L}_{RGB}$) for selected areas shown as numbers in brackets.

and pores where there was a significant increase in porosity, see UV luminance values in **Fig. 13a**. Localized damage at the fibre-matrix interface did not seem to induce a substantial transformation of the bulk cement paste adjacent to the fibre (see **Fig. 13c**). Despite that there was a narrow zone directly in contact to the steel surface, i.e. approx. 1 – 5 µm, rich in portlandite that showed in some cases a higher porosity compared to the bulk paste, see UV luminance values in **Fig. 13d**.

5.3 Deterioration, fibre corrosion inside the crack

This section covers the comparison of macroscopic results describing the relation between fibre corrosion and ingress profiles, the comparison of corrosion thresholds with former studies and the discussion of the local conditions leading to corrosion of steel fibres in concrete.

5.3.1 Corrosion threshold values

The conditions inside the crack leading to fibre corrosion have been plotted in **Fig. 14** as the pH (x-axis) and water-soluble chloride concentration $[Cl^-]_{ws}$ expressed in mmol/l (y-axis), at the location of each fibre, based on the data presented in **section 4.2**. The fibres are plotted as dots, categorized in colours by the level of corrosion, as described in **Fig. 1**. Additionally, the results are compared to threshold values for initiation of corrosion in fibres exposed to chlorides proposed in former studies for embedded fibres [48] and fibres tested in artificial pore solution [5], which have been plotted as dotted and dashed lines. Fibres not exposed to chlorides were included in the plot, assuming a $[Cl^-]_{ws}$ = 2.5 mmol/l at the surface, equal to the values measured in the freshwater solution used.

The results presented in **Fig. 14** show that there is a correlation between the pH and $[Cl^-]_{ws}$ values measured in specimens exposed to chlorides, i.e. note the shape of the distribution of points, which mostly cover the upper-right diagonal of the plot. Such correlation is expected since the ingress of Cl^- and egress of OH^- are complementary transport processes that lead to higher $[Cl^-]_{ws}$ and lower pH values at the outermost regions of the crack, which decrease and increase correspondingly deeper into the crack. A similar discussion was presented in [5] for fibres embedded in concrete exposed to chlorides, which observed fibre corrosion at the outer 10 mm of the crack, and did not consider the $[Cl^-]_{ws}$ as the main factor contributing to corrosion.

Corrosion of steel fibres exposed to chlorides occurred primarily at pH values below pH 10 – 11, corresponding to $[Cl^-]_{ws}$ values of 80 – 100 mmol/l. Those results correspond reasonably well to threshold values for fibres embedded in concrete presented in [48], i.e. $[Cl^-]/[OH^-] \approx 320$. However, these are significantly higher than the threshold values for depassivation of steel fibres in pore solution presented in [5], which correspond to $[Cl^-]/[OH^-] \approx$ 2.5 – 50 for pH values in the range 10 – 13.

Discrepancies between corrosion threshold values measured for fibres in artificial pore solution and embedded in concrete have been discussed in the literature [5], presenting total $[Cl^-]$ threshold values for steel fibres embedded in concrete larger than 5-6 wt.%-cem; compared to equivalent values of approx. 2 wt.%-cem in artificial pore solution. A recent discussion proposed that the cement matrix surrounding the fibres plays an important role on preventing fibre corrosion, primarily by limiting oxygen and ionic mobility around the fibre and maintaining a high $[OH^-]$ at the steel surface [1]; similarly to as discussed for reinforcing steel bars [49].

Furthermore, the comparison of the abovementioned results to those for fibres not exposed to chlorides shows that overall the pH at the location of the fibre might be the dominant factor among the two, see values at $[Cl^-]_{ws} \approx 2.5$ mmol/l in **Fig. 14**. Noting that the presence of chloride leads to more severe corrosion damage at the exposed fibres and a larger number of fibres corroding compared to fibres not exposed to chlorides.

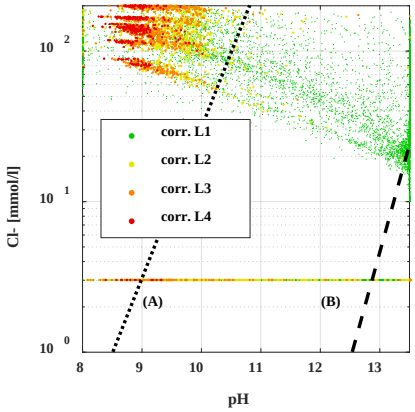

Fig. 14. Fibre corrosion (corrosion level L1 to L4) vs pH vs $[Cl^-]_{ws}$ for specimens exposed to chlorides and fresh water. Measured values are compared with threshold values proposed for: (A) fibres embedded in concrete [48] and (B) fibres tested in pore solution [5]. The specimens not exposed to chlorides included in the plot are plotted for a $[Cl^-]_{ws}$ = 2.5 mmol/l, plotted horizontally in the lower edge of the plot.

5.3.2 Local conditions influencing fibre corrosion

Petrographic observations of steel fibres embedded in uncracked concrete have shown that chloride-induced corrosion of fibres primarily appears at voids or defects at the steel-matrix interface, provided that the fibre is close to the surface, see **Fig. 15a**. No signs of

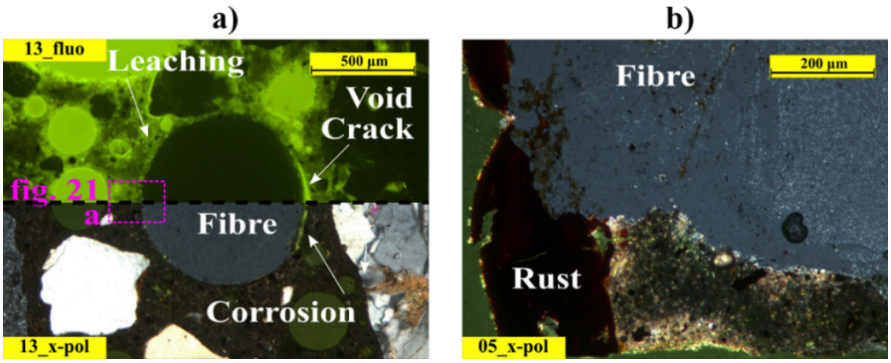

Fig. 15. Corrosion of steel fibres on: a) fibre embedded in the matrix at approx. 10 mm from the surface and exposed to chlorides, in specimens w30s7c0B, under cross-polarized light and UV-fluorescent light; and b) fibre directly exposed at limewater solution, in specimen w30s0c0A, under cross-polarized light.

spalling or substantial cross-sectional reduction were identified for fibres embedded in uncracked concrete in this study. These observations in thin-sections are in agreement with macroscopic observations and results reported in [46,50].

There was no consistent observation of localized corrosion at the deformed regions of the fibres (i.e. at the hook), which was only visible in a few fibres; which contradicts the observations form previous studies in uncracked [51] and cracked SFRC [44]. Whereas, the deterioration phenomena reported in this paper still agrees with the corrosion initiation and propagation mechanisms described at smaller scales in [5]; which described that corrosion of the steel fibres would initiate at the drawing trenches of the cold-drawn steel wire, i.e. due to lower potentials and imperfect passivation state relative to the rest of the steel surface.

Corrosion of fibres in contact with the external environment (i.e. fibres at the surface or crossing cracks) occurred mainly at the exposed steel surfaces regardless of the presence of chlorides (**Fig. 15b)**. Corrosion did not extend deep inside the composite and did not cause any further damage to the matrix, i.e. cracking or spalling, similarly to what was observed in [50]. Corrosion of fibres crossing the cracks was localized at the intersection with the crack, and the adjacent 1 – 2 mm embedded in the matrix, as shown in the examples presented in **Fig. 1**. Petrographic observations presented in **Fig. 18a-d** show that corrosion spots form at surfaces exposed to the crack, but carbonate precipitation and corrosion products tend to block those paths when exposed to wet-dry cycles.

All in all, there is evidence suggesting that the local conditions provided by the cement matrix at the steel-matrix interface (e.g. high pH, limited access to water, low oxygen concentrations and low ionic diffusion) play a critical role in preventing and controlling fibre corrosion, as discussed in [1]. It was observed that alteration of these conditions led to corrosion initiation of steel fibres embedded in chloride-contaminated concrete; by observing signs of active corrosion at steel fibres after a few hours after splitting the specimens and exposing the fibres to the laboratory air, corresponding to observations in former studies [48].

5.4 Recovery: secondary reactions and precipitation inside the crack

Based on the conceptual deterioration model proposed in **section 5.1**, there are recovery processes opposing the deterioration processes, which prevent and reduce the extent of damage of the cement matrix and are expected to have a positive effect on the resistance to transport and/or mechanical performance of the cracked SFRC.

The processes described in this section comprise structural changes at the bulk matrix and at the matrix surrounding the steel fibres and are affected by three mechanisms: i) transport of species inside the bulk matrix which both reduce the concentration of aggressive species in the solution at the crack, and maintain a high pH in the pore solution at the crack ii) binding of aggressive ions at the cement matrix around the crack, that reduce the bulk concentration at the solution in the crack, and release of hydroxyl ions from cement phases that maintain high alkalinity; iii) precipitation of secondary phases in pores and cracks that reduce moisture and ionic transport in the micro-cracked matrix.

5.4.1 Transport of species within the matrix

The main crack serves as a preferential path for transport of species into the matrix adjacent to the crack. These processes, discussed in **section 5.4.1**, comprise a complex combination of diffusion of dissolved and gaseous species, advection of dissolved species and transport of moisture. Yet, the transport of species does not only take place inside the main crack, the matrix surrounding the crack is expected to play an important role for the overall concentration of dissolved species inside the crack.

As extrinsic ions are transported inside the crack, e.g. Cl^-, a concentration gradient relative to the adjacent matrix will promote the diffusion of those ions deeper into the matrix. Thus, lowering the bulk concentration of these inside the crack and distributing these species

over a larger paste volume. Elemental Cl maps presented in **Fig. 5** show this effect, as the elemental Cl content inside the crack decreases progressively both along and transversal to the crack, i.e. approx. 10 – 15 mm into the matrix surrounding the crack. A similar but inverse effect is expected to take place for intrinsic ions, e.g. OH^- or Ca^{2+}, which are transported outwards.

The aforementioned transport processes are generally competing with the bulk transport processes inside the crack, described in **Section 5.2.1**. However, the matrix adjacent to the crack comprises a large volume of pores that act as a "buffer" to the transport inside the crack, which generally slows the bulk ingress of aggressive species (e.g. Cl^-) and maintains stable concentrations of intrinsic species (e.g. OH^-).

5.4.2 Reactivity of the matrix: binding of Cl^- and release of OH^-

The cement matrix surrounding the crack reacts with the solution inside the crack, maintaining chemical equilibrium. Therefore, acting as a chemical buffer of dissolved species, that maintains stable concentrations of extrinsic ions (e.g. Cl^-) by means of binding processes, and intrinsic ions (OH^-) through dissolution processes.

First, the dissolved Cl^- that ingresses through the crack is bound by the surrounding cement paste through the mechanisms described in [7]. Water-soluble chloride values measured at the faces of the crack reached values up to approx. 0.5 – 0.6 wt.%-cem at the outermost locations, decreasing up to values close to 0.01 – 0.05 wt.%-cem deeper inside the crack, see **Fig. 4**. Whereas, corresponding values for total Cl reached values in the range 1.5 – 2.5 wt.%-cem, reaching still moderate Cl content in the cement paste adjacent to the crack at deeper regions after two-years exposure (i.e. Cl ≈ 0.1 – 0.2 wt.%-cem), as shown in **Fig. 5**. Equivalent regions of the cement paste inspected in thin-sections, see **Fig. 12**, showed changes in the coloration under cross-polarized light, that indicate transformation of the microstructure and composition of the cement-paste.

The comparison of the water-soluble Cl^- profiles presented in **Section 4.2** and elemental Cl maps presented in **Section 4.3**, shows that the total chlorine-to-water soluble chloride ratio ($[Cl]/[Cl^-]$) reaches values in the range $[Cl]/[Cl^-] \approx 2 – 4$ at the outermost 10 mm of the concrete, whereas these values decrease down to $[Cl]/[Cl^-] \approx 1 – 1.5$ deeper inside the crack. There is therefore still substantial capacity for binding of Cl^- in the cement paste surrounding the crack, which may delay chloride-induced corrosion initiation of the steel fibres. Yet, this discussion does not aim at describing these processes in detail, being the reader aware of the large complexity of the binding and transport mechanisms involved in Cl^- ingress in concrete [7].

Secondly, alteration of equilibrium conditions in the pore solution at the matrix adjacent to the crack lead to the dissolution of primary phases (e.g. portlandite or sulfoaluminates), as described in **Section 5.2.2**; which result in the release of intrinsic ions (e.g. OH^- and Ca^{2+}) that enforce equilibrium conditions inside the matrix and at the crack. There is insight of this behaviour in the data presented in **Fig. 10-12**, which shows leaching of portlandite in the matrix adjacent to the crack, particularly at the outer 10 – 20 mm of the crack.

These recovery mechanisms generally contribute to stabilize the bulk ionic concentration of ionic species of the pore solution, and counteract the bulk transport processes (i.e. ingress and leaching) inside the crack, described in **Section 5.2.1**. Ultimately, these may contribute to prevent corrosion of the steel fibres inside the crack. Yet, understanding and predicting the evolution of these processes over time require the use of complex modelling techniques, involving reactive mass-transport models.

5.4.3 Precipitation of secondary phases

The ingress of extrinsic species (e.g. Cl^- or CO_2) and dissolution of primary phases lead, under some conditions to the precipitation of secondary phases, typically inside moist voids and cracks. Macroscopic observations presented in **Fig. 9** show a precipitate covering the entire section of the crack for all the exposed specimens, regardless of the exposure type. The composition of this precipitate varies from a primarily carbonate phase at the outermost regions of the crack, to mostly ettringite and some ASR gel (i.e. from mechanically-fractured aggregates) deeper inside the crack (see **Section 5.2**).

The structure of the precipitate did not close entirely the crack throughout the whole section under any of the investigated exposures. The precipitate blocked the outer crack path of specimens under wet-dry cycle exposure to chlorides and to freshwater, see **Fig. 16a-b**; but not of specimens exposed to limewater cycles, see **Fig. 16c**. The profile where the pH drops below pH 9 – 10 into the crack of specimens exposed to wet-dry cycles of chlorides and freshwater did not progress with exposure time and showed a gradual drop over the depth of the crack (see **Fig. 16d)**. While, the pH profile progressively decreased over time for specimens exposed to limewater cycles (see **Fig. 3**).

This contradictory behaviour may be explained by the role of leaching at the matrix surrounding the crack in specimens exposed to freshwater or saltwater; which facilitates precipitation of carbonates, as described in

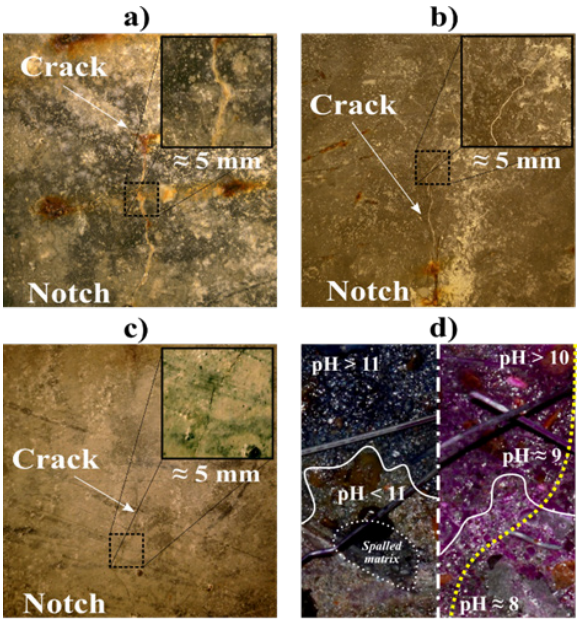

Fig. 16. Precipitate at crack edge for: a) chloride exposure, s7c0; b) carbon dioxide exposure, s0c5; and c) limewater exposure, s0c0.

[18,52]. Instead, under saturated limewater exposure Ca^{2+} may be stable in solution as $Ca(OH)_{2(aq)}$ or as $CaCO_{3(s)}$ in suspension if carbonating.

Further investigation inside the crack, showed that initially fibre reinforcement may have reduced the average crack width substantially due to branching and splitting of the main crack into smaller ones, see **Fig. 17a**; as well as due to blocking of the crack locally with debris from the cracking process, see **Fig. 17b**. During exposure, both narrow cracks and debris tend to be preferential locations for precipitation of calcite and ettringite, as shown in **Fig. 17a-b**; which reduce the connectivity inside the crack and therefore hinder ionic and moisture transport. Precipitation of calcite occurred preferentially at the outer region of the main crack under salt-water (see **Fig. 12c**) and fresh-water exposure (see **Fig. 17d**), and blocked almost completely the access of moisture and ions to the crack; but it was minimum for specimens exposed to limewater, see **Fig. 10a**.

Deeper inside the crack mostly ettringite formed (see **Fig. 17c)**, which did not seem to impede transport of moisture and ions (**Fig. 17a)**; but served as a preferential location for the precipitation of portlandite and calcite, which may limit transport inside the crack (**Fig. 17c)**. At these regions, there was also a thin layer of ASR gel lining parts of the crack, typically near the surface of some reactive aggregate that was mechanically fractured or exposed to the crack before the exposure, see **Fig. 17b**. Yet, this is not expected to have any significant impact on the transport through the crack or in the overall integrity of the cracked composite.

These observations at the meso-scale complement the results presented in **Section 4.3**, which showed that ionic and fluid ingress (i.e. based on Cl profiles and resin impregnation respectively) at the central section of the crack (see **Fig. 5a**) were substantially lower compared to the values registered at the specimen surface (see **Fig. 5b**). Similar macroscopic observations were reported in [53] for comparable crack widths, i.e. 0.05 – 0.2 mm, where ingress of moisture and dissolved species trough non-coalesced or disconnected cracks was delayed at 40 – 50 mm inside the crack.

Precipitation of secondary phases also occurred around fibres crossing the crack, shown in **Fig. 18**, which covered partially the exposed surface of the fibre, but did not fully isolate the steel surface from

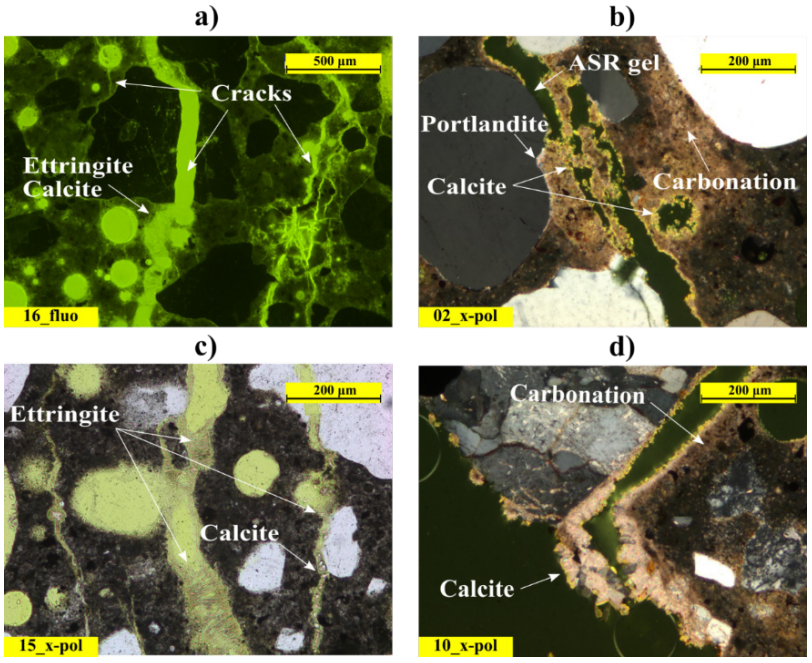

Fig. 17. Recovery phenomena inside cracks, showing precipitation of secondary phases at selected locations: a) crack branching and precipitation of calcite and ettringite inside crack observed under UV-fluorescent light, for specimen w30s7c0B; b) calcite precipitation and carbonation at debris blocking partially the crack at 7mm depth observed under cross-polarized light, for specimen w30s0c0A; c) formation of ettringite needles at 28 mm inside the crack observed under polarized light, for specimen w30s7c0B; d) precipitation of calcite at crack mouth under cross-polarized light, for specimen w30s0c5B.

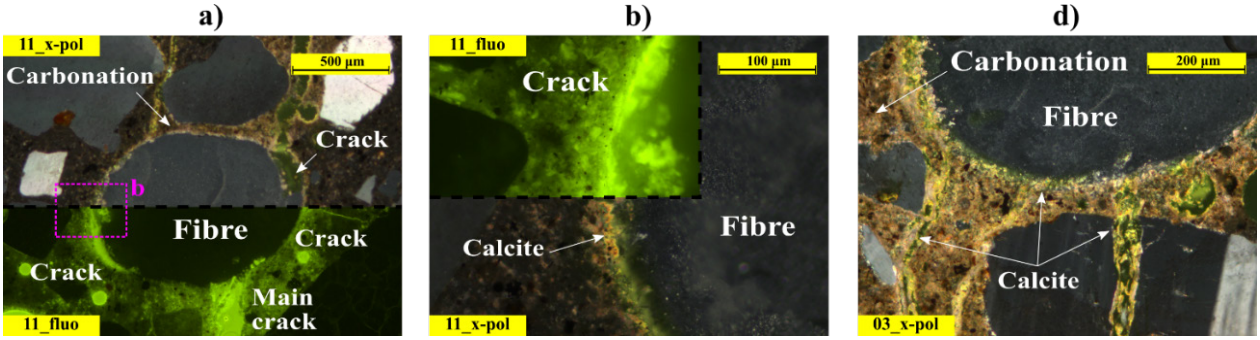

Fig. 18. Recovery phenomena at fibres crossing the crack, showing precipitation of secondary phases at selected locations: a) fibre crossing crack at 15 mm depth for specimen w30s0c5B, under cross-polarized light and UV-fluorescent light; b) detail of left part of corresponding fibre presented in "a" under cross-polarized light and UV fluorescent light; c) fibre crossing crack at 20 mm depth, for specimen exposed to limewater, w30s0c0A, under cross-polarized light.

the solution inside the crack, as shown in **Fig. 18a,b,e,f**. Observations presented in **Fig. 18c** showed that fibre corrosion might occur preferentially at the exposed steel surfaces, which would be gradually covered by corrosion products and calcite; whereas, the rest of the steel would be isolated from the solution inside the crack.

Leaching from the adjacent matrix is expected to provide sufficient Ca^{2+} to facilitate the precipitation of calcite observed, as noted by the lower quantity of CH in the non-carbonated paste around fibre and lower density of paste under fluorescent light in **Fig. 18c**. Furthermore, precipitation of calcite is expected to seal with time the main crack at discrete locations around the fibre, as observed in **Fig. 18d**, therefore reducing substantially the transport around the steel surface and maintaining a high pH value at these locations. Similarly, studies investigating corrosion of steel in seawater have shown that calcareous deposits at cathodic sites reduce substantially corrosion rates at anodic sites [54], yet there is limited research available for cement-based materials [55].

The results reported in this study give insight on the formation of secondary phases at the fractured fibre-matrix interface of fibres crossing the crack near the crack region (i.e. described in **Section 5.2.2**), yet the composition and formation mechanisms are not clear, see **Fig. 19**.

Initially, the interface of a fibre not crossing the crack showed a similar structure compared to the bulk matrix, except for a slightly larger concentration of portlandite at the adjacent 20 – 50 µm, as shown in **Fig. 19a**, contrarily to what was reported in former research [4]. Nevertheless, the interface is not homogeneous, and local defects, such as voids, are expected as shown in **Fig. 15a** for the same fibre. Whereas, the fibre-matrix interface of steel fibres bridging cracks show a distinct structure, see **Fig. 13d**, characterized by significant mechanical damage, i.e. multiple cracking, and seemingly crushing at the interface, as shown in **Fig. 13a**.

For most of the partially-pulled fibres, there is a band of 5 – 10 µm of matrix adjacent to the fibre rich in

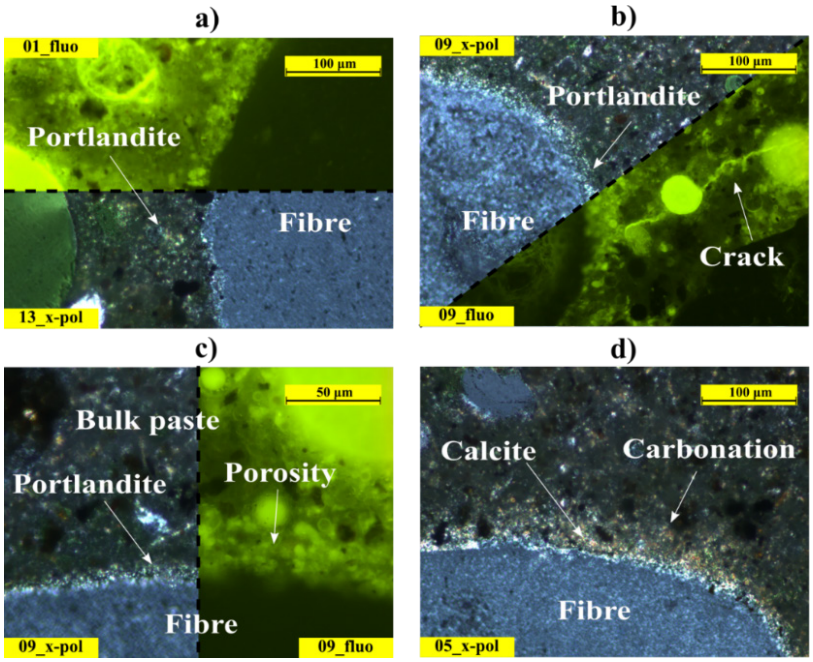

Fig. 19. Characteristics at the fibre-matrix ITZ for: a) fibre embedded in uncracked concrete matrix at 20 mm from the crack, under polarized light and UV-fluorescent light, for the specimen w30s7c0B; b) fibre crossing crack at 20 mm depth, for the specimen w30s7c0A, under cross-polarized light and UV-fluorescent light; c) closer detail of corresponding fibre presented in "b" under cross-polarized light and UV-fluorescent light; and d) carbonation at interface of embedded part of fibre adjacent to the notch, for the specimen w30s0c0A, under cross-polarized light.

fine-grained CH, which was surrounded by approx. 50 µm of cement paste that presented a larger porosity compared to the bulk matrix (see **Fig. 19c** and **Fig. 13d)**. In other cases, this region was filled with a fine-grained layer of calcite instead, as shown in **Fig. 19d**, which may be the result of the carbonation process of the abovementioned CH layer.

The source and nature of this CH-rich layer at the cracked interface is not well understood, and there is insufficient data to allow a discussion on the topic. Yet, finely grained portlandite and calcite precipitated inside micro-cracks has been reported in some studies investigating self-healing phenomena in cracked lime-based mortar specimens [56,57]. As well as at the fibre-matrix interface of glass-fibre strands in uncracked aged Glass-fibre Reinforced Concrete (GRC) [58].

However, based on the limited data available, there is no definite insight to suggest which is the nature and composition of the phases found at the damaged fibre-matrix interface after exposure. And whether these phases may be related to the increase in residual performance observed in cracked SFRC exposed to wet-dry cycles discussed in [1] and recently observed in companion specimens of this study [4].

6. Conclusion

This paper investigates the main processes taking place during the exposure of cracked SFRC to wet-dry cycles involving chloride and/or CO_2 exposure for one and two years. These main processes comprise changes in the cracked concrete matrix due to mass transport and the damage to the steel fibres due to corrosion. The discussion presents a conceptual deterioration model that describes the deterioration and recovery mechanisms concurring inside the crack.

The results presented show that corrosion of fibres crossing the crack occurred mainly at the steel located directly in the crack and was highly influenced by the pH inside the crack, also in the presence of chlorides.

The deterioration model described proposes that concurring dissolution and precipitation processes at the crack and at the matrix surrounding it may have a strong influence on the chemical composition of the solution inside the crack and may reduce transport of moisture and ions inside the crack; ultimately governing the corrosion damage of the steel fibres crossing the crack.

At the fibre scale, precipitation of calcite at the intersection between the fibre and the crack sealed partially the surface of the steel and the damaged fibre-matrix interface was lined by a CH rich layer that may be related to healing processes.

Further research focusing on quantifying the correlation of those transport and chemical processes inside cracks is needed to understand the long-term impact of corrosive exposures on the performance of cracked fibre reinforced composites.

Acknowledgements

The first author would like to express his gratitude to: CowiFonden, InnovationsFonden, the German association of steel fibre producers (VDS), VejDirektoratet and Mapei-Denmark, for supporting this project. The Norwegian Public Roads Administration (NPRA) Ferry Free E39 coastal route project is acknowledged for funding the Norwegian contribution.

References

[1] V. Marcos-Meson, A. Michel, A. Solgaard, G. Fischer, C. Edvardsen, T.L. Skovhus, Corrosion resistance of steel fibre reinforced concrete - A literature review, Cem. Concr. Res. 103 (2018) 1–20. doi:10.1016/j.cemconres.2017.05.016.

[2] E.S. Bernard, Durability of cracked fibre reinforced shotcrete, in: E.S. Bernard (Ed.), Shotcrete More Eng. Dev. Proc. Second Int. Conf. Eng. Dev. Shotcrete, A.A. Balkema Publishers, Sydney, Australia, 2004: pp. 59–66.

[3] E.S. Bernard, Effect of Exposure on Post-crack Performance of FRC for Tunnel Segments, in: I. Vrkljan, Z. Dekovic, M. Dobrilovic, J. Likar, P. Miscevic (Eds.), SEE TunnelPromoting Tunneling SEE Reg. - ITA WTC 2015, ITA-AITES, Dubrovnik, Croatia, 2015: p. 13.

[4] V. Marcos-Meson, G. Fischer, C. Edvardsen, A. Solgaard, A. Michel, Mechanical performance of steel fibre reinforced concrete exposed to chlorides and carbon dioxide: results after one year (Unpublished), J. Sustain. Cem. Mater. (2018).

[5] C. Dauberschmidt, Untersuchungen zu den Korrosionsmechanismen von Stahlfasern in chloridhaltigem Beton, Munich University, 2006.

[6] E. Nordström, Durability of Sprayed Concrete Steel fibre corrosion in cracks, Lulea University of Technology, 2005.

[7] F.P. Glasser, J. Marchand, E. Samson, Durability of concrete — Degradation phenomena involving detrimental chemical reactions, Cem. Concr. Res. 38 (2008) 226–246. doi:10.1016/j.cemconres.2007.09.015.

[8] H. Ye, Y. Tian, N. Jin, X. Jin, C. Fu, Influence of cracking on chloride diffusivity and moisture influential depth in concrete subjected to simulated environmental conditions, Constr. Build. Mater. 47 (2013) 66–79. doi:10.1016/j.conbuildmat.2013.04.024.

[9] X. Du, L. Jin, R. Zhang, Y. Li, Effect of cracks on concrete diffusivity: A meso-scale numerical study, Ocean Eng. 108 (2015) 539–551.

doi:10.1016/j.oceaneng.2015.08.054.

[10] H. Ye, N. Jin, X. Jin, C. Fu, Model of chloride penetration into cracked concrete subject to drying–wetting cycles, Constr. Build. Mater. 36 (2012) 259–269. doi:10.1016/j.conbuildmat.2012.05.027.

[11] Q.F. Liu, J. Yang, J. Xia, D. Easterbrook, L.Y. Li, X.Y. Lu, A numerical study on chloride migration in cracked concrete using multi-component ionic transport models, Comput. Mater. Sci. 99 (2015) 396–416. doi:10.1016/j.commatsci.2015.01.013.

[12] Y.C. Wu, J. Xiao, The effect of microscopic cracks on chloride diffusivity of recycled aggregate concrete, Constr. Build. Mater. 170 (2018) 326–346. doi:10.1016/j.conbuildmat.2018.03.045.

[13] J. Perko, K.U. Mayer, G. Kosakowski, L. De Windt, J. Govaerts, D. Jacques, D. Su, J.C.L. Meeussen, Decalcification of cracked cement structures, Comput. Geosci. 19 (2015) 673–693. doi:10.1007/s10596-014-9467-2.

[14] T. Ishida, P.O.N. Iqbal, H.T.L. Anh, Modeling of chloride diffusivity coupled with non-linear binding capacity in sound and cracked concrete, Cem. Concr. Res. 39 (2009) 913–923. doi:10.1016/j.cemconres.2009.07.014.

[15] Q. Yuan, C. Shi, G. De Schutter, K. Audenaert, Effect of temperature on transport of chloride ions in concrete, Concr. Repair, Rehabil. Retrofit. II. 1 (2009) 345–352.

[16] S. Alahmad, A. Toumi, J. Verdier, R. François, Effect of crack opening on carbon dioxide penetration in cracked mortar samples, Mater. Struct. Constr. 42 (2009) 559–566. doi:10.1617/s11527-008-9402-x.

[17] J. Han, W. Liu, S. Wang, D. Du, F. Xu, W. Li, G. De Schutter, Effects of crack and ITZ and aggregate on carbonation penetration based on 3D micro X-ray CT microstructure evolution, Constr. Build. Mater. 128 (2016) 256–271. doi:10.1016/j.conbuildmat.2016.10.062.

[18] D. Palin, V. Wiktor, H.M.M. Jonkers, Autogenous healing of marine exposed concrete: Characterization and quantification through visual crack closure, Cem. Concr. Res. 73 (2015) 17–24. doi:10.1016/j.cemconres.2015.02.021.

[19] M. Maes, D. Snoeck, N. De Belie, Chloride penetration in cracked mortar and the influence of autogenous crack healing, Constr. Build. Mater. 115 (2016) 114–124. doi:10.1016/j.conbuildmat.2016.03.180.

[20] T. Danner, M.R. Geiker, K. De Weerdt, μ -XRF characterisation of chloride ingress and self-healing in cracked concrete, XXIII Symp. Nord. Concr. Res. Dev. (2017) 3–6.

[21] P.D. Nieuwoudt, A.J. Babafemi, W.P. Boshoff, The response of cracked steel fibre reinforced concrete under various sustained stress levels on both the macro and single fibre level, Constr. Build. Mater. 156 (2017) 828–843. doi:10.1016/j.conbuildmat.2017.09.022.

[22] A. Bentur, S. Mindess, S. Diamond, Pull-out processes in steel fibre reinforced cement, Int. J. Cem. Compos. Light. Concr. 7 (1985) 29–37. doi:10.1016/0262-5075(85)90024-7.

[23] T.H. Ahn, D.J. Kim, S.H. Kang, Crack Self-Healing Behavior of High Performance Fiber Reinforced Cement Composites Under Various Environmental Conditions, in: Kris Zacny, R.B. Malla, W. Binienda (Eds.), Earth Sp. 2012, ASCE, Pasadena, United States, 2012: pp. 635–640.

[24] L. Ferrara, V. Krelani, F. Moretti, M. Roig Flores, P. Serna Ros, Effects of autogenous healing on the recovery of mechanical performance of High Performance Fibre Reinforced Cementitious Composites (HPFRCCs): Part 1, Cem. Concr. Compos. 83 (2017) 76–100. doi:10.1016/j.cemconcomp.2017.07.010.

[25] D. Homma, H. Mihashi, T. Nishiwaki, Self-Healing Capability of Fibre Reinforced Cementitious Composites, J. Adv. Concr. Technol. 7 (2009) 217–228. doi:10.3151/jact.7.217.

[26] Concrete - Materials - Rules for the use of EN 206-1 in Denmark, 2011.

[27] European Commitee for Standardization (CEN), Fibres for concrete - Part 1: Steel fibres - Definitions, specifications and conformity, EN 14889-1:2006, European Union, 2006.

[28] European Commitee for Standardization (CEN), Test method for metallic fibre concrete - Measuring the flexural tensile strenght (limit of proportionality (LOP), residual), EN 14651:2006 +A1, European Union, 2006.

[29] N. Otsuki, S. Nagataki, K. Nakashita, Evaluation of the AgNO3solution spray method for measurement of chloride penetration into hardened cementitious matrix materials, Constr. Build. Mater. 7 (1993) 195–201. doi:10.1016/0950-0618(93)90002-T.

[30] D.H. Campbell, R.D. Sturm, S.H. Kosmatka, Detecting Carbonation, Concr. Technol. Today (Portl. Cem. Assoc. 12 (1991) 1–6.

[31] I. The MathWorks, MATLAB Image Processing Toolbox release R2017, (2017).

[32] M. Castellote, C. Alonso, C. Andrade, P. Castro, M. Echeverría, Alkaline leaching method for the determination of the chloride content in the aqueous phase of hardened cementitious materials, Cem. Concr. Res. 31 (2001) 233–238. doi:10.1016/S0008-8846(00)00449-X.

[33] T. Chaussadent, G. Arliguie, AFREM test procedures concerning chlorides in concrete: Extraction and titration methods, Mater. Struct. 32 (1999) 230–234. doi:10.1007/BF02481520.

[34] M. Nixon, A. Aguado, Feature extraction and image processing, Featur. Extr. Image Process. Comput. Vision, Second Ed. (2008) 161–216. doi:10.1016/B978-0-12-396549-3.00001-X.

[35] M. Khanzadeh Moradllo, B. Sudbrink, Q. Hu, M. Aboustait, B. Tabb, M.T. Ley, J.M. Davis, Using

micro X-ray fluorescence to image chloride profiles in concrete, Cem. Concr. Res. 92 (2017) 128–141. doi:10.1016/j.cemconres.2016.11.014.

[36] R.J. Detwiler, L.J. Powers, U.H. Jakobsen, W.U. Ahmed, K.L. Scrivener, K.O. Kjellsen, Preparing specimens for microscopy, Concr. Int. 23 (2001) 51–58.

[37] U.H. Jakobsen, L. Laugesen, N. Thaulow, Determination of water to cement ratio in hardened concrete by optical fluorescence microscopy, in: M.S. Khan (Ed.), SP-191 Water-Cement Ratio Other Durab. Parameters, 1st., American Concrete Institute (ACI), Farmington Hills, USA, 1999: pp. 27–41.

[38] U.H. Jakobsen, K. De Weerdt, M.R. Geiker, Elemental zonation in marine concrete, Cem. Concr. Res. 85 (2016) 12–27. doi:10.1016/j.cemconres.2016.02.006.

[39] J. D'Errico, Inpaint nans (Matlab), (2004).

[40] F. He, C. Shi, Q. Yuan, C. Chen, K. Zheng, AgNO3-based colorimetric methods for measurement of chloride penetration in concrete, Constr. Build. Mater. 26 (2012) 1–8. doi:10.1016/j.conbuildmat.2011.06.003.

[41] F. He, C. Shi, Q. Yuan, K. Zheng, Q. Zou, Factors influencing chloride concentration at the color change boundary using AgNO3 colorimetric method, Kuei Suan Jen Hsueh Pao/ J. Chinese Ceram. Soc. 36 (2008).

[42] J.K. Nielsen, J. Maiboe, Epofix and Vacuum : an Easy Method To Make Casts of Hard Substrates, Palaeontol. Electron. 3 (2000) 10.

[43] H. Shim, Corner effect on chloride ion diffusion in rectangular concrete media, KSCE J. Civ. Eng. 6 (2002) 19–24. doi:10.1007/BF02829036.

[44] J.-L. Granju, S.U. Balouch, Corrosion of steel fibre reinforced concrete from the cracks, Cem. Concr. Res. 35 (2005) 572–577. doi:10.1016/j.cemconres.2004.06.032.

[45] C. Frazão, J. Barros, A. Camões, A.C. Alves, L. Rocha, Corrosion effects on pullout behavior of hooked steel fibers in self-compacting concrete, Cem. Concr. Res. 79 (2016) 112–122. doi:10.1016/j.cemconres.2015.09.005.

[46] E. O'Neil, J.T. Devlin, Durability of Fiber-Reinforced Concrete Under Flexural Stress in a Severe Marine Environment, Defense Technical Information Center, Vicksburg, US, 1999.

[47] I. Markovich, J.G.M. Van Mier, J.C. Walraven, Single fiber pullout from hybrid fiber reinforced concrete, Heron. 46 (2001) 191–200.

[48] P.S. Mangat, K. Gurusamy, Corrosion resistance of steel fibres in concrete under marine exposure, Cem. Concr. Res. 18 (1988) 44–54. doi:10.1016/0008-8846(88)90120-2.

[49] U.M. Angst, M.R. Geiker, A. Michel, C. Gehlen, H. Wong, O.B. Isgor, B. Elsener, C.M. Hansson, R. François, K. Hornbostel, R. Polder, M.C. Alonso, M. Sanchez, M.J. Correia, M. Criado, A. Sagüés, N. Buenfeld, The steel–concrete interface, Mater. Struct. 50 (2017) 143. doi:10.1617/s11527-017-1010-1.

[50] S.U. Balouch, J.P. Forth, J.-L. Granju, Surface corrosion of steel fibre reinforced concrete, Cem. Concr. Res. 40 (2010) 410–414. doi:10.1016/j.cemconres.2009.10.001.

[51] A. Beglarigale, H. Yazıcı, Electrochemical corrosion monitoring of steel fiber embedded in cement based composites, Cem. Concr. Compos. 83 (2017) 427–446. doi:10.1016/j.cemconcomp.2017.08.004.

[52] C. Edvardsen, Water permeability and autogenous healing of cracks in concrete, ACI Mater. J. 96 (1999) 448–454. doi:10.14359/645.

[53] B.J. Pease, Influence of concrete cracking on ingress and reinforcement corrosion, DTU, 2010.

[54] S. Elbeik, A.C.C. Tseung, A.L. Mackay, The formation of calcareous deposits during the corrosion of mild steel in sea water, Corros. Sci. 26 (1986) 669–680. doi:10.1016/0010-938X(86)90032-6.

[55] V. Achal, A. Mukherjee, S. Goyal, M.S. Reddy, Corrosion prevention of reinforced concrete with microbial calcite precipitation, ACI Mater. J. 109 (2012) 157–164. doi:10.14359/51683702.

[56] B. Lubelli, T.G. Nijland, R.P.J. Van Hees, Self-healing of lime based mortars: microscopy observations on case studies, in: Proc. First Int. Conf. Self Heal. Mater., Springer, Noordwijk aan Zee, NL, 2011.

[57] T.G. Nijland, J. a Larbi, R.P.J. Van Hees, B. Lubelli, Self Healing Phenomena in Concretes and Masonry Mortars: A Microscopic Study, in: A.J.M. Schmets, S. van der Zwaag (Eds.), First Int. Conf. Self Heal. Mater., Springer, Noordwijk aan Zee, NL, 2007: pp. 76–91.

[58] P. Purnell, N.. Short, C.. Page, A.. Majumdar, Microstructural observations in new matrix glass fibre reinforced cement, Cem. Concr. Res. 30 (2000) 1747–1753. doi:10.1016/S0008-8846(00)00407-5.

5.2 Paper VII. Deterioration phenomena of steel fibres in cracked concrete under wet-dry exposure conditions

The following publication, referred as “paper VII”, in in press in Magazine of Concrete Research.

Marcos-Meson, V., Solgaard, A., Skovhus, T.L., Jakobsen, U.H., Fischer, G., Edvardsen, C., Michel, A. 2020. Pull-out behaviour of steel fibres in cracked concrete under wet-dry cycles – deterioration phenomena. Mag. Concr. Res. (2020) 1–32. doi:10.1680/jmacr.19.00448.

Printed in this thesis as the original manuscript with the authors’ formatting.

Published in Magazine of Concrete Research (2020)

Pull-out behaviour of steel fibres in cracked concrete exposed to wet-dry cycles – deterioration phenomena

V. Marcos-Meson[1,2,3*], A. Solgaard[2], T.L. Skovhus[3], U.H. Jakobsen[4], G. Fischer[1], C. Edvardsen[2] and A. Michel[1]

[1] Department of Civil Engineering, Technical University of Denmark, Copenhagen, Denmark

[2] COWI A/S, Copenhagen, Denmark

[3] VIA Building, Energy, Water & Climate, VIA University College, Horsens, Denmark

[4]Danish Technological Institute, Taastrup, Denmark

* Corresponding author: vicmes@byg.dtu.dk

Abstract

This paper presents observations and results of an experimental investigation on the mechanisms altering the pull-out behaviour of partially pulled hooked-end steel fibres inside an artificial crack exposed to wet-dry cycles for six months. Mechanical and corrosion damage at the surface of the steel fibre were investigated by 3D optical interferometric profiling and petrographic analyses to describe mechanical damage and healing processes at the matrix surrounding the fibre. Mechanical damage observed in the cementitious matrix and at the fibre confirmed that, after debonding, the pull-out process was governed by yielding of the fibre hook, fracture of the adjacent matrix and friction between the hook and the matrix. The partial restoration of the adhesive bond after exposure was attributed to a combination of autogenous healing around the fractured fibre-matrix interface and accumulation of corrosion products around the intersection of the fibre with the crack. The increase of the mechanical bond strength was ascribed to autogenous healing processes at the mechanically damaged matrix around the fibre hook. Results of this study support the hypothesis that the increase of the pull-out force transferred by hooked-end steel fibres bridging cracks in concrete exposed to wet-dry cycles is mainly related to autogenous healing and carbonation of the damaged matrix around the fibre than corrosion damage of the steel.

Keywords

Steel Fibre Reinforced Concrete (SFRC); cracks; chlorides; carbonation; corrosion; petrography; autogenous healing; pull-out

1. Introduction

There is disagreement regarding the role of fibre corrosion in the long-term mechanical performance of cracked Steel Fibre Reinforced Concrete (SFRC) under exposures involving wet-dry conditions [1]. Studies investigating the mechanical performance of SFRC reinforced with hooked-end fibres have reported considerable alteration of the residual tensile strength of the cracked SFRC, which was generally attributed to an increase of the fibre-matrix bond strength due to corrosion [2] or to additional hydration of the cement matrix [3,4]. Yet, recent investigations suggest that increases of the residual tensile strength of cracked SFRC may be related instead to autogenous healing of damage in the cement matrix around partially-pulled fibres [5,6].

Investigation of the cause for such variations of the residual tensile strength of the cracked SFRC require a detailed understanding of the pull-out behaviour of hooked-end fibres in concrete, i.e. the fibre matrix bond. The bond of an aligned hooked-end fibre embedded in a cementitious matrix is ascribed to three bond mechanisms, that partly overlap during the

pull-out process of hooked-end fibres: the adhesive bond, and the mechanical and frictional bond [7,8]. After the utilization of the adhesive bond, at displacement values of approx. 20 – 30 µm [9], the pull-out behaviour of the fibre is primarily governed by the mechanical and frictional anchorage transferred trough the hook. These result in substantial mechanical damage to the cement matrix surrounding the hook [10–13], which facilitates the pull-out process of the fibre.

Studies investigating the pull-out behaviour of aligned fibres bridging an artificial crack in a cementitious matrix exposed to wet-dry cycles of saltwater have reported increases in the maximum pull-out force after the exposure [14,15]. A recent investigation on partially-pulled fibres exposed to wet-dry cycles of saltwater and freshwater described a partial recovery of the adhesive bond between the fibre and the matrix, and a significant increase of the mechanical bond strength [9].

Former studies ascribed the increase of the fibre-matrix bond strength after exposure to an increase of the frictional resistance due to fibre corrosion, i.e. due to localized expansion of corrosion products at the hook [15] or an increase of the fibre roughness over the whole fibre surface [14]. The latter hypothesis was also suggested in a study investigating pre-corroded fibres embedded in mortar [16]. However, these hypotheses are not fully consistent with the increases of the fibre-matrix bond strength shown in experiments that did not involve corrosion damage, such as for de-bonded steel and polymer fibres cured in freshwater [17–19]. Other studies propose instead that the increase of the fibre-matrix bond strength is governed by an alteration of the microstructure of the damaged matrix around the fibre, referred to as autogenous healing processes [9,17].

This investigation aims at describing the deterioration processes that govern the changes in the pull-out behaviour of partially pulled steel fibres from concrete exposed to wet-dry cycles reported in [9], testing the compatibility and validity of the aforementioned hypotheses. The studies herein describe the alteration of the surface of the steel fibre due to mechanical and corrosion damage and the mechanical damage and microstructural changes at the matrix surrounding the fibre.

2. Methodology

The investigations covered the preparation, exposure and inspection of single fibre pull-out specimens, partially pulled-out to induce mechanical damage equivalent to crack widths in the range of 0.2 – 0.3 mm and exposed to wet-dry cycles for six months. The exposures investigated comprise wet-dry cycles of saltwater and freshwater with a high carbon dioxide concentration. Single-fibre specimens were investigated in a single-sided test, based on the setup described in [9,20]. The specimens inspected in this study corresponded to companion specimens to the ones investigated in [9]. Inspection of damage in the matrix was undertaken by means of petrographic analysis, whereas measurement of the extent of corrosion damage and accumulation of corrosion products was done by 3D optical interferometric profiling.

Table 1. Mix-design. After [9].

Component	Quantity (kg/m^3)
Cement (CEM I 52.5N)	326.3
Fly Ash	100
Water	145
Sand 00/02	787.4
Sea gravel 04/08	1036.5
Entrained air	3%

2.1 Preparation of specimens

The pull-out specimens investigated were cast using the mix-design presented in [9]. The total binder content was 426.3 kg/m^3 with 31 -wt.% fly ash replacement of the Portland cement, and the water to binder ratio was 0.34, see **Table 1**. The superplasticizer content was adjusted in the subsequent mixes to reach a flow diameter of 120±20 mm, measured according to EN 1015-3:1999 [21] and the air-entrainer content was adjusted to reach a level of entrained air of 3.0±0.5 vol.%, measured according to EN 413-2:2016 [22]. The steel fibre investigated was made of cold-drawn carbon-steel wire with a characteristic tensile strength of 1800 MPa, hooked ends (type 1 according to EN 14889-1:2006 [23]), a length of 60 mm and a diameter of 0.75 mm, see **Fig. 1a**.

The specimens were mixed using a 60 L planetary mixer, cast using PVC formworks over a vibration table. The fibres were held to the bottom plate of the PVC formwork using a perforated rubber plug

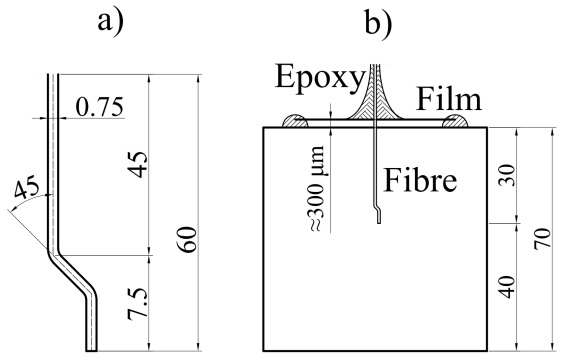

Fig. 1. Dimensions of a) steel fibre and b) pull-out specimen. Dimensions are expressed in mm. After [9].

inserted into a conic gap at the centre of the bottom surface of the form, maintaining a 90° angle with the bottom of the formwork.

The specimens exposed to saltwater and freshwater were partially pulled-out up to a slip value of 0.15 mm before the exposure. The upper surface of the specimens was covered with a 50×50 mm acetate film, leaving a separation between the film and the concrete surface of approx. 0.3±0.1 mm, mimicking exposure of a single fibre in cracked concrete environment. The part of the fibre exposed to the surface out was covered with heavy-duty marine-grade epoxy paint, see **Fig. 1b**.

2.2 Exposure setup

The investigated specimens were coded according to the number of sample (from 1 to 4) and the type of study including thin-sections (T), polished sections (P) and 3D optical profiles (O). The exposure environments are described in **Table 2** and comprised wet-dry cycles exposure of partially pulled specimens exposed to saltwater and freshwater. Reference specimens were also tested after curing immersed in limewater for 56 days.

The specimens cured in limewater were immersed in the solution at all times. The wet-dry exposure setup consisted of two rectangular polyethylene containers of approx. 200 L each, one used for each exposure. The wet-dry cycles for the freshwater and saltwater exposure were controlled automatically, with a total cycle length of four days, as described in [9].

During the wet cycle (two days), the specimens were covered completely with the solution. The solution was replaced every two weeks during the first two months of exposure and every month up to 6 months, and was checked weekly by means of electrical resistivity and pH measurements. Non-chlorinated water (pH = 7.5 – 8.0, Cl^- < 100 mg/l, 16 – 17 °dH) was used as exposure media for the specimens subjected to freshwater cycles and to prepare the saltwater brine. The solution of specimens cured in limewater was not replaced, and the pH value in the solution was kept in the range of 10 – 13 by addition of approx. 25 cl of saturated solution of calcium hydroxide every two weeks.

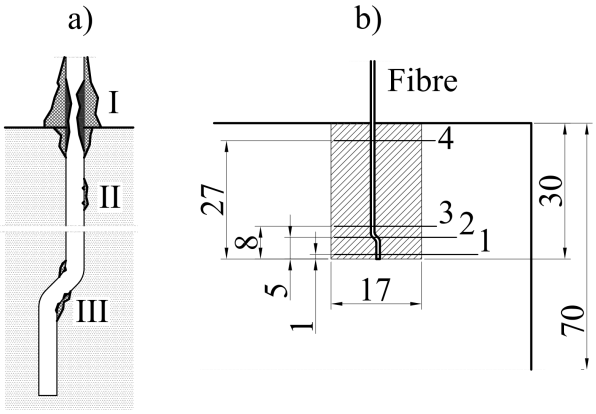

Fig. 2. Location of inspection areas of specimens: a) inspection areas for 3D optical profiles, after [9], and b) location of thin-sections and inspection area of polished sections.

The drying cycle for the specimens exposed to laboratory air was provided by two inlet fans with a total nominal flow of 100 m^3/h and two outlets placed at opposite ends at the top of the tank. The air was kept at stable temperature, humidity and CO_2 concentration by the ventilation system of the building and was monitored weekly, being 20±2 °C, 50±10 % and 0.05±0.01 -vol.% respectively. The drying cycle of the carbon dioxide exposure had a nominal flow of approx. 90 m^3/h, running through a closed loop and utilized a cooled heat exchanger to condensate moisture from the air flux. The CO_2 concentration inside the carbon dioxide loop was measured weekly and was approx. 0.5±0.1 -vol.%.

2.3 Experimental studies

2.3.1 Optical inspection of fibres

The surface of pulled-out steel fibres from selected specimens was inspected using a 3D optical

Table 2. Test samples and exposure conditions. After [9].

Sample		Study	Presented	Pull (mm)	Wet cycle	Dry cycle
1	T	Thin-section	x	0.15	7 -wt.% NaCl	0.05 -vol.% CO_2
	P	Polished-section	x			
	O	3D profile	x			
2	T	Thin-section	x	0.15	Freshwater	0.5 -vol.% CO_2
	P	Polished-section				
	O	3D profile	x			
3	T	Thin-section	x	0.15	Limewater	-
	P	Polished-section				
	O	3D profile	x			
4	T	Thin-section	x	0	Limewater	-
	O	3D profile *	x			

Note: Each sample corresponds to a separate specimen, prepared and tested as the others. Except for (5S):
** The fibre scanned was tested as supplied, before being embedded in the matrix.*

interferometry profiler (Keyence VR-3000 G2) with a resolution of 0.1 µm. The inspection was done on three locations of the fibre, shown in **Fig. 2a**: I) the steel exposed to the solution inside the artificial crack, II) the central part of the fibre stem, III) the intermediate part of the hook.

The analysis focused on describing the roughness and volume of corrosion products to determine whether an alteration of the steel surface due to corrosion damage may have an impact on the pull-out behaviour of the fibre. The analysis of the corrosion damage and accumulation of corrosion products on the exposed steel surface (Location I in **Fig. 2a**) was done on a 3D reconstruction of approx. 1/3 of the fibre's cross-section, due to limitations in the maximum scan area. The analysis of the surface roughness of the steel at the embedded parts of the fibre (Locations II and III in **Fig. 2a**) was done on a flattened surface profile, reconstructed from a 3D scan, as shown **Fig. 3**. The analysis of the surface roughness was done on an average surface of 1.5 x 0.5 mm, characterized according to selected parameters described in ISO 25178-2: 2012:

i) The arithmetical mean height (S_a) that describes an absolute value of the sum of the height difference of each point to the arithmetical mean of the surface.
ii) The maximum height (S_z) that represents the sum of the largest peak height value and the largest pit depth.
iii) The root mean square height (S_q) that corresponds to the root mean square value of the absolute height values within the area, comparable to the standard deviation of the heights.
iv) The density of peaks (S_{pd}) that describes the average number of peaks per unit area.

2.3.2 Petrographic study

The preparation techniques for the petrographic specimens corresponded to those described in [24,25]. The stabilization and initial preparation process comprised the following: i) drying of pull-out specimens in laboratory air for 2 weeks, ii) vacuum resin impregnation of the pull-out specimens to stabilize the fibre, iii) sawing of the specimen at the central section surrounding the embedded fibre (i.e. 10 x 10 x 40 mm prism) and drying in oven at 35°C for approx. 10 hours. After this process, two types of specimens were prepared, i.e. polished sections longitudinal to the fibre axis and thin-sections transversal to the fibre axis, respectively.

Polished sections were prepared on a plane parallel to the longitudinal axis of the fibre, from the intersection of the fibre with the artificial crack to the hooked-end,

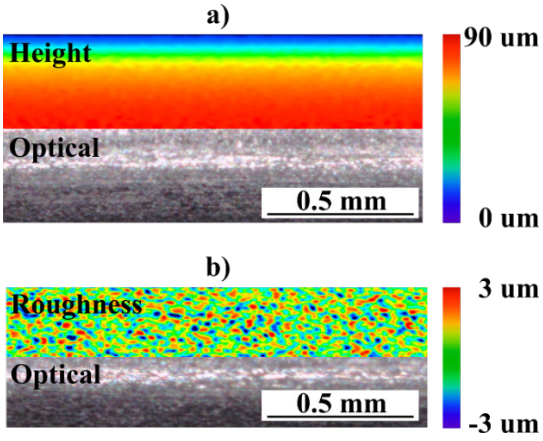

Fig. 3. 3D scans of fibre surface embedded in concrete, at the fibre stem, showing: a) original 3D scan with height profile, b) flattened surface with roughness profile.

shown as a shaded area in **Fig. 2b**. The preparation process comprised: i) sawing of the specimen longitudinal to the fibre, at approx. 1 mm to the surface of the fibre, ii) vacuum resin impregnation, iii) grinding of the specimen surface until reaching the steel fibre, iv) vacuum resin impregnation, v) lapping and polishing until reaching the central axis of the fibre.

Thin-sections were prepared on four consecutive slices, perpendicular to the direction of the fibre, at the locations shown in **Fig. 2b**. The preparation process consisted on: i) sawing off four slices perpendicular to the direction of the fibre, ii) vacuum resin impregnation, iii) mounting of four slices into one section, iii) subsequent grinding, lapping and polishing to prepare the thin-section.

The polished sections were photographed under UV light at 50 MP resolution using a 65mm f/2.8 1-5x macro lens. The thin-sections were analysed by optical polarizing microscopy, using a Leica DM2500P optical polarizing microscope equipped with a UV fluorescent light source. The fluorescent filter combination used was a BG12 excitation filter and a K530 yellow blocking filter, as utilized in [26].

3. Experimental results

3.1 Inspection of fibre surface

Selected steel fibres were inspected after pull-out and before being embedded in the matrix. The results presented comprise two groups of measurements: i) characterization of the variation of the cross-section of the fibre at the area where the fibre intersects with the crack due to corrosion, and ii) characterization of surface roughness of the steel embedded in the matrix.

Accumulation of corrosion products was observed around the intersection between the fibre and the artificial crack, extending approximately 1 – 2 mm

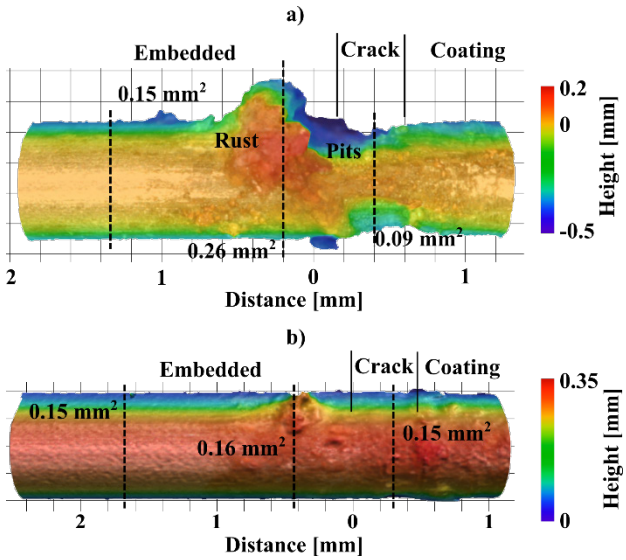

Fig. 4. 3D scan of fibre exposed to saltwater at the intersection with the crack for: a) specimen exposed to saltwater wet-dry cycles, and b) specimen exposed to freshwater wet-dry cycles. The colour map shows the relative height of the surface. The scanned cross-section at three locations was calculated in mm^2 (the cross-section inspected was approx. 1/3 of the total cross-section of the fibre).

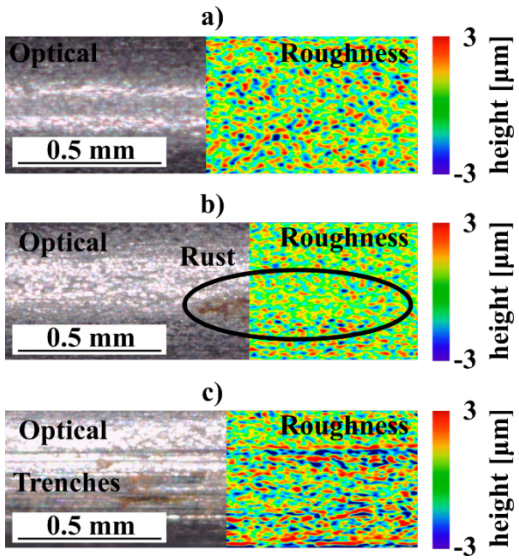

Fig. 5. 3D scans of fibre surface embedded in concrete: a) surface roughness at the stem of an exposed fibre (2S-I); b) surface roughness around a rust spot at the stem of an unexposed fibre (4S-I), c) surface roughness at the straightened section of the hook of a pulled-out fibre (2S-II).

inside the matrix. Formation of corrosion products (i.e. rust) in this area for the specimen exposed to saltwater, led to an effective increase of the fibre cross-section (i.e. up to ≈ 70% increase in cross-section), see **Fig. 4a**. Alongside, there was a substantial reduction of the fibre's cross-section exposed inside the crack (i.e. up to ≈ 40% reduction of cross-section), which spread slightly into the matrix and the epoxy coating. This was not the case for specimens exposed to freshwater, see **Fig. 4b**, which showed a minor variation in the fibre cross-section due to corrosion.

Inspection of the surface roughness of the embedded fibre parts was done on a flattened profile, levelled to the mean profile of the 3D scan (as shown in **Fig. 3**). The analysis was done on two representative locations of the steel fibre: at the fibre stem (see **Fig. 5a-b**) and at the straightened part of the hook after pull-out (see **Fig. 5c**). Surface roughness parameters calculated according to (ISO 25178-2: 2012) are presented in **Table 3**.

Table 3. Roughness parameters from flattened of 3D scans at the embedded parts of the fibre, calculated according to ISO 25178.

Specimen		S_a	S_z	S_q	S_{pd}
		µm	*µm*	*µm*	*1/mm²*
1S	I	0.98	11.7	1.25	1245
1S	II	1.07	23.9	1.49	1269
2S	I	1.03	13.0	1.30	1387
2S	II	1.26	18.1	1.62	1294
3S	I	0.93	12.1	1.19	1442
4S	I	1.06	16.2	1.37	1449

Abbreviations: (S_a) arithmetical mean height, (S_z) maximum height, (S_q) root mean square height, and (S_{pd}) density of peaks.

The steel surface showed a generally uniform distribution of peaks and pits at the steel surface, see **Fig. 5a**. Localized areas presenting rust stains were found in exposed and unexposed specimens, in the latter these were attributed to oxygen corrosion during storage, handling and preparation of the specimens. Yet, the presence of rust spots did not alter substantially the average roughness measured of the inspected surface, slight decrease of roughness was observed instead (see **Fig. 5b**). Conversely, there was a clear difference in roughness of the fibres after pull-out in the hook region, as shown in **Fig. 5c**. The steel presented deep longitudinal "trenches" at the straightened hook, which can be attributed to the friction between the steel surface and the surrounding matrix during the pull-out process. Thus, indicating that this area transferred most of the friction during pull-out. The roughness parameters presented in **Table 3** confirm that, at the fibre stem, fibres are similar to each other, regardless of the exposure conditions; while major increase in roughness was measured at the hook region of pulled-out fibres, regardless of the exposure conditions as well.

3.2 Petrographic study

A petrographic study was carried out to assess the extent of mechanical damage and microstructural alteration of the matrix surrounding the partially-pulled steel fibres before and after exposure. Focus was set on connecting macro- and micro-structural damage in the matrix surrounding the fibre and the pull-out mechanisms of the fibre. Selected results from one specimen exposed to freshwater cycles (specimen 2P in **Table 2**) are presented below. The extent and nature of the mechanical damage along a

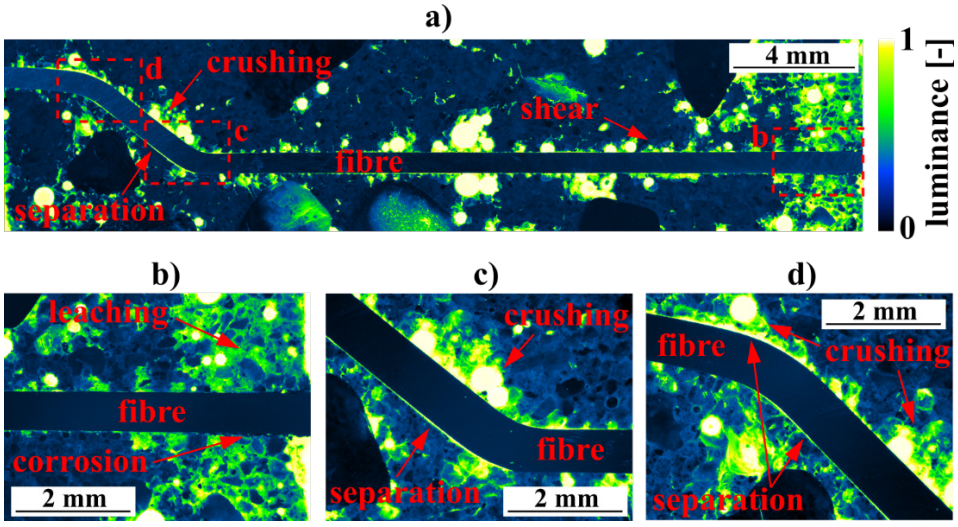

Fig. 6. Polished section of partially pulled-out steel fibre, exposed to freshwater wet-dry cycles (specimen 2P), showing relative UV luminance values for: a) overview of the fibre with indication of local damage; b) intersection of the fibre with the artificial crack; c) first bend of the hook; d) second bend of the hook. The annotations in red indicate damage and features observed in the section under visible and UV light up to x5 magnification.

partially-pulled fibre is shown in **Fig. 6** as the relative luminance values of a micrograph under UV fluorescent light. The results show areas with voids, higher porosity or mechanical damage in light green/yellow colour and denser areas in darker blue colour.

The results presented in **Fig. 6a** show that there is an increase in porosity at the outermost 2 – 3 mm of the specimen, inside the artificial crack, which are attributed to leaching and carbonation of the matrix during the exposure. In this case, there is accumulation of corrosion products at the outermost 2 mm of the fibre, which block separation damage and pores in the matrix around this part of the fibre, see **Fig. 6b**. There is substantial porosity and damage along the stem of the fibre, yet the damage does not seem to form a continuous path along the fibre stem, see **Fig. 6a**. Most of the mechanically-induced damage to the matrix concentrates around the fibre hook, see **Fig. 6a**. The side of the hook that faces the pull-out direction generally presents crushing damage, while the opposite side is separated a few micrometres from the matrix, as shown in **Fig. 6 c,d**. This damage is localized around the hook bends, see **Fig. 6c,d**. There was no indication of additional transformation of the matrix around the fibre due to exposure at this scale, e.g. autogenous healing or carbonation of the cement paste.

Results from the inspection of thin-sections are presented for selected cross-sections of the fibre in one specimen exposed to wet-dry cycles of saltwater (see **Fig. 7**), and selected features of various exposed and unexposed specimens (see **Fig. 8**). The micrographs presented comprise overlays of the inspected areas under cross-polarized and UV-fluorescent light, denoted in the figures as "x-pol" and "fluo", respectively.

The inspection of the specimen exposed to wet-dry cycles of saltwater was done at the locations described in **Fig. 2**: I) at approximately 2 mm from the intersection of the fibre with the artificial crack (**Fig. 7a**), II) at the end of the stem, close to the first bend of the hook (**Fig. 7b**), III) at the second bend of the hook (**Fig. 7c**), IV) at the straight end of the hook (**Fig. 7d**).

The micrographs taken under UV fluorescent light show substantial mechanical damage at the matrix adjacent to the fibre, particularly at the hook bends (**Fig. 7b,c**) and at the intersection of the fibre with the crack (**Fig. 7a**). This damage generally comprises well-defined radial cracks smaller than 10 µm (**Fig. 7a**), and overall increase in porosity (**Fig. 7b,c**). The latter may be related to crushing of the matrix around the fibre, which appears smeared in the thin-section and cannot be fully investigated at the scales observed

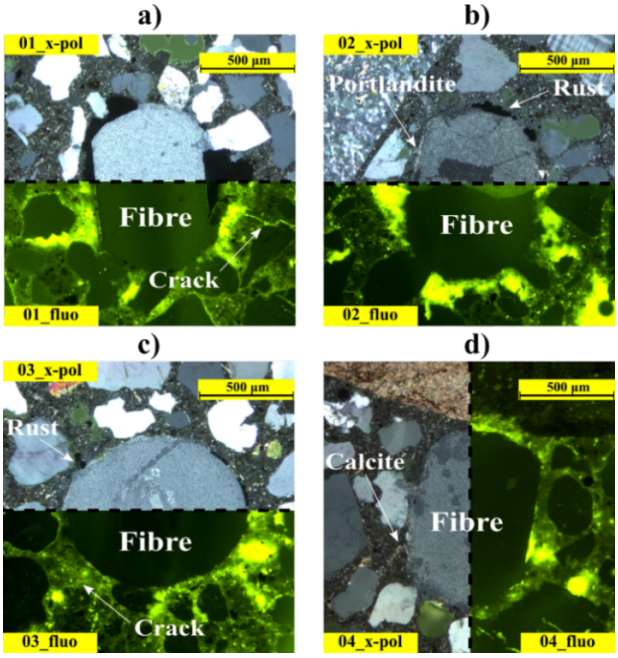

Fig. 7. Thin-section of partially pulled-out fibre exposed to saltwater (specimen 1T), under cross-polarized and UV fluorescent light, at selected locations: a) at the intersection of the fibre with the simulated crack (location I); b) at the stem of the fibre (location II); c) at the centre of the fibre hook (location III); and d) at the end of the fibre hook (location IV). Locations correspond to the ones described in **Fig. 2**.

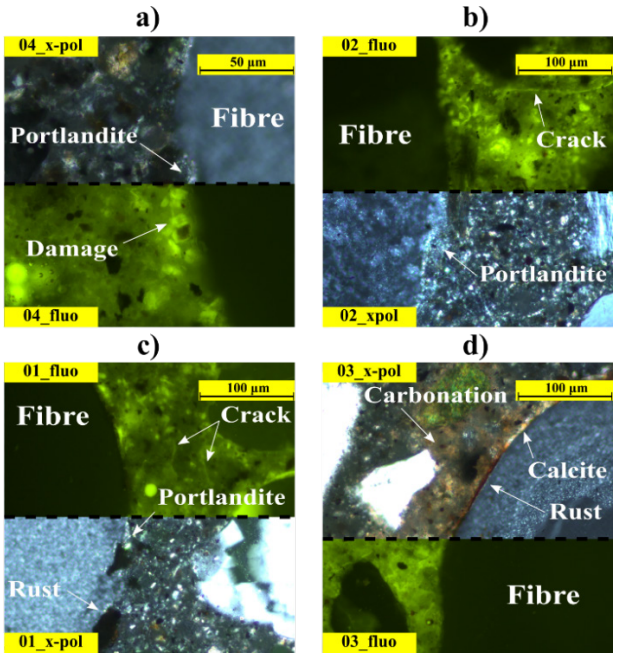

Fig. 8. Thin-section of steel partially pulled-out fibre under cross-polarized and UV fluorescent light, for selected exposures: a) unexposed specimen (specimen 3T at location II); b) specimen exposed to freshwater (specimen 2T at location III); c) specimen exposed to saltwater (specimen 1T at location II); and d) specimen exposed to saltwater (specimen 1T at location III).

with this method. Part of the additional porosity observed at the outermost section (**Fig. 7a**), may be as well linked to leaching processes in the matrix adjacent to the crack, as shown in **Fig. 6a**.

Corrosion products were found at the intersection of the fibre with the crack (**Fig. 7a**), filling porosity and damage around the fibre. There is also smaller accumulation of rust at some locations in the hook region, filling as well separation between the matrix around the steel, see **Fig. 7b,c**. Portlandite and calcite were observed at the interface between the matrix and the fibre, which correspond to dissolution and precipitation and of calcium-based phases (i.e. reprecipitation), that eventually carbonated.

A closer inspection of the damage and reprecipitation processes at the interface between the fibre and the matrix is presented in **Fig. 8**. The interface of an unexposed fibre, see **Fig. 8a**, generally did not show a distinctive microstructure compared to the bulk paste or the interface of an aggregate; nonetheless, local defects such a pores or mechanical damage were also found. There was limited mechanical damage to the matrix around the stem of the fibre (**Fig. 8a**), which presented minor re-precipitation of cryptocrystalline portlandite in some cases. In the case of the exposed specimens, most of the voids generated along the fibre surface during pull-out were generally lined with either cryptocrystalline portlandite (see **Fig. 8b**), and corrosion products (iron oxides) in fewer cases (**Fig. 8c**). Some locations showed carbonation of the matrix around the fibre at damaged areas, where the interface and surrounding voids were filled by a combination of corrosion products and calcite (**Fig. 8d**).

4. Discussion

The observations presented in the results section described the global and local damage observed at the steel fibre and in the matrix surrounding the fibre. The results are discussed below in order to clarify whether variations in the pull-out behaviour of partially-pulled fibres exposed to wet-dry cycles may be due to accumulation of corrosion products [2,14,27] or healing processes in the matrix around the fibres [9,17]. Results from pull-out experiments on specimens re-tested after exposure to freshwater or saltwater cycles performed in [9] were used as reference, see **Fig. 9**. There were three main aspects that indicated an alteration of the pull-out behaviour of corresponding specimens: i) a partial restoration of the adhesive bond after exposure, ii) an increase of the maximum pull-out force at a slip of approximately 0.5 mm (i.e. an increase in the range of 50 – 100 N), and iii) the unexpected rupture of some fibres at slip values much larger than the one corresponding to the maximum force.

4.1 Pull-out behaviour and mechanical damage

The observations presented in the results section show that most of the load transfer in the fibres investigated occurred at the hook. Most of the mechanical damage in the matrix were also observed at the hook region; corresponding to crushing of the matrix at one side of the hook, and separation at the

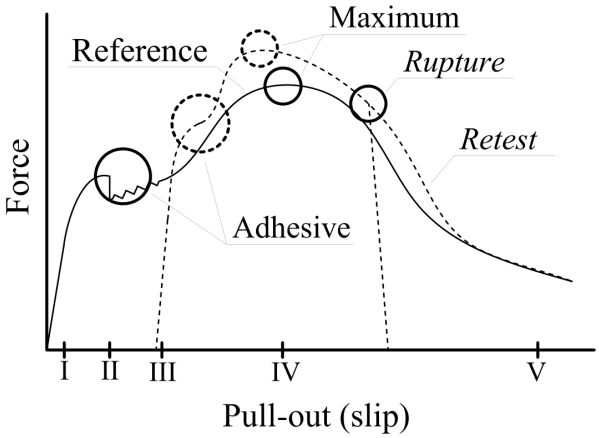

Slip values (indicative)

I : 20 - 50 µm	IV : 0.5 - 1 mm
II : 50 - 100 µm	V : 5 - 6 mm
III :100 - 200 µm	

Fig. 9. Representation of changes in the pull-out forces transferred in partially pulled steel fibres exposed to wet-dry cycles, after [9].

opposite side. There was substantial abrasion of the steel at the straightened hook after the pull-out process; while the surface roughness at the stem did not vary regardless of presence of rust spots or compared to the original fibre (e.g. non-embedded).

These arguments support that most of the pull-out process of hooked-end steel fibres is actually governed by yielding of steel at the hook, fracture of the matrix around the hook and friction between the hook and the matrix, which is in agreement with former studies [12,28].

4.2 Deterioration processes

Accumulation of corrosion products occurred mainly at the intersection of the fibre with the crack extending approximately 1 – 2 mm into the matrix. Rust filled adjacent voids/damage and pores and was more abundant under chloride exposure. Small accumulation of corrosion products was observed in the hook region, which partly filled some of the voids/damage around the hook.

There were no signs of alteration of the bulk fibre roughness due to corrosion, for the exposures investigated in this study. Alteration of the matrix around the fibre and re-precipitation processes were found along the whole fibre but were more pronounced at the intersection of the fibre and the crack and at the hook. Sings of re-precipitation inside cracks, voids and separation damage around the fibre, comprising portlandite and calcite, indicate initial stages of autogenous healing of damage around the fibre, as also discussed in [29] at the composite scale.

Additionally, signs of carbonation of the cement paste surrounding the fibre were found, which may alter the mechanical properties of the adjacent matrix over time, e.g. stiffness, hardness and strength [30].

4.3 Relating deterioration processes and pull-out behaviour

Based on the observations discussed above, the pull-out process of hooked-end fibres in concrete described in [9] and the deterioration processes discussed in [29,31] may be connected, as shown in **Fig. 10**. The pull-out path of an unexposed fibre may follow the steps shown in **Fig. 10a-b**, while, exposure of the fibre and matrix after partial pull-out (**Fig. 10a**) may lead to variations in the pull-out process, as shown in (**Fig. 10c-d**) and discussed hereafter.

The partial restoration of the adhesive bond reported after exposure may be explained by a combination of precipitation of portlandite and formation of calcite around the fractured fibre-matrix interface and formation (and localized expansion) of corrosion products at the intersection of the fibre with the matrix, see **Fig. 10c**. Subsequent strain and fracture of these under axial re-loading of the fibre may provide sufficient bond at small slip values, e.g. below 30 µm. In this aspect, accumulation of rust at the intersection with the crack could have an important role, considering that for example an increase in the pull-out force of up to 10 N distributed along approx. 2 mm of the fibre investigated would be equivalent to an average additional shear stress localized in this region of approx. 2 MPa. That is in agreement with values presented for corroded reinforcement bars (approx. 2 – 4 MPa) [32,33], also measured at small slip values during the de-bonding phase.

The increase of the mechanical bond strength, e.g. observed by an increase of the pull-out force by 50 – 100 N at slip values up to approx. 0.5 mm, is expected to be governed by the accumulation of solid phases (e.g. portlandite, calcite and iron oxides) at voids and cracks around the fibre (**Fig. 10d**). Filling up of voids

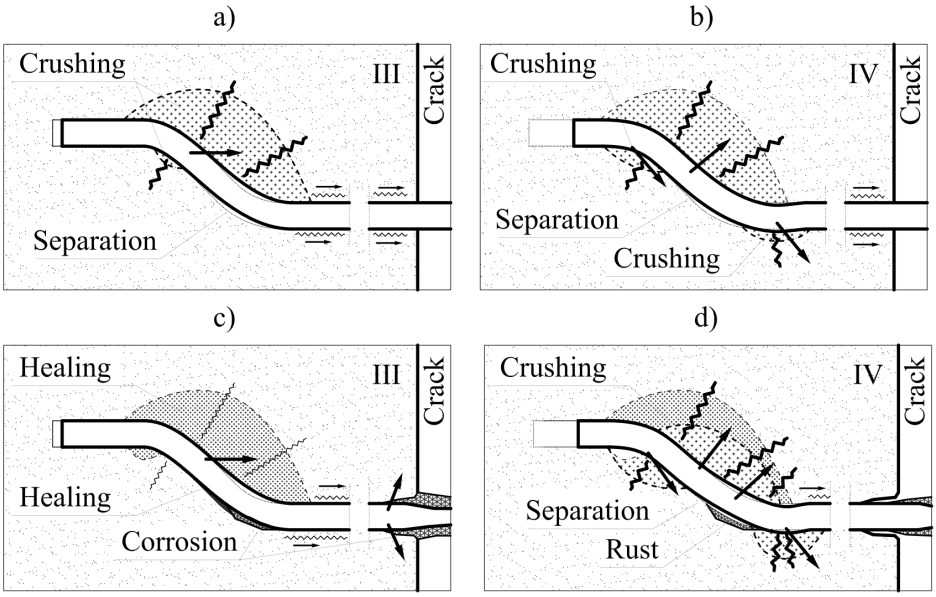

Fig. 10. Conceptual representation of the pull-out process of a fibre at various stages: a) initial damage after debonding, b) utilization of mechanical bond under normal conditions, c) reactivation of the adhesive bond after exposure, d) utilization of mechanical bond after exposure.

and damage around the fibre alters the pull-out path of the fibre, leaving a narrower channel for the hook to bend afterwards. Carbonation of the cement matrix around the fibre and the precipitated portlandite may increase the hardness of the paste around the fibre, thus increasing friction. In this case, the hypothesis suggesting that the increase of the maximum pull-out force was due to additional friction caused by accumulation of rust at the outermost 2 mm of the fibre was discarded. Such an increase in the force would be equivalent to an additional frictional stress over that area in the range 10 – 20 MPa, that should lead instead to failure of the matrix. Yet, the contribution of accumulation of rust at voids and separation damage around the hook, despite minor, may have a contribution to the increase of pull-out forces transferred.

Rupture of the fibre at the hook in the descending branch of the pull out process, e.g. at 2.5 – 4 mm slip, could be explained as well by the mechanisms governing the increase of the mechanical bond strength. The alteration of the pull-out path of the fibre increases the frictional forces transferred through the hook, which leads to accumulation of additional yield strain at the hook bends and exceeds the local tensile limit of the steel at the deforming regions of the fibre. Corrosion damage at the hook could contribute to an early rupture of the fibres at the hook, but the extent of this contribution is not clear from the data available. Small corrosion spots, of approx. 1 mm^2, were observed at the hook, but these did not entail a measurable reduction of the cross-section at the steel surface with the methods used.

5. Conclusion

This paper investigated the governing processes taking place during the exposure of partially pulled-out steel fibres to wet-dry cycles of chlorides and CO_2. The discussion described the processes that altered the pull-out behaviour of hooked-end steel fibres in companion specimens, which did not solely comprise corrosion damage of the fibre, and led to the following conclusions:

- Corrosion damage occurred mainly in the fibre region exposed directly to the crack and corrosion products precipitated in the matrix surrounding the fibre and adjacent to the crack. Limited corrosion damage was observed in the fibre region embedded in the matrix, which did not alter the surface roughness of the fibre.
- Mechanical damage observed in the matrix and at the fibre confirmed that the pull-out process is governed by yielding of the hook and fracture of the adjacent matrix. Most of the friction between the fibre and matrix was transferred through the hook.
- The partial restoration of the adhesive bond reported in companion specimens was attributed to a combination of autogenous healing around the fractured fibre-matrix interface and accumulation of corrosion products around the intersection of the fibre with the matrix.
- The increase of the mechanical bond strength reported in companion specimens was ascribed to the precipitation of solid phases, e.g. portlandite, calcite and to a lesser extent iron oxides, in voids and cracks of the matrix around the fibre hook. The accumulation of these phases reduced the free-space available for the fibre hook to yield, and led in some cases to premature rupture of the fibre at the hook bends.

These conclusions support recent hypotheses, which suggest that corrosion damage may not dominate the deterioration of the residual tensile strength of cracked SFRC exposed to wet-dry cycles, contrary to what was reported in former studies. However, further experimental and numerical investigations are needed in order to quantify the role of healing and deterioration processes at the fibre-matrix interface on the variations of the pull-out performance of hooked-end fibres in cracked concrete.

Acknowledgements

The first author would like to express his gratitude to: CowiFonden, InnovationsFonden, the German association of steel fibre producers (VDS), VejDirektoratet and Mapei-Denmark, for supporting this project.

References

[1] V. Marcos-Meson, A. Michel, A. Solgaard, G. Fischer, C. Edvardsen, T.L. Skovhus, Corrosion resistance of steel fibre reinforced concrete - A literature review, Cem. Concr. Res. 103 (2018) 1–20. doi:10.1016/j.cemconres.2017.05.016.

[2] J.-L. Granju, S.U. Balouch, Corrosion of steel fibre reinforced concrete from the cracks, Cem. Concr. Res. 35 (2005) 572–577. doi:10.1016/j.cemconres.2004.06.032.

[3] E.S. Bernard, Age-dependent changes in post-crack performance of fibre reinforced shotcrete linings, Tunn. Undergr. Sp. Technol. 49 (2015) 241–248. doi:10.1016/j.tust.2015.05.006.

[4] E.S. Bernard, Effect of Exposure on Post-crack Performance of FRC for Tunnel Segments, in: I. Vrkljan, Z. Dekovic, M. Dobrilovic, J. Likar, P. Miscevic (Eds.), SEE TunnelPromoting Tunneling SEE Reg. - ITA WTC 2015, ITA-AITES,

Dubrovnik, Croatia, 2015: p. 13.

[5] V. Marcos-Meson, G. Fischer, C. Edvardsen, A. Solgaard, A. Michel, Mechanical performance of steel fibre reinforced concrete exposed to chlorides and carbon dioxide: results after one year (Manuscript submitted for publication), Mag. Concr. Res. (2018).

[6] V. Marcos-Meson, G. Fischer, A. Solgaard, C. Edvardsen, A. Michel, Development of the mechanical performance of steel fibre reinforced concrete exposed to wet-dry cycles of chlorides and carbon dioxide: results after two years (Manuscript submitted for publication), Mag. Concr. Res. (2019).

[7] R.J. Gray, Experimental techniques for measuring fibre/matrix interfacial bond shear strength, Int. J. Adhes. Adhes. 3 (1983) 197–202. doi:10.1016/0143-7496(83)90094-5.

[8] C. DiFrancia, T.C. Ward, R.O. Claus, The single-fibre pull-out test. 1: Review and interpretation, Compos. Part A Appl. Sci. Manuf. 27 (1996) 597–612. doi:10.1016/1359-835X(95)00069-E.

[9] V. Marcos-Meson, G. Fischer, C. Edvardsen, A. Solgaard, A. Michel, Pull-out behaviour of hooked-end steel fibres in cracked concrete exposed to wet-dry cycles of chlorides and carbon dioxide – mechanical performance (Manuscript submitted for publication), Constr. Build. Mater. (2019).

[10] I. Markovich, J.G.M. Van Mier, J.C. Walraven, Single fiber pullout from hybrid fiber reinforced concrete, Heron. 46 (2001) 191–200.

[11] P.D. Nieuwoudt, A.J. Babafemi, W.P. Boshoff, The response of cracked steel fibre reinforced concrete under various sustained stress levels on both the macro and single fibre level, Constr. Build. Mater. 156 (2017) 828–843. doi:10.1016/j.conbuildmat.2017.09.022.

[12] A. Bentur, S. Mindess, S. Diamond, Pull-out processes in steel fibre reinforced cement, Int. J. Cem. Compos. Light. Concr. 7 (1985) 29–37. doi:10.1016/0262-5075(85)90024-7.

[13] T.H. Ahn, D.J. Kim, S.H. Kang, Crack Self-Healing Behavior of High Performance Fiber Reinforced Cement Composites Under Various Environmental Conditions, in: Kris Zacny, R.B. Malla, W. Binienda (Eds.), Earth Sp. 2012, ASCE, Pasadena, United States, 2012: pp. 635–640.

[14] C. Frazão, J. Barros, A. Camões, A.C. Alves, L. Rocha, Corrosion effects on pullout behavior of hooked steel fibers in self-compacting concrete, Cem. Concr. Res. (2015). doi:10.1016/j.cemconres.2015.09.005.

[15] N. Banthia, C. Foy, Marine Curing of Steel Fiber Composites, J. Mater. Civ. Eng. 1 (1989) 86–96. doi:10.1061/(ASCE)0899-1561(1989)1:2(86).

[16] E. Alizade, F.J. Alaee, S. Zabihi, Effect of Steel Fiber Corrosion on Mechanical properties of Steel Fiber Reinforced Concrete, Asian J. Civ. Eng. 17 (2016) 147–158.

[17] R.J. Gray, Autogenous healing of fibre/matrix interfacial bond in fibre-reinforced mortar, Cem. Concr. Res. 14 (1984) 315–317. doi:10.1016/0008-8846(84)90047-4.

[18] T. Nishiwaki, S. Kwon, D. Homma, M. Yamada, H. Mihashi, Self-healing capability of fiber-reinforced cementitious composites for recovery of watertightness and mechanical properties, Materials (Basel). 7 (2014) 2141–2154. doi:10.3390/ma7032141.

[19] D. Homma, H. Mihashi, T. Nishiwaki, Self-Healing Capability of Fibre Reinforced Cementitious Composites, J. Adv. Concr. Technol. 7 (2009) 217–228. doi:10.3151/jact.7.217.

[20] A.K. Kragh, M.E. Carlsen, Development of fibre-matrix bond over time, Technical University of Denmark, 2017.

[21] European Commitee for Standardization (CEN), Methods of test for mortar for masonry. Determination of consistence of fresh mortar, European Union, 1999.

[22] European Commitee for Standardization (CEN), Masonry cement. Test methods, European Union, 2016.

[23] European Commitee for Standardization (CEN), Fibres for concrete - Part 1: Steel fibres - Definitions, specifications and conformity, EN 14889-1:2006, European Union, 2006.

[24] R.J. Detwiler, L.J. Powers, U.H. Jakobsen, W.U. Ahmed, K.L. Scrivener, K.O. Kjellsen, Preparing specimens for microscopy, Concr. Int. 23 (2001) 51–58.

[25] U.H. Jakobsen, L. Laugesen, N. Thaulow, Determination of water to cement ratio in hardened concrete by optical fluorescence microscopy., Sp 191. Water-Ceme (2000) 27–41.

[26] U.H. Jakobsen, K. De Weerdt, M.R. Geiker, Elemental zonation in marine concrete, Cem. Concr. Res. 85 (2016) 12–27. doi:10.1016/j.cemconres.2016.02.006.

[27] E.S. Bernard, Durability of cracked fibre reinforced shotcrete, in: E.S. Bernard (Ed.), Shotcrete More Eng. Dev. Proc. Second Int. Conf. Eng. Dev. Shotcrete, A.A. Balkema Publishers, Sydney, Australia, 2004: pp. 59–66.

[28] K. Georgiadi-Stefanidi, E. Mistakidis, D. Pantousa, M. Zygomalas, Numerical modelling of the pull-out of hooked steel fibres from high-strength cementitious matrix, supplemented by experimental results, Constr. Build. Mater. 24 (2010) 2489–2506. doi:10.1016/j.conbuildmat.2010.06.007.

[29] V. Marcos-Meson, M. Geiker, G. Fischer, A. Solgaard, U.H. Jakobsen, C. Edvardsen, T. Danner, T.L. Skovhus, A. Michel, Durability of cracked SFRC exposed to wet-dry cycles of chlorides and carbon dioxide – multiscale deterioration phenomena (Manuscript submitted for publication), Cem. Concr. Res. (2019).

[30] B. Šavija, M. Luković, Carbonation of cement paste: Understanding, challenges, and opportunities,

Constr. Build. Mater. 117 (2016) 285–301. doi:10.1016/j.conbuildmat.2016.04.138.

[31] V. Marcos-meson, A. Michel, A. Solgaard, G. Fischer, C. Edvardsen, T.L. Skovhus, Corrosion Resistance of Steel Fibre Reinforced Concrete – a Literature Review, in: H. Beushausen (Ed.), Fib Symp. 2016. Performance-Based Approaches Concr. Struct., FIB, Cape Town, ZA, 2016: pp. 121–122.

[32] A.A. Almusallam, A.S. Al-Gahtani, A.R. Aziz, Rasheeduzzafar, Effect of reinforcement corrosion on bond strength, Constr. Build. Mater. 10 (1996) 123–129. doi:10.1016/0950-0618(95)00077-1.

[33] H. Yalciner, O. Eren, S. Sensoy, An experimental study on the bond strength between reinforcement bars and concrete as a function of concrete cover, strength and corrosion level, Cem. Concr. Res. 42 (2012) 643–655. doi:10.1016/j.cemconres.2012.01.003.

Chapter 6
A multiscale modelling approach to link corrosion damage and mechanical performance of SFRC

The discussion initiated in Chapter 3 and Chapter 4, indicated that there are significant changes in the mechanical performance of cracked SFRC over time when exposed to wet-dry cycles (Chapter 3). These changes in the mechanical performance have been related both to corrosion damage of the steel fibres and changes in the fibre-matrix bond strength over time (Chapter 4). However, a link between these investigations is still missing.

Results at the single-fibre level provide a detailed description of the actual pull-out mechanisms of the fibre, including the eventual rupture of fibres when the tensile capacity of the steel is exceeded, either due to corrosion damage or an increase of the bond strength. Yet, interactions inside the crack at the composite level are complex, and involve considerable number of fibres with different orientations, degrees of corrosion damage and embedment lengths. Therefore, extrapolation of the pull-out behaviour from the single-fibre level to residual forces at the composite level is needed in order to provide an explanation for the changes in mechanical performance observed on the cracked SFRC specimens.

In Paper VII, experimental results from single-fibre pull-out tests (Chapter 4) were used to discretize the pull-out behaviour of single fibres as a spring-slider model, which were up-scaled to the composite level based on a probabilistic approach of the fibre bundle model. Model predictions were then compared to results from uniaxial tension tests of cracked SFRC exposed to wet-dry cycles of saltwater (Chapter 3).

The model output showed comparable trends with respect to the experimental observations. Modelled and experimental results concurred that measured increases in

the fibre-matrix bond strength of partially pulled fibres after exposure to wet-dry cycles corresponded to the measured increases of the tensile stress observed in uniaxial tensile samples. Limitations in the model regarding the description of the fibre rupture process and the pull-out behaviour of inclined fibres were identified and discussed. The discussion confirmed that both the increase of the fibre-matrix bond strength and the reduction of fibre cross-section due to corrosion, may lead to a decrease in the residual tensile strength of the composite at larger crack openings. The model was capable of describing the non-linear relationship between the aforementioned parameters and variations in the toughness of cracked SFRC.

These conclusions support the hypotheses discussed in the previous chapters of this thesis, confirming that corrosion damage of the steel fibres may not be the only mechanism responsible for the deterioration reported in cracked SFRC exposed to chlorides and carbon dioxide in former studies. In particular, an unaccounted increase of the fibre-matrix bond strength during the exposure, likely due to alteration of the cement matrix around the fibre, may lead to either an increase of the toughness or a dramatic reduction of it due to rupture of most fibres crossing the crack.

6.1 Paper VIII. A multiscale mechanical model for SFRC

The following publication, referred as “paper VIII”, has been published in Construction and Building Materials.

Marcos-Meson, V., Fischer, G., Edvardsen, C., Solgaard, A., Michel, A., 2020. Mechanical performance of cracked SFRC exposed to corrosive environments – a multiscale modelling approach. Constr. Build. Mater. 234 (2020) 117847.doi:10.1016/j.conbuildmat.2019.117847.

Construction and Building Materials 234 (2020) 117847

Contents lists available at ScienceDirect

Construction and Building Materials

journal homepage: www.elsevier.com/locate/conbuildmat

Mechanical performance and corrosion damage of steel fibre reinforced concrete – A multiscale modelling approach

Victor Marcos-Meson [a,b,c,*], Gregor Fischer [a], Anders Solgaard [b], Carola Edvardsen [b], Alexander Michel [a]

[a] Department of Civil Engineering, Technical University of Denmark, Copenhagen, Denmark
[b] COWI A/S, Copenhagen, Denmark
[c] VIA Building, Energy, Water & Climate, VIA University College, Horsens, Denmark

HIGHLIGHTS

- Fibre bundle models can describe variations in the toughness of cracked SFRC.
- The tensile strength of SFRC increased due to an increase of fibre bond strength.
- Corrosion damage of steel fibres is not the only deterioration mechanism of SFRC.
- Excessive increase of the fibre bond strength result in toughness loss of SFRC.

ARTICLE INFO

Article history:
Received 18 July 2019
Received in revised form 6 December 2019
Accepted 10 December 2019
Available online 26 December 2019

Keywords:
Steel fibre reinforced concrete (SFRC)
Corrosion
Single fibre pull-out
Fibre bundle model

ABSTRACT

This paper investigates variations in the tensile toughness of cracked steel fibre reinforced concrete (SFRC) subjected to corrosion damage, by means of a multiscale modelling framework. Experimental results were used to discretise the pull-out behaviour of single fibres using a spring-slider model, which were then upscaled to the composite level by means of a probabilistic fibre bundle approach. The model described the alteration of the residual tensile performance of the composite due to variations of the fibre-matrix bond strength and corrosion damage of the steel fibres, observed experimentally. This investigation supports recent hypotheses suggesting that corrosion damage of the steel fibres may not be the only mechanism responsible for the deterioration reported in cracked SFRC exposed to corrosive environments. The strengthening of the fibre-matrix bond over time may entail a decrease of the tensile toughness of the composite due to fibre rupture.

1. Introduction

The effects of corrosion of carbon-steel fibres on the residual tensile performance of cracked steel fibre reinforced concrete (SFRC) are in focus and under discussion both at the technical and scientific level [1]. There is discrepancy among studies that suggest that the variations in the tensile toughness observed for the cracked composite are solely due to corrosion damage at the steel fibres [2,3] or else that additional mechanisms are responsible for variations in the fibre-matrix bond strength over time [4,5].

Most of the discussion regarding corrosion damage of steel fibres is based on experiments at the composite scale, where cracked SFRC was exposed to corrosive environments (e.g. saltwater, freshwater or CO_2) under field or laboratory conditions and tested afterwards [1]. However, the interpretation of the nature of the changes in the residual tensile performance of the composite by means of macroscopic investigations is limited. Alternatively, investigations at the single-fibre scale provided more detailed hypotheses for the nature of the changes in the residual tensile performance of cracked SFRC over time [6,7]. A number of studies have approached the modelling of the pull-out behaviour of single fibres in concrete, as critically discussed in [8,9]. These approaches used generally comprise: i) semi-analytical solutions [10–13], numerical methods [14,15] or mixed approaches [9]. Investigations have mainly focused in aspects such as the role of fibre inclination [10,16–19], embedment length [9,16,18], geometry [11,13,20] or mechanical failure at the fibre and surrounding matrix [12,14]. Yet, extrapolation of results at the single-fibre scale to the performance of the cracked composite is hindered by the still limited development of multiscale models.

Most of the current model approaches that describe the tensile behaviour of SFRC at the composite scale are either based on:

* Corresponding author at: Technical University of Denmark, Department of Civil Engineering. Brovej 118, Kgs. Lyngby, (2800) Denmark.
E-mail address: vicmes@byg.dtu.dk (V. Marcos-Meson).

https://doi.org/10.1016/j.conbuildmat.2019.117847
0950-0618/

multilinear stress-opening laws adjusted to the composite response by means of inverse analysis [21–23]; or else the discrete modelling of fibres in finite element formulations [9,13,24,25] and lattice models [15,26,27]. The first group of models provides a computationally efficient solution to model the tensile behaviour of the material, but it lacks upscaling capabilities; while the second group of models allows the upscaling but entails a large computational demand. Other upscaling methods, based on the fibre bundle model approach, have been used in the literature to model failure of cementitious [9,18,28] fibre reinforced composites. These methods provide a computationally efficient method to upscale the performance of single fibres to the composite level. Yet, there is room for development of such modelling approaches for the prediction of the stress-opening relation in tension of concrete reinforced with mechanically anchored fibres (e.g. hooked-end fibres), to date only described analytically in [9].

This paper presents the implementation of a semi-empirical model framework based on the fibre bundle model approach and plasticity theory that describes the traction-opening behaviour of cracked and uncracked SFRC based on the pull-out behaviour of single fibres. The model framework is used to investigate the relation between fibre rupture, fibre corrosion and variations in the mechanical performance at the composite and single-fibre scale.

2. Methodology

The investigation presented in this paper covers the development and verification of a semi-analytical model to describe the tensile behaviour of uncracked and cracked SFRC in tension at the composite scale based on the pull-out behaviour at the single-fibre scale. The methodology hereafter covers the description of the experimental methods used and the modelling framework developed.

2.1. Experimental

2.1.1. Materials

The mix design used for the uniaxial tension specimens was specified in compliance with the recommendations of [29] for the exposure classes XC4 and XS3. The total binder content was 426.3 kg/m^3 with 31% fly ash replacement of the Portland cement (CEM I 52.5 N). Chemical and physical properties of the binders used are given in [30] as: (K1) for the cement and (V) for the fly ash. The water to binder ratio (w/b) was 0.34 and the equivalent water to cement ratio (w/c_{eq}) was 0.40. The pull-out specimens were cast following the same mix-design as the one used for the uniaxial tension specimens, but adjusting the maximum aggregate size to 8 mm, see Table 1. The characteristic compressive strength at 28 days of the concrete mixes used was equivalent to a strength class C70/85 [31]. Average values and Coefficient of Variation (COV) of selected mechanical properties of the hardened concrete mixes, tested at the end of the curing period (i.e. 56 days) are included in Table 1.

Table 1
Mix-design and mechanical properties.

Component	Quantity (kg/m^3)	
	Composite	Pull-out
Aalborg Rapid Cement (CEM I 52.5 N)	326.3	326.3
Emineral Fly Ash	100	100
Water	145	145
Sand (00/02 mm)	626.5	752.3
Gravel (04/08 mm)	175.1	990.3
Gravel (08/16 mm)	933.6	–
Steel fibre	40.0	–
Entrained air	4.5%	3%
Mechanical properties [*1]		
Compressive strength (MPa) [*2]	87 (11%)	85 (8%)
Tensile strength (MPa) [*3]	2.6 (18%)	–
Young's modulus (GPa) [*4]	44.0 (8%)	45.0 (6%)

[*1] Mechanical properties measured at the end of the curing period (i.e. 56 days). COV values calculated assuming normally distributed values, and reported as a percentage rounded to nearest integer, in brackets.
[*2] Compressive-strength values (from 6 test-replicates), measured and reported as per EN 12390-3 [32].
[*3] Tensile-strength values calculated as the limit of proportionality from uniaxial-tension results (from 10 test-replicates), tested according to [5].
[*4] Stabilised elastic modulus in compression (from 6 test-replicates), measured and reported according to EN 12390-13 [33].

The steel fibres used were made of high-carbon cold-drawn wire with hooked ends (type 1 according to EN 14889-1:2006 [34]); with a length of 60 mm and a diameter of 0.75 mm and were mixed in a proportion of 40 kg/m^3. One of the fibres had a single hook and a characteristic tensile strength of 1900 MPa and the other fibre had a double hook and a characteristic tensile strength of 1800 MPa, see Fig. 1a. The single-hooked fibre was specified for a concrete strength class superior to the one used, and the double-hooked fibre was specified for a strength class no larger than the one used in the study. Additional information about the geometry and properties of the steel fibres used can be found in [6].

The pull-out specimens were cast in the laboratory with a 60-l planetary mixer over a vibration table, using tailored PVC formworks, as used in [6]. The fibres were held at the bottom plate of the PVC formwork using a perforated rubber plug inserted into a conic gap at the centre of the bottom surface of the form. The pull-out specimens were 70 mm cubes with a single fibre embedded 30 mm, see Fig. 2a.

The uniaxial tension specimens were prepared in a laboratory, mixed with a 300-l planetary mixer and cast over a vibration table. The specimens were 150 mm cubes, with a 35 mm deep and 5 mm wide notch cut along the central perimeter, leaving an effective cross-section of 80 × 80 mm inside the notch, see Fig. 2b.

The uniaxial tension and pull-out specimens were grouped in samples of ten replicates. The specimens were distributed uniformly in the samples from the individual batches.

2.1.2. Mechanical tests

The workflow of the experiments comprised: i) testing of reference specimens at 56 days; ii) cracking of the specimens at 56 days and preparation for exposure; iii) exposure; iv) testing after exposure. The data presented in this paper covers the experimental results after one-year exposure for the uniaxial tension specimens and six-months exposure for the single-fibre pull-out specimens [5].

The testing of the uniaxial tension test specimens was done in a 500 kN capacity universal test frame. The uniaxial tension setup was described in [5], and is based on the design presented in [35], see Fig. 1b. The opening displacement at the notch ($CMOD_N$) was measured by two clip gages placed onto two steel pins glued to the centre of opposite faces of the specimen.

Single-fibre-pull-out tests were performed on a 25 kN universal test frame, equipped with a 10 kN load-cell, using a tailored clamping setup and following the test methodology described in [6]. The pull-out displacement of the fibre was measured as the displacement of the clamp relative to the surface of the concrete cube with three extensometers.

The displacement rates used for the experiments are shown in Table 2, and were based on the ones specified in EN 14889-1:2006 for 3-point bending tests; using a sampling frequency rate of 100 Hz. The test was controlled by the displacement of the crosshead.

Upon testing, the load – CMOD and load – slip data from each specimen was first resampled to a resolution of 1 μm. Then, the data was filtered and smoothed, using a 1-dimensional median filter and a moving average filter, following a similar scheme as described in [5]. The opening displacement at the crack mouth ($CMOD_M$) for the uniaxial tension specimens was calculated as the mean value from the two $CMOD_N$ measurements. Hereafter, crack opening values discussed in this paper will only refer to the opening displacement at the crack mouth (i.e. $CMOD_M \rightarrow CMOD$). The pull-out slip of the fibre was calculated as the average displacement of the

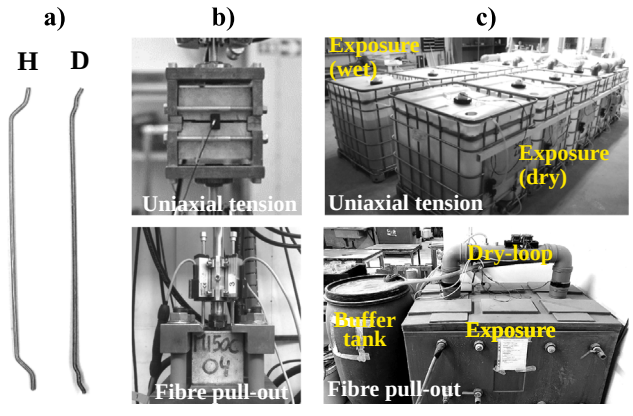

Fig. 1. Description of experiments: a) steel fibres used, b) mechanical tests for uniaxial-tension specimens and single-fibre specimens, after [5,6], and c) exposure setups after [5,6].

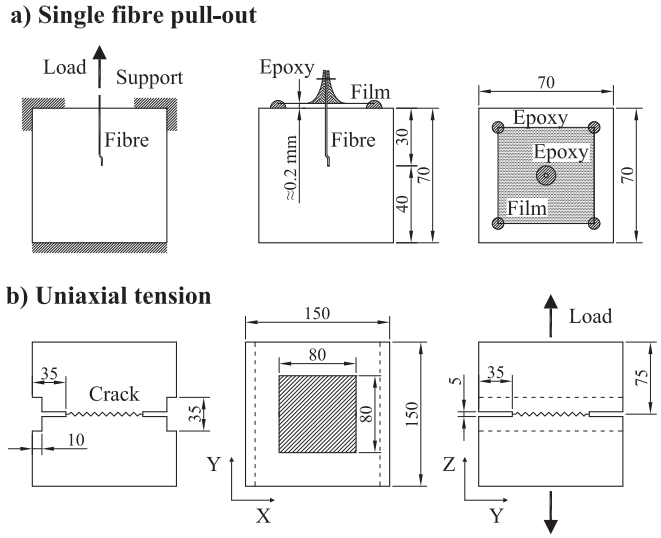

Fig. 2. Description of test specimens: a) single-fibre pull-out specimen and exposure configuration, after [6]; and b) uniaxial tension specimen, after [5].

three extensometers, hereafter referred to as "slip". The final filtered data for each sample (i.e. a group of specimens) was fitted by a lognormal probability distribution and presented as the mean value of the load at each CMOD value with its upper and lower confidence bounds at a 90% confidence interval (CI).

2.1.3. Exposure tests

The exposure environments comprised wet-dry cycles (i.e. two days each) of cracked specimens (uniaxial tension) and partially pulled specimens (single-fibre pull-out) to a saltwater (7 wt-% NaCl) solution. The exposure setups are described in [5,6], see Fig. 1c. The uniaxial-tension samples were exposed pre-cracked at 0.3 mm, holding the crack open by means of 4 polyethylene inserts in the notch. The single-fibre pull-out specimens were partially pulled-out up to a slip value of 0.15 mm, corresponding to the beginning of the mechanical anchorage phase of the fibre hook. The crack was simulated by covering the upper surface of the specimen with a rigid plastic film, leaving a separation between the film and the concrete surface of approx. 0.3 ± 0.1 mm, and coating the rest of the steel surface with epoxy.

2.2. Numerical model

The numerical model presented in this paper was constructed as a semi-empirical model, combining plasticity theory and a probabilistic implementation of the fibre bundle model. The single fibre pull-out was modelled based on plasticity theory, discretised as two spring-slider systems connected in series, which replicated the data from single-sided single-fibre pull-out tests and upscaled it to a double-sided pull-out. The fibre pull-out model was upscaled to the composite level by means of the fibre bundle model. A probabilistic approach to the fibre bundle model was used to generate synthetic data at the composite scale, based on the single-fibre pull-out experiments.

2.2.1. Single-sided fibre pull-out model

The data from the single-sided single-fibre pull-out tests was fitted to a multi-linear elastic-plastic model, discretised as a linear elastic spring element (elastic law) with a stiffness "k_a" connected in series to a frictional block element with a variable stiffness "r_a" (residual law), following a similar approach to [22], see Fig. 3a. The constitutive law of the elastic-plastic force-slip relation $F(\gamma, u)$ is given by Eq. (1):

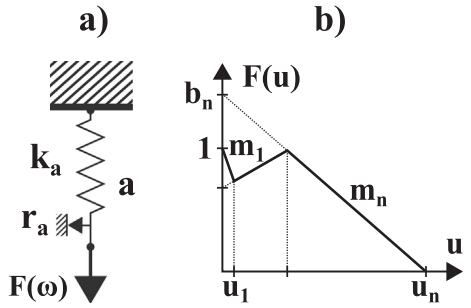

Fig. 3. Single-fibre single-sided pull-out model: a) equivalent spring-slider model system; and b) definition of parameters of the n-linear force-slip (F-u) relationship of the friction-slider.

$$F(\gamma,u)=\begin{cases} F(\gamma)=\int_0^l G\gamma 2\pi r dl & (I)\ elastic\ term \\ F_\varepsilon(u)=\tau(u)F_\tau & (II)\ residual\ term \end{cases} \quad (1)$$

where $F(\gamma)$ describes the force-deformation relationship of the linear-elastic term (I), being G the effective shear modulus of the fibre-matrix bond, γ is the shear strain, and l is the embedded length; $F_u(u)$ describes the force-slip relationship of the residual term (II), whose shape is defined by a function $\tau(u)$ of the pull-out displacement u normalised to the limit shear force F_τ of the elastic law. In this case, the residual term of the model (II) is described by a multi-linear law $F(u)$, written as:

$$F(u)=b_i-a_iu=\begin{cases} b_1-m_1u, & 0\le u<u_1 \\ b_i-m_iu, & u_{i-1}\le u<u_i \end{cases} \quad (2)$$

where $b_1\equiv 1$, m_1 and m_i are the slopes of the segments, and the limits u_1 and u_i are given by the intersection of the adjacent line segments, and the intersection of the second line segment and the abscissa, respectively, as shown in Fig. 3b.

The constitutive law of the fibres, in this example a linear elastic law (I) and a 5-linear residual law (II) was considered, were calibrated to experimental data by least-square minimisation, as shown in Fig. 4.

The terms G, γ of the elastic term $F(\gamma)$ of the function and the limit of proportionality F_τ were calibrated to the initial branch of the force-slip diagram of the experiments. The fit was done assuming that the end of linear-elastic branch of the force-slip diagram corresponds to the coordinate $F(\gamma)$ where the deviation of the local stiffness G is larger than 10% of the average stiffness.

For example, the terms a_i and b_i of the 5-linear residual law $F(u)$ were calibrated in Fig. 4 to: i) the peak debonding force, ii) the full debonding, iii) the ascending branch, iv) the maximum pull-out force, and v) the end of the tail at 4 mm.

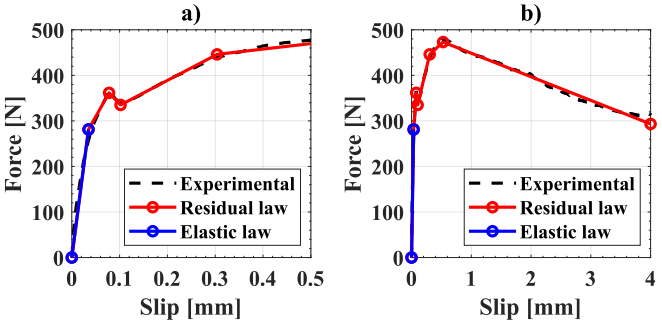

Fig. 4. Example of single-sided elastic-plastic law, compared to experimental data: a) up to slip values of 0.5 mm, b) up to a slip value of 4 mm.

Table 2
Load rates for uniaxial tension and fibre pull-out tests.

		Uniaxial tension		Fibre pull-out	
Step		Displacement rate (mm/min)	Range (kN)/(mm)	Displacement rate (mm/min)	Range (N)/(mm)
1	Preload	0.10	0–10 kN	0.10	0–10 N
2	Initial	0.05	0–0.1 mm	0.05	0–0.1 mm
3	Residual	0.20	0.1–5 mm	0.25	0.1–5.5 mm
4	Finish	1.00	>5 mm	1.00	5.5–>35 mm

2.2.2. Double-sided fibre pull-out model

The single-sided fibre pull-out model was upscaled to a double-sided case by calculating the equivalent Force-Crack Opening Displacement (henceforth "Force-COD") relation of the system's traction-opening law $F_c(\gamma,\omega)$. The system considered consists of two sets of the serial spring-slider model described above connected in series, see Fig. 5. So that the following relation is satisfied:

$$F_{ab}(\gamma,\omega) = F_a(\gamma,u) = F_b(\gamma,u) \tag{3}$$

where $F_a(\gamma,u)$ and $F_b(\gamma,u)$ are the constitutive laws of each of the sides. So that the elastic term of the traction-opening law $F_{ab}(\gamma)$ is the equivalent stiffness of both springs in series and the residual term $F_{ab}(\omega)$ is the combination of the residual term of the two models $F_a(u)$ and $F_b(u)$.

The equivalent elastic stiffness (elastic term), e.g. k_{ab} in Fig. 5, is calculated analytically as the equivalent spring constant from Hooke's law, see Eq. (4). And the slopes of the residual term for the frictional block, e.g. r^{ij}_{ab} in Fig. 5, are calculated stepwise considering the frictional component as a non-reversible process, according to Eq. (5).

$$k_{ab} = k_a k_b/(k_a + k_b) \tag{4}$$

$$r^{ij}_{ab} = r^i_a r^j_b/(r^i_a + r^j_b) \tag{5}$$

where k_a and k_b are the stiffness of the two fibre laws, according to Eq. (2); and the terms r^i_a and r^j_b correspond to the slopes of the ith and jth segments of the residual term for the two fibre laws.

For example, the resulting constitutive law $F_c(\gamma,\omega)$ of the combination of the example above with a second fibre, results in a linear-elastic law (I) and an 8-linear residual law (II), according to Eq. (1), since the last two branches of the tail in the first law were not activated in this case, see Fig. 6.

2.2.3. Pull-out parameters

The double-sided pull-out law described above by the model is based on the semi-empirical law described in (Eq. (1)), which is based on a limited number of experiments. Therefore, extrapolation of the model to general conditions at the composite scale is done by means of corrections of the force-slip law. These comprise: i) the fibre orientation, ii) the embedment length, iii) the load bearing capacity of the fibre and matrix and iv) variations in the fibre-matrix bond-strength.

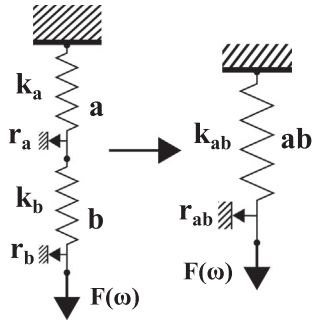

Fig. 5. Two-sided mechanical model, showing the equivalent system (ab) of two serial spring-slider model in series (a and b).

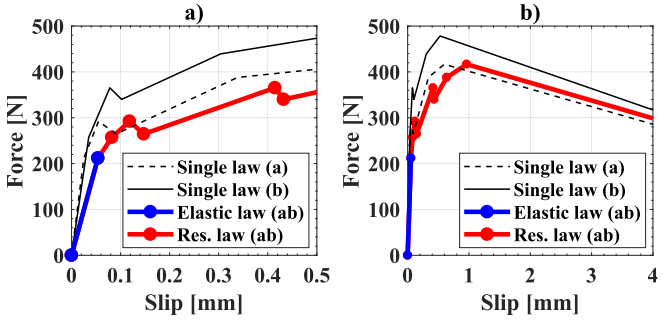

Fig. 6. Example of single-sided to double-sided law: a) up to slip values of 0.5 mm, b) up to slip values of 4 mm.

2.2.3.1. Fibre orientation. The variation of the force-slip relation due to the orientation of the fibre was accounted for by the decomposition of the force $F(\gamma,\omega)$ and slip (γ,ω) vectors into a 2-dimensional Cartesian components (i.e. disregarding the orientation of the fibre within the crack plane): $F_{xy}(\gamma,\omega)$ and $\left(\gamma_{xy},\omega_{xy}\right)$, according to:

$$F_x(\gamma,\omega) = \sin\alpha F_{ab}(\gamma,\omega), \quad F_y(\gamma,\omega) = \cos\alpha F_{ab}(\gamma,\omega) \tag{6}$$

$$(\gamma_x,\omega_x) = \sin\alpha(\gamma,\omega), \quad \left(\gamma_y,\omega_y\right) = \cos\alpha(\gamma,\omega) \tag{7}$$

where α is the deviation of the angle perpendicular to the crack plane, and the components x and y represent the horizontal and vertical components of the vectors, respectively (Fig. 7).

This approach disregards additional variations in the force-slip relation of inclined fibres, attributed to localised deformations at the fibre-crack intersection in [36]. Being the authors are aware of the additional bond-slip mechanisms affecting inclined fibres, i.e. the "snubbing effect" as modelled in [10,12,18,36]; those were not included due to limitations of current test-methods describing those in deformed fibres [37].

2.2.3.2. Embedment length. The shear bond strength $F_\tau(\gamma)$ of the fibre during the debonding phase was expected to vary linearly with the embedment length of the fibre e, as discussed in [38,39]. Therefore, the equivalent shear bond strength term $F'_\tau(\gamma)$ described in the force-slip relation (Eq. (1)) is re-calculated as follows:

$$F'_\tau(\gamma) = \frac{e}{e_0} F_\tau(\gamma) \tag{8}$$

where e is the embedment length of the fibre, and $F_\tau(\gamma)$ is the shear bond strength of the law measured at an embedment e_0, which is equal to 30 mm in this study.

Variations of the frictional bond strength in the residual term of the constitutive law (Eq. (1)) due to the embedment length are neglected in this model, assuming that the contribution of the straight part of the fibre to the frictional forces is trivial compared to the mechanical anchorage at the slip values investigated (e.g. up to 4 mm). Whereas, semi-analytical models can be used to describe such variation [10].

2.2.3.3. The load-bearing capacity of the fibre and the matrix. The pull-out process of the fibre relies on the ultimate strength of the fibre and the matrix transferring the forces to the adjacent composite. Exceeding these leads to: i) tensile failure of the steel fibre (i.e. fibre rupture), or ii) fracture of the matrix where the fibre is embedded (i.e. matrix spalling). This model accounts for these failure types by means of a simplification, where the model assumes that the resulting force-COD relation $F'_{ab}(\gamma,\omega)$ of the fibre remains unaltered, unless the equivalent pull-out force $F_{ab}(\gamma,\omega)$ at the slip value i exceeds either of the load-bearing capacity of the steel or the matrix, as follows:

$$F'_{ab}(i) = \begin{cases} F_{ab}(i), & \text{if } F_{ab}(i) < F^s_t \wedge F^m_t \\ 0, & \text{if } F_{ab}(i) \geq F^s_t \wedge F^m_t \end{cases} \tag{9}$$

where F^s_t is the load bearing capacity of the steel fibre and f^c_t is the equivalent load-bearing capacity of the matrix surrounding the fibre. The load bearing capacity of the steel fibre F^s_t was calculated as the tensile capacity of a circular cross-section in tension:

$$F^s_t = K_c A^s_k f^s_{tk} \tag{10}$$

where f^s_{tk} is the characteristic tensile strength of the steel fibre and $(K_c A^s_k)$ represents the effective cross-section of the fibre; which is calculated as the product of the characteristic cross-section A^s_k and a damage coefficient K_c (that satisfies $0 < K_c < 1$) that accounts for e.g. corrosion damage. The load bearing capacity of the matrix surrounding the fibre F^m_t was calculated based on the approach described in [12], as:

$$F^m_t = \pi e^2 \tan\Phi f^c_t \tag{11}$$

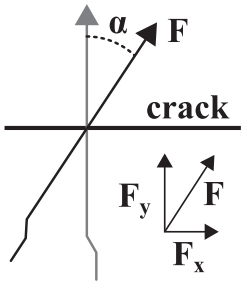

Fig. 7. Inclination of the fibre relative to the crack plane.

where f_t^c is the average tensile strength of the matrix; and ($\pi e^2 tan\Phi$) represents the lateral surface of a right cone with a height equal to the embedment length e of the fibre and a radius equal to ($e \tan\Phi$), where Φ is the internal friction angle of the matrix, assumed as 45° in this paper.

2.2.3.4. Variations in the fibre-matrix bond-strength. Variations in the fibre-matrix bond strength, e.g. increases due to hydration of the matrix or else deterioration due to weakening of the matrix, have been accounted for in the model as a variation of the maximum pull-out force $F(u)_{max}$, which is calculated as:

$$F(u)_{max} = k_h F(u)^0_{max} \tag{12}$$

where $F(u)^0_{max}$ is the maximum pull-out force of the original law for the single-side fibre and k_h is a coefficient that can be experimentally determined based on single-fibre pull-out tests.

2.2.4. Fibre composite model

The single-fibre model was upscaled to the composite level by means of the fibre bundle model approach [40], where n fibres are combined into a single composite; calculated as a system of "n" spring-slider elements (Eq. (3)) aligned in parallel connected to a perfectly rigid body, as shown in Fig. 8.

The physical model assumes that there is a single crack with a uniform COD (ω); and that the matrix adjacent to the crack is an infinitely stiff body, only subject to a uniform COD ω, longitudinal to the spring-slider elements.

The equivalent total force transferred by the system of fibres $F'(\gamma,\omega)$ depending of the number of fibres crossing the crack is calculated according to the principle of superposition, as follows:

$$F'(\gamma,\omega) = \sum_n F'_y\left(\gamma_y,\omega_y\right)_n \tag{13}$$

where n is the number of spring-slider elements and $F_y(\gamma,\omega)_n$ is the traction-crack opening relationship of the n-element, calculated according to Eq. (3). The resulting equivalent system may be represented once again, as a spring-slider element with an equivalent stiffness in the elastic term and a higher order of non-linearity in the residual term.

An example of the average force transferred by a system of two spring-slider elements connected in parallel is given in Fig. 9. The model assumes that the horizontal component of the force in the individual fibres counteract each other and maintain equilibrium of forces and moments in the cross-section, thus neglecting them.

Finally, the equivalent stress-COD relation of the composite $\sigma(\varepsilon,\omega)$ was calculated by superposition of the equivalent stress-COD of the fibre bundle model and the corresponding stress-COD relation of the matrix, assuming compliant strains and COD values (ε,ω) within the composite:

$$\sigma(\varepsilon,\omega) = (1-A_f)\sigma_m(\varepsilon,\omega) + \frac{1}{A}F'(\gamma,\omega) \tag{14}$$

where A is the total crack area, A_f is the fraction of the total area covered by the fibres, $F'(\gamma,\omega)$ is the equivalent force-COD relation of the bundle of fibres and $\sigma_m(\varepsilon,\omega)$ is the stress-COD relation of the plain matrix, calculated based on the approach described in Eq. (1), as follows:

$$\sigma_m(\varepsilon,\omega) = \begin{cases} \sigma(\varepsilon) = E\varepsilon & (I) elastic\ term \\ \sigma_\omega(\omega) = g(\omega) f_t^c & (II) residual\ term \end{cases} \tag{15}$$

where $\sigma(\varepsilon)$ is the equivalent stress-strain relation under the elastic term (I), E is the elastic modulus of the uncracked concrete and ε is the equivalent tensile strain at the crack plane; $\sigma_\omega(\omega)$ is the equivalent stress-COD relation of the residual term (II), described by the stress-COD relation $g(\omega)$, which is normalised to the limit tensile strength f_t^c of the elastic term:

$$g(\omega) = b_1 - m_i\omega = \begin{cases} b_1 - m_1\omega, & if\ 0 \le \omega < \omega_1 \\ b_i - m_i\omega, & if\ \omega_{i-1} \le \omega < \omega_i \end{cases} \tag{16}$$

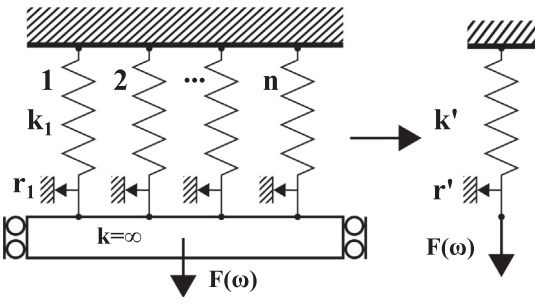

Fig. 8. Fibre bundle model, with n spring-slider elements.

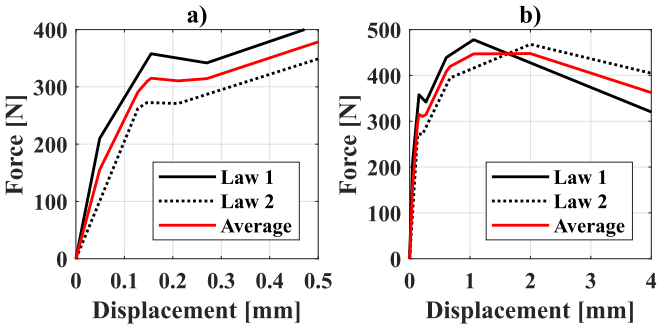

Fig. 9. Example of fibre bundle model, combination of two laws into an average law: a) up to displacement values of 0.5 mm, b) up to displacement values of 4 mm.

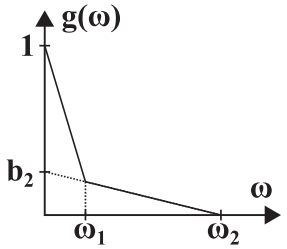

Fig. 10. Bilinear Stress-COD relation for plain concrete in uniaxial tension.

where $b_i \equiv 1$, m_1 and m_i are the slopes of the segments, and the limits ω_1 and ω_i are given by the intersection of adjacent line segments, and the intersection of the second line segment and the abscissa, e.g. see Fig. 10.

2.2.5. Probabilistic model

The model described above was used to generate random synthetic stress-COD relations for a steel-fibre reinforced composite, utilising the Monte-Carlo method [41]. The main parameters describing the performance of the composite material were described as probability distributions, approximated based on experimental results and former studies.

The fibre pull-out laws were calculated from single-fibre pull-out test experiments and were adjusted to a two-dimensional mixture-Gaussian distribution, which accounted for self-correlation at the force-slip dimensions but assumed that the pull-out parameters were uncorrelated. The example shown in Fig. 11 shows the probability distribution functions of a penta-linear residual law, where the first four terms are two-dimensional Gaussian distributions, and the last term is a one-dimensional normal distribution function, at a slip value equal to 4 mm.

The parameters involved in the model described above where also modelled as discrete distributions that were assumed uncorrelated and normally distributed. The distributions considered for the examples presented in the paper are given in Table 3. The distributions chosen were truncated to an upper and lower limit to produce random values within a reasonable range.

The synthetic stress-COD data was generated with 50 runs, which were fitted by a lognormal distribution and presented as the mean value with its upper and lower confidence bounds at a 90% CI, following the procedure described in Section 2.1.2 for the experimental data, e.g. see Fig. 12.

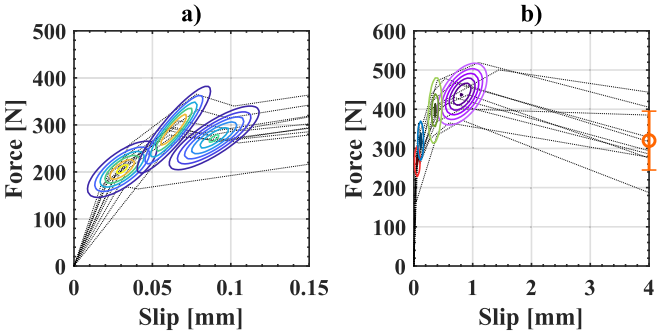

Fig. 11. Example of probability distributions for fibre law, for a penta-linear residual law, at: a) a slip range of 0–0.15 mm; and b) a slip range of 0–4 mm.

Table 3
Distributions assumed for model variables and limits (truncation).

Parameter		Units	Distribution	Limits	
				Lower	Upper
1	Fibre content	$1/m^2$	Normal	-inf	+inf
2	Fibre orientation	°	Normal	0	90
3	Embedment length	mm	Normal	0	30
4	Fibre bond strength	–	Normal	0	+inf
5	Matrix strength	MPa	Normal	0	+inf
6	Corrosion damage *	–	Mixture normal (4)	0	1

* Gaussian mixture distribution parameter weights (p) vary depending on the amount of corrosion damage simulated, e.g. p = (0.5, 0.2, 0.2, 0.1).

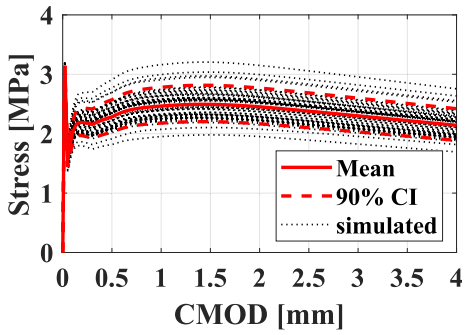

Fig. 12. Example of synthetic stress-CMOD data, for 50 runs and calculation of mean value and 90% CI for lognormal distribution.

2.2.6. Model cases

The model was compared to experimental data by means of four examples, where a set of 50 synthetic laws on an 80 mm square section was generated based on the model parameters given in Table 4. The fibre pull-out laws used for each case were calculated from the experimental data provided in [6]. The matrix strength law was described by the tensile strength of the concrete and a tri-linear residual law, where stress values were allowed to vary but strain and opening values were kept constant, being: 0.005, 0.03, 0.3 and 0.5 mm for the elastic deformation and the three residual terms respectively (being stress in the last term zero). Specific values for the stress levels are given in Table 4.

3. Results

The results described in this section are separated into experimental and model results. Experimental results are given at the single-fibre scale and at the composite scale. The numerical results are given at the composite scale, as a stress-COD law.

3.1. Experimental results

The results of the single-fibre pull-out tests are presented in Fig. 13 for unexposed reference specimens (Ref) and exposed pre-pulled specimens (Exp), after the experimental data presented in [6]. The results show a moderate increase in the pull-out forces at small slip values up to the maximum pull-out force (e.g. at approx. 1 mm slip) of the exposed samples (Exp) compared to their corresponding reference sample (Ref). While the pull-out forces at the end of the tail are similar for the exposed (Exp) and reference (Ref) samples. None of the single-hooked fibres rupture during pull-out, despite of corrosion damage; while 50% of the double-hooked fibres exposed to wet-dry cycles (Exp) ruptured during the pull-out process.

The results of the uniaxial tension tests are presented in Fig. 14 for unexposed reference specimens (Ref) and exposed pre-pulled specimens (Exp), after the experimental data presented in [5]. The results show a moderate increase in the residual tensile stress of the exposed samples (Exp) for CMOD values in the range 0.5–1.5 mm, relative to the uncracked reference samples (Ref). There is a progressive decrease of the residual stress of the exposed samples (Exp) at CMOD values larger than approx. 1.5 mm, which corresponds to rupture of the fibres bridging the cracks. The decrease in the residual strength is gradual in the case of the single-hooked fibre (Fig. 14a) and much sharper in the case of the double-hooked fibre (Fig. 14b).

3.2. Numerical results

The numerical results for the stress-COD response of the composite for the two fibre types modelled under uncracked and exposed cracked conditions are shown in Fig. 15. The synthetic data presented shows similar trends to the ones described in Fig. 14 for the reference and the exposed cracked composite; while discrepancies between the experimental and the synthetic data are noticeable.

Comparison of the synthetic stress-COD law of the uncracked reference (Ref) to the stress-CMOD results of the experimental data, shows that the simulated data (Fig. 15) does not fully

Table 4
Model parameters for probability distributions.

Parameter		Units	Mean		Sd		p	
			Ref	Exp	Ref	Exp	Ref	Exp
1	Fibre content	$1/m^2$	10,000		500			
2	Fibre orientation	deg	45		15			
3	Embedment length	mm	15		5			
4	Fibre bond strength	–	1	1.2	0.1	0.2		
5	Matrix strength law *1	MPa (–)	2.5		0.25			
			(1.1)		0.1			
			(0.2)		0.02			
6	Corrosion damage *2	–	1		0.01		0.4	1
			0.95		0.05		0.3	0
			0.7		0.1		0.2	0
			0.3		0.1		0.1	0

Notes:
*1 Strength law for the matrix strength component is given as the elastic term as a tensile stress of the concrete at the limit of proportionality and the residual law as a proportion of the tensile strength "()". Values correspond to displacements: 0.005, 0.03 and 0.3 mm.
*2 Gaussian mixture distribution parameter weights (p) described for each exposure based on results presented in [5].

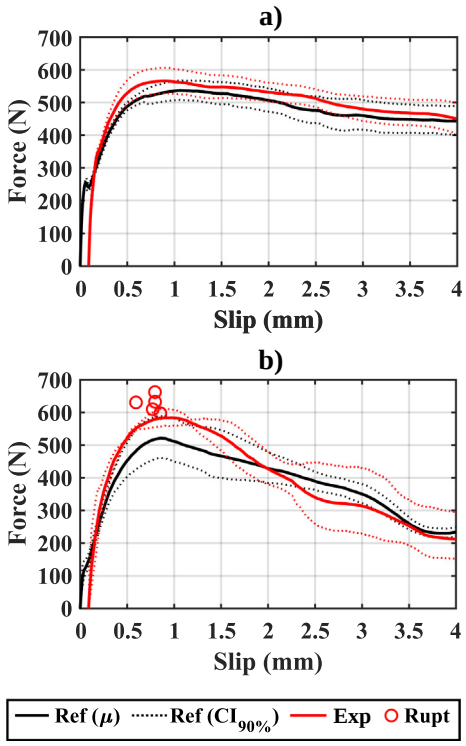

Fig. 13. Single fibre pull-out tests, load-slip plot for samples: a) Single-hooked fibre, b) Double-hooked fibre. Full lines represent the log-mean value (μ) of the sample and dotted lines represent the upper- and lower- confidence bounds at 90% CI, for lognormal distribution. Sample names correspond to code names described in: (Ref) Un-pulled reference specimens, (Exp) Pre-pulled exposed specimens. The maximum force of the specimens that ruptured during the pull-out test were marked with 'o' in the plots. After [6].

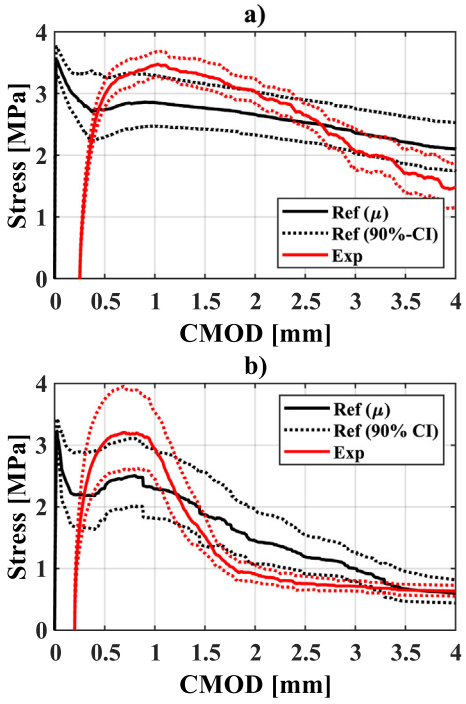

Fig. 14. Uniaxial tension tests, stress-CMOD plot for samples: a) Single-hooked fibre, b) Double-hooked fibre. Full lines represent the log-mean value (μ) of the sample and dotted lines represent the upper- and lower-confidence bounds at 90% CI, for lognormal distribution. Sample names correspond to code names described in: (Ref) Uncracked reference specimens, (Exp) Cracked exposed specimens. After [5].

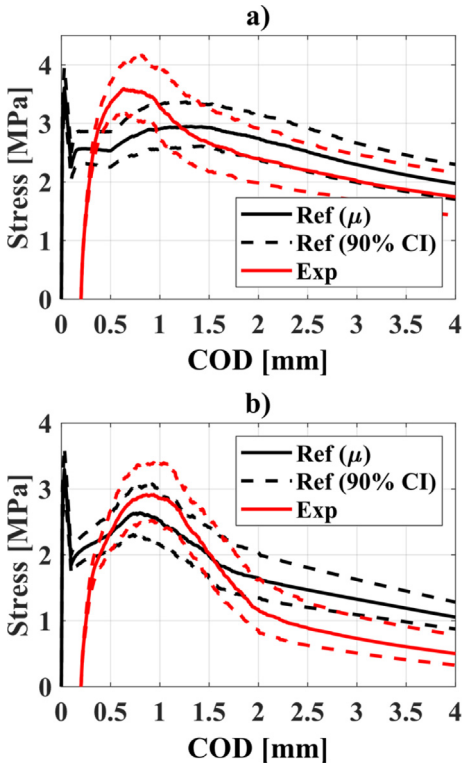

Fig. 15. Modelled stress-COD response for samples: a) Single-hooked fibre, b) Double-hooked fibre. Full lines represent the log-mean value (μ) of the sample and dotted lines represent the upper- and lower- confidence bounds at 90% CI, for lognormal distribution. Sample names correspond to code names: (Ref) Uncracked reference specimens, (Exp) Cracked exposed specimens.

describe the smoother decrease in stress at the transition between the uncracked and cracked state, observed in the experimental data at CMOD up to 0.5 mm (Fig. 14). Correspondingly, the slope of the reloading branch of the stress-COD curve of the synthetic data corresponding to the exposed samples (Exp) appears to be smaller compared to the experimental data.

Discrepancies were also observed in the tail of the stress-CMOD curve, since the model was not fully capable of capturing the progressive rupture of the fibres during the crack opening observed e.g. in Fig. 14a. The decrease in the stress due to fibre rupture is modelled instead as a sharper process that occurs at the maximum pull-out forces, see Fig. 15, which is in better agreement with the data presented in Fig. 14b.

4. Discussion

The results presented above showed that there is an increase in the pull-out forces of partially pulled fibres after exposure to wet-dry cycles at slip values below 1 mm; which corresponds well to the increase of the tensile stress observed in uniaxial tensile samples within the CMOD range 0.5–1.5 mm. Whereas, both an excessive increase in the pull-out forces transferred by the fibres and a reduction of the fibres' cross-section due to corrosion may lead to a decrease in the residual tensile strength of the composite at CMOD values larger than 1.5–2 mm.

4.1. Model validation and limitations

Results from the numerical model shown in Fig. 15 are generally in agreement with the experimental observations presented in Fig. 14. Both sets of data showed corresponding increase after

exposure in the maximum residual tensile stresses transferred at the crack for CMOD values in the range 0.5–1.5 mm, followed by a decrease in the stresses transferred up to 4 mm CMOD. However, the predicted behaviour at the composite scale still shows some discrepancy with the experimental data; which may be explained by current limitations of the model when describing the average stress transferred through the crack at small deformations and the occurrence of fibre rupture.

First, the results produced by the model showed a sharper transition between the uncracked and the cracked composite states compared to the experimental data. Such discrepancy is expected to be dominated by limitations in the experimental methods used and a lack of understanding of the pull-out process of inclined steel fibres in concrete.

i) Corresponding experiments in uniaxial tension specimens presented branching, multiple cracking, and substantial rotation as the crack formed progressively over the cross-section [42,43]; which were expected to smooth sudden drops in the tensile forces transferred through the crack, as also discussed for similar SFRC specimens in [44]. Yet, a sudden drop in the stiffness of the composite was still observed after cracking, leading to a rapid increase of the CMOD over time during the first 0.2 mm of opening. Otherwise, the model was capable of describing the drop of stiffness after cracking; since it describes a single and uniform crack, perpendicular to the applied forces and opening monotonously.
ii) The contribution of fibre inclination to the pull-out forces transferred by the fibres is currently accounted for in the model as a geometrical transformation of the force and displacement vectors; which is a limited simplification of the actual pull-out behaviour of the fibre, otherwise subject to large lateral forces, additional yielding of the steel and cracking of the matrix around the fibre [36,45]. There is discrepancy within literature regarding the impact of fibre inclination in the force-slip behaviour of steel fibres, particularly at low slip values [10,36,37,45], since experiments cannot reproduce the actual lateral stiffness at the composite scale. Inclined fibres statistically comprise the vast majority of the fibres bridging cracks in specimens with uniformly distributed fibres [46].

Second, the stress-CMOD data generated by the model showed fibre rupture occurring at the ascending branch and maximum stress region of the uniaxial law, at CMOD < 1.5 mm. Whereas, the experimental data showed that fibre rupture may also occur at much larger CMOD values, e.g. up to CMOD = 4 mm in Fig. 14a.

This discrepancy corresponds to the still limited understanding of the fibre rupture process; which in this case was modelled as a deterministic process, based on the characteristic yield strength of the material. Available data has shown that fibres may not necessarily rupture at the highest pull-out force (e.g. due to loss of tensile capacity), but can also rupture at the descending branch of the pull-out curve, as reported in [6,47]. Such failure corresponded to the rupture observed at the deformed parts of the hooked-end fibres, which are expected to perform above the yielding point to allow pull-out. Rupture under such conditions could be simulated by more advanced failure models that account for the accumulated damage during the pull-out process, based on e.g. cumulative damage theory [48]; yet additional data is needed to better understand the failure process.

Additional development of the pull-out models utilised in this paper may be based on alternative approaches, critically discussed in [8,9]; in order to further describe the role of fibre inclination [10,16–19] or failure of the matrix and fibre [12,14]. The simulated results at the composite scale (e.g. stress-COD response) may be then discretised and implemented as a non-linear traction-separation (e.g. multilinear) relation in numerical solutions, for example based on: fictitious crack propagation models [22], damage plasticity models [49] or cohesive models in FEM formulations [50].

4.2. Model capabilities

In spite of the abovementioned limitations and discrepancy with the experimental data, the modelling approach described in this paper facilitates the evaluation of the combined effects on the mechanical performance at the composite scale of a number of parameters affecting the pull-out performance of steel fibres in concrete, among them: the fibre content, fibre orientation, the fibre dimensions, fibre damage and the fibre matrix bond strength. Within these, the impact of the fibre damage and alteration of the fibre matrix bond on the residual toughness of cracked SFRC subject to corrosive environments is currently in focus [1].

Results from a parametric study are presented in Fig. 16 for the two types of fibres investigated under exposed conditions on a cross-section of 1 m^2, where the parameters described in Table 4 were fixed and two parameters were swept: i) the extent of corrosion damage and ii) the increase of the maximum pull-out force. The plot shows the variation of the composite toughness (i.e. described as the integration of the area below the stress-CMOD curve in the CMOD range 0.3–4 mm) relative to the toughness value at the coordinates (1,0), plotted as "toughness ratio" in the z-axis of the plot. The predicted ratio of fibres rupturing in the

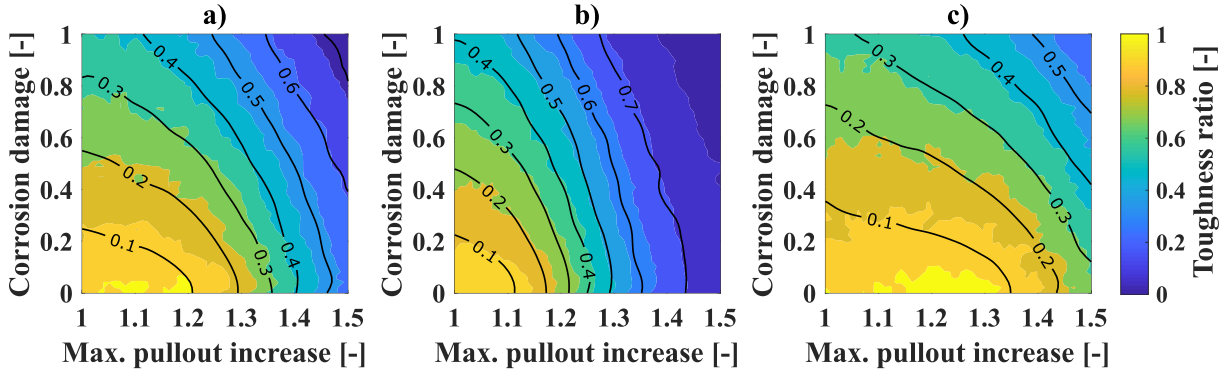

Fig. 16. Variation of the mean toughness (i.e. work) with increase in the maximum pull-out force and corrosion damage, relative to value at coordinates [10] and ratio of fibres rupturing for: a) Single-hooked fibre in cracked concrete, b) Double-hooked fibre in cracked concrete, and c) Single-hooked fibre in cracked concrete assuming a characteristic steel strength of 2200 MPa. The toughness ratio is plotted as a coloured filled contour and the ratio of fibres rupturing is plotted as black contours.

composite (in the range 0–1) is also plotted as an overlay contour in black.

The data presented in Fig. 16 highlights the importance of understanding the evolution of the fibre-matrix bond strength over time due to e.g. exposure to wet-dry cycles. Results are calculated for three scenarios: i) the single hooked fibre of the experimental study, see Fig. 16a, ii) the double-hooked fibre of the experimental study, see Fig. 16b, and iii) the single hooked fibre with a characteristic strength of 2200 MPa, see Fig. 16c. Results indicate that variations in the type and strength of the steel fibre may result in a limited decrease of the residual strength of the composite despite that e.g. 20% of the fibres would corrode (Fig. 16a), or else a rapid decrease in the toughness of the cracked composite over time despite of the number of fibres corroding (Fig. 16b). Extrapolation of the data to a higher tensile strength of the steel would yield a larger allowance for increase to the bond-strength without affecting the toughness of the composite.

These predictions correspond well to observations at the composite scale [5] and at the single-fibre scale [6]; which suggest that fibre corrosion does not necessarily play a dominant role in the mechanical performance of cracked SFRC, provided that: i) an adequate steel fibre (e.g. fibre strength and bond strength) is selected for the application, ii) increases in the fibre-matrix bond strength over time are foreseen at the design phase, and iii) the extent of fibre corrosion through the total cross-section of the crack is moderate, such as observed in cracks below 0.3 mm for cross-sections larger than 100 mm subject to wet-dry cycles [5].

Overall, this discussion supports the argumentation given in [1], which suggested that a share of the deterioration reported for cracked SFRC exposed to chlorides and carbon dioxide in former studies could correspond to an increase in the fibre-matrix bond strength over time, rather than solely corrosion damage; as experimentally also presented in [51,52].

5. Conclusions

This paper investigated the tensile performance of uncracked and cracked SFRC at the single-fibre and composite scale. A semi-empirical multiscale modelling framework was developed to describe the stress-opening behaviour of cracked and uncracked SFRC at the composite scale, from the force-slip behaviour of single steel fibres calibrated to experimental data.

The modelling framework developed was based a discretisation of the single-fibre pull-out behaviour based on a serial spring-slider model with a multilinear plastic law. Results at the single-fibre level were upscaled to the composite level based on a probabilistic approach to Daniels model in combination with the Monte-Carlo method. The model was used to generate sets of synthetic stress-COD data, based on probability distribution functions of experimentally measured input model parameters.

Results confirmed that measured increases of the tensile stress observed in cracked uniaxial tensile samples exposed to wet-dry cycles corresponded to an increase of the fibre-matrix bond strength of the fibres bridging the crack.

Decrease in the residual tensile strength of cracked SFRC at large crack openings may correspond to both an excessive increase of the fibre-matrix bond strength and to the reduction of the fibres' cross-section due to corrosion. The model was capable of describing the non-linear relationship between the aforementioned parameters and variations in the toughness of cracked SFRC.

The results presented in this paper support recent hypotheses, which suggest that corrosion damage of the steel fibres may not be the only mechanism responsible for the deterioration reported in cracked SFRC exposed to chlorides and carbon dioxide in former studies. Unpredicted increase of the fibre-matrix bond strength over time and exposure due to various alterations of the matrix around the fibre may lead to either an increase of the toughness or a dramatic reduction of it due to fibre rupture.

Modelled results corresponded well to the experimental results, showing comparable trends. Nonetheless, there were limitations in the model regarding the description of the fibre rupture process and the pull-out behaviour of inclined fibres. Further work focusing on a better understanding of the fibre pull-out process of hooked-end fibres in concrete is needed to improve the proposed modelling approach.

CRediT authorship contribution statement

Victor Marcos-Meson: Conceptualization, Methodology, Software, Validation, Formal analysis, Investigation, Writing - original draft, Writing - review & editing, Visualization, Project administration. **Gregor Fischer:** Conceptualization, Writing - review & editing, Supervision, Funding acquisition. **Anders Solgaard:** Conceptualization, Writing - review & editing, Supervision, Funding acquisition. **Carola Edvardsen:** Conceptualization, Writing - review & editing, Supervision, Funding acquisition. **Alexander Michel:** Conceptualization, Writing - review & editing, Supervision, Project administration, Funding acquisition.

Declaration of Competing Interest

The authors declare that they have no known competing financial interests or personal relationships that could have appeared to influence the work reported in this paper.

Acknowledgements

The first author would like to express his gratitude to: CowiFonden, InnovationsFonden, the German association of steel fibre producers (VDS), VejDirektoratet and Mapei-Denmark, for supporting this project; and Dr. Torben Lund Skovhus for his contribution to supervision during this project.

Appendix A. Supplementary data

Supplementary data to this article can be found online at https://doi.org/10.1016/j.conbuildmat.2019.117847.

References

[1] V. Marcos-Meson, A. Michel, A. Solgaard, G. Fischer, C. Edvardsen, T.L. Skovhus, Corrosion resistance of steel fibre reinforced concrete – a literature review, Cem. Concr. Res. 103 (2018) 1–20, https://doi.org/10.1016/j.cemconres.2017.05.016.
[2] P.S. Mangat, K. Gurusamy, Permissible crack widths in steel fibre reinforced marine concrete, Mater. Struct. 20 (1987) 338–347, https://doi.org/10.1007/BF02472580.
[3] R. Roque, N. Kim, B. Kim, G. Lopp, Durability of Fiber-Reinforced Concrete in Florida Environments, Florida, USA, 2009.
[4] E.S. Bernard, Effect of exposure on post-crack performance of FRC for tunnel segments, in: I. Vrkljan, Z. Dekovic, M. Dobrilovic, J. Likar, P. Miscevic (Eds.), SEE TunnelPromoting Tunneling SEE Reg. – ITA WTC 2015, ITA-AITES, Dubrovnik, Croatia, 2015, p. 13.
[5] V. Marcos-Meson, G. Fischer, C. Edvardsen, A. Solgaard, A. Michel, Mechanical performance of steel fibre reinforced concrete exposed to chlorides and carbon dioxide: results after one year (Unpublished), J. Sustain. Cem. Mater. (2018).
[6] V. Marcos-Meson, G. Fischer, C. Edvardsen, A. Solgaard, A. Michel, Pull-out behaviour of hooked-end steel fibres in cracked concrete exposed to wet-dry cycles of chlorides and carbon dioxide – mechanical performance (In press), Constr. Build. Mater. (2019).
[7] C. Frazão, J. Barros, A. Camões, A.C. Alves, L. Rocha, Corrosion effects on pullout behavior of hooked steel fibers in self-compacting concrete, Cem. Concr. Res. (2015), https://doi.org/10.1016/j.cemconres.2015.09.005.
[8] F. Aslani, S. Nejadi, Bond characteristics of steel fibre reinforced self-compacting concrete, Can. J. Civ. Eng. 39 (2012) 834–848, https://doi.org/10.1139/l2012-069.

[9] T. Soetens, S. Matthys, Different methods to model the post-cracking behaviour of hooked-end steel fibre reinforced concrete, Constr. Build. Mater. 73 (2014) 458–471, https://doi.org/10.1016/j.conbuildmat.2014.09.093.
[10] T. Soetens, A. Van Gysel, S. Matthys, L. Taerwe, A semi-analytical model to predict the pull-out behaviour of inclined hooked-end steel fibres, Constr. Build. Mater. 43 (2013) 253–265, https://doi.org/10.1016/j.conbuildmat.2013.01.034.
[11] G. Chanvillard, Modeling the pullout of wire-drawn steel fibers, Cem. Concr. Res. 29 (1999) 1027–1037, https://doi.org/10.1016/S0008-8846(99)00081-2.
[12] A.P. Fantilli, P. Vallini, A cohesive interface model for the pullout of inclined steel fibers in cementitious matrixes, J. Adv. Concr. Technol. 5 (2007) 247–258, https://doi.org/10.3151/jact.5.247.
[13] E. Zile, O. Zile, Effect of the fiber geometry on the pullout response of mechanically deformed steel fibers, Cem. Concr. Res. 44 (2013) 18–24, https://doi.org/10.1016/j.cemconres.2012.10.014.
[14] K. Georgiadi-Stefanidi, E. Mistakidis, D. Pantousa, M. Zygomalas, Numerical modelling of the pull-out of hooked steel fibres from high-strength cementitious matrix, supplemented by experimental results, Constr. Build. Mater. 24 (2010) 2489–2506, https://doi.org/10.1016/j.conbuildmat.2010.06.007.
[15] F. Montero-Chacón, E. Schlangen, F. Medina, A lattice-particle approach for the simulation of fracture processes in fiber-reinforced high-performance concrete, in: VIII Int. Conf. Fract. Mech. Concr. Concr. Struct. Fram. (2013) 1249–1256. doi:10.13140/RG.2.1.3969.9362.
[16] J. Zhang, V.C. Li, Effect of inclination angle on fiber rupture load in fiber reinforced cementitious composites, Compos. Sci. Technol. 62 (2002) 775–781, https://doi.org/10.1016/S0266-3538(02)00045-3.
[17] E. Cailleux, T. Cutard, G. Bernhart, Pullout of steel fibres from a refractory castable: experiment and modelling, Mech. Mater. 37 (2005) 427–445, https://doi.org/10.1016/j.mechmat.2004.02.001.
[18] V.C. Li, Y. Wang, S. Backer, A micromechanical model of tension-softening and bridging toughening of short random fiber reinforced brittle matrix composites, J. Mech. Phys. Solids 39 (1991) 607–625, https://doi.org/10.1016/0022-5096(91)90043-N.
[19] F. Laranjeira, A. Aguado, C. Molins, Predicting the pullout response of inclined straight steel fibers, Mater. Struct. 43 (2010) 875–895, https://doi.org/10.1617/s11527-009-9553-4.
[20] J. Alwan, A. Naaman, P. Guerrero, Effect of mechanical clamping on the pull-out response of hooked steel fibers embedded in cementitious matrices, Concr. Sci. Eng. 1 (1999) 15–25. http://rilem.net/gene/main.php?base=600026&id_publication=391&id_papier=7278.
[21] I. Paegle, Characterization and modeling of fiber reinforced concrete for structural applications in beams and plates, 2015.
[22] J.F. Olesen, Fictitious crack propagation in fiber-reinforced concrete beams, J. Eng. Mech. March (2001) 272–280. doi:10.1061/(ASCE)0733-9399(2001)127:3(272).
[23] H. Tlemat, K. Pilakoutas, K. Neocleous, Modelling of SFRC using inverse finite element analysis, Mater. Struct. 39 (2006) 221–233, https://doi.org/10.1617/s11527-005-9010-y.
[24] H. Zhang, Y.J. Huang, Z.J. Yang, S.L. Xu, X.W. Chen, A discrete-continuum coupled finite element modelling approach for fibre reinforced concrete, Cem. Concr. Res. 106 (2018) 130–143, https://doi.org/10.1016/j.cemconres.2018.01.010.
[25] V.M.C.F. Cunha, J.A.O. Barros, J.M. Sena-Cruz, A finite element model with discrete embedded elements for fibre reinforced composites, Comput. Struct. 94–95 (2012) 22–33, https://doi.org/10.1016/J.COMPSTRUC.2011.12.005.
[26] F. Montero-Chacón, H. Cifuentes, F. Medina, Mesoscale characterization of fracture properties of steel fiber-reinforced concrete using a lattice-particle model, Materials (Basel) 10 (2017) 207, https://doi.org/10.3390/ma10020207.
[27] J. Kang, K. Kim, Y.M. Lim, J.E. Bolander, Modeling of fiber-reinforced cement composites: discrete representation of fiber pullout, Int. J. Solids Struct. 51 (2014) 1970–1979, https://doi.org/10.1016/j.ijsolstr.2014.02.006.
[28] M. Maalej, V.C. Li, T. Hashida, Effect of fiber rupture on tensile properties of short fiber composites, J. Eng. Mech. 121 (1995) 903–913, https://doi.org/10.1061/(asce)0733-9399(1995) 121:8(903).
[29] European Committee for Standardization (CEN), Concrete. Specification, performance, production and conformity. EN 206, European Union, 2013.
[30] M.R. Geiker, K. De Weerdt, S.F. Garzon, M.M. Jensen, B. Johannesson, A. Michel, Screening of low clinker binders, compressive strength and chloride ingress, Nord. Concr. Res. 57 (2017) 23–38.
[31] European Committee for Standardization (CEN), Eurocode 2: Design of concrete structures - Part 1-1: General rules and rules for buildings, ENV 1992-1-1:1993, European Union, 1993.
[32] European Committee for Standardization (CEN), Testing hardened concrete - Part 3: Compressive strength of test specimens, EN 12390-3 + AC:2012, European Union, 2012.
[33] European Committee for Standardization (CEN), Testing hardened concrete. Determination of secant modulus of elasticity in compression, European Union, 2013.
[34] European Committee for Standardization (CEN), Fibres for concrete - Part 1: Steel fibres - Definitions, specifications and conformity, EN 14889-1:2006, European Union, 2006. http://www.en-standard.eu/csn-en-14889-1 (accessed February 15, 2016).
[35] I. Paegle, F. Minelli, G. Fischer, Cracking and load-deformation behavior of fiber reinforced concrete: influence of testing method, Cem. Concr. Compos. 73 (2016) 147–163, https://doi.org/10.1016/j.cemconcomp.2016.06.012.
[36] R. Breitenbücher, G. Meschke, F. Song, Y. Zhan, Experimental, analytical and numerical analysis of the pullout behaviour of steel fibres considering different fibre types, inclinations and concrete strengths, Struct. Concr. 15 (2014) 126–135, https://doi.org/10.1002/suco.201300058.
[37] V.D. Mois, V. Chiriac, Response of single fibers to pull-out forces at different embedment angles, Technical University of Denmark, 2017. https://findit.dtu.dk/en/catalog/2385161887 (accessed February 7, 2019).
[38] C. DiFrancia, T.C. Ward, R.O. Claus, The single-fibre pull-out test. 1: review and interpretation, Compos. Part A Appl. Sci. Manuf. 27 (1996) 597–612, https://doi.org/10.1016/1359-835X(95)00069-E.
[39] R.J. Gray, Analysis of the effect of embedded fibre length on fibre debonding and pull-out from an elastic matrix, J. Mater. Sci. 19 (1984) 1680–1691, https://doi.org/10.1007/BF00563066.
[40] H.E. Daniels, The statistical theory of the strength of bundles of threads. I, Proc. R. Soc. London. Ser. A. Math. Phys. Sci. 183 (1945) 405–435. doi:10.1098/rspa.1945.0011.
[41] N. Metropolis, S. Ulam, The Monte Carlo method, J. Am. Stat. Assoc. 44 (1949) 335–341, https://doi.org/10.1080/01621459.1949.10483310.
[42] A. Adamczyk, Influence of rotation on uni-axial tension tests of SFRC, Technical University of Denmark, 2017. https://findit.dtu.dk/en/catalog/2385162056 (accessed May 16, 2019).
[43] L. Alm, Investigation of crack propagation in SFRC using an experimental approach, Technical University of Denmark, 2017. https://findit.dtu.dk/en/catalog/2372287874 (accessed May 16, 2019).
[44] I. Löfgren, Fibre-reinforced concrete for Industrial Construction – a fracture mechanics approach to material testing and structural analysis, 2005.
[45] F. Isla, G. Ruano, B. Luccioni, Analysis of steel fibers pull-out. Experimental study, Constr. Build. Mater. 100 (2015) 183–193, https://doi.org/10.1016/j.conbuildmat.2015.09.034.
[46] J.P. Suuronen, A. Kallonen, M. Eik, J. Puttonen, R. Serimaa, H. Herrmann, Analysis of short fibres orientation in steel fibre-reinforced concrete (SFRC) by X-ray tomography, J. Mater. Sci. 48 (2013) 1358–1367, https://doi.org/10.1007/s10853-012-6882-4.
[47] J.A.O. Barros, Steel fibre reinforced concrete: Material properties and structural applications, Fibrous Compos. Mater. Civ. Eng. Appl. (2011) 95–155, https://doi.org/10.1533/9780857095583.2.95.
[48] L. Yang, A. Fatemi, Cumulative fatigue damage mechanisms and quantifying parameters: a literature review, J. Test. Eval. 26 (1998) 89, https://doi.org/10.1520/JTE11978J.
[49] G.H. Mahmud, Z. Yang, A.M.T. Hassan, Experimental and numerical studies of size effects of Ultra High Performance Steel Fibre Reinforced Concrete (UHPFRC) beams, Constr. Build. Mater. 48 (2013) 1027–1034, https://doi.org/10.1016/J.CONBUILDMAT.2013.07.061.
[50] S. Tarasovs, J. Krūmiņš, V. Tamužs, Modelling of the fracture toughness anisotropy in fiber reinforced concrete, Frat. Ed Integrità Strutt. 35 (2016) 271–277, https://doi.org/10.3221/IGF-ESIS.35.31.
[51] E.S. Bernard, Durability of cracked fibre reinforced shotcrete, in: E.S. Bernard (Ed.), Shotcrete More Eng. Dev. Proc. Second Int. Conf. Eng. Dev. Shotcrete, A.A. Balkema Publishers, Sydney, Australia, 2004: pp. 59–66.
[52] E.S. Bernard, Age-dependent changes in post-crack performance of fibre reinforced shotcrete linings, Tunn. Undergr. Sp. Technol. 49 (2015) 241–248, https://doi.org/10.1016/j.tust.2015.05.006.

Chapter 7
Discussion, design implications and perspectives for development

The investigations presented in this thesis were initiated to address discrepancies observed within design guidelines regarding the applicability of cracked SFRC in corrosive exposure conditions. These discrepancies appeared to be motivated by inconsistencies within former research in the case of chloride (e.g. XD and XS exposure classes in EN-206) and carbonation exposure classes (XC exposure class), and to a general lack of research in the case of chemical attack (e.g. XA exposure class).

The specification of a critical crack width for SFRC exposed to wet-dry cycles involving chlorides and carbon dioxide was of particular interest to practitioners, but was also the main subject of concern and disagreement among academics. Strong disagreement was found among researchers when describing variations in the performance of SFRC with cracks in the range of 0.1 – 0.3 mm subject to wet-dry cycles involving chlorides and carbon dioxide. Studies reported either a substantial increase of the residual tensile strength of the cracked SFRC or else a dramatic drop of it. Yet, some studies pointed out that part of these changes may be due to an excessive development of the fibre-matrix bond strength during exposure.

An experimental campaign exposing cracked SFRC and single-fibre specimens was carried out within this thesis in order to investigate the extent of damage and deterioration mechanisms inside cracks in the range of 0.15 – 0.3 mm under such wet-dry conditions involving chloride and carbon dioxide exposure. The exposure time was limited to a maximum of two years under laboratory conditions, yet the investigations identified key deterioration mechanisms affecting the long-term performance of cracked SFRC.

The discussion below begins with a critical comparison of the findings of this study with the background presented in Chapter 1 and Chapter 2. Final remarks about the

implications of these findings on the design of uncracked and cracked SFRC are given as a closing discussion.

7.1 Deterioration phenomena and mechanical performance of SFRC

The discussion presented in Chapter 1 and Chapter 2 of this thesis showed that traditional deterioration models proposed for corrosion deterioration of steel reinforcement in concrete (Tuutti, 1982), (shown indicatively in **Figure 1**) may not be fully applicable to SFRC. The model assumes corrosion damage as the governing deterioration mechanism affecting the performance of SFRC. However, these assumptions are not fully coherent with the increases of the mechanical performance reported in former studies (Chapter 2) and presented in this thesis at the composite level (Chapter 3).

The discussion below describes and connects the experimental observations presented at the composite level and at the single-fibre level in Chapter 3 and Chapter 4, respectively, with the deterioration model proposed in Chapter 5. Observations at the single-fibre level and composite level were connected by the multiscale mechanical model presented in Chapter 6.

7.1.1 A conceptual deterioration model for SFRC

A simplified representation of the conceptual deterioration model described in Chapter 5 of this thesis is presented in **Figure 3**. The model describes two types of mechanisms affecting the durability of the SFRC under these exposures: deterioration and recovery mechanisms. These mainly affect two elements in the fibre reinforced composite: i) the steel fibre, that can be damaged due to corrosion, and ii) the porous cement matrix, where the transport of species and moisture occur, and thus alter microstructure and chemical composition of the matrix. The combination of these processes leads, for example, to variations of the tensile performance of the SFRC, that are identified in **Figure 3** as “global deterioration”.

The model considers that alterations of the mechanical performance of SFRC reported in Chapter 3 (mainly in the cracked state) can be related to changes in the pull-out performance of the individual fibres crossing the crack (Chapter 4).

The connection of the pull-out performance at the single-fibre level and the tensile performance at the composite level was done in Chapter 6 by means of a semi-empirical multiscale model based on the fibre-bundle approach. This model framework explained alterations of the tensile strength and toughness measured at the composite level (Chapter 3) to reductions of the tensile capacity of the fibre and variations of the fibre-matrix bond strength reported in Chapter 4.

The two main features that governed the variations of the pull-out behaviour of the fibres were the tensile capacity of the steel fibre and the fibre-matrix bond strength. So that, a critical decrease of the first, or an excessive increase of the second can lead to a premature rupture of the fibre, as discussed in Chapter 4. The tensile capacity of the fibre is governed by the reduction of the cross-section of the fibre due to corrosion. Variations of the fibre-matrix bond strength are related to microstructural changes of the cement matrix around the steel fibres. Thus, the three groups of processes shown in **Figure 3** govern the changes in the pull-out behaviour and thus the tensile performance of the exposed SFRC.

i) Ingress and transport of species and moisture leads to changes in the composition of the pore solution inside the cement matrix and the crack. Transport processes inside the cement matrix and cracks did not have a direct impact on the mechanical performance of the SFRC in this study, but promoted the alteration of the matrix composition and microstructure (e.g. carbonation, leaching, healing) and eventually the corrosion of the steel fibres.

ii) Dissolution and formation of new phases of the cement matrix around the fibres alters the fibre-matrix bond, for example leading to a stronger fibre-matrix bond in the experiments carried out in this thesis. This "autogenous healing" process was attributed in this work to precipitation and subsequent carbonation of portlandite in cracks and damage in the cement matrix around the steel fibre due to exposure. An excessive increase of the strength of this bond leads to rupture of the fibre during pull-out or fracture of the concrete matrix.

iii) Critical changes in the composition of the solution in contact with the surface of the steel fibres (e.g. pH or Cl^-) promote the depassivation of the steel and the reduction of the cross-section due to corrosion. Corrosion of fibres embedded in uncracked SFRC was found at voids and local defects in the cement matrix around the fibre, while corrosion of fibres crossing cracks occurred at an area of approx. 2 – 4 mm around the intersection between the fibre and the crack. A critical reduction of the fibre cross-section due to corrosion leads to premature rupture.

7.1.2 Corrosion damage and mechanical performance of SFRC

The relative contribution of the processes described above to the global deterioration of the mechanical performance of the composite is expected to vary depending on a number of parameters, for example: presence and size of cracks, dimensions and geometry of the cross-section, exposure conditions or matrix and type of fibre. The

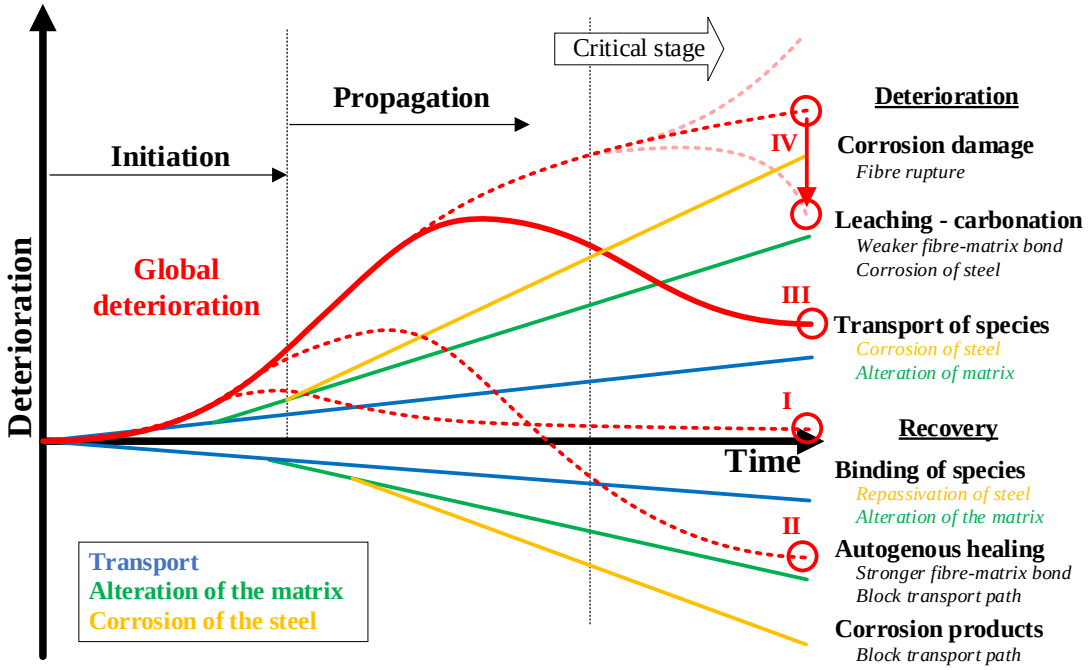

Figure 3 Updated conceptual deterioration model. Individual mechanisms are separated into deterioration and recovery processes and are depicted as linear processes, while the global damage process is presented as a non-linear process. Distances and trends presented in the graphic are indicative. Indicative points of the "global deterioration" function are shown in roman numbers. After (Marcos-Meson et al., 2019).

impact of these parameters on the corrosion damage and mechanical performance of SFRC are discussed briefly below in the context of this study and former research.

Presence of cracks and crack width

According to the deterioration model described above, the presence and width of cracks in SFRC contributes to the deterioration and recovery processes occurring at the composite and fibre level:

At the composite level, cracks facilitate the access of species trough the cross-section of the SFRC. Transport processes in uncracked concrete are hindered by the tortuosity of the pore microstructure, and thus corrosion damage of the fibres only occurs at the surface, where the cement matrix is altered by the exposure. Larger crack widths extend the transport of species inside the crack leading to alteration of the matrix and eventually corrosion of the steel fibres. Autogenous healing processes at the crack can block the access of species and moisture, but its effectiveness decreases, among others, with increasing crack width.

At the single-fibre level, there is limited porosity and voids at the matrix surrounding the fibres in uncracked concrete, and thus limited access of species to induce corrosion of the steel and alter the fibre-matrix bond. As the concrete cracks, this interface is damaged allowing access of species. Larger crack widths entail larger mechanical damage to the fibre-matrix interface, thus higher probability of corrosion damage around the fibre and lower probability of autogenous healing at the interface and surrounding matrix.

Exposure of uncracked SFRC in this study resulted in limited corrosion damage and moderate alteration of the uncracked concrete matrix, e.g. within a few centimetres from the exposed surface, as also reported in former studies (O'Neil and Devlin, 1999). These conditions led to negligible changes in the performance of the SFRC, see "I" in **Figure 3**. The presence of cracks resulted in a substantial increase of corrosion damage through the cross-section of the specimens, but also to large variations of the fibre-matrix bond strength regardless of the exposure conditions, see "III" or "IV" in **Figure 3**. Similar variations in the deterioration trends in the presence of cracks were reported in former research, leading in some cases to an increase of the tensile performance over time (Granju and Balouch, 2005) or a decrease (Roque et al., 2009) relative to uncracked SFRC.

As described above, the crack width is expected to have a critical impact on the deterioration and performance of SFRC. Experimental investigations of this study showed a clear detriment in tensile performance with increasing crack width when comparing cracks of 0.15 and 0.3 mm, but being still larger than for uncracked reference specimens, e.g. equivalent to "III" or "IV" in **Figure 3**. Similar conclusions were drawn in the literature review (Chapter 2), which showed general agreement regarding critical deterioration during exposure when cracks were wider than approx. 0.5 mm.

Summarising, the presence of cracks in SFRC is expected to "stimulate" most of the deterioration and recovery processes described in **Figure 3**. Larger crack widths will reduce the effectiveness of the healing processes occurring at the cement matrix and at the crack while increasing the impact of the deterioration processes occurring at the fibre and cement matrix.

Dimensions and geometry of the cross-section

The contribution of the deterioration processes described by the model varies depending on the transport processes inside the pore structure of the cement matrix or inside cracks. So that, reductions of the tensile capacity of the fibres and variation of the fibre-matrix bond strength are not necessarily uniform throughout the cross-section of the exposed elements.

Results from this study (Chapter 3) showed that corrosion damage inside uncracked SFRC was limited to fibres located at the surface of the specimen, e.g. within the carbonated concrete matrix at a distance of approx. less than 5 mm to the surface. Former research generally showed similar results for cross-sections comparable to the ones investigated here, e.g. in the order of 100 cm^2 (Balouch et al., 2010; O'Neil and Devlin, 1999). Studies investigating much smaller cross-sections, e.g. in the order of 10 cm^2 (Kosa and Naaman, 1990), showed a substantial drop of the tensile performance (e.g. "II" in **Figure 3**).

Corrosion damage of steel fibres inside the cracks investigated in this study was observed within the outer 20 – 40 mm of the crack (Chapter 3), generally corresponding to the fibres located within the carbonated zones of the crack, the presence of chlorides increased the degree of corrosion damage (Chapter 5). The depth inside the crack where corrosion was found mainly varied with the crack width and type of exposure, but not substantially over time. Similar conclusions were drawn in former studies that investigated comparable cross-sections and crack widths (Granju and Balouch, 2005; Mangat and Gurusamy, 1988; Nemegeer et al., 2000; Nordström, 2005). Investigations of SFRC with smaller cross-sections, e.g. up to one order of magnitude smaller showed critical corrosion damage and substantial decrease of the tensile performance of the cracked SFRC (Kosa and Naaman, 1990).

Therefore, both the reduction of the tensile capacity of the fibres due to corrosion and the variations of the fibre-matrix bond strength must be addressed as a size-dependent phenomena that affects the outermost fibres crossing cracks or embedded in the uncracked concrete matrix. The depth inside the cross-section where these alterations occur is directly linked to transport and reaction processes inside the cement matrix and cracks, so that its progress can be estimated over time based on interpolation of experimental data or predicted by means of mechanistic models (e.g. reactive mass transport models). This appreciation has a critical implication in traditional design approaches: the concept of a critical crack width cannot be strictly applied to SFRC, since any "critical crack width" would necessarily imply a "critical crack depth" that increases over time, where deterioration and recovery processes concur.

The size-dependency of these phenomena explain some of the divergence reported in former studies, which generally showed much larger deterioration of the tensile performance of the cracked or uncracked SFRC when smaller cross-sections were investigated, as discussed above. The implications of such size-dependency to the structural behaviour of typical structural applications, for example: comprising hyperstatic structural elements with cross-sections of 300 – 600 mm (e.g. tunnel segments or ground-supported slabs), are still not fully described. However, limited damage is expected in such an element when negligible detriment in the bending strength is for example observed on a three-point bending notched element with a cross-section depth of 150 mm.

Exposure conditions

The exposure conditions define the chemical composition and saturation degree of the solution inside pores and cracks. These conditions govern the alteration processes occurring at the cement matrix (e.g. carbonation, leaching and healing) and ultimately the initiation and propagation of corrosion of steel fibres. The relative contribution of the deterioration and recovery processes on the global deterioration of the mechanical performance of the SFRC varies depending on the exposure conditions.

Exposure to wet-dry cycles of cracked SFRC investigated in this study resulted in considerable corrosion damage at the outer cross-section of the specimens (Chapter 3). The exposure led to substantial alteration of the cement matrix adjacent to the crack and around fibres, e.g. involving leaching and carbonation of the cement matrix, but also autogenous healing of cracks and damage. These processes occurring in the cement matrix resulted in a substantial increase of the fibre-matrix bond strength, see "III" in **Figure 3**. The residual tensile strength of the SFRC specimens tested varied similarly, regardless of the exposure conditions tested (e.g. chloride or freshwater exposure). However, it changed consistently when increasing the crack width. This showed, that under the exposure conditions investigated in this thesis, deterioration and healing at the matrix dominated over corrosion damage; yet this is not necessarily true for every exposure scenario.

Other exposure factors, such as the cycle length of the wet-dry cycles, the relative humidity or the temperature were discussed in Chapter 2, but were not experimentally investigated in this thesis. Changes in the exposure conditions, for example involving a different degree of saturation, a significant flow velocity of the solution or a much lower pH encompass large variations in the performance, not solely due to corrosion damage.

Exposures involving stable moisture conditions at the specimen surface or inside cracks have been linked to minor corrosion damage and alteration of the cement matrix. These entailed small variations of the tensile performance of cracked SFRC, for example, under exposure to chlorides under fully immersed conditions (Roque et al., 2009), or airborne chlorides (Bernard, 2015b) see "I" in **Figure 3**.

Percolation of saltwater solution through cracks resulted in substantial ingress of chlorides and leaching damage of the cement matrix, which led to both substantial corrosion damage and deterioration of the cement matrix around the fibres (Hagelia, 2011b), and entailed critical reductions of the tensile performance in some studies (Batson, 1977; Rider and Heidersbach, 1978), see "II" in **Figure 3**.

Exposure to agents aggressive to the cement matrix, such as exposure of cracked SFRC to acetic acid (Roque et al., 2009) or sulphuric acid (Kaufmann, 2014), promoted large deterioration of the concrete matrix as well as corrosion damage, which resulted in a strong decrease of the tensile performance, even for uncracked SFRC (Roque et al., 2009), corresponding to "II" in **Figure 3**.

These examples show that, deterioration modelling approaches cannot only consider corrosion of the steel, e.g. described by the concentration of chlorides or the pH in pore solution, as the governing factor for deterioration of the mechanical performance of the SFRC in all cases. Under some exposures, deterioration and recovery processes occurring at the cement matrix and inside cracks (e.g. leaching, carbonation or autogenous healing) may dominate over corrosion damage. Additional understanding

of these processes is needed to identify the governing deterioration mechanism in different exposure scenarios.

Matrix and fibre type

The tensile performance of SFRC reinforced with hooked-end fibres is governed by the balance between the tensile capacity of the fibre and the strength of the bond between the fibre and the cement matrix. The combination of these parameters is optimized during the design of the SFRC mix (Vandewalle, 1999). However, these parameters may change over time due to the exposure, which can lead to either increase or decrease of the tensile performance of the SFRC.

From current understanding, the tensile capacity of the fibre can only be reduced due to corrosion, but this reduction is not necessarily critical. Accordingly, fibre corrosion can only be related to a reduction of the maximum pull-out force and tensile strength of SFRC. The study presented in Chapter 3 showed a correlation between fibre corrosion and rupture of fibres during pull-out, but still having a negligible impact on the total count of fibres rupturing during the experiment.

Conversely, the fibre-matrix bond strength can either increase or decrease due to exposure. Deterioration of the cement matrix around the fibre (e.g. due to leaching or mechanical damage) leads to a decrease of the bond strength; while hydration processes or healing processes may increase it. Under the exposure conditions and mix-design variables covered in this study, rupture of fibres was correlated with measured increases of the residual tensile strength and tensile toughness of the SFRC, see "III" in **Figure 3**. These observations were explained by the strengthening of the mechanical bond between the fibre and the concrete matrix in Chapter 4.

The discussion presented in Chapter 4 and Chapter 6 confirmed that an insufficient tensile capacity of the steel fibre, e.g. that cannot accommodate moderate increases of the fibre-matrix bond strength over time, may result in critical reductions of the tensile toughness of SFRC over time, e.g. leading to "IV" in **Figure 3**. This behaviour would be characterized by an increase of the maximum tensile strength of the SFRC followed by a steep decrease of it afterwards.

This argument may explain some of the inconsistency in the literature that investigated corrosion damage and performance in cracks in the range 0.1 – 0.3 mm, as discussed in Chapter 2. However, few authors reported clearly these effects (Bernard, 2015b, 2004). It is not fully clear, which is the share of the literature that might have misinterpreted corrosion damage with variations of the fibre-matrix bond strength. Yet, based on the insight presented in this thesis, a share of the decrease of toughness in studies reporting increases of the peak strength are likely to be related to increases of the fibre-matrix bond strength during the exposure.

7.2 Design implications

In most aspects, traditional models may produce conservative estimations that do not compromise the service-life of the structure due to corrosion damage of the steel fibre; but some aspects such as variations of the fibre-matrix bond strength during exposure time are not addressed. The approach of most design guidelines was to specify a crack width limitation similar to conventional reinforcement (e.g. $w_{k,crit}$ = 0.1 – 0.3 mm) or else enforce uncracked conditions in service. Additional recommendations such as sacrificial layers in the range of Δ_h = 10 – 40 mm, or special measures (e.g. use of non-corroding steel alloys or design by testing) were specified in few guidelines.

7.2.1 Uncracked SFRC

The discussion presented above confirm the conclusions of former research and support the current design approach for uncracked SFRC, where a nil or minimal sacrificial layer to account for fibre corrosion is considered in the design of SFRC under chloride (e.g. XS and XD exposure classes) or carbonation (e.g. XC exposure class) exposure. A sacrificial design layer of, e.g. up to one-half of the fibre length could be prescribed for deemed-to-satisfy design approaches, to disregard the mechanical contribution of fibres in contact with the surface that would corrode. Performance-based service-life design approaches may consider the depth of carbonation as the governing factor for estimation of corrosion initiation of embedded fibres, yet it is not clear whether corroding fibres embedded in uncracked SFRC may reach a critical loss of their tensile capacity.

For other corrosive exposures, such as in the case of acid attack, design criteria are imprecise or not specified. Based on the literature review in Paper II, fibre corrosion is not expected to dominate the deterioration of the mechanical performance of the composite. Consideration of a sacrificial layer for uncracked SFRC exposed to acids (e.g. XA exposure class) would mainly depend on the degradation of the concrete matrix that could be calculated as for plain concrete, e.g. disregarding the contribution of the steel fibres. Yet, experiments were not performed in this aspect and the discussion is based on conclusions from former research. Alternatively, the use of advanced modelling tools such as reactive-mass transport models may provide a more detailed description of the deterioration of the concrete matrix (e.g. pH, porosity) over time, yet research is needed to develop these further.

7.2.2 Cracked SFRC

The experimental observations and discussion presented in this thesis indicates that, design approaches based solely on disregarding the contribution of the outermost fibres crossing the crack, selecting a critical crack width or enforcing the use of non-corroding steel alloys, may only approach the corrosion damage issue. In this regard, increases in the fibre-matrix bond strength could eventually lead to critical reductions of the material toughness if the tensile capacity of the fibre is not correctly selected (e.g. steel strength, fibre cross-section and bond strength). A simplified design strategy may entail, for example, the overestimation of the concrete strength class when selecting the steel fibre in the pre-design phase; but still disregarding the contribution of the additional strength gained during exposure, which would result in a conservative approach.

Calculation of a critical crack width and sacrificial layer for carbon-steel fibres could be approached by means of extrapolation of experiments in cracked SFRC or plain concrete or by comparing carbonation/chloride ingress depths of plain concrete structures. In this regard, chloride threshold values have been proposed in former studies, yet $[Cl^-]$ or $[Cl^-]/[OH^-]$ thresholds would vary within one order of magnitude. Results in this study indicate that specification of these parameters (e.g. critical crack width and sacrificial layer) based on the expected pH in the solution of the crack may provide a more reliable estimation instead, considering either the presence or absence of chlorides as a factor leading to critical fibre corrosion or not.

Under other corrosive exposures, such as acids (e.g. XA exposure class), fibre corrosion may be as well a secondary source of damage, yet hypotheses and conclusions from former studies were not tested in this investigation. Fibre corrosion may be addressed as in the case of carbonation induced corrosion, where a critical crack width and

sacrificial layer accounting for fibre corrosion may be estimated based on the decrease of the pH inside the crack below a specific threshold (e.g. pH < 9). The penetration depth of this front over time may be predicted based on, for example: experience in plain cracked concrete, semi-empirical modes or advanced modelling approaches such as reactive mass transport models. Again, in this case the main source of performance loss is expected to be related to the alteration of the cement matrix surrounding the fibres that bridge the crack; but specifying design recommendations in this regard is limited by the lack of data available.

7.3 Perspective for development and final remarks

A more advanced approach for specifying the long-term mechanical performance of the cracked or uncracked composite under these conditions may comprise the estimation of a constitutive law based on the predicted performance at the single-fibre level, as presented in Chapter 6. This approach may result in a unique constitutive law for each part of the material analysed, depending on the level of damage estimated from fibre corrosion and variations in the fibre-matrix bond strength due to exposure. Corrosion damage may be estimated based on the chemical composition of the pore solution or inside the crack (e.g. pH or $[Cl^-]$), which could be predicted based on semi-empirical models or reactive mass transport models. Thus, providing a holistic modelling approach to the mechanical performance of SFRC under corrosive exposures. Despite the completeness and predictive capabilities of this approach, practical implementation of such model would require a large amount of development and additional data, in addition to a large computational demand.

Finally, it must be emphasised that the discussion presented herein covered results from a limited share of the types of steel fibres and alloys, as well as mix-designs available. Parameters such as the duration of the exposure or the length of the wet-dry cycles could not be fully investigated, nor validated to field exposure tests. Other exposure scenarios, such as the case of fully immersed elements, spray/atmospheric exposure to chlorides or percolation through cracks were not covered in this study and were only discussed based on former literature.

Among these, the case of percolation of water through cracks (e.g. neutral, acidic or saline) is lightly covered in the literature; yet it represents a critical exposure scenario for e.g. the design of tunnel linings, that must be investigated in depth before providing guidance. Despite these limitations, conditions inside the crack may be as well studied based on results from plain concrete, as suggested above.

All things considered, the results and design implications discussed above must not be considered as a design guideline or design recommendations. The discussion herein is based on a limited number of experiments under controlled conditions, for a relatively short period of time compared to the expected service life of typical infrastructure. The results and discussion presented in this thesis are not intended to be used for extrapolation to structural applications, but to serve as a basis for a better understanding of the material performance under these exposures.

Chapter 8
Conclusions and future work

In Chapter 2, the literature review revealed inconsistencies in design guidelines and former studies regarding the durability of cracked SFRC under corrosive exposures. A conceptual deterioration model was proposed to clarify the deterioration mechanisms affecting cracked SRFC.

- There is no general concern regarding durability of uncracked SFRC under corrosive exposures. Chloride and carbonation induced corrosion of steel fibres resulted in aesthetical damage at the surface. Corrosion damage of the steel fibres under acidic exposure is expected secondary compared to deterioration of the cement matrix. General agreement was found in design guidelines.
- There is disagreement in former studies regarding the performance of cracked SFRC under wet-dry exposure to chlorides and carbon dioxide. There is limited research covering the performance of cracked SFRC under acidic exposures. Inconsistent recommendations in design guidelines were attributed to discrepancy in research.

In Chapter 3, investigation of the performance of SFRC under wet-dry cycles of chlorides and carbon dioxide determined that fibre corrosion may not be the dominant deterioration mechanism affecting the mechanical performance of cracked SFRC during exposure.

- Corrosion damage of steel fibres in uncracked SFRC affected the outermost fibres, directly exposed to the solution or embedded within few mm from the surface, where the concrete matrix was carbonated. The presence of chlorides only increase the corrosion damage at the surface. There was no measurable variation of the compressive strength of the uncracked SFRC within the time-span investigated.
- Corrosion damage only affected the fibres located at the outermost area of the crack, close to the surface of the specimen. The depth inside the crack where

corroding fibres were found increased for larger crack widths but did not vary significantly over time comparing one- and two-year exposure.

- Corrosion damage of fibres inside cracks had a moderate impact on the residual strength of the specimens tested. There was a clear size-dependency to the detriment of the mechanical performance of cracked SFRC over time.
- Variations of the fibre distribution in the cross-section of the specimens investigated had a dominant impact on the toughness of the cracked composite compared to corrosion damage of the fibres or the exposure time.
- Fibre rupture was generally related to an increase of the residual tensile capacity of the cracked SFRC. The impact of corrosion damage on the amount of fibres rupturing during pull-out was secondary compared to the increase in the fibre-matrix bond strength over the exposure.

In Chapter 3 and Chapter 4, investigations of the damage mechanisms involved in the deterioration of cracked SFRC under wet-dry cycles indicated that the alteration of the cement matrix surrounding the fibres may account for most of the changes of the mechanical performance of the cracked SFRC.

- Investigations at the single-fibre level confirmed that, a large share of the fibres rupture due to an increase of the fibre-matrix bond strength during the exposure to wet-dry cycles. Corrosion damage at the exposed surface of the steel had a considerable, but secondary, contribution to the rupture of fibres during pull-out.
- Corrosion of fibres crossing the crack mainly occurred at the steel exposed in the crack and was dominated by the pH inside the crack, also in the presence of chlorides. Data regarding the chloride concentration and pH in the solution around the fibres crossing the crack showed partial agreement with the threshold values proposed in the literature.
- The conceptual deterioration model proposed in the literature review, was compared and extended according to experimental observations. The model suggests that concurring dissolution and precipitation processes inside the crack and at the adjacent cement matrix have a dominant influence on the overall deterioration process.
- The increase of the fibre-matrix bond strength was attributed to an alteration of the cement matrix surrounding the fibres during the exposure. Autogenous healing at the fibre-matrix interface was proposed as the main mechanism responsible.

In Chapter 6, a multi-scale modelling approach was used to correlate results at the single-fibre and composite level; confirming that increase of the fibre-matrix bond strength was responsible for a large share of the variations observed in the toughness of the cracked SFRC.

- The model confirmed that measured increases of the toughness of the cracked composite are due to an increase in the fibre-matrix bond strength of partially pulled fibres during exposure.
- The study supports that corrosion of the steel fibres is not the only mechanism that may decrease the toughness of cracked SFRC under corrosive exposures.

An increase of the fibre-matrix bond strength over the exposure time may result as well in a critical decrease of the toughness of the cracked SFRC.

- The study concludes that design recommendations shall address the issue of deterioration of cracked SFRC under wet-dry exposure by considering both the corrosion damage of the outermost fibres crossing cracks and by accounting for increases in the fibre-matrix bond strength during the exposure time.

8.1 Future work

Investigations presented in this thesis focused on describing the global picture concerning the deterioration of cracked SFRC under corrosive exposures. The study could not fully cover all aspects of the issue, such as:

Understanding and predicting the transport and reaction processes inside cracks. Prediction of the transport of aggressive species inside cracks over periods corresponding to service-life prescriptions of large infrastructure (e.g. over 100 years) are limited by current modelling approaches, which in many aspects are based on experience with conventional structures. Development in the following areas is needed:

- Inspection of existing infrastructure built of SFRC under aggressive environments, and public reporting of the results is key to correlate observations in SFRC to the data available for plain and reinforced concrete. To date, few studies are available (Hagelia, 2011a; Nordström, 2005). Development of long-term laboratory and field experiments including non-destructive monitoring techniques is key to further development in the field.

- Development of more advanced modelling techniques, such as reactive mass transport modelling approaches (Michel et al., 2019, 2018), will contribute to a better understanding of the deterioration and (in many cases) healing processes concurring inside cracked concrete subject to aggressive exposures. Tailored experiments are also needed to verify and calibrate such models, as discussed in (Michel et al., 2019).

Describing the mechanisms involved in the corrosion of steel fibres crossing cracks. Observations in this study and former research have highlighted the limited corrosion damage of carbon-steel fibres in cracked SFRC. However, discussion of the corrosion mechanisms involved is scarce and, to date, mainly covers steel fibres in artificial pore solution with added chlorides (Dauberschmidt, 2006).

- Future experimental studies must focus on describing the relation between corrosion rates of steel fibres and: the chemical conditions at the steel surface, precipitation processes taking place at the exposed steel surface and the microstructural damage and healing at the fibre-matrix interface. Continuation of the development in these techniques presented at the composite level (Mangat and Gurusamy, 1988; Raupach et al., 2004) and in single fibres (Beglarigale and Yazıcı, 2017; Frazão et al., 2016) is needed.

- Development of tools for monitoring the electrochemical state of steel fibres embedded in cracked and uncracked SFRC are needed. Such tools could be used to instrument coupons and structures exposed under laboratory or field conditions over long time-spans. Development of such corrosion sensors was initiated in former studies (Nemegeer et al., 2000).

Describing variations in the pull-out performance of steel fibres in cracked SFRC. This study has shown the impact of alterations of the cement matrix surrounding fibres in the pull-out behaviour of these over time. However, results presented in this study only covered a small share of the parameters that could be investigated. Parameters such as the type and material of the fibre, the fibre orientation or the concrete composition must be covered.

- Experimental investigations covering other types of cold-drawn wire fibre (e.g. straight, crimped or helicoidal fibres), other fibre materials (e.g. glass, polymer or composite) as well as other design parameters (e.g. fibre orientation or concrete composition); are key for further understanding of the long-term performance of Fibre Reinforced Concrete (FRC) infrastructure.
- Development of multi-scale modelling approaches may facilitate the extrapolation of results at the single-fibre level to the tensile performance of the FRC composite. Such tools are key to the development of optimized fibre solutions that may overcome some of the issues presented in this study, e.g. premature fibre rupture due to an increase of the fibre-matrix bond strength.

List of references

The references below are included in the core of the thesis. References in the appended papers are included at the end of each publication.

Abbas, S., 2014. Structural and Durability Performance of Precast Segmental Tunnel Linings. University of Western Ontario.

Abbas, S., Soliman, A.M., Nehdi, M.L., 2015. Exploring mechanical and durability properties of ultra-high performance concrete incorporating various steel fiber lengths and dosages. Constr. Build. Mater. 75, 429–441. https://doi.org/10.1016/j.conbuildmat.2014.11.017

Abbas, S., Soliman, A.M., Nehdi, M.L., 2014. Chloride Ion Penetration in Reinforced Concrete and Steel Fiber-Reinforced Concrete Precast Tunnel Lining Segments. ACI Mater. J. 111, 613–622. https://doi.org/10.14359/51686991

ACI Committee 544, 2010. ACI 544.5R-10 - Report on the Physical Properties and Durability of Fiber-Reinforced Concrete, ACI Structural Journal. Farmington Hills, USA.

ACI Committee 544, 2002. State-of-the-Art Report on Fiber Reinforced Concrete. ACI 544.1R-96. United States.

Addassi, M., Michel, A., Meson, V.M., Kunther, W., 2019. MODELLING AND TESTING OF CARBONATION EFFECTS ON HYDRATED OIL-WELL CEMENTS, in: IFFSAR (Ed.), International Workshop. CO2 Storage in Concrete. Marne La Vallée, FR.

AFTES, 2013. AFTES-GT38R1A1. Design, dimensioning and execution of precast steel fibre reinforced concrete arch segments. France.

Angst, U., Elsener, B., Larsen, C.K., Vennesland, Ø., 2009. Critical chloride content in reinforced concrete — A review. Cem. Concr. Res. 39, 1122–1138. https://doi.org/10.1016/j.cemconres.2009.08.006

Balouch, S.U., Forth, J.P., Granju, J.-L., 2010. Surface corrosion of steel fibre reinforced concrete. Cem. Concr. Res. 40, 410–414. https://doi.org/10.1016/j.cemconres.2009.10.001

Batson, G.B., 1977. Strength of Steel Fiber Concrete in Adverse Environments. Champaign, Illinois (US).

Beglarigale, A., Yazıcı, H., 2017. Electrochemical corrosion monitoring of steel fiber embedded in cement based composites. Cem. Concr. Compos. 83, 427–446. https://doi.org/10.1016/j.cemconcomp.2017.08.004

Bernard, E.S., 2015a. Age-dependent changes in post-crack performance of fibre reinforced shotcrete linings. Tunn. Undergr. Sp. Technol. 49, 241–248. https://doi.org/10.1016/j.tust.2015.05.006

Bernard, E.S., 2015b. Effect of Exposure on Post-crack Performance of FRC for Tunnel Segments, in: Vrkljan, I., Dekovic, Z., Dobrilovic, M., Likar, J., Miscevic, P. (Eds.), SEE Tunnel:Promoting Tunneling in SEE Region - ITA WTC 2015. ITA-AITES, Dubrovnik, Croatia, p. 13.

Bernard, E.S., 2008. Embrinlement of Fiber-Reinforced Shotcrete. Shotcrete 16–21.

Bernard, E.S., 2004. Durability of cracked fibre reinforced shotcrete, in: Bernard, E.S. (Ed.), Shotcrete: More Engineering Developments: Proceedings of the Second International Conference on Engineering Developments in Shotcrete. A.A. Balkema Publishers, Sydney, Australia, pp. 59–66.

Berrocal, C.G.I.L., 2015. Chloride Induced Corrosion of Steel Bars in Fibre Reinforced Concrete. Chalmers University of Technology SE-412.

Bertolini, L., Elsener, B., Pedeferri, P., Redaelli, E., Polder, R.B., 2013. Corrosion of Steel in Concrete: Prevention, Diagnosis, Repair, Second. ed. John Wiley & Sons.

Cangiano, S., Plizzari, G. a, Cadoni, E., Frigeri, G., Teruzzi, T., 2005. On durability of steel fibre reinforced concrete, in: Dhir, R.K., Harrison, T.A., Newlands, M.D. (Eds.), International Conference of Cement Combinations for Durable Concrete. Thomas Telford, Dundee, Scotland, pp. 477–486. https://doi.org/10.1680/ccfdc.34013

CRN, 2006. Guide for the Design and Construction of Fiber-Reinforced Concrete Structures. Italy.

DAfStb, 2012. DAfStb Stahlfaserbeton. Deutscher Ausschuss für Stahlbeton e. V. - DAfStb, Germany.

Dauberschmidt, C., 2012. Corrosion mechanism of steel fibres in concrete. München.

Dauberschmidt, C., 2006. Untersuchungen zu den Korrosionsmechanismen von Stahlfasern in chloridhaltigem Beton. Munich University.

de Rivaz, B., 2009. Steel fiber reinforced concrete (SFRC): The use of SFRC in precast segment for tunnel lining, in: Kanjlia, V.K. (Ed.), Water and Energy International. Indian Central Board of Irrigation & Power, Bekaert (France), pp. 75–84.

European Commitee for Standardization (CEN), 2013. Concrete. Specification, performance, production and conformity. EN 206. European Union.

European Commitee for Standardization (CEN), 1993. Eurocode 2: Design of concrete structures - Part 1-1: General rules and rules for buildings. ENV 1992-1-1:1993, European Union.

Frazão, C., Barros, J., Camões, A., Alves, A.C., Rocha, L., 2016. Corrosion effects on pullout behavior of hooked steel fibers in self-compacting concrete. Cem. Concr. Res. 79, 112–122. https://doi.org/10.1016/j.cemconres.2015.09.005

Frazão, C., Camões, A., Barros, J., Gonçalves, D., 2015. Durability of steel fiber reinforced self-compacting concrete. Constr. Build. Mater. 80, 155–166. https://doi.org/10.1016/j.conbuildmat.2015.01.061

Frazão, C.M. V., Camões, A., Barros, J.A.O., Gonçalves, D., 2013. Durability of steel fiber reinforced self-compacting concrete, in: Cavaleiro, V., Pinto, I., Gomes, L.M.F., Gomes, C., Lopes, S., Bernardo, L. (Eds.), 5th International Conference on the Concrete Future. CI-Premier Pte Ltd, Covilhã, Portugal, pp. 93–102.

German Society for Concrete and Construction Technology, 2001. Guide to Good Practice: Steel fibre concrete. Germany.

Granju, J.-L., Balouch, S.U., 2005. Corrosion of steel fibre reinforced concrete from the cracks. Cem. Concr. Res. 35, 572–577.

https://doi.org/10.1016/j.cemconres.2004.06.032

Hagelia, P., 2011a. Deterioration Mechanisms and Durability of Sprayed Concrete for Rock Support in Tunnels. Technical University of Deltf.

Hagelia, P., 2011b. Sprayed concrete in aggressive subsea environment the Oslofjord test site, in: 6th International Symposium on Sprayed Concrete - Modern Use of Wet Mix Sprayed Concrete for Underground Support. Tromsø, Norway, p. 15.

Havlik, R., Galik, I., 2017. Creep Behavior of Fiber Reinforced Concrete. Technical University of Denmark.

Hwang, J.P., Jung, M.S., Kim, M., Ann, K.Y., 2015. Corrosion risk of steel fibre in concrete. Constr. Build. Mater. 101, 239–245. https://doi.org/10.1016/j.conbuildmat.2015.10.072

International Federation for Structural Concrete, 2010. FIB Model Code for concrete structures 2010. Lausanne, Switzerland.

Kamal, M.M., El-Refai, F.E., 1987. Durability of steel fibre reinforced concrete, in: Proceedings of the Fourth International Conference on Durability of Building Materials and Components. Elsevier, Singapore, pp. 235–247. https://doi.org/10.1016/B978-1-4832-8386-9.50034-6

Kaufmann, J.P., 2014. Durability performance of fiber reinforced shotcrete in aggressive environment, in: Negro, A., Bilfinger, W., Cecilio, M.O. (Eds.), WTC 2014 – Tunnels for a Better Life. ITA-AITES, Iguaçu, Brazil, pp. 1–7.

Kosa, K., Naaman, A.E., 1990. Corrosion of Steel Fiber Reinforced Concrete. ACI Mater. J. 87, 27–37.

Kragh, A.K., Carlsen, M.E., 2017. Development of fibre-matrix bond over time. Technical University of Denmark.

Kragh, A.K., Carlsen, M.E., Marcos-Meson, V., Fischer, G., Michel, A., 2019. The influence of concrete maturity on the pull-out behaviour of steel fibres at early-ages, in: Derkowski, W., Gwoździewicz, P., Hojdys, Ł., Krajewski, P., Pańtak, M. (Eds.), Proceedings of the Symposium 2019. Concrete - Innovations in Materials, Design and Structures. Fédération Internationale du Béton (fib), Krakow, Poland, pp. 471–479.

Mangat, P.S., Gurusamy, K., 1988. Corrosion resistance of steel fibres in concrete under marine exposure. Cem. Concr. Res. 18, 44–54. https://doi.org/10.1016/0008-8846(88)90120-2

Mangat, P.S., Gurusamy, K., 1987a. Chloride diffusion in steel fibre reinforced marine concrete. Cem. Concr. Res. 17, 385–396. https://doi.org/10.1016/0008-8846(87)90002-0

Mangat, P.S., Gurusamy, K., 1987b. Permissible crack widths in steel fibre reinforced marine concrete. Mater. Struct. 20, 338–347. https://doi.org/10.1007/BF02472580

Marcos-Meson, V., Geiker, M., Fischer, G., Solgaard, A., Jakobsen, U.H., Edvardsen, C., Danner, T., Skovhus, T.L., Michel, A., 2019. Durability of cracked SFRC exposed to wet-dry cycles of chlorides and carbon dioxide – multiscale deterioration phenomena (Unpublished). Cem. Concr. Res.

Marcos-Meson, V., Michel, A., Solgaard, A., Fischer, G., Edvardsen, C., Skovhus, T.L., 2018. Corrosion resistance of steel fibre reinforced concrete - A literature

review. Cem. Concr. Res. 103, 1–20. https://doi.org/10.1016/j.cemconres.2017.05.016

Meda, A., Plizzari, G.A., 2005. New Design Approach for Steel Fiber-Reinforced Concrete Slabs-on-Ground Based on Fracture Mechanics. ACI Struct. J. 101, 3–8.

Michel, A., Marcos-Meson, V., Geiker, M., 2019. Microstructural changes and mass transport in cement-based materials: a modeling approach (Unpublished). Cem. Concr. Res.

Michel, A., Meson, V.M., Stang, H., Geiker, M.R., Lepech, M., 2018. Coupled mass transport, chemical, and mechanical modelling in cementitious materials: A dual-lattice approach, in: Caspeele, R., Taerwe, L., Frangopol, D.M. (Eds.), Life Cycle Analysis and Assessment in Civil Engineering: Towards an Integrated Vision: Proceedings of the Sixth International Symposium on Life-Cycle Civil Engineering (IALCCE 2018). CRC Press, Ghent, Belgium, pp. 965–972.

Mois, V.D., Chiriac, V., 2017. Response of single fibers to pull-out forces at different embedment angles. Technical University of Denmark.

Nemegeer, D., Vanbrabant, J., Stang, H., 2000. Final report on Durability of Steel Fibre Reinforced Concrete. Copenhagen, Denmark.

New Zealand Standards, 2006. Concrete Structures Standard. NZS 3101:2006. New Zealand.

Nordström, E., 2005. Durability of Sprayed Concrete Steel fibre corrosion in cracks. Lulea University of Technology.

Norsk Beton, 2011. Sprayed Concrete for Rock Support. Publication no. 7. Norway.

O'Neil, E., Devlin, J.T., 1999. Durability of Fiber-Reinforced Concrete Under Flexural Stress in a Severe Marine Environment. Defense Technical Information Center, Vicksburg, US.

Raupach, M., Dauberschmidt, C., Eichler, T., 2004. Corrosion behaviour of steel fibres in concrete containing chlorides, in: EUROCORR 2004. CEFRACOR, Nice, FR, pp. 20–54.

Rider, R., Heidersbach, R., 1978. Degradation of Metal-Fiber Reinforced Concrete Exposed to a Marine Environment, in: Tonini, D.E., Gaidis, J.M. (Eds.), Corrosion of Reinforcing Steel in Concrete. ASTM International, Philadelphia, US, pp. 75–92.

RILEM, 2000. Test and design methods for steel fibre reinforced concrete, RILEM TC 162-TDF Workshop. France.

Roque, R., Kim, N., Kim, B., Lopp, G., 2009. Durability of Fiber-Reinforced Concrete in Florida Environments. Florida, USA.

Schupack, M., 1985. Steel Fiber Concrete, in: Shah, S.P., Skarendahl, A. (Eds.), Steel Fiber Concrete, US-Sweden Joint Seminar (NSF-STU). Elsevier, Stockholm, sweden, pp. 479–496.

SFRC Consortium, 2013. Design guideline for structural applications of steel fibre reinforced concrete. SFRC Consortium, Copenhagen, Denmark, Denmark.

Solgaard, A.O.S., 2014. Corrosion of reinforcement bars in steel fibre reinforced concrete structures. BYG Rapport. Technical University of Denmark, Department

of Civil Engineering.

Solgaard, A.O.S., Carsana, M., Geiker, M.R., Küter, A., Bertolini, L., 2013. Experimental observations of stray current effects on steel fibres embedded in mortar. Corros. Sci. 74, 1–12. https://doi.org/10.1016/j.corsci.2013.03.014

Spanish Development Ministry, 2009. Instrucción de hormigón estructural. EHE-08. EHE-2008, Spain.

Stefanoni, M., Angst, U., Elsener, B., 2018. Corrosion rate of carbon steel in carbonated concrete – A critical review. Cem. Concr. Res. 103, 35–48. https://doi.org/10.1016/j.cemconres.2017.10.007

Šušteršič, J., Ukrainczyk, V., Zajc, A., Aljosa, S., 2000. Ageing effect on post-crack behaviour of SFRC, in: Rossi, P., Chanvillard, G. (Eds.), Fifth RILEM Symposium on Fibre-Reinforced Concretes (FRC). RILEM Publications SARL, Lyon, France, pp. 623–631.

Swedish Standards Institute, 2014. SS 812310:2014. Fibre Concrete – Design of Fibre Concrete Structures. Sweden.

T. Teruzzi, Cadoni, E., Frigeri, G., Cangiano, S., Plizzari, G.A. a., Teruzzi, T., Cadoni, E., Frigeri, G., Cangiano, S., Plizzari, G.A. a., 2004. Durability aspects of steel fibre reinforced concrete, in: Prisco, M. Di, Felicetti, R., Plizzari, G.A. (Eds.), 6th International RILEM Symposium on Fibre Reinforced Concretes. RILEM Publications SARL, Varenna, Italy, pp. 625–634. https://doi.org/2912143748

Teixeira Buttignol, T.E., Colombo, M., di Prisco, M., 2016. Long-term aging effects on tensile characterization of steel fibre reinforced concrete. Struct. Concr. 17, 1082–1093. https://doi.org/10.1002/suco.201500149

The Concrete Society, 2007. TR-63. Guidance for the design of steel-fibre-reinforced concrete. TR63, United Kingdom.

Thorsen, M.S., Christensen, P., 2018. Impact of w/c-ratio on development of fibre-matrix bond in steel fibre reinforced concrete over time - DTU Findit. Technical University of Denmark.

Tuutti, K., 1982. Corrosion of steel in concrete, First. ed. Swedish Cement and Concrete Research Institute, Stockholm.

Vandewalle, L., 1999. Influence of tensile strength of steel fibre on toughness of high strength concrete. High Perform. Fiber Reinf. Cem. Compos. 6, 331–337.

Weydert, R., Schiessl, P., 1998. Korrosion von Stahlfasern in gerissenem und ungerissenem Stahlfaserbeton. Abschlussbericht. Bergisch Gladbach (Germany).